CRANFIELD INSTITUTE OF TECHNOLOGY

SCHOOL OF MECHANICAL ENGINEERING

Ph. D. Thesis

Erol Kilik

THE INFLUENCE OF SWIRLER DESIGN PARAMETERS ON THE AERODYNAMICS OF THE DOWNSTREAM RECIRCULATION REGION.

Supervisors: Professor A.H. Lefebvre
K.W. Ramsden.

May, 1976.

SUMMARY

The influence of swirler design parameters namely , vane shape (flat or curved), vane outlet angle, aspect ratio and space-to-chord ratio (number of vanes) , on the pressure drop-mass flow characteristics and the size and turbulence characteristics of the downstream recirculation region has been determined experimentally. A five-hole spherical pressure probe and hot-wire anemometry have been used for the investigation. A technique for simple and reasonably accurate interpretation of the signals from the hot-wire anemometer has been formulated. Its performance has been tested at first in round jets for which experimental turbulence data are already available for comparison purposes. The method has been applied subsequently to swirling flows issuing from the swirlers; the mean and turbulence characteristics of the flow fields have been determined in this way. In addition to these, the turbulent viscosities μ_{rr}, μ_{rz} , $\mu_{r\theta}$ and $\mu_{\theta\theta}$ have been calculated.Also,detailed accounts of the previous experimental work on swirling flows and of some finite difference procedures for the computation of weakly and strongly swirling flows have been given.

It has been shown that the hot-wire formulation developed provides a simple,economic and efficient procedure for the measurement of the turbulence quantities in swirling flows.

The results have shown that curved vane type swirlers operate more efficiently than flat vane types such that a larger recirculation region and a stronger shear zone are induced at a lower pressure drop.

The pressure drop through both the flat and curved vane type swirlers increases with increasing vane angle,decreasing aspect ratio and decreasing space-to-chord ratio.

The size of the downstream recirculation region,the reverse mass flow and the decay rates of the axial and swirl velocities increase with increasing vane angle and decreasing aspect ratio in the case of curved vane type swirlers. The effect of the space-to-chord ratio has not been found very significant in the cases of I6 and I2 vanes for the vane angle of 60°and the aspect ratio of 0.4 .

Higher turbulence and stronger shear zones can be obtained in swirling flows with increasing vane angle, decreasing aspect ratio and decreasing space-to-chord ratios.

Turbulence is anisotropic in strongly swirling jets issuing from vane type swirlers. The most dominant stresses

are in turn $\overline{ww}$, $\overline{uw}$ and $\overline{uu}$; all the other stresses are smaller . In parallel to the anisotropy in the stresses , the turbulent viscosities are also anisotropic ; the turbulent viscosity $\mu_{\theta\theta}$ has shown domination among the four viscosities which have been calculated. μ_{rr} values have shown too much scatter.

For these reasons, curved vane type swirlers should prove much more efficient than flat vane types in the application to combustion process.

ACKNOWLEDGEMENTS

Many thanks are due to Prof.A.H.Lefebvre and Mr.K.W. Ramsden for making this research possible, sincere supervision and continuous encouragement during the course of this work. I also would like to take this opportunity to thank Prof.R.S. Fletcher for further support during the completion period of the thesis.

Acknowledgement is also made to the Academic and Workshop Staff of the School of Mechanical Engineering of C.I.T..Skilful works, on the swirlers and the test rig, of Mr.Nobby Beatee, Mr.Charles Smith and Mr.Derek Brown are to be commended.

Many thanks go very gratefully to Dr.D.G.Lilley for long hours of discussion on several subjects.His very helpful suggestions and continuous support to keep up with the recent literature are unforgettable.

I am thankful to my wife, Sevim Kilik, for her help in typing this thesis.

LIST OF FIGURES

No.	TITLE
I.I	Air flow pattern in a conventional combustion chamber
I.2	Conventional flat vane type swirler with central blading and the related notation
I.3	Conventional flat vane type swirler with off-central blading
I.4	Variation of air outlet angle for flat plate cascades
I.5	Curved vane type swirler
I.6	Coordinate axes for the swirling flow
I.7	Recirculation region in a pipe step
I.8	Recirculation region in a swirling flow field
I.9	Typical profiles of the axial and swirl velocities in a strongly swirling flow field
4.I	The small volume (area) element over which integration is performed
4.2	Boundary conditions for free swirling jet
5.I	Test rig assembly
5.2	Orifice plate and flange for mass flow measurement
5.3	The settling chamber
5.4	B.S. Nozzle
5.5	B.S. Nozzle and the protrector mechanism
5.6	The test rig and the hot-wire anemometer system
5.7	The platform and the five-hole spherical pressure probe
5.8	The five-hole spherical pressure probe in position in the hole on the platform
5.9	Three types of vane swirler
5.I0	Picture of the swirler in Fig.5.9
5.II	Flat and curved vane type swirler
5.IIa	Picture of the swirlers in Fig.5.II
5.I2	Hub bullets
5.I3	Arrangement of the five holes on the head of the spherical pressure probe
5.I4	Structure of the head of the five-hole spherical pressure probe
5.I5	Calibration chart for directional sensitivity of the pressure probe
5.I6	Calibration chart for the calculation of static pressure
5.I7	An example of a traversing mesh
5.I8	Notation for the calculation of static pressure and the components of absolute velocity
6.I	Hot-wire probe head and the notation
6.2	Operation principle of hot-wire anemometer in constant temperature mode

6.3 Effective cooling velocity in the cosine cooling law
6.4a Cross section of the hot-wire placed perpendicularly in the flow field
6.4b The hot-wire placed obliquely into the flow field
6.5 Variation of the yaw coefficient with the length-to-diameter ratio of the wire
6.6 Variation of k_1 with yaw angle
6.7 Variation of the relative error in the calculation of velocity with yaw angle
6.8 Overall directional characteristics of a hot-wire probe
6.9 Increase in the velocity due to the thickness of the prong ends
6.10 Variation of k_2 with pitch angle
6.11 Variation of the relative error in the calculation of velocity with the pitch angle
6.12 Measurement of Reynolds stresses using an X-type hot-wire probe
6.13 Orientation of the hot-wires in six-orientation measurement technique
6.14 Application of the six-orientation method to the recirculation region in a swirling flow field
6.15 Application of the four-orientation technique to a swirling flow field with recirculation
6.16 The square wave form assumed for instantaneous wire voltage
6.17 Orientation of the hot-wire probe in a swirling flow field with recirculation
6.18 Variation of instantaneous wire voltage for three orientations of a hot-wire probe placed in the recirculation region
6.19 The three voltages are assumed to occur simultaneously with the assumption of stationary turbulence
6.20 A typical calibration curve for the hot-wire probe
6.21 Variation of heat transfer from the wire with yaw and pitch angles
6.22 Distribution of axial velocity in a straight round jet
6.23 Radial distribution of normalized axial velocity
6.24 Distribution of the shear stress $\overline{uv}$ in a straight round jet
6.25 Radial distribution of the normalized shear stress
6.26 Distribution of the kinetic energy of turbulence in a straight round jet
6.27 Radial distribution of the normalized turbulence kinetic energy
6.28 Distribution of the longitudinal turbulence intensity and normalized axial velocity on the axis of the straight jet
6.29 Profiles of the longitudinal turbulence intensity in the immediate downstream region of the nozzle

7.1 Typical profiles of the axial velocity component at the exit from the three types of swirler
7.2 Radial distribution of the swirl velocity component at the exit of the three types of swirler

7.3a Circumferantial distribution of the axial velocity component in the swirler
7.3b Radial distribution of the axial velocity component in the swirler
7.4 Pressure drop for vane type swirlers
7.5 Variation of the pressure drop coefficient with mass flow for flat and curved vane type swirlers
7.6 Variation of the pressure drop coefficient with mass flow for flat and curved vane type swirlers
7.6a Profile loss coefficient for conventional section blades at zero incidence
7.6b Variation of loss coefficient with the aspect ratio
7.7 Normalized pressure drop coefficient for flat and curved vane type swirlers
7.8 Comparison of the pressure drop coefficient for flat and curved vane type swirlers
7.9 Variation of the pressure drop coefficient with vane angle for flat and curved vane type swirlers
7.I0 Variation of the static pressure drop with mass flow for the swirlers
7.II Variation of the static pressure drop coefficient with mass flow for flat and curved vane type swirlers
7.I2 Variation of the static pressure drop coefficient with mass flow for flat and curved vane type swirlers
7.I3 Variation of the static pressure drop coefficient with vane angle for flat and curved vane type swirlers
7.I4 Distribution of static pressure along the jet axis for curved and flat vane type swirlers
7.I5 Distribution of the axial velocity in the jet issuing from the swirler S.I
7.I6 Distribution of the axial velocity in the jet issuing from the swirler S.4
7.I7 Distribution of the axial velocity in the jet issuing from the swirler S.6
7.I8 Distribution of the axial velocity in the jet issuing from the swirler S.9
7.I9 Distribution of the axial velocity in the jet issuing from the swirler S.I0
7.20 Distribution of the axial velocity in the jet issuing from the swirler S.II
7.2I Distribution of the axial velocity in the jet issuing from the swirler S.I2
7.22 Variation of the profiles of the normalized axial velocity in the flow field of the swirler S.I
7.23 Variation of the profiles of the normalized axial velocity in the flow field of the swirler S.4
7.24 Variation of the profiles of the normalized axial velocity in the flow field of the swirler S.6
7.25 Variation of the profiles of the normalized axial velocity in the flow field of the swirler S.I0
7.26 Variation of the axial velocity on the jet axis for different swirlers
7.27 Variation of the reverse mass flow along the jet axis for different swirlers

7.28 Variation of maximum reverse mass flow with swirl number
7.29 Variation of reverse mass flow with vane angle
7.30 Decay of the maximum axial velocities along the jet axis for different swirlers
7.3I Profiles of the axial velocity for different swirlers at z/D=I.0
7.32 Profiles of the axial velocity for different swirlers at z/D=I.75
7.33 Profiles of the axial velocity for different swirlers at z/D=2.5
7.34 Profiles of the axial velocity for different swirlers at z/D=3.25
7.35 Comparison of the size of the recirculation regions for different swirlers
7.36 Comparison of the size of the reverse flow zones for different swirlers
7.37 Distribution of the swirl velocity in the jet issuing from the swirler S.I
7.38 Distribution of the swirl velocity in the jet issuing from the swirler S.4
7.39 Distribution of the swirl velocity in the jet issuing from the swirler S.6
7.40 Distribution of the swirl velocity in the jet issuing from the swirler S.9
7.4I Distribution of the swirl velocity in the jet issuing from the swirler S.IO
7.42 Distribution of the swirl velocity in the jet issuing from the swirler S.II
7.43 Distribution of the swirl velocity in the jet issuing from the swirler S.I2
7.44 Variation of the profiles of the normalized swirl velocity in the flow field of the swirler S.I
7.45 Variation of the profiles of the normalized swirl velocity in the flow field of the swirler S.4
7.46 Variation of the profiles of the normalized swirl velocity in the flow field of the swirler S.6
7.47 Variation of the profiles of the normalized swirl velocity in the flow field of the swirler S.IO
7.48 Profiles of the swirl velocity for different swirlers at z/D=I.0
7.49 Profiles of the swirl velocity for different swirlers at z/D=I.75
7.50 Profiles of the swirl velocity for different swirlers at z/D=2.5
7.5I Profiles of the swirl velocity for different swirlers at z/D=3.25
7.52 Decay of the maximum swirl velocities along the jet axis for different swirlers
7.53 Distribution of the kinetic energy of turbulence in the jet issuing from the swirler S.I
7.54 Distribution of the kinetic energy of turbulence in the jet issuing from the swirler S.4
7.55 Distribution of the kinetic energy of turbulence in the jet issuing from the swirler S.6

7.56 Distribution of the kinetic energy of turbulence in the jet issuing from the swirler S.9
7.57 Distribution of the kinetic energy of turbulence in the jet issuing from the swirler S.IO
7.58 Distribution of the kinetic energy of turbulence in the jet issuing from the swirler S.II
7.59 Distribution of the kinetic energy of turbulence in the jet issuing from the swirler S.I2
7.60 Profiles of the kinetic energy of turbulence for different swirlers at z/D=I.0
7.6I Profiles of the kinetic energy of turbulence for different swirlers at z/D=2.5
7.62 Decay of the maximum kinetic energy of turbulence along the jet axis for different swirlers
7.63 Profiles of the Reynolds stresses at z/D=0.25 in the flow field of the swirler S.9
7.64 Profiles of the Reynolds stresses at z/D=I.0 in the flow field of the swirler S.9
7.65 Profiles of the Reynolds stresses at z/D=2.5 in the flow field of the swirler S.9
7.66 Profiles of the Reynolds stresses at z/D=3.25 in the flow field of the swirler S.9
7.67 Profiles of the Reynolds stresses at z/D=I.0 in the flow field of the swirler S.IO
7.68 Profiles of the Reynolds stresses at z/D=2.5 in the flow field of the swirler S.IO
7.69 Profiles of the Reynolds stresses at z/D=I.0 in the flow field of the swirler S.II
7.70 Profiles of the Reynolds stresses at z/D=I.0 in the flow field of the swirler S.I2
7.7I Profiles of the Reynolds stresses at z/D=I.0 in the flow field of the swirler S.I
7.72 Profiles of the Reynolds stresses at z/D=3.25 in the flow field of the swirler S.I
7.73 Profiles of the dominant stress $\overline{ww}$ for different swirlers at z/D=I.0
7.74 Profiles of the dominant stress $\overline{ww}$ for different swirlers at z/D=2.5
7.75 Profiles of the second dominant stress $\overline{uw}$ for different swirlers at z/D=I.0
7.76 Profiles of the second dominant stress $\overline{uw}$ for different swirlers at z/D=2.5
7.77 Profiles of the third dominant stress $\overline{uu}$ for different swirlers at z/D=I.0
7.78 Profiles of the third dominant stress $\overline{uu}$ for different swirlers at z/D=2.5
7.79 Profiles of the turbulent viscosity $\mu_{\theta\theta}$ in the flow field of the swirler S.9
7.80 Profiles of the turbulent viscosity $\mu_{\theta\theta}$ in the flow field of the swirler S.IO
7.8I Profiles of the turbulent viscosity $\mu_{\theta\theta}$ in the flow field of the swirler S.II
7.82 Profiles of the turbulent viscosity $\mu_{\theta\theta}$ in the flow field of the swirler S.I2

7.83 Profiles of the turbulent viscosity $\mu_{r\theta}$ in the flow field of the swirler S.9
7.84 Profiles of the turbulent viscosity $\mu_{r\theta}$ in the flow field of the swirler S.I0
7.85 Profiles of the turbulent viscosity $\mu_{r\theta}$ in the flow field of the swirler S.II
7.86 Profiles of the turbulent viscosity $\mu_{r\theta}$ in the flow field of the swirler S.I2
7.87 Profiles of the turbulent viscosity μ_{rr} in the flow field of the swirler S.9
7.88 Profiles of the turbulent viscosity μ_{rr} in the flow field of the swirler S.I0
7.89 Profiles of the turbulent viscosity μ_{rr} in the flow field of the swirler S.II
7.90 Profiles of the turbulent viscosity μ_{rr} in the flow field of the swirler S.I2
7.9I Profiles of the turbulent viscosity μ_{rz} in the flow field of the swirler S.9
7.92 Profiles of the turbulent viscosity μ_{rz} in the flow field of the swirler S.I0
7.93 Profiles of the turbulent viscosity μ_{rz} in the flow field of the swirler S.II
7.94 Profiles of the turbulent viscosity μ_{rz} in the flow field of the swirler S.I2
7.95 Comparison of the four turbulent viscosities at z/D=0.25 in the flow field of the swirler S.9
7.96 Comparison of the four turbulent viscosities at z/D=I.0 in the flow field of the swirler S.9
7.97 Comparison of the four turbulent viscosities at z/D=0.083 in the flow field of the swirler S.I0
7.98 Comparison of the four turbulent viscosities at z/D=I.5 in the flow field of the swirler S.I0
7.99 Comparison of the four turbulent viscosities at z/D=2.5 in the flow field of the swirler S.II
7.I00 Comparison of the four turbulent viscosities at z/D=I.75 in the flow field of the swirler S.I2
7.I0I Comparison of the dominant viscosity $\mu_{\theta\theta}$ for different swirlers
7.I02 Comparison of the dominant viscosity $\mu_{\theta\theta}$ for different swirlers
7.I03 Comparison of the turbulent viscosity $\mu_{r\theta}$ for different swirlers
7.I04 Comparison of the turbulent viscosity $\mu_{r\theta}$ for different swirlers
7.I05 Comparison of the turbulent viscosity μ_{rz} for different swirlers
7.I06 Comparison of the turbulent viscosity μ_{rz} for different swirlers

LIST OF TABLES

No.	TITLE
I	Effect of the change in the coefficients of the hot-wire calibration equation on the experimental results
2	Effect of the change in the coefficients of the hot-wire calibration equation on the experimental results
3	Effect of the change in the yaw correction factor on the experimental results
4	Effect of the change in the yaw correction factor on the experimental results

NOTATION

a	: Overheating ratio;the distance of the origin of the jet from the orifice;slope of the hot-wire calibration curve
A,B,C	: Calibration constants for the hot-wire probe
b_j	: Pressure recovery factor
c	: Chord
C_μ, C_k	: Constants in the turbulence model
C_1, C_2	: Constants in the turbulence model
C_p	: Specific heat at constant pressure
d	: Hub diameter
d_e	: Effective nozzle diameter
d_{or}	: Diameter of the hole on the orifice meter (2.75")
D	: Outer diameter of the swirlers (3")
e	: Fluctuating part of E
e'	: RMS value of e
E	: Instantaneous voltage drop across the hot-wire
$\bar{E}$	: Mean value of E
E_0	: Value of E at zero velocity
E_L	: Linearizer output voltage
E,F,G	: Swirl velocity profile constants
$\vec{F}$	: Body force per unit volume
G	: Nozzle thrust
Gr	: Grashof number
h	: Aspect
Δh	: Pressure difference for mass flow measurement(H_2O")
i	: Incidence
k	: Thermal conductivity;kinetic energy of turbulence; error curve constant
k_1	: Yaw correction factor
k_2	: Pitch correction factor
k_e	: Entrainment rate constant
k_p	: Static pressure profile constant
k_t	: Temperature profile coefficient
k_u	: Axial velocity profile constant
K_1, K_2	: Coefficients of pressure drop due to friction and acceleration through the swirler
K	: Total pressure drop coefficient
k_L, K_L	: Linearizer transfer coefficients

l : Length of the hot-wire
ℓ : Mixing length
m : Entrainment rate; mass flow rate
M : Mach number
M_Θ : Angular momentum flux
M_z : Axial momentum flux
Nu : Nusselt number
p : Instantaneous static pressure
$\bar{p}$: Mean part of p
p' : Fluctuating part of p
P : Total pressure; heat loss from the hot-wire to the surroundings
P_k : Production of the kinetic energy of turbulence
Pr : Prandtl number
Q : Dependent variable
$Q(E)$: A function of instantaneous voltage drops
r, θ, z : Cylindrical polar coordinates
Re : Reynolds number
Re_n : Reynolds number based on the velocity component normal to the wire
s : Space
S : Swirl number
S_1, S_2 : Proportionality constants for an X-type probe
t : Time
$\bar{\bar{T}}$: Stress tensor
T : Stress (with indices); temperature; nozzle torque; period of the square wave
u, v, w : Fluctuating parts of V_z, V_r and V_θ, respectively.
U, V, W : Mean parts of V_z, V_r and V_θ, respectively.
U_e : Effective cooling velocity
$\vec{V}$: Instantaneous absolute velocity vector
$\tilde{V}$: Magnitude of the absolute velocity vector
V_r : Radial component of the instantaneous absolute velocity
V_θ : Swirl component of the instantaneous absolute velocity
V_z : Axial component of the instantaneous absolute velocity
x, y, z : Cartesian coordinates
X : Directional coefficient for the pressure probe
z : Hub ratio

Greek letters

α	: Half jet angle; yaw angle
β	: Pitch angle
ϵ	: Rate of dissipation of the kinetic energy of turbulence
δ	: Dihedral angle between the flow plane and the meridian plane (the plane containing 2,0 and 4th holes) on the pressure probe
δ_c	: Convergence criteria
σ_k	: Prandtl number for the kinetic energy of turbulence
σ_ϵ	: Prandtl number for dissipation rate
Ω	: Circulation
η	: Normalized stream function
ω	: Vorticity
ξ	: r/(z+a)
θ	: Vane outlet angle;conical angle between the velocity vector and the probe axis
ρ	: Density
η_p	: Pressure loss coefficient
Ψ	: see Eqn.6.31
W	: Stream function
μ	: Laminar viscosity
μ_t	: Turbulent viscosity
μ_e	: Effective viscosity
ν	: Kinematic viscosity

Subscripts

a	: Atmospheric conditions
i	: Inlet conditions
j	: Relating to the j th hole (0,1,2,3,4)
m	: Maximum value at a station
n	: Normal component;relating to nozzle
o	: Outlet conditions
s,∞	: Relating to the free stream
t	: Tangential component
w	: Relating to the wire
.5	: Relating to the radial station where the axial velocity component assumes half of its maximum value at that station

CONTENTS

SUMMARY
ACKNOWLEDGEMENTS
LIST OF FIGURES
LIST OF TABLES
NOTATION

Page

Chapter 1. INTRODUCTION 1

1.1. The Combustion Process and Swirling Flows

1.2. Methods of Obtaining Swirling Flows

1.3. Types of Vane Swirlers and Design Parameters for Conventional Flat Vane Type Swirlers

1.4. Reasons for the Present Work

1.5. Scope of the Present Work

1.6. Notation Relating to a Swirling Flow Field

1.7. Structure of the Recirculation Region

Chapter 2. GENERAL TRANSPORT EQUATIONS 9

2.1. Form of the General Transport Equations

2.2. Gross Integral Equations

2.3. Momentum Flux Relations for Laminar Flow

2.4. Turbulence and Transport Equations for Characteristic Quantities

2.5. Momentum Flux Relations for Turbulent Flow

Chapter 3. LITERATURE SURVEY 18

3.1. Introduction

3.2. Swirling Jets Generated by Several Means

3.3. Swirling Jets Generated by Vane Type Swirlers

3.4. Conclusions

Chapter 4. PREDICTION OF FLOW FIELDS 32

4.1. Introduction

4.1.1. Prediction of Boundary Layer Type Swirling Flows

4.1.2. Prediction of Swirling Flows with Recirculation

4.2.Primitive Pressure-Velocity Approach
4.3.Vorticity-Stream Function Approach
4.3.1.Governing Transport Equations
4.3.2.Common Form for the Transport Equations
4.3.3.A General Finite Difference Solution Procedure
4.3.4.Solution of the Algebraic Equations
4.4.Turbulence Modelling
4.5.Boundary Conditions for the Strongly Swirling Free Flows
4.6.Computational Procedure
Chapter 5. DESCRIPTION OF EXPERIMENTAL FACILITY 56
5.1.Test Rig
5.2.Design of Swirlers
5.3.Instrumentation
5.3.1.Five-Hole Spherical Pressure Probe
5.3.1.a.Calibration Procedure
5.3.1.b.Measurement Procedure
5.3.2.Hot-Wire Anemometer
Chapter 6. HOT-WIRE TECHNIQUE 64
6.1.Choice of Hot-Wire Anemometry
6.2.Basic Principles of Hot-Wire Anemometry
6.3.Directional Sensitivity of Hot-Wire Probes
6.4.Methods for the Interpretation of Signals from Hot-Wire Anemometer
6.5.Conclusions
6.6.Formulation for the Present Work
6.6.1.Assumptions
6.6.2.Choice of the Orientations
6.6.3.Formulation
6.7.Experimental Procedure
6.7.1.Some Considerations
6.7.2. Calibration of the Anemometer Unit
6.7.3.Calibration of the Temperature Compensated Hot-Wire Probe
6.7.4.Directional Sensitivity Tests

6.7.5.Measurement Procedure
6.8.Test Application to a Straight Round Jet
6.9.Advantages and Disadvatages of the Method
Chapter 7. RESULTS AND DISCUSSION 100
7.I.Introduction
7.2.Flow Characteristics at Swirler Exit
7.3.Pressure Drop-Mass Flow Characteristics
7.4.Variation of Static Pressure along Jet Axis
7.5.Velocity Distributions
7.5.I.Axial Velocity Distributions,Recirculation Regions and Reverse Flow Zones
7.5.2.Swirl Velocity Distributions
7.6.Turbulence Characteristics
7.6.I.Kinetic Energy of Turbulence
7.6.2.Reynolds Stresses
7.6.3.Effect of Swirler Type on the Dominant Reynolds Stresses
7.6.4.Turbulent Viscosities
7.6.5.Effect of Swirler Type on the Turbulent Viscosities
7.7.Discussion of Errors
Chapter 8. CONCLUSIONS 135
Chapter 9. SUGGESTIONS FOR FURTHER WORK 138
REFERENCES 141
TABLES 148
FIGURES 152

CHAPTER 1. INTRODUCTION

1.1.COMBUSTION PROCESS AND SWIRLING FLOWS

The combustion process is employed in thermodynamic cycles in order to increase the internal energy of the fluid.This process is performed in combustors or furnaces. A conventional aircraft gas turbine combustor is shown in Fig.1.1 (Ref.s.1,2).Three main zones can be distinguished, namely,primary,intermediate and dilution zones. Fuel is injected and ignited in the primary zone.Combustion is completed in the intermediate zone and hot gases are cooled to a lower temperature in the dilution zone before expanding through the turbine.

Combustors are designed to meet several requirements. These are briefly : acceptable size,low emission of pollutants,high combustion intensity,high combustion efficiency,ease of ignition,good combustion stability, good cross sectional distribution of temperature, durability and low pressure loss.

A pressure loss coefficient in a combustion chamber is defined either by

$$\eta_p = \frac{P_2 - P_1}{P_1}$$

or

$$\eta_p = \frac{P_2 - P_1}{.5\rho V_2^2}$$

where the indices 2 and 1 refer to combustor inlet and outlet conditions,respectively.Although ideally it is assumed that combustion takes at constant pressure, a pressure loss,typically of around 5% occurs (Ref.3). In the early types of combustors this pressure loss has been associated only with the friction on the walls and with heat addition.For the conventional types,however, the total pressure losses comprise those due to (Ref.4) : swirler,mixing,heat addition and miscellaneous (losses due to bends,corrugated spacers and frictional losses).Swirler losses constitute usually about 25% of the total losses according to approximate loss calculations.As is well known,any loss in the combustion process decreases the net output of a thermodynamic cycle,and therefore its efficiency.

Combustion efficiency is defined as the ratio of the actual temperature rise to the theoretical temperature rise.It is,therefore, a measure of the completeness of combustion.

The term 'combustion stability' applies to the range of fuel-to-air ratios over which a stable flame can be maintained.An alternative definition for combustion stability considers maximum air velocity obtainable without flame extinction and is closely related to the flame speeds for the existing fuels.Due to the rather wide range of operational conditions in aircraft combustors (very low pressures and temperatures) combustion stability is an important factor to be considered.

Another requirement of increasing current importance is for low emission of pollutants from combustors. Due to incomplete mixing of fuel with air,high air velocities and the requirement of short length for combustors,several undesired combustion products are emitted.Among these are CO,CO_2,NO_x,smoke and SO_2. Existance of these products indicates low combustion efficiency and has a detrimental effect on public health.

Combustion efficiency and stability are inversely proportional to the mean axial velocity in the combustor (Ref.1).In fact,a combustor must be capable of running, without flame-out or with very high reliability for relighting, over a wide range of air-to-fuel ratios.The only way of achieving this is by creating low velocity and good mixing regions (i.e.,recirculation) in the combustor.The recirculation region provides a continuous hot source for a stable combustion since the hot combustion products flow in the upstream direction and give rise to the ignition of incoming fresh fuel-air mixture.Creation of low velocities is also essential since the flame speeds for the most widely available fuels are much lower than the average velocities in combustion chambers.

. In early combustors,baffle type flame stabilizers have have been used (Ref.5).These have not been,however, very successful at high mass flows.The structure of the flow field behind such a baffle is also examined later in this work.It suffices here to say that turbulence intensities are also relatively low for these flows. Can type flame stabilizers have also not been very efficient because of the 'trapped' form of the recirculation region at the beginning of the combustor.

A better way of flame stabilization at high mass flows can be attained by swirling the incoming flow to the combustor (Ref.5). Vortex breakdown is a well known phenomenon in swirling flows,causing a recirculation region (a standing eddy) to occur in the core region of the flow when the amount of rotation imparted to the flow is high.This type of recirculation region provides a better mixing than that obtained by the other means,such as bluff bodies,due to the presence of swirl velocity component.Higher turbulence intensities and stronger shear regions are,therefore, expected causing better atomization for the liquid-fuel particles already atomized by the injector.Since the flow

possesses a swirl velocity component,lower axial velocities occur even outside the recirculation region in the combustor.This considerably increases the residence time of the fuel and subsequently the combustion products in the chamber.Furthermore,more complete combustion is achieved thus reducing the level of the pollutants.Due to the better mixing,higher turbulence intensities,stronger shear regions and in consequence provision for better atomization of the fuel particles,superiority of swirling flows in flame stabilization,combustion efficiency,reduction of pollutants and good combustion stability becomes apparent. These features of swirling flows have long been known and have been widely utilized in order to control the stability and intensity of combustion,the shape of the flame and the rate of reaction .

Apart from the combustion process,swirling flows have also found application in general for flow cases in which strong shear regions are required,such as paint guns. Vortex flow separators is a further example of swirling flows where use is made of the centrifugal force field of swirling flows.

When sufficient swirl is introduced to cause recirculation, a 'strong swirl' situation is said to exist.'Weak swirl',therefore,induces no recirculation.The type of swirling flow is characterized by'the swirl number'.The mathematical definition of the swirl number will be given in Chapter 3.All the swirling flows investigated in this work are vane generated type,strong and particularly suitable for combustor applications.

1.2.METHODS OF OBTAINING SWIRLING FLOWS

Swirling flows can be obtained in the following ways:-

a)Pipe bends ; a rather weak swirl is created as the flow moves through a pipe bend.
b)Spiral strips in a tube.
c)Surrounding pipe is rotated at a fixed rpm.
d)Tangential flow is injected.
e)Vane type swirlers.

Swirling flows obtained using the first three methods have been employed mainly for experimental purposes. Tangential-flow-entry type swirlers are generally used in furnaces.Vane type swirlers have been the common practice as flame stabilizers in aircraft gas turbine combustors,but can be used equally well in furnaces.

1.3. TYPES OF VANE SWIRLERS AND DESIGN PARAMETERS FOR CONVENTIONAL FLAT VANE TYPE SWIRLERS

There are several types of vane swirlers, namely :-

a) Constant-angle flat vane type ; these are the most widely used swirlers due to their ease of manufacture.
b) Constant-angle curved vane type ; more difficult to manufacture, but the improvement in performance over the flat vane type may be very considerable.
c) Variable-angle curved vane type ; these are very diffucult to manufacture and the improvement over the constant angle curved vane type is only slight. This type is, therefore, not widely used.

A conventional flat vane type swirler and the related notation are shown in Fig.1.2 .This type is referred here as 'central blading' where the centre line of the blade in the spanwise sense passes through the axis of the swirler (z-z axis). Fig.1.3 shows the alternative 'off-central blading' type .The former type is easier to manufacture because, at the inner ends of the vanes, an almost circular shape is required. The latter necessitates an irregular shape, causing serious manufacturing difficulties, especially when the aspect ratio is high.

1.4. REASONS FOR THE PRESENT WORK

A vane swirler performs the task of turning the incoming flow to the combustor from a rather low absolute axial velocity to a higher absolute velocity having swirl and radial components. Due to this acceleration, a pressure drop occurs through the swirler. Additionally, profile and secondary losses occur within the swirler due to the vanes.

In the case of flat vanes the turning through the swirler is incomplete for high values of the space-to-chord ratio, because the air outlet angle becomes much smaller than the geometrical vane outlet angle. Relevant information on this deviation is widely available for turbine type cascades as shown typically in Fig.1.4 .Ineffective turning of air through the swirler results in lower swirl and in consequence, lower radial velocity components. In other words, less angular momentum is imparted to the incoming axial flow. A smaller recirculation region and less turbulence intensities are, therefore, induced. Inherently, the amount of recirculating mass flow drops.

The ineffective turning can be partly obviated by reducing the space-to-chord ratio. To obtain a tight swirl, therefore, a space-to-chord ratio of about .7 is used together with vane outlet angles 65° to 85° for flat vanes (Ref.4) .This, however, increases both the profile and secon-

dary losses excessively.Additionally,it may introduce blockage problems.All these resulting excessive losses eventually manifest themselves in the form of an excessive pressure drop through the swirler and the whole process of turning becomes quite inefficient.

Whatever the value of the space-to-chord ratio,the inefficient operation inevitably accompanies flat vanes,because they always run under 'stalled' conditions.Aerodynamically curved vanes are,therefore,employed in which the turning is gradually imparted to the incoming axial flow (see Fig.1.5).In this way,flow separation is greatly reduced on the suction (convex) side of the vanes.This results in a cosiderable reduction in the profile loss.Thus,more complete turning and higher swirl and radial velocity components can be obtained at the exit of the swirler at the cost of a reduced pressure drop.

Although it is expected that smaller aspect ratios would produce larger recirculation regions and higher recirculating mass flows,it is clear that this would only be achieved at the cost of a larger pressure drop,due to the increasing blockage.Although known qualitatively, no quantitative information is available on the influence of the aspect ratio.The present information covers the influence of the vane outlet angle on the size of recirculation region and the pressure drop for flat vane types (Ref.s.6,7,8,9,10).Also,information on hubbless swirlers with flat vanes has been reported in Ref.s.8,9 and 10 .It is obvious that available information is far from being complete.Some other works on the subject represent only discrete cases (Ref.s.11,12).Matching a swirler to a combustion chamber is,therefore,still a trial-and-error process even when the flat vane types are employed. For curved vane type swirlers,however,as far as the author is aware,very little experimental evidence exists.

It was predicted that because of the higher efficiency of air flow turning obtained by using curved vanes, the same size recirculation region should be obtainable for a smaller vane outlet angle.This,in turn,would involve a lower corresponding pressure drop.

1.5.SCOPE OF THE PRESENT WORK

The aim of this work is to determine,experimentally,the influence of swirler geometric parameters,namely,vane angle, space-to-chord ratio and aspect ratio,on the size and turbulence characteristics of the downstream recirculation region.Both flat and curved vane types are considered.In particular,the pressure drop-mass flow characteristic is to be established for each swirler configuration together with the corresponding shape and size of the recirculation region.

Special attention was also to be given to establish the maximum shear stress regions.Experiments are carried out under isothermal conditions.

1.6.NOTATION RELATING TO A SWIRLING FLOW FIELD

The flow field and coordinate axes employed in this work are shown in Fig.1.6 .In order to facilitate the mathematical treatment of the problem,cylindrical polar coordinates are used.The z-axis coincides with the axis of symmetry of the flow field.

The flow is considered axisymmetrical,therefore,no variation in the θ direction is assumed.The three components of the absolute velocity at a point P in the flow field are also shown in Fig.1.6 .

1.7.STRUCTURE OF THE RECIRCULATION REGION

The word recirculation is generally used for flow reversal in the main flow direction in a two-dimensional field.Three dimensional recirculation regions are also possible.Recirculation is caused by several factors.

The cause of the recirculation phenomenon occuring in swirling flows is totally different from those of the recirculations encountered on the walls,for instance in diffusers,and behind bluff bodies,such as baffle type flame stabilizers.In the latter cases the recirculation is due to flow separation from a surface,caused mainly by adverse pressure gradients or sharp surface discontinuities and ,therefore,the inability of the flow to remain attached. In the former case,however,the recirculation is due entirely to the rotation of the flow field.When the strength of the rotation is high enough,vortex breakdown takes place. More precisely,when there is strong swirl the axial gradient of the swirl velocity component is high.This causes the value of the vorticity to decrease considerably in the core region of the flow.Examination of the definition of the vorticity leads to the deduction that recirculation occurs in the core region of the flow field (see Chapter 4).

Except for the purposes of combustion stability,a recirculation region is generally undesirable in a flow field because it extracts considerable energy from the main flow. The consequent momentum loss manifests itself as a total pressure drop through the system.Even for the combustion application,therefore,an optimum case,that is,a reasonable size at the cost of an acceptable pressure drop, is sought.

A recirculation region in a pipe step is shown in Fig.1.7 .The incoming flow separates from the surface AB

at B due to the sharp discontinuity,i.e., the corner,and attaches to the surface DE at C.The point C is called the stagnation point .The flow in the central part of the step is the main flow.The length of the recirculation,DC,depends on the inlet velocity profile,that is,the state of the incoming flow (laminar or turbulent) and the step ratio (the ratio of the small pipe diameter to the large pipe diameter) The rotation inside the DBC loop is driven through the application of shear stresses along the solid BC line (the boundary of the recirculation region) by the main flow. Along the DC line,where a wall exists as a boundary, the energy gained from the main flow is dissipated through viscous shear stresses.The same kind of wall dissipation continues along the line DB.Therefore,near the point B,the recirculating flow has been slown down considerably. As a result the maximum shear stress between the main flow and the recirculation region is expected near the point B on the recirculation boundary.Although,mathematically, the value of the stream function on the wall is assumed the same along the recirculation boundary (which physically means that the recirculating flow is confined in the DBC loop in terms of mass),a mass transfer from the main flow to the recirculation region occurs through diffusion at the downstream section of the recirculation region boundary. The same rate of mass transfer occurs at the upstream end of the recirculation region to the main flow to maintain conservation of mass in the recirculation region.The dashed line between B and C represents the zero velocity line below which the axial velocities assume positive values and above which negative values exist indicating reverse mass flows.

The recirculation region in a free swirling flow is shown in Fig.1.8 .Since the flow is assumed to be axisymmetric,only half the plane of the jet is considered. If a zero value for the stream function is accepted along the Oz axis,it assumes the same value on the solid line AB. Therefore,the OAB loop encloses the recirculation region in this plane.The point B is called the stagnation point. The flow outside the OAB loop is the main flow.If a line is drawn parallel to the Oy axisthrough the vortex centre C,together with the zero velocity line AB (dashed),four zones can be distinguished inside the recirculation region. The 1st and 4th zones represent the flow reversal zones. Obviously in the other half of the Oyz plane,a similar flow configuration is co-existant.More precisely,recalling the assumption of axisymmetric flow,the existance of a toroidal recirculation region becomes obvious.The above remarks about the recirculation in a pipe step equally apply to this flow field.The main flow derives the recirculation along the solid AB line;the maximum shear stresses are, therefore,expected near the point A along the recirculation boundary.Typical axial and swirl velocity profiles are shown in Fig.1.9 .All the velocity components decay in

the downstream direction. After the stagnation point, reverse axial velocities disappear and further downstream the peak of the axial velocity profiles shifts towards the centreline as the effect of swirling diminishes. The swirl velocity profiles assume a forced vortex form in the core region of the flow and are, therefore, proportional to the radius. After the peak in the radial direction, however they assume a free vortex form, varying inversely with the radius.

CHAPTER 2. GENERAL TRANSPORT EQUATIONS

This chapter is intended to provide, in the volume, the basic background for the general mathematical understanding of the following chapters. Most of the equations presented can be found, in a simpler or similar form, in most textbooks on fluid mechanics or heat transfer (Ref.13).

2.1. FORM OF THE GENERAL TRANSPORT EQUATIONS

The basic physical laws of conservation of mass and momentum when applied to finite volumes yield integral forms of the general equations of fluid dynamics. When this volume is chosen as an infinitesimal element of the flow field, the differential forms which are used to predict point-to-point variations in the flow field, are obtained (Ref.13).

Conservation of mass is expressed as the continuity equation. In vectorial notation this takes the form :-

$$\frac{D\rho}{Dt} + \rho(\nabla.\vec{V}) = \frac{\partial\rho}{\partial t} + \nabla.(\rho\vec{V}) = 0 \qquad (2.1)$$

Conservation of momentum is expressed as the momentum equation from Newton's 2nd law of motion :-

$$\rho \frac{D\vec{V}}{Dt} = \vec{F} - \vec{\nabla p} + \nabla.\bar{\bar{T}} \qquad (2.2)$$

It is seen in Eqn.2.2 that pressure terms have been considered separately from the normal stress terms.

In cylindrical polar coordinates for axially symmetric flow Eqn.s.2.1 and 2.2 can be written as:-

$$\frac{\partial\rho}{\partial t} + \frac{1}{r}\frac{\partial}{\partial r}(\rho r\, V_r) + \frac{\partial}{\partial z}(\rho\, V_z) = 0 \qquad (2.3a)$$

$$\rho\left(\frac{\partial V_r}{\partial t}+V_r\frac{\partial V_r}{\partial r}+V_z\frac{\partial V_r}{\partial z}-\frac{V_\theta^2}{r}\right)=F_r-\frac{\partial p}{\partial r}+\frac{1}{r}\frac{\partial}{\partial r}(r\,T_{rr})+\frac{\partial T_{rz}}{\partial z}-\frac{T_{\theta\theta}}{r} \qquad (2.3b)$$

$$\rho\left(\frac{\partial V_\theta}{\partial t}+V_r\frac{\partial V_\theta}{\partial r}+V_z\frac{\partial V_\theta}{\partial z}+\frac{V_rV_\theta}{r}\right)=F_\theta+\frac{1}{r^2}\frac{\partial}{\partial r}(r^2T_{r\theta})+\frac{\partial T_{\theta z}}{\partial z} \qquad (2.3c)$$

$$\rho\left(\frac{\partial V_z}{\partial t}+V_r\frac{\partial V_z}{\partial r}+V_z\frac{\partial V_z}{\partial z}\right)=F_z-\frac{\partial p}{\partial z}+\frac{1}{r}\frac{\partial}{\partial r}(r\,T_{rz})+\frac{\partial T_{zz}}{\partial z} \qquad (2.3d)$$

It is seen that Eqn.s.2.3 form a system of strongly coupled non-linear partial differential equations. They are not closed in their present form because if the components of the absolute velocity, that is, V_r, V_θ, V_z and static pressure, p, are considered as unknowns, it is seen that the components of the stress tensor still remain as the quantities that must be determined. Further relations expressing the components of the stress tensor in terms of the other quantities, for instance, velocity components, are required for closure.

Eqn.2.3a can be expressed in terms of the stream function :

$$V_z=\frac{1}{\rho r}\frac{\partial W}{\partial z} \qquad (2.4a)$$

$$V_r=-\frac{1}{\rho r}\frac{\partial W}{\partial r} \qquad (2.4b)$$

Introduction of the stream function into Eqn.s.2.3 through Eqn.2.4 reduces the number of the unknowns by one. Further relations are still required for their closure.

2.2.GROSS INTEGRAL EQUATIONS

Eqn.s.2.3 can be integrated with the assumption of negligible body force over a cross section of the flow field to obtain the gross integral forms of the equations of motion. The mathematical procedure is similar in all the cases : grouping the derivative terms with respect to the same variable and integrating over a cross section (see Fig.1.9), we obtain

$$\frac{d}{dz}\int_0^\infty(\rho r\,V_z)\,dr=-\left|\rho r\,V_r\right|_0^\infty \qquad (2.5a)$$

$$\frac{d}{dz}\int_0^\infty (\rho V_z^2+p-T_{zz})r\,dr = \left|r(T_{rz}-\rho V_r V_z)\right|_0^\infty \qquad (2.5d)$$

$$\frac{d}{dz}\int_0^\infty (\rho V_\theta V_z-T_{\theta z})r^2 dr = \left|r^2(T_{r\theta}-\rho V_r V_\theta)\right|_0^\infty \qquad (2.5c)$$

$$\frac{d}{dz}\int_0^\infty (\rho V_r V_z-T_{rz})r\,dr = \int_0^\infty (\rho V_\theta^2-T_{\theta\theta}+p)dr + \left|r(T_{rr}-p-\rho V_r^2)\right|_0^\infty \qquad (2.5b)$$

The similarity in the form of these equations must be underlined. They can be employed to determine the stress terms when the velocity and pressure profiles are known. This form of the equations, together with some proper simplifications, is largely used in boundary layer theory (Ref.14).

For application to swirling flows issuing into stagnant atmosphere, the required boundary conditions are :-

$$r=0 \;\ldots\ldots\; V_r=V_\theta=\frac{\partial p}{\partial r}=\frac{\partial V_z}{\partial r}=0 \qquad (2.5e)$$

$$r=0 \;\ldots\ldots\; V_z=V_r=V_\theta=r^2T_{r\theta}=r\,T_{rz}=p-p_a=0$$

Applying these conditions, Eqn.s.2.5c and 2.5d can be written as

$$\frac{d}{dz}\int_0^\infty (\rho V_\theta V_z-T_{\theta z})\,r^2 dr = 0 \qquad (2.5f)$$

$$\frac{d}{dz}\int_0^\infty (\rho V_z^2+p-T_{zz})\,r\,dr = 0 \qquad (2.5g)$$

which means that the variations of these integrals along the z-axis is zero. These integrals are, therefore, conserved at various cross sections of the free jet. Examination of Eqn.s.2.5f and 2.5g reveals that these are the angular (moment of tangential momentum) and axial momenta of the jet, respectively. Therefore,

$$M_\Phi = \int_0^\infty (\rho V_\theta V_z-T_{\theta z})\,r^2 dr = \text{constant} \qquad (2.5h)$$

$$M_z = \int_0^\infty (\rho V_z^2 + p - T_{zz})\, r\, dr = \text{constant} \qquad (2.5i)$$

These are the parameters characterizing the state of a swirling jet, i.e., either recirculation occurs or not.

2.3. MOMENTUM FLUX RELATIONS FOR LAMINAR FLOW

In Eqn.s.2.3 , T's represent the stresses acting on the surfaces of the infinitesimal volume with sides dr, dz and r dθ. For Newtonian fluids the stresses are linearly related to the rates of strain. In the case of laminar axisymmetric flow , they can be expressed as :-

$$T_{rr} = \mu \left(2 \frac{\partial V_r}{\partial r} - \frac{2}{3} \nabla . \vec{V} \right) \qquad (2.6a)$$

$$T_{\theta\theta} = \mu \left(2 \frac{V_r}{r} - \frac{2}{3} \nabla . \vec{V} \right) \qquad (2.6b)$$

$$T_{zz} = \mu \left(2 \frac{\partial V_z}{\partial z} - \frac{2}{3} \nabla . \vec{V} \right) \qquad (2.6c)$$

$$T_{r\theta} = \mu \left(r \frac{\partial}{\partial r} \left(\frac{V_\theta}{r} \right) \right) \qquad (2.6d)$$

$$T_{\theta z} = \mu \left(\frac{\partial V_\theta}{\partial z} \right) \qquad (2.6e)$$

$$T_{rz} = \mu \left(\frac{\partial V_r}{\partial z} + \frac{\partial V_z}{\partial r} \right) \qquad (2.6f)$$

The ratio of proportionality between shear stresses and the rates of strain is called the momentum transport coefficient or viscosity. It is assumed constant in the case of laminar isothermal flows. It is known that only molecular transport is important for laminar flows. The molecular viscosity can then be expressed as

$$\mu = \rho \nu \qquad (2.7)$$

where ν is called the diffusivity coefficient of momentum or kinematic viscosity. The similarity between the expressions for momentum, heat and mass transfer are strong. For example,

in the case of mass transfer,

$$\Gamma_j = \rho D_j \qquad (2.8)$$

where Γ_j is the transport coefficient of chemical species j , say, oxidant in a combustion process, and D_j is the diffusivity coefficient of chemical species j . Since cold conditions are considered in this work, the transport equations for heat and mass transfer are not presented here.

2.4.TURBULENCE AND TRANSPORT EQUATIONS FOR CHARACTERISTIC QUANTITIES

In Eqn.s.2.3 any flow variable,in general,is a function of the position in space and time,that is, $V_r=V_r(r,z,t)$,$p=p(r,z,t)$ and so on.The θ dependence has been omitted due to the assumption of axisymmetric flow.If a certain point of the flow field is considered,the flow variables at that point depend only on time. Therefore,at any position in the flow field,the variables can be separated to a mean value and a fluctuating component about this mean value.The instantaneous values can then be expressed as

$$\begin{aligned} V_r &= \bar{V} + v \\ V_\theta &= W + w \\ V_z &= U + u \\ p &= \bar{p} + p' \end{aligned} \qquad (2.9)$$

Because of the low velocities (Mach number-0.3) and cold flow conditions employed in this work,the assumption of incompressible flow is reasonable.Density fluctuations are,therefore, not considered.

Introducing Eqn.s.2.9 into Eqn.s.2.3b,c,d ,making use of the continuity equation, Eqn.2.3a, and taking time average, we obtain

$$\frac{1}{r}\frac{\partial}{\partial r}(\rho r\bar{V})+\frac{\partial}{\partial z}(\rho U)=0 \qquad (2.10a)$$

$$\rho\left(\bar{V}\frac{\partial \bar{V}}{\partial r}+U\frac{\partial \bar{V}}{\partial z}-\frac{\bar{W}^2}{r}\right)=-\frac{\partial \bar{p}}{\partial r}+\frac{1}{r}\frac{\partial}{\partial r}(rT_{rr}-\rho r\,\overline{v^2})+\frac{\partial}{\partial z}(T_{rz}-\rho\,\overline{uv})-\frac{T_{\theta\theta}-\rho\,\overline{w^2}}{r} \qquad (2.10b)$$

$$\rho\left(V\frac{\partial W}{\partial r}+U\frac{\partial W}{\partial z}+\frac{VW}{r}\right)=\frac{1}{r^2}\frac{\partial}{\partial r}\left(r^2T_{r\theta}-\rho r^2\overline{vw}\right)+\frac{\partial}{\partial z}\left(T_{\theta z}-\rho\,\overline{uw}\right) \qquad (2.10c)$$

$$\rho\left(V\frac{\partial U}{\partial r}+U\frac{\partial U}{\partial z}\right)=-\frac{\partial \bar{p}}{\partial z}+\frac{1}{r}\frac{\partial}{\partial r}\left(rT_{rz}-\rho r\,\overline{uv}\right)+\frac{\partial}{\partial z}\left(T_{zz}-\rho\,\overline{u^2}\right) \qquad (2.10d)$$

It is seen that the stresses are augmented by some amount with the quantities $\rho\overline{uv}$, $\rho\overline{uw}$,etc. for turbulent flow case. These quantities result from applying time averaging to the convection terms and cause the total stresses in turbulent flows to increase very considerably. They are called 'appareni' or 'Reynolds stresses' and Eqn.s.2.10 are called 'Reynolds equations' .

Similar transport equations can be derived for Reynolds stresses. Introducing Eqn.s.2.9 into Eqn.2.3b ,multiplying by v and taking time average,we get

$$\rho\left(\frac{V}{2}\frac{\partial\overline{v^2}}{\partial r}+\frac{U}{2}\frac{\partial\overline{v^2}}{\partial z}+\frac{v}{2}\frac{\partial\overline{v^2}}{\partial r}+\frac{u}{2}\frac{\partial\overline{v^2}}{\partial z}\right)=-v\frac{\overline{\partial p'}}{\partial r}-\overline{v^2}\frac{\partial V}{\partial r}-\overline{uv}\frac{\partial V}{\partial z}+\frac{2W}{r}\overline{vw}+\frac{\overline{vw^2}}{r}+(v.d.t)^{*} \qquad (2.11a)$$

In a similar manner, from Eqn.s.2.3c and 2.3d

$$\rho\left(\frac{V}{2}\frac{\partial\overline{w^2}}{\partial r}+\frac{U}{2}\frac{\partial\overline{w^2}}{\partial z}+\frac{v}{2}\frac{\partial\overline{w^2}}{\partial r}+\frac{u}{2}\frac{\partial\overline{w^2}}{\partial z}\right)=-\overline{vw}\frac{\partial W}{\partial r}-\overline{uw}\frac{\partial W}{\partial z}-\frac{V}{r}\overline{vw}-\frac{\overline{vw^2}}{r}+(v.d.t) \qquad (2.11b)$$

$$\rho\left(\frac{V}{2}\frac{\partial\overline{u^2}}{\partial r}+\frac{U}{2}\frac{\partial\overline{u^2}}{\partial z}+\frac{v}{2}\frac{\partial\overline{u^2}}{\partial r}+\frac{u}{2}\frac{\partial\overline{u^2}}{\partial z}\right)=-u\frac{\overline{\partial p'}}{\partial z}-\overline{uv}\frac{\partial U}{\partial r}-\overline{u^2}\frac{\partial U}{\partial z}+(v.d.t.) \qquad (2.11c)$$

are obtained.

Defining the kinetic energy of turbulence as

$$k=\frac{\overline{u^2}+\overline{v^2}+\overline{w^2}}{2} \qquad (2.12)$$

and combining Eqn.s.2.11 yield the transport equation for the kinetic energy of turbulence :-

* : v.d.t. stands for viscous dissipation terms.

$$\rho\left(V\frac{\partial k}{\partial r}+U\frac{\partial k}{\partial z}+\overline{v\frac{\partial k}{\partial r}}+\overline{u\frac{\partial k}{\partial z}}\right)=-\overline{v\frac{\partial p'}{\partial r}}-\overline{u\frac{\partial p'}{\partial z}} \qquad (2.13)$$

$$-\overline{u^2}\frac{\partial U}{\partial z}-\overline{v^2}\frac{\partial V}{\partial r}-\overline{w^2}\frac{V}{r}-\overline{uv}\left(\frac{\partial V}{\partial z}+\frac{\partial U}{\partial r}\right)-\overline{uw}\,\frac{\partial W}{\partial z}-\overline{vw}\left(\frac{\partial W}{\partial r}-\frac{W}{r}\right)$$

$$-(\text{v.d.t})$$

The left hand side of this equation represents transportation of the kinetic energy of turbulence by convection. It appears from Eqn.2.13 that transportation by convection is due to both the mean and turbulent part of the fluid motion. However, it can be shown that

$$\overline{v\frac{\partial k}{\partial r}}+\overline{u\frac{\partial k}{\partial z}}=0 \qquad (2.14)$$

Eqn.2.14 implies that transportation of the kinetic energy of turbulence through convection is only by the mean part of the fluid motion.The derivation of Eqn.2.14 is quite lengthy, therefore,is not presented here. The first line on the right hand side of Eqn.2.13 shows how the kinetic energy of turbulence is transported by the pressure fluctuations.The second line represents production of the kinetic energy of turbulence by Reynolds stresses in corporation with the mean flow field. The last line stands for the decay of the kinetic energy of turbulence due to the molecular viscosity of the fluid.

It is also possible to derive transport equations for the shear stresses in a similar manner to that of Eqn.s.2.11. The difficulty with all these equations is that they contain correlation terms between pressure and velocity fluctuations.Very little is known about the behaviour of these terms.It is this difficulty that is hindering the development of a universal turbulence modelling for isothermal flows. The viscous dissipation term,however,can be represented in terms of the kinetic energy of turbulence and can be determined experimentally.

The transport equations presented above are for the correlations of the fluctuations at a single point and all the fluctuations are considered at the same time.Time average is taken for a short period of time.Alternatively,time correlation can be applied to the fluctuating parts of the velocity components, that is,such quantities as

$$\overline{u(r,z,t)\;u(r,z,t+\tau)}$$

etc.,where τ is the time delay, can be formed and applying to

Eqn.s.2.3 , the transport equations can be obtained for these quantities. It is also possible to form such quantities as

$$\overline{u(r,z,t)\ u(r+\Delta r,z,t)}$$

etc. , where Δr is the space displacement,in order to deal with space correlations.However, the direct engineering interest is the determination of the Reynolds stresses in a flow field, because their spatial distribution indicates the regions where maximum shear stresses occur.The knowledge of such regions is important in several applications.Fuel injection is one of them and good fuel atomization can be obtained when the fuel is injected towards high shear stress regions.

It would be very much desirable to be able to calculate the amount and position of the maximum values of the Reynolds stresses in any given turbulent flow configuration . The transport equations presented above are used for this purpose together with a numerical solution technique. However,the universality of such a calculation procedure is greatly obviated by the difficulty explained above.Therefore,a formulation valid for a flow case can not be used reliably for a different flow case.

2.5.MOMENTUM FLUX RELATIONS FOR TURBULENT FLOW

Turbulent flows can be calculated as time dependent laminar flows with a constant viscosity.This approach,however, gives the details of the flow field in terms of velocities and pressure,but does not yield results about the statistical properties of the flow field,such as Reynolds stresses.

The Reynolds equations,Eqn.s.2.10,govern the momentum transport phenomena in an axisymmetrical turbulent flow field. It can be seen from these equations that the total stresses in a turbulent flow field are higher than those in a laminar flow.Therefore,in order to close the equation system,Eqn.s.2.10, for a solution, Eqn.s.2.6 with constant viscosity are not suitable.

One method of closure is to assume an augmented 'isotropic viscosity' and then substitute for the total stress terms in Eqn.s.2.10 some relations similar in form to Eqn.s.2.6 ,but with the exception that velocities are mean values and viscosity is an 'effective viscosity'. Then , a total shear stress in a turbulent flow field is represented,for example, as

$$\tau_{\theta z}-\rho\overline{uw} = (\mu + \mu_t)\frac{\partial \overline{w}}{\partial z} = \mu_e \frac{\partial \overline{w}}{\partial z} \qquad (2.15)$$

This is the simplest and most economical solution to the closure problem of Eqn.s.2.10 .

It is also possible,however,to obtain a solution,for instance, by keeping the Reynolds stresses in Eqn.s.2.10 and writing a transport equation for each of the stresses (see Eqn.2.11). Assumptions are then made for the correlation terms between pressure and velocity fluctuations in terms of,say,velocity gradients.This procedure,however,results in an increased number of transport equations and even for a reasonable mesh system taxes the limits of storage capacity of the most widely available computers. Therefore, this procedure is not considered in this work.

CHAPTER 3. LITERATURE SURVEY

3.1.INTRODUCTION

Ever since the strong and useful effects of swirl on combustion efficiency,stability and flame length were known, extensive research has been carried out on swirling flows. While some investigators have studied the subject only experimentally,others have done theoretical work.Theoretical works can further be divided into laminar and turbulent flow cases. Mostly analytical procedures have been employed for the former, while application of numerical procedures are necessary for the latter.The latter class is more relevant for combustion applications and will be reviewed briefly in Chapter 4 . Since some detailed reviews are already present (Ref.s.15,16,17,18 and 19),this chapter is intended to present briefly the experimental work done on turbulent swirling flows and vane type swirlers.Emphasis has been mainly on the basic definitions,the type of flow considered,experimental procedure and the instrumentation employed, rather than results since some of the relevant will be included in Chapter 7 for direct comparison purposes.

3.2.SWIRLING JETS GENERATED BY VARIOUS MEANS

One of the earliest investigations into isothermal turbulent swirling flows was due to ROSE (Ref.20). He carried out mean flow and turbulence measurements in a swirling flow obtained by rotating a pipe.The flow was,therefore, of the boundary layer type.Hot-wire anemometry was used for turbulence measurements. The hot-wire probe aligned in the direction of the mean absolute velocity was employed with a technique to measure also the velocity fluctuation.This technique was observed to be successful under such weak swirling flow conditions.

CHIGIER BEER (Ref.21) made mean flow measurements in swirling flows obtained with tangential-air-entry type swirl generator,using a hemispherical impact tube and a disc-type static pressure probe.The rates of both tangential and axial air flow could be controlled. In this way it was possible to change, within a wide range,the amount of rotation imparted to the axial flow. The amount of rotation was characterized by the swirl number defined as

$$S = \frac{2\,M_{\Phi}}{M_Z\,D} \qquad (3.1$$

where D is the diameter at the nozzle exit.They varied the swirl number between 0 and 1.57 .For high values of swirl number ($S>.6$), a recirculation region was present at the nozzle exit.Its size varied as the swirl number was increased. Flow

inside the tangential-air-entry type generator showed almost solid body rotation, therefore, radial equilibrium could be assumed there with the equation

$$\frac{\partial p}{\partial r} = \rho \frac{W^2}{r} \qquad (3.2)$$

for especially high swirl numbers. When issued into atmosphere, the flow expanded more rapidly as the swirl number was creased. The static pressure in the jets were always sub-atmospheric and decreased progressively as the swirl number was increased. Decay rates of the velocity components were proportional to swirl number. It was found from the integration of the velocity profiles that the axial and angular momentum fluxes are conserved along the length of the jets. Finally , two convergent and a convergent-divergent nozzles were fixed at the exit of the swirl generator. It was found that the addition of a divergent nozzle increases the size of the recirculation region and facilitates its occurance.

CHIGIER and CHERVINSKY (Ref.22) used a five-hole spherical pressure probe for the investigation of swirling flows obtained from a tangential-air-entry type swirl generator. Although they varied the swirl number up to .64 , no recirculation was reported. All the flows investigated were of the boundary layer type. These allowed them to use the reduced (boundary layer) form of the momentum equations from which they derived

$$M_z = 2\pi\rho \int_0^\infty r\left(U^2 - \frac{W^2}{2} \right) dr \qquad (3.3)$$

for the axial momentum flux by assuming that the quantity

$$u^2 - \frac{v^2+w^2}{2}$$

is small. Further, in the fully developed region they assumed that the axial and swirl velocity components are of the similarity form :

$$U(r,z) = U_m(z) . U(\xi) \qquad (3.4a)$$

$$W(r,z) = W_m(z) . W(\xi) \qquad (3.4b)$$

where

$$\xi = \frac{r}{z+a} \qquad (3.5)$$

These assumptions led to ordinary differential equations from which analytical expressions for the decay of the maximum values at each station , of the axial and swirl velocity component and static pressure were obtained. Experimental results showed that the profiles of the axial and swirl velocity components and static pressure can be expressed as

$$U/U_m = \exp(-k_u \xi^2) \tag{3.6}$$

$$W/W_m = E\,\xi + F\,\xi^2 + G\,\xi^3 \tag{3.7}$$

$$(p-p_a)/(p_m-p_a) = \exp(-k_p \xi^2) \tag{3.8}$$

where the axial velocity and static pressure profile constants are given as functions of swirl number :

$$k_u = \frac{92}{1+6S} \tag{3.9}$$

$$k_p = \frac{150}{1+8S} \tag{3.10}$$

It has not been possible,however,to express the swirl velocity profile constants E,F and G as functions of the swirl number. They vary irregularly with swirl number.The axial velocity profiles assumed the form of the Gaussian curve (Eqn.3.6) only after a distance of ten nozzle diameters for high swirl numbers (S-.5) .In closer regions to the nozzle exit,maximum of the velocity was shifted from the axis. Finally, the entrainment rate was expressed as

$$m = k_e\, m_o\, \frac{z}{D} \tag{3.11}$$

where k_e ,the entrainment constant, was given as

$$k_e = 0.32 + 0.8\,S \tag{3.12}$$

It was pointed out ,however, that this linear relation for the entrainment constant is valid only for swirl numbers up to approximately 1. A similar work was also reported by CHERVINSKY (Ref.23) where it was found that two similarity scales are

possible in swirling jets depending on whether the flow is controlled by the axial or angular momentum. It was also stated that high axial pressure gradients distort the velocity profiles and similarity can not be obtained in such regions.

CHIGIER and CHERVINSKY (Ref.24) also examined weakly swirling flows under burning conditions. Same swirl generator as that in Ref.22 was used for the investigation.However, gas fuel was injected into the axial air. A wator cooled five-hole hemispherical impact probe and a bare Platinum/Platinum-Rhodium thermocouple were used for the measurements of the mean velocity components and temperature.Boundary layer analysis was also extended to include the energy equation with the similarity assumptions

$$U = U_m(z).U(\xi) \tag{3.4a}$$

$$W = W_m(z).U(\xi) \tag{3.4b}$$

$$\rho-\rho_a = (\rho_m-\rho_a).o(\xi) \tag{3.13}$$

$$T-T_a = (T_m-T_a).T(\xi) \tag{3.14}$$

and analytic expressions for the decay of the maximum values at each axial station,of the axial and swirl velocity components and temperature were obtained.Experimental results showed that these similarity assumptions are reasonably good far downstream from the nozzle exit and the radial profiles of the axial velocity component and temperature can be represented in the form of Gaussian error curve as

$$U/U_m = \exp(-k_u.\xi^2) \tag{3.15}$$

$$(T-T_a)/(T_m-T_a) = \exp(-k_t.(\xi-\xi_{Tm})^2) \tag{3.16}$$

where ku, the axial velocity profile coefficient, has a different value from that given by Eqn.3.9 .The swirl velocity component showed a forced vortex type rotation in the core region of the jet and a free vortex type rotation in the outer part. The decay rates along the centreline of the jet were given as

$$\frac{U_m}{U_{mo}} = \Lambda_u \frac{D}{z+a} \left(\frac{\rho_a}{\rho_m} \right)^{0.5} \tag{3.17}$$

$$\frac{W_m}{W_{mo}} = B_w \left(\frac{D}{z+a} \right)^2 \left(\frac{\rho_a}{\rho_m} \right)^{0.5} \qquad (3.18)$$

$$\frac{T_m - T_a}{T_a} = C_t \frac{D}{z+a} \left(\frac{\rho_a}{\rho_m} \right)^{0.5} \qquad (3.19)$$

where A_u, B_w and C_t are constants determined experimentally.

PRATTE and KEFFER (Ref.25) made measurements of turbulence quantities and mean velocity components in a turbulent swirling jet. Only a single swirl number case was considered.Their way of obtaining swirl was the same as Rose's (Ref.20) : a round pipe with axial air flow inside was rotated at a fixed rpm . In this way, only a weakly swirling flow was obtained.Hot-wire anemometry was used for turbulence measurements. A normal type probe was rotated in the direction of the mean absolute velocity at each spatial position in the flow field.This was relatively easy because of the boundary layer character of the flow. With the probe aligned in the direction of the mean absolute velocity, one-dimensional turbulent kinetic energy spectra were also measured using a frequency analyzer. The distribution of static pressure was measured on the axis of the jet using a disc-type static pressure probe and a conventional needle type probe. For the measurement of the radial distribution of static pressure,however, only disc-type probe was used. On the axis , measurements with the disc-type probe showed a 15% difference (higher) from those with the conventional type. They presented a boundary layer type analysis using the similarity form in the same way of Ref.22 .Experimental axial velocity profiles showed a Gaussian error curve distribution and could be expressed as

$$U(\eta) / U_o = \exp(-45\,\eta^2) \qquad (3.20)$$

where $\eta = r/l$ and l is the lateral length scale. Swirl velocity profiles were of a Rankine vortex type ,i.e., solid body rotation in the core of the jet (forced vortex) and free vortex in the outer region. The radial distributions of the normal stresses showed peaks shifted from the jet axis in the initial region of the jet.Further downstream in the similarity region the peaks were shifted back to the axis .The dominant shear stress was ouw and this was proven using the transport equation for this quantity. Finally,they emphasized the formidable difficulties in obtaining reliable data in highly turbulent flows.

SYRED,CHIGIER and BEER (Ref.26) made investigation in the recirculation region set up at the exit of a tangential-air-entry type swirl generator . Hot and cold conditions were considered. The components of the mean absolute velocity were

measured under both hot and cold conditions, using an impact probe.In flames,temperatures were determined using a Platinum/ Platinum-Rhodium thermocouple. Turbulence measurements were carried out under cold conditions, employing a hot-wire anemometer .A new method for the interpretation of the signals from the hot-wire anemometer was used in the investigation. In these method,six orientations of the hot-wire were required at each point in the flow field.Turbulence intensities as high as 160% occured at the exit of the swirl generator.The size of the recirculation region was slightly smaller under hot conditions.Maximum reverse mass flow rates are 1o% higher under cold conditions than those under hot cases.The recirculation region occupied almost 75% of the generator exit.Maximum reverse velocities were of the same order of the nozzle exit velocities.It was found that temperature decay closely followed the decay of the kinetic energy of turbulence.It was concluded that for strong swirl cases,the aerodynamics dominate the flow field rather than the chemical reaction.For strong swirl,therefore,tests can be carried out under cold conditions to determine approximately the aerodynamic structure of the flow field under hot conditions.

CHIGIER and DVORAK (Ref.27) used a Laser Doppler anemometer for the investigation of a recirculation region in a swirling flow issuing from a tangential-air-entry type swirl generator. Hot and cold cases were considered at a swirl number of 0.3 . Natur l gas was used as fuel and was fed into the swirling flow field through a central pipe in the swirl generator such a diffusion flame was obtained.The Laser anemometer was operated in the 'double Doppler mode' .Since the Laser anemometer could not detect reverse flows without frequency shifting, it was applied by using a rotating diffraction grating.Magnesium oxide was used for seeding the flowing air.It was observed from the measured profiles of the axial velocity component that the length of the recirculation was larger under hot conditions than that under cold conditions. The width of the recirculation region,however, was not altered.These results were in contrary to the results of Ref,26 where hot conditions decreased both the length and width of the recirculation region.Hot conditions increased the rate of entrainment.Radial profiles of the swirl velocity component possessed a step before a peak in the recirculation region.Further downstream, however,they assumed a form similar to that of Rankine vortex. Finally it was found out that higher turbulence intensities occur under hot conditions.Turbulence intensities of the order of 100% were observed in the recirculation region.

3.3.SWIRLING JETS GENERATED BY VANE TYPE SWIRLERS

KERR and FRASER (Ref.6) made mean flow measurements in swirling jets issuing into a furnace atmosphere.The furnace burner had a special design such that inner flow passed through a flat vane type swirler and outer flow through angled slots.

Swirlers with vane angles of $0°, \pm 45°, \pm 60°$ were available. The angle of the slots could be varied as $0°$ or $30°$. No mention was made of the number of vanes employed on the swirlers. In this way, a wide range of swirl could be obtained. Only six combinations, however, were investigated in the furnace burner. A model burner was also designed in order to measure the nozzle torque and the nozzle thrust. The components of the absolute velocity were measured in the jets issuing from both the furnace and the model burners, using a Hiett and Powell pressure probe. All of the measurements were taken far downstream. No recirculation was, therefore, reported even for high vane angles. It was found from the integrated velocity profiles that axial and angular momentum fluxes are conserved along the length of the jets and are approximately equal to the measured nozzle thrust and torque, respectively. In this way, swirl number could be expressed as

$$S = \frac{T}{G d_e} \tag{3.21}$$

where d_e, the effective nozzle diameter, is defined for annular swirlers as

$$d_e = (D^2 - d^2)^{0.5} \tag{3.22}$$

It is seen that for hubless vane type or tangential-air-entry type swirlers $d_e = D$. Using Eqn.3.22 the swirl number becomes

$$S = \frac{1-z^3}{(1-z^2)^{3/2}} \cdot \frac{tg\theta}{3} \tag{3.23}$$

assuming that at the swirler exit the axial and swirl velocity components have uniform distributions and all along the vane span

$$W_o = U_o \, tg\theta \tag{3.24}$$

holds. Examination of Ref.21, however, reveals that these assumptions are not completely true, although swirl was obtained there with a tangential-air-entry type swirl generator. In particular, at high swirl numbers most of the flow accumulates near the outer wall in the in the swirler and almost no axial flow occurs in the central region, i.e., the axial velocity profile possesses a sharp peak near the outer wall. Also, the axial and swirl velocity profiles are not linearly related all along the vane span as it is suggested by Eqn.3.24. With these

assumptions,however,it is seen from Eqn.3.23 that swirl number depends only on the swirler geometry.The efficiency of swirl generation was also given as : for a given blade form the higher the swirl number for a fixed pressure loss, or the lower the pressure loss for a fixed swirl number,the higher is the efficiency of the swirl generation.For the acceleration of the flow through the swirler from U_i to a value of $U_i/\cos\theta$,the pressure drop is proportional to

$$\Delta P \sim tg^2\theta . U_i^2 \qquad (3.25)$$

and for a fixed inlet velocity

$$\Delta P \sim tg^2\theta \qquad (3.26)$$

On the other hand, for a fixed swirl number, using Eqn.3.23

$$\Delta P \sim \frac{(1-z^2)^3}{(1-z^3)^2} \qquad (3.27)$$

that is,if the hub ratio, z, is increased with the aim of obtaining a fixed swirl number, a smaller value of the vane angle is required and less pressure drop is incurred as it is seen from Eqn.3.26 or Eqn.3.27 .On the other hand, for a fixed pressure drop,that is,vane angle, if the hub ratio is increased, the swirl number increases. It is also obvious that the influence of the vane angle on the swirl number is much more than that of hub ratio.The entrainment rate was given as

$$\frac{m}{m_o} = (k_{e1}+k_{e2}S)\,\frac{z}{D} \qquad (3.28)$$

where for S=0 , the entrainment rate in a straight jet is obtained as a special case. The constants were expressed as

$$\frac{tg\alpha}{tg\alpha_{S=0}} = \frac{U_{mS=0}}{U_m} = \left(\frac{k_{S=0}}{k}\right)^{0.5} = \frac{r_{.5}}{r_{.5S=0}} = 1+\frac{k_{e2}}{k_{e1}}S \qquad (3.29)$$

where

$$r_{.5} = z \,.\, tg\alpha \qquad (3.30)$$

therefore,

$$r_{.5} = z\left(1+\frac{k_{e2}}{k_{e1}}S\right) tg\alpha_{S=0} \qquad (3.31)$$

Experiments showed that at the stations where measurements were taken, axial velocity profiles assumed the form of the Gaussian error curve

$$\frac{U}{U_m} = \exp(-\ln 2 \,(\frac{r}{r_{.5}})^2) = \exp(-k\,(\frac{r}{z})^2) \qquad (3.32)$$

where the error curve constant is

$$k = (\frac{z}{r_{.5}})^2 \ln 2 \qquad (3.33)$$

or from Eqn.3.31

$$k = \frac{\ln 2}{(1+k_{e2}/k_{e1}\ S)^2\ tg^2\alpha_{S=0}} \qquad (3.34)$$

The error curve constant k was also determined experimentally as (compare with Eqn.3.9)

$$k = \frac{96}{(1+4.8\ S)^2} \qquad (3.35)$$

in terms of swirl number. Finally, the entrainment rate was found experimentally as (see Eqn.3.28)

$$\frac{m}{m_o} = (\ 0.35+1.4\ S)\ \frac{z}{d_e} \qquad (3.36)$$

Later, KERR extended this study to include combustion conditions (Ref.7).

MATHUR and MACCALUM (Ref.8) examined isothermal free swirling flows issuing from vane type swirlers. Flat vanes with the outlet angles of 15°, 30°, 45°, 60°, 70° and 75° were considered. The swirlers were designed in two types : annular and hubless. To facilitate the manufacturing of the hubless swirlers, all the vanes were designed in the form of a segments of a circle, such that their sharp ends met on the axis of the swirler. Eight vanes were employed on each swirler and their trailing edges were not at the exit plane of the swirler. All the vanes were symmetrical and their chord lengths were so selected that on all the swirlers except those with vane angles of 15° and 30°, they formed an overlap of 30°. The overlaps on the latter two were -13° and 27°, respectively. Effective

turning of air through the swirler was provided in this way. No attempt was made, however, to decrease the pressure drop. The definition of the swirl number was given in a similar way to that of Ref.21 .The outer radius of the swirlers was used as the non-dimensionalizing length parameter. Thus , the swirl number could be expressed in terms of the geometric parameters of the swirlers as

$$S = \frac{2}{3}\,\frac{1-z^3}{1-z^2}\,tg\theta \qquad (3.37)$$

However, the same assumptions made in Ref.6 were used : uniform axial and swirl velocity distributions at the swirler exit and the relation

$$W_o = U_o\ tg\theta \qquad (3.24)$$

holds all along the vane span. For hubless swirlers, the swirl number becomes

$$S = \frac{2}{3}\ tg\theta \qquad (3.38)$$

It is seen from an examination of Eqn.s.3.38 and 3.37 that annular swirlers have larger swirl numbers, since always

$$1 \leq f(z) = \frac{1-z^3}{1-z^2} \leq 1.5$$

for practical values of the hub ratio. It is seen that the the effect of the hub ratio on the swirl number is very slight. The swirl number is increased by increasing the vane angle . The theoretical total pressure drop through the swirler has been expressed as

$$\Delta P = \Delta P_1 + \Delta P_2 = \frac{\rho U_i^2}{2}\left(K_1 + K_2\ tg^2\theta \right) = \frac{\rho U_i^2}{2} K \qquad (3.39)$$

where the first part, ΔP_1 , is the frictional loss with the vane angle of θ . When the flow accelerates through the swirler vanes with an angle of θ , from an average axial velocity U_i to $U_i/\cos\theta$, the additional pressure drop, ΔP_2 , occurs. The frictional pressure drop coefficient K_1 depends on surface roughness, wetted area and thickness of the vanes. K_2 is dependent mainly upon the design of vanes, i.e., the effectiveness of the vanes in turning the flow through the swirler. For vane

angles 45° or higher, K_1 can be neglected. If all the losses are neglected, the theoretical value of K2 becomes unity. For a swirler imparting complete turning to the flow passing through, the efficiency of swirl generation was given as

$$\text{efficiency} = \frac{\text{theoretical pressure drop}}{\text{actual pressure drop}} \approx \frac{1}{K_2}$$

for vane angles 45° or higher. A Hiett and Powell pressure probe was used for the measurement of velocity components. The distribution of static pressure was measured using a disc-type static pressure probe. The static pressure drop through the swirlers was defined as

$$\Delta p = p_i - (p_o)_{axis} \qquad (3.40)$$

and mass flow-pressure drop characteristics were presented. It was found that the pressure drop increased with increasing mass flow rate and vane angle. The distribution of the static pressure along the axis of the jets for different swirlers showed that for hubless swirlers, sub-atmospheric pressures were set up in the core region of the jets and their values increased gradually towards atmospheric pressure far downstream. The minimum values which occured in the immediate downstream of the swirlers, decreased with increasing vane angle. The distribution of static pressure was directly proportional to $U_i^2 \, tg\theta$. For annular swirlers, however, such a direct gradual increase towards the atmospheric pressure was not observed. Instead, for vane angles below 45°, the sub-atmospheric value at the exit from the swirlers increased towards a maximum and this was followed by a minimum. Subsequently, it increased gradually towards the atmospheric pressure. For the vane angles of 45° or higher, however, the initial maximum was not observed. The sub-atmospheric pressure at the exit dropped further to a minimum and then increased gradually towards the atmospheric value, thus indicating the formation of a recirculation region. Similar to the hubless swirlers, the minimum values of the static pressure decreased with increasing vane angles, also for annular swirlers. Distribution of the axial velocity profiles showed that the size of the recirculation region (both the length and width) increases with increasing vane angle in the case of hubless swirlers. For the annular swirlers, however, the length of the recirculation region was reduced, while its width being increased considerably with increasing vane angle. The amount of the recirculating mass flow was measured for the annular type swirlers and it was found that

$$\frac{\text{maximum recirculating mass flow}}{\text{nozzle flow}} \approx 0.06 \, tg^2\theta \qquad (3.41)$$

Finally,it was shown that swirling jets expand very rapidly after issuing into atmosphere and the rate of expansion increases with vane angle. It was concluded that tgθ can be taken,instead of the swirl number,as a measure of swirl for flat vane type swirlers.

BAFUWA and MACCALUM (Ref.9) examined the performance of the flat vane type swirlers of Ref.8,under burning conditions. Only the swirlers with vane angles of 15,30,45 and 60 were tested. Velocity,static pressure and temperature measurements were carried out. A water-cooled Hiett and Powell probe was used for the measurement of velocity components. A water-cooled disc type static pressure was employed for static pressure measurements. Temperature profiles were determined using a Platinum-5%Rhodium/Platinum-20%Rhodium bare thermocouple. It was that the recirculation region is lengthened and widened with increasing vane angle for both hubless and annular swirlers under also hot conditions. Flame length was,however, reduced considerably with increasing vane angle. A comparison with cold tests for a fixed vane angle showed that combustion shortened and widened the recirculation region. Further,it was observed that burning jets expand initially more rapidly than cold jets for a fixed vane angle. This was because of the expansion of the hot gases due to combustion. Further downstream, however, the expansion rate of the burning jets decreased to that of cold jets. Also, a finite difference method,the vorticity stream function approach,was employed to predict the turbulent swirling flow fields. No turbulence model was incorporated,however,into the calculation procedure. The extension of this work to swirling flows in furnaces was carried out by BELTAGUI and MACCALUM (Ref.10). Also,among the measurements made in swirling flames within confinements are those due to YOUSSEF (Ref.11) and HUTCHINSON et.al (Ref.12). In the former, the swirling flow in a combustion chamber,generated by a vane swirler was examined experimentally under both hot and isothermal flow conditions. A combined velocity,pressure and temperature probe was used for the investigation. It was found that,combustion reduced the rates of reverse flow,while also decreasing slightly the size of the recirculation region.These findings were partly consistent with that of Ref.9 , where it was also faund that the length of the recirculation region decreases with combustion. There,however,the width of the recirculation region was increased. Here,the decrease in the width of the recirculation was probably due to the strong radia penatration of the dilution air in the combustion chamber. In the latter study(Ref.12),the swirling flow in a cylidrical furnace was considered under diffusion flame conditions. Axial velocity profiles and corresponding normal Reynols stress were measured using a Laser Doppler anemometer. Temperature measurements were taken with a suction pyrometer in the furnace and with chromel-alumel thermocouples on the walls. Some experimental results were also predicted using a finite difference method (the primitive pressure-velocity approach). Swirl was obtained with a vane type swirler and the effects of a burner quarl was investigated. It was found that the presence of the quarl decreased the length of the flame considerably. Only a

single type swirler was,however,used in the investigation.

3.4. CONCLUSIONS

The following main conclusions are drawn from the literature survey:-

a)The axial momentum flux is conserved in the free jet region of a swirling flow and is equal to the nozzle thrust.
b)The angular momentum flux is conserved and is equal to the nozzle torque.
c)The degree of rotation in a swirling flow can be characterized with a non-dimensional parameter,the swirl number.
d)Swirling flows expand much more rapidly than corresponding straight jets and the rate of expansion increases with swirl number.
e)The rate of entrainment of a swirling flow from ambient is larger than a corresponding straight jet and increases with swirl number.
f)A core region with a sub-atmospheric pressure is induced in the central region of swirling flows.When the swirl number increases and reaches a critical value, the sub-atmospheric value of the pressure becomes low enough to induce a recirculation region where reverse flow velocities occur.
g)When there is no recirculation,swirling flow is said to have 'weak swirl' ($S \leq 0.4$) .When the streamlines start diverging considerably, but there is still no recirculation, it is called 'moderate swirl' ($S \leq 0.6$). When recirculation occurs ($S > 0.6$), it is called 'strong swirl' .
h)Higher turbulence intensities and stronger shear stress regions are created in swirling flows due to the presence of swirl velocity component.However,this high intensity turbulence makes very difficult all turbulence measurements in swirling flows.Therefore, information on the turbulent behaviour of swirling flows,especially with recirculation,is quite scanty. Knowledge about the distribution of the kinetic energy of turbulence,shear stresses, etc., is quite necessary for both direct practical problems (fuel injection,for instance) and academic interest (flow modelling).
j)The most common way of obtaining swirl is by employing tangential-air-entry or vane type swirl generators. In the former aerodynamic, in the latter physical blokage is created.The latter has been the most common practice in aircraft gas turbine combustion chambers.
k)For a swirler with flat vanes, $tg\theta$ can be taken,instead of the swirl number, as the degree of swirl since the hub ratio has only a minor effect on the swirl number.
l)A recirculation region of considerable size from a flat vane type annular swirler can be obtained at a vane

angle of around 45°. When the vane angle is increased, the length of the recirculation region decreases, while, however, its width is increasing.

m) The pressure drop through a flat vane type swirler is proportional to $tg^2\theta$, for a fixed inlet velocity. As the vane angle is increased, the blockage created and the resulting pressure drop increase very rapidly.

n) Flat vanes always run under stalled conditions, causing, therefore, excessive momentum loss through the swirler.

o) The effectiveness of turning by curved vanes, therefore, becomes quite obvious. However, very little information is available in the literature about curved vane type swirlers.

p) Although known qualitatively, no quantitative information is available about the effect of hub ratio on the size of recirculation region or other flow properties. The influence of the number of the vanes on the efficiency of the air turning through the swirler has also not been investigated.

q) The influence of varying the main swirler design parameter, that is, the vane angle, is the same under both hot and cold conditions; as it is increased, the length of the recirculation region decreases and its width increases. Therefore, in order to investigate swirler performance, tests can be carried out under cold conditions.

CHAPTER 4. PREDICTION OF FLOW FIELDS

4.1.INTRODUCTION

Reynolds equations,Eqn.s.2.10 ,have to be solved for the prediction of turbulent axisymmetrical swirling flows.For free turbulent flows,it is well known that the contribution to the momentum flux by molecular transport is negligible (Ref.28).Therefore,the laminar stresses in Eqn.s.2.10 can be neglected.If we denote the Reynolds stresses as

$$-\rho\overline{uv} = T_{rz} \quad , \quad -\rho\overline{u^2} = T_{zz}$$

,etc.,for convinience and after manipulating Eqn.s.2.10b,c,d with Eqn.2.10a ,they can be written for incompressible flow as :-

$$\rho\left(\frac{1}{r}\frac{\partial}{\partial r}(rV^2)+\frac{\partial}{\partial z}(UV)-\frac{W^2}{r}\right)=-\frac{\partial p}{\partial r}+\frac{1}{r}\frac{\partial}{\partial r}(rT_{rr})+\frac{\partial}{\partial z}T_{rz}-\frac{T_{\theta\theta}}{r} \qquad (4.1a)$$

$$\rho\left(\frac{1}{r}\frac{\partial}{\partial r}(rVW)+\frac{\partial}{\partial z}(UW)+\frac{VW}{r}\right)=\frac{1}{r^2}\frac{\partial}{\partial r}(r^2T_{r\theta})+\frac{\partial}{\partial z}T_{\theta z} \qquad (4.1b)$$

$$\rho\left(\frac{1}{r}\frac{\partial}{\partial r}(rUV)+\frac{\partial}{\partial z}(U^2)\right)=-\frac{\partial p}{\partial z}+\frac{1}{r}\frac{\partial}{\partial r}(rT_{rz})+\frac{\partial}{\partial z}T_{zz} \qquad (4.1c)$$

where the bar on p has been dropped for convinience.It is seen that Eqn.s.4.1 constitute a system of strongly coupled non-linear elliptic partial differential equations.Actually they are in exactly the same form as the momentum equations.Therefore,if the momentum flux relations for laminar flow,Eqn.s.2.6 are used for closure,they represent the equations governing the laminar swirling flow field of a viscous fluid.As a special case,if the viscosity is set to zero,the inviscid flow form of the equations are obtained.For turbulent flows,however,as was stated before,one simple way of solution is to employ an effective viscosity varying with the position in the flow field.

4.1.1.Prediction of boundary layer type swirling flows

Before starting the solution procedures for Eqn.s.4.1 , which must be solved for swirling flows with recirculation , a reduced form of them will be considered.For weakly swirling flows, the axial pressure gradient is not strong enough to cause recirculation.Therefore,the flow can be treated as a boundary layer flow. Comparing the order of magnitudes of the terms in Eqn.s.4.1 ,they can be reduced to the boundary layer form as :-

$$\rho\left(\frac{W^2}{r}\right)=\frac{\partial p}{\partial r} \tag{4.2a}$$

$$\rho\left(\frac{1}{r}\frac{\partial}{\partial r}(rVW)+\frac{\partial}{\partial z}(UW)+\frac{VW}{r}\right)=\frac{1}{r^2}\frac{\partial}{\partial r}(r^2T_{r\theta}) \tag{4.2b}$$

$$\rho\left(\frac{1}{r}\frac{\partial}{\partial r}(rUV)+\frac{\partial}{\partial z}(U^2)\right)=-\frac{\partial p}{\partial z}+\frac{1}{r}\frac{\partial}{\partial r}(rT_{rz}) \tag{4.2c}$$

Then only the fluxes in the radial direction become important and the equations assume a parabolic character. Because in the solution of parabolic partial differential equations, further (downstream) events do not influence previous (upstream) events, the solution procedure becomes easier than those of the elliptic equations. Solution is facilitated further by transforming Eqn.s.4.2 to (z-W) coordinates, using von-Mises transformation (Ref.29 and 30). Eqn., say, 4.2c then becomes :-

$$\frac{\partial U}{\partial z}=\frac{\partial}{\partial W}(rT_{rz})-\frac{1}{\rho U}\frac{\partial p}{\partial z} \tag{4.3}$$

Also, non-dimensionalizing the stream function W, computations can be carried out for only the region of interest in the flow field.

In general, there are two methods for the solution of the parabolic equations of boundary layer type flows, namely :-

1) Explicit integral types,
2) Complete theories. This class can be further divided into three cases :

a) Cross stream integration ,
b) Parametric integral methods,
c) Marching integral methods.

No detailed explanation of respective methods will be given here. It is considered sufficient to say that marching integral methods employing finite differences in their formulations have proven the most efficient amongst the others, as it is substantiated by the rapid developments using this way (Ref.s.29 ,30). The reader is referred to the same references for the explanation concerning the above methods.

Marching integral methods, too, can be subdivided into two cases : explicit and implicit formulations. Explicit formulations, although more straightforward than the implicit methods, may be unstable for some mesh configurations. Considering also the strong non-linearity of Eqn.s.4.2 , it can be deduced that

a fully implicit numerical marching integral method should be used for their solution.Such a numerical solution method has been formulated (Ref.29) ,developed (Ref.30) and has been modified for boundary layer type swirling flows (Ref.31). An extensoin of Prandtl's mixing length hypothesis has been used in the latter work.Also, some other turbulence models, say,k-kℓ model, have been tested with the procedure (Ref.32) and quite consistent results with those of experiments have been obtained.

In this computational procedure, Eqn.s.4.2 are at first transformed to von-Mises coordinates (see Eqn.4.3) and then they are cast into the common form of

$$\frac{\partial Q}{\partial z}+(\alpha+\beta\eta)\frac{\partial Q}{\partial \eta} = \frac{\partial}{\partial \eta}(\gamma \frac{\partial Q}{\partial \eta})+ \epsilon \qquad (4.4)$$

where Q might be considered as U ,rW and,say,in the case of employing k-kℓ model of turbulence, k and kℓ . η represents the non-dimensional stream function defined for convinience as

$$\eta = \frac{W - W_I}{W_E - W_I} \qquad (4.5)$$

where I and E represent the value of the stream function at the internal and external boundaries of the flow region. In this way, it becomes possible to give η values between 0 and 1 in order to focus attention on the particular region of interest in the flow field.In further stages of the procedure, Eqn.4.4 is integrated over finite volumes, employing a micro integral method, to obtain the implicit finite difference equation of the form

$$Q_i = A\, Q_{i+1} + B\, Q_{i-1} + C \qquad (4.6)$$

This is used to solve with stability,all the equations of interest, for each forward step.A simple successive substitution technique,controlled by i for scanning the mesh points in the cross stream direction, is adequate for the following algebraic computations. A,B and C in Eqn.4.6 are functions of η differences,the values of Q's at the upstream step and the coefficients a,b,c and d in Eqn.4.4 .Thus linearization is obtained and iteration in the downstream direction is avoided.However, a forward extrapolation is used for higher accuracy in the representation of the source term d.

The swirl equation,Eqn.4.2b, does not fall exactly into the

form of Eqn.4.4 ,having the variable rW as its argument Q . It is, therefore, put into the form of (Ref.31)

$$\frac{\partial}{\partial z}(rW)+(\alpha+\beta\eta)\frac{\partial}{\partial \eta}(rW) = \frac{\partial}{\partial \eta}(\gamma r^2 \frac{\partial}{\partial \eta}(\frac{W}{r})) \qquad (4.7)$$

In this way,the troublesome source term d in Eqn.4.4 is eliminated for swirl equation, Eqn.4.2b .

Calculations start at the upstream end of the region of interest usually employing experimental profiles for the required variables. For non-swirling boundary layer type flows, the calculation procedure tends to smooth out the profiles in the downstream direction (Ref.29). Similar results are also expected for swirling flows.Computations can be extended as far as desired in the downstream direction.The computational procedure has been tested extensively,therefore,its general accuracy is exceptionally good.Using also the modified procedure for swirl (Ref.31), turbulent swirling flows with combustion have been predicted (Ref.33).

Implicit formulation of the numerical marching methods is used to provide stability for the computational procedure, with the downstream step length.However,some instability problems still arise due to entrainment at the free boundary of the flow. In such circumstances the usual practice is that the step length for each downstream station is chosen in such a way that the mass flow rate increases,due to entrainment,by a very small amount,say, 0.01 .When the boundary layer flow is confined ,however,this problem does not exist .

With a careful choice of downstream step length the instabilities in an explicit formulation can be obviated (Ref.34,35). Considering this point,boundary layer type problems can also be calculated by the use of explicit formulation.Using this approach,boundary layer type confined swirling flows,with and without combustion,have been calculated (Ref.36,37).The advantage of explicit formulation is that no iteration in the cross stream is required.The computation proceeds in the stream direction in a straightforward manner.In order to obtain stability,however,the downstream step length should be extremely small.Thus,if calculations are to be carried out for a long distance in the stream direction,computational time becomes quite large.This can be partlyavoided by choosing larger step lengths in the cross stream direction.However,this introduces errors into the computations.The implicit formulation,on the other hand, does not suffer this disadvantage.The structure of Eqn.s.4.2 governing a weakly swirling turbulent flow field, makes them amenable to another treatment : inverse solution procedures.Since a single stress component exists in each equation, Eqn.s.4.2b and 4.2c can also be written as

$$\rho r^2\left(V\frac{\partial W}{\partial r}+U\frac{\partial W}{\partial z}+\frac{VW}{r}\right) = \frac{\partial}{\partial r}(r^2 T_{r\theta}) \qquad (4.8a)$$

$$r\left(\rho\left(V\frac{\partial U}{\partial r}+U\frac{\partial U}{\partial z}\right)+\frac{\partial p}{\partial z}\right) = \frac{\partial}{\partial r}(r\,T_{rz}) \qquad (4.8b)$$

Then it is seen that if the left hand sides of these equations are known, the stresses can be calculated as a function of r only. Two different paths may be followed subsequently . Firstly, analytic inverse procedure (Ref.39) may be applied by adopting analytic curves, fitted to experimentally determined velocity and pressure profiles, of the form of Eqn.s.3.6 to 3.8 , together with Eqn.s.3.9 and 3.10 .Substituting them into Eqn.s.4.8 shows that it then becomes possible to obtain analytic curves for the stresses, in terms of position in the flow field and swirl number.

Secondly, a complete numerical method is used to perform the inverse solution procedure (Ref.39). At first, Eqn.s.4.8 are expressed in finite difference form, say, using three, five or seven-point difference formulae. Then integrations are performed using numerical integration methods, say, Simpson rule. Experimental time-mean data are required as input to the procedure. In order to obtain reliable results, the mesh system on which experimental data are collected must be quite detailed. This, however, necessitates excessive computer storage. Hence, a special grid configuration is used in the procedure in order to alleviate this prohibitive requirement. In this way (see Ref.s.31 and 39), stresses in Eqn.s.4.8 may be calculated from the detailed measurements of velocity components and pressure (Ref.40). Because the velocity gradients are already calculated before the results about the stresses are obtained, it also becomes possible to compute other turbulence modelling parameters, say, turbulent viscosity and mixing length when, for instance, Prandtl's mixing length theory is employed. The mathematical procedure can be extended (Ref.41) by the addition of transport equations for heat and mass transfer to calculate their fluxes (and associated exchange coefficients) which have but one component in the radial direction when the boundary layer assumptions are applied to these equations.

Whatever method, analytical or numerical, is employed in an inverse solution procedure, it is an intermediate step towards an actual solution procedure in that it allows turbulent fluxes and associated exchange coefficients to be calculated from time mean data. Comparison of these calculations with the actual measurements of fluxes, say, Reynolds stresses, throws light about the accuracy or inaccuracy of measurements and such inverse solution procedures. The results produced about the exchange coefficients are used to elucidate the validity, or otherwise, of hypothes s, derived or devised to simulate the physical phenomena. It must be emphasized that an inverse solu-

tion procedure is feasible only due to the reduced structure of Eqn.s.4.2 .

When interest is in the strongly swirling flows, that is, flows with recirculation, the full elliptic equations , Eqn.s.4.1 ,have to be solved.The existance of several stresses in each equation then makes an inverse solution procedure impossible.Therefore, direct solution procedures have to be followed,together with hypotheses to represent the physical phenomena.The accuracy of hypotheses can then be checked only by trial-and-error calculations,according to the results of these direct solution procedures. However, examination of weakly swirling flows,both theoretically and experimentally, aids greatly in an understanding of the occurance of the recirculation phenomena taking place in strongly swirling flows, such that the results of the former have to be generalized for the latter case. Inverse solution procedures offer an invaluable tool for such an examination.

Measurements of time-mean flow properties (velocity and static pressure) and their interpretation with the inverse solution procedures has yielded anisotropic turbulent fluxes and exchange coefficients in weakly swirling flows (Ref.31). The existance of anisotropic fluxes was also proven experimentally in Ref.25 where the turbulent momentum fluxes,that is, Reynolds stresses, were measured in a weakly swirling flow using hot-wire anemometry. The tendency,therefore, in the modelling of turbulence in weakly swirling flows has been towards the use of anisotropic exchange coefficients (see Ref.32) . In this way, it is asumed that the two dominant Reynolds stresses can be expressed as

$$T_{rz} = \mu_{rz} \frac{\partial U}{\partial r} \quad , \quad T_{r\theta} = \mu_{r\theta}\, r \frac{\partial}{\partial r}\left(\frac{W}{r}\right) \tag{4.9}$$

and μ_{rz} and $\mu_{r\theta}$ can be written down using an extension of Prandtl's mixing length hypothesis,for instance, as

$$\mu_{rz} = \varrho\, \ell_{rz}^2 \left(\left(\frac{\partial U}{\partial r}\right)^2 + \left(r \frac{\partial}{\partial r}\left(\frac{W}{r}\right)\right)^2\right)^{.5} \tag{4.10}$$

where the mixing length ℓ_{rz} is expressed in terms of the thickness of the flow field r_{max} :-

$$\ell_{rz} = \lambda_{rz}\, r_{max} \quad , \quad \lambda_{rz} = \text{a constant} \tag{4.11}$$

Anisotropy is allowed for either by the definition of rθ-viscosity number $\sigma_{r\theta}$

$$\mu_{rz} = \mu_{r\theta}\, \sigma_{r\theta} \qquad (4.12)$$

which is mostly assigned a constant value, or, by applying Eqn.s.4.10 and 4.11 to $\mu_{r\theta}$, such that

$$\mu_{r\theta} = \rho\, \ell_{r\theta}^2 \left(\left(\frac{\partial U}{\partial r}\right)^2 + \left(r \frac{\partial}{\partial r}\left(\frac{W}{r}\right)\right)^2\right)^{.5} \qquad (4.13)$$

where

$$\ell_{r\theta} = \lambda_{r\theta}\, r_{max} \quad , \qquad \lambda_{r\theta} = \text{a constant} \qquad (4.14)$$

Other ways of incorporating anisotropic exchange coefficients into the analysis are also possible. For instance, writing down transport equations for the parameters of a turbulence model, say, k and $k\ell$, and calculating μ_{rz} from a relation like

$$\mu_{rz} = \rho\, \ell\, k^{1/2}$$

then employing a relation similar to Eqn.4.12 to allow for anisotropy. It is reported that more realistic predictions of weakly swirling flows have been made, employing such anisotropic models (Ref.32). Especially swirl velocity profiles have been predicted much more accurately in this way. However, it is also reported in the literature that quite good predictions of weakly swirling flows, with and without combustion, have been made, using isotropic exchange coefficients (Ref.32,36,37). An extension of Prandtl's mixing length hypothesis has been employed in most cases (see Ref.36,37). It should also be added that these predictions were more consistent with the experimental results in the far downstream region of the flow field.

Modelling of the flow field, using anisotropic exchange coefficients, does not present severe computational difficulties in the case of weakly swirling flows since there are only a couple of parameters , such as those in Eqn.4.9 and 4.11, to be adjusted in the calculation procedure. This fact is surely caused by the simpler structure of the flow field and consequently the reduced form of the governing equations. Therefore, only two stresses appear in the governing equations and boundary layer type hypotheses, such as Prandtl's mixing length, are available for the calculations.

For strongly swirling flows, however, distribution of mixing length is not known across the flow field and relations like Eqn.4.11 are not available. More elaborate models are, therefore, required. The appearence of full stress tensor in the governing elliptic equations makes the modelling quite difficult. Espec-

cially if a model with anisotropic exchange coefficients is attempted, the number of parameters to be adjusted becomes so excessive that the whole process becomes tedious and very expensive.

In a strongly swirling flow, all the members of the stress tensor have different significance in the structure of the recirculation region (see Eqn.s.2.11 and 2.13). The profile of each stress is created by the turbulence structure of the flow field. On the turbulence structure of the flow field, the geometry of the initial confinement and the method of producing swirl have quite strong influences. For instance, if a strong swirl is produced with tangential-air-entry in a rather long nozzle and the flow is allowed to mix well before it issues to the atmosphere, more uniformities are expected in the recirculation region obtained this way than that obtained by placing a vane type swirler at the exit of the nozzle. In the former case, the turbulence structure in the recirculation region occuring at the immediate downstream of the nozzle exit is more strongly dependent upon the properties of the flow just upstream and is quite free from the confinement effects for upstream, due to the thorough mixing taking place in the nozzle. In the latter case, however, the turbulence structure in the recirculation region is quite strongly dependent on the geometry of the vanes, surface roughness, etc., that is, it is not largely created due to pure aerodynamic development of the flow, but the geometry has great influences on it.

In this work, several vane type swirlers are involved. As it will be explained in Chapter 5, quite severe difficulties have been encountered even in the uniform production and fixing of the vanes on a single swirler. Also, for instance, it was actually impossible to produce vanes with equal surface roughnesses. For all these reasons, it is obvious that the turbulence structure in each recirculation region produced by each swirler would also be dependent to a large extent on the minor geometric properties, such as, small burrs, surface roughness, of the specific swirler. An anisotropic turbulence model, although could be successful in the prediction of stresses in in a recirculation region of a specific swirler, would not be valid for another swirler. Reconsidering also the large number of parameters to be adjusted when such a model is attempted , even for a single flow field, the use of an isotropic viscosity seems reasonable for the aim of predicting the sizes of the recirculation regions.

It must be noted, however, that in the modelling of strongly swirling flows there is still much to be gained from the examination of the structure of turbulence in weakly swirling flows. More elaborate models simulating the physical phenomenon more realistically must be developed and after appropriate fitting to weakly swirling flows, must be generalized to strongly swirling flows.

4.1.2.Prediction of swirling flows with recirculation

The full momentum equations,Eqn.s.4.1 ,have to be solved for the prediction of strongly swirling flows.For turbulent flows,it was stated that all the variables in this equation system are time-mean values (see Section 2.4).The Reynolds stresses are the second order correlations between the fluctuating parts of the velocity components,multiplied by density (for incompressible flows).Turbulence in this way has been treated as quasi-steady,that is,mean velocity components do not vary with time.The form of the quasi-steady Eqn.s.4.1 is exactly the same as that of the momentum equations, Eqn.s.2.3 ,apart from the existance of the time dependence terms in the latter.Together with the closure relations Eqn.s.2.6 ,the latter represent unsteady motion of a viscous fluid.Using such a formulation for the flow field,the prediction of strongly swirling flows has been made in Ref.s.42 and 43 ,where also some other references about simpler approaches to the problem can be found.In such a time dependant formulation, solution for the steady flow case is obtained when the time goes to infinity.The equations are of parabolic form with respect to time, for which numerical solution procedures were reviewed briefly in the previous section. Constant viscosities have been used in the calculations of these references and no simulation of turbulence has been made.

In order to calculate turbulent flows the quasi-steady Eqn.s.4.1 have to be solved together with some closure assumptions,like Eqn.2.15 ,and a turbulence model.The reasons why isotropic exchange coefficients are considered as reasonable were explained in the previous section. Directly,therefore, the solution procedures will be examined here.

There are two approaches to the solution of the equation system,Eqn.s.4.1, in fluid dynamics. Firstly,they are treated in the same form as they are. This is called the primitive pressure-velocity approach.Secondly, the pressure terms in Eqn.s.4.1a and 4.1c are eliminated by taking cross derivatives and the resulting two equations are combined to obtain the transport equation for the tangential component of vorticity defined as

$$\omega = \frac{\partial V}{\partial z} - \frac{\partial U}{\partial r} \qquad (4.15)$$

Eqn.4.15 itself provides the necessary transport equation for the mean stream function W ,with the insertion of Eqn.s.2.4 . This,therefore,is called the vorticity-stream function approach. For swirling flows,Eqn.4.1b is solved in addition to the vorticity and stream function equations to calculate the circulation or swirl velocity component. Circulation is defined as

$$\Gamma = 2 \pi W r \qquad (4.16)$$

for a path around the axis of symmetry of the flow.

In both approaches, the full transport equations are so complicated that the use of some approximate (numerical) methods is inevitable for a solution. Several of these methods are available. Among these are finite difference, finite element and others. In each case, a solution is sought to a boundary value problem. (For time dependent equations, however, the solution procedure becomes an initial value problem. Again several choices are available for a solution : finite difference, finite element, Galerkin procedures, integral differential forms and several others.)

Whatever the method is employed for an approximate solution of the transport equations of both approaches, the similarity already existant (see Eqn.s.4.1) or obtainable (in the second approach) with some manipulations in their form, aids greatly towards a simpler construction of the formulation of the method. Because swirl characterizes the flow field in this work, the similarity forms of the two approaches will be shown using the swirl equation, Eqn.4.1b , in the following sections.

4.2. PRIMITIVE PRESSURE-VELOCITY APPROACH

Substituting the momentum flux relations, Eqn.s.2.6 , after similar modifications to those in Eqn.2.15 , into Eqn.4.1b , the following form results :-

$$\frac{1}{r}\left[\frac{\partial}{\partial r}\left(\rho rVW-\mu_e r\frac{\partial W}{\partial r}\right)+\frac{\partial}{\partial z}\left(\rho rUW-\mu_e r\frac{\partial W}{\partial z}\right)\right]=\frac{W}{r}\left[\rho V+\frac{1}{r}\frac{\partial}{\partial r}(r\mu_e)\right] \qquad (4.17)$$

Alternatively, it can be put to the same form, using the definition of circulation, Eqn.4.16 :-

$$\frac{1}{r}\left[\frac{\partial}{or}\left(\rho rV\Omega-\mu_e r\frac{\partial \Omega}{\partial r}\right)+\frac{\partial}{\partial z}\left(\rho rU\Omega-\mu_e r\frac{\partial \Omega}{\partial z}\right)\right]=\frac{2}{r}\frac{\partial}{\partial r}(\mu_e\Omega) \qquad (4.18)$$

Assuming incompressible flow, Eqn.s.4.1a and 4.1c can also be put into the similar form :-

$$\frac{1}{r}\left[\frac{\partial}{\partial r}\left(\rho rVV-\mu_e r\frac{\partial V}{\partial r}\right)+\frac{\partial}{\partial z}\left(\rho rUV-\mu_e r\frac{\partial V}{\partial z}\right)\right]=\frac{\partial p}{\partial r}+\frac{\rho W^2}{r}-\frac{2\mu_e V}{r^2}+\frac{\partial}{\partial z}\left(\mu_e\frac{\partial U}{\partial r}\right)+\frac{1}{r}\frac{\partial}{\partial r}\left(\mu_e r\frac{\partial V}{\partial r}\right) \qquad (4.19)$$

$$\frac{1}{r}\left[\frac{\partial}{\partial r}\left(\rho rVU-\mu_e r\frac{\partial U}{\partial r}\right)+\frac{\partial}{\partial z}\left(\rho rUU-\mu_e r\frac{\partial U}{\partial z}\right)\right]=-\frac{\partial p}{\partial z}$$
$$+\frac{\partial}{\partial z}\left(\mu_e\frac{\partial U}{\partial z}\right)+\frac{1}{r}\frac{\partial}{\partial r}\left(\mu_e r\frac{\partial V}{\partial z}\right) \qquad (4.20)$$

It is seen that Eqn.s. 4.17,18,19 and 20 all have the same form :

$$\frac{1}{r}\left[\frac{\partial}{\partial r}\left(\rho rVQ-\mu_e r\frac{\partial Q}{\partial r}\right)+\frac{\partial}{\partial z}\left(\rho rUQ-\mu_e r\frac{\partial Q}{\partial z}\right)\right]=S_Q \qquad (4.21)$$

where Q stands for W or Ω , V and U .If Eqn.4.21 can be solved, the solution can then be applied to each of the equations that represents transportation of a flow variable.Such a solution is possible using Gauss's divergenge theorem (Ref.44). In this solution procedure,Eqn.4.21 is converted to an algebraic form using a finite difference method.Then,this algebraic equation is used for a line-by-line iterative technique in the flow domain.The procedure employs a staggered grid for U and V velocity components.However, the results of this procedure yield velocity components and turbulence quantities.The axial velocity profiles must then be integrated to obtain the radial distribution of the stream function at several stations along the jet axis in order to find the size of the recirculation region. Such information,however,becomes directly available in the case of the use of the vorticity-stream function approach. The latter is,therefore,given more detailed consideration in this work.The author,however,has very good acquaintance also with the primitive pressure-velocity approach. Work on the calculation of combusting swirling flows in a cylindrical chamber with dilution air injection is already in progress.

4.3.VORTICITY-STREAM FUNCTION APPROACH

4.3.1.Governing transport equations

Also for this approach (ref.45), the general form into which all the transport equations are cast will be shown initially using swirl component of the Reynolds equations.In order to do so,every term in Eqn.4.1b is multiplied by r^2 .The third term on the left hand side is combined with the first one.Turbulent momentum flux relations, like Eqn.2.15, are then substituted for the stresses.Using also the definition, Eqn.4.16 , of circulation, Eqn.4.1b takes the following form :

$$\frac{\partial}{\partial z}(\rho r^2 UW)+\frac{\partial}{\partial r}(\rho r^2 VW)=\frac{\partial}{\partial r}(\mu_e r^3\frac{\partial}{\partial r}(\frac{\Omega}{r^2}))+\frac{\partial}{\partial z}(\mu_e r^3\frac{\partial}{\partial z}(\frac{\Omega}{r^2})) \qquad (4.22)$$

Further, introducing the mean velocity-stream function relations, Eqn.s.2.4, into Eqn.4.22 yields

$$\frac{\partial}{\partial z}(\Omega\frac{\partial W}{\partial r})-\frac{\partial}{\partial r}(\Omega\frac{\partial W}{\partial z})=\frac{\partial}{\partial r}(\mu_e r^3\frac{\partial}{\partial r}(\frac{\Omega}{r^2}))+\frac{\partial}{\partial z}(\mu_e r^3\frac{\partial}{\partial z}(\frac{\Omega}{r^2})) \qquad (4.23)$$

The vorticity transport equation is obtained by combining Eqn.s.4.1a and 4.1c after cross derivation. This results in the elimination of the troublesome pressure terms. Substituting the turbulent momentum flux relations for the stress terms and after some manupulation it becomes,

$$r^2\left[\frac{\partial}{\partial z}(\rho U\omega)+\frac{\partial}{\partial r}(\rho V\omega)\right]=\frac{\partial}{\partial z}\left[r^3\frac{\partial}{\partial z}(\frac{\mu_e\omega}{r})\right]+\frac{\partial}{\partial r}\left[r^3\frac{\partial}{\partial r}(\frac{\mu_e\omega}{r})\right]+r\frac{\partial}{\partial z}(\rho W^2)+r^3 S_\omega \qquad (4.24)$$

where for compressible flow

$$S_\omega=\frac{2}{r}\left[\frac{\partial V_z}{\partial r}\frac{\partial^2\mu_e}{\partial z^2}-\frac{\partial V_r}{\partial z}\frac{\partial^2\mu_e}{\partial r^2}+\frac{\partial^2\mu_e}{\partial r\partial z}(2\frac{\partial V_r}{\partial r}+\frac{V_r}{r})\right] \qquad (4.25a)$$

or

$$S_\omega=\frac{2}{r}\left[\frac{\partial V_z}{\partial r}\frac{\partial^2\mu_e}{\partial z^2}-\frac{\partial V_r}{\partial z}\frac{\partial^2\mu_e}{\partial r^2}-\frac{\partial^2\mu_e}{\partial r\partial z}(2\frac{\partial V_z}{\partial z}+\frac{V_r}{r})\right] \qquad (4.25b)$$

Substituting Eqn.s.2.4 into the vorticity transport equation, Eqn.2.24, it can be shown that :-

$$r^2\left[\frac{\partial}{\partial z}(\frac{\omega}{r}\frac{\partial W}{\partial r})-\frac{\partial}{\partial r}(\frac{\omega}{r}\frac{\partial W}{\partial z})\right]=\frac{\partial}{\partial z}\left[r^3\frac{\partial}{\partial z}(\frac{\mu_e\omega}{r})\right]+\frac{\partial}{\partial r}\left[r^3\frac{\partial}{\partial r}(\frac{\mu_e\omega}{r})\right]+r\frac{\partial}{\partial z}(\rho W^2)+r^3 S_\omega \qquad (4.26)$$

The transport equation for the stream function is obtained from the definition of vorticity, Eqn.4.15 .Introducing Eqn.2.4 into Eqn.4.15 yields :

$$\frac{\partial}{\partial z}\left(\frac{1}{r}\frac{\partial W}{\partial z}\right)+\frac{\partial}{\partial r}\left(\frac{1}{r}\frac{\partial W}{\partial r}\right)=-\omega \qquad (4.27)$$

which is known in fluid dynamics as Poisson's equation for the stream function.

4.3.2.Common form for the transport equations

Examination of Eqn.s.4.23 , 4.26 and 4.27 reveals that they all can be expressed in the form of the partial differential equation

$$\alpha\left[\frac{\partial}{\partial z}\left(Q\frac{\partial W}{\partial r}\right)-\frac{\partial}{\partial r}\left(Q\frac{\partial W}{\partial z}\right)\right]-\frac{\partial}{\partial z}\left[\beta r\frac{\partial}{\partial z}(\gamma Q)\right]-\frac{\partial}{\partial r}\left[\beta r\frac{\partial}{\partial r}(\gamma Q)\right]-r\epsilon=0 \qquad (4.28)$$

The required changes in the coefficients of Eqn.4.28 for each of the transport equations for Ω , ω/r and W are tabulated below :

Q	α	β	γ	ϵ
ω/r	r^2	r^2	μ_e	$\frac{\rho}{r^2}\frac{\partial}{\partial z}(\Omega^2)+r^2 S_\omega$
W	0	$1/\rho r^2$	1	ω/r
Ω	1	$r^2\mu_e$	$1/r^2$	0

Existance of a common form, like Eqn.4.28, for all the transport equations greatly facilitates the formulation and organization of a solution procedure.It then becomes possible to use,with appropriate changes presented above,the same integration formula for all the transport equations.

4.3.3.A general finite difference solution procedure

There are several numerical methods for the solution of an equation like Eqn.4.28 . The method of finite differences is the most commonly used.Others,such as finite element

using calculus of variations,are being very rapidly developed. The finite difference method has been used in this solution procedure(Ref.45).Two ways of producing finite difference equations from a differential equation are available : Taylor series expansions and micro integral forms.It is known (Ref.46) that the latter gives better accuracy.Also,it has been applied to parabolic type partial differential equations quite successfully (Ref.30).Therefore, it has been employed in this procedure.

Integration of Eqn.4.28 is performed in a small element chosen from the finite difference mesh system adopted for the solution procedure (Fig.4.1). Sides of this small element (points e,w,n,s) lie midway between the actual mesh points, that is,points P,E,W,N,S as shown in Fig.4.1 .Integration is carried out as follows :

$$\int_{r_s}^{r_n}\int_{z_w}^{z_e} \alpha\left[\frac{\partial}{\partial z}\left(Q\frac{\partial W}{\partial r}\right)-\frac{\partial}{\partial r}\left(Q\frac{\partial W}{\partial z}\right)\right] dr\,dz -$$

$$\int_{r_s}^{r_n}\int_{z_w}^{z_e}\left[\frac{\partial}{\partial z}\left(\beta r\frac{\partial}{\partial z}(\gamma Q)\right)+\frac{\partial}{\partial r}\left(\beta r\frac{\partial}{\partial r}(\gamma Q)\right)\right]dr\,dz=\int_{r_s}^{r_n}\int_{z_w}^{z_e}\epsilon\, r\, dr\, dz \qquad (4.29)$$

o is a variable only in the case of ω/r .Therefore,it can be assumed that in the small element α assumes a value equal to the value at the point P. Thus,integration can be performed as

$$\alpha_P\left\{\int_{r_s}^{r_n}\left[Q_e\left(\frac{\partial W}{\partial r}\right)_e-Q_w\left(\frac{\partial W}{\partial r}\right)_w\right]dr-\int_{z_w}^{z_e}\left[Q_n\left(\frac{\partial W}{\partial z}\right)_n-Q_s\left(\frac{\partial W}{\partial z}\right)_s\right]dz\right\}$$

Term 1 Term 2

$$-\int_{r_s}^{r_n}\left[\left(\beta r\frac{\partial}{\partial z}(\gamma Q)\right)_e-\left(\beta r\frac{\partial}{\partial z}(\gamma Q)\right)_w\right]dr \qquad (4.30)$$

Term 3

$$-\int_{z_w}^{z_e}\left[\left(\beta r\frac{\partial}{\partial r}(\gamma Q)\right)_n-\left(\beta r\frac{\partial}{\partial r}(\gamma Q)\right)_s\right]dz = \int_{r_s}^{r_n}\int_{z_w}^{z_e}\epsilon\, r\, dr\, dz$$

Term 4 Term 5

Terms 1 and 2 are the convection terms.Their second integ-

ration is performed in a special way: If the first part in the term 1 is considered

$$T_{11} = \alpha_P \int_{r_s}^{r_n} Q_e \left(\frac{\partial W}{\partial r}\right)_e dr \qquad (4.31)$$

Assuming that Q_e remains constant over the east face of the small element, this integration can be approximated as

$$T_{11} = \alpha_P \, Q_e \, (W_{ne} - W_{se}) \qquad (4.32)$$

Here arises the problem of expressing Q_e and $(W_{ne} - W_{se})$ in terms of the values at the mesh points. For instance, Q_e can be expressed simply in terms of Q_E and Q_P. It is known, however, that this formulation introduces instabilities into the calculation procedure, especially at high velocities. Therfore, a formulation called 'upwind differences' in atmospheric aerodynamics (Ref.46) is used in the procedure. In this formulation, it is assumed that

$Q_e = Q_P$ if the axial velocity at e is positive,

$Q_e = Q_E$ if the axial velocity at e is negative.

In other words, it is assumed that Q_e always takes the value at the upstream side of the e face of the small element. These points can mathematically be expressed in Eqn.4.32 as

$$T_{11} = \frac{\alpha_P}{2}\left[Q_E(W_{ne} - W_{se} - |W_{ne} - W_{se}|) + Q_P(W_{ne} - W_{se} + |W_{ne} - W_{se}|)\right] \qquad (4.33)$$

Similarly, the other part in term 1 and the two parts in term 2 are expressed as

$$T_{12} = \frac{\alpha_P}{2}\left[Q_W(W_{nw} - W_{sw} + |W_{nw} - W_{sw}|) + Q_P(W_{nw} - W_{sw} - |W_{nw} - W_{sw}|)\right] \qquad (4.34)$$

$$T_{21} = \frac{\alpha_P}{2}\left[Q_N(W_{ne} - W_{nw} + |W_{ne} - W_{nw}|) + Q_P(W_{ne} - W_{nw} - |W_{ne} - W_{nw}|)\right] \qquad (4.35)$$

$$T_{22} = \frac{\alpha_P}{2}\left[Q_S(W_{se} - W_{sw} - |W_{se} - W_{sw}|) + Q_P(W_{se} - W_{sw} + |W_{se} - W_{sw}|)\right] \qquad (4.36)$$

Summation of Eqn.s.4.33 to 4.36 ,after some manipulation, yield the integration of the convection terms 1 and 2 in Eqn.4.30 :

$$T_{11}+T_{12}+T_{21}+T_{22} =$$
$$A_E(Q_P-Q_E)+A_W(Q_P-Q_W)+A_N(Q_P-Q_N)+A_S(Q_P-Q_S) \qquad (4.37)$$

where A_E, A_W, A_N and A_S represent, after the assumptions

$$W_{ne} = \frac{W_N + W_{NE} + W_P + W_E}{4} \qquad (4.38)$$

$$W_{nw} = \frac{W_N + W_{NW} + W_P + W_W}{4} \qquad (4.38b)$$

the convection coefficients

$$A_E = \frac{\alpha_P}{8} (Q_1 + |Q_1|) \qquad (4.39a)$$

$$A_W = \frac{\alpha_P}{8} (Q_2 + |Q_2|) \qquad (4.39b)$$

$$A_N = \frac{\alpha_P}{8} (Q_3 + |Q_3|) \qquad (4.39c)$$

$$A_S = \frac{\alpha_P}{8} (Q_4 + |Q_4|) \qquad (4.39d)$$

where

$$Q_1 = W_S + W_{SE} - W_N - W_{NE} \qquad (4.40a)$$

$$Q_2 = W_N + W_{NW} - W_S - W_{SW} \qquad (4.40b)$$

$$Q_3 = W_E + W_{NE} - W_W - W_{NW} \qquad (4.40c)$$

$$Q_4 = W_W + W_{SW} - W_E - W_{SE} \qquad (4.40d)$$

In Eqn.4.30 ,terms 3 and 4 represent the diffusion terms. Their integration is made as follows; the first part of term 3 can be written as

$$T_{31} = \int_{r_s}^{r_n} (\beta r)_e \left(\frac{\partial(\gamma Q)}{\partial z}\right)_e dr \qquad (4.41)$$

where the integration can be carried out numerically by assuming

$$\beta_e = \frac{\beta_E+\beta_P}{2}$$

$$r_e = \frac{r_E+r_P}{2}$$

$$\left(\frac{\partial(\gamma Q)}{\partial z}\right)_e = \frac{\gamma_E Q_E-\gamma_P Q_P}{z_E-z_P} .$$

such that the complete term is

$$T_{31} = \frac{\beta_E+\beta_P}{2}\ \frac{r_E+r_P}{2}\ \frac{\gamma_E Q_E-\gamma_P Q_P}{z_E-z_P}\ \frac{r_N-r_S}{2} \qquad (4.42)$$

If the integration is performed for the second part of term 3 and also for both parts of term 4, then diffusion terms become

$$T_{31}+T_{32}+T_{41}+T_{42} = \qquad (4.43)$$

$$B_E(\gamma_E Q_E-\gamma_P Q_P)+B_W(\gamma_W Q_W-\gamma_P Q_P)+B_N(\gamma_N Q_N-\gamma_P Q_P)+B_S(\gamma_S Q_S-\gamma_P Q_P)$$

where

$$B_E = \frac{(r_E+r_P)(r_N-r_S)}{8\,(z_E-z_P)}\ (\beta_E+\beta_P) \qquad (4.44a)$$

$$B_W = \frac{(r_W+r_P)(r_N-r_S)}{8\,(z_P-z_W)}\ (\beta_W+\beta_P) \qquad (4.44b)$$

$$B_N = \frac{(r_N+r_P)(z_E-z_W)}{8(r_N-r_P)}(\beta_N+\beta_P) \qquad (4.44c)$$

$$B_S = \frac{(r_S+r_P)(z_E-z_W)}{8(r_P-r_S)}(\beta_S+\beta_P) \qquad (4.44d)$$

Term 4 in Eqn.4.30 is called the source term.For its integration,the best approximations are r=rp , ϵ=constant in the small element.Thus it becomes

$$T_5=\int_{r_s}^{r_n}\int_{z_W}^{z_e} \epsilon\, r\, dr\, dz = \epsilon\, V_P \qquad (4.45)$$

where

$$V_P= \frac{r_P}{4}(z_E-z_W)(r_N-r_S) \qquad (4.46)$$

Integration of Eqn.4.29 is completed summing up all the terms in Eqn.4.30 :-

$$T_{11}+T_{12}+T_{21}+T_{22}+T_{31}+T_{32}+T_{41}+T_{42}+T_5 = 0$$

and this yields

$$A_E(Q_P-Q_E)+A_W(Q_P-Q_W)+A_N(Q_P-Q_N)+A_S(Q_P-Q_S) \qquad (4.47)$$
$$-B_E(\gamma_E Q_E-\gamma_P Q_P)-B_W(\gamma_W Q_W-\gamma_P Q_P)-B_N(\gamma_N Q_N-\gamma_P Q_P)-B_S(\gamma_S Q_S-\gamma_P Q_P)=\epsilon\, V_P$$

Eqn.4.47 can further be arranged as

$$Q_P\left[A_E+A_W+A_N+A_S+\gamma_P(B_E+B_W+B_N+B_S)\right]= \qquad (4.48)$$
$$Q_E(A_E+B_E\gamma_E)+Q_W(A_W+B_W\gamma_W)+Q_N(A_N+B_N\gamma_N)+Q_S(A_S+B_S\gamma_S)+\epsilon\, V_P$$

It is seen that Eqn.4.48 can be expressed in a brief form as

$$Q_P = C_E Q_E+C_W Q_W+C_N Q_N+C_S Q_S+D \qquad (4.49)$$

where

$$H = A_E+A_W+A_N+A_S+\gamma_P(B_E+B_W+B_N+B_S)$$

$$C_E = (A_E+B_E\gamma_E)/H$$

$$C_W = (A_W+B_W\gamma_W)/H$$

$$C_N = (A_N+B_N\gamma_N)/H$$

$$C_S = (A_S+B_S\gamma_S)/H$$

Examination of Fig.4.1 ,from which Eqn.4.49 was derived reveals that for every interior point in the mesh system such an equation exists.It simply connects the value of the variable Q at that point to its values at the four surrounding mesh points.A system of algebraic equations is,therefore, obtained for the interior points of the complete mesh net. However,since the coefficients C_E,C_W,C_N and C_S are functions of exchange coefficients and stream function,the latter of which Q also stands for,the algebraic system is strongly non-linear.Therefore, an iterative technique must be used for their solution.

4.3.4.Solution of the algebraic equations

There are several methods for the solution of a system of algebraic equations.If the equations of the system are linear, direct methods may be employed.These comprise Gaussian elimination,row interchanges,recurrence relationships and matrix inversion.In the case of non-linear equations,however,iterative methods have to be employed.

Amongst the iterative methods,several choices are also available:point iterative methods,block iterative methods and the alternating direction method.In the block iterative methods,use is made of matrix inversion as part of the iteration cycle.Basically,direct methods are employed for chosen grid sections in these methods.Organization of a computer program, therefore,becomesquite difficult.The same remarks also apply to the third class of iterative method concerning the difficulty of organization.Point iterative methods,however,do not present similar difficulties through the use of the procedure of successive substitution such that a substitution formula derived for an interior point is used for all the other interior points.Therefore,organization of a computational scheme becomes much simpler.There are several applications of the point iterative methods.The Jacobi method employs only the values of the previous iteration in order to calculate the values in the new iteration.Therefore,both sets of values, that is,of the previous and present iterations must be kept in the memory.In consequence,this method doubles the computer storage requirement of that called Gauss-Seidel method.In the latter method,new values calculated for a point in an iteration is used immediately in the same iteration for the calculation

of the value at a neighbouring mesh point.In this way,convergence rate is increased.The convergence rate of the Gauss-Seidel can be further improved by using a procedure called SOR (successive over-relaxation).It is applied in the following way : if Q_N indicates the value of Q in the Nth iteration and Q_{N+1} in the (N+1)th iteration,then the value taken eventually for Q in the (N+1)th iteration is

$$Q_{N+1} = \varkappa\, Q_{N+1} + (1-\varkappa)\, Q_N \qquad (4.50)$$

where $\varkappa$ is the over-relaxation parameter which takes values between 1 and 2 .However,for flow problems, SOR is applied in a different form due to the strong coupling between the transport equations for the vorticity and stream function-It is then called SUR (successive under-relaxation) and $\varkappa$ assumes values between 0 and 1 in order to suppress the values of the quantities which undergo rapid changes.Actually SUR is applied for any flow quantity which procure divergence because of large changes in its value from one iteration to the other.

Gauss-Seidel point iterative method together with SUR is used in this solution procedure in a stationary manner,that is,the same cycle of iterations are used.In this way,organization of the computer programme is facilitated greatly. Eqn.4.49 is used as the successive substitution formula,the coefficients of which are updated before each iteration.

4.4.TURBULENCE MODELLING

Several turbulence models have been developed for the prediction of both confined and free turbulent flows.For a general review of these models,the reader is referred to Ref.47 .A two-equation model,for instance, the energy-dissipation rate model (Ref.48),can be employed for the calculation of turbulence quantities.In this model,the turbulent viscosity is calculated from

$$u_t = C_u \rho \frac{k^2}{\epsilon} \qquad (4.51)$$

Then, relations like Eqn.2.15 are used to calculate the stresses in the flow field.Turbulence kinetic energy and dissipation rate are determined from two transport equations for these quantities :-

$$\rho\left(\frac{1}{r}\frac{\partial}{\partial r}(rVk)+\frac{\partial}{\partial z}(Uk)\right)=\frac{1}{r}\frac{\partial}{\partial r}\left(\frac{r\mu_e}{\sigma_k}\frac{\partial k}{\partial r}\right)+\frac{\partial}{\partial z}\left(\frac{\mu_e}{\sigma_k}\frac{\partial k}{\partial z}\right)+P_k-C_k\rho\epsilon \qquad (4.52)$$

$$\rho\left(\frac{1}{r}\frac{\partial}{\partial r}(rV\epsilon)+\frac{\partial}{\partial z}(U\epsilon)\right)=\frac{1}{r}\frac{\partial}{\partial r}\left(\frac{r\mu_e}{\sigma_\epsilon}\frac{\partial \epsilon}{\partial r}\right)+\frac{\partial}{\partial z}\left(\frac{\mu_e}{\sigma_\epsilon}\frac{\partial \epsilon}{\partial z}\right)+C_1P_k\frac{\epsilon}{k}-C_2\rho\frac{\epsilon^2}{k} \qquad (4.53)$$

where P_k represents production of the kinetic energy of turbulence through the interaction of Reynolds stresses with the mean motion (see Eqn.2.13). With the assumption that Reynolds stresses can be expressed in terms of the turbulent viscosity, P_k can be calculated from

$$P_k=\mu_t\left[2\left\{\left(\frac{\partial V}{\partial r}\right)^2+\frac{V^2}{r^2}+\left(\frac{\partial U}{\partial z}\right)^2\right\}+\left(\frac{\partial U}{\partial r}+\frac{\partial V}{\partial z}\right)^2+\left(\frac{\partial W}{\partial r}\frac{W}{r}\right)^2+\left(\frac{\partial W}{\partial z}\right)^2\right] \qquad (4.54)$$

The constants appearing in the model has been determined in Ref.49 as

$$\begin{aligned} C_u &= 0.09 \\ C_k &= 1.00 \\ C_1 &= 1.4 \\ C_2 &= 1.95 \\ \sigma_k &= 1.00 \\ \sigma_\epsilon &= 1.30 \end{aligned} \qquad (4.55)$$

In this way, transportation of both k and e are allowed in the flow field by using transport equations for these quantities. When these equations are fitted to the common form, the required changes in the coefficients of Eqn.4.28 are

Q	α	β	γ	ϵ
k	1	μ_t/σ_k	1	$P_k-C_k\rho\epsilon$
ϵ	1	μ_t/σ_ϵ	1	$C_1P_k\frac{\epsilon}{k}-C_2\rho\frac{\epsilon^2}{k}$

Then, the same substitution formula, Eqn.4.49, can also be used for the calculation of k and ϵ at grid points with appropriate changes in the coefficients.

4.5.BOUNDARY CONDITIONS FOR STRONGLY SWIRLING FREE FLOWS

Boundary conditions have also to be specified for the solution of the elliptic equations of Sections 4.3 and 4.4 , using the finite difference technique presented in Section 4.3.3.Actually this is characteristic requirement for the solution of all elliptic equations and boundary conditions have to be prescribed for all the variables all around the region of interest.This is not the case,however,for parabolic equations for which only initial conditions and subsequently upstream values and side boundary conditions are required. In some cases when the values are not known on the boundary nodes before calculations,they are computed during each iteration.

The following boundary conditions can be applied for the present problem of prediction of free swirling jets.At the exit from The nozzle (Fig.4.2),mostly experimental profiles are used:The axial velocity profile is integrated to obtain distribution of the stream function. ω/r profile can also be obtained from the axial velocity profile.Kinetic energy of turbulence and dissipation rate are determined from

$$k = 0.03\ U^2 \tag{4.56}$$

$$\epsilon = 2\ k^{3/2}/0.005\ D \tag{4.57}$$

The other boundary conditions are seen in Fig.4.2 and need not be explained except for the vorticity calculation on the wall.Normally for isothermal laminar flow,vorticity on a wall is calculated using a relation like (Ref.50)

$$\left(\frac{\omega}{r}\right)_W = \frac{3(W_{NW}-W_W)}{\rho\ r_W^2\ n_{NW}^2} - \left(\frac{\omega}{r}\right)_{NW}\ \frac{1}{2} \tag{4.58}$$

where indices W and NW indicate wall and near-wall grid points and n_{NW} represent the distance between the wall and inner grid point. By choosing this distance very small,near-wall grid points can be located in the viscous sub-layer.In this way, turbulent boundary layer calculations need not be incorporated. However,Eqn.4.58 is only an approximate formula and sometimes may introduce discontinuity to the coupling between stream function and vorticity transport equations;this may cause divergence.In this case,wall vortices are incorporated into the calculation process implicitly.For this purpose,Eqn.4.58 is introduced into the successive substitution formula, Eqn.4.49 ,to eliminate wall vortices when the latter is applied to a near-wall grid point.When,for instance,the method

is applied to a near-wall grid point lying in the east of the wall, the successive substitution formula for such grid points becomes

$$\left(\frac{\omega}{r}\right)_P = \frac{C_N\left(\frac{\omega}{r}\right)_N + C_S\left(\frac{\omega}{r}\right)_S + C_E\left(\frac{\omega}{r}\right)_E - 3C_W(U_P - U_W)/\rho_W n_P^2 r_W^2 + D}{1+0.5\ C_W} \qquad (4.59)$$

In this way, the use of Eqn.4.58 can be avoided, that is, the wall vortices are excluded from the iteration process. If they are required, however, they can be calculated at the end of the iteration process, using again Eqn.4.58 .

4.6. COMPUTATIONAL PROCEDURE

Computation starts with the initial estimates and boundary conditions of the dependent variables ω/r, W, Ω, k and ϵ . Their transport equations are solved in the order they are mentioned, using the finite difference formulation presented in Section 4.3.3 . Successive substitution formula, Eqn.4.49, is applied for each transport equation with appropriate changes in its coefficients and the whole grid system is scanned point-by-point. However, an examination of Eqn.4.49 shows that every time computations are performed at a grid point for each variable, same geometrical calculations are repeated. In order to avoid waste of computer time in this way, such geometrical terms are separated and calculated for each grid point at the beginning of computations, once and for all. Afterwards, such values are simply called for whenever they are needed. This can be achieved by changing Eqn.4.49 into the following form :

$$Q_P = \frac{\sum_{j=N,S,E,W} \left\{A'_j + \gamma_j(\beta_j+\beta_P)B'_j\right\} Q_j + C}{\sum_{j=N,S,E,W} \left\{A'_j + \gamma_P(\beta_j+\beta_P)B'_j\right\}} \qquad (4.60)$$

where

$$A'_j = \frac{A_j}{V_P} \quad , \quad j=N,S,E,W \qquad (4.61)$$

$$B'_j = \frac{B_j}{V_P(\beta_j+\beta_P)} \quad , \quad j=N,S,E,W \qquad (4.62)$$

Eqn.s.4.62 are calculated at the beginning of a computation and stored for later use.

In this way, the grid system is scanned point-by-point for each dependent variable and at each point new values of the dependent variables are calculated using Eqn.4.60 . Following is the calculation of the other variables, such as , viscosity, depending on the values of the dependent variables at the grid points. These new values are then used for the next iteration and so on. The whole process is iterated as much as required. When the changes in the values of the variables between two iterations are within a specified limit, it is assumed that the equations have been solved. Very frequently this limit is expressed as

$$\frac{Q_P^{N+1} - Q_P^N}{Q_P^{N+1}} \leq \delta_c$$

where Q_P^{N+1} is the value of Q_p in the (N+1)th iteration and Q_P^N is the value in the Nth iteration. The convergence criteria, δ_c, is generally chosen 0.01 or less.

For the organization of a computer programme, the reader is referred to Ref.45 .

CHAPTER 5. DESCRIPTION OF EXPERIMENTAL FACILITY

5.1.TEST RIG

The general layout of the test rig is shown in Fig.5.1 . The downstream pipe was vertical and about 11ft high to reduce the amount of dust sucked through the system.The mass flow was measured with an orifice meter (Fig.5.2) designed according to British Standard BS1042 (Ref.51).The formula used for mass flow calculation has the following form :-

$$m = 0.059434\ d_{or.}^{2}\ (\ \Delta h\ \rho\ )^{0.5} \qquad (5.1)$$

The fan was capable of producing 0.33 lb/sec at a maximum available pressure of 44" static water gauge.As the mass flow was increased,this pressure decreased.This drop was quite rapid after a mass flow of about 0.761 lb/sec .

The settling chamber was to the design of Ref.52 (Fig.5.3). A honeycomb cell was used to straighten the flow in the chamber. The nozzle into which the swirlers were fitted was fixed at the end of the settling chamber (Fig.5.4). The nozzle length was kept short in the design procedure in order to avoid boundary layer development on the walls.In this way,the flat velocity profile obtained at the nozzle throat could be maintained up to the entry to the swirlers.

The swirlers were placed into the nest in the nozzle (see Fig.5.4) and clamped with a large ring which was screwed to the annular wall of the nozzle at the exit.This clamping was strong enough to prevent rotation of the swirlers when the rig was running. The inner diameter of the ring was the same as that of the swirlers.

The protractor mechanism was built on the nozzle (Fig.5.5). The height of the end of the Pitot tube was altered using different spacers to match the aspect ratios of different swirlers.

In order to accurately scan the flow fields generated by the swirlers, use has been made of the traversing mechanism of a large size lathe. To this end, the settling chamber and the nozzle were fixed on the lathe (Fig.5.6). Geometrical alignment of the nozzle and the settling chamber on the lathe,of better than 0.003"/4.166"was performed.Subsequently aerodynamic alignment was carried out,using a Pitot tube.The traversing mechanism allowed the probes to be located to the desired position in the flow fields with an accuracy better than 0.001"in the radial direction.In the axial direction, this was about 0.05" .

On the bare surface of the traversing mechanism a metal platform was built.It could turn around the axis (vertical) of its clamp mechanism.This rotation was used for the calibration of the five-hole spherical pressure probe (Fig.5.7).

A hole with a diameter to fit the probe arms were drilled on the platform.A clamp mechanism was provided to tighten the probes to the platform when they are placed in the hole (see Fig.s.5.8 and 5.6).

5.2.DESIGN OF SWIRLERS

Several factors have been considered in the design of swirlers.Firstly,they have been designed with a size directly suitable for combustor applications.The alternative large size,similar to nozzle inlet guide vanes,for instance,would facilitate some part of the experimental investigation to a certain extent.However,excessive mass flow rates would then be required in order to achieve the required velocity level at the exit of the swirlers.Furthermore,scale effects would be involved.With these points in mind,the outer diameter of the swirlers was fixed at 3".

Secondly,the mass flow rate,rather than inlet and outlet velocities of the swirler, is important from the combustion point of view.Accordingly,comparative swirler performance (recirculation size) at the same mass flow rate was required. Since the aspect ratio was also changed for the investigation, i.e.,h/c=0.4 and 1,swirler inlet and exit velocities varied from one swirler to the other for the same mass flow rate. At this mass flow rate,however,the range of Reynolds number for the swirlers with different design parameters was similar to that employed by other investigators,for instance,Ref.8 (see Section 7.5).In this way,chord length was fixed at 1" to yield exit velocities giving the above range of the Reynolds number.In all the cases,exit velocities were also low enough to avoid compressibility effects.

The three swirlers manufactured initially with these considerations are shown in Fig.5.9 .One of them is with flat, the other two are with curved vanes.Central and of central designs were employed for the two curved vane type swirlers. The profile of the curved vanes is a circular arc.The profile geometry for curved vanes is also shown in Fig.5.9 .It is seen that the vane stagger angle in each case is one half the vane outlet angle for curved vanes.The incidence was zero on all the curved vanes.All vanes were fabricated from standard 0.04" sheet steel with constant 1" chord and sharpened leading and trailing edges.A photograph of these three swirlers is shown in Fig.5.10 .All three swirlers were designed with a vane angle of 60° and an aspect ratio of unity.They were tested initially at a mass flow rate of about 0.323 lb/sec .For this value of mass flow,the nozzle velocity was about 86 ft/sec .With an aspect ratio of 1 and vane angle of 60°,the swirler inlet and outlet velocities were 96 and 192 ft/sec,respectively. In this way,compressibility limit was not exceeded.

After testing the first three swirlers it was found that the off-central design gave a larger recirculation region . However,its manufacture,as was explained in Section 1.3, was quite difficult.Therefore,all the other curved and flat vane type swirlers (Fig.5.11) were designed with central blading. In this way, eight more swirlers,four with flat,four with curved vanes (Fig.5.11a) were manufactured.A value of aspect ratio of 0.4 was used.Chord length,however, was kept constant at 1".The other design parameters can be seen in Fig.5.11 . The maximum mass flow rate which can pass through the flat vane type swirler with vane angle 70°,aspect ratio 0.4 and space-to-chord ratio corresponding to 16 vanes, was about 0.136 lb/sec .Therefore,this mass flow was used as the constant mass flow rate for the tests with all the other swirlers.It gave a nozzle velocity of 36 ft/sec . Swirler inlet velocity, however, varied with the aspect ratio : for 0.4 , swirler inlet velocity was 78 ft/sec ; for 1 , it was 41 ft/sec .The former value gave the maximum exit velocity 228 ft/sec with the swirler having 70° vanes, which was also below the compressibility limit.

Great difficulties were encountered in the manufacture of the swirlers. It is quite obvious that complete uniformity can not be obtained in the manufacture of the vanes.Their surface roughness, for instance, was slightly different from one vane to the other. The vanes were braised. This fixing method was also not completely perfect. However, the asymmetry was only slight.

The centre of all the swirlers were fitted with the hub bullets (Fig.5.12).They are geometrically similar.They were intended to simulate a fuel injector in the hub. Also, they provided a smooth acceleration for the air from the nozzle velocity to the swirler inlet velocity.

5.3.INSTRUMENTATION

In order to measure distributions of the components of the absolute velocity,static pressure and turbulence characteristics a five-hole spherical pressure probe and a 55D00 type hot-wire anemometer together with a 55P81 type temperature compensated probe were employed (see Fig.5.6,7 and 8). Traversings were made with the lathe mechanism described in Section 5.1 .

5.3.1.Five-hole spherical pressure probe

Operation of the five-hole spherical pressure probe is based on the flow around a sphere.Behaviour of this type of flow is well known and can be found in any classical textbook,such as Ref.14 .Depending on the range of Reynolds number,four flow regimes can be distinguished.If $Re<1$,the flow has a creeping character and no separation occurs.If $1<Re<10^3$ separation starts on the upstream surface of the sphere. As the Reynolds number is increased towards 10^3,small eddies form at the rear stagnation of the sphere .At higher values of the Reynolds number,these eddies grow to the point where they separate from the sphere and are swept downstream into the wake.This is called von Karman vortex street and the flow has an unsteady character in the downstream region. When Reynolds number is increased further to the range between 10^3 and $6x10^5$, separation stabilizes at a point about 80° from the forward stagnation point.If the Reynolds number is increased more ,the separation point moves further downstream on the sphere,to about 120° from the forward stagnation point.The conclusion from this explanation is that if a sphere with several holes is to be used as a probe,the central angle between the symmetrical holes must not be more than 80° if the flow is almost laminar.If the flow is highly turbulent,this angle can be increased up to 120°.If higher values are used under laminar or turbulent flow conditions,one of the holes falls into the separation region on the sphere and in consequence,no relation can be formed between the pressure values obtained from this hole and the others.

A general arrangement of the probe head is shown in Fig.5.13 .The central angle between the symmetric holes is 80 ;the head diameter is 0.2".Each of the five holes has been drilled with a diameter of 0.018".The inner structure of the probe head is shown in Fig.5.14 .Pressure holes have been connected to pressure lines with standard tubing.

For measurements in flow fields with three velocity components,a five-hole spherical probe can be used in two ways. Firstly,it is turned in the yaw direction (see Fig.5.13; in the plane passing through the holes numbered 2,0 and 4) or in the pitch direction (in the plane of the holes 1,0 and 3) according to the geometry of the flow field under investigation.Then,two dimensional calibration curves are used for the

interpretation of the actual measurements.These calibration curves are obtained by rotating the probe in the direction other than that using for the measurements.Calibration in this way is quite easy.However,when the number of measurements are excessively large (which is the case,for instance, when scanning of flow fields is intended),it becomes quite tedious and time consuming to rotate the probe to find the direction of flow at every point in the flow field.Secondly, therefore,the probe can be used in a fixed position.Three dimensional calibration curves are required for this way of application.

The latter approach has been adopted in this work (Ref.54) and therefore,only that will be explained here.When the probe is placed in a flow field,if the absolute velocity at a point P falls on the sphere at the point A (see Fig.5.13),five different pressure values can be read from the five holes.Application of the Bernoulli equation to the free stream and the jth hole yields

$$\frac{V_s^2}{2} + \frac{p_s}{\rho} = \frac{V_j^2}{2} + \frac{p_j}{\rho} \qquad (5.2)$$

from which

$$p_j = p_s + \rho\, b_j \frac{V_s^2}{2} \qquad (5.3)$$

can be written. In Eqn.5.3

$$b_j = 1 - \frac{V_j^2}{V_s^2} \qquad (5.4)$$

is called the pressure recovery factor for the jth hole.It is a function of Reynolds number and the position of the point A on the sphere.After the careful examination of the states of flow around the sphere as a function of Reynolds number and also considering the positioning of the pressure holes,the effect of Reynolds number is neglected.The position of the point A on the sphere can be represented by two spherical parameters, δ and θ (see Fig.5.13).Therefore, $b_j = f(\delta,\theta)$.

If the following ratios are formed for $0° \leq \delta \leq 180°$,

$$\frac{b_1 - b_3}{b_0 - b_3} = \frac{p_1 - p_3}{p_0 - p_3} = X_{133}(\delta,\theta) \qquad (5.5a)$$

$$\frac{b_2 - b_4}{b_0 - b_3} = \frac{p_2 - p_4}{p_0 - p_3} = X_{243}(\delta,\theta) \qquad (5.5b)$$

it is then seen that these coefficients can be determined experimentally for a known orientation of the probe.For the range of $-180° \leq \delta \leq 0°$, a different set of pressure coefficients are required :

$$\frac{b_1-b_3}{b_0-b_1} = \frac{p_1-p_3}{p_0-p_1} = X_{131}(\delta,\theta) \qquad (5.5c)$$

$$\frac{b_2-b_4}{b_0-b_1} = \frac{p_2-p_4}{p_0-p_1} = X_{241}(\delta,\theta) \qquad (5.5d)$$

Eqn.s.5.5 are used to determine the direction of the absolute velocity.Applying Eqn.5.3 once to the central hole and once to the third hole,then taking their difference , we obtain

$$p_0-p_3 = 0.5\,\rho\,(b_0-b_3)\,V_s^2 \qquad (5.6)$$

where only the free stream velocity, V_s , is not known.The static pressure of the free stream can be calculated by applying Eqn.5.3 directly to the centre hole

$$p_s = p_0 - 0.5\,\rho\,b_0 V_s^2 \qquad (5.7)$$

5.3.1.a.Calibration procedure

Calibration of the five-hole spherical pressure probe was carried out on the same test rig in the position as shown in Fig.5.7 .The straight jet necessary for the calibration was obtained without the swirlers in position in the nozzle.Calibration velocity was about 100ft/sec corresponding to a Reynolds number of approximately 10^4,based on the probe head diameter.

The values of δ were changed with intervals of 15°. θ values were changed according to the requirement to provide an accurate reading from the calibration charts (Fig.5.15,16). An interval of 3° provided required accuracy.

The following steps were taken during the calibration procedure.The rig was run.After obtaining a steady flow (this was checked by observing temperature and the dynamic head in the jet), δ and θ were altered at the intervals mentioned

above.At each setting of the probe five pressure values were recorded.These readings were evaluated using Eqn.s.5.3 to 5.7 and calibration charts were obtained. Day-to-day changes during calibration can be compensated most easily by adjusting the dynamic head to a reference value.

In order to investigate the influence of Reynolds number on the calibration charts,several curves were drawn at different velocity levels.It was observed that no considerable change occured.This is also reported in Ref.54 that calibration charts were not effected considerably up to a Mach number of 0.4 .In this work,Mach number was always well below 0.3 .

5.3.1.b.Measurement procedure

After tests with the firstly available three swirlers and determination of recirculation regions it was decided to scan the flow fields in the following manner : Radial traversings were made with intervals of 0.25"at 13 points. This length of mesh in the radial direction proved large enough to accommodate recirculation regions from all the swirlers.An example mesh system is shown in Fig.5.17. The axial stations were chosen according to the requirement of different swirlers. The five-hole spherical pressure probe, after fixed to the hole on the platform (see Fig.5.8),were located to the required position in the flow field using the traversing mechanism of the lathe.

The procedure followed during measurements was as follows: The rig was run and after obtaining a steady flow (this was checked by observing temperature and dynamic head),the probe was placed to the mesh points.Five pressure values were recorded at each point .

In order to obtain velocity components and static pressure from these pressure readings,two steps were required.Firstly, directional coefficients defined by Eqn.s.5.5 were calculated. Using these results, δ, θ, b_0 and (b_0-b_3) values were read from the calibration charts.The magnitude of the absolute velocity was calculated from Eqn.5.6 .Subsequently,the fcllowing formulae have been used for the calculation of the other quantities :

$$\begin{aligned} W &= \tilde{V}\cos\theta \\ V &= \tilde{V}\sin\theta\cos\delta \\ U &= \tilde{V}\sin\theta\sin\delta \\ p &= p_0 - b_0 \rho V^2/2 \end{aligned} \qquad (5.8)$$

The notation for Eqn.s.5.8 is shown in Fig.5.18 .

5.3.2.Hot-wire anemometer

A DISA 55D00 type hot-wire anemometer system has been used for turbulence measurements. The choice of hot-wire anemometry,its principles,previous interpretation techniques and the new formulation are presented in Chapter 6 .

CHAPTER 6. HOT-WIRE TECHNIQUE

6.1.CHOICE OF HOT-WIRE ANEMOMETRY

The rates of transport phenomena occuring in flow fields are strongly dependent upon the state of the flow.In the case of turbulent flows,these rates are enhanced very considerably. They represent,therefore,the type of flow which is mostly encountered in industrial applications.Despite the rapid strides in the prediction methods for this class of flow,they have not achieved perfectness yet,especially for more complex flow fields, such as turbulent swirling flows with recirculation.All the prediction methods are based on some constants that must be determined experimentally and separately for different types of flow configurations and for different calculation methods. Therefore, knowledge about the structure of these flows is still obtained by actual turbulence measurements.

Due to their utmost importance,several measurement techniques have been developed for the investigation of turbulent flow fields.These include hot-wire,pulsed wire,Laser Doppler, Glow and Corona discharge anemometers,some optical techniques and a few others (Ref.s.55,56 and 57).Most of them are either still in the development stage or suitable for a particular application.Hot-wire type is the most established and general purpose anemometer.It is,therefore,one of the most popular and widely available instrumentation for turbulence research.

For flows with reaction, laser Doppler anemometer should be employed due to the lack of necessity for using probes with this instrument.However, rather complicated and consequently expensive test rigs are required with this instrument if the flow field under investigation is of a complex type where,for instance,measurement of the complete stress tensor is necessary.Even with the very sophisticated test rigs,only four components of the stress tensor can be measured readily. Knowledge about the distributions of the other two stresses is,however,also required to determine the maximum shear stress regions.Therefore, laser Doppler system presents formidable difficulties in the measurement of shear stresses despite its claimed accuracy due to recent developments (Ref.58).

For the isothermal flow case in this work, hot-wire anemometry has been used for its longer availability,ease of operation and higher performance to measure the complete stress tensor.

6.2.BASIC PRINCIPLES OF HOT-WIRE ANEMOMETRY

Hot-wire anemometry constitutesone of the best instruments developed so far for the experimental investigation of space and time variables of the micro structure of flow fields. By the micro structure of flow fields, the instantaneous flow variable of small fluid particles is meant.This small fluid

particle is a finite volume element of the fluid.It is small compared to complete flow field,but large compared to the distance between the individual fluid molecules.Such experimental field structure investigations are of much importance for both understanding and utilizing micro characteristics of flow fields in both direct engineering and academic interests.

A very small sensitive element having a very short response time,sufficient sensitivity and as little as possible disturbance on the original flow is necessary for measurements of the micro structure of flow fields.Hot-wire anemometry employs a very thin wire as its sensing element,supported between two prongs.This thin wire is electrically heated and the operation of the hot-wire anemometry depends upon the heat transfer from this wire to the surroundings (Fig.6.1) .The mean and fluctuating parts of the heat transfer rate are indicated in the form of two separate voltages.

Heat transfer in such a flow configuration depends upon fluid velocity,density and temperature.Apart from the geometrical and material properties of the wire,therefore,hot-wire anemometry is sensitive to a heat flux produced by any of these flow properties.At constant pressure and temperature, it is primaraly sensitive to flow velocity.However, it is also used for temperature measurements.

Because the wire diameter is taken very small,of the order of a few microns,to reduce the thermal capacity of the wire and consequently to increase frequency response,Reynolds number based on wire diameter becomes small.The flow around the wire can,therefore,be considered as laminar even at rather high velocities.The exact solution to the convective heat transfer is by solving the equations of momentum and energy

$$\rho\left(\frac{\partial U}{\partial t}+U\frac{\partial U}{\partial z}+V\frac{\partial U}{\partial r}\right)=-\frac{\partial p}{\partial z}+v\left(\frac{\partial^2 U}{\partial z^2}+\frac{\partial^2 U}{\partial r^2}\right) \tag{6.1}$$

$$\rho\left(\frac{\partial V}{\partial t}+U\frac{\partial V}{\partial z}+V\frac{\partial V}{\partial r}\right)=-\frac{\partial p}{\partial r}+v\left(\frac{\partial^2 V}{\partial z^2}+\frac{\partial^2 V}{\partial r^2}\right) \tag{6.2}$$

$$\rho\left(\frac{\partial T}{\partial t}+U\frac{\partial T}{\partial z}+V\frac{\partial T}{\partial r}\right)=\frac{k}{C_p}\left(\frac{\partial^2 T}{\partial z^2}+\frac{\partial^2 T}{\partial r^2}\right) \tag{6.3}$$

for two dimensional (that is,the wire is considered of infinite length) laminar flow case around the wire.In fact, the wire acting as the sensor element is suspended between two prongs. Therefore,the first deviation from the pure two dimensional convection problem is caused by conduction heat transfer to the prongs.Secondly,because of the complexity of prong ends,

where the wire is connected generally by electroplating, the convective heat transfer problem assumes a three-dimensional form.This requires the addition of the third component of the momentum equations to the problem.A theoretical solution,therefore, becomes very difficult.Another fact is that every probe can not be manufactured exactly in the same geometric shape.Even if a theoretical solution was possible to predict the heat transfer rate from a specific probe,it would not be possible to use it for another probe.For all these reasons, solution is obtained experimentally,using the laws of similarity.

Nusselt number is the non-dimensional parameter characterizing forced convective heat transfer from a body to the surroundings.Natural convection characterized by Grashof number becomes important compared to forced convection at very low velocities.Therefore,for very low velocities

$$Nu = f(Gr,Re,Pr) \qquad (6.4)$$

In the higher velocity range, forced convection becomes dominant and natural convection can be neglected.Therefore,

$$Nu = f(Re,Pr) \qquad (6.5)$$

For air, in the moderate range of temparature, Prandtl number can be taken as a constant since it is simply a property of the fluid.In this way,its effect on the heat transfer rate can also be omitted :-

$$Nu = f(Re) \qquad (6.6)$$

At higher velocities,that is, for Mach number ≥ 0.3 ,compressibility effects must be taken into consideration.In consequence, both temperature and velocity effects are incorporated into the heat transfer relation :-

$$Nu = f(Re,Pr,M) \qquad (6.7)$$

One of the earliest investigations into the form of this heat transfer relation for the flow around a uniformly heated cylinder has been made by L.v.King (Ref.59), assuming two dimensional,potential,incompressible flow conditions.His theoretical derivation can be expressed as

$$Nu = A + B\,(Re)^{0.5} \qquad (6.8a)$$

or

$$P = (A_1 + B_1 U_e^{0.5})\,(T - T_s) \qquad (6.8b)$$

where P represents the heat loss from the wire to the surrounding flow.

The half power dependence of the heat transfer on Reynolds number given by King has been investigated by several authors. Besides, dependence of the heat transfer on the temperature difference between the wire and enviroment has been considered. The most comprehensive work on both these effects is that of Ref.50 .The final relation given is

$$Nu = \left(\frac{T_w}{T_s}\right)^{0.17} (0.24+0.56\ Re^{0.15}) \qquad (6.9)$$

where T_w is the average wire temperature.This equation gives the best fit to the heat transfer relation for hot-wires operating in air for the range of $0.22<Re<44$ .At $Re=44$,vortex shedding starts behind the wire and the heat transfer characteristics change.The constants 0.24 , 0.56 and 0.45 should , therefore, be replaced by 0 ,0.48 and 0.51,respectively, for a range of $44<Re<140$.

Similar results have also been reported in the literature (Ref.56). They can be summarized as :-

$$E^2 = A + B\ U_e^n \qquad (6.10)$$

assuming constant temperature and density for a specific application.The exponent n has,over a wide range of Reynolds number ($0.1<Re<10^5$), an almost constant value of approximately 0.4 to 0.5 .For more details on the subject, the reader is referred to Ref.s.56 and 59.It should be added,however, that most of the heat transfer relations have been derived theoretically for an infinitely large length-to-diameter ratio.On standard probes,however, this is of the order of a few hundreds.For the best accuracy in the measurements, the constants in Eqn.6.10 should be determined experimentally for each specific probe to be used.

The length-to-diameter ratio is one of the most important characteristics of hot-wire probes .It has several influences on the operation of the anemometer. A reduction in the wire diameter for a certain value of wire length increases signal-to-noise ratio,directionality and frequency response since its thermal capacity decreases.Also,such a reduction in diameter cause a decrease in end effects,flow interference,radiation errors and current consumption , while worsening the strength of the wire and sensitivity to dirt accumulation.Increasing the wire length improves the strength of the anemometer,directionality , while decreasing end effects,the strength of the wire and space resolution. An important point is that in a free stream turbulence the wire length should be smaller than

the micro scale of turbulence. As it is well known, micro scale closely related to the smallest eddy sizes in the turbulent flow field which are dissipated due to viscosity effects during the final period of the decay of turbulence. For more details the reader is referred to Ref.s.61 and 62 . Another very important influence of the length-to-diameter ratio is that on the effective cooling velocity.This will be examined in detail in Section 6.3 .

The heating of the wire is accomplished by placing it in one of the arms of a Wheatstone bridge.There are two modes of operation for the system : In the constant current mode, the bridge is operated from a source of current in series with an adjustable resistance.The value of this resistance should be high compared to the bridge resistance.The bridge current can then be kept constant.The bridge direct current unbalance voltage is a measure of mean velocity.The alternative component of the bridge unbalance voltage provides a true picture of the low frequency velocity components only. A single network can be used to compensate for the distortion of signals.For the compensation to be correct,the time constant of the compensating network must be equal to the time constant of the wire.The latter is a function of mean flow velocity.The compensating network should,therefore,be readjusted when the mean velocity changes.In this mode of operation,another drawback is caused when a hot-film probe is required for the measurements.The frequency response of a hot-film probe is not characterized by a single time constant. It is,therefore,very difficult to design a compensating amplifier having the inverse dynamic characteristics of a hot-film probe.Consequently, a hot-film is not applicable to measurements of velocity fluctuations when using the constant current mode of operation.Advantages of the constant current method are : The electronic circuit is simpler;it is possible to keep electronic noise at a low level through the use of transformer coupling,which makes it possible to measure small velocity fluctuations.

In the constant temperature mode,the temperature of the sensor,in consequence,its temperature is kept constant.Under this condition, the bridge voltage provides a measure of the heat transfer from the wire.Its operation (see Fig.6.2) can be explained in the following way : The bridge is in balance at a certain bridge voltage from the servo-amplifier (that is, at a certain heat transfer rate from the wire).A change in the temperature (resistance) of the wire due to a change in the heat transfer rate causes an unbalance in the bridge. This introduces an error voltage at the input of the servo amplifier.This voltage, after having undergone a considerable amplification, is used to adjust the bridge voltage at the bridge top. This increases the current through the wire and heats it up. In this way, its temperature,consequently resisttance increases.Therefore, bridge balance is restored and wire temperature variations are kept very small.This minimizes

the effect of the thermal inertia of the wire, even when high frequences of the fluctuating velocity occur. All these features make the method well suited for measurements of fluctuations at high frequencies,using both hot-wire and hot-film probes and for measurements under conditions of greatly varying velocity. The DISA system has a bandwith of 0 to 5 kc/sec at velocities near zero and this increases to 0 to 50 kc/sec at about 300 ft/sec . Improvement of the frequency response by increasing the transconductance is limited because high frequency oscillations appear in the closed loop system. Such types of instability are well known from all feedback systems. Constant temperature anemometry is, therefore,based on the design and operation of a stable servo system having a high closed loop gain.Frequency response can be increased by increasing over heating ratio which is defined as the ratio of the operating temperature to the ambient temperature. This is again limited,however, by the temperature endurance of the wire material (Ref.63). The constant temperature anemometer has the following advantages : Since no frequency compensation is necessary, operation in this mode is easier. It is possible to obtain greater flow sensitivity using high overheating with no risk of probe burn-out owing to sudden velocity decrease.

6.3.DIRECTIONAL SENSITIVITY OF HOT-WIRE PROBES

Hot-wire probes have directional characteristics due to their structure.The cylindrical wire is primarly sensitive to the component of absolute velocity normal to the wire axis. When the wire is normal to the mean flow direction,maximum heat transfer occurs. If the wire is inclined at some angle to the mean flow direction,the heat transfer drops for the same velocity.For the inclined positioning of the wire, initially it has been usual to adopt a simle cosine relationship for the normal cooling component of velocity (Ref.s.56 and 64).This can be expressed as (Fig.6.3)

$$U_e = U_\infty \cos\alpha \qquad (6.11)$$

In this case, King's heat transfer relation can be expressed as

$$Nu = A + B\,(Re\,\cos\alpha)^{.5} = A + B\,Re_n^{.5} \qquad (6.12)$$

Such a relation is accurate only for wires.with infinitely large length-to-diameter ratios. As the length-to-diameter

ratio is reduced,deviation from this simple cosine cooling law becomes quite significant. The reason is that decreasing the length-to-diameter ratio causes the percentage of the conduction heat losses to the prongs to increase in the total heat losses. In consequence, a non-uniform temperature distribution is created along the wire length. The smallest permissible value for the length-to-diameter ratio is around 200 and this gives the largest deviation from the simple cosine cooling law.

All these points could be explained in a theoretical way: For the flow field around a uniformly heated wire of infinite length placed perpendicularly to a uniform velocity stream (see Fig.6.4a), only Eqn.s.6.1,2 and 3 must be solved.The problem is two dimensional and heat transfer from the wire depends upon the velocity components normal to the wire,assuming the other variables as constant.That is,

$$U_e = (U^2 + V^2)^{.5} \qquad (6.13)$$

If this infinitely long wire is placed into the stream obliquely, a third velocity component develops along its axis (Fig.6.4b). The problem assumes a three dimensional character and full momentum equations together with the energy equation have to be solved.

Because the wire of infinite length is heated uniformly, the term $W\partial T/\partial z$ disappears although the velocity component along the wire,W, is not zero.This means that temperature distribution and consequently, convective heat transfer is independent of W and depends only on the normal velocity components,U and V. Thus, the simple cosine cooling law,Eqn.6.11, can be assumed for an infinitely long wire.The heat transfer relation then becomes

$$Nu = f(Re \cos\alpha, Pr, a) \qquad (6.14)$$

However, if the wire is of finite length,that is,if it is suspended between two prongs,conduction heat transfer occurs to the prongs.The temperature distribution along the wire is then determined by the heat generated in the wire,the convective heat transfer to the flow and additionally,the end conduction heat transfer to the prongs.(Radiation is neglected due to its very small order of magnitude.) Since the prongs are much longer than the wire,they are assumed to be effectively at ambient temperature and cause the non-uniform temperature distribution along the wire.This means that $\partial T/\partial z=0$ and the term including the velocity component along the wire does not vanish in the energy equation.The implication is that the temperature distribution,in cosequence,the convective heat transfer depends also on the velocity component

along the wire,W.The flow around the wire can still be assumed two dimensional, at least with a first approximation,due to the large values of the length-to-diameter ratio employed in practice.

These remarks explain whyheat loss from an inclined wire is larger then that from a wire normal to the flow with the same normal velocity component.Inclined and normal wires have nearly identical end conduction losses, although the temperature distribution on an inclined wire is slightly asymmetrical. Therefore,a deviation from the simple cosine cooling law is caused by an increase in the convective heat transfer which can be, by the above discussion, attributed to the velocity component along the wire.Thus,the effective cooling velocity should take into account this effect :-

$$U_e^2 = U_\infty^2 (\cos^2\alpha + k_1^2 \sin^2\alpha) = U_n^2 + k_1^2 U_t^2 \qquad (6.15)$$

where k_1 is called the yaw correction factor.

Similar relations were reported by several authors(Ref.s. 65,66,67 and 68). It is the most realistic way of treatment for the deviation from the simple cosine cooling law since it is based on both theoretical and experimental evidence. Different formulations have,however, also been suggested,for instance (Ref.69),

$$U_e = U_\infty^n \cos^m\alpha \qquad (6.16)$$

where

$$m = n - 0.05 \quad , \quad n,m=f(U_\infty)$$

Another example is Ref.70 where for the deviation from the simple cosine cooling law , account has been taken as

$$U_e = U_\infty \cos\alpha + 1.2 \sin^2\alpha \, (d_w/l_w)^{.5} \qquad (6.17)$$

Superiority of Eqn.6.15 in expressing deviation from the simple cosine cooling law is obvious since it also takes into account the effect of the velocity component along wire length. Therefore,it is the usually accepted form.The value of k_1 in this equation must be determined experimentally.Ref.59 gives k_1 as 0.2 at a velocity of about 150 ft/sec . k_1 is mainly dependent on the length-to-diameter ratio according to Ref.67 (Fig.6.5),where several probes with different length-to-diameter ratios have been tested.It is also reported that yaw

correction factor k_1 does not depend significantly on Reynolds number for the range of 2.5 to 11.7 .The effect of temperature distribution along the wire was also investigated and it was found that no significant effect was evident.

One of the most comprehensive work on the subject is Ref.71 where tests were carried out to determine the directional characteristics of two types of hot-wire and a fiber-film probe.It has been found out that yaw corection factor k_1 depends on the free stream velocity (magnitude and direction, that is, yaw angle) and probe shape.However, the effect of the magnitude of the free stream velocity is very slight for all the three probes,especially at high values of yaw angle. This finding is quite consistent with that of Ref.67 .The influence of the magnitude of free stream velocity becomes important as the length-to-diameter ratio of the wire is decreased considerably.This was the case for the fiber-film probe for which the length-to-diameter ratio was 18 .For a specific probe, the value of k_1 can be considered as a constant,between 0.2 and 0.14 ,for a wide range of the yaw angle when the probe has long prongs supporting a wire having a large length-to-diameter ratio (about 250).This is shown clearly in Fig.6.6 .Also, the relative error due to the selection of a specific value for the determination of the free stream velocity impinging obliquely on the wire has been reported.It has been found that choosing for k_1 the value at the yaw angle of 90° (see Fig.6.6) produces an error of maximum 3% in the determination of the free stream velocity (Fig.6.7).If the value at 60° is chosen,an error of 15% is caused at rather high values of the yaw angle. Approximately zero relative error for a wide range of yaw angle should be noted when the value of k_1 at the yaw angle of 60° is used.

It was so far considered that the free stream velocity lies in the plane of the wire and prongs,that is,only yaw sensitivity was examined.If the velocity,however, lies outside the plane of the wire and prongs (Fig.6.8), namely,for $B<90°$, the heat transfer from the wire increases (Ref.72).In order to see this more clearly, the simpler case of $\alpha=0°$ can be considered. For the same stream velocity,maximum heat transfer compared to that occuring at $\alpha=0°$, $\beta=90°$,takes place at $\beta=0°$ (Fig.6.9).This is due to two reasons : Firstly, when the probe is rotated around the wire axis (z-axis in Fig.6.8), a blockage effect is induced due to the larger diameter of the prongs and velocity increases around the connection regions. This increases the heat transfer from the wire. Secondly,some of the heat created electrically in the wire is transferred to the prongs by conduction. This increases the temperature at the ends of the prongs.In consequence, heat is also transferred to the surroundings by convection from these hot prong ends.This convective heat transfer increases if the prongs are orientated perpendicularly to the direction of the stream velocity.

It is quite obvious that as the length of the wire is increased on a probe while keeping the other dimensions constant,

the ratio of the convective heat transfer at the prong ends to the total convective heat transfer from the probe decreases. This means that as the length of the wire is increased, end effects become negligible. Similar to this situation, the yaw sensitivity could be expressed by the simple cosine cooling law and the end effects of the prong ends could be neglected for the length-to-diameter ratio of about 600 (see Fig.6.5). Therefore, if the stream velocity is out of the wire-prongs plane, a correction factor similar to that in Eqn.6.15 is also required in order to express the increase in the heat transfer rate. The effective cooling velocity can be written as

$$U_e^2 = U_\infty^2 (\sin^2\beta + k_2 \cos^2\beta) \qquad (6.18)$$

for $\alpha=0°$, where k_2 is called the pitch correction factor. k_2 is given as 1.15 at a velocity of 150 ft/sec in Ref.59 . A more detailed examination of k_2 is reported in Ref.71 for a probe similar to that used in this work. It has been found that k_2 depends very slightly on the magnitude of the stream velocity. It can also be seen from Fig.6.10 that k_2 does not change considerably with the pitch angle. Only a slight increase occurs as the pitch angle is increased. k_2 is mainly dependent on the shape of the probe. Its value increases , for instance, if the length-to-diameter ratio is reduced. Sensitivity to pitch decreases with increasing distance between the prongs and with increasing prong length. Relative order of magnitude of the error in the determination of the free stream velocity due to the selection of the value of k_2 at the pitch angle of 90° has been found less than 1% (Fig.6.11). This error, however, increases as the length of the prongs or the length-to-diameter ratio of the wire are reduced on a specific probe. From Fig.6.11 , it can also be seen that neglecting k_2 might result in errors of around 5% . It should also be noted that the values of k_1 and k_2 have been calculated in Ref.71 , using a heat transfer relation similar to Eqn.6.10 .

Combining these two factors to represent the general case in which the free stream velocity falls on the wire with a yaw angle of α and a pitch angle of β (see Fig.6.8), the effective cooling velocity can then be expressed as

$$U_e^2 = U^2 + k_1^2 W^2 + k_2^2 V^2 \qquad (6.19)$$

In an overall sense, by choosing k_1 and k_2 at the yaw and pitch angles of 90°, the total error in the evaluation of the free stream velocity should be of the order of 6 to 8% . However, neglecting one of these, for instance, yaw sensitivity, as it is mostly applied on X-type probes by assuming the simple cosine cooling law, introduces errors of the order of 40 to 60% in the determination of the free stream velocity (Ref.71).

Therefore, they should be considered if the free stream velocity has a yaw direction and is out of the wire-prongs plane.

The directional characteristics can be interpreted as the relative difference between the true velocity of the fluid and the effective cooling velocity acting on the wire. The cooling velocity is obtained from the calibration curve by means of the voltage signal measured with the wire in the direction of its original orientation.

6.4. METHODS FOR THE INTERPRETATION OF SIGNALS FROM HOT-WIRE ANEMOMETER

After a probe is connected to an anemometer unit and the bridge is balanced, two voltage values can be read from the anemometer unit if this probe is inserted into a flow field.

All of the analyses of the electrical signals from hot-wire anemometers start with an equation relating the voltage drop across the wire (that is, the heat transfer) to the effective cooling velocity acting on the wire. For the purpose of a general discussion in what follows, let us consider a heat transfer relation of the form

$$E^2 = f(U_e) \qquad (6.20)$$

where the function contains calibration constants determined experimentally in laminar flow conditions. A crucial assumption made at this point is that this relation is also valid in the case of turbulent flow. Then, E and Ue become instantaneous voltage drop and effective cooling velocity, respectively. This assumption is quite reasonable since Reynolds number based on the diameter of the wire is very low even at rather high velocities.

Most of the methods available are restricted to flow cases with low turbulence intensities (less than 20%). For flows with a higher level of turbulence intensity different methods have been developed. Here only the general trends will be explained.

It is indeed quite difficult to classify these methods for several reasons. Firstly, some of them are applicable to highly turbulent flows as well as to low turbulence cases. Some are, however, adequate for only a single case. Secondly, some methods require a single sensor probe, while in some others a multi-sensor probe must be used. In some cases, however, both must be employed. Thirdly, probes must be rotated in some applications despite the unnecessity in some others to orientate them again. due to the simplicity of the application. No classification will, therefore, be made here and the order will follow, in the author's opinion, the procedures from the simplest to the most developed and widely applicable one.

In the earliest application of hot-wire tecnique(Ref.59) the flow is assumed completely one-dimensional (on the axis of a pipe flow,for instance),that is,only U and u exist;v and w can be neglected.Actually these lateral fluctuating velocity components are not zero even the flow is one-dimensional and they create an additional cooling effect on the heat transfer from the wire. In this method,a heat transfer relation of the form

$$E^2 = E_0^2 + B\,U^n \qquad , \quad 0.45 \leq n \leq 0.5 \qquad (6.10)$$

can be used to determine the mean velocity U .The turbulence intensity can be evaluated (see the sketch) from

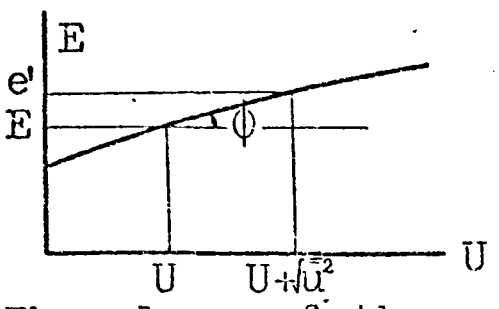

$$T.I. = 100\ u^2/U = 100\ e'/aU \qquad (6.21)$$

where

$$a = tg\phi = e'/\sqrt{u^2} \qquad (6.21a)$$

The slope of the curve at the required velocity can be obtained from the heat transfer relation Eqn.6.10 .By taking derivative with respect to velocity and assuming n=0.5

$$a = \frac{dE}{dU} = \frac{B}{4EU^{.5}}$$

and

$$aU = \frac{BU^{.5}}{4E}$$

Substituting for $U^{.5}$ from Eqn.6.10

$$aU = \frac{E^2 - E_0^2}{4E}$$

Then,substituting into Eqn.6.21 , we get

$$T.I. = 100\ e' \frac{4E}{E^2 - E_0^2} \qquad (6.22)$$

The important point to remember is that the slope of the curve at the velocity U has been represented by Eqn.6.21a which is only an approximation.In general,this curve is not straight.Therefore,this expression for the slope of the curve is correct only for low values of the velocity fluctuations. In other words,this method is correct for low level of turbu-

lence.However,this difficulties can be overcome by using a linearizer.Its main function is to cancel out the anemometer output voltage at zero flow velocity and to raise the output voltages by a suitable exponent depending on the velocity level.It has a variable gain.Hence,its transfer function results in a voltage that varies depending on the flow velocity.In order to provide an optimum linearization,logarithmic amplifiers are used.In this way,continuous linearization of the anemometer output voltage can be achieved.It is actually an analog correlator and its transfer function can be written as

$$E_L = K_L\,(E^2-E_0^2)^m = K_L(B\,U^n)^m$$

If m is chosen equal to 1/n ,then

$$E_L = K_L\,B^m\,U = k_L\,U$$

Using a linearizer,therefore, the slope of the heat transfer curve can be represented in a linear form for higher values of $\sqrt{u^2}$ .However,because of the drift occuring in the electronics, a linearizer is not usually desired (see Ref.59) in a measuring system for turbulence intensities of less than 10% and the direct calibration curve is used.For higher values of turbulence level,it should be used.It can be recalled that v and w have been neglected in the method.This worsenes the applicability range of the method for multi-dimensional flow cases and it is generally assumed that it can be used for one dimensional flows with a turbulence intensity up to 20% .When the measurements are to be carried out in a two-dimensional field (away from the axis in a pipe flow,for instance), the method can be applied by inserting the probe into the flow field perpendicularly to the flow axis so that the wire faces the absolute velocity (pitch correction must be considered in this case).Even in this case the third component of the fluctuating velocity,w, has to be neglected.The method does not give the required data when it is applied to complex flow fields where turbulence intensities are high and lateral components of the mean and fluctuating parts of the absolute velocity can not be neglected.

When more information is necessary for a flow field,for instance,in a boundary layer flow where not only $\sqrt{u^2}/U$ but also $\sqrt{v^2}/U$ and $\overline{uv}/U^2$ are required (see the sketch),an X-type probe can be employed.Two anemometer units are required for its operation.The probe should be orientated in the flow in such a way that the mean velocity U must bisect the angle between the two wires. When the values of v and w are small, that is, at low turbulence levels(less than 10%),this orientation can be performed quite easily.If $\alpha(t)$ and

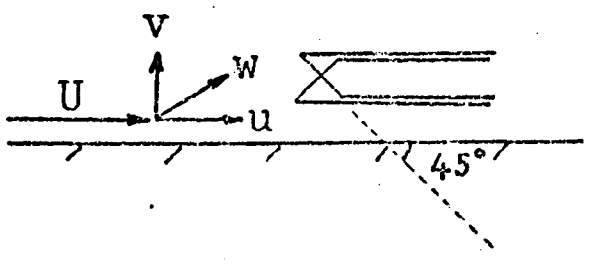

$\beta(t)$ are the output voltages obtained from the wires 1 and 2, then by assuming that the simple cosine cooling law holds for both wires, it can be shown that

$$\alpha(t) = S_1' (u-v)$$

$$\beta(t) = S_2' (u+v)$$

If the signals are adjusted such that $S_1'=S_2'$, the following relations can be obtained :

$$u = \frac{0.5(\alpha(t)+\beta(t))}{S_1'}$$

$$v = \frac{0.5(\alpha(t)-\beta(t))}{S_2'}$$

$$\sqrt{\overline{u^2}} = \frac{0.5((\alpha(t)+\beta(t))^2)^{0.5}}{S_1'}$$

$$\sqrt{\overline{v^2}} = \frac{0.5((\alpha(t)-\beta(t))^2)^{0.5}}{S_1'}$$

$$\overline{uv} = \frac{0.5(\alpha^2(t)-\beta^2(t))}{S_1'^2}$$

The two wires must be connected to two separate anemometer units the output voltages of which are fed into a dual summing unit. Addition and difference of these two voltages can be obtained at the output of the dual summing unit. Subsequently, they are fed to the two channels of a correlator to obtain the above quantities (Fig.6.12). Changing the orientation of the probe to the other two planes, $\sqrt{\overline{w^2}}$, $\overline{uw}$ and $\overline{vw}$ can also be measured. However, the assumption of the simple cosine cooling law might cause quite serious errors in the experimental data. Additional assumptions are that the probe is adjusted according to the main flow direction and w fluctuating component exerts same cooling effect on the two wires. These assumtions are never completely true, for instance, in highly turbulent flows the probe can not be adjusted readily to obtain an angle of 45° between each of the two wires and the mean flow direction. Also, the two wires can never be completely equal. Furthermore, because they must be fixed with some distance between them not to interfere with each other, the spatial resolution of the probe becomes worse. Besides,

because of the need to employ two anemometer units with the same sensitivity, the procedure becomes quite unattractive. Yet it has been used quite frequently, especially in boundary layer research. For more information, the reader is referred to Ref.s.55 and 64 .

In order to dispense with the two anemometer units required in the previous procedure and to improve spatial resolution, a 45° slanting single wire probe can be used (see the sketch). The probe axis is fixed parallel to the direction of flow. After determining the voltages in the first orientation, the probe is rotated 180 degrees around its axis to the second orientation. It is assumed that the effect of w on the cooling of the wire for the two orientations are equal. If the simple cosine cooling law is assumed for the wire, the shear stress can then be measured using the formula

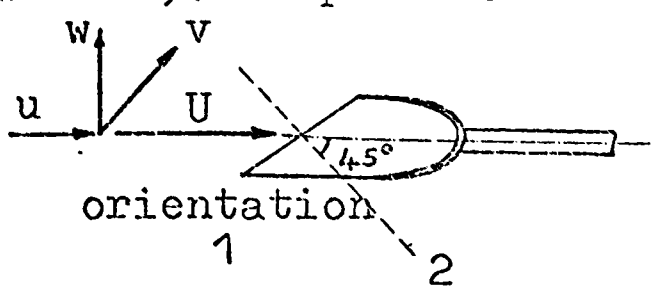

$$-\rho\overline{uv} = \frac{\rho U^2}{4 S_1'} - 4\left(\left(\frac{E^2 e'}{E^2 - E_0^2}\right)_1^2 - \left(\frac{E^2 e'}{E^2 - E_0^2}\right)_2^2\right)$$

Another important assumption made here is that the flow field is assumed stationary from one orientation to the other. This measurement procedure also necessitates the knowledge of the main flow direction so that the probe can be aligned properly. Besides, most of the assumtions of X-type probe must still be used. Therefore, the method can be used in flows with low turbulence intensities. For more details, the reader is referred to Ref.73 .

In more complex flow fields, such as, three dimensional or two dimensional flows with three velocity components , more information is required from measurements. A direct approach to the measurements for such cases may seem that a three-dimensional probe should be used. Three wires fixed perpendicularly to each other are used on this probe. Operation, therefore, requires three anemometers. In order to avoid interference and in consequence, inaccuracy in the readings due to thermal wakes of the wires, the probe should be orientated to the flow direction in such a way that the absolute velocity falls within the octant formed by the three perpendicular wires (see the sketch). If then the simple cosine cooling law is assumed for each of the wires, the components of the absolute velocity U, V and W in the direction of the wires can be found as

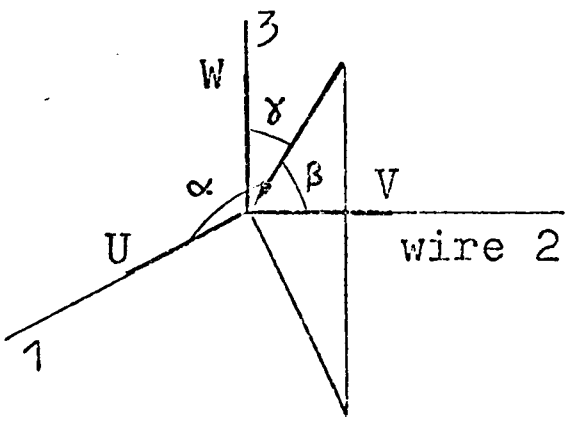

$$U = \sqrt{-E_1^2+E_2^2+E_3^2} \;/\; S\sqrt{2}$$

$$V = \sqrt{E_1^2+E_2^2+E_3^2} \;/\; S\sqrt{2}$$

$$W = \sqrt{E_1^2+E_2^2-E_3^2} \;/\; S\sqrt{2}$$

where S is the sensitivity of the linearized anemometers and E_1, E_2 and E_3 are the linearized output voltages.This method is possible for flows with up to 10% turbulence intensity. If,however,the yaw sensitivity of the wires is included in the cooling law,the effective cooling velocity of each wire is written as

$$U_{e1}^2 = V\,(\sin^2\alpha + k_{11}^2\cos^2\alpha)$$
$$U_{e2}^2 = V\,(\sin^2\beta + k_{12}^2\cos^2\beta) \qquad (6.23)$$
$$U_{e2}^2 = V\,(\sin^2\gamma + k_{13}^2\cos^2\gamma)$$

and assuming $k_{11}=k_{12}=k_{13}=k$ for all the wires

$$V^2 = \frac{U_{e1}^2+U_{e2}^2+U_{e3}^2}{2+k^2} \qquad (6.24)$$

After the absolute velocity is found from Eqn.6.24 ,its direction is determined from Eqn.6.23 .The method in this way provides instantaneous magnitude and direction.Several reasons,however,make the method quite unattractive.First of all,the use of three wires on the probe causes a poor spatial resolution,especially in the flows with large velocity gradients.Actually the interference between them deveagainst spatial resolution.One gets poorer as the other gets better.The hree wires can never be made comletely equal. Furthermore,three anemometer units are required and they must have the same electronic sensitivity,which is very difficult to acquire.Application is quite difficult because the approximate direction of the velocity should be known and the level of turbulence should be relatively low in order to keep the absolute velocity in the octant of the wires. When there is reverse flow zones in the flow field,the method can not be used readily,because the direction of velocity is not known.It should be noted that if the structure of the reverse

flow zones are approximately known for a specific case,the probe can be manufactured according to the requirements to include the absolute velocity in the octant formed by the wires.The remarks mentioned above,however,still makes the procedure quite unfavourable.

A special type probe,called split film probe has been developed recently.On this probe,two separate films have been deposited around a single quartz rod (Ref.74).Therefore, two anemometers are required for its operation.The principle of its operation is that the variation of heat transfer around the sensor is examined.It is generally used for direction determination in two-dimensional flow fields.It can be used in place of X-type probes even for flows with a high turbulence intensity.It provides better spatial resolution in comparison to X-type probes. Due to insensitivity to the velocity component along the rod axis,however,it can not be used properly in flow fields with three velocity components.

Using three split film sensors,that is,six films deposited on three quartz rods,a three dimensional probe can be constructed(Ref.74). Such a probe is quite sensitive to flow reversals.However,it requires six anemometer units with the same sensitivity.Alternatively, a single unit providing all the required voltages for all the films is also available, while being prohibitively expensive.If the flow has a dominant direction,that is,it is of the boundary layer type, the use of a three-sensor probe is acceptable with a suitable orientation of the probe. When there are flow reversals , however,it is almost impossible to avoid wake interference from one sensor or film,to the other while scanning in the flow reversal zone.This can be obviated designing the probe with a longer distance between the sensors.However,this worsens he spatial resolution which is already poor for flow with large velocity gradients.

In a group of interpretation techniques,the so called conventional methods,the heat transfer relation,Eqn.6.20, is written as

$$E = (f(U_e))^{0.5} \qquad (6.25)$$

by taking square root of both sides (Ref.s.65,68,75). Then, binomial expansion is applied to the right hand side,neglecting all high order terms.Time average of both sides are taken and neglecting all correlation terms (Reynolds stresses) the mean voltage is obtained in terms of mean velocity. In order to obtain Reynolds stresses ,

$$\overline{e^2} = (\overline{E^2} - \bar{E}^2)$$

is formed from the relations already obtained.The main assumption of several procedures are that third and higher order

correlation terms, such as, $\overline{uv^2}$, $\overline{u^2v}$ or $\overline{w^2v^2}$, are negligible in comparison to second order terms(Reynolds stresses) and also some normal Reynolds stresses are negligible with respect to the mean velocity.Due to the assumptions mentioned above,these methods are generally applicable to flows with up to 20% turbulence intensity.They can be applied employing either single sensor or X-type probes.These methods have been widely applied in boundary layer flows where most attention is directed to the $\overline{u^2}$, $\overline{v^2}$, $\overline{w^2}$ and $\overline{uv}$ due to the exitance of a strongly dominant flow direction.A recent version of this group has been developed for three-dimensional flow field However,it is still applicable to flow fields with low turbulence intensity (10%) and with a strongly dominant flow direction (Ref.76).

Two recent methods (Ref.77 and 78) are also very similar to the conventional methods just described.In the former, the procedure is dependent on the determination of the direction of the mean absolute velocity with the hot-wire itself. This can be achieved rather readily in a boundary layer type flow, such as,a straight jet which has already been chosen to demonstrate the capability of the procedure in this reference. Because the turbulence intensity in such a flow is not very high,the determined flow direction can be quite reliable. However,for a flow field where turbulence intensity is higher, say,60% or more,the determination of the direction of the flow becomes quite unreliable.Therefore,it is seen that the method is not applicable to recirculation regions.Just for the sake of completing the discussion,it is worth noting that more general assumptions have been made in this method. Third and higher order correlations have been neglected with respect to the mean velocity.The method calculates the mean absolute velocity from the normal signal in a very similar manner to the conventional methods.On the other hand,the components of the fluctuating velocity are determined from the squared electrical signals.Another difficulty with the method is that the use of two hot-wire probes are required for its application.This is most undesirable when a flow field is to be scanned.Changing the probes during an experimentation is quite troublesome since it must also be accompanied by the changes of the settings of the anemometer unit. Alternatively,scanning the field with the probes one-by-one is also not a very good solution to the problem since a change in the state of the flow may occur with time.Therefore, an ideal procedure must include the use of only one probe and measurement at a spatial point in a possible shortest time.It has been reported by the authors that the method is also not applicable to flows with low turbulence intensity (less than 25%) and is very time consuming.The latter method has also been applied to a boundary layer type flow,in consequence,approximate direction of the flow was known.In this way, use could be made of a Pitot tube to determine the direction of the mean flow.It was also possible,however, to do this with the hot-wire.In the mothod,lateral component of the

mean velocity should either be neglected or be determined from the continuity equation.Both methods can not be applied to complex flow fields because the approximate direction of the mean flow is not known.Even it is known,it is not reliable because of the high turbulence intensity encountered in such flows.

As examples of more developed methods,two works employing six orientations of hot-wire probes at a spatial point can be shown (Ref.s.79 and 80).The latter method is based on an improved heat transfer relation which has a quadratic form in square root of velocity.It has been shown that this heat transfer relation represents the cooling of the hot-wire better than King's law for a wider velocity range (Ref.81). In the method,it was assumed that the fluctuating component of the instantaneous voltage drop across the hot-wire is of the form of a square wave.The period and phasing of the wave were assumed to be independent of the wire orientation at a given point in the flow field.With these assumptions,the mean value of a function of the instantaneous wire voltages could be expressed in terms of anemometer output voltages.The orientations of the wires are shown in Fig.6.13 .In order to obtain readily these six orientations at every point in the flow field two probes having normal and 45 slanting wires have been used. Orientations 1,2,3 and 4 have been obtained using the latter probe inserted to the flow field parallel to the z-axis.In order to obtain orientations 5 and 6, the former probe has been used.The necessity,in this way, to change the probes at every point in the flow field is quite troublesome.The alternative,using the probes one-by-one,might result in a change of the state of the flow field. A more important point in the method can be seen when it is appled to flow reversal zones (Fig.6.14).The point where the hot-wire has been located is in the recirculation region.When the orientation 3 is applied at such points,the hot-wire lies in the wake of the upstream prong,i.e.,the one on the right in the figure.Therefore,RMS readings taken at such points for the orientation 3 of the hot-wire are spuriously high and DC voltage readings are small.Obviously,another orientation causes similar false signals in the other zones of the recirculation region (see also Fig.1.8).Another difficulty is that the two hot-wires can not be placed exactly at the same point in the flow field.In an overall sense,therefore, the method can be assumed quite unattractive for the present application.

Finally,before starting the present formulation,another method (Ref.15) employing four orientations at every point in the flow field will be examined.These four orientations, when applied to a swirling flow field with recirculation is shown in Fig.6.15 .They all can be obtained with a single normal sensor probe inserted into the flow field parallel to the x-axis.The improved heat transfer relation suggested by Ref.81 has been used in the formulation.The same assumptions

employed in the six-orientation methods about the electrical signals,have been made.In this way, response equation have written for every orientation and instantaneous velocities in terms of output voltages have been obtained.Reynolds stresses have been obtained by correlating these quantities. It must also be noted that orientation 3 has been used to calculate the assumed phase difference between the orientation 2 and 4 .It was reported that some ambiguity was existant in the results,especially for the area around the boundary of the reverse flow zones.This occured probably due to the following reasons : Firstly,just at the boundary between the zones 3 and 4 , U=0 .The absolute velocity,therefore,lies in the plane of the orientation 3, leaving the wire completely in the wake of the top prong,especially in the zone 3 of the recirculation region near the reverse flow boundary.If it is recalled that the voltage taken at this orientation was being used to determine the assumed phase difference,it becomes obvious that this point might be introducing some error. Secondly,in the zone 3,for instance,where the axial velocity component is not zero,but almost equal to the magnitude of the swirl velocity component at some points,the voltage readings taken at the orientation 4 might be spurious since the wire itself remains in the wake of the prong at the higher position.A similar situation is observed,for instance,in the zone 4 for the orientation 2.Also,another very serious difficulty in the method is that the direction (sign) of the mean velocity components should be known in order to calculate the Reynolds shear stresses.However,a close examination of the formulation of the method reveals that,even from the experimental data,it is impossible to determine the direction (sign) of the velocity components.For all these reasons, the the method is quite difficult to apply to a recirculation region.

6.5.CONCLUSIONS

It is concluded that,as far as the author is aware,the lack of a hot-wire technique to examine easily,quickly and cheaply recirculation regions in swirling flows is obvious. All the available methods for the hot-wire anemometry are bound to give erroneous signals at some orientations of the probe when applied to recirculation regions. These erroneous signals may cause a wrong interpretation of the mean flow direction.Therefore,all the effort has to be exercised in this direction to eliminate the effects caused by the prongs, rather than the treatment of signals.

6.6.FORMULATION FOR THE PRESENT WORK

The most attention in the present work has been given to

the structure of the flow field in order to rotate the probe in the most suitable way such that the hot-wire always faces directly the mean absolute velocity.

6.6.1.Assumptions

The following assumtions have been made for the present analysis :-

a)Turbulence is assumed stationary.Thus,the state of the flow at a point in the field does not change from one orientation to the other.Actually such an assumption is compulsory for any technique requiring probe orientation.

b)The relation between the voltage drop across the wire and the effective cooling velocity normal to the wire in laminar flows is of the form of a quadratic equation (Ref.81)

$$E^2 = A + B\,U_e^{0.5} + C\,U_e \qquad (6.26)$$

The advantage of this formula over King's law is that it represents the experimental heat transfer-voltage drop relation with better accuracy.It can be used,therefore,for a wider cooling range.It is also assumed to be valid for turbulent flows.In that case, E represents the instantaneous wire voltage and U_e ,the instantaneous effective cooling velocity.Obviously,a linearizer can not be used in the procedure because of the quadratic form of this equation.It can also be written as

$$C\,U_e + B\,U_e^{0.5} + (A-E^2) = 0 \qquad (6.27)$$

Therefore,

$$U_e^{0.5} = \frac{-B + \left(B^2+4C(E^2-A)\right)^{0.5}}{2C} \qquad (6.28)$$

The magnitude of the velocity determined from Eqn.6.28 depends upon the values of A,B and C .B is generally positive and C is negative (Ref.81).They were similarly determined in this work.

c)The effective cooling velocity for the description of the directional sensitivity of the hot-wire is assumed to be of the form of

$$U_e^2 = k_2^2\,U^2 + k_1^2\,V^2 + W^2 \qquad (6.29)$$

d)The fluctuating component of the voltage drop across the hot-wire is assumed to be of the form of a square wave (Fig.6.16).Its period,T, and phase are assumed to remain constant for all the orientations of the probe.In this way,it becomes possible to calculate the time average of a function of the instantaneous voltages in terms of the measured DC and RMS voltages. If such a function is $\mathcal{T}=\mathbb{D}(E)$,its time average becomes

$$\overline{\mathcal{T}}=\overline{\mathbb{D}(E)}=\frac{1}{T}\int_0^T \mathbb{D}(E)\,dt$$

which can be separated as

$$\overline{\mathcal{T}}=\overline{\mathbb{D}(E)}=\frac{1}{T}\left[\int_0^{.5T}\mathbb{D}(E)\,dt+\int_{.5T}^{T}\mathbb{D}(E)\,dt\right]$$

Therefore

$$\overline{\mathcal{T}}=\overline{\mathbb{D}(E)}=\frac{1}{T}\left[\int_0^{.5T}\mathbb{D}(\overline{E}+e)\,dt+\int_{.5T}^{T}\mathbb{D}(\overline{E}+e)\,dt\right]$$

$$=\frac{1}{T}\left[\mathbb{D}(\overline{E}+e_m)\ 0.5T+\mathbb{D}(\overline{E}-e_m)\ 0.5T\right]$$

$$=0.5\left[\mathbb{D}(\overline{E}+e_m)+\mathbb{D}(\overline{E}-e_m)\right] \qquad (6.30)$$

From Fig.6.16 it can be seen that $e_m=e'$. Eqn.6.30 therefore becomes

$$\overline{\mathcal{T}}=\overline{\mathbb{D}(E)}=0.5\left[\mathbb{D}(\overline{E}-e')+\mathbb{D}(\overline{E}+e')\right] \qquad (6.31)$$

The importance of Eqn.6.31 is that it allows the calculation of the mean values of the instantaneous effective cooling velocity from the output voltage values.If it is applied to Eqn.6.28 ,after squaring

$$\overline{\mathcal{T}}=\overline{\mathbb{D}(E)}=\overline{U_e^2}=0.5\left[U_e^2(\overline{E}+e')+U_e^2(\overline{E}-e')\right] \qquad (6.32)$$

The effective instantaneous cooling velocity in Eqn.6.32 can be written in terms of the components of the instantaneous absolute velocity for a specific orientation of the hot-wire.Such an equation,however,contains three unknowns (the three components of the instantaneous abso-

lute velocity).Therefore, it should be accompanied by two others for a solution to be possible.If such equations are written for two other orientations then the instantaneous velocity components can be solved from the equation set.It is apparent that the rigth hand sides of these equations vary as the voltages read from the anemometer change for each orientation.

6.6.2.Choice of the orientations

In order to find out the best three orientations,consideration is now to be given to the structure of the flow field in the recirculation region occuring in a swirling flow (Fig.6.17).As it was explained before,four zones can be distinguished inside the recirculation region. The swirl velocity component is always positive (in one direction) everywhere in the flow field.Therefore,only axial and radial velocity components characterize the rotation in the recirculation region. Reverse axial velocities occur in the zones 1 and 4 .These zones are separated from zones 2 and 3 by the zero velocity line.The radial velocity component is positive in the zones 2 and 1 .At the points,like point 5 and 7, where the main flow is diverging, the direction of the resultant velocity in the z-r plane is close to that in the zone 2 . At the points like 6, the direction of the resultant velocity in the z-r plane is close to that in the zone 3. It can be concluded that the consideration of the flow directions only in the recirculation region is sufficient to cover all possible cases in the complete flow field.

It becomes obvious from these remarks that the hot-wire should be rotated in the plane containing the axial and radial velocity components in order to detect the flow direction and to avoid the hot-wire to fall in the wake of one of the prongs for some orientations of the probe in the flow field.The three orientations chosen are shown in Fig.6.17 .It is seen that for all the orientations, the absolute velocity always faces the hot-wire and it never remains in the wake of the prongs anywhere in the flow field.

6.6.3.Formulation

After the choice of the three orientations,the effective cooling velocity is determined for each case.For the orientation 1 (see Fig.6.17),the effective cooling velocity can be expressed as

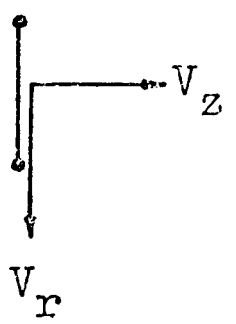

orientation 1

$$V_z^2+V_\theta^2+k_1^2V_r^2=U_{e1}^2=\mathfrak{T}_1 \qquad (6.33)$$

where

$$\mathfrak{T}_1=\frac{-B+\left[B^2+4C(E_1^2-A)\right]^{0.5}}{2C} \qquad (6.34)$$

In Eqn.6.34 , E_1 represents the instantaneous voltage drop at the orientation 1 .It can be read directly from anemometer indicators in the form of DC and RMS voltages.

For the orientation 2,which is obtained by rotating the probe 45° with respect to orientation 1, the effective cooling velocity is

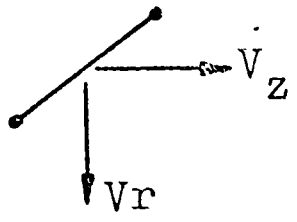

$$(V_z+V_r)^2+2V_\theta^2+k_1^2(V_z-V_r)^2=2U_{e2}^2=2\mathfrak{T}_2 \qquad (6.35)$$

where $\mathfrak{T}_2$ is expressed similar to Eqn.6.34 .

For the orientation 3 ,at 90° to the orientation 2 ,effective cooling velocity is expressed as

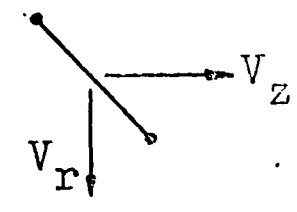

$$(V_z-V_r)^2+2V_\theta^2+k_1^2(V_z+V_r)^2=2U_{e3}^2=2\mathfrak{T}_3 \qquad (6.36)$$

where $\mathfrak{T}_3$ is expressed similar to Eqn.6.34 .

It may be recalled that for a constant stream velocity, the heat transfer from a hot-wire is maximum if it is located perpendicularly to the flow direction.As it is inclined,the heat transfer drops and becomes minimum when the hot-wire is parallel to the flow direction.This feature of the variation of the heat transfer can be used to determine the flow direction in this procedure. For instance, the voltage reading at the orientation 3 is larger than that at the orientation 2 when the wire is in the zone 3 .The opposite occurs when the wire is in zone 2,etc.

Eqn.s.6.33,35 and 36 can be written as

$$V_z^2+V_\theta^2+k_1^2V_r^2=\mathfrak{T}_1$$

$$(1+k_1^2)V_z^2+2V_\theta^2+(1-k_1^2)2V_rV_z=2\mathfrak{T}_2$$

$$(1+k_1^2)V_z^2+2V_\theta^2-(1-k_1^2)2V_rV_z=2\mathfrak{T}_3$$

from which

$$V_rV_z=\frac{\mathfrak{T}_2-\mathfrak{T}_3}{2(1-k_1^2)} \qquad (6.37a)$$

$$V_z^2+V_\theta^2+k_1^2V_r^2=f_1 \tag{6.37b}$$

$$V_z^2(1+k_1^2)+2V_\theta^2+V_r^2(1+k_1^2)=f_2+f_3 \tag{6.37c}$$

can be derived.Rearranging Eqn.6.37 ,we can obtain

$$V_r^4+\frac{2f_1-f_2-f_3}{1-k_1^2}V_r^2-\frac{(f_2-f_3)^2}{4(1-k_1^2)^2}=0 \tag{6.38}$$

which is a quadratic form with respect to V_r^2 .Since V_r^2 is a positive value,it should be the positive root of Eqn.6.38 and this yields

$$V_r^2=\frac{-2f_1+f_2+f_3+2^{\frac{1}{2}}\left[(f_1-f_2)^2+(f_1-f_3)^2\right]^{\frac{1}{2}}}{2(1-k_1^2)} \tag{6.39}$$

which can be represented as

$$V_r^2=Q_r(f_1,f_2,f_3) \tag{6.39a}$$

From Eqn.s.6.37b and 6.37c

$$V_\theta^2=\frac{1+k_1^2}{k_1^2-1}f_1-\frac{f_2+f_3}{k_1^2-1}-(k_1^2+1)V_r^2 \tag{6.40}$$

can be obtained.Introducing Eqn.6.39 into Eqn.6.40 and after some manipulations

$$V_\theta^2=\frac{f_2+f_3}{2}-\frac{(1+k_1^2)}{2^{\frac{1}{2}}(1-k_1^2)}\left[(f_1-f_3)^2+(f_1-f_2)^2\right]^{\frac{1}{2}} \tag{6.41}$$

is obtained.Eqn.6.41 can be represented as

$$V_\theta^2=Q_\theta(f_1,f_2,f_3) \tag{6.42}$$

Finally, V_z^2 can be obtained from Eqn.6.37b and can be shown as

$$V_z^2 = Q_z(T_1, T_2, T_3) \tag{6.42a}$$

If, now, the components of the instantaneous absolute velocity are separated into a mean and a fluctuating value (see Eqn.s.2.9) and after squaring and taking time average

$$\overline{V_r^2} = V^2 + \overline{v^2} = \overline{Q_r(T_1, T_2, T_3)} \tag{6.43a}$$

$$\overline{V_\theta^2} = W^2 + \overline{w^2} = \overline{Q_\theta(T_1, T_2, T_3)} \tag{6.43b}$$

$$\overline{V_z^2} = U^2 + \overline{u^2} = \overline{Q_z(T_1, T_2, T_3)} \tag{6.43c}$$

can be obtained. The mean values of the functions Q_r, Q_θ and Q_z are obtained, making use of Eqn.6.31

$$\begin{aligned}
\overline{Q_r(T_1, T_2, T_3)} &= 0.5 \left[Q_{rP}(T_1, T_2, T_3) + Q_{rN}(T_1, T_2, T_3) \right] \\
\overline{Q_\theta(T_1, T_2, T_3)} &= 0.5 \left[Q_{\theta P}(T_1, T_2, T_3) + Q_{\theta N}(T_1, T_2, T_3) \right] \\
\overline{Q_z(T_1, T_2, T_3)} &= 0.5 \left[Q_{zP}(T_1, T_2, T_3) + Q_{zN}(T_1, T_2, T_3) \right]
\end{aligned} \tag{6.44}$$

where the additional indices P and N are used to denote the function values calculated by substituting DC voltage plus RMS voltage and DC voltage minus RMS voltage, respectively.

In order to determine the normal Reynolds stresses from Eqn.s.6.43 , the mean velocity components must be known. They can readily be obtained from Pitot tube measurements in the case of simple flow fields. If this is, however, not readily feasible due to the complexity, for instance, of the flow field under investigation, it is desired that the mean velocity components are also determined from hot-wire data. They can be obtained in the following way : from Eqn.s.6.39a, 6.41a and 6.42a

$$\begin{aligned}
V_r &= \left[Q_r(T_1, T_2, T_3) \right]^{\frac{1}{2}} \\
V_\theta &= \left[Q_\theta(T_1, T_2, T_3) \right]^{\frac{1}{2}} \\
V_z &= \left[Q_z(T_1, T_2, T_3) \right]^{\frac{1}{2}}
\end{aligned} \tag{6.45}$$

can be written.Taking also time average yields

$$V = \overline{\left[Q_r(T_1,T_2,T_3)\right]^{\frac{1}{2}}} = \overline{\left[Q_R(E_1,E_2,E_3)\right]^{\frac{1}{2}}}$$
$$W = \overline{\left[Q_\theta(T_1,T_2,T_3)\right]^{\frac{1}{2}}} = \overline{\left[Q_\theta(E_1,E_2,E_3)\right]^{\frac{1}{2}}} \qquad (6.46)$$
$$U = \overline{\left[Q_z(T_1,T_2,T_3)\right]^{\frac{1}{2}}} = \overline{\left[Q_Z(E_1,E_2,E_3)\right]^{\frac{1}{2}}}$$

In order to take time average of Eqn.6.45 ,however,consideration has to be given to the contents of the functions Q_R, Q_Z and Q_θ .They are the functions of three instantaneous voltages,E_1,E_2 and E_3 .These three voltages are created across the wire by the instantaneous heat transfer rates at the orientations 1,2 and 3 of the probe.The three voltages occuring across the wire placed at a point in the zone 2 , for instance, have been shown in Fig.6.18 .It has been assumed that the rotain of the probe starts with the orientation 2 . The variation of the instantaneous voltage E_2 during the measurement time at the orientation 2 has been shown in the figure with a square wave.Its period is denoted by T .When the probe is rotated to orientation 1 ,the mean value of the instantaneous voltage drops (see the previous chapter for the reason).However,the centre of the hot-wire is still at the same point in the flow field.Therefore,although the heat transfer rate has changed (different $\bar{E}_1$ and e'_1 from $\bar{E}_2$ and e'_2)because of the rotation,its fluctuating character does not change (stationary turbulence).Thus,it still has a period of T .Similar remarks also apply when the probe is rotated to the orientation 3 .

Choosing the common period T as the integration period from arbitrary initial times $t_1=t_2=t_3=0$ for the three orientations,it is seen that all the fluctuations are in phase (Fig.6.19).Time averaging can then be performed in Eqn.s.6.46 in the following manner :

$$V = \frac{1}{T}\int_0^T \left[Q_r(T_1,T_2,T_3)\right]^{\frac{1}{2}}\,dt$$
$$= \frac{1}{T}\int_0^{.5T} \left[Q_r(T_1,T_2,T_3)\right]^{\frac{1}{2}}\,dt + \frac{1}{T}\int_{.5T}^{T} \left[Q_r(T_1,T_2,T_3)\right]^{\frac{1}{2}}dt$$

Therefore,

$$V = \overline{\left[Q_r(T_1,T_2,T_3)\right]^{\frac{1}{2}}} = \frac{1}{2}\left[Q_{rP}(T_1,T_2,T_3)^{\frac{1}{2}} + Q_{rN}(T_1,T_2,T_3)^{\frac{1}{2}}\right] \qquad (6.47)$$

Similarly, for the other velocity components

$$W=\overline{\left[Q_\theta(\mathfrak{T}_1,\mathfrak{T}_2,\mathfrak{T}_3)\right]^{\frac{1}{2}}}=\frac{1}{2}\left[Q_{\theta P}(\mathfrak{T}_1,\mathfrak{T}_2,\mathfrak{T}_3)^{\frac{1}{2}}+Q_{\theta N}(\mathfrak{T}_1,\mathfrak{T}_2,\mathfrak{T}_3)^{\frac{1}{2}}\right] \quad (6.48)$$

$$U=\overline{\left[Q_z(\mathfrak{T}_1,\mathfrak{T}_2,\mathfrak{T}_3)\right]^{\frac{1}{2}}}=\frac{1}{2}\left[Q_{zP}(\mathfrak{T}_1,\mathfrak{T}_2,\mathfrak{T}_3)^{\frac{1}{2}}+Q_{zN}(\mathfrak{T}_1,\mathfrak{T}_2,\mathfrak{T}_3)^{\frac{1}{2}}\right] \quad (6.49)$$

where tha additional indices P and N have been used in the same meaning as that in Eqn.6.44. It is worth noting that the direction of the mean velocity components are not required for the determination of the normal Reynolds stresses since they are squared in Eqn.s.6.43 .

In order to obtain Reynolds shear stresses, the following products are formed from Eqn.s.6.45

$$V_rV_z=\left[\,Q_r(\mathfrak{T}_1,\mathfrak{T}_2,\mathfrak{T}_3)\;Q_z(\mathfrak{T}_1,\mathfrak{T}_2,\mathfrak{T}_3)\,\right]^{\frac{1}{2}}$$

$$V_rV_\theta=\left[\,Q_r(\mathfrak{T}_1,\mathfrak{T}_2,\mathfrak{T}_3)\;Q_\theta(\mathfrak{T}_1,\mathfrak{T}_2,\mathfrak{T}_3)\,\right]^{\frac{1}{2}} \quad (6.50)$$

$$V_zV_\theta=\left[\,Q_z(\mathfrak{T}_1,\mathfrak{T}_2,\mathfrak{T}_3)\;Q_\theta(\mathfrak{T}_1,\mathfrak{T}_2,\mathfrak{T}_3)\,\right]^{\frac{1}{2}}$$

Substituting into Eqn.s.6.50 from Eqn.s.2.9 and then taking time average,

$$\begin{aligned}
UV+\overline{uv}&=\overline{\left[Q_r(\mathfrak{T}_1,\mathfrak{T}_2,\mathfrak{T}_3)\;Q_z(\mathfrak{T}_1,\mathfrak{T}_2,\mathfrak{T}_3)\right]^{\frac{1}{2}}}\\
&=\frac{1}{2}\left\{\left[Q_{rP}(\mathfrak{T}_1,\mathfrak{T}_2,\mathfrak{T}_3)\;Q_{zP}(\mathfrak{T}_1,\mathfrak{T}_2,\mathfrak{T}_3)\right]^{\frac{1}{2}}\right.\\
&\qquad\left.+\left[Q_{rN}(\mathfrak{T}_1,\mathfrak{T}_2,\mathfrak{T}_3)\;Q_{zN}(\mathfrak{T}_1,\mathfrak{T}_2,\mathfrak{T}_3)\right]^{\frac{1}{2}}\right\}\\
VW+\overline{vw}&=\frac{1}{2}\left\{\left[Q_{rP}(\mathfrak{T}_1,\mathfrak{T}_2,\mathfrak{T}_3)\;Q_{\theta P}(\mathfrak{T}_1,\mathfrak{T}_2,\mathfrak{T}_3)\right]^{\frac{1}{2}}\right.\\
&\qquad\left.+\left[Q_{rN}(\mathfrak{T}_1,\mathfrak{T}_2,\mathfrak{T}_3)\;Q_{\theta N}(\mathfrak{T}_1,\mathfrak{T}_2,\mathfrak{T}_3)\right]^{\frac{1}{2}}\right\} \quad (6.51)\\
UW+\overline{uw}&=\frac{1}{2}\left\{\left[Q_{zP}(\mathfrak{T}_1,\mathfrak{T}_2,\mathfrak{T}_3)\;Q_{\theta P}(\mathfrak{T}_1,\mathfrak{T}_2,\mathfrak{T}_3)\right]^{\frac{1}{2}}\right.\\
&\qquad\left.+\left[Q_{zN}(\mathfrak{T}_1,\mathfrak{T}_2,\mathfrak{T}_3)\;Q_{\theta N}(\mathfrak{T}_1,\mathfrak{T}_2,\mathfrak{T}_3)\right]^{\frac{1}{2}}\right\}
\end{aligned}$$

Reynolds shear stresses can be determined from Eqn.s.6.51 substituting for the mean velocity components.

6.7.EXPERIMENTAL PROCEDURE

6.7.1.Some considerations

It is well known that hot-wire measurements suffer from two major factors :

a)Drift on the readings due to temperature gradients and fluctuations :This might be caused on the present test rig due to the heating of the flow by the fan.Hot-wire anemometer measures the heat transfer loss from the wire to the surroundings.If the flow temperature increases, the heat transfer decreases and the voltage drops.This leads,therefore,to the indication of smaller velocities than the actual values. This can be compensated in two ways.Firstly,temperature measurements are made prior to hot-wire measurements.Then,the latter data are corrected according to the former.This way doubles the measurement time and effort.Besides,it can not be sufficiently correct since both the mean temperatures may change during the period from temperature measurements to hot-wire measurements and temperature fluctuations can not be compensated.Secondly, a temperature compensated probe is used.This has been the practice in this work (see Fig.6.2).The principle of this probe is that ,instead of using the variable bridge arm resistance of the anemometer unit,a resistance providing a recommended overheating has been fixed on the probe.When scanning the flow field,if the mean temperature is higher at some point than the other points the value of the compensation resistance increases.This causes the wire temperature to rise . In this way,the amount of heat transfer becomes proportional only to the velocity at that point. However,compensation of the temperature fluctuations can be achieved up to a moderate frequency level.Further errors,if any,due to this effect is neglected.The reason for this will be explained in Section 6.7.2 .

b)Drift on the readings due to ageing of probes :Ageing is caused due to the contamination of the hot-wire suspended in the flowing fluid.Normally,filtering is required. In this work,however,air was sucked by the fan with an orifice meter at a height of almost 11 ft.The incoming flow was,therefore, rather clean.Tests were still carried out, however,in order to check the effect of ageing.Since a calibration was intended before each scanning of a flow field,ageing would be effective during the time required for this purpose (see Fig.5.17).To this end,the temperature compensated hot-wire probe was left several times in the flow for long periods of time,such as,6 or 8 hours

and the voltages of the anemometer were examined frequently.It was observed that they showed no variation for this length of time.Besides,the voltage readings at zero velocity were quite constant even when severe day-to-day changes of atmospheric pressure and temperature occured.Clearly,this was also aided by the employment of a temperature compensated probe.However,it also showed that there was no ageing.For both reasons,it was decided that aging was not effective.

6.7.2.Calibration of the anemometer unit

A DISA 55D01 type anemometer was employed for the investigation.DC and RMS voltages were recorded from 55D31 and 55D35 type digital voltmeters.

When using a single sensor type probe,calibration of the anemometer unit is performed as follows :

a)Voltage measurement is made.
b)Current passing through the wire is measured (a suitable value is 3.5 mA).
c)Resistance of the connection lead is compensated.
d)Resistance of the hot-wire is measured.
e)Overheating ratio is adjusted.Care must be taken during this operation not to increase the wire temperature more than 300,otherwise the wire material starts oxidation. For most types of probes,the recommended value for the overheating ratio is 1.8 .
f)Anemometer is turned on to operation.The voltage value which is now readable from the DC voltmeter is due to the heat transfer from the wire by natural convection.In general,this value is taken as the voltage value at zero velocity.In fact,a smaller value must be determined from calibration since free convection causes a flow around the wire and this value is not the actual value at zero velocity.

This calibration is carried out at 1/20 bridge ratio and it is compulsory to use the adjustable resistance built in the anemometer unit.When the measurements are required in a flow field with temperature gradients,either several calibrations have to be made for the required temperatures or the hot-wire readings have to be corrected for the temperature differences from the calibration temperature. In both cases,hot-wire measurements must be preceded by temperature measurements.It is obvious that both procedures are very tedious and time consuming;also,temperature fluctuations can never be compensated.It is,therefore,much more suitable to use a temperature compensated probe.

Although a temperature compensated probe provides more correct and easier measurements and considerable time saving,it has a minor disadvantage.Because there are two sensors on this probe,two leads are required to connect it

to the anemometer unit.Since the adjustable bridge arm resistance is not used in this case,the anemometer unit operates at 1/1 bridge ratio.The two leads should,therefore,be completely identical.Otherwise, oscillations occur at high frequencies,causing a lower frequency response from the overall system.This has been checked by feeding a signal from a square wave generator (DISA 55D25 type Auxiliary Unit) and the frequency response has been found around 20 kHz at zero velocity.However,it is known that under non-zero velocity condition the frequency response increases considerably (Ref.59).It is expected that it becomes in the range of 30 to 40 kHz.This range is considered sufficient for the present case since it is known that contribution to the Reynolds stresses by the high frequencies more than 20 kHz is already negligible.

Calibration of the anemometer unit for the temperature compensated probe has been made as follows :

a)Voltage measurement is made.
b)Probe current is measured and adjusted.
c)Compensation for the resistance of the first lead is made at 1/20 bridge ratio,using a shorting probe and probe support relevant to the temperature compensated probe.Without changing the settings,the second lead is connected and is checked.If there is no change in the in the meter deflection,both leads have the same resistance.Proper setting can be achieved only after several trials.
d)It is always better to check the resistance values of both the wire and the temperature sensor,at least against the possibility that the latter is defective or broken.This can be performed in the usual way,using the adjustable bridge arm resistance at 1/20 bridge ratio.Failure to do this check will burn out the wire if the temperature sensor is defective or broken.
e)The probe is connected with the two leads to the probe and compensation resistance terminals on the anemometer unit.
f)The bridge ratio is adjusted to 1/1 .
g)The anemometer is turned on to operation.For the value of the voltage which is read on the DC voltmeter,the remarks in the item f) of the simple operational procedure apply equally.

6.7.3.Calibration of the temperature compensated hot-wire probe

Calibration of the temperature compensated hot-wire probe (type 55P81) was performed on the same test rig in the straight jet obtained without the swirlers in position in the nozzle. Turbulence intensity was approximately o.o2 (calculated according to the simple procedure,Eqn.6.22) in the straight jet at the nozzle exit.Calibration has been

carried out with the probe in horizontal position and the wire itself facing the velocity vector at a perpendicular direction (see Eqn.6.29).

The experimental procedure for the calibration of the hot-wire probe was as follows :

1)Atmospheric pressure was recorded.
2)The rig was run at maximum mass flow until a steady flow is obtained.This was achieved by checking the temperature and mass flow until they assume a constant value.Their values were recorded.The temperature probe was then taken out for it was increasing the level of turbulence in the straight jet at the nozzle exit to approximately 0.05 .
3)Starting from maximum mass flow rate,it was reduced to zero value.For each value of the mass flow, dynamic pressure and the corresponding voltage from the anemometer were taken.
4)A typical plot of these values,voltage squared versus root velocity, is shown in Fig.6.20 .Probably because of temperature compensation,no significant changes were observed in the calibration curve due to daily changes in atmospheric conditions.
5)It is known (Ref.81) that a curve of the form of Eqn.6.26 provides a better fit to the calibration curve.Fig.6.26. The coefficients of Eqn.6.26 were determined using the method of least squares.It was applied in the following manner (Ref.82):

$$\sum C\ U_e+\sum B\ U_e^{\frac{1}{2}}+K\ A\ =\sum \bar{E}^2$$

$$\sum C\ U_e^{\frac{3}{2}}+\sum B\ U_e+\sum A\ U_e^{\frac{1}{2}}=\sum \bar{E}^2 U_e^{\frac{1}{2}}$$

$$\sum C\ U_e^2+\sum B\ U_e^{\frac{3}{2}}+\sum A\ U_e=\sum \bar{E}^2 U_e$$

where K is the number of measurements during calibration. This equation system was solved to obtain the coefficients of Eqn.6.26 ,using determinant expansion.It should be noted that a better accuracy can be obtained as the number of measurements is increased.A value of K between 30 and 40 should prove enough for most applications.

An important point to remember is that in Eqn.6.26 , A should not be taken as the voltage value at zero velocity. It should be determined from calculation,performed excluding the voltage value at zero velocity from the experimental data. The reason is that at zero velocity the voltage indicated by the anemometer is spuriously higher than the actual value.This is due to the free convection from the wire.

A good fit to the calibration curve which is very essential in the whole procedure can be obtained in this way.

It was mentioned above that the effect of daily atmospheric conditions on the calibration curve was insignificant. Only slight changes occured in the calculated values of coefficients A,B and C. The coefficient B was most influenced by these changes. The differences in the values of A and C were very small.The important point is that how these changes in the values of A,B and C influence the results. An example is given in Tables 1 and 2 .It is seen that the variations in the determined velocity or stress terms are quite negligible.Clearly this was provided by the use of a temperature compensated probe.

6.7.4.Directional sensitivity tests

Tests were also carried out to determine the directional sensitivity of the temperature compensated hot-wire probe . It was rotated in the straight jet in the yaw and pitch directions (see Fig.6.8) to determine the variation of the heat transfer,that is,the voltage drop across the hot-wire (Fig.6.21).Variation was significant only in the yaw direction.The difference could increase up to 24% with respect to the voltage value at the initial straight orientation. The sensitivity in the pitchwise direction was,however, very insignificant.It was not therefore considered in this study and the pitch correction factor was taken as equal to unity. In Ref.71,it is reported as approximately 1.03 .If desired, however, incorporation of the pitch correction factor into the procedure does not present any diff culty at all.

The yaw correction factor was taken as 0.17 .This choice is substantiated by Ref.71 for a hot-wire probe with similar structure.It is reported as about 0.2 in Ref.59 .The effect of the choice of the yaw correction factor on the results were investigated.It can be seen from Tables 3 and 4 that the choice of the yaw correction factor does not influence the results significantly.In fact,the difference in the results are so small that a much larger difference in the value of the yaw correction factor would not change the general tendency in the graphs.

6.7.5.Measurement procedure

The hot-wire probe was located to the required position in the flow field using the traversing mechanism of the lathe. The probe arm was fixed to the same hole on the platform where the five-hole spherical pressure probe was also fixed for measurements (Fig.6.6).

The procedure for the measurement of a flow field was as follows :-

1)The rig was run until a steady flow was obtained.This was checked by observing the mass flow and temperature.These were recorded.

2)The probe was then located to the measurement points in the flow field as shown typically in Fig.6.17 .It was then rotated three times at every point.For each orientation, DC and RMS voltages were recorded.
3)Then,these values were fed into a computer program to make the calculations presented in Section 6.6 .

6.8.TEST APPLICATION TO A STRAIGHT ROUND JET

The procedure was applied to a straight jet obtained without the swirlers in position in the nozzle of the test rig.Nozzle velocity was approximately 100 ft/sec .Traverses were made at several stations along the jet axis. The variation of the axial velocity profile is shown in Fig.6.22 where the spread of the jet and decay of the velocities are observed.Normalized axial velocity profiles with respect to the maximum axial velocity at each axial station is shown in Fig.6.23 .It is seen that at the nozzle exit, a laminar velocity profile in a pipe is observed.Further downstream, the velocity profile expands and become similar to that occuring in the similarity region.Comparison is given with Ref.83 where the measurements were made in the similarity region of the jet (z/D>20).It is seen that quite good results are obtained with the present formulation.Integrating the axial velocity profile at the nozzle exit, mass flow was checked.Calculated mass flow was 96% of the measured mass flow with the orifice meter.Integration was performed by fitting a curve to the axial velocity profile.

The distribution of the shear stress $\overline{uv}$ is shown in Fig.6.24 .The potential flow region where the shear stress is not important can be observed quite clearly.Examination of Fig.6.22 also reveals a similar region at the boundary of which the axial velocity profiles start to deviate from their flat form.The decay of the shear stress in the flow field can be seen from Fig.6.24 .Its profile varies towards that existing in the similarity region. Normalized shear stress profile at station z/D=6.0 has been shown in Fig.6.25. Its maximum value is of the order of 0.003 which may seem a bit low .However,firstly the nozzle geometry,in the form two steps, causes the average flow velocity to decrease considerably apart from the other geometrical effects on the turbulence properties of the flow field.When the flow velocity decreases,the shear stresses decrease all over the flow field. Secondly,the value of shear stress in a flow field depends on the position of the fluid in the flow field.For a point further downstream region,its value is smaller. In Ref.84 , for instance,where the nozzle exit region of a round jet is examined,the maximum value in a profile of the normalized shear stress is 0.01 at z/D=2 ,0.009 at z/D=4 and 0.0074 at z/D=7.5 .It can be deduced,therefore,that at z/D=6 normalised

shear stress should be of the order of 0.008 .However, the nozzle velocity in this work was very high corresponding to a Mach number 0.3 .In the present straight jet, it is about 0.1 .Also,considering the effect of the nozzle geometry,this lower value of the normalized shear stress is justified.Distribution of the kinetic energy of turbulence is shown in Fig.6.26 .The peaks in the second and third profile curves develop due to the disturbance produced by the step at the nozzle exit.As it is seen,however, it decays rapidly at a distance of about six nozzle diameters and the profile of the turbulence kinetic energy becomes almost similar to that in the similarity region.Normalized values of the kinetic energy of turbulence is shown in Fig.6.27 where the transition from off-central peak form to central peak form can clearly be observed.Comparison has also been given with Ref.83 .However, the higher values of $\sqrt{k}/U_m$ in this reference is due to the measurements in the similarity region where the level of turbulence is higher. The increase in the level of longitudinal turbulence intensity has been plotted in Fig.6.28 where the decay of axial velocity along the jet axis has also been shown.Exactly similar results are reported in Ref.85 .The radial distribution of the longitudinal turbulence intensity is shown in Fig.6.29 where it is seen that turbulence increases in the downstream direction. Comparison is also given to indicate the qualitative similarity .However, complete quantitative consistency can not be expected because of the nozzle geometry in the present work.Also, in the reference given for comparison, the nozzle velocity was about three times larger than that in the present investigation.On the other hand,it is worth noting that there is even a good consistency in the quantitative form,especially in the central region of the straight jet where the flow was not effected much by the step in the immediate downstream region of the nozzle.

The purpose of this section was,rather than carrying out a complete investigation of straight round jets ,only to test the performance of the hot-wire formulation presented in Section 6.6 . As it was shown, it produced quite reasonable results.The differences from the other works were due to the step in the nozzle of the test rig.

6.9.ADVANTAGES AND DISADVANTAGES OF THE METHOD

Advantages can be outlined as follows :-

1)Easy to apply.
2)Single probe is used.Both calibration and measurement times are ,therefore,shorter.Operation during the measurements are significantly more convenient.
3)Recirculation zones can be detected rather easily.
4)Since it is sufficient to use a single wire probe,temperature compensation can be effected readily by using a

temperature compensated probe.

5)Since the number of orientations are as little as possible, the state of the flow can be considered as constant during the three orientations.

Disadvantages are :-

1)The assumption that the three voltages are square wave form and in phase.This might not be completely true. However,the mass flow obtained integrating the velocity profiles was quite consistent with the measured values. For this reason,the above assumptions can be considered as reasonable.

2)The formulation has not given zero swirl velocity on the jet axes.This might be,however, not due to an unrealistic formulation,but due to a slight asymmetry in the flow field.Also, the structure of the hot-wire probe can also cause the detection of non-zero swirl velocity on the axis.

CHAPTER 7. RESULTS AND DISCUSSION

7.1.INTRODUCTION

One of the most common ways of obtaining swirling flows is to employ a vane type swirler.Because the swirler is the main component dominating the flow in the primary zone of a conventional combustor, knowledge of the effects of its design parameters on the structure of the flow field where all the reactions of the combustion process are taking place,is vitally important to the combustor designer.Despite its importance,not much work has been done on swirlers.Currently,flat vane types are used most frequently.However,even for those,design data are not complete (see Chapter 1).

In this chapter results of the tests carried out to elucidate the influence of the swirler design parameters on the mass flow-pressure drop characteristics and the size and turbulence characteristics of the resulting recirculation region,are presented.Eleven swirlers with different design parameters,with either flat or curved vanes,were tested.They are shown in Fig.s.5.9 to 5.12 . The parameters for each swirler are listed below :-

Details of Swirlers

SWIRLER NUMBER	VANE TYPE	VANE ANGLE	ASPECT RATIO	SPACE-TO-CHORD RATIO
S.1	flat (C.)*	60	1	16 vanes
S.2	curved(O.C.)	60	1	16 vanes
S.3	curved(C.)	60	1	16 vanes
S.4	curved(C.)	60	1	12 vanes
S.5	flat (C.)	50	.4	16 vanes
S.6	flat (C.)	60	.4	16 vanes
S.7	flat (C.)	60	.4	12 vanes
S.8	flat (C.)	70	.4	16 vanes
S.9	curved(C.)	50	.4	16 vanes
S.10	curved(C.)	60	.4	16 vanes
S.11	curved(C.)	60	.4	12 vanes
S.12	curved(C.)	70	.4	16 vanes

7.2.FLOW CHARACTERISTICS AT SWIRLER EXIT

The flow characteristics inside the swirlers have not

* . C stands for central, O.C. for off-central See

been examined specifically.All attention has been focused on the exit conditions and the resulting flow field.However, a close examinations of the velocity profiles at the exit gives quite a reliable insight into the flow occuring within the swirler itself.

All measurements at the exit of the swirlers have been taken at an axial distance of .25" .The heads of the two probes have been placed in the middle of two vanes at the swirler exit.Typical axial velocity profiles at the exit of the three types of swirlers, S.1 , S.2 and S.4 , are shown in Fig.7.1 .The efficiency of curved vanes can be seen readily : more angular momentum can be imparted to the axial flow by using curved vanes.Therefore,most of the flow leaves the swirler near the outer wall of the swirler,that is,sharp peaks in the axial velocity profiles are obtained near the outer wall.These results are exactly consistent with those of Ref.21 ,where also almost flat axial velocity profiles were obtained at the exit of a tangential-air-entry type swirl generator for moderate and weak swirl cases.For strong swirl,however,the profiles had a sharp peak near the outer wall,similar to those obtained from the curved vane type swirlers in Fig.7.1 .Mostly, exit velocities in the immediate downstream of the vane type swirlers are not reported in the literature,for instance Ref.9 and 12 . This is because the flow is very complex and of small size in the immediate downstream of the swirler,with respect to the dimensions of the heads of the two probes.Any error due to this is neglected.

Examination of the other components of the absolute exit velocity aids more the understanding of the flow structure in the swirler and also explains the better performance of curved vanes,that is, addition of more angular momentum to the incoming purely axial flow. The radial distribution of the swirl velocity component at the exit from the same swirlers as those in Fig.7.1 is shown in Fig.7.2 .The ability of the curved vane type swirlers to impart a larger swirl velocity to the incoming axial flow is apparent.This means that for the same vane angle as that of a corresponding flat vane type swirler,a larger swirl number is created with curved vane type swirlers. Therefore, a larger recirculation region is inherently expected from a curved vane type swirler.

It can be deduced from examination of Fig.7.1 and 7.2 that the axial velocity profiles inside the swirler follows the following pattern (Fig.7.3a,b) : both circumferantial and radial distributions start with almost flat profiles. However,because of the swirl velocity component imparted to the flow a centrifugal force acts on each fluid particle in the swirler.Therefore,every fluid particle at the inlet tends to move radially outwaed along the length of the swirler (Fig.7.3b).Thus,most of the flow leaves the swirler near the outer wall.Circumferentially,accumulation of the flow occurs on the pressure surface (concave side) of the

vanes (Fig.7.3a) and the majority of the flow in a passage leaves the swirler close to the pressure side of the one of the surrounding vanes.In the immediate exit from the swirler,the flow is not axisymmetrical.However,because of the strong mixing characteristics of swirling flows such discontinuities are smoothed out very rapidly and the flow field can be assumed axisymmetric within a short distance from the swirler.If the swirl number is to be calculated by integrating velocity profiles it would be more proper to use profiles at some distance downstream from the swirler.

7.3.PRESSURE DROP-MASS FLOW CHARACTERISTICS

One of the most important performance parameters for a vane type swirler is its pressure drop-mass flow characteristic,more precisely,the knowledge of what pressure drop occurs through the swirler at a certain mass flow. The total pressure is here defined as

$$\Delta P = P_i - P_a \qquad (7.1)$$

This is plotted against mass flow in Fig.7.4 .It is obseved quite clearly that in all the cases flat vane type swirlers,for a given vane angle,aspect ratio and vane numbers (that is,space-to-chord ratio) produce larger pressure drop than the corresponding curved vane type swirlers (compare S.8 to S.12,S.6 to S.10,S.7 to S.11 and S.5 to S.9).For a larger value of aspect ratio (1.) similar results were obtained: flat vanes produced larger pressure drop (compare S.1 to S.4).However, the off-central design with curved vanes gave larger pressure drop (see S.2). Increasing vane number (that is,decreasing space-to-chord ratio) increases pressure drop for both flat and curved vane type swirlers.Its influence is more pronounced in the case of curved vane type swirlers (compare S.10 to S.11).Its effect ,however, is only slight for flat vane type swirlers (compare S.6 to S.7).Decreasing aspect ratio increases pressure drop in the case of both curved (compare S.4 to S.11) and flat vane type swirlers (compare S.1 to S.6).These results can be summarized as follows :-

a)Pressure drop is decreased by the use of curved vanes. However, off-central design gives larger pressure drop than the corresponding flat vane type.
b)Incresing vane angle increases pressure drop for both flat and curved vane type swirlers.
c)Increasing space-to-chord ratio decreases the pressure drop.Its effect is much more significant for curved type swirlers.

d)Increasing aspect ratio reduces the pressure drop very considerably.

Normalized values of the total pressure drop with the nozzle dynamic head has been shown in Fig.7.5.The same remarks as those mentioned above for Fig.7.4 apply. Furthermore,it is observed that all the curves tend towards a constant value above a mass flow of approximately .15 lb/sec .

The pressure drop normalized by the swirler inlet dynamic head is shown in Fig.7.6. It is observed that the flat vane type swirlers produce larger pressure drop coefficients than the corresponding curved vane type swirlers (compare S.8 to S.12,S.6 to S.10,S.7 to S.11 and S.5 to S.9). Increasing the space-to-chord ratio decreases the pressure drop coefficient for both flat (compare S.6 to S.7) and curved vane type swirlers (compare S.10 to S.11). Increasing the vane angle increases the pressure drop coefficient for both flat (compare S.5,S.6,S.7 and S.8) and curved vane type swirlers (compare S.9,S.10,S.11 and S.12). Decreasing the aspect ratio increases the pressure drop coefficient for both flat (compare S.1 to S.6) and curved vane type swirlers (compare S.4 to S.11). It is again observed that above a mass flow of about .15 lb/sec ,the pressure drop coefficient tends towards a constant value for each swirler.

The reasons for these results can be explained as follows : according to Ref. 86 ,where a method is presented to calculate the pressure drop coefficient in blade rows of axial flow turbines,the losses in blade rows can be divided to :-

a)Profile loss :This is due to the skin friction on and separation of flow from the blades.
b)Secondary loss :This is due to the three dimensional effects,particularly due to the interaction between the blade ends and the boundary layer on the annulus walls.
c)Tip clearance loss :This is due to the clearence between the blade ends and annulus wall.There is not such a loss in the swirlers of this work.
d)Annulus loss:This is due to the boundary layer friction on the annulus walls.In fact,the annulus loss is very much related to the secondary loss.For analyzing purposes purposes,however,they are considered separately.Because axial length of the swirlers in this work are rather short (less than 1"), this loss is considered very small.

The profile and secondary losses are, then,the main losses occuring in vane type swirlers.In the case of flat vanes,the profile losses are excessively large because the vanes run always under stalled conditions. A recirculation (separation) region is formed behind each vane and extracts

considerable energy from the main flow in the passages as it was explained in the Section 1.7.Additionally, such a separation region in a passage blocks the main flow area and increases the velocity gradients in the main flow region of the passage. Therefore,it causes the frictional loss to rise up rapidly. In the case of curved vanes,however, these energy dissipating eddies are not present over the substantial part of the vanes since they do not occur near the leading edge. Separation might occur over the suction (convex) side of the vanes near the trailing edge. It is seen,however, that the blokage in a passage due to a separation region has been avoided and this consequently reduces the frictional loss through the blade row extensively due to the resulting smaller velocity gradients. Secondly, the vanes do not run under stalled conditions and separation region which may occur near the trailing edge is expected to have much less influences on the flow field in the passage. Therefore, it does not cause energy dissipation through the swirler. A slight increase in the overall frictional loss which is due to the increased wetted area in the case of curved vanes in comparison to flat vanes is obvious. On the other hand, the total frictional loss is larger in the case of flat vanes due to the resulting separation regions. These are the reasons why less pressure drop is incurred in the case of the curved vane type swirlers. This can be seen from Fig.7.6 ,comparing the curves for S.8,S.6,S.7 and S.5 to S.12,S.10,S.11 and S.9, respectively.

The reason why the pressure drop increases for both flat and curved vane type swirlers with decreasing space-to-chord ratio (that is, increasing vane number) is simply that the wetted area increases. This increases both the frictional losses and the number of separation regions behind the vanes.All these factors cause more energy to be dissipated through the swirlers (see Fig.7.6, comparing S.7 to S.6 and S.11 to S.10).Similar results are also reported by Ref.86 (see Fig.7.6a).A point of minumum is observed on each curve.The increase on the right side of the curves are due to increasing separation losses at high space-to-chord ratios.For such high values of the space-to-chord ratio ,a proper overlap of the vanes can not be obtained and the turning flow separates from the convex surfaces of the vanes,while also increasing the pressure loss.For the lower values of the space-to-chord ratio,this inefficiency in turning the axial flow decreases .However,the wetted area increases,together with the velocity gradients in the passages.Both these factors increase the frictional loss rapidly as the space-to-chord ratio decreases,in consistent with the results presented above.The swirlers employed in this work had the following space-to-chord ratios (at blade mean heights) :-

number of vanes	16	12
aspect ratio : 1	.393	.523
.4	.511	.681

Comparing to Fig.7.6a,it is seen that all the swirlers run on the frictional loss side of the curves.It is also observed that they all lie in the region where losses are the least for practical vane anles,that is, 50,60 and 70.

Finally, the effect of the aspect ratio that increasing it reduces the pressure drop for both flat and curved vane type swirlers, can be explained as follows : If the aspect is increased while keeping the chord constant, the effect of the boundary layer on the main flow in the passage decreases. The secondary loss is, therefore, reduced.This means that increasing aspect ratio reduces the pressure drop (see Fig.7.6 comparing S.6 to S.1 and S.11 to S.4). Similar results have also been obtained in Ref.86 (see Fig.7.6b),where it is reported that changing the aspect ratio by changing the length of the chord and keeping aspect constant does not produce the same effect,since the secondary losses then are altered very insignificantly.

The pressure drop coefficient devided by both $tg\theta$ or $tg^2\theta$ and accordingly shown in Fig.7.7 by the curves numbered as S.8.1 and S.8.2 for the swirler S.8,etc., indicates that it is proportional to $tg\theta$ .For flat vane type swirlers

$$\frac{P_i - P_a}{.5\rho V_i^2 tg^2\theta} = 4. \quad \text{(for } h/c=.4\text{)} \qquad (7.2)$$

can be assumed roughly. Then, using Eqn.7.2 it is possible to calculate the total pressure drop from a flat vane type swirler for a given vane angle. For curved vane type swirlers with the aspect ratio of .4 ,however, the value of this constant reduces roughly to 1.25 . When the aspect ratio is increased, the deviation from the constant value, 1.25 , is only slight for the curved vane type swirlers (compare S.12.2 , S.11.2 , S.10.2 and S.9.2 to S.4.2) . However, the deviation for the flat vane type swirlers is excessively large (compare S.8.2 , S.7.2 , S.6.2 and S.5.2 to S.1.2). Therefore, Eqn.7.2 can not be used to calculate even roughly the total pressure drop for the flat vane type swirlers. For a different aspect ratio, a completely different constant must be determined experimentally. For curved vane type swirlers,however, it can be used with relatively good accuracy irrespective of the aspect ratio, only by replacing the constant 4 by 1.25 .

Much less pressure drop created by the curved vane type

swirlers can be seen more clearly by plotting the pressure drop from the curved vane type swirlers normalized by the pressure drop from the flat vane type swirlers versus vana angle for the corresponding swirlers (Fig.7.8). It is seen that all the values are below .4 and the curved vane type swirlers yield much less pressure drop than the flat vane type swirlers.

The constant values of the pressure drop coefficient for each swirler (see Fig.7.6) over a mass flow of .15 lb/sec are shown in Fig.7.9 as a function of the vane angle. It is seen quite clearly that the curved vane type swirlers produce much less total pressure drop than the flat vane type swirlers. The difference increases very rapidly as the vane angle is increased. For the both types of swirler , increasing the space-to-chord ratio decreases the total pressure drop coefficient. This is more pronounced for the curved vane type swirlers.

The static pressure drop through the swirlers, which is defined as

$$\Delta p = p_i - (p_e)_{axis}$$

was also investigated. It is observed from Fig.7.10 that the curved vane type swirlers induce much less static pressure drop in comparison to the corresponding flat vane type swirlers (compare S.8 to S.12, S.6 to S.10, S.7 to S.11 and S.5 to S.9). The influence of reducing the number of the vanes (or, increasing the space-to-chord ratio) is the same for both the curved (compare S.10 to S.11) and the flat vane type swirlers (compare S.6 to S.7), such that it decreases the static pressure drop. However, this effect was much more pronounced for the curved vane type swirlers. Increasing the aspect ratio reduces the static pressure drop for both the flat (compare S.6 to S.1) and the curved vane type swirlers (compare S.11 to S.4). The effect of increasing the vane angle is to increase the static pressure drop for both the curved (compare S.12, S.10 and S.9) and the flat vane type swirlers (compare S.8, S.6 and S.5). The normalized values of static pressure drop with the avarage nozzle dynamic head is given in Fig.7.11 . The same remarks as above also apply to this figure. It should be noted that above a mass floww of .15 lb/sec , all the curves tend towards constant values. This shows that the static pressure drop is not dependent on the mass flow rate any more.

The normalized values of the static pressure drop with the swirler inlet dynamic head is given in Fig.7.12. It is seen that all the curves tend towards constant values. Actually it can be assumed that above a mass flow

of .13 lb/sec , they are not dependent on the mass flow. As for the total pressure drop, the static pressure drop coefficient is much higher for flat vane type swirler in comparison to the curved vane type swirlers (compare S.8 to S.12 , S.6 to S.10 , S.7 to S.11 and S.5 to S.9) . Increasing the vane angle increases the static pressure drop coefficient both for the flat (see S.5 , S.6 and S.8) and the curved vane type swirlers (see S.9 , S.10 and S.12). Increasing the space-to-chord ratio decreases the static pressure drop coefficient for both the flat (compare S.6 to S.7) and the curved vane type swirlers (compare S.10 to S.11). For the flat vane type swirlers, if the aspect ratio is increased, the static pressure drop coefficient decreases (compare S.6 to S.1). For the curved vane type swirlers,however, it increases (compare S.11 to S.4). This is due to the less blokage created by the curved vane type swirlers than those having flat vanes. For the latter,increasing the aspect ratio decreases the blokage very rapidly.For the former,however, the decrease in the blokage is much less. Therefore,the static pressure drop is smaller than that of the flat vane type swirler for a given mass flow (see Fig.7.10 and 11).However, the inlet dynamic head drops very considerably in both types for increased aspect ratios. Thus, increasing the aspect ratio increases the static pressure drop coefficient for the curved vane type swirlers.

The constant values of the static pressure drop coefficient for each swirler (see Fig.7.12) above a mass flow of .13 lb/sec are shown in Fig.7.13 as a function of the vane angle. It is again observed that the curved vane type swirlers produce much less static pressure drop than the flat vane type. For both the curved and flat vane type swirlers the pressure drop increases with increasing vane angle and decreasing space-to-chord ratios.

7.4.VARIATION OF THE STATIC PRESSURE ALONG THE AXIS

The distributions of the static pressure along the axes of the jets issuing from the flat and curved vane type swirlers are shown in Fig.7.14 .For all the swirlers , except for S.1 , the distribution starts with a decrease towards a minumum (the peaks). After this minumum value , the static pressure increases towards atmospheric pressure asmthotically.The peaks coincide with the position of the centre of the recirculation region for each swirler. Therefore, the position of the peak of each curve along the axis gives insight into the size of the recirculation region created by that swirler.It is observed that the centre of the recirculation region is shifted slightly

in the downstream direction as the vane angle is increased for the flat vane type swirlers (see S.5 , S.6 and S.8) . It is also accompanied by a decrease in the minimum value of the static pressure . These results are completely in consistent with those of Ref.8 . If the space-to-chord ratio is increased (compare S.6 with S.7) ,the centre of the recirculation region moves further downstream and the value of the minimum static pressure increases . In the case of the curved vane type swirlers , however , the centre of the recirculation region moves downstream as the vane angle increases (see S.9 , S.IO and S.I2) . It is also observed that the value of the minimum static pressure increases as the vane number increases . When the aspect ratio is increased to I in the case of the flat vane type swirlers , the normalized static pressure increases considerably (compare S.6 with S.I) . Also , no peak is observed. For the curved vane type swirlers , however , the peaks appear in the distribution of the static pressure (see S.4 and S.II) and their positions are shifted in the upstream direction . It is concluded that distribution of the static pressure along the axis of the jets is rather irregular for the different types of swirlers with different design parameters and can not be formulated in a simple mathematical form . Similar irregular distributions are also reported in Ref. 9 .

7.5.VELOCITY DISTRIBUTIONS

It is appearent from Section I.I that flame stabilization in a flow strongly depends on its structure;the structure of a flow field is determined from profiles of the flow properties. The size of a recirculation region in a flow field can be determined,for instance,from the axial velocity profiles;forced vortex core is observed from the swirl velocity distributions. These will be presented in this section to examine the structure of the flow fields.

All the field investigations in the flows issuing from the swirlers S.I,S.4,S.6,S.9,S.IO,S.II and S.I2 have been made at a constant mass flow of O.I36 lb/sec .This mass flow has produced an average nozzle velocity of 36 ft/sec .This nozzle velocity corresponds to an average swirler inlet velocity of 4I ft/sec for the swirlers having the aspect ratio of I and to 78 ft/sec for those having the aspect ratio of 0.4 .Defining several Reynolds numbers as

$$Re_{de} = \frac{U_i (D-d)}{\nu} \qquad \text{(Ref.8)}$$

$$Re_{ci} = \frac{U_i \, c}{\nu} \qquad (7.3)$$

$$Re_{co} = \frac{V_o \, c}{\nu}$$

corresponding flow parameters for the swirlers can be calculated as follows:

Swirler	B.R.*=$(\frac{d}{D})^2$	U_i	V_o	$Re_{de}I\bar{O}^4$	$Re_{ci}I\bar{O}^4$	$Re_{co}I\bar{O}^4$	S
S.I	0.II	4I	82	4.3	2.I	4.3	I.25
S.4	0.II	4I	82	4.3	2.I	4.3	I.25
S.6	0.537	78	I56	3.3	4.I	8.2	I.5I
S.9	0.537	78	I2I	3.3	4.I	6.3	I.04
S.I0	0.537	78	I56	3.3	4.I	8.2	I.5I
S.II	0.537	78	I56	3.3	4.I	8.2	I.5I
S.I2	0.537	78	228	3.3	4.I	I2.0	2.40

The swirl number S has been calculated here according to Mathur and Maccalum's definition for a vane type swirler,Eqn.3.37 (Ref.8).It is seen from this table that the range of Rede is between 33000 and 43000 .This range is consistent with the range investigated in other works;for instance,Mathur and Maccalum tested their annular swirlers in the range of Rede from I7000 to 600000 .Since the primary concern in this study is the immediate downstream region of the swirlers,the measurement range extended up to a maximum distance of 4D in the axial direction.

A convention in the form of writing has been adopted to provide convinience in the comparisons to the reader:in the comparison section of a sentence the order of the swirlers has been arranged in the direction of what is said in the main part of that sentence.For instance,when saying 'The length of the recirculation region increases as the vane angle is increased (compare S.9 with S.I0 and S.I2).',the vane angle increases from S.9 to S.I2 .

7.5.I.Axial Velocity Distributions

Profiles of the axial velocity in the jets issuing from the swirlers S.I,S.4,S.6,S.9,S.I0,S.II and S.I2 are shown in Fig.s.7.I5 to 2I .Degree of swirl is high in all the cases ; there is therefore a toroidal recirculation region in every flow field.The core of the recirculation region is occupied by a reverse flow zone on the boundary of which the axial velocity is zero.The boundary of the reverse flow zone which is also called as zero velocity line has been shown with dashed lines in the figures.Solid line shows the boundary of the recircula-

*: B.R. stands for blokage ratio.

tion region where the stream function which is calculated with

$$U = \rho \int_0^r U\, r\, dr \qquad (7.4)$$

has zero value and forward mass flow is equal to reverse mass flow.The strong swirl in the flow and the consequent toroidal recirculation distorts the shape of the axial velocity profiles from the Gaussian form encountered in a straight jet at axial distances beyond 8D .Considering also the other half of the plane (-r side),it is seen that there are always in the profiles of the axial velocity two peaks with a trough in the middle.The profiles do not tend to Gaussian form within the range of investigations,up to 4D.Gaussian form in the axial velocity profiles is encountered at the axial station of z/D=I.0 in the case of a weakly swirling flow obtained by rotating a pipe (Ref.25).In the case of more strongly swirling jets it has been observed that the Gaussian form occurs at axial distances beyond z/D=I2(Ref.6). It is also reported by Mathur and Maccalum (Ref.8) that the Gaussian form is not encountered within axial distances of up to z/D=7.0 in strongly swirling jets issuing from flat vane type swirlers.Domination of the two-peak profile form prevails over longer distances in the downstream direction as the swirl number increases,for instance in the case of S.I0 and S.I2 (see Fig.s. 5.I9 and 2I).This is also reported by Mathur and Maccalum for flat vane type swirlers(Ref.8).The shape of the profiles change rapidly in both the axial and radial directions.The positions of the maximum gradients in the axial velocity profiles coincide with the boundary of the reverse flow zone in every flow field. In particular close to swirler exit,these gradients are of the order between 2 and $5xI0^{-4}sec^{-1}$.Values of the reverse velocities are of the same order of the values of the forward velocities for every flow case.

Variation of the profiles of the normalized (with respect to swirler inlet velocity) axial velocity along the jet axis of the swirler S.I is shown in Fig.7.22 .It is seen that reverse velocities are present in the profiles close to the swirler exit.The jet expands in the downstream direction and the peak values in the profiles drop continuously.The reverse velocities disappear and the profiles tend to a flat form at the axial station of z/D=2.5 .It is expected that they take the form of the Gaussian curve further downstream.It is seen that the width of the reverse flow zone decreases in the downstream direction.Similar trends are observed in the variation of the profiles of the normalized axial velocity in the flow field of the swirler S.4 (Fig.7.23). This swirler has curved vanes and can produce therefore better swirl on the flow than that of S.I .The consequence of this is that a larger reverse flow zone is induced and the peak value of the normalized axial velocity at the swirler exit,for instance at z/D=I.0 is less (about I.2) than that of S.I which is about I.42 .Also,the positions of the peaks at the corresponding axial stations are further away from the jet axis and the jet expands more rapidly in the latter case.The peak values drop in the down-

stream direction for this swirler as well.Profiles of the normalized axial velocity at several axial stations in the flow fields of S.6 and S.IO are shown in Fig.s.7.24 and 25 ,respectively . Exactly a similar picture is observed.Since these swirlers have larger swirl numbers,larger reverse flow zones are induced; the peak values are less than those of S.I and S.4 and the negative values do not disappear in the profiles within the range of investigations.The peaks similarly drop in the downstream direction following the expansion of the jets.Also S.IO can produce more swirl than S.6 since it has curved vanes;the result is that its peak value is less than that produced by the swirler S.6 .

Variation of the normalized axial velocity on the jet axis for different swirlers are shown in Fig.7.26 .For every swirler, reverse velocities occur on the jet axis in the immediate downstream region and the flow moves in the upstream direction.The reverse velocities disappear further downstream at a distance depending on the degree of swirl imparted to the flow and the flow moves in the downstream direction.The positions of the peak reverse velocities are at about z/D=I.0 and this does not seem changing considerably with the degree of swirl (except for S.I).Similar results are reported by Mathur and Maccalum (Ref.8) for swirling jets issuing from flat vane type swirlers,who have found that the peak reverse velocities are observed to occur at about z/D=I.0 (see the dashed lines).Decreasing the aspect ratio from I to 0.4 (reducing the area of the gap) increases the peak reverse velocity considerably in the case of flat vanes (compare S.I with S.6).In the case of curved vanes,however,decreasing the aspect ratio reduces the peak reverse velocity (compare S.4 with S.II).Effect of vane type is such that curved vane type swirler produces less reverse axial velocity (compare S.6 with S.IO);this may be due to larger reverse flow zone produced by the curved vane type swirler S.IO;consequently lower velocities are obtained. Increasing the vane angle firstly increases the maximum reverse velocity for curved vanes (compare S.9 with S.IO).Further rise, however,decreases the peak reverse velocity (see S.I2). Mathur and Maccalum (Ref.8) reports that the peak reverse velocity drops if the vane angle is increased from 60° to 75° for the case of flat vanes.Comparison of S.I with the corresponding (same blockage ratio,vane number and vane type) 60° swirler of Ref.8 shows that the latter induces larger reverse velocities. This is due to the fact that the swirler S.I can not produce as much swirl as the other since the latter swirler has good overlap on the vanes although the number of vanes is less in the latter case.The values and positions of the maximum reverse velocities for different swirlers are given in the table below:

VANE SWIRLER (curved)	$(\frac{U}{U_i})_{max}$	Position z/D	VANE SWIRLER (flat)	$(\frac{U}{U_i})_{max}$	Position z/D
S.4 (60,I2,d/D=.33)	0.69	0.5	45,8,d/D=.324	0.35	I.0
S.9 (50,I6, .73)	0.55	0.8	60,8, .324	0.77	I.0
S.IO(60,I6, .73)	0.65	I.0	70,8, .324	0.76	I.0
S.II(60,I2, .73)	0.565	I.0	75,8, .324	0.72	I.0
S.I2(70,I6, .73)	0.60	I.0	(all swirlers above from Ref.8		
			S.I(60,I6,.33)	0.29	0.25
			S.6(60,I6,.73)	0.83	I.0

Variation of the normalized mass flow in the reverse flow zone along the jet axis is shown in Fig.7.27 for the swirlers of this work.The maximum values of the reverse mass flows occuring in the jets of Mathur and Maccalum's (Ref.8) flat vane type swirlers are also shown in the figure (since the positions of the maximum reverse mass flows have not been given in this referance,they have been shown in Fig.7.27 at an arbitrary axial station,z/D=I.3 ,around which the width of the reverse flow zone is maximum for different swirlers). Amount of the reverse mass flow is closely related to the strength of recirculation.In flame stabilization with vortex flows,since the heat transferred to the fresh fuel-air mixture by the hot combustion products from the reverse flow zone is directly proportional to the amount of the reverse mass flow, its determination is particularly important for combustion applications.Axial distribution of the normalized reverse mass flow has been calculated with the numerical integration of the equation

$$\frac{m_r}{m_o} = \frac{2\pi\rho\int_o^{r_o} U\, r\, dr}{m_o} = \frac{W_r}{W_o} \qquad (7.5)$$

at several axial stations in the reverse flow zone. In Eqn.7.5, r_o is the radius of the boundary of the reverse flow zone at a particular axial station.The maximum reverse mass flow occurs in a flow at the axial position of the eye of the recirculation region.It is observed from Fig.7.27 that the maximum values always occur between z/D=0.6 and I.0 for the swirlers in this work.The recirculating mass flow increases :
a)with increasing vane angle in the case of curved(compare S.9, S.IO with S.I2) and flat vanes (compare 45°,60°,70° and 75°flat vane swirlers of Ref.8),
b)with decreasing aspect ratio in the case of curved (compare S.4 with S.II) and flat vanes (compare S.I with S.6),
c)with the use of curved vanes (compare S.6 with S.IO),
d)with increasing number of vanes (compare S.II with S.IO).
Comparison of the 60° flat vane swirler of Ref.8 with the corresponding 60° flat vane swirler S.I (both have the blockage ratio of O.II) shows that the reverse mass flow is higher in the case of the former although there are more vanes in the latter.The difference is due to the better overlap on the vanes of the swirlers of Ref.8 .If curved vanes are employed,however, the reverse mass flow increases (see S.4) since curved vanes can provide a better overlap and a consequent swirl on the flow. Comparison of 70° flat vane swirler of Ref.8 with S.I2 shows that much more reverse mass flow is induced by the latter ; apart from curved vanes,much larger blockage ratio on the swirler S.I2 may cause the difference.

Variation of the normalized reverse mass flow along the jet axis of a tangential-air-entry type swirl generator investigated

by Syred et al.(Ref.26) is also shown in Fig.7.27 .This flow has a swirl number of 2.2 and the maximum value of the normalized reverse mass flow is $0.83m_o$ .The position of this maximum reverse mass flow is very close to swirler exit due to the type of this swirl generator;there is not a physical blockage such as a hub,obstructing the way of the reverse flow at the swirler exit.The reverse flow can therefore penerate the swirl generator and the position of the maximum reverse mass flow nears the swirler exit.It must be noted that a similar amount ($0.76\ m_o$) of reverse mass flow can be obtained with a curved vane type swirler, S.IO ,which has a much smaller swirl number, I.5I .Also shown in this figure are the distributions of the reverse mass flow in the wakes of three baffles,B.I,B.2 and B.3,investigated by Davies (Ref.79).The baffles have the blockage ratios of 0.II,0.25 and 0.54,respectively.For the swirlers in this work the aspect ratio of I corresponds to a blockage ratio of 0.II and 0.4 to 0.537 .If a comparison is made between a corresponding (in terms of B.R.) baffle and a swirler, significance of the blockage ratio in obtaining higher reverse mass flow is revealed.For the B.R.=0.II if S.I and B.I are compared,the latter recirculates the same maximum reverse mass flow although there is swirl in the case of S.I .The length of the recirculation region of the swirler S.I,however,is more than that of B.I due to swirl.For the same blockage ratio,as the swirl imparted to the flow is increased (for instance,using curved vanes) the maximum reverse mass flow increases rapidly (compare S.4 with S.I and B.I).If the B.R. is increased to 0.54, the reverse mass flow increases proportionally in the case of baffles (see B.I,B.2 and B.3).If a comparison is made between a swirler,S.9, and a corresponding baffle,B.3, for the blockage ratio of 0.54 ,it is seen that the same maximum reverse mass flow is induced.The size of the recirculation region,however. is larger and the position of the peak is further away from the exit in the case of the swirler S.9 as it is the case for the blockage ratio of 0.II .For these reasons,the average velocity normal to the boundary of the reverse flow zone near the swirler exit (before the eye of the recirculation) is less in the case of swirlers in addition to the decrease in the level of axial velocities due to swirl.All these factors show why better flame stabilization at high mass flows can be achieved when vane type swirlers are employed. As in the case of the blockage ratio of 0.II ,for the blockage ratio of 0.54 as well,the reverse mass flow increases very rapidly with swirlers having higher swirl numbers (from $0.26m_o$ for the baffle B.3 and the swirler S.9 up to $I.6m_o$ for the swirler S.I2 having 70° curved vanes).

Variation of the maximum reverse mass flow with the swirl number for Mathur and Maccalum's (Ref.8) flat vane type swirlers and for the swirlers of this work is shown in Fig.7.28.It is seen that the maximum reverse mass flow increases with increasing swirl number in the case of both flat and curved vanes.It is also observed that curved vanes produce larger reverse mass flows for a certain swirl number (see S.9,S.IO and S.I2).It must be recalled,however,that these swirlers namely S.9,S.IO and S.I2, have a much larger blockage ratio than that of 60°,70° and 75°

flat vane swirlers of Ref.8 .Actually it seems that this differance in the blockage ratio causes the increase in the maximum reverse mass flow in the case of the swirlers S.9,S.IO and S.I2 .The reason for this is explained as follows : the swirler S.I and 60° swirler of Ref.8 have almost the same blockage ratio,the vane angle and flat vanes;the latter,however,has a better overlap of the vanes and can therefore produce better swirl than that of S.I .The indications for this can be seen from Fig.7.26,32 and 48;for instance,S.I has a much smaller reverse velocity (see Fig.7.26) and a much larger axial velocity peak at the swirler exit (see Fig.7.32).The maximum reverse mass flow is therefore less in the case of S.I .The swirler S.4, on the other hand,have similar parameters to those of S.I ,but it has I2 curved vanes;the curved vanes can provide a good overlap as in the case of the 60° swirler of Ref.8 and S.4 has a similar maximum reverse mass flow to that of the 60° swirler of Ref.8 .The fact that S.I and the 60° flat vane swirler of Ref.8 have very similar flow structures can be seen from the examination of Fig.s.7.26,32 and 48 .The actual effect of the vane type on the reverse mass flow is seen from the examination of the swirlers S.6 and S.IO both of which have exactly the same parameters .It is seen that keeping the other parameters constant,the curved vane type swirler S.IO produces larger reverse mass flow .

Variation of the reverse mass flow with the vane angle is shown in Fig.7.29 .This figure is very similar to Fig.7.28; it shows that maximum reverse mass flow increases with increasing vane angle in the case of both curved (see S.9 ,S.IO and S.I2) and flat vanes (see 60°,70° and 75° swirlers of Ref.8).The use of this figure is to show the net effect of the blockage ratio which is also included in the definition of swirl number according to Eqn.3.37 .It is seen that increasing the blockage ratio increases the maximum reverse mass flow in the case of both flat (compare S.I with S.6) and curved vane type swirlers (compare S.4 with S.II).Comparison of S.6 with S.IO shows that maximum reverse mass flow increases when curved vanes are employed. All the remarks about the difference in the two curves in Fig.7.28 equally apply to the curves in Fig.7.29 .Briefly,the difference is a combined effect of vane type and blockage ratio;in fact , mostly due to the latter since for the same blockage ratio the type of vane is not very effective (see S.4 and S.I).

The jets expand more rapidly as the degree of swirl is increased.In every flow field,the positions of the peaks in the axial velocity profiles move continuously outwards in the downstream direction due to this expansion while their values also decay.As it is well known this decay of the axial velocity profiles is very significant for combustion applications since when the decay rate is high,this increases the residence time of the fuel-air mixture in the combustor and therefore aids towards more complete burning.Decay of the peak values in the axial velocity profiles is faster as the degree of swirl is increased;this is shown in Fig.7.30 .Similar results are also

reported by Mathur and Maccalum (Ref.8) for flat vane type swirlers (see the dashed lines in the figure).The rate of decay increases :
a)as the vane angle is increased in the case of curved (compare S.9,S.I0 and S.I2) and flat vanes (see the dashed lines for the 60°,70° and 75° flat vane swirlers of Ref.8),
b)as the aspect ratio is reduced in the case of flat (compare S.I with S.6) and curved vanes (see S.4 and S.II),
c)as the number of vanes is increased for the curved type (compare S.II with S.I0).
Influence of the vane type on the decay of the peak values does not seem very pronounced for the initial region up to z/D=2.75; further downstream,however,the decay is faster for the swirler having curved vanes(see S.6 and S.I0).The 60° swirler of Ref.8 can be compared with the corresponding swirler S.I which has the same vane angle,vane type and blockage ratio;the decay rate is faster for the former since it has better overlap of the vanes and can produce consequently more swirl on the flow.If more swirl is produced,for instance using curved vanes,the decay increases for the same blockage ratio as that of S.I (see S.4).

Sufficient residence time for fuel and combustion products is required for the completion of burning in the combustor. Residence time decreases as the level of velocities increases in the combustor.In swirl flow combustors,residence time depends on the level of axial velocities.In order to increase the residence time and also to promote the stability of the flame, smaller axial velocities are desired. Comparison of the normalized axial velocity profiles for different swirlers at several axial stations are shown in Fig.s.7.3I to 34 .Also included in these figures are the relevant profiles from Ref.8 .It is seen from Fig.7.3I that as the degree of swirl is increased with either increasing the vane angle or decreasing the aspect ratio, the reverse flow zone expands;also,the peak value of the axial velocity decreases and occurs at a larger radial distance. For instance,as the vane angle is increased from 50° to 70° in the case of curved vanes (see S.9,S.I0 and S.I2),the peak value of the axial velocity at the exit of the swirler drops from I.0 to about 0.4 and the reverse flow zone expands considerably from r/D=0.29 to 0.7 .The position of the peak value moves from about r/D=0.5 for S.9 to more than r/D=I.0 for S.I2 .Effect of the aspect ratio is similar in the case of both flat and curved vanes:decreasing the aspect ratio from I to 0.4 decreases the peak forward velocity and shifts its position to a larger radial distance in the case of both flat (see S.I and S.6) and curved vanes (see S.4 and S.II) .A comparison of the profiles of S.6 and S.I0 shows that curved vane type swirlers can produce larger reverse flow zone with almost equal peak forward velocities. In the case of curved vanes,a larger reverse flow zone can be obtained by increasing the vane number (see S.II and S.I0). It is also seen that the 75° flat vane swirler of Ref.8 has quite a similar profile to that of S.I2 in the reverse flow zone, however,the reverse flow zone is larger for the former.

These trends are also observed in the axial velocity profiles further downstream at z/D=I.75 for the swirlers in this work

(Fig.7.32) .Profiles of the axial velocity at the axial station z/D=2.07 for 60°,70° and 75° flat vane swirlers of Ref.8 have also been included.It is seen that the peak values drop and the width of the reverse flow zone increases in the case of flat vanes as well,as the vane angle is increased.Comparison of the 60° swirler of Ref.8 with the corresponding flat vane swirler S.I shows that smaller forward and larger reverse velocities and a larger reverse flow width are obtained from the former . This may be due to better overlap of the vanes on the 60° swirler of Ref.8 .However,the difference in the axial positions of the profiles must be noted .Comparison of 60° swirler of Ref.8 with S.4 shows that peak values are quite similar and curved vanes can turn the flow quite efficiently;the reverse velocity is,however,slightly higher in the case of flat vanes.

Profiles of the axial velocity at the axial station of z/D=2.5 are shown in Fig.7.33 .A comparison of the general appearance of this figure with those of Fig.s.7.3I and 32 clearly shows the rapid expansion of the jets,such that the range of measurements in the radial direction (up to r/D=I.0) can not accommodate the peaks in the case of some swirlers , for instance S.I2 .The trend of the profiles are similar to that at the axial station of z/D=I.0 .

Profiles of the axial velocity at the axial station of z/D=3.25 are shown in Fig.7.34 where the axial velocity profiles at the axial station z/D=3.I for the 60° and 70° swirlers of Ref.8 are also included.It is seen that the jets have expanded and the peaks are beyond the range of measurements in the radial direction.The peak values have decreased rapidly and the reverse velocities in the profiles have disappeared at this axial station,for instance for the swirlers S.I,S.4 and S.9 .

A recirculation region is set up in the flow field of every swirler.The upstream stagnation point of the recirculation region is always at the hub exit;position of the downstream stagnation point depends on the degree of swirl given to the flow and is not very stable.The level of velocities is low around the downstream stagnation point.There is no any indication of the closure of the recirculation region within the range of investigations in the case of some swirlers, for instance S.I2 .The stream function has zero value at the boundary of the recirculation region and it can be calculated using Eqn.7.4 .A comparison of the size of the recirculation regions induced in the flow fields of the swirlers in this study has been made in Fig.7.35 .It is observed that :
a)increasing the vane angle increases the size of the recirculation region in the case of curved vanes (compare S.9 and S.IO with S.I2),
b)decreasing the aspect ratio increases the size of the recirculation region in the case of both curved (compare S.4 and S.II) and flat vane type swirlers (see S.I and S.6),
c)curved vane type swirler produces larger recirculation region than that of the corresponding flat vane type (see S.IO and S.6),

d)effect of the number of vanes does not seem very pronounced in the case of curved vanes;the length of the recirculation is altered slightly.The width,however,is more strongly affected and increased with increasing number of vanes (compare S.II with S.IO).From Ref.s.2I and 79,three recirculation regions are also included into Fig.7.28 (see the dashed lines).The short ones are produced with two baffles having the blockage ratios of 0.54 and 0.II,respectively (Ref.79);these are also the values of the blockage ratio in this work.The third recirculation region has been obtained with a tangential-air-entry type swirl generator (Ref.2I) and the issuing swirling flow has a swirl number of I.57 .It is seen that a baffle produces a very small recirculation region for small values of the blockage ratio,that is,for 0.II (see B.I).If a swirl is introduced to the flow at the same blockage ratio as that of B.I,the size of the recirculation region increases rapidly (see B.I and S.I);the width,however, seems to remain almost constant.If the swirl imparted to the flow is increased keeping the blockage ratio constant,for instance using curved vanes,the size of the recirculation region (both width and length) increases considerably (see B.I and S.4). In the case of baffles,increasing the blockage ratio to 0.54 increases both the length and width of the recirculation region (see B.I and B.3).If a moderate swirl is introduced to the flow at this blockage ratio,an exactly similar situation to that of B.I and S.I is observed:the length of the recirculation region increases quite rapidly while its width remains almost constant (see B.3 and S.9 comparing their relation with that of B.I and S.I). If a higher swirl is introduced to the flow at this blockage ratio,the size of the recirculation region (both length and width) increases very rapidly (see S.6,S.IO,S.II and S.I2 and compare with B.3 and S.9).Also,it is seen that tangential-air-entry type swirlers produce quite compact recirculation regions.Although the swirl number for this swirler is higher than those of the vane swirlers S.6 and S.IO,its recirculation region is much smaller than those of these vane swirlers.The peak of the curve is close to the swirler exit due to unpresence of hub in the case of the tangential-air-entry type swirler as explained previously.

A reverse flow zone occupies the core of every recirculation region.In combustion applications,hot combustion products flow in the upstream direction from this reverse flow zone and ignites the fuel-air mixture.It is therefore very important for flame stabilization and its characteristics play a significant role on the shape of the flame.A comparison of the sizes of these reverse flow zones is given in Fig.7.36 .It is seen that the size of the reverse flow zone increases :
a)with increasing vane angle in the case of curved vanes (see S.9,S.IO and S.I2),
b)with decreasing aspect ratio in the case of flat (see S.I and S.6) and curved vanes (see S.4 and S.II),
c)with the use of curved vanes (see S.6 and S.IO).
The length and width of the reverse flow zone are not influenced significantly with the number of curved vanes investigated in this work (I2 and I6 vanes for the swirlers S.II and S.IO , respectively);it altered slightly the shape of the reverse flow zone.The position of the maximum width of the reverse flow zone is closer to swirler exit in the case of the swirler S.IO since it has more vanes than S.II and can therefore give a tighter

swirl to the flow;this can also be seen from a comparison of the decay rates of axial velocity and of the reverse mass flows for these two swirlers (Fig.7.27);it is seen that both the decay rate and the reverse mass flow are larger in the case of the swirler S.IO .The influence on the size is,however, not very significant and this may be due to very close values of the number of vanes investigated.Also shown in this figure are the boundaries of five reverse flow zones in swirling jets of Ref.s.8,2I and 87.The reverse flow zones occuring in the jets issuing from Mathur and Maccalum's (Ref.8) flat vane type swirlers are rather long;it is seen from the curves for these swirlers that the size of the reverse flow zone increases with increasing vane angle.Chigier and Beer (Ref.2I) and Syred et al. (Ref.26),on the other hand,have obtained quite compact reverse flow zones (see the dashed lines) with high reverse mass flows using tangential-air-entry type swirl generators;it is seen that in this case the length of the reverse flow zone is shortened and its width is increased with increasing swirl numbers.It is known (Ref.s.I5 and I7) that in flame stabilization with recirculatory flows,compact reverse flow zones with high rates of reverse mass flow are desirable to obtain good efficiency and performance from the combustion.(Combustion efficiency is defined as the ratio of the actual temperature rise in the combustor to the theoretical rise.)The reason for this is explained as follows :the principle of flame stabilization with recirculatory flows is that the reverse flow zone occuring in such flows acts as a source of heat and active species;the region becomes,therefore,a continuous igniter for the fresh fuel-air mixture.This ignition is caused by a heat trasfer from the hot combustion products in the reverse flow zone to the fresh fuel-air mixture.The amount of this heat transferred can be calculated with

$$Q = m_r C_p (T_r - T_m) \qquad (7.6)$$

where C_p is the specific heat,m_r is the reverse mass flow rate and T_m and T_r are the temperatures of the fuel-air mixture and reverse flow zone,respectively. It is seen from Eqn.7.6 that for a certain mixture temperature, the heat trasfer necessary to ignite a certain rate of fuel-air mixture depends on the rate of reverse mass flow and the average temperature in the reverse flow zone.In order to be able to burn more fuel ,to this end,to increase Q , the reverse mass flow must be increased. It is alsc obvious that as the mean temperature in the reverse flow zone increases,that is, as the reverse flow zone gets hotter ,more heat can be supplied from this zone and flame stabilization is improved. In the case of long reverse flow zones,however, cooled combustion products recirculate in the upstream direction and give rise to a drop in the mean temperature of the reverse flow zone.This appearently impairs flame stabilization,giving rise to a lower rate of heat transfer and decreases combustion efficiency since the actual temperature rise in the combustor drops due tc this decrease in the temperature of the reverse flow zone. If high turbulence and low

velocities are created around the area where this heat transfer to the fresh fuel-air mixture occurs, the former factor promotes mixing and increases the heat transfer while the latter increases the residence time of the fuel-air mixture. In this way, the heat transfer to the unburnt fuel-air mixture can occur within a shorter distance and the combustion can be completed; in consequence, the length of the flame is shortened. It should be appearent from the explanation so far that the width of the flame increases with increasing reverse flow zone width.

In these respects, the vane type swirlers S.6, S.9, S.IO and S.II are in between the tangential-air-entry type and flat vane type swirlers of Ref.8 such that they do not induce very long reverse flow zones and their reverse mass flows are higher than those of the corresponding flat vane type swirlers of Ref.8 ; especially the values of the reverse mass flows of the swirlers S.6, S.IO and S.II are close to the value of the reverse mass flow induced by the tangential-air-entry type swirler (Fig.7.27). Using these swirlers, therefore, it is expected that better performance, shorter flame lengths and higher temperatures , in consequence, better combustion efficiency can be obtained.

The characteristics of the recirculation region and reverse flow zone for all the swirlers are given in the table below :

SWIRLER NO.	SWIRL	LENGTH of R.R.	MAX.WIDTH of R.R.	MAX.WIDTH of R.F.Zone	MAX. REV. Mass Flow	AXIAL.POS. of Max.Rev. Mass Flow
S.I	I.25	2.0 D	0.I83 D	0.I24 D	0.05 m_o	0.50 D
S.4	I.25	3.0 D	0.373 D	0.29 D	0.I5 m_o	0.70 D
S.6	I.5I	3.9 D	0.6I4 D	0.40 D	0.59 m_o	0.65 D
S.9	I.04	3.2 D	0.390 D	0.29 D	0.26 m_o	0.90 D
S.IO	I.5I	4.I D	0.640 D	0.448 D	0.76 m_o	0.64 D
S.II	I.5I	4.05D	0.540 D	0.4II D	0.44 m_o	I.00 D
S.I2	2.40	7.5 D	0.888 D	0.697 D	I.60 m_o	0.75 D

Corresponding results for Mathur and Maccalum's (Ref.8) flat vane type annular swirlers have been given below :

45^o	0.72	3.7 D	0.23 D	0.039m_o
60^o	I.25	5.0 D	0.33 D	0.I57m_o
70^o	I.98	5.2 D	0.44 D	0.434m_o
75^o	2.68	5.2 D	0.92 D	I.53 m_o

7.5.2.Swirl Velocity Distributions

Profiles of the swirl velocity in the flows issuing from the swirlers S.I,S.4,S.6,S.9,S.IO,S.II and S.I2 are shown in Fig.s.7.37 to 43. The boundaries of the reverse flow zone and the recirculation region are also shown in every flow field. Irregular profiles have been measured in the immediate downstream in the case of the swirlers S.I and S.6 (see the profiles at the axial station of z/D=0.25 in Fig.s.7.37 and 39). These are due to the wakes behind the vanes of the swirlers and this is proven by the fact that both S.I and S.6 are flat vane type swirlers for which these vane wakes are larger than those produced by curved vanes.All the curved vane type swirlers,that is,S.4,S.9,S.IO,S.II and S.I2 produce almost a Rankine type swirl velocity profile (with single peak; forced-vortex form in the core of the flow where the swirl velocity is proportional to r and free-vortex form beyond the peak where the swirl velocity is proportional to I/r) at the swirler exit.In the case of the swirlers S.IO and S.II ,however,there is another smaller peak on the profile towards the jet axis (see the profiles at the axial station of z/D=0.25 in Fig.s.7.4I and 42).The mixing of the wakes behind the vanes with the main stream is completed for all the swirlers at z/D=I.O and further downstream;all the profiles assume the form of the Rankine type.The radial position of the peak in the swirl velocity profile moves outwards in the downstream direction as a general trend in the flow fields.The thickness of the forced-vortex core do not remain constant along the jet axis as it is reported by Mathur and Maccalum (Ref.8) who have found that this thickness is almost equal to the swirler outer radius. In this work,its variation with the swirler is irregular.

The swirl velocity should have zero value on the jet axis. The measurements,however,did not show zero value.This is due to the following reasons (Ref.I7) :firstly,reverse velocities on the axis are irregular and intermittent;a low frequence noise has been superimposed upon it.Secondly,actual turbulence levels on the jet axis are often higher than 60% due to axial and sometimes radial velocity fluctuations since mean swirl and radial velocities are zero on the axis.In addition to these,it is impossible to manufacture the vanes of a swirler with an arrangement of exact axisymmetry around the hub;this obviously has an effect on the problem of non-zero mean swirl velocity on the jet axis.

Variation of the normalized swirl velocity profiles in the flow field of the swirler S.I is shown in Fig.7.44 .It is seen that the profiles decay and flatten in the downstream direction. They are of the Rankine type swirl profile and the peak moves continuously outwards following the expansion of the jet.Near the swirler exit especially in the core region of the jet up to about r/D=0.5 ,the profiles show a continuous drop.This means that a term like $\partial W^2/\partial z$ (one of the source terms in the vorticity transport equation;page 43,Eqn.4.24) is negative in this region.This causes the value of the vorticity to become

negative as well.Since the vorticity is the source term in the stream function transport equation,Eqn.4.27, the stream function tends to have negative values in this region.The recirculation region is thus created.

Profiles of the normalized swirl velocity in the flow fields of the swirlers S.4,S.6 and S.IO are shown in Fig.s.7.45 to 47 .They show exactly the same behaviour as that in the flow field of the swirler S.I : the peaks drop continuously in the downstream direction while they are also shifted outwards. The profiles close to the swirler exit tend to flat profiles as the swirl number of the swirler increases (see Fig.s.7.46 and 47 for the swirlers S.6 and S.IO ,respectively).

Comparison of the normalized swirl velocity profiles at the axial station z/D=I.O for different swirlers has been made in Fig.7.48 .It is seen that :
a)as the vane angle is increased in the case of curved vanes position of the peak is shifted outwards and the peak value of the normalized swirl velocity imparted to the flow drops at this axial station (see S.9,S.IO and S.I2);
b)effect of the aspect ratio is similar in the case of both curved and flat vanes : decreasing the aspect ratio reduces the normalized swirl velocity (compare S.I with S.6 for flat, S.4 with S.II for curved vanes);
c)the normalized swirl velocity decreases if curved vanes are employed on a swirler for the constant values of other parameters (see S.6 and S.IO).
Profiles of the normalized swirl velocity at the axial station z/D=I.036 in the flow fields of Mathur and Maccalum's (Ref.8) flat vane swirlers are also shown in this figure (the dashed lines).It is expected that in accordance with the case for the curved vanes,the normalized swirl velocity should drop also for flat vanes at the swirler exit as the vane angle is increased from 60° to 75°;70° flat vane swirler of Ref.8 ,however, has given larger swirl velocity than that of 60° swirler in contrast to this order.Comparison of the 60° flat vane swirler of Ref.8 with S.I which also has 60° flat vanes,shows that the normalized swirl velocity is less in the former case;its positic however,is further away from the axis.

Similar trends are observed at the following axial station in the downstream direction (see Fig.7.49) such that with increasing vane angle,for instance,the maximum value of the normalized swirl velocity drops in the case of both curved (see S.9,S.IO and S.I2) and flat vane type swirlers (see 60°, 70° and 75° flat vane swirlers of Ref.8).Comparison of S.IO with S.I2 in this figure to see the effect of the vane angle shows very similar values for these two swirlers;this is because the profile of the swirler S.IO is given at the axial station of z/D=2.0 ,on the other hand,that of S.I2 at z/D=I.75. The profile of S.IO decays with the axial distance ;it is seen that its peak value at the axial station of z/D=2.0 is still slightly higher than that of S.I2 at the axial station z/D=I.75. If the peak value of the profile of S.IO at the axial station

of z/D=2.0 is greater than that of S.I2 at the axial station of z/D=I.75,the peak value of the profile of S.IO at the axial station z/D=I.75 should be considerably higher than that of S.I2 at the same station.Such differences in the axial positions of the profiles have been taken into consideration in the comparisons.Effect of the other parameters are exactly similar at this axial station as well.

Comparison of the normalized swirl velocity profiles at the axial station of z/D=2.5 is shown in Fig.7.50.The general trend in the profiles do not change;for instance,decreasing the aspect ratio reduces the normalized swirl velocity in the case of both curved (see S.4 and S.II) and flat vane type swirlers (see S.I and S.6);also,increasing the vane angle reduces the peak value for both curved (see S.9,S.IO and S.I2) and flat vane type swirlers (see 60°,70°and 75° flat vane swirlers of Ref.8). It must be noted that the profile of the 70°swirler of Ref.8 is at the axial station of z/D=2.07 ;its profile at the axial station of z/D=3.I should consist of smaller values,in consequence,what is said about the effect of the vane angle is justified.For this figure,no mention of a comparison of the peak values of the profiles of the swirlers of this work and those of Ref.8 is made since the profiles are at different axial stations;also,such a comparison is made in Fig.7.52.A comparison of the profiles of the normalized swirl velocity at the axial station of z/D=3.25 for different swirlers is given in Fig.7.5I and shows the same effects of the swirler parameters.

Since the swirl velocity is not desired at the exit of a can type combustor, variation of the decay of the swirl velocity for different swirlers is also of concern.The decay of the swirl velocity profiles in the flow fields of the swirlers S.I,S.4,S.6 and S.IO are shown in Fig.s.7.44 to 47.The decay of the peak values of the swirl velocity profiles along the jet axis for different swirlers is shown in Fig.7.52.Also included are the decay rates of the normalized swirl velocity in the flow fields of Mathur and Maccalum's (Ref.8) 60°,70° and 75° flat vane type swirlers.It is observed that the decay of the normalized swirl velocity increases :

a)with increasing vane angle in the case of curved (see S.9,S.IO and S.I2) and flat vane type swirlers (compare 60°,70° and 75° swirlers of Ref.8),

b)with decreasing aspect ratio in the case of both curved (see S.4 and S.II) and flat vanes(compare S.I with S.6),

c)with the use of curved vanes (compare S.6 with S.IO),

d)with increasing number of vanes (compare S.II with S.IO).

It must be noted that the decay of the normalized swirl velocity for the corresponding swirlers S.I and 60° flat vane swirler of Ref.8 have very similar values beyond z/D=I.0 .It is also seen from this figure that at about z/D=3.5,the peak values of the swirl velocity are almost the same for all the vane swirlers; this is due to the fact that the swirl is already strong in all the cases.In the case of tangential-air-entry type swirler investigated by Syred (Ref.87),however,the decay is much faster in the initial region up to about z/D=I.5 .

Radial velocities are small with respect to axial and swirl velocities in all the flow fields as it is also reported in the literature,for instance by Syred(Ref.87);they are not given, therefore, any further consideration.

7.6. TURBULENCE CHARACTERISTICS

7.6.I.Kinetic Energy of Turbulence

It is possible to measure the six components of the Reynolds stress tensor using the hot-wire technique presented in Chapter 6 .Kinetic energy of turbulence is defined with Eqn.2.I2 as the half of the sum of the three normal components of the Reynolds stress tensor.Profiles of the kinetic energy of turbulence in the flow fields of the swirlers S.I,S.4,S.6, S.9,S.I0,S.II and S.I2 are shown in Fig.s.7.53 to 59 .In every flow field,boundaries of the reverse flow zone and the recirculation region are also shown with dashed and solid lines , respectively.These figures with the absolute values of the kinetic energy of turbulence have been presented for direct comparison between the flow fields.The two-peak form is common in the immediate downstream of all the swirlers.Maximum amount of turbulence in a flow field is always created in this immediate downstream region up to the axial distance of z/D=I.O ; in the cases of the swirlers S.I0 and S.I2 ,maximum turbulence occurs just at the exit. In every flow field,the lower peak in the profiles of the kinetic energy of turbulence is around the boundary of the recirculation region and between this and the zero velocity line (reverse flow zone boundary).This means that this area is a source of turbulence.Creation of turbulence around the boundary of the recirculation region is also reported by Davies for baffle flows (Ref.79) and by Syred for swirling flows (Ref.87).Further downstream,turbulence kinetic energy decays rapidly in both the radial and axial directions and one of the two peaks in the profiles vanishes;they tend to possess a form with a single peak which is shifted from the jet axis similar to that in the initial region of a weakly swirling flow (see the dashed lines at z/D=I.O in Fig.7.6I).

Although the relative kinetic energy of turbulence is defined using the local axial velocity in turbulence literature, the absolute value of the kinetic energy of turbulence is more of interest in combustion applications.Also, a definition with the local axial velocity goes tc infinity on the boundary of the reverse flow zone and comparisons with such a definition do not become very elucidating about the variation of the kinetic energy of turbulence.For these reasons,a relative kinetic energy of turbulence is defined using the average nozzle velocity :

$$K = \frac{\overline{u^2} + \overline{v^2} + \overline{w^2}}{V_n^2} \qquad (7.7)$$

Here, V_n has been used for normalization instead of U_i,the swirler inlet velocity which is dependent on the aspect ratio,

in order that this definition becom s consistent with that mostly used in the combustion literature and in this way, a direct comparison of the magnitude of the relative kinetic energy of turbulence can be made.

A comparison of the profiles of the relative kinetic energy of turbulence ,K, for different swirlers at the axial station of z/D=I.O is shown in Fig.7.60 .The dashed line in this figure shows Pratte and Keffer's (Ref.25) measurements in the initial region ,at z/D=I.O , of a weakly swirling flow (with no recirculation),using a method involving the alignement of probe along the velocity vector.Also shown in the figure is an approximate profile of K obtained from Syred's (Ref.87) contour plots for this quantity in a strongly swirling jet with a swirl number of 2.2 .It is seen that the peaks in the profiles are not on the jet axis at the swirler exit for the cases of weakly or strongly swirling flows.The profiles have two-peak form and the turbulence kinetic energy is higher in the strong swirl case.It is seen that the relative kinetic energy of turbulence increases at this axial station :
a)with decreasing vane angle in the case of curved vanes (see S.I2 , S.IO and S.9 ;actually more turbulence kinetic energy is created at the immediate exit of the swirlers having larger vane angles,see Fig.s.7.56 , 57 and 59 ;as it will be seen from Fig.7.62 ,however,the decay of turbulence kinetic energy becomes more rapid as the vane angle increases and lower values of the relative kinetic energy of turbulence result at the axial station z/D=I.O for higher vane angles);
b)with decreasing aspect ratio in the case of both flat (see S.I and S.6) and curved vanes (see S.4 and S.II);
c)in the case of using flat vanes (see S.IO and S.6 ;actually more relative turbulence kinetic energy is created at the immediate exit of the swirlers having curved vanes as it is seen from Fig.7.62 ; however,the decay is faster in the case of S.IO and a smaller value results at the axial station of z/D=I.O for curved vanes);
d)with decreasing number of vanes (compare S.IO with S.II).
It is also seen from this figure that tangential-air-entry type swirlers (Ref.87) produce very high turbulence (compare S.I2 and tangential-air-entry type swirler of Ref.87 for which the swirl numbers are 2.4 and 2.2 , respectively).

Profiles of the relative kinetic energy of turbulence at the axial station of z/D=2,5 for different swirlers are shown in Fig.7.6I . Also included are the profiles of K from Pratte and Keffer's (Ref.25) measurements in a weakly swirling flow at the axial stations z/D=I.O and 6.0 (the dashed lines) and from Carmody's (Ref.88) measurements in a baffle flow . Profiles of the relative kinetic energy of turbulence at the axial stations z/D=2.0 and 6.0 (from Fig.6.27) in the straight jet

obtained to test the performance of the hot-wire technique without the swirlers in position in the nozzle,are also shown in this figure with dash and dot lines . It is observed that turbulence kinetic energy increases in the downstream direction in the case of straight jets;the peak of the profile is on the jet axis at about z/D=6.0 .For the weakly swirling flow of Ref.25 ,it is seen that the peak of the profile at the axial station of z/D=I.0 is not on the jet axis and kinetic energy of turbulence drops towards the axis;the kinetic energy of turbulence increases in the downstream direction similar to the case for straight jets and the peak lies on the jet axis at about z/D=6.0 .Comparison of the profiles of the kinetic energy of turbulence at the axial station z/D=2.0 for straight jet and z/D=I.0 for the swirling jet of Ref.25 shows that much higher kinetic energy of turbulence occurs in swirling flows. Kinetic energy of turbulence increases in the downstream direction in both types of flow and its production is faster in the case of swirling flows (see the profiles at the axial station of z/D=6.0 for both flows).In the case of baffles,it is seen that turbulence level is not very high,even lower than that in weakly swirling flows (at the corresponding axial stations).Examination of the profiles of the kinetic energy of turbulence for the swirlers of this work shows that the peak values decay very rapidly within a distance of I.5D to the level of turbulence at the axial station of z/D=6.0 in weakly swirling flows;for instance,turbulence kinetic energy drops from about 0.8 at the axial station of z/D=I.0 to about 0.25 at z/D=2.5 in the case of the swirlers S.9 and S.6 .Also, all the profiles assume a single-peak form at the axial station of z/D=2.5 ,similar to that in the initial region of weakly swirling flow;only for S.I ,there is a second peak in the profile.

Variation of the peak values in the profiles of the relative kinetic energy of turbulence along the jet axis for different swirlers is shown in Fig.7.62 .In the case of the swirlers S.9, S.II,S.6 and S.4 ,there is an initial increase in the relative kinetic energy of turbulence near the swirler exit up to about z/D=I.0 .In other cases,the peak values occur at the swirler exit and then decay continuously in the downstream direction (see S.I,S.IO and S.I2).For all the swirlers,the level of the relative kinetic energy of turbulence drops rapidly to about 0.2 at about z/D=2.5 .The rate of decay of the peaks increases with increasing swirl number,that is,

a)with increasing vane angle (see S.9,S.IO and S.I2) in the case of curved vanes,

b)with decreasing aspect ratio for curved (compare S.4 with S.II) and flat vanes(see S.I and S.6),

c)with increasing number of vanes (see S.II and S.IO),

d)in the case of the use of curved vanes instead of flat vanes (see S.6 and S.IO).

Decay of the peaks of the relative kinetic energy of turbulence in a strongly swirling jet (S=2.2) issuing from Syred's (Ref.26) tangential-air-entry type generator is also shown in Fig.7.62 . It is seen that much higher turbulence is created at the exit

of a tangential-air-entry type generator;it decays ,however, very rapidly to a value of 0.25 within an axial distance of z/D=I.5 similarly to those vane swirlers having such high swirl numbers (see S.I0 and S.I2).

7.6.2.Reynolds Stresses

Interpretation of the hot-wire signals with the method presented in Chapter 6 yields the six Reynolds stresses.Profiles of the normalized Reynolds stresses at several axial stations in the flow field of the swirler S.9 are given in Fig.s.7.63 to 66 .The vertical dashed and solid lines in these figures show the boundaries of the reverse flow zone and the recirculation,respectively,for this swirler at these axial stations. It is clearly seen from every figure that turbulence is strongly anisotropic; $\overline{ww}$, $\overline{uw}$ and $\overline{uu}$ (ρ has been dropped for convinience) are the dominant stresses. $\overline{uu}$ is slightly larger than $\overline{ww}$ and $\overline{uw}$ near the swirler exit at z/D=0.25 (see Fig.7.63). They are all,however, of the same order of magnitude,about 0.27 . $\overline{uu}$ has a peak on the jet axis as well and dominates in the reverse flow zone.This is due to closeness of this axial station to the upstream stagnation point which is at the hub end. $\overline{uu}$ increases similarly in the reverse flow zone around the upstream stagnation point in baffle flows (Ref.s.79 and 88). A similar situation is reported by Syred et al.(Ref.87) for the region around the axis near the upstream stagnation point in a tangential-air-entry type swirler.In this reference at the axial station of z/D=0.25 ,the peak in the profile of $\overline{uu}/V_n^2$ has a value of about 2.54 ,$\overline{ww}/V_n^2$ about I.6 and $\overline{uw}/V_n^2$ about I.I . In this work,however, these normalized dominant stresses have the maximum values 0.33 , 0.29 and 0.28 ,respectively, at the exit of the swirler S.9 .It is seen that the order of domination is the same as that in Ref.87 .The discrepancy in the level of the values might be due to either the difference in the degree of swirl (it is 2.2 in Ref.87 and 1.25 for the swirler S.9) or the type of swirl generation.It is also seen from this figure that $\overline{uu}/V_n^2$ values are much lower in baffle flows (Ref.88). Further downstream at z/D=I.0 (Fig.7.64), $\overline{ww}$ starts increasing and becomes more dominant than the other two dominant stresses, $\overline{uu}$ and $\overline{uw}$, over the whole of the cross section of the jet. Further downstream at z/D=2.5 and 3.25 (see Fig.s.7.65 and 66), the domination of $\overline{ww}$ continues.Between the other two dominant stresses, $\overline{uw}$ is greater than $\overline{uu}$ in all the cases over the whole cross section of the jet (see Fig.s.7.64,65 and 66). These results at the axial station z/D=I.0 and further downstream are in contrast to Syred's results (Ref.87);he found the order of domination of the Reynolds stresses at the axial station z/D=I.0 as $\overline{uu}/V_n^2$=0.42 (the peak value in the profile), $\overline{ww}/V_n^2$=0.28 and $\overline{uw}/V_n^2$=0.06 .The order of domination has been shown below for the two works :

Ref.87 z/D=0.25	S.9 z/D=0.25	S.9 z/D=I.0	Ref.87 z/D=I.0
$\overline{uu}$	$\overline{uu}$	$\overline{ww}$	$\overline{uu}$
$\overline{ww}$	$\overline{ww}$	$\overline{uw}$	$\overline{ww}$
$\overline{uw}$	$\overline{uw}$	$\overline{uu}$	$\overline{uw}$

All the other stresses $\overline{uv}$,$\overline{wv}$ and $\overline{uv}$ are considerably smaller in the most part of the flow field.Among these smaller stresses, $\overline{wv}$ looks the most dominant one.It is also seen from Fig.s.7.63 and 64 that near the swirler exit,the Reynolds stresses are much higher than those created in baffle flows at the corres - ponding stations.Further downstream at z/D=2.5 and beyond (Fig.7.65 and 66),however,the Reynolds stresses,for instance $\overline{uu}$ and $\overline{uv}$, in the swirling flow drop to the values induced in baffle flows.

The same trends are also observed in the flow field of the swirler S.IO .Turbulence is strongly anisotropic;profiles of the Reynolds stresses at the axial stations of z/D=I.0 and 2.5 are shown in Fig.s.7.67 and 68 . $\overline{ww}$ is the most dominant stress similarly to the case at z/D=I.0 in the flow field of S.9 . $\overline{uw}$ is the second, $\overline{uu}$ is the third dominant stress.It is observed again that near the swirler exit,the Reynolds stresses are higher than those in baffle flows (compare $\overline{uu}$ and $\overline{vu}$ for baffle and swirl flow cases in Fig.7.67).Further downstream at z/D=2.5, however, $\overline{uu}$ and $\overline{uv}$ in the swirling case drop again to the level in the case of baffle flow (see Fig.7.68).

These trends also do not change significantly at several axial stations in the flow fields of the swirlers S.II,S.I2 and S.I (the last one has been given as an example for flat vane type swirlers ;see Fig.s.7.69 and 70).

7.6.3.Effect of Swirler Type on the Dominant Reynolds Stresses

The main conclusion from the previous section is that in a swirling flow issuing from a vane swirler,the most dominant stresses are in turn $\overline{ww}$,$\overline{uw}$ and $\overline{uu}$ irrespective of the type of the vanes;the others are considerably smaller.It is therefore these dominant stresses that determine the positions of high shear and high turbulence regions in swirling flows. It can also be concluded that higher Reynolds stresses occur in swirling flows than those in baffle flows near the exit;further downstream the Reynolds stresses in swirling flows decrease to the level of the Reynolds stresses occuring in baffle flows.

Effect of the swirler design parameters on the most dominant stress $\overline{ww}$ at the axial station z/D=I.0 is shown in Fig.7.73 .It is observed that :
a)increasing the vane angle from 50° to 60° decreases at first the values of $\overline{ww}$ (compare S.9 with S.IO),however,further increase to 70° increases this dominant stress (compare S.IO with S.I2);
b)decreasing the aspect ratio increases the magnitude of the dominant stress in the case of both flat (compare S.I with S.6) and curved vanes (compare S.4 with S.II);
c)values of this stress are higher at this axial station for flat vane type swirler than those for curved vane type (see S.6 and S.IO);
d)increasing the vane number decreases the maximum value of the dominant stress $\overline{ww}$ and flattens its profile (see S.II and S.IO).
It is seen from Pratte and Keffer's (Ref.25) measurements that

in a weakly swirling flow, $\overline{ww}$ values are much lower than those created in strong swirl cases.

Similar trends are observed at the axial station of z/D=2.5 (Fig.7.74) .For instance, in the case of flat vanes the effect of the aspect ratio is the same as that at z/D=I.O :decreasing the aspect ratio increases the dominant stresses (see S.I and S.6);for curved vanes,however,the situation is not the same as that at the axial station of z/D=I.O (see S.4 and S.II): decreasing the aspect ratio decreases the values of $\overline{ww}$ .Also, decreasing the vane number causes the values of the dominant stress $\overline{ww}$ to decay very rapidly (see S.IO and S.II).It is also seen that $\overline{ww}$ has lower values (except for S.II) in weakly swirling flows (Ref.25) and baffle flows (Ref.88) .

Effect of the swirler design parameters on the second dominant stress $\overline{uw}$ at the axial station of z/D=I.O is shown in Fig.7.75 .It is seen that :
a)increasing the vane angle decreases $\overline{uw}$ values at this axial station in the case of curved vanes (see S.9,S.IO and S.I2);
b)decreasing the aspect ratio increases this shear stress in the case of both curved (see S.4 and S.II) and flat vane type swirlers (see S.4 and S.6);
c)increasing the number of vanes does not influence very considerably the maximum value of $\overline{uw}$ (see S.II and S.IO),it slightly decreases it;
d)flat vane type swirler can produce higher shear stress than that of curved vane type at this axial station (see S.6 and S.IO).
It is seen from Fig.7.75 that much larger shear stress $\overline{uw}$ is created in strongly swirling flows than that occuring in weakly swirling flows (Ref.25).Also included in this figure are the profiles of the dominant shear stress $\overline{uv}$ in baffle flows investigated by Davies (Ref.79) and Carmody (Ref.88); comparison of the dominant shear stress $\overline{uw}$ in swirling flows with the dominant shear stress $\overline{uv}$ in baffle flows shows that much stronger shear regions can be created by strongly swirling flows. The position of the maximum shear stresses are nearly always around r/D=0.75 in both swirling and baffle type flows at the axial station of z/D=I.O .

The trends are quite similar at the axial station of z/D=2.5 (Fig.7.76).It is seen,however,that $\overline{uw}$ in the field of the curved vane type swirler S.II decays very rapidly and in contrast to the case with flat vanes,decreasing the aspect ratio decreases this shear stress in the case of curved vanes (see S.4 and S.II). Also,decreasing the number of the vanes give rise to the decay of this shear stress very rapidly (see S.IO and S.II).It is seen again that the dominant shear stress $\overline{uw}$ is larger in the case of strongly swirling flows than that in weakly swirling case (Ref.25).Besides,the dominant shear stress $\overline{uw}$ for swirling flows is much higher than the dominant shear stress $\overline{uv}$ in the case of baffle flows (Ref.88).

Profiles of the third dominant stress $\overline{uu}$ at the axial station z/D=I.O are shown in Fig.7.77 for different swirlers. All the

profiles have two peaks. As it is in the case of the other dominant stresses, increasing the vane angle reduces the peak value of $\overline{uu}$ when curved vanes are employed (see S.9, S.I0 and S.I2); decreasing the aspect ratio increases this stress in the case of both flat (see S.I and S.6) and curved vanes (compare S.4 and S.II). Varying the number of vanes from I2 to I6 does not influence the peak values of $\overline{uu}$ very considerably (see S.I0 and S.II). As it is for the other dominant stresses, flat vanes produce larger values of $\overline{uu}$ (see S.6 and S.I0). Also included in this figure is the profile of $\overline{uu}$ in the wake of a baffle at the axial station z/D=I.0 , determined by Carmody (Ref.88); it is seen that much larger $\overline{uu}$ values are created in strongly swirling flows. Comparison of the profile of $\overline{uu}$ determined by Pratte and Keffer (Ref.25) in a weakly swirling flow with the other profiles shows that much larger values of the stress $\overline{uu}$ are created in strongly swirling flows.

These remarks also apply to the profiles of the normal stress $\overline{uu}$ at the axial station z/D=2.5 and similar trends are observed (Fig.7.78). The fast decay in the values of the swirler S.II, however, outstands again; it is seen that the values of $\overline{uu}$ decay rapidly from the axial station z/D=I.0 to the axial station z/D=2.5 and the peak values are of the order created in the nearly well developed region of weakly swirling flows (Ref.25). Comparison with the profiles of $\overline{uu}$ in a baffle flow investigated by Carmody (Ref.88) shows that in swirling flows the level of the values of $\overline{uu}$ drops very rapidly (up to the axial distance of z/D=2.5) to the level created in baffle flows at the axial station of z/D=2.0 .

7.6.4. Turbulent Viscosities

The anisotropic turbulent viscosities μ_{rr}, $\mu_{\theta\theta}$, $\mu_{r\theta}$ and μ_{rz} have been calculated from the measured Reynolds stress and mean velocity profiles using Eqn.s.2.6 . The measurements have been taken with I.5" intervals in the z direction ; this has made it impossible to calculate accurately the derivatives with respect to z direction in Eqn.s.2.6 such as $\partial U/\partial z$, $\partial W/\partial z$, etc. In consequence, the turbulent viscosities $\mu_{z\theta}$ and μ_{zz} could not be calculated.

After some trials with several procedures to fit curves to the experimental profiles of the mean velocity components and to calculate the derivatives with respect to radial coordinate appearing in Eqn.s.2.6 , Lagrange's interpolation formula (Ref.89) has been decided as the best choice for this purpose. It has been applied to every five experimental point in the radial direction, that is, a fourth-order polynomial curve has been used and the derivative has been calculated at the middle point. This method has proved to be the most correct among the others. This method is simple, therefore, is not presented here.

Profiles of the turbulent viscosity $\mu_{\theta\theta}$ at several axial stations in the flow fields of the swirlers S.9,S.I0,S.II and S.I2 are shown in Fig.s.7.79 to 82 .The profile of $\mu_{\theta\theta}$ in the flow field of a tangential-air-entry type swirl generator investigated by Syred (Ref.87) is also shown in these figures; it is seen that its values are very similar to those obtained in this work. In Fig.7.79 for the swirler S.9 ,the jet has not fully expanded yet near the swirler exit at z/D=0.25 ; around the boundary of the jet at a radial distance of r/D=0.65 , therefore, the turbulent viscosity $\mu_{\theta\theta}$ drops rapidly to a value of $I0^{I.96}\mu$.Further downstream ,the value of $\mu_{\theta\theta}$ increases following the expansion of the jet and beyond z/D=I.75,reaches an average value of $I0^{4.3}\mu$ .The trend of $\mu_{\theta\theta}$ in the case of the swirler S.I0 is not altered considerably (see Fig.7.80); the constant value near the swirler exit beyond about r/D=0.6 is about $I0^{2.44}\mu$ .For the axial stations further downstream, an average value of $I0^{4}\mu$ can be assumed. For the case of the swirler S.II ,however, there is an obvious flattening in the profiles at z/D=2.5 although a similar shape is observed in the immediate downstream of the swirler exit; the flat form in the profiles continues in the downstream direction. An average value of $I0^{3.I}\mu$ can be used for $\mu_{\theta\theta}$ for the swirler S.II .Due to very rapid expansion of the flow from the swirler S.I2 (see Fig.7.82) even in the immediate downstream of the exit,the level of the turbulent viscosity $\mu_{\theta\theta}$ does not drop within the range of radial distance investigated as in the cases of the other swirlers;all the profiles accumulate around an average value of $I0^{4}\mu$ .This average value can also be used for the prediction of the flows from the swirlers S.9 and S.I0 .

Profiles of the turbulent viscosity $\mu_{r\theta}$ in the jets of the swirlers S.9,S.I0,S.II and S.I2 are shown in Fig.s.7.83 to 86. Although there is quite much scatter in the curves, they mostly show two-peak profiles .For the swirler S.9 (Fig.7.83) , an average value of $I0^{2.7}\mu$ can be used .For the swirler S.I0 (Fig.7.84), the scatter is much more and an average value of about $I0^{2.5}\mu$ can be used for the turbulent viscosity $\mu_{r\theta}$. A considerable drop in the value of $\mu_{r\theta}$ in the flow field of the swirler S.II is observed in consistent with the drop in the value of $\mu_{\theta\theta}$ (Fig.7.85); an average value of I00μ can be assumed for $\mu_{r\theta}$ .In the case of the swirler S.I2 (Fig.7.86), the scatter is again quite much and a value of $I0^{2.4}\mu$ can be used for $\mu_{r\theta}$.

Variation of the turbulent viscosity μ_{rr} in the flow fields of the swirlers S.9,S.IO,S.II and S.I2 is shown in Fig.s.7.87 to 90 .Also shown in these figures is a profile of μ_{rr} in the flow field of a tangential-air-entry type swirl generator investigated by Syred (Ref.87).It is seen that the values show too much scatter;they are,therefore,left with no further treatment.

Profiles of the turbulent viscosity μ_{rz} in the flow fields of the swirlers S.9,S.IO,S.II and S.I2 are shown in Fig.s.7.9I to 94 . Also, a profile of μ_{rz} calculated by Syred (Ref.87) from measurements in a strongly swirling flow issuing from a tangential-air-entry type generator is shown in these figures. Scatter is again very much for the case of every swirler. For this turbulent viscosity,however,this scatter might be due to neglecting in its calculation the term $\partial V/\partial z$ in the velocity gradients (see Eqn.s.2.6).A characteristic case is seen in the case of the swirler S.II (see Fig.7.93).This swirler has I2 vanes and in consequence,can not turn the flow as much as the corresponding swirler S.IO which has I6 vanes;the flow can pass through more readily and a higher shear stress $\overline{uv}$ can be created.At the exit of the swirler S.II ,therefore, μ_{rz} has considerably higher values;further downstream, this viscosity decays much more rapidly than it does in the case of the other swirlers.An average value of $I0^{2.4}\mu$ for the swirler S.9 (see Fig.7.9I), $I0^{2.2}\mu$ for the swirler S.IO (see Fig.7.92) and $I0^{2}\mu$ for the swirler S.I2 (see Fig.7.94) can be used for μ_{rz} . In the case of S.II (see Fig.7.93) ,an average value of $I0I.4\mu$ can be used for μ_{rz} in the region beyond z/D=I.0 .

The results of this section have been summarized in the following table :

SWIRLER	S.9	S.IO	S.II	S.I2
VISCOSITY				
$\mu_{\theta\theta}$	$I0^{4}$	$I0^{4}$	$I0^{3.I}$	$I0^{4}$
$\mu_{r\theta}$	$I0^{2.7}$	$I0^{2.5}$	$I0^{2}$	$I0^{2.4}$
μ_{rz}	$I0^{2.4}$	$I0^{2.2}$	$I0^{I.4}$	$I0^{2}$

From the examination of this table,it is seen that $\mu_{\theta\theta}$ is the most dominant viscosity among the turbulent viscosities calculated in this work;the order of domination is $\mu_{\theta\theta}$,$\mu_{r\theta}$ and μ_{rz} (μ_{rr} has been left out of this order due to too much scatter and probably unreliability in its values).More detailed comparison with the profiles of the turbulent viscosities will be given now;although the values of μ_{rr} have been included into

the following figures, they have been excluded from the following discussion due to the scatter in its values.

Comparison of the profiles of the four turbulent viscosities at the axial station z/D=0.25 in the flow field of the swirler S.9 is shown in Fig.7.95 .The short vertical dashed and solid lines show the positions of the boundaries of the reverse flow zone and the recirculation region, respectively. Among the four viscosities calculated, domination of $\mu_{\theta\theta}$ over the whole cross section of the jet, within and outside of the recirculation region, is appearent. The values of the other viscosities $\mu_{r\theta}$, μ_{rr} and μ_{rz} values are quite close to each other. Also at the axial station of z/D=I.0 , similar trends are observed in the profiles; the domination of $\mu_{\theta\theta}$ still continues at this axial station (see Fig.7.96). Among the other turbulent viscosities, however, $\mu_{r\theta}$ starts increasing especially in the central region.

A similar trend is observed in the profiles of the turbulent viscosities at the immediate exit of the swirler S.IO (Fig.7.97); $\mu_{\theta\theta}$ is the most dominant viscosity again over the most part of the cross section of the jet. $\mu_{\theta\theta}$ is followed by $\mu_{r\theta}$. μ_{rr} and have quite scattered values. The same trends exist for the turbulent viscosities in the flow fields of the swirlers S.IO at z/D=I.5 (Fig.7.98), S.II at z/D=2.5 (Fig.7.99) and S.I2 at z/D=I.75 (Fig.7.I00).

The final conclusion from this section is that among the four viscosities which could be calculated in this work, $\mu_{\theta\theta}$ is the most dominant turbulent viscosity in a swirling flow field up to an axial distance of z/D=3.25 ; this does not vary with the swirler. $\mu_{\theta\theta}$ is followed by $\mu_{r\theta}$.

7.6.5. Effect of Swirler Type on the Turbulent Viscosities

Comparison of the dominant viscosity $\mu_{\theta\theta}$ is shown in Fig.7.I0I for the immediate downstream region of the swirlers S.9, S.IO, S.II and S.I2 .In all the cases, the peaks are around r/D=0.5 .The maximum values in the viscosity profiles are not influenced very much with the type of the swirlers. It is seen, however, that the values of $\mu_{\theta\theta}$ drop slightly in the core region of the jets with increasing swirl number (that is, with increasing vane angle for the swirlers S.9, S.IO, S.I2). In the outer region of the jets, however, an exactly opposite trend is observed. Due to slower expansion of the jet from the swirler S.9 , $\mu_{\theta\theta}$ drops very rapidly to a value of about $IO^{I.96}\mu$ at a radial distance of r/D=0.65 .In the case of S.IO , this drop in the value of the turbulent viscosity $\mu_{\theta\theta}$ is slower; the constant value towards

the boundary is about $I0^{2.44}\mu$ .In the case of S.I2 ,the peak moves considerably outwards since the jet expands very rapidly for this swirler.Also shown in the figure is the profile of $\mu_{\theta\theta}$ in the flow field of tangential-air-entry type swirl generator investigated by Syred (Ref.87) ; a considerable difference is observed in the values,however, the profile form is quite similar.The position of the peaks are nearly coincident at about r/D=0.5 as well.

Further downstream at z/D=I.0 (Fig.7.I02), profiles of the viscosity $\mu_{\theta\theta}$ are flattened considerably especially in the core region of the jets.The values of $\mu_{\theta\theta}$ drop in the outer part of the flows in the case of the swirlers S.9 and S.II due to less expansion of the flow fields in these cases. An average value of $I0^{4}\mu$ can be used especially for the core region of the flow for z/D=I.0 and further downstream in the predictive calculations.It is seen that the profile of the viscosity $\mu_{\theta\theta}$ determined by Syred (Ref.87) has an average value of $I0^{4.6}\mu$ and the difference from the value $I0^{4}\mu$ in this work might be due to the type of swirl generation.

Comparison of the profiles of $\mu_{r\theta}$ at the exit from the swirlers is shown in Fig.7.I03 .The $\mu_{r\theta}$ trend is that increasing the swirl number (that is,increasing the vane angle from 50^{o} to 70^{o} with the swirlers S.9,S.I0 and S.I2) increases the peak values of the viscosity $\mu_{r\theta}$ and the peak moves continuously outwards (the profile for the swirler S.I0 is at the axial station of z/D=0.083;the values of $\mu_{r\theta}$ at the axial station of z/D=0.25 should be slightly smaller).If the number of vanes are decreased (see S.I0 and S.II),the values of $\mu_{r\theta}$ decrease. Further downstream,the profiles of $\mu_{r\theta}$ assume two-peak form (Fig.7.I04) and although the peak values near the axis drop with increasing swirl numbers (with increasing vane angles for the swirlers S.9,S.I0 and S.I2),the outer peak of the profiles changes irregularly.In the case of decreasing vane numbers , $\mu_{r\theta}$ increases near the axis but decreases away from the axis.

Comparison of the turbulent viscosity μ_{rz} in the immediate downstream region of the swirlers S.9,S.I0 ,S.II and S.I2 is shown in Fig.7.I05 .Also shown in this figure is the profile of μ_{rz} determined by Syred (Ref.87) in a swirling flow issuing from a tangential-air-entry type swirl generator.Scatter is quite much in all the profiles for the swirlers;this is considered to be due to the neglect of the term $\partial V/\partial z$ in the velocity gradients in the calculation of its profiles.The values do not show a constant trend with varying swirl numbers.Syred's profile is in quite good agreement with the profile for the swirler S.I2 which has a swirl number 2.4 ,a value similar to the swirl number 2.2 in this referance.Profiles of the viscosity μ_{rz} show a similar trend at the axial station of z/D=I.0 (Fig.7.I06).

Profiles of the viscosity μ_{rr} have not been compared for different swirlers since they show too much scatter.

7.7.DISCUSSION OF ERRORS

Several factors might cause errors in this procedure. Firstly,the assumptions for the hot-wire formulation may not be completely true .However, experimental evidence and comparison of the experimental results with those of others (see Sections 6.6 and 6.8) show that they are not very unrealistic , either . All these factors are in fact within the limitations of the hot-wire anemometry .The state of the flow at a point in the flow field might be changing from one orientation to the other . In this case ,it is clear that measurement of the fluctuating quantities u , v and w should be made separately and possibly at the same time for more exactness . A single channel Laser system is sufficient in the former case , but three different Laser systems with different colours (wavelengths) are required for the latter. Laser systems must be of the type providing continuous signals. As it is well known, such systems have their own troubles.

The performance of the hot-wire and the pressure probe has not been examined.They might involve some order of error when applied to the flow fields with high velocity gradients. Everything possible has been made , however , in order to decrease this source of error.The pressure probe has been manufactured with a head as small as possible within the manufacturing limitations .The hot-wire employed is of a standard type with a length of I.2 mm which gives quite a reasonable space resolution.Further errors due to this source has been neglected .Also,locating the probes to the points of the flow fields has been performed with quite a good accuracy (see Section 5.I). Some draughting errors might be involved in the hot-wire measurements; such a kind of error is common to all hot-wire measurements (see Ref.25). Since most of the measurements have been taken,however, well inside the boundaries of the flow fields , they are considered as negligible.

Finally,some measurements have been repeated. The general appearance of the profiles has not changed significantly;maximum change it the values of the required quantities is of the order of I0 to I5% .Although this range of repeatibility seems a bit high, it is well consistent with the highly fluctuating behaviour of the flow fields.

CHAPTER 8. CONCLUSIONS

CONCLUSIONS

Although effects of the swirler design parameters on the pressure drop-mass flow characteristics and the mean flow characteristics of the downstream recirculation region have been investigated in the case of flat vanes (Ref.8), not much is known about the effects of these parameters in the case of curved vane type swirlers; it is known (Ref.17) that curved vane swirlers operate more efficiently than flat vane type and only discrete cases have been examined in a few works , for instance Ref.12 .Also,turbulence characteristics have not been investigated fully in the case of curved vane swirlers.In fact,there is a dearth of turbulence data for swirling flows issuing from flat vane swirlers as well.

The present work is in this direction to elucidate the effects of swirler design parameters,namely, vane shape,vane angle,aspect ratio and space-to-chord ratio on the pressure drop-mass flow characteristics and mean flow and turbulence characteristics of the downstream recirculation region .The following conclusions are drawn from the investigation :

I) Recirculation region obtained in a swirling flow is an ideal flow configuration for the primary zone in a combustor.
2) One of the best ways of obtaining such a swirling flow and a recirculation region required for flame stabilization is to employ a vane,preferably curved,swirler.
3) Efficient numerical methods are being developed for the solution of the governing transport equations to predict the structure of such strongly swirling flows.
4) The formulation for the interpretation of the hot-wire anemometer signals is quite versatile and can be readily used for the measurement of swirling flows.
5) Curved vanes operate much more efficiently than flat vanes do due to the fact that the latter always run under 'stalled' conditions;much larger wakes are created behind flat vanes and the momentum loss,therefore,becomes higher than that in the case of curved vanes.Since the momentum loss manifests itself in the form of a pressure drop,conventional flat vane swirlers give rise to much higher pressure drops than curved vane swirlers do.
6) The total pressure drop through a vane swirler can be decreased by decreasing the vane angle,decreasing the number of vanes and increasing the aspect ratio in the cases of both flat and curved vanes.
7) These remarks apply equally for the static pressure drop through flat and curved vane type swirlers;this is because a much higher blockage is created to the axial flow by flat vanes.Its consequence is that flat vane swirlers are choked at a much lower mass flow.

8) The flow is turned more efficiently by curved vanes; in consequence,a higher angular momentum is imparted to the axial flow by curved vane type swirlers.This results in a higher swirl number and a larger recirculation region is induced.
Size of the recirculation region can be increased by increasing vane angle,decreasing aspect ratio and increasing vane number in the cases of both flat and curved vane type swirlers.

9) Curved vane swirlers produce larger reverse flow zones than the corresponding flat vane type swirlers.Additionally, size of the reverse flow zone can be increased with increasing vane angle and decreasing aspect ratio;number of vanes does not influence the size of the reverse flow zone considerably,however,it alters only its shape.

I0) Axial velocity profiles from all the swirlers possess a two-peak form with a trough in the middle;reverse velocities are of the same order of magnitude as that of forward velocities .

II) Curved vane type swirlers induce larger reverse mass flows than the corresponding flat vane types;also,reverse mass flow increases with increasing vane angles,decreasing aspect ratios and increasing vane number.

I2) Maximum reverse axial velocities increase with decreasing vane angles,decreasing aspect ratios and with increasing number of vanes.

I3) Different shapes are observed in the swirl velocity profiles just at the immediate downstream of the swirlers.All the profiles assume a Rankine type swirl velocity profile at and beyond the axial station of z/D=I.0 .

I4) Decay of the axial and swirl velocities increases with the use of curved vane type swirlers;in the cases of both flat and curved vane type swirlers,decay rate increases with increasing vane angles,decreasing aspect ratios and increasing number of vanes.

I5) The level of the kinetic energy of turbulence can be increased by using curved vane type swirlers.Profiles of the kinetic energy of turbulence possess four-peak forms near the swirler exit;further downstream,two-peak form is observed and the position of this variation depends on the type of swirler.In the case of both flat and curved vane type swirlers, the level of the kinetic energy of turbulence increases as the number of vanes and vane angle are increased;it increases,however, as the aspect ratio is reduced.Decay of the kinetic energy of turbulence increases with increasing vane angles,decreasing aspect ratios and increasing number of vanes;the use of curved vanes also increases the decay of the kinetic energy of turbulence.

I6) It is observed that turbulence is anisotropic in swirling flows.The most dominant Reynolds stresses are $\overline{ww}$, $\overline{uw}$ and $\overline{uu}$ over the whole cross section of the jets.It can,therefore, be assumed that the position of the maxima of the quantities $\overline{uu}+\overline{ww}$ and $\overline{uw}$ show the position of the maximum turbulence and maximum shear regions,respectively.

I7) Shear region in a swirling flow can be strengthened by using curved vane type swirlers; increasing vane angles, decreasing aspect ratios and increasing number of vanes also increases the level of shear stresses.

I8) In parallel to the anisotropy in turbulence, effective viscosities also show an anisotropic case. Among the four viscosities μ_{rr}, $\mu_{r\theta}$, μ_{rz} and $\mu_{\theta\theta}$ the calculations of which have been possible, $\mu_{\theta\theta}$ is the most dominant one; in domination, $\mu_{\theta\theta}$ is followed by $\mu_{r\theta}$ and μ_{rz}. The values of μ_{rr} have shown too much scatter and have not been considered, therefore, any further.

I9) It is clear from these results that curved vane type swirlers operate more efficiently than flat vane type such that a larger recirculation region, a larger reverse mass flow and stronger shear zones are obtained at a lower pressure drop. For a required recirculation size, therefore, a curved vane type swirler with a lower vane can be used and this provides a further reduction in the pressure loss incurred in the case of using a flat vane type swirler to obtain the same size of the recirculation region. Thus, with the capability of producing a larger recirculation region, a larger reverse mass flow and stronger shear zones, curved vane swirlers can be more helpful in the realization of achievement a better combustion.

20) Since better mixing and longer residence times occur in the case of curved vane swirlers due to increasing turbulence and decreasing axial velocities, a more complete combustion and consequently less pollutant production can be expected from the combustion chambers employing this type of swirlers

CHAPTER 9. SUGGESTIONS FOR FURTHER WORK

SUGGESTIONS FOR FURTHER WORK

The useful effects of vane swirlers on combustion process have long been known and they have been widely employed on burners.In spite of their importance in the planning of the combustion process, not enough investigations for the production of swirler design charts have been made due to mainly quite serious experimental difficulties and there is a dearth for such data in the literature.

The present work makes only a moderately significant stride towards filling this gap;it is by no means claimed herewith that research on swirlers or swirling flows has been completed.In fact,the author believes that in general, the end of a thesis is very likely to open an era of new questions. Although this may generally be more true for the works with mostly experimental concern, this has not been exactly the case here : the trends caused by the swirler design characteristics have been examined and found out using the hot-wire formulation developed and the test rig designed and manufactured. What is left to be done is to quantify the results in more detail ; for instance,effect of the aspect ratio has been examined for only two values,namely, 0.4 and I .It is suggested that additional tests should be carried out with the swirlers having an aspect ratio between 0.6 and 0.7 .In such tests , the pressure drop caused by the aspect ratio will obviously be smaller than that in the case of the aspect ratio of 0.4 . Also,the effect of the number of vanes has not been examined in detail; only the cases of I2 and I6 vanes which are quite close values,have been investigated.In the case of the aspect ratio of 0.4 and vane angle 60^{o}, the effect of the vane number does not seem very much pronounced;this can be seen from a comparison of the swirlers S.I0 and S.II .It may be that by decreasing the number of vanes,for instance to 8 ,and by selecting an aspect ratio of 0.7 ,the pressure drop due to this characteristics can be reduced while the decrease in the swirl number and consequently the size of the recirculation region can be compensated with small increases in the vane angle.In order to complete the present comparative tests for the aspect ratio of I.0 , it is suggested that the swirlers with the characteristics

60^{o}, I2 flat vanes , I.0

60^{o}, I6 curved vanes , I.0

should be tested.It has not been possible to manufacture these swirlers during the course of this work.Significance of these swirlers can be seen from a comparison of their characteristics with those of the present ones .Comparison of the former with

S.I would show the effect of the vane number in the case of flat vanes ; a comparison of the former with the swirler S.4 would show the effect of the curved vanes in the case of I2 vanes . A comparison of the latter swirler with S.I would show the effect of the curved vanes in the case of I6 vanes ; its comparison with the swirler S.4 would show the effect of the number of vanes in the case of the curved vanes . Also , testing of the swirler with the characteristics(70°,I6 curved vanes, I.0) is recommended to find out the effect of the vane angle for the curved vanes in the case of the aspect ratio of I.0 .Further,for the first step towards swirler design charts it is suggested that the swirlers with the following parameters should be tested :

40°, I6 curved vanes , 0.7
50°, I2 curved vanes , 0.7
50°, I6 curved vanes , 0.7
60°, 8 curved vanes , 0.7
60°, I2 curved vanes , 0.7
60°, I6 curved vanes , 0.7
70°, I6 curved vanes , 0.7

Extending the values of these characteristics and with further tests, many more details about the flow fields can be deter - mined and design charts can be prepared .Obviously,many more swirlers are required for this purpose .

All the consideration in this work has been given to the examination of the interaction between the swirler geometry and the aerodynamic properties of the downstream recirculation region .The flow inside the swirler,however, has not been examined .The distribution of the static pressure along the vanes can be investigated and separation from the vanes can be detected .All this information can then be used for more efficient swirler design .

It has been observed by Syred (Ref.87) and in this work that the Reynolds stresses $\overline{ww}$, $\overline{uw}$ and $\overline{uu}$ are the most dominant stresses in strongly swirling flows and the corresponding viscosities are the most dominant viscosities .Among these dominant viscosities,however, calculation of the viscosity $\mu_{z\theta}$ has not been possible in this work due to the I.5" intervals between the radial traverses in the z direction ; with more detailed measurements in this direction,that is,making many more radial traverses, its variation should be calculated . Such detailed measurements would also aid more correct calculation of the viscosity μ_{rz} since determination of the term $\partial V/\partial z$ would then be possible(see Eqn.s.2.6) .

Although anisotropic turbulence and momentum exchange coefficients have been observed both theoretically and experimentally in swirling flows, to the best knowledge of

the author the best turbulence models developed so far for the calculation of such turbulent flows, for instance the so called k--ε model, employ a single relation connecting the isotropic momentum exchange coefficient with a turbulence quantity, for instance turbulence kinetic energy ;anisotropy for the momentum exchange coefficients can be allowed simply with some constants .In order to be able to obtain better predictions with the computational methods for swirling flows, more elaborate turbulence models taking the anisotropy into account in a more realistic way are required.All such models would be devised by making use of experimental turbulence data .The dearth for turbulence data in strongly swirling flows ,however, is much more severe than that for the mean data ;this is because it poses formidable difficulties to obtain reliable turbulence data in swirling flows and these difficulties are obviously due to the higher turbulence intensities present than those in the corresponding straight jets for which turbulence data are quite abundant .Therefore, more detailed measurements ,especially with different measuring techniques from that employed in this work for comparison purposes, are recommended.The results of all such measurements should then be used for the establishment of a more developed turbulence model.Since the measurements could not be much detailed due to the comparative character of this work, such an attempt was not tried at all; this may be attempted ,however, taking more detailed measurements in a few flow fields using the already existing test rig and swirlers .

In this study tests have been carried out under isothermal conditions .The investigations can be extended to include the hot conditions as well . A Laser Doppler anemometer is clearly much more convinient for such a purpose .Thus ,the influence of the hot conditions on the aerodynamic characteristics of the downstream recirculation region can be determined .

Only the case of free jet flows has been considered in this work in order to eliminate the effects of a confinement on the recirculation region. Confined flow geometries,also with air dilution can be examined .

REFERENCES

No.	Author	Title
1	Lefebvre,A.H.	'Lecture notes on Combustion Applications',School of Mechanical Engineering,C.I.T.,1974
2	Khalil,M.I.	'Study of Pollutant Formation in a Gas Turbine Combustor',Ms.C.Thesis, C.I.T.,1974
3	Durham,F.P.	'Aircraft Jet Powerplants', Prentice-Hall Inc.,New York,1951
4	Knight,H.A. Walker,R.B.	'The Component Pressure Losses in Combustion Chambers',N.G.T.E. Report R.143,Nov.,1953
5	Schetinkov, Ye.,S.	'The Physics of Combustion of Gases', N.T.I.S.,U.S. Department of Commerce,1969
6	Kerr,N.M. Fraser,D.	'Swirl.Part 1:Effect on Axisymmetrical Turbulent Jets',J.Ins. Fuel, Dec., 1965,38,p.19-526
7	Kerr,N.M.	'Swirl.Part 2:Effect on Flame Performance and the Modelling of the Swirling Flames',J.Ins. Fuel, Dec., 1965,38,p.527-538
8	Mathur,M.L. Maccalum,N.R.L.	'Swirling Air Jets Issuing from Vane Swirlers.Part 1.Free Jets', J.Ins. Fuel,May,1967,40,p.21
9	Bafuwa,G.G. Maccalum,N.R.L.	'Turbulent Swirling Flames Issuing from Vane Swirlers',18th Meeting of Aerodynamics Panel,I.F.R.F.,1970
10	Beltagui,S.A. Maccalum,N.R.L.	'Vane Swirled Flames in Furnaces', 15th Combustion Symposium,Sept.,1975
11	Youssef,T.E.A.	'Experimental Determination of the Velocity and Pressure Profiles in the Combustion Zone in a Model of a Gas Turbine Combustion Chamber', Faculty of Engineering, Cairo University
12	Hutchinson,P Khalil,E.E. Whitelaw,J.H. Wigley,G.	'Influence of Burner Geometry on the Performance of Small Furnaces',15th Combustion Symposium,1975

13 Welty,J.R. Wicks,C.E. Wilson,R.E. 'Fundamentals of Momentum,Heat and Mass Transfer',Wiley,1969

14 Schlichting,H. 'Boundary Layer Theory',4th Edition, Mc Graw Hill Comp.,1960

15 Beer,J.M. Chigier,N.A. 'Combustion Aerodynamics',Applied Science Publishers,London,1972

16 Goldman,Y. Manheimer-Timnat,Y. Weiser,S. 'Influence of Geometric and Kinematic Factors on Combustion Performance',Progress Report 1. T.A.E. Report No.255,Technion-Israel Ins. of Tech. Haifa,Israel

17 Syred,N. Beer,J.M. 'Combustion in Swirling Flows : A Review',Combustion and Flame,23, p.143-201,1974

18 Lefebvre,A.H. Ramsden,K.W. Kilik,E. 'First and Second Progress Reports on the Influence of Swirler Design Parameters on the Aerodynamics of the Downstream Recirculation Region', School of Mechanical Engineering, C.I.T.,1973-74

19 Chigier,N.A. 'Gasdynamics of Swirling Flow in Combustion Systems',Astronautica Acta,Vol.17,p.387-395,Pergamon Press,1972

20 Rose,W.S. 'A Swirling Round Turbulent Jet', J.Appl.Mech.,Vol.29,Trans.ASME, Ser.E,p.615-625,1962

21 Chigier,N.A. Beer,J.M. 'Velocity and Static Pressure Distribution in Swirling Air Jets Issuing from Annular and Divergent Nozzles',J.Basic Eng.,Trans.ASME, Ser.D,Vol.86,p.788-798,1964

22 Chigier,N.A. Chervinsky,A. 'Experimental Investigation of Swirling Vortex Motion in Jets', J.Appl.Mech.,Vol.34,Trans.ASME, Ser.E,p.443-451,1966

23 Chervinsky,A. 'Similarity of Turbulent Axisymmetrical Swirling Jets',AIAA Journal, Vol.6,No.5,p.912-914,May,1968

24 Chigier,N.A. Chervinsky,A. 'Aerodynamic Study of Turbulent Burning Free Jets with Swirl',11th Int.Symp. on Combustion,The Combustion Institute,p.489-499,1967

25 Pratte,B.D. Keffer,J.F. 'The Swirling Turbulent Jet', J.Basic Eng.,Trans.ASME,Ser.D, Vol.94,p.739-748,1972

26	Syred,N. Chigier,N.A. Beer,J.M.	'Flame Stabilization in Recirculation Zones of Jets with Swirl', 13th Int. Combustion Symposium, The Combustion Institute, p.563-570,1971
27	Chigier,N.A. Dvorak,K.	'Laser Anemometer Measurements in Flames with Swirl',15th Int.Symp. on Combustion,The Combustion Institute,Tokyo,August,1974
28	Pai,S.I.	'Fluid Dynamics of Jets',Van Nostrand, New York,1954
29	Patankar,S.V. Spalding,D.B.	'Heat and Mass Transfer in Boundary Layers',Morgan-Grampion,London,1967
30	Patankar,S.V. Spalding,D.B.	'Heat and Mass Transfer in Boundary Layers',2nd Edition,Intertext Books, London,1970
31	Lilley,D.G.	'Theoretical Study of Turbulent Swirling Boundary Layer Flow with Combustion',Ph.D.Thesis,Dept. of Chem.Eng. and Fuel Tech.,Sheffield Univ.,1970
32	Lilley,D.G.	'Prediction of Inert Turbulent Swirl Flows',AIAA Paper,No.72-699, AIAA 5th Fluid and Plasma Dynamics Conference,Boston,Massachusetts, June,1972
33	Lilley,D.G.	'Turbulent Swirling Flame Prediction', AIAA Journal,Vol.12,No.2,p.219-223, Feb.,1974
34	Bayley,F.J. Owen,J.M. Turner,A.B.	'Heat Transfer',T.Nelsonad Sons Lmt., London,1972
35	Mitchell,A.R.	'Computational Methods in Partial Differential Equations',Wiley,London, 1969
36	Rubel,A.	'Some Effects of Swirl on Turbulent Mixing and Combustion',NASA CR-1956, Feb.,1972
37	Rubel,A.	'Swirling Jet Turbulent Mixing and Combustion Computations',NASA CR-2231,1973
38	Lilley,D.G.	'Analytic Inverse of the Turbulent Swirl Flow Boundary Layer Equations', AIAA Paper No.75-856,AIAA 8th Fluid and Plasma Dynamics Conference, Hartford,Connecticut,June,1975

39	Lilley,D.G. Chigier,N.A.	'An Inverse Solution Procedure for Turbulent Swirling Boundary Layer Combustion Flow',Dept. of Chem. Eng. and Fuel Tech.,Sheffield Univ.
40	Lilley,D.G. Chigier,N.A.	'Nonisotropic Turbulent Stress Distribution in Swirling Flows from Mean Value Distributions', Int. J. Heat and Mass Transfer, Vol.14 , p.573-585,1971
41	Lilley,D.G. Chigier,N.A.	'Nonisotropic Exchange Coefficients in Turbulent Swirling Flames from Mean Value Distributions',Dept. of Chem. Eng. and Fuel Tech.,Sheffield Univ.,also 13th Symp. (int.) on Combustion,Salt Lake City, August,1970
42	Torrance,K.E. Kopecky,K.M.	'Numerical Study of Axisymmetrical Vortex Breakdowns', NASA CR-1865, August,1971
43	Torrance,K.E.	'Mass Diffusion in a Self-confined Rotating Flow', NASA CR-2172 , November,1972
44	Lilley,D.G.	'Computing Strongly Swirling Flows with a Primitive Pressure-Velocity Code',AIAA Paper No.75-872, AIAA 8th Fluid and Plasma Dynamics Conference,Hartford,Connecticut, June,1975
45	Gosman,A.D. Pun,W.M. Runchal,A.K. Spalding,D.B. Wolfshtein,M.W.	'Heat and Mass Transfer in Recirculating Flows',Academic Press, London,1969
46	Forsyth,G.E. Wasow,W.R.	'Finite Difference Methods for Partial Differential Equations', Wiley,New York,1960
47	Launder,B.E. Spalding,D.B.	'Mathematical Models of Turbulence', Academic Press,London,1972
48	Jones,W.P. Launder,B.E.	'The Prediction of Laminarization with a Two Equation Model of Turbulence', Int. J. Heat and Mass Transfer, Vol.15,p.301,1972
49	Kubo,I. Goulding,F.C.	'Numerical Calculations of Turbulent Swirling Flow', Fluid Mechanics of Combustion,A.S.M.E.,New York,1974

50	Roache, P.J.	'Computational Fluid Dynamics', Hermosa Pub., Albuquerque, N.Mex., 1972
51	British Standards Institution	'B.S.1042'
52	Binks, D.	'Compressible Flow in Ducts', Ms.C.Thesis, C.I.T., 1970
54	Lee, J.C. Ash, J.E.	'A Three Dimensional Spherical Pitot Probe', Trans.ASME, Vol.78, p.603-608, April, 1956
55	Slingsby, B.	'Lecture Notes on Boundary Layers and Turbulence', School of Mechanical Engineering, C.I.T., 1974
56	Bradshaw, P.	'An Introduction to Turbulence and its Measurement', Pergamon Press, 1971
57	Ladenburg, R.W.	'Physical Measurements in Gas Dynamics and Combustion', Princeton University Press, 1954
58	Durst, F. Melling, A. Whitelaw, J.H.	'Laser Anemometry : A Report on EUROMECH 36 ', J. of Fluid Mech., Vol.56, Part 1, p.143-160, Nov., 1972
59	DISA	'Instruction and Service Manual for Type 55D01 Anemometer Unit'
60	Collis, D.C. Williams, M.J.	'Two-Dimensional Convection from Heated Wires at Low Reynolds Numbers', J. of Fluid Mech. , Vol.6 , p.357, 1959
61	Frankiel, F.N.	'The Influence of the Length of a Hot-Wire on the Measurement of Turbulence', Phys. Rev. , Vol.75, April, 1949
62	Frankiel, F.N.	'On the Hot-Wire Length Correction', Phys. Rev. , Vol.76, Oct., 1949
63	DISA	'Probe Manual', Feb., 1973
64	Klatt, F.	'The X-Hot-Wire Probe in a Plane Flow Field', DISA Information, No.8 , July, 1969
65	Hinze, J.O.	'Turbulence, An Introduction to Its Mechanism and Theory', McGraw-Hill Book Co., Inc., New York, 1959

66	Webster,C.A.G.	'A Note on the Sensitivity to Yaw of a Hot-Wire Anemometer', J. of Fluid Mech., Vol.13,p.307,1962
67	Champagne,F.H. Sleicher,C.A.	'Turbulence Measurements with Inclined Hot-Wires', J. of Fluid Mech.,Vol.28,Part 1,p.152-176, 1967
68	Champagne,F.H. Sleicher,C.A.	'Turbulence Measurements with Inclined Hot-Wires', J. of Fluid Mech.,Vol.28,Part 2,p.177-182, 1967
69	Davies,P.O.A.L. Bruun,H.	'The Performance of Yawed Hot-Wires', I.S.V.R.,University of Southampton, England
70	Kronauer,R.E.	Pratt and Whitney Research Report ,No.137, 1953
71	Jorgensen,F.E.	'Directional Sensitivity of Wire and Fiber Film Probes', DISA Information ,No.11,p.31-37,1970
72	Dahm,M. Rasmussen,C.G.	'Effect of Wire Mounting System on Hot-Wire Probe Characteristics', DISA Information ,No.7 ,p.19-24, Jan., 1969
73	Kjellstrom,B. Hedberg,S.	'Calibration of a DISA Hot-Wire Anemometer and Measurements in a Circular Channel for Confirmation of the Calibration', DISA Information,No.9,p.8-14,Feb.,1970
74	TSI	'Anemometry'
75	Heskestad,G.	'Hot-Wire Measurements in a Plane Turbulent Jet',J. Appl. Mech., Vol.32,Trans.ASME,Ser.E,p.721-734, Dec.,1965
76	Mojola,O.O.	'A Hot-Wire Method for Three Dimensional Shear Flows',DISA Information,No.16 ,p.11-14,July,1974
77	Rodi,W.	'A New Method of Analysing Hot-Wire Signals in Highly Turbulent Flow and Its Evaluation in a Round Jet', DISA Information,No.17,p.9-18, Feb.,1975
78	Durao,D. Whitelaw,J.H.	'Turbulent Mixing in the Developing Region of Coaxial Jets', J. Fluids Eng.,Vol.95,Trans.ASME,Ser.1,No.3, p.467-473,Sept.,1973
79	Davies,T.W.	'A Study of the Aerodynamics of the Recirculation Zone Formed in a Free Annular Air Jet', Ph.D. Thesis, Sheffield Univ.,1968

80	Davies,P.O.A.L.	'Recent Developments in Hot-Wire Anemometry', Int. Sem. on Heat and Mass Transfer,Hercey Novi, Yugoslavia,1969
81	Siddall,R.G. Dawies,T.W.	'An Improved Response Equation for Hot-Wire Anemometry', Int. J. Heat and Mass Transfer, Vol.15 , No.2, p.367-368,Feb.,1972
82	McCracken,D. Dorn,W.S.	'Numerical Methods and Fortran Programming with Application in Engineering and Science', John Wiley and Sons, Inc.
83	Wygnansky,I. Fiedler,H.E.	'Some Measurements in the Self-Preserving Jet', J. Fluid Mech., Vol.38,p.577,1969
84	Bradshaw,P. Ferris,D.H. Johnson,R.F.	'Turbulence in the Noise Producing Region of a Circular Jet',J. Fluid Mech.,Vol.19,p.591,1964
85	Durst,F. Whitelaw,J.H.	'Measurements of Mean Velocity, Fluctuating Velocity and Shear Stress in air Using a Single Channel Optical Anemometer',DISA Information,No.12,p.11,Nov.,1971
86	Ainley,D.G. Mathieson,G.C.R.	'An Examination of the Flow and Pressure Losses in Blade Rows of Axial-Flow Turbines',Ministry of Supply,Reports and Memorenda, No.2891,March,1951
87	Syred,N. Beer,J.M. Chigier,N.A.	'Turbulence Measurements in Swirling Recirculating Flows',Inst.of Mech. Engineers,London.Symp.on Internal Flow,Univ. of Salford,paper I3, B 27-36,April,I97I
88	Carmody,T.	'Establishment of the Wake Behind a Disc',Trans. ASME,J. Basic Eng., 86 D,4,p.869,I964
89	Kopal,Z.	'Numerical Analysis',John Wiley and Sons Inc.,I955

TABLES

TABLE 1. Effect of the change in the coefficients of the hot-wire calibration equation on the experimental results (compare with TABLE 2)

A= 0.7177
B= 1.4676
C= -0.0017

RMS= 0.1700 ✓

VIN= 69.8569 ✓

RADIAL DISTRIBUTIONS OF REYNOLDS STRESSES AND MEAN VELOCITIES AT AXIAL STATION 1

VII	UM	UII	V2	W2	U2	UV	VW	UW	RAD.STA
11.8343	17.3458	0.0001	23.1582	74.4785	0.0000	0.0002	41.5305	0.0003	1
9.7061	17.6191	1.8734	14.7736	81.7974	1.3373	4.4449	34.7627	10.4590	2
5.3797	20.5264	4.4896	0.9697	98.9785	11.2987	3.3100	9.7969	33.4415	3
2.7194	26.1464	14.2984	4.9624	134.0096	26.7785	11.5276	25.7877	59.9048	4
55.3845	67.4551	82.2937	19.5521	298.6186	481.2224	96.9499	76.3717	379.0804	5
67.2536	128.2691	142.4561	38.9713	109.8462	0.3037	3.4402	65.4282	5.7757	6
37.5062	132.9107	149.6164	0.1671	54.3013	1.2206	-0.4516	-3.0121	8.1411	7
14.5788	3.8244	3.9092	13.8245	5.5853	0.5697	2.8064	8.6284	1.7516	8

TABLE 2. Effect of the change in the coefficients of the hot-wire calibration equation on the experimental results (compare with TABLE 1)

A= 0.7177
B= 1.4712
C= -0.0017

FK= 0.1700 ✓

VIN= 88.8560 ✓

RADIAL DISTRIBUTIONS OF REYNOLDS STRESSES AND MEAN VELOCITIES AT AXIAL STATION 1 .

VM	UM	UN	V2	W2	U2	UV	VW	UW	RAD.STA
11.7744	17.2586	0.0000	22.9207	73.7246	0.0000	0.0001	41.1074	0.0001	1
9.6570	17.5305	1.8639	14.6219	80.9692	1.3237	4.3994	34.4082	10.3527	2
5.3525	20.4230	4.4670	0.9595	97.9736	11.1836	3.2757	9.6955	33.1013	3
2.7055	26.0143	14.2255	4.9116	132.6423	26.5007	-11.4088	25.5241	59.2884	4
55.0916	67.1987	81.8620	19.3084	295.4974	476.0309	95.8717	75.5352	375.0545	5
66.8921	127.5406	141.6918	38.5398	108.6554	0.2988	3.3937	64.7114	5.6983	6
37.3051	132.2188	148.8106	0.1656	53.7133	1.2046	-0.4469	-2.9821	8.0439	7
14.5057	3.8058	3.8395	13.6846	5.3314	0.5639	2.7778	8.5415	1.7338	8

TABLE 3. Effect of the change in the yaw correction factor, k_1 , on the experimental results (compare with TABLE 4)

RADIAL DISTRIBUTIONS OF REYNOLDS STRESSES AND MEAN VELOCITIES AT AXIAL STATION 1

V1	W1	U1	V2	W2	U2	UV	VW	UW	RAD.STA
4.750	-23.152	9.746	0.456	119.550	52.157	4.877	7.383	78.964	1
2.581	24.470	14.702	4.468	128.282	80.602	18.976	23.940	101.685	2
14.817	29.332	17.333	39.012	184.747	111.931	66.081	84.896	143.801	3
24.683	53.543	18.566	9.025	634.733	98.770	29.857	75.688	250.385	4
57.807	126.872	131.092	2.928	186.439	91.016	-16.326	-23.366	130.265	5
41.840	124.104	130.747	2.407	40.045	5.567	3.661	9.819	14.931	6
12.474	106.879	103.910	1.789	199.959	0.076	-0.368	-18.913	3.892	7
12.813	7.494	3.839	22.186	16.418	1.891	6.478	19.085	5.572	8
8.641	4.198	2.799	11.617	4.348	0.863	3.166	7.107	1.937	9
8.928	4.082	2.190	13.704	4.210	0.573	2.802	7.596	1.553	10

TABLE 4. Effect of the change in the yaw correction factor, k_1 , on the experimental results (compare with TABLE 3)

RADIAL DISTRIBUTIONS OF REYNOLDS STRESSES AND MEAN VELOCITIES AT AXIAL STATION 1

VM	UM	U1	V2	W2	U2	UV	VW	UW	RAD.STA
4.759	23.142	9.764	0.458	119.403	52.346	4.894	7.392	79.058	1
2.386	24.453	14.729	4.484	128.001	80.894	19.045	23.957	101.757	2
14.844	29.299	17.364	39.153	184.232	112.336	66.320	84.931	143.861	3
24.727	53.308	16.599	9.058	634.698	99.127	29.965	75.823	250.831	4
57.911	128.678	131.329	2.939	186.406	91.345	-16.385	-23.406	130.489	5
41.926	123.798	130.998	2.416	40.098	5.587	3.674	9.843	14.968	6
12.498	106.672	109.113	1.795	200.723	0.076	-0.369	-18.983	3.907	7
12.837	7.647	3.846	22.266	16.364	1.398	6.501	19.088	5.573	8
8.650	4.161	2.796	11.659	4.308	0.866	3.178	7.087	1.931	9
8.944	4.044	2.202	13.754	4.162	0.575	2.812	7.566	1.547	10

FIGURES

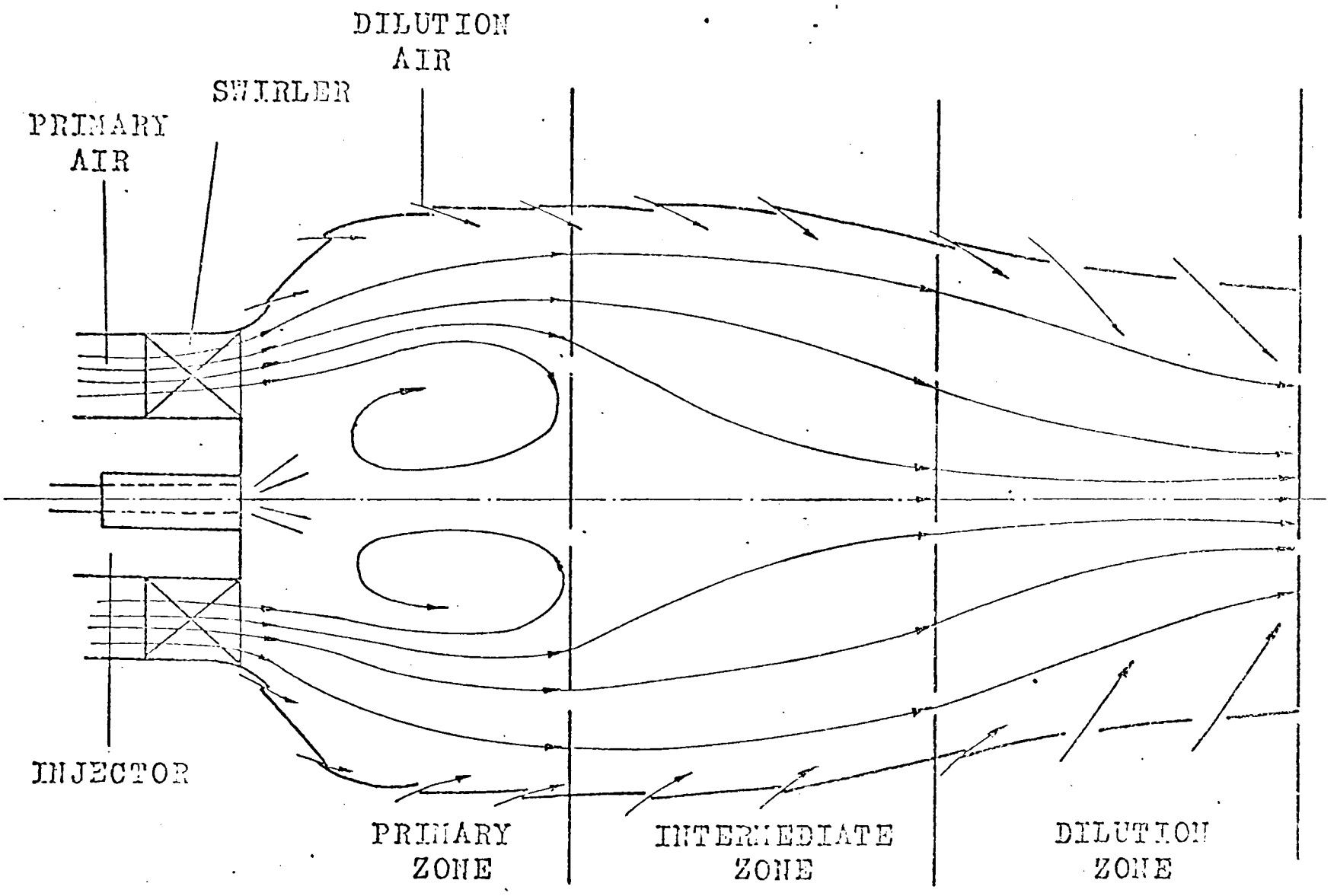

Fig. 1.1. Air flow pattern in a conventional combustion chamber.

θ : vane outlet angle

c : chord

s : space

h/c : aspect ratio

s/c : space-to-chord ratio

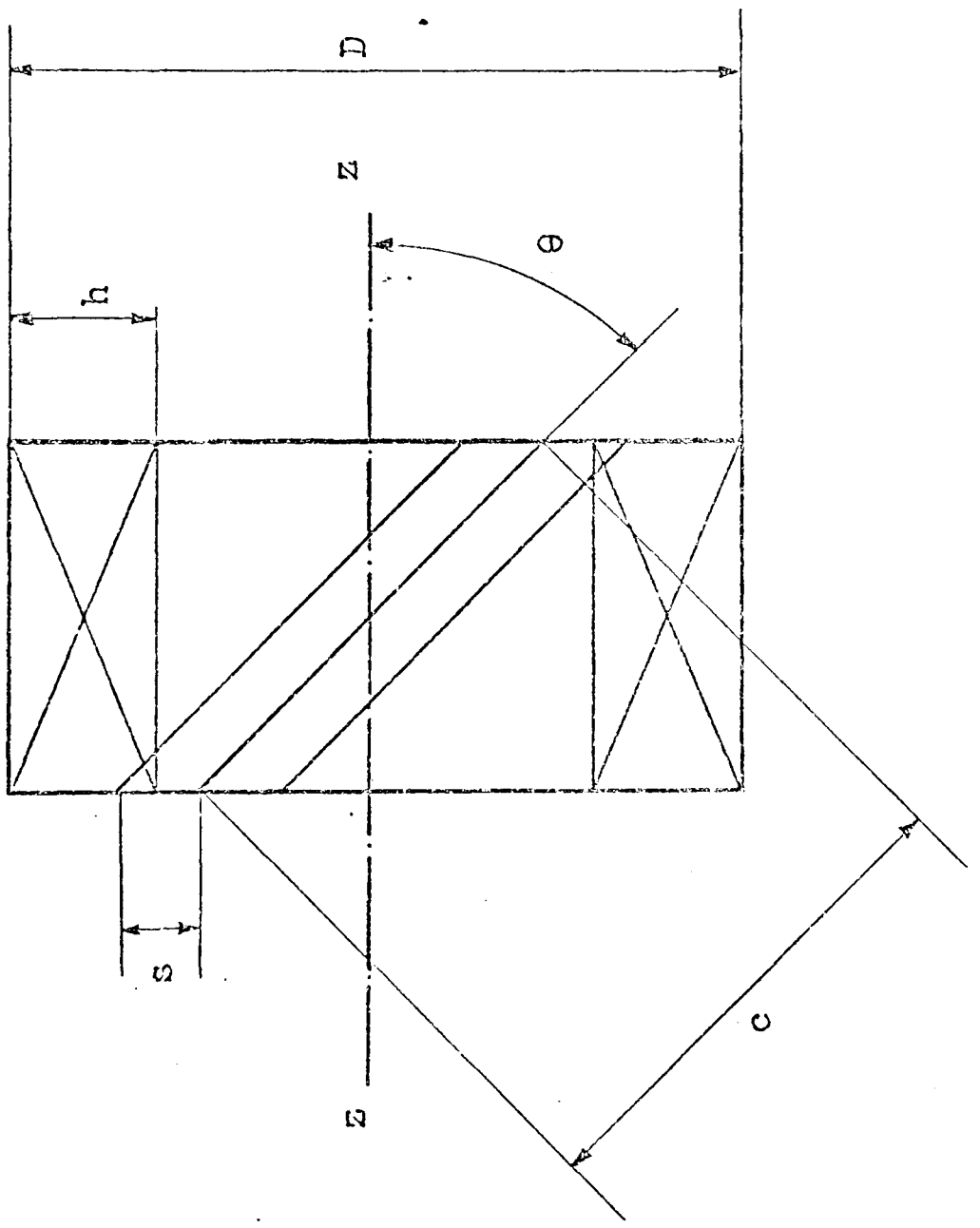

Fig. I.2. Conventional flat vane type swirler with central blading and related notation (only three vanes have been shown)

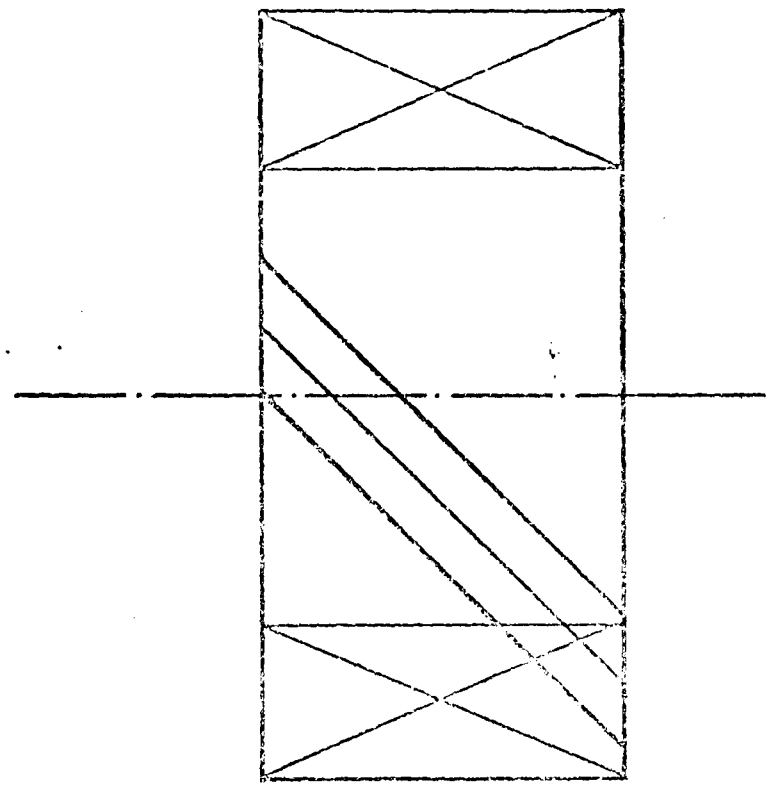

Fig.I.3.Conventional flat vane type swirler with off-central blading(only three vanes have been shown)

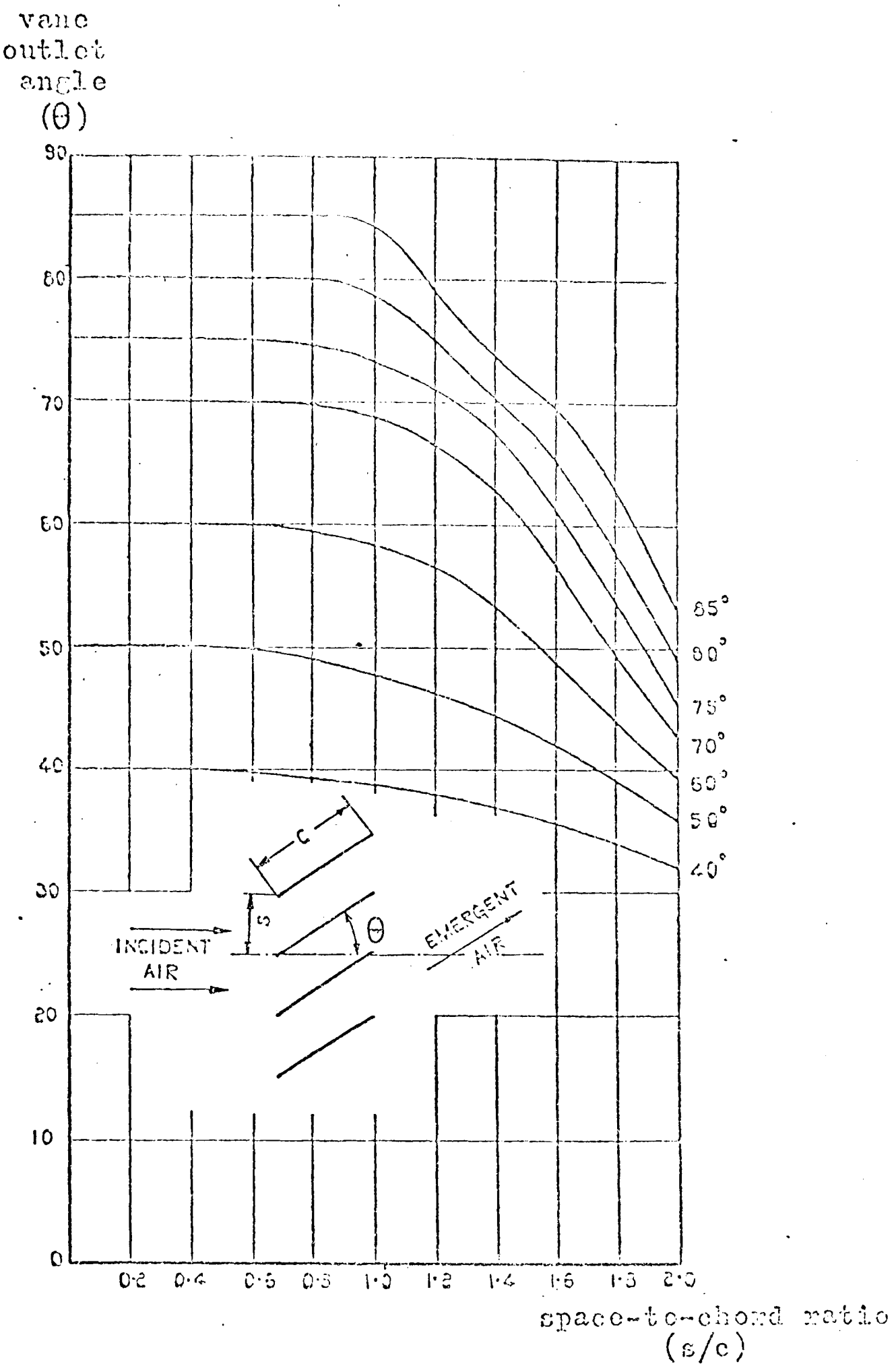

Fig.I.4.Variation of air outlet angle
for flat plate cascades

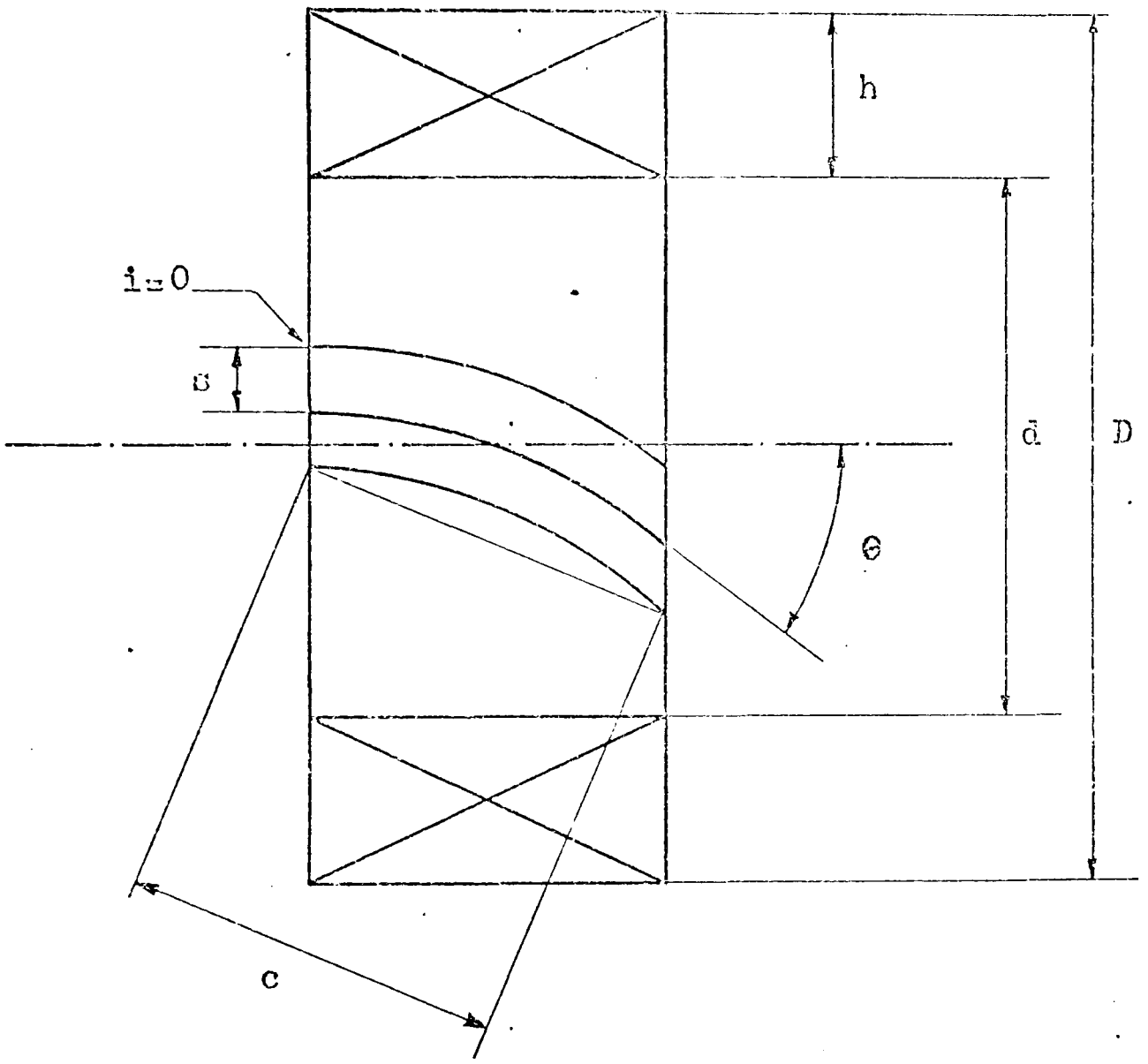

Fig.I.5.Curved vane type swirler (central blading)

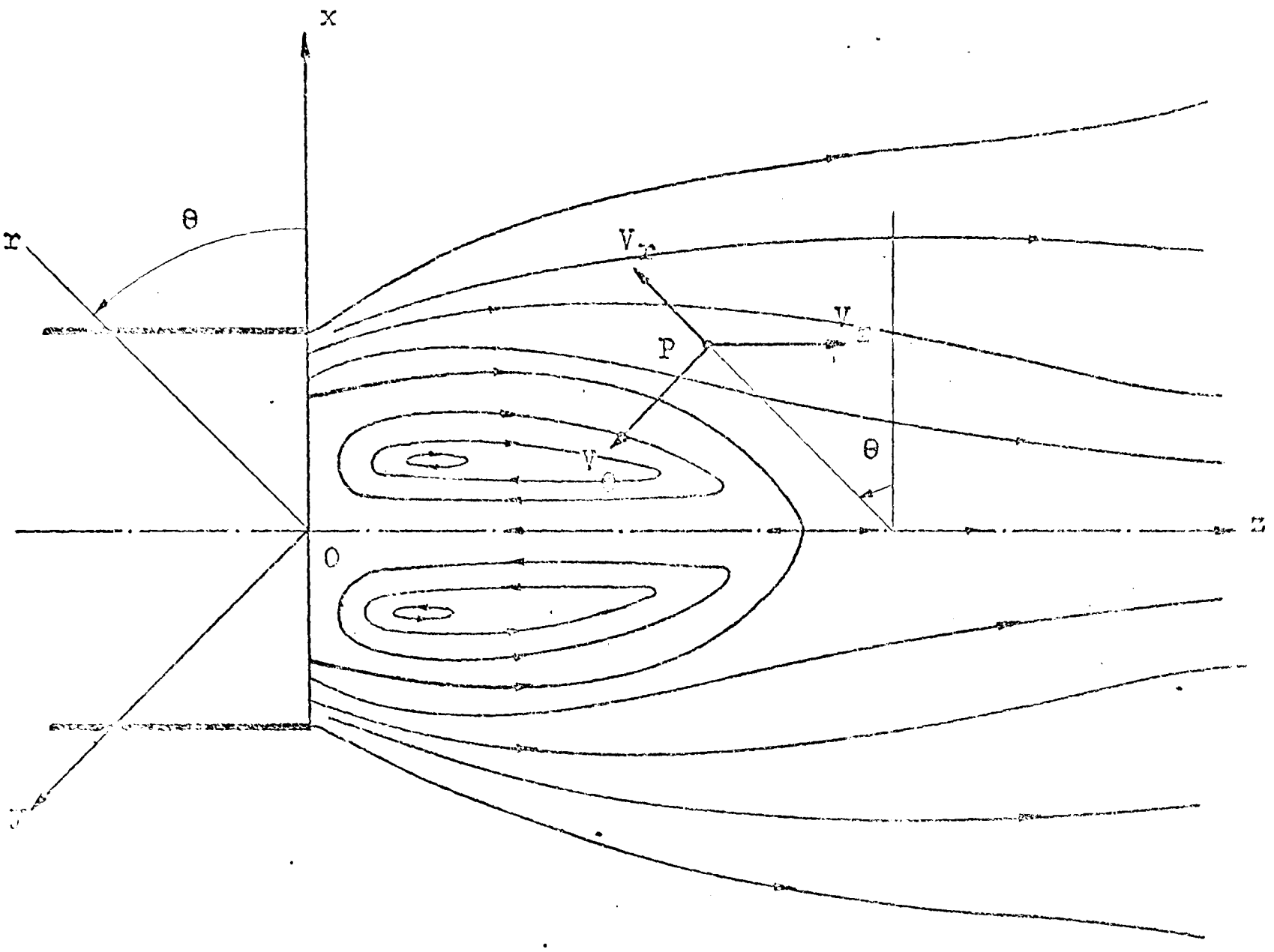

Fig.I.6.Coordinate axes for the swirling flow

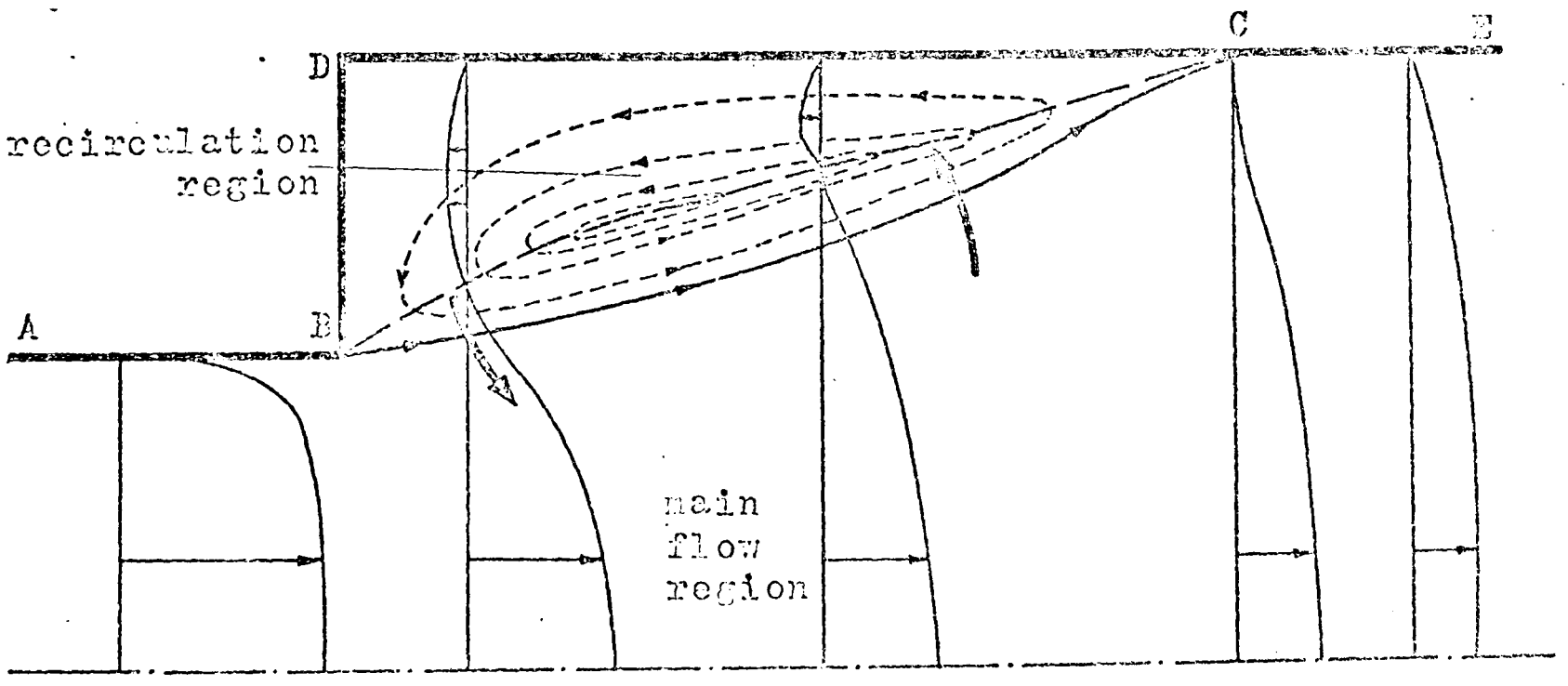

Fig.I.7.Recirculation region in a pipe step

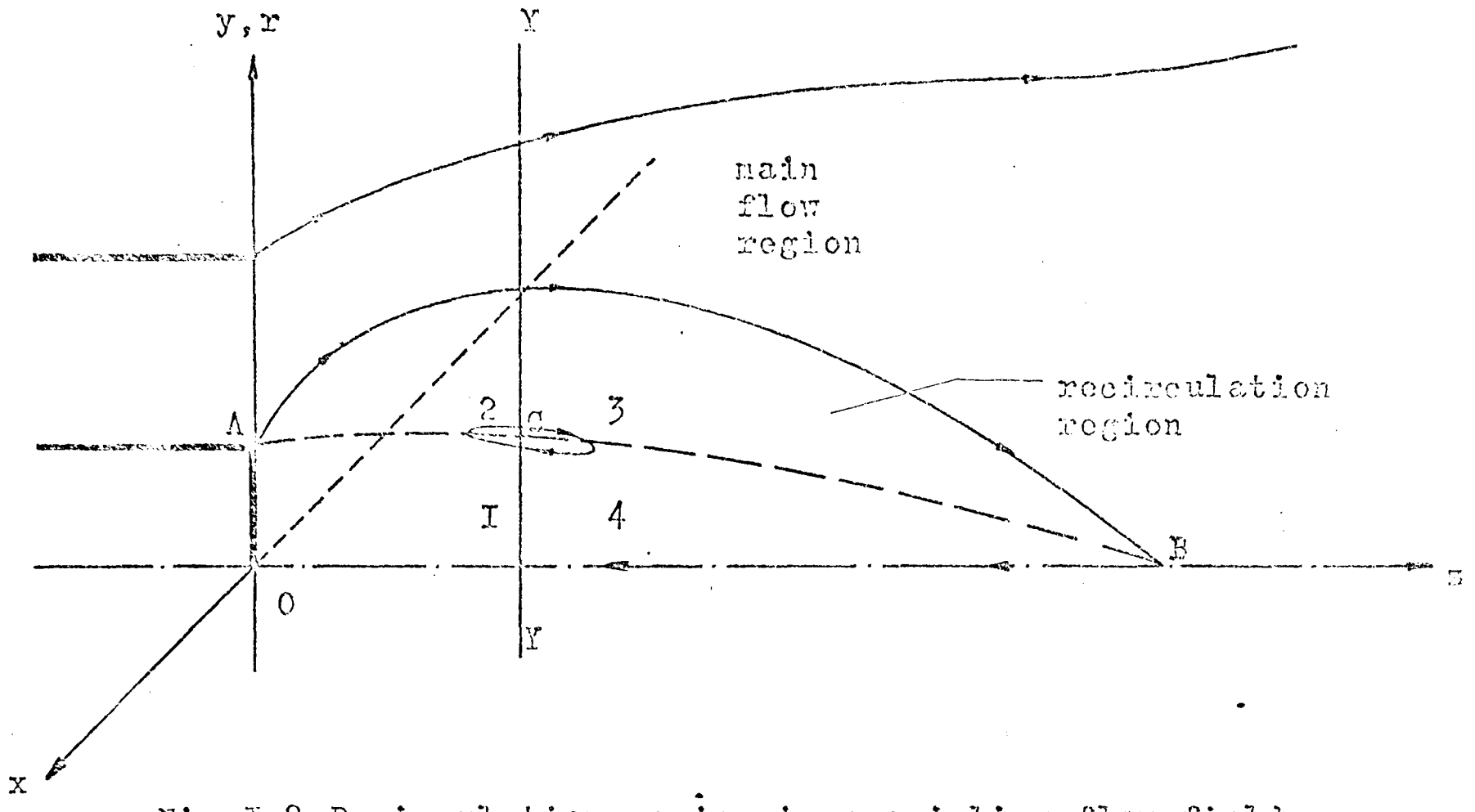

Fig.I.8.Recirculation region in a swirling flow field

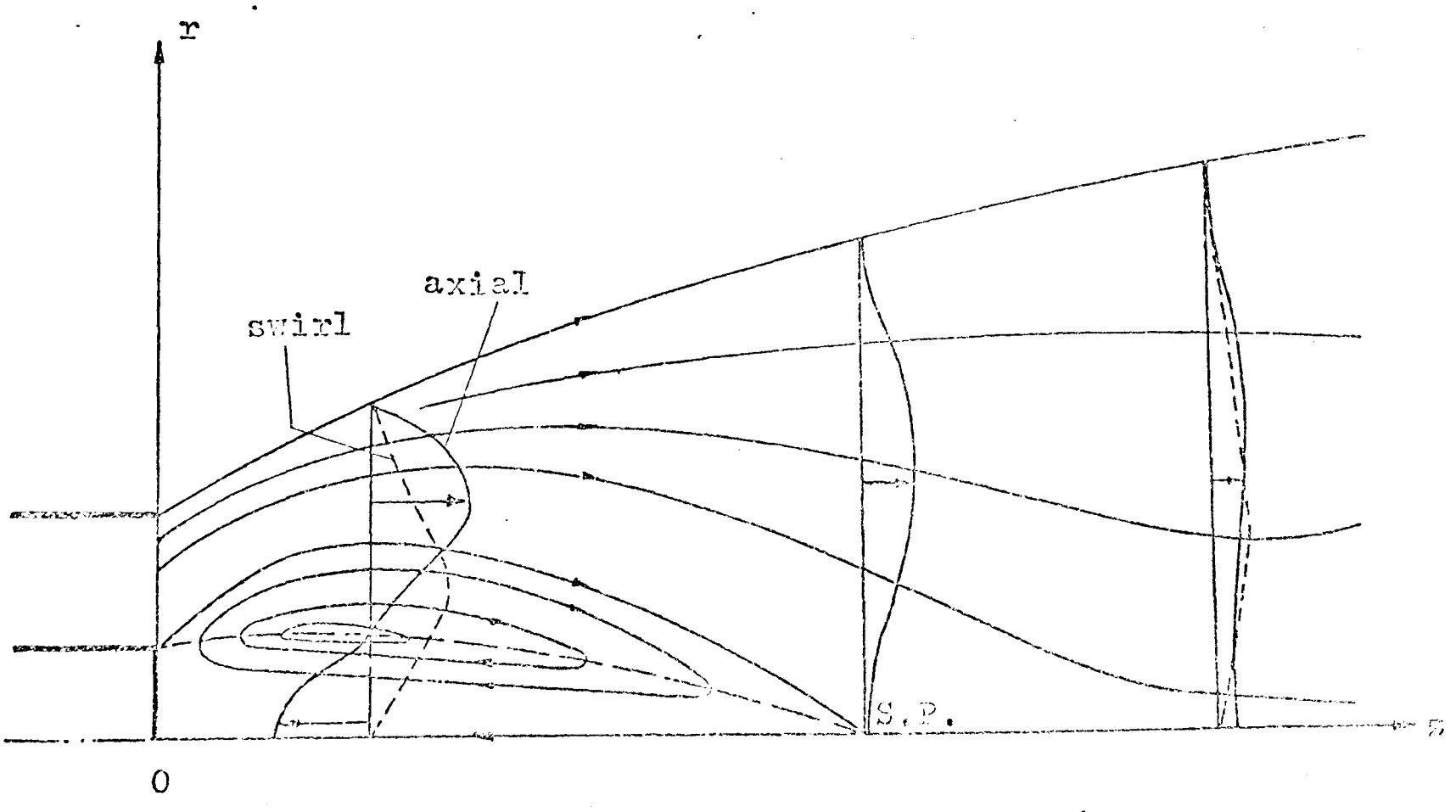

Fig.I.9.Typical profiles of axial and swirl velocity components in a strongly swirling flow field

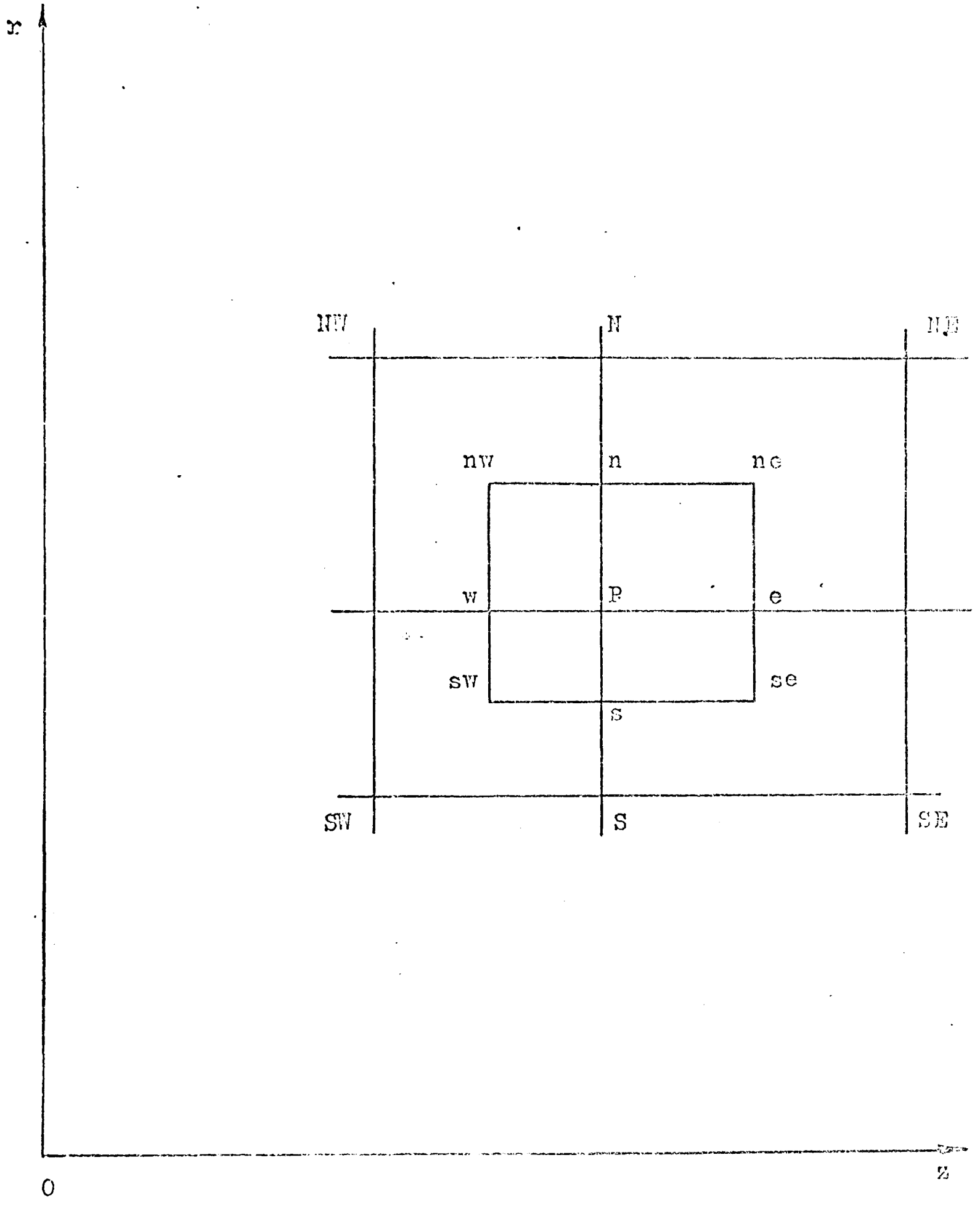

Fig.4.I.The small volume (area) element over which integration is performed

free boundary:
$\partial(\omega/r)/\partial z = 0$

$\partial W/\partial z = 0$

$\Omega = 0$

$\partial k/\partial z = 0$

$\partial \varepsilon/\partial z = 0$

free boundary:
$\partial(\omega/r)/\partial r$, $\partial W/\partial r$, Ω , k , $\varepsilon = 0$

outlet:

$\partial(\omega/r)/\partial z = 0$
$\partial W/\partial n = 0$
$\partial\Omega/\partial z = 0$
$\partial k/\partial n = 0$
$\partial\varepsilon/\partial z = 0$

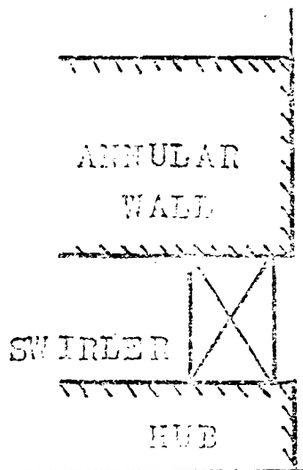

wall:
ω/r :from wall formula
$W = W_{max}$
$\Omega = 0$
$k = 0$
$\varepsilon = 0$

inlet:
ω/r : from U profile
W : from U profile
Ω : from W profile
$k = 0.03\ U^2$
$\varepsilon = 2\ k^{1.5}/0.005\ D$

symmetry axis:
$\omega/r, W, \Omega, \partial k/\partial r, \partial\varepsilon/\partial r = 0$

Fig.4.2. Boundary conditions for free swirling jet

DRAWING No. PD10231

ISSUE	MODIFICATION
A	—

ALL DIMENSIONS IN MILLIMETRES UNLESS OTHERWISE STATED.

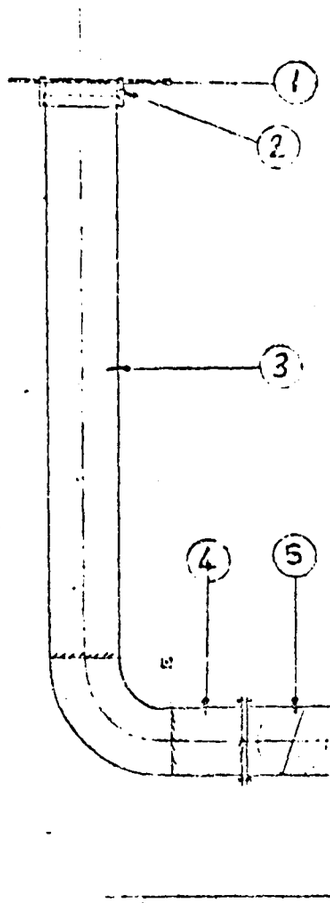

ITEM	PART No.	DESCRIPTION	No. OFF	MATS	SPEC.	REMARKS
13	PD10234	SPINDLE	45			
12	PD10232	BODY FLANGE	1			
11	—	SETTLING CHAMBER	1		3 DIA.	EXISTING
10	—	FLANGED PIPE	1		4 DIA.	
9	—	FLEXIBLE PIPE	1		4 DIA.	
8	—	PIPE	1		4 DIA.	
7	—	FAN	1			KEITH-BLACKMAN
6	—	DIFFUSER	1		6" x 6" DIA 6 DIA	
5	—	BUTTERFLY VALVE	1		6	
4	—	PIPE and FLANGE	1		6 DIA.	
3	—	DOWNSTREAM PIPE	1		6 DIA 4" LONG	
2	PD10233	SUPPORT FRAME	1			
1	PD10231	ORIFICE PLATE	1			

THIRD ANGLE PROJECTION

SHEET SIZE A3

GENERAL TOLERANCE ON DIMENSIONS
MACHINED
UNMACHINED
OTHER DIMENSIONS AS STATED

WELD WHERE SHOWN THUS

MACHINE WHERE SHOWN THUS

JOB No.

No. OF SETS REQD 1

USED ON DRG. —

SCALE 1/10

FINISH

DRAWN

CHKD

APPVD

DATES APPVD

TITLE:- (FIG.42) TEST RIG ASSEMBLY

ISSUED BY SCHOOL OF MECHANICAL ENGINEERING
CRANFIELD INSTITUTE OF TECHNOLOGY
CRANFIELD.

DRAWING No. PD10231

SHT. 1 OF 1 SHEETS

Fig.5.1. Test rig assembly

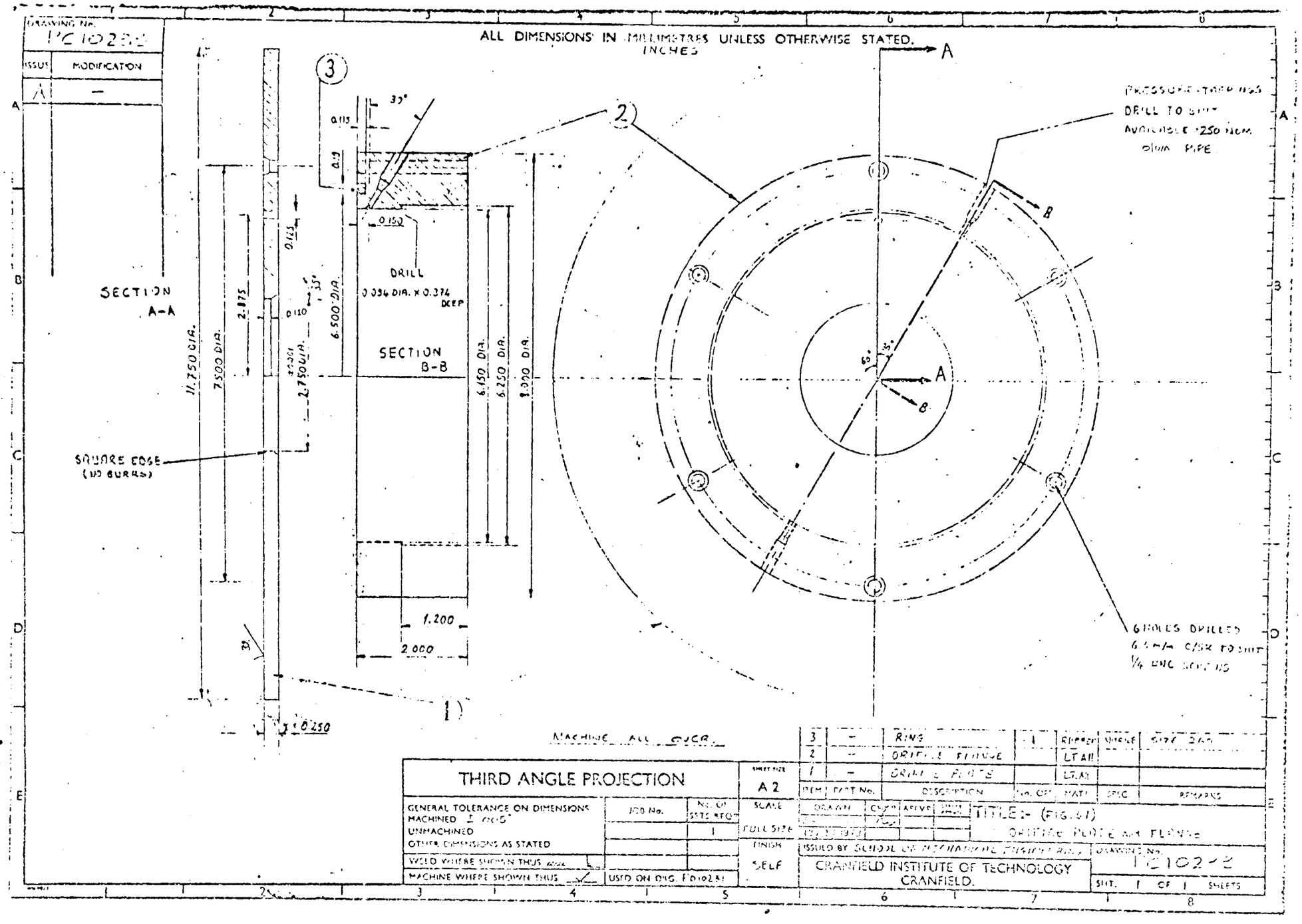

Fig.5.2. Orifice plate and flange for mass flow measurement

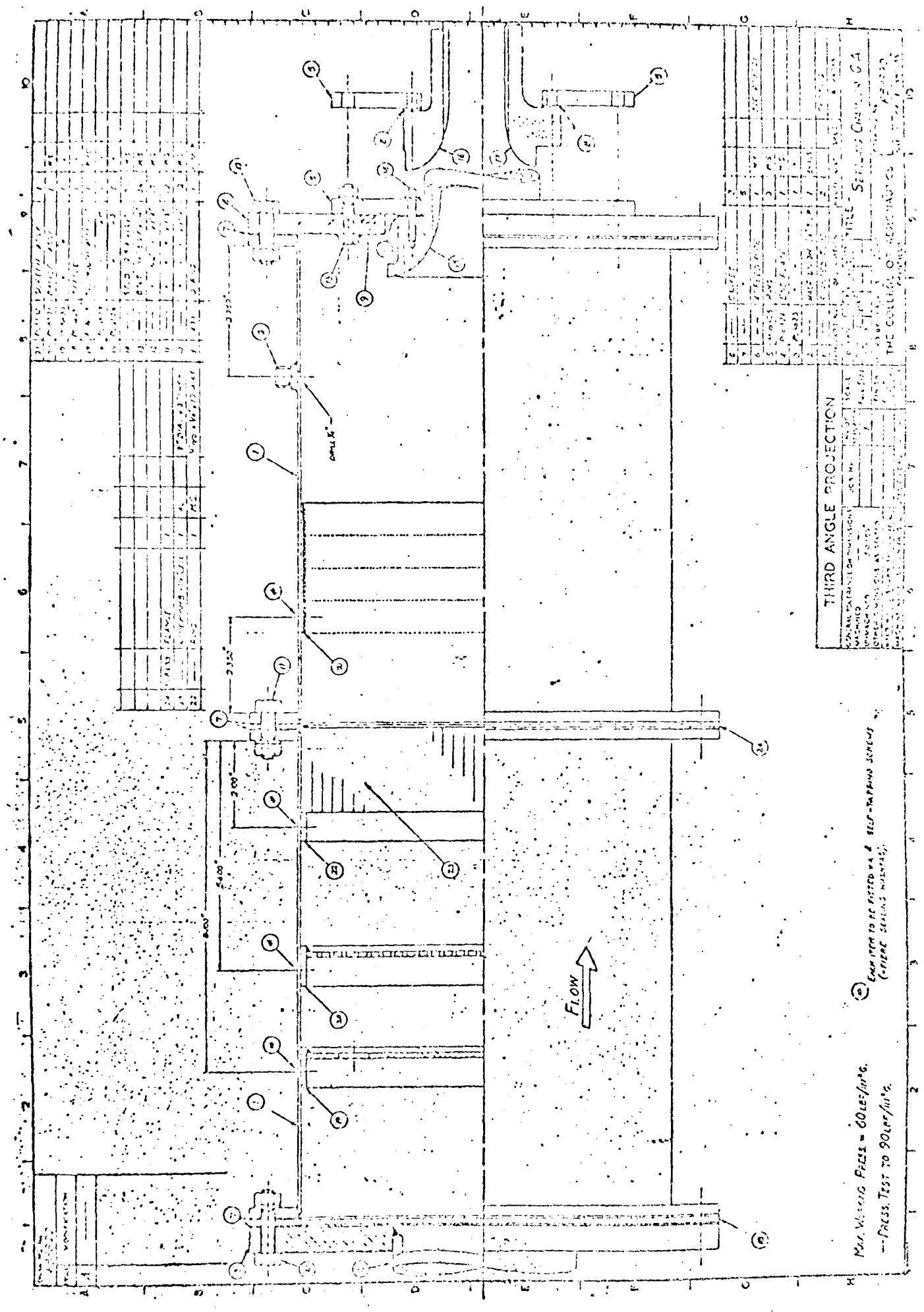

Fig.5.7. The settling chamber

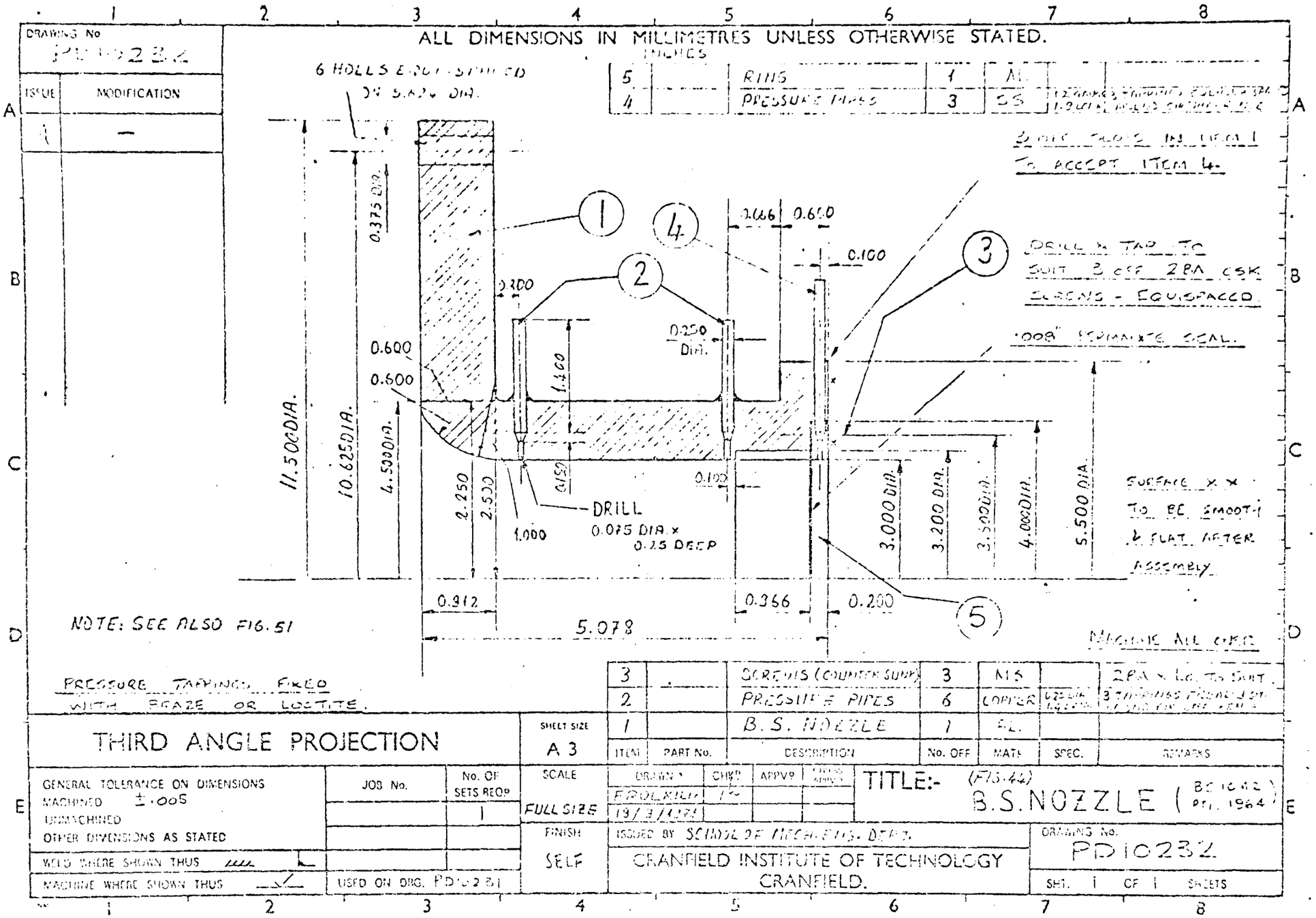

Fig.5.4. B.S. Nozzle

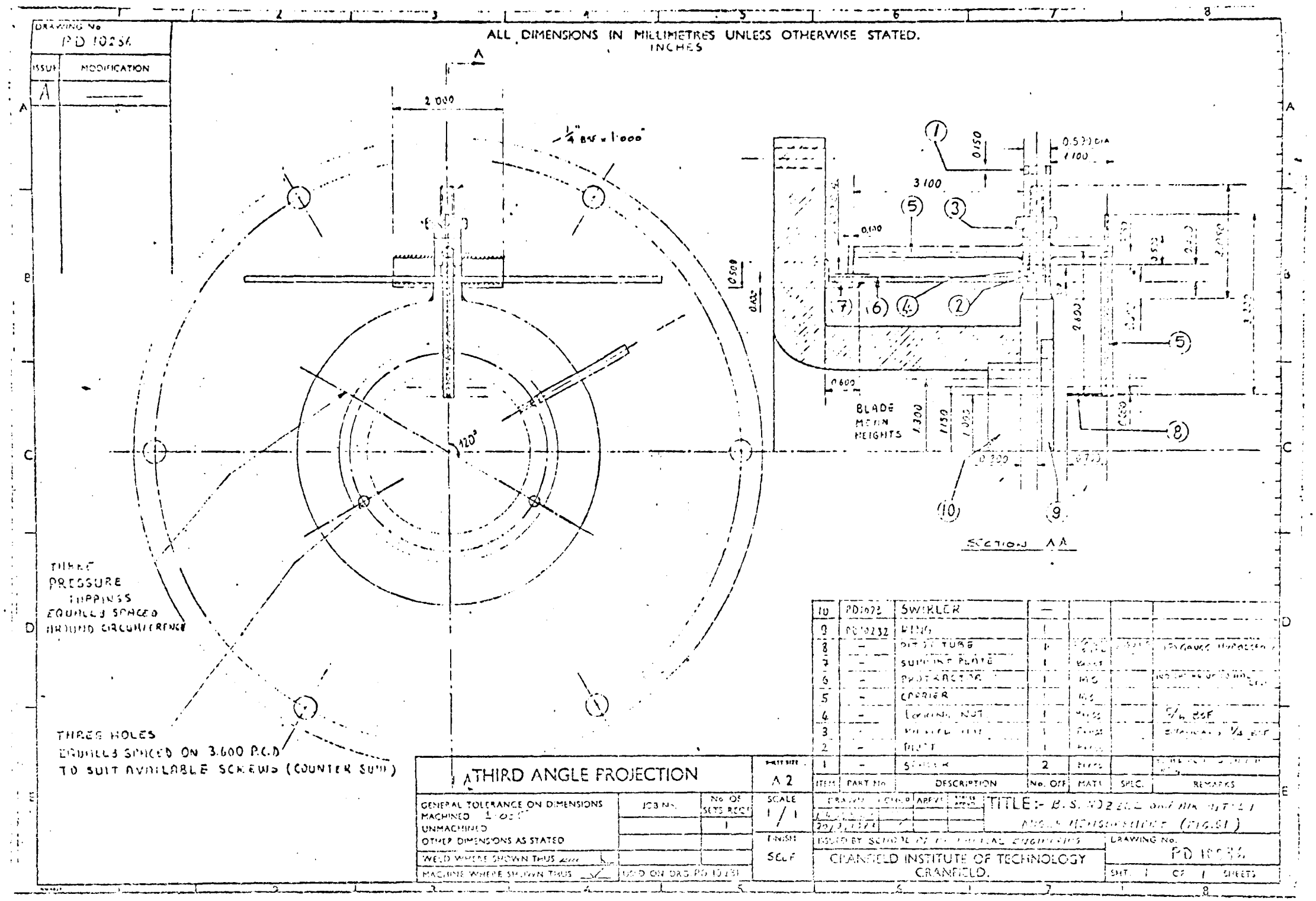

Fig.5.5. B.S. Nozzle and the traversing mechanism

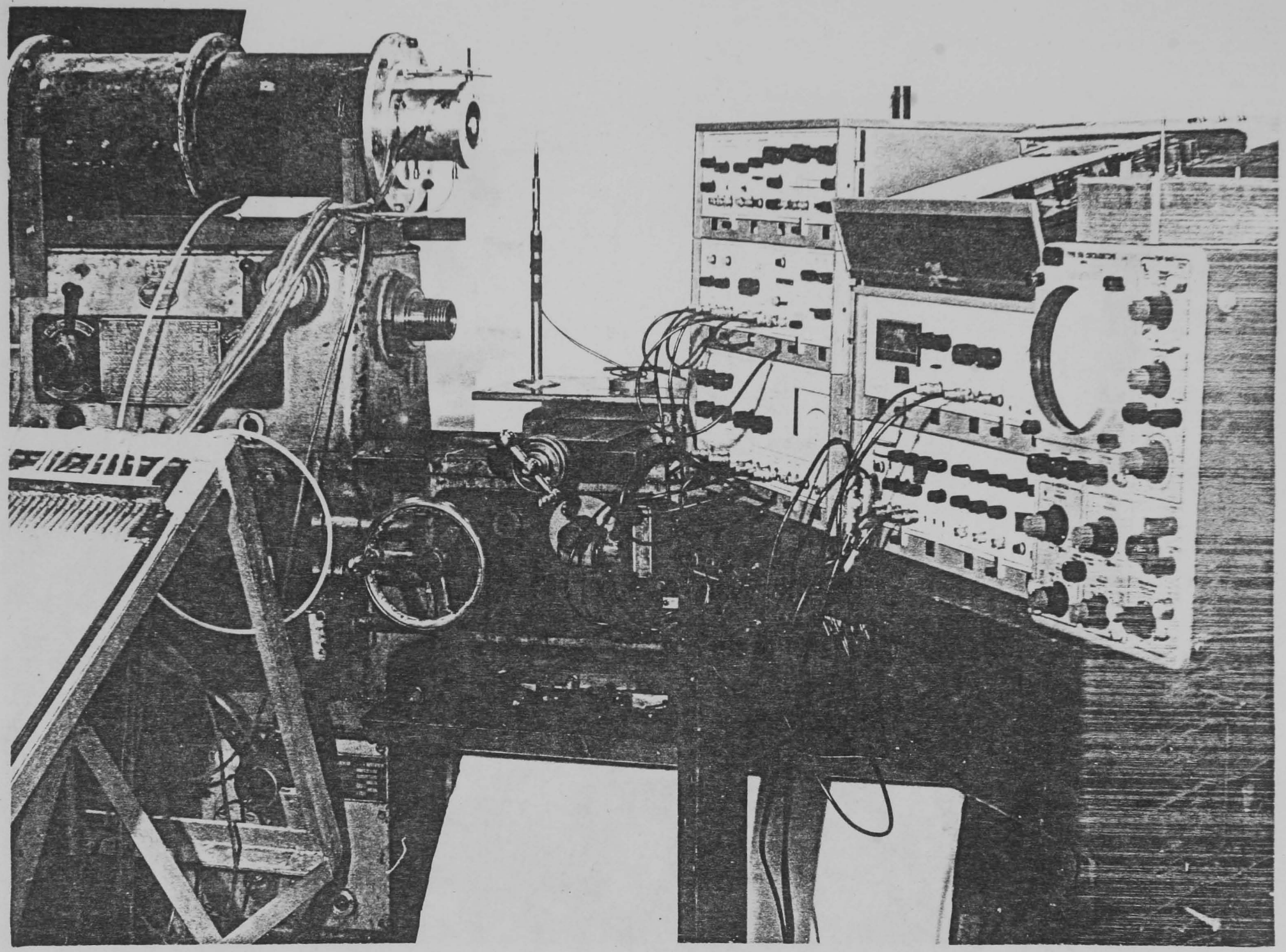

Fig.5.6.The test rig and the hot-wire anemometer system

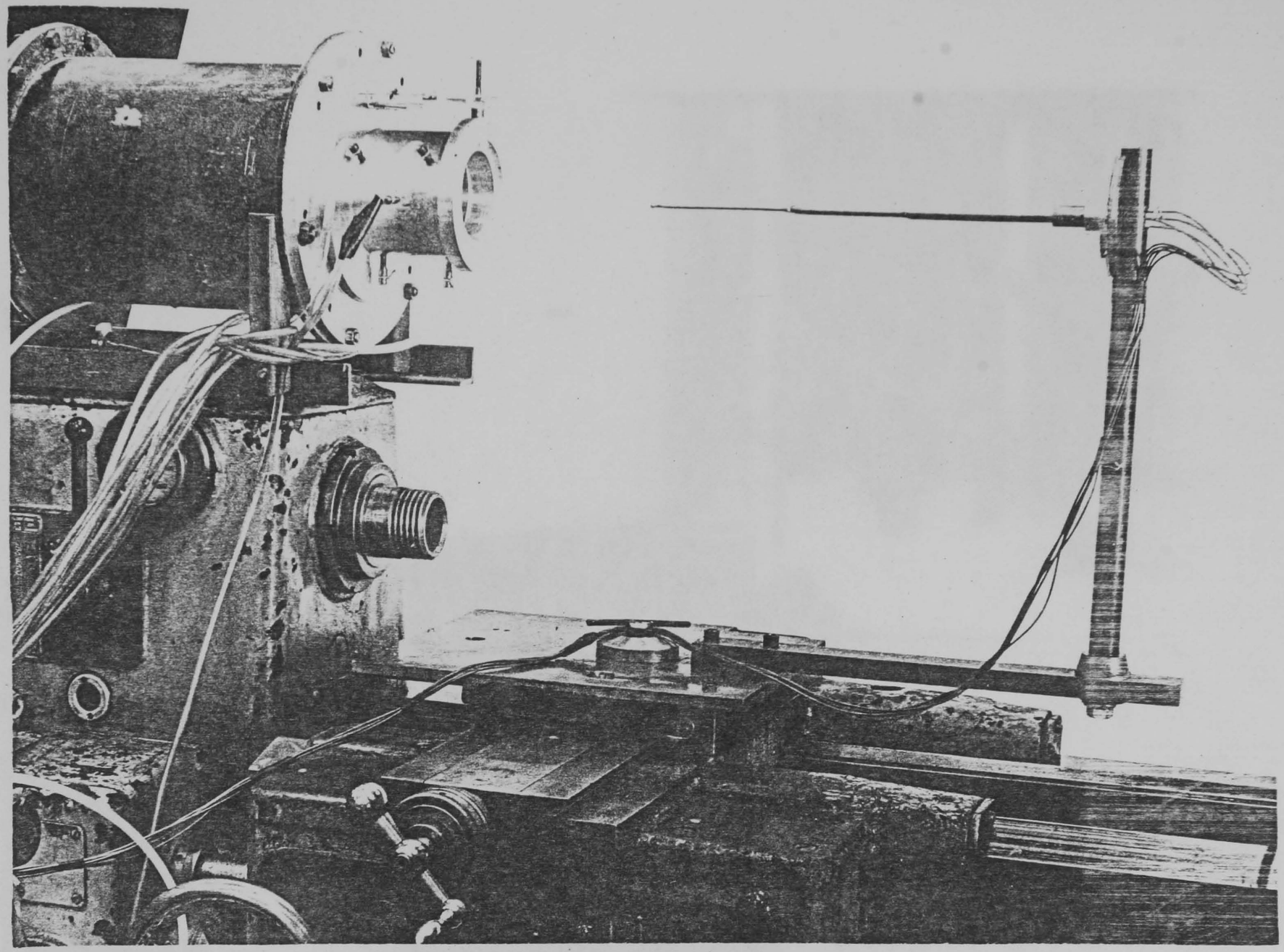

Fig.5.7.The platform and the five-hole spherical pressure probe

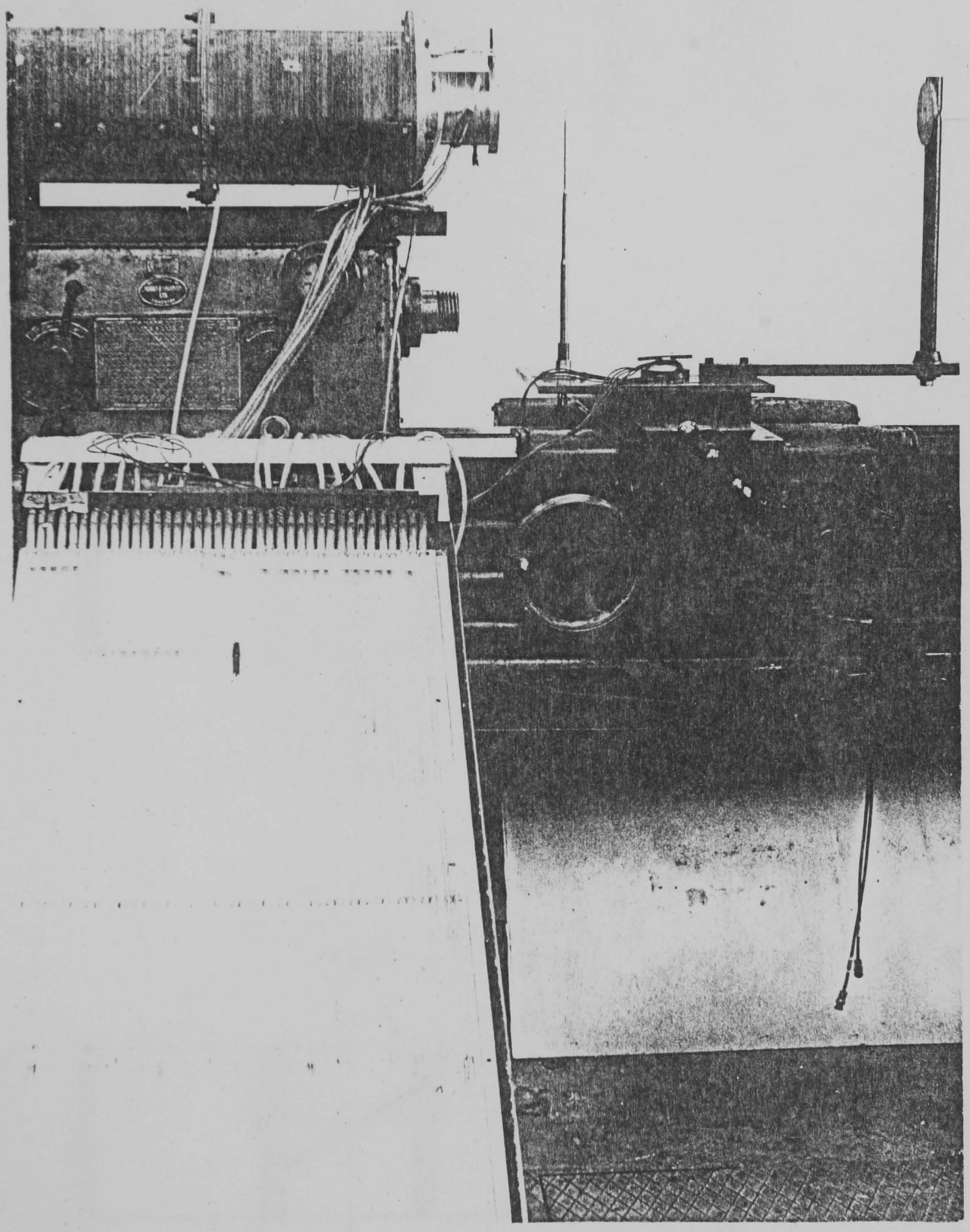

Fig.5.8.The five-hole spherical pressure probe in position in the hole on the platform

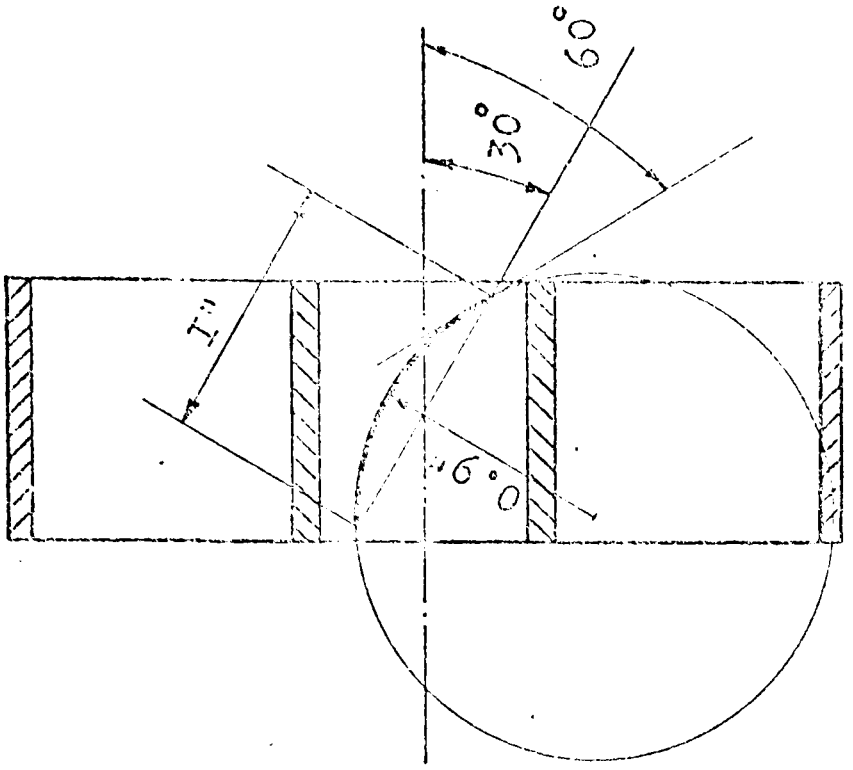

curved vane
(circular arc)
CENTRAL BLADING

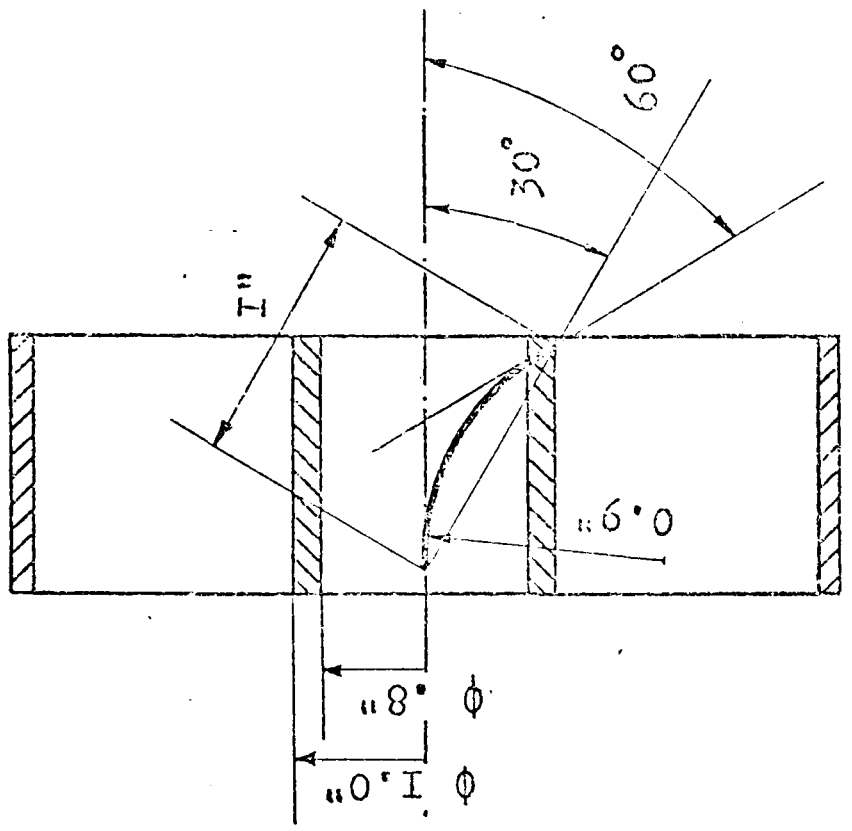

curved vane
(circular arc)
OFF-CENTRAL BLADING

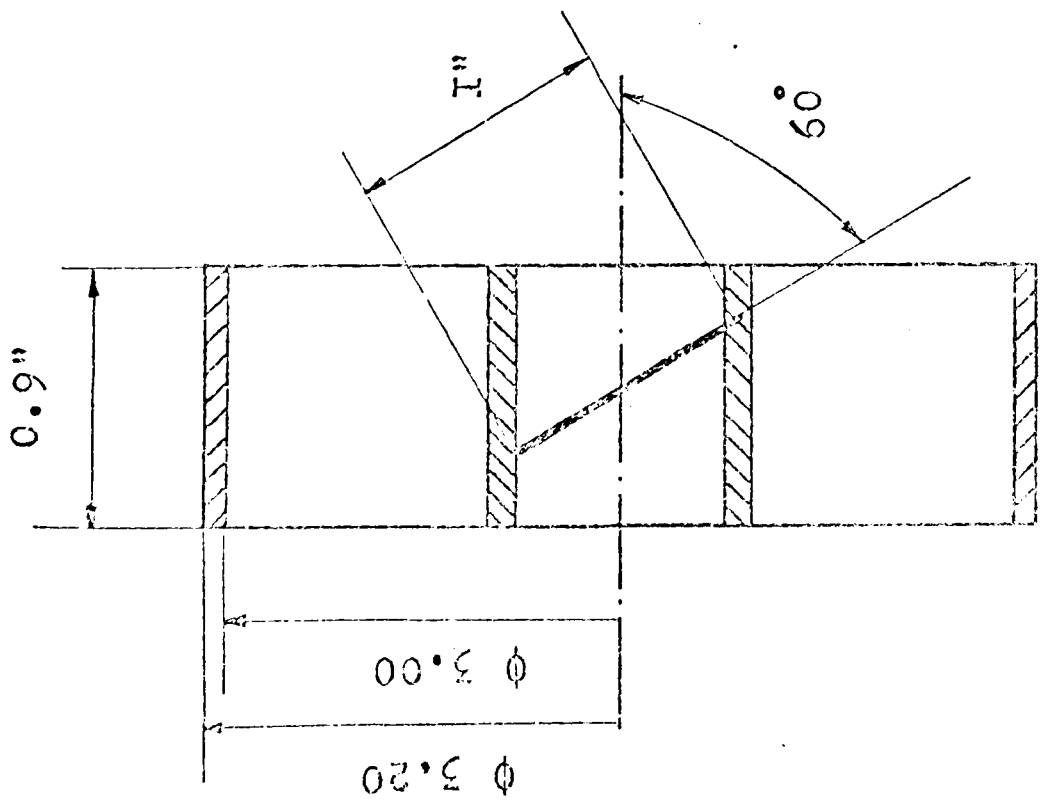

flat vane
CENTRAL BLADING

Fig.5.9.Three types of vane swirler

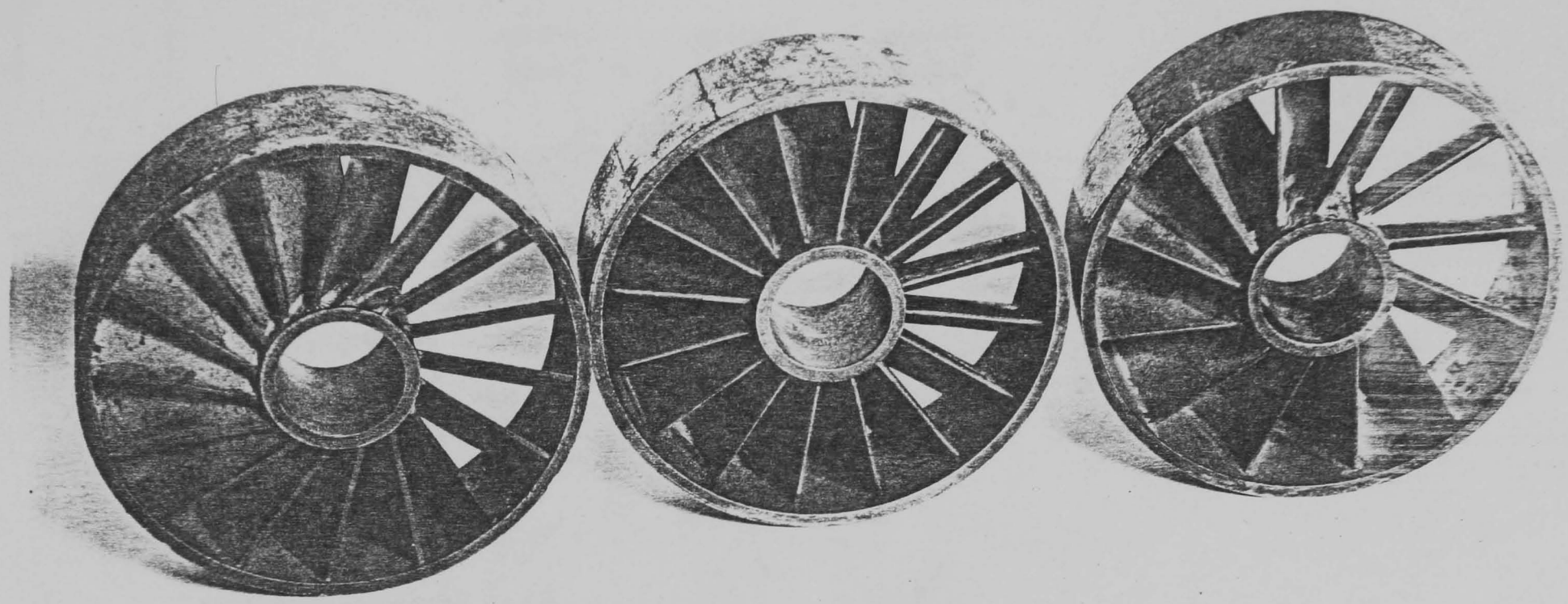

Fig.5.10.Picture of the swirlers in Fig.5.9

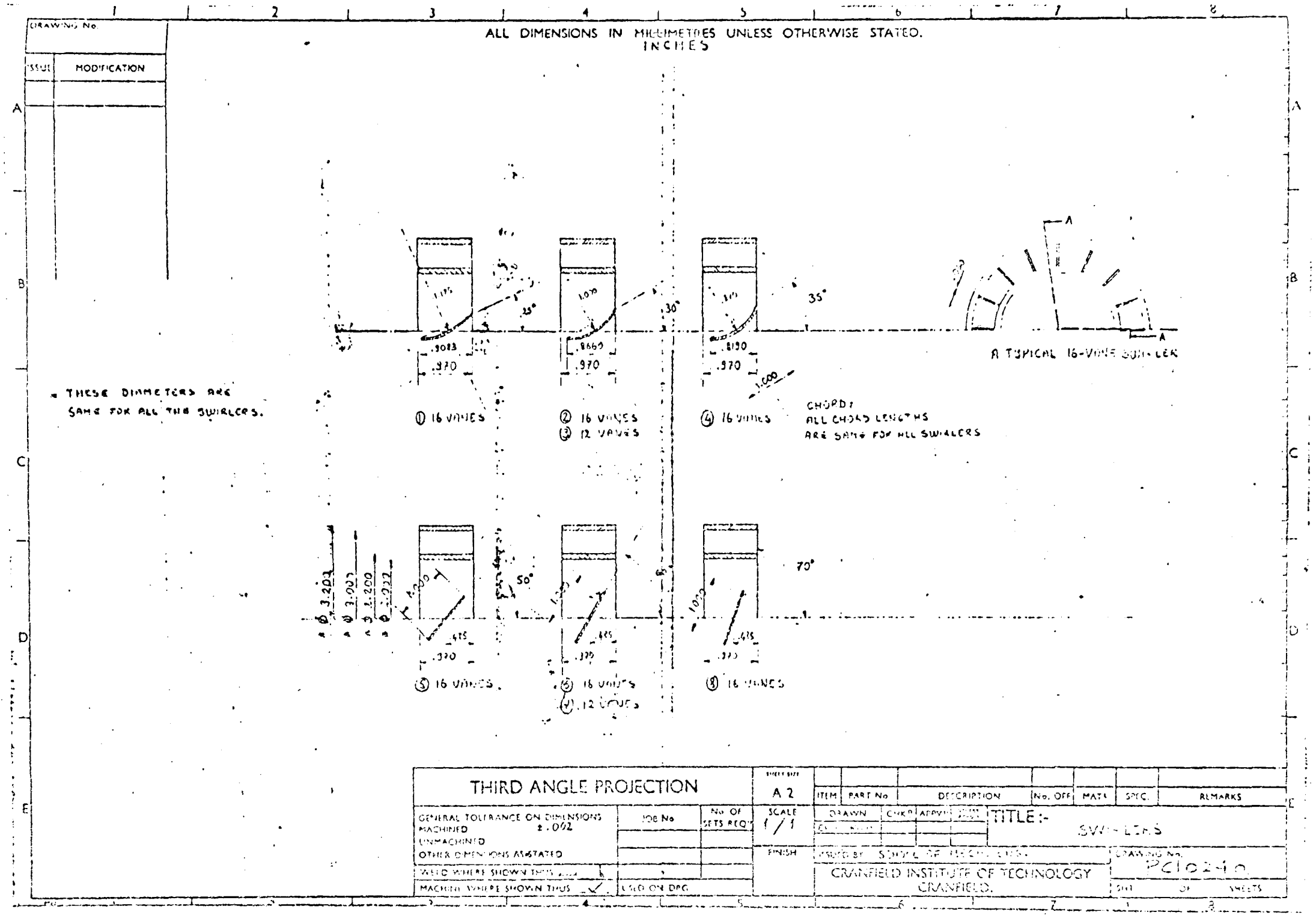

Fig.5.II. Flat and curved vane type swirlers

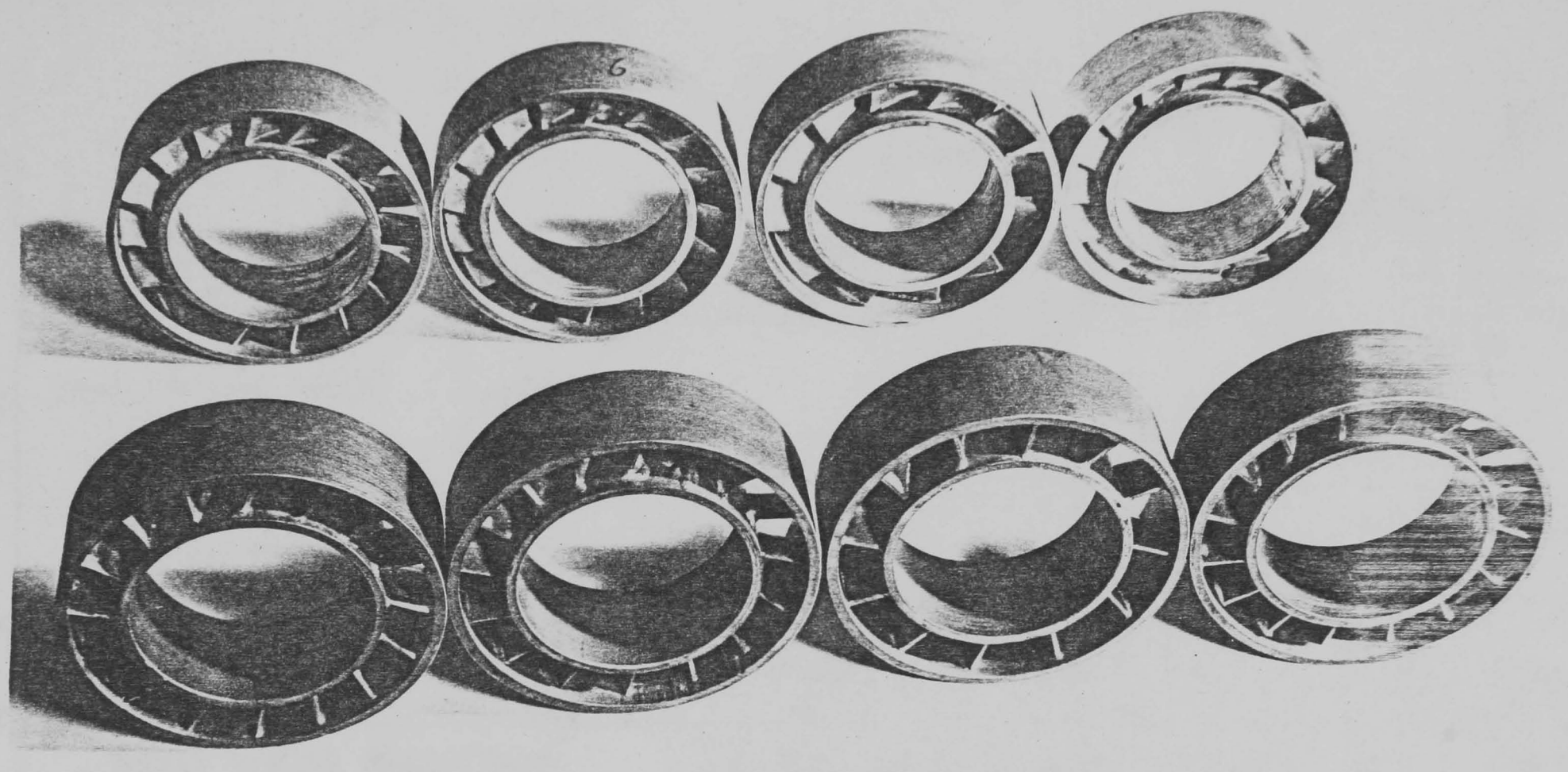

Fig.5.11a.Picture of the swirlers in Fig.5.11

DRAWING No. PD 10235

ISSUE	MODIFICATION
A	----

ALL DIMENSIONS IN MILLIMETRES UNLESS OTHERWISE STATED.
INCHES

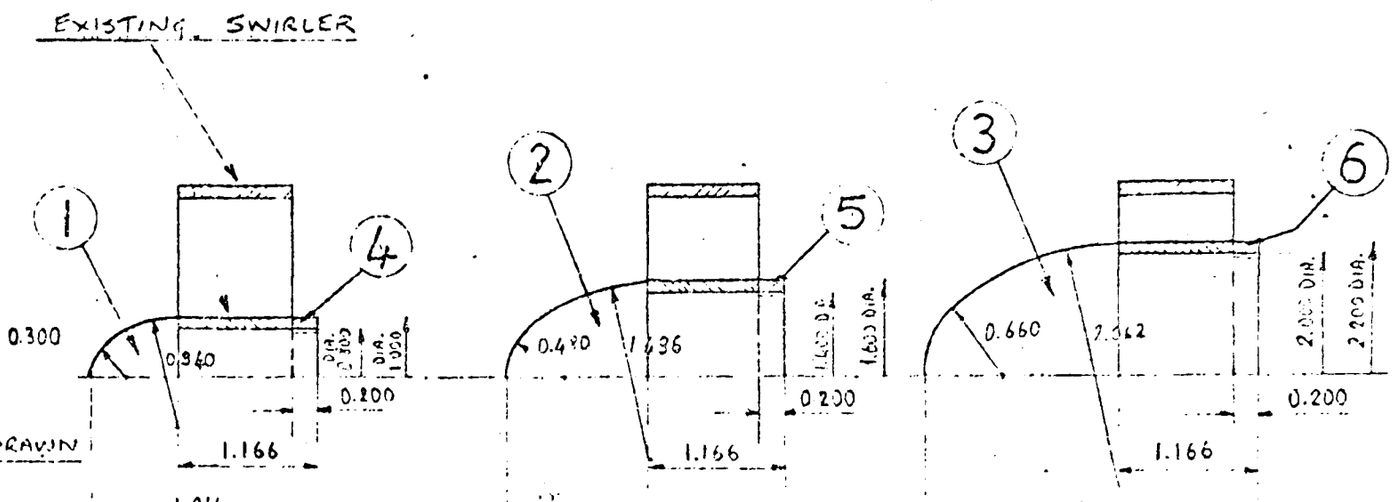

HALF SECTIONS DRAWN

ITEMS 4 5 & 6 TO BE
THREADED ON TO ITEMS
1 2 & 3 26 TPI RH WHIT FORM

ITEM	PART No	DESCRIPTION	No OFF	MATS	SPEC.	REMARKS
6	–	RING FOR h/c=0.4	1	145		
5	–	RING FOR h/c=0.7	1	"		
4	–	RING FOR h/c=1	1	"		
3	–	BULLET FOR h/c=0.4	1	STEEL	[illegible]	PROFILE $x^{2}/_{0.5} + y^{2}/_{1.1} = 1$
2	–	BULLET FOR h/c=0.7	1	"	"	PROFILE $x^{2}/_{1.2} + y^{2}/_{2} = 1$
1	–	BULLET FOR h/c=1	1	"	"	PROFILE $x^{2}/_{1.2} + y^{2}/_{2} = 1$

THIRD ANGLE PROJECTION

SHEET SIZE A 3

SCALE 1 / 1

FINISH SELF

GENERAL TOLERANCE ON DIMENSIONS
MACHINED ± .005"
UNMACHINED
OTHER DIMENSIONS AS STATED
WELD WHERE SHOWN THUS
MACHINE WHERE SHOWN THUS ✓

JOB No	No. OF SETS REQD
	1
USED ON DRG. PD 10231	

DRAWN	CHKD	APPVD	ISSUE AUTH
EROL KILIN			
21 [illegible] 72			

TITLE:- HUB BULLETS (FIG. 5.12)

ISSUED BY SCHOOL OF MECHANICAL ENGINEERING
CRANFIELD INSTITUTE OF TECHNOLOGY
CRANFIELD.

DRAWING No. PD 10235

SHT. 1 OF 1 SHEETS

Fig.5.12. Hub bullets

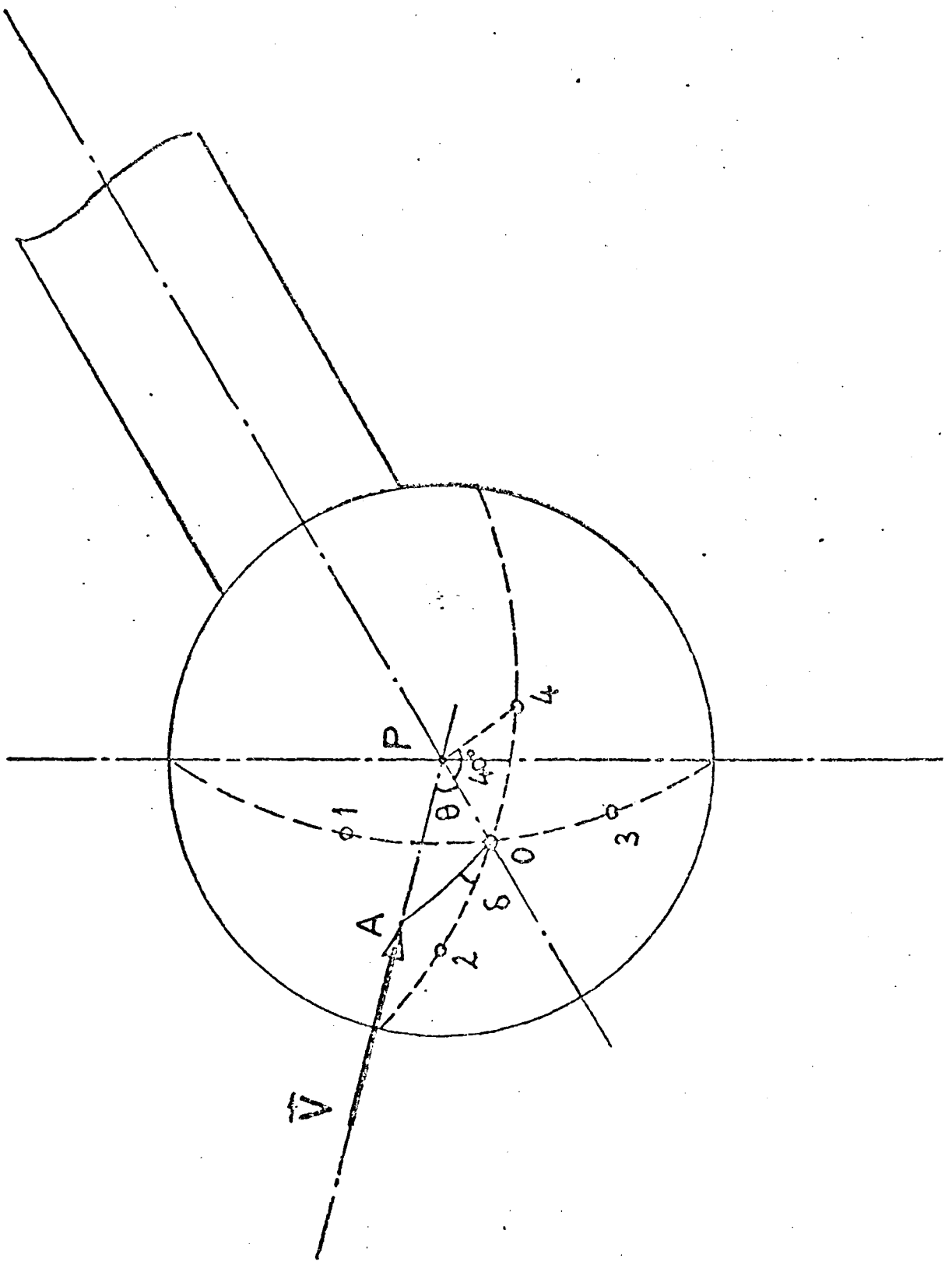

Fig.5.13. Arrangement of the five holes on the head of the spherical pressure probe

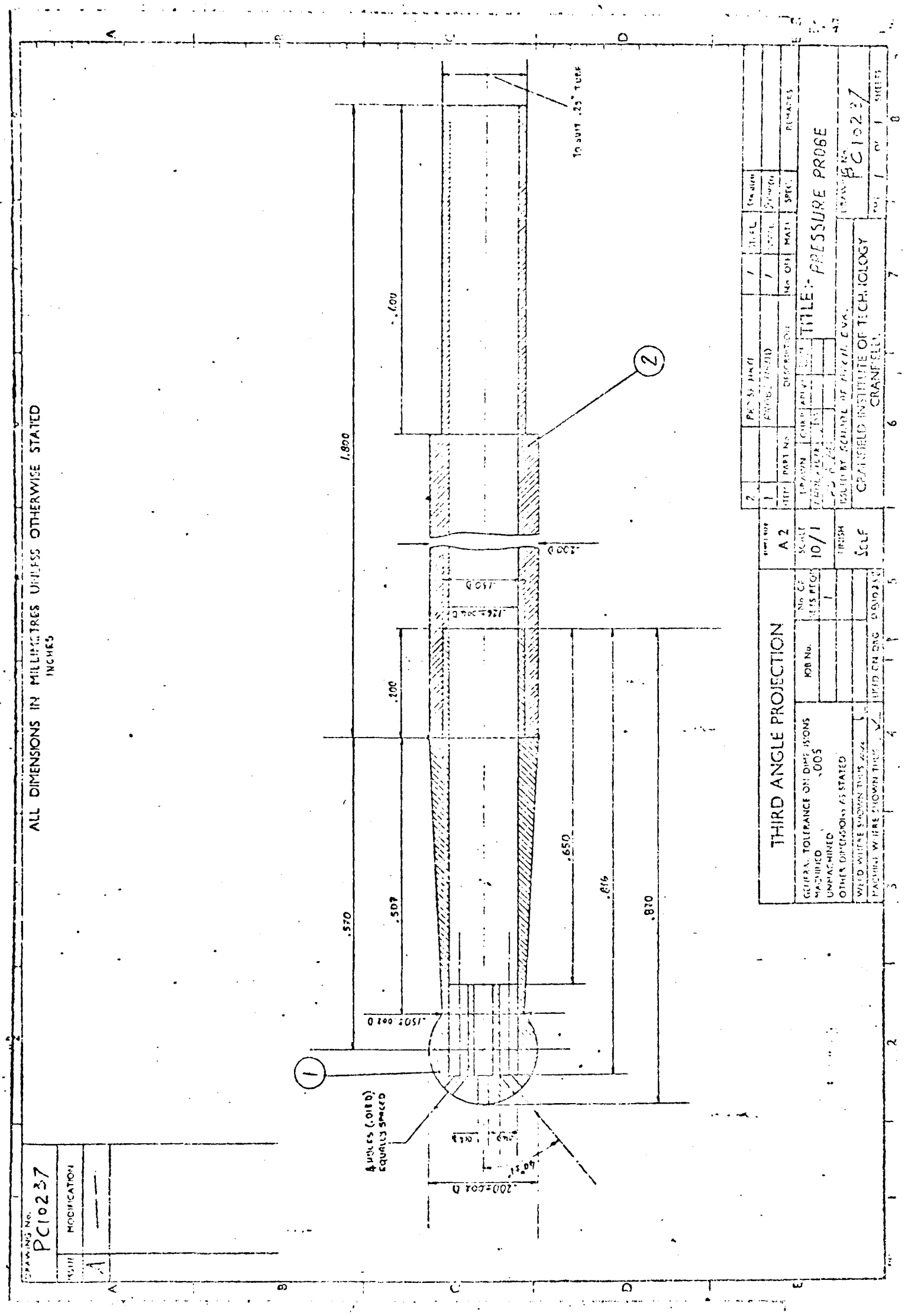

Fig. 5.14. Structure of the head of a pressure probe

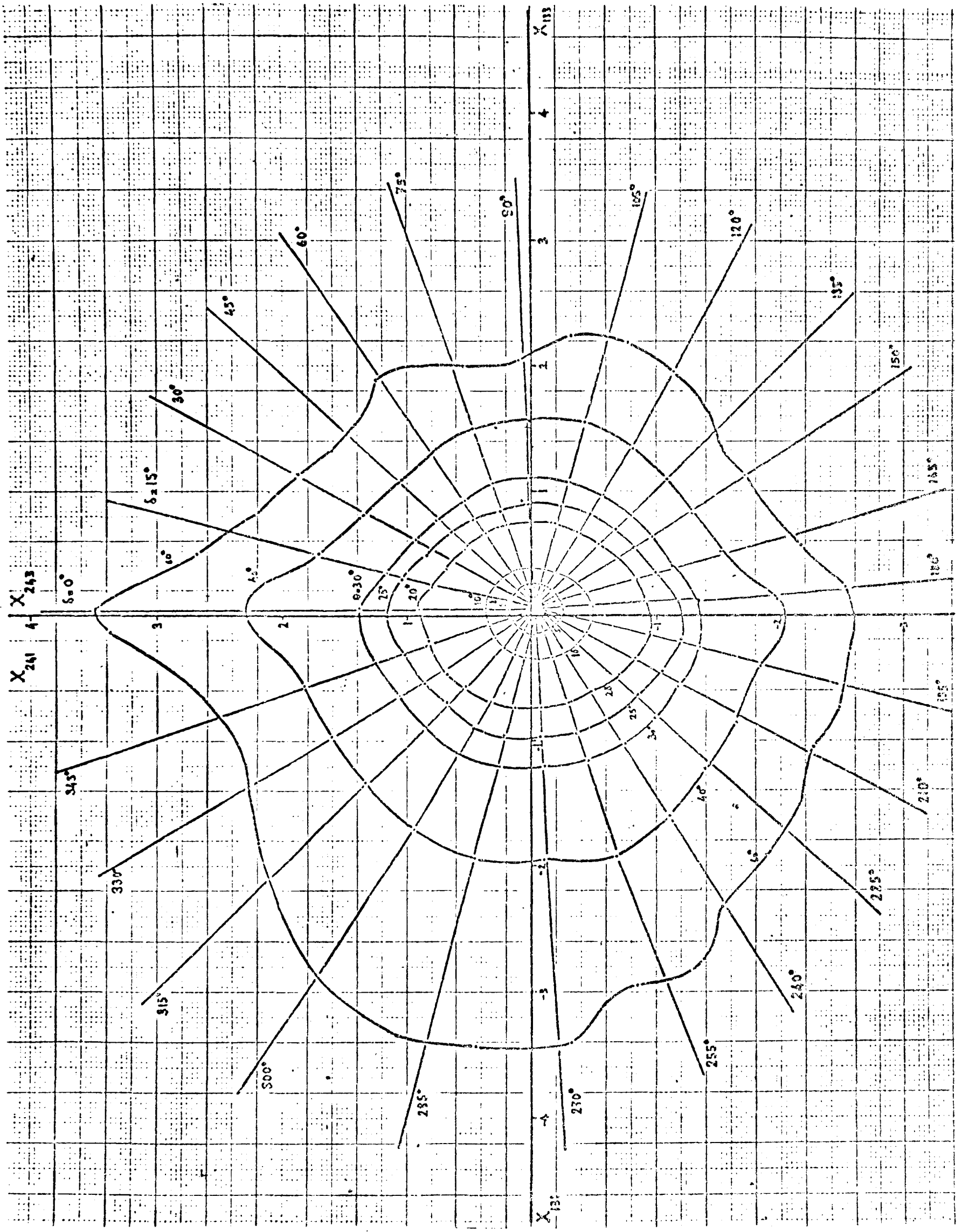

Fig. 5.15. Calibration chart for direction

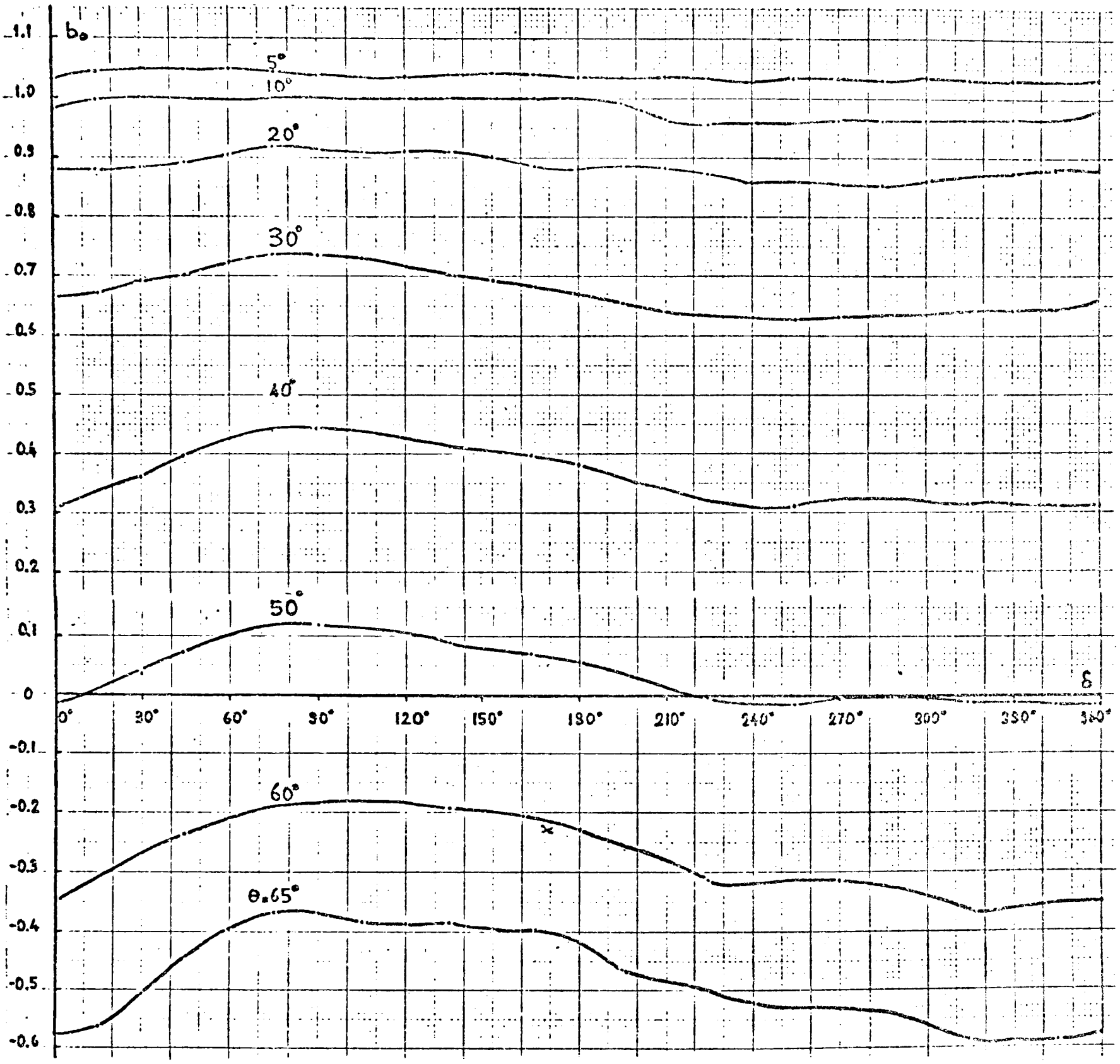

Fig.5.16.Calibration chart for the calculation of static pressure

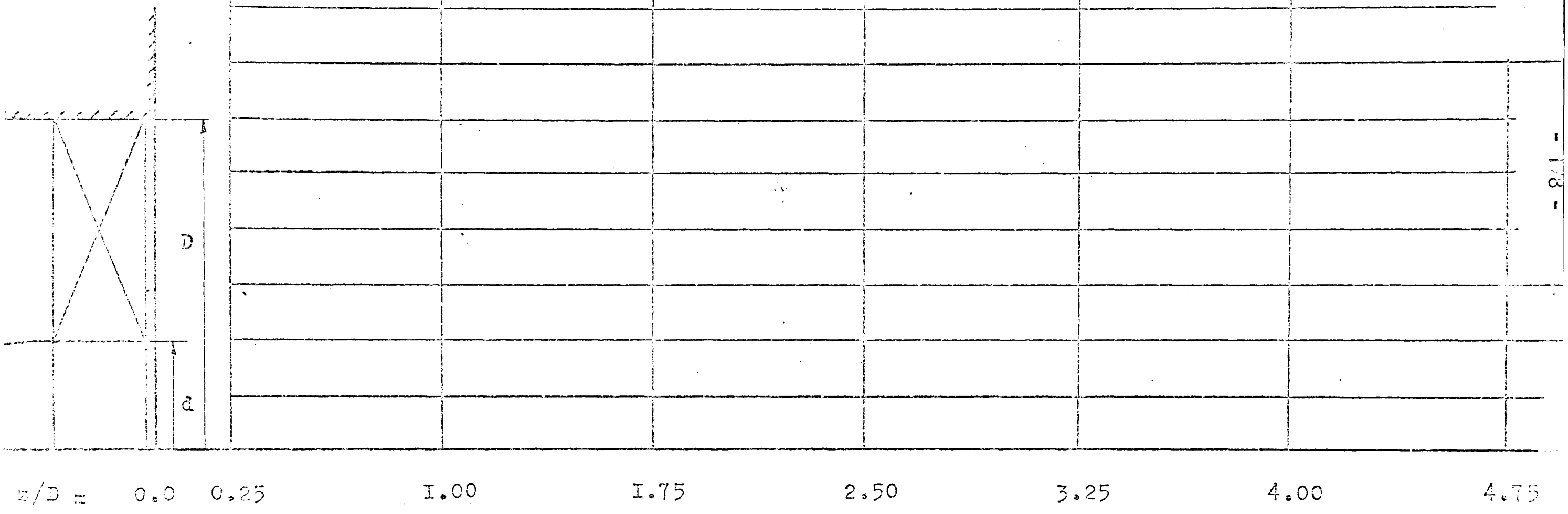

Fig.5.I7.An example of a traversing mesh

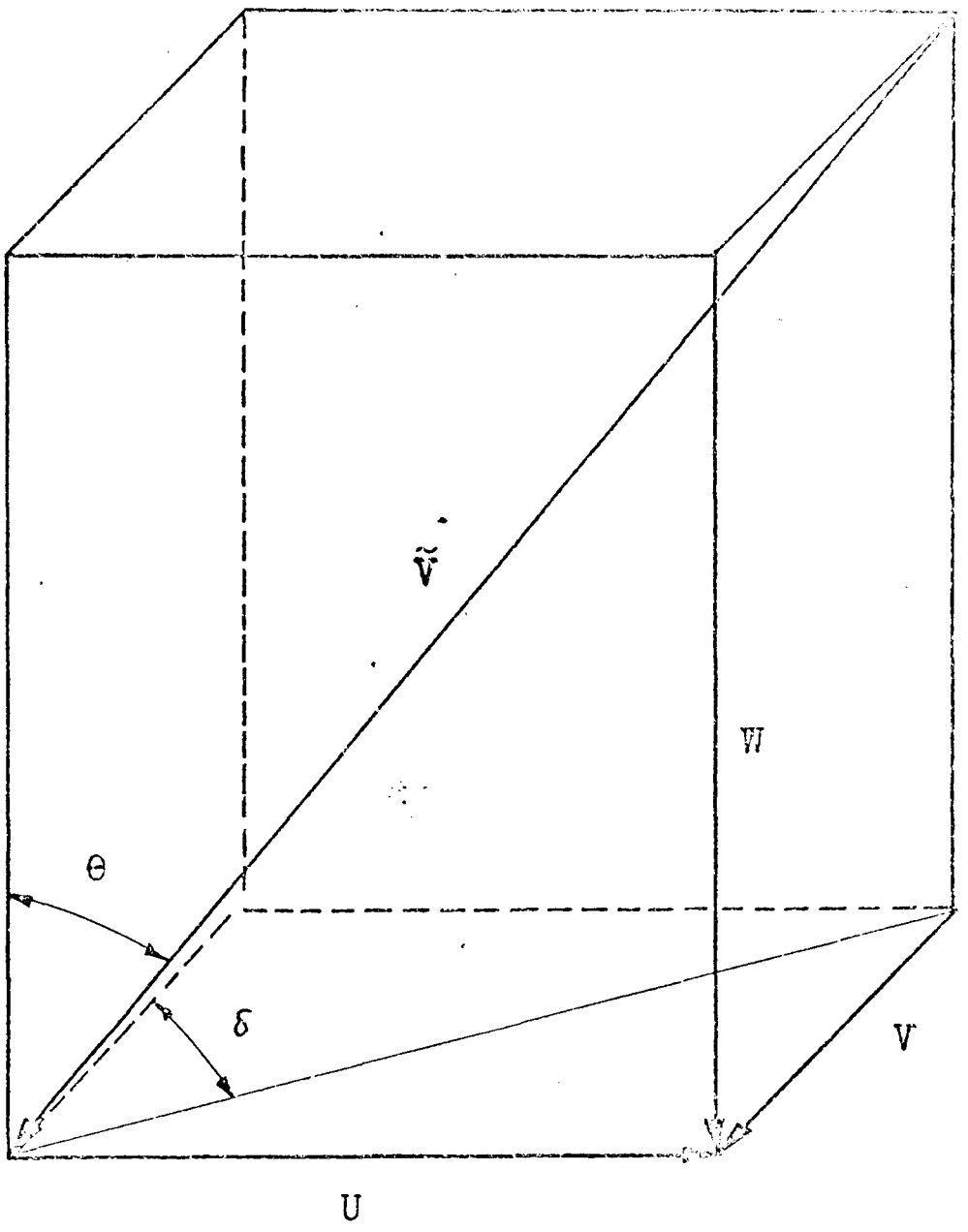

Fig.5.18.Notation for the calculation of static pressure and the components of absolute velocity

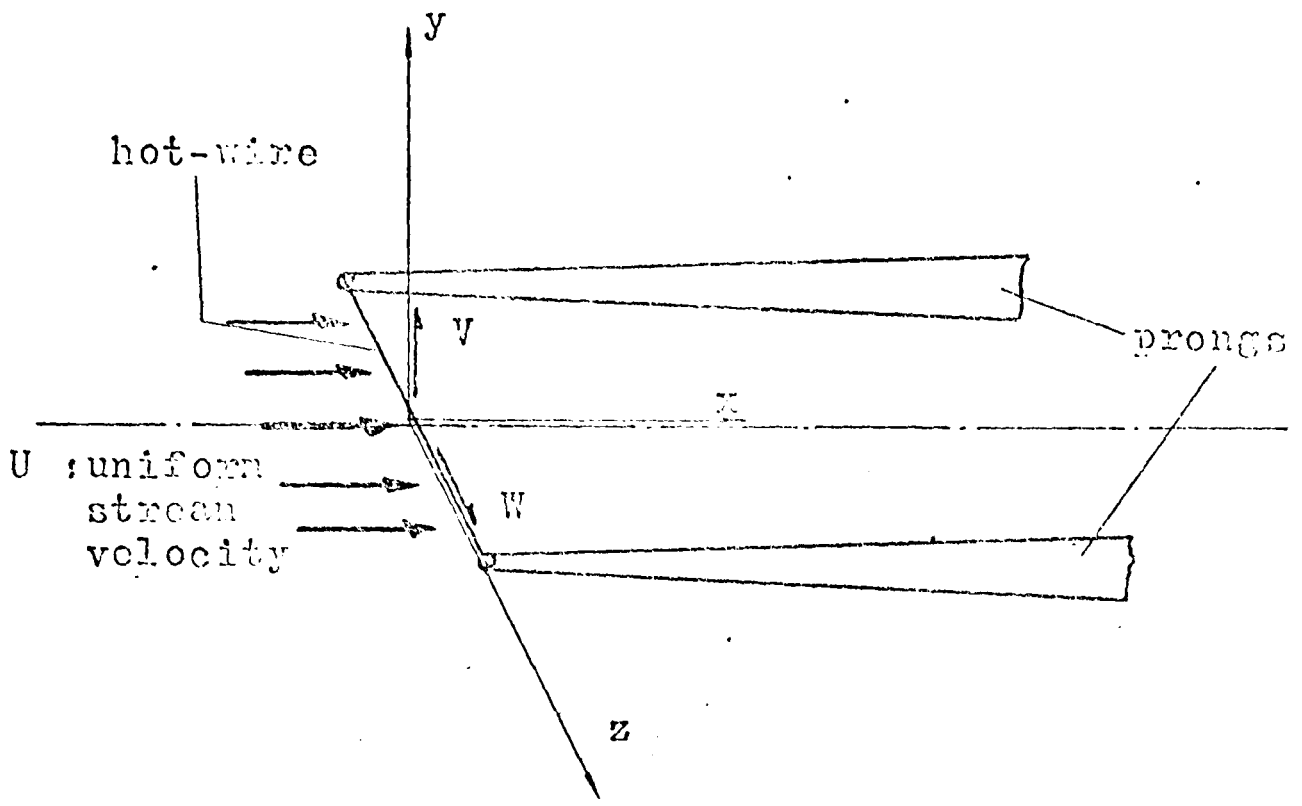

Fig.6.I.Hot-wire probe head and notation

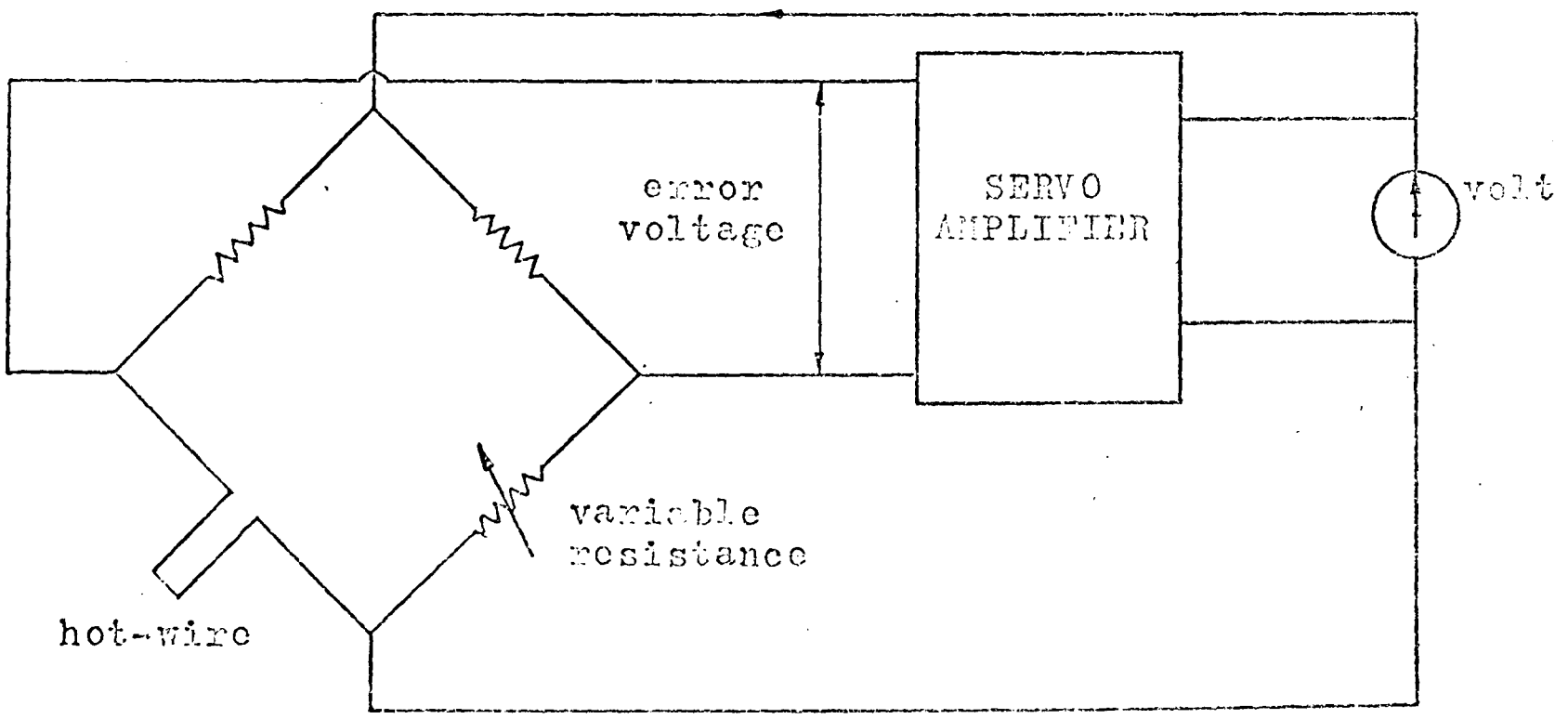

Fig.6.2.Operating principle of hot-wire anemometer in constant temperature (resistance) mode

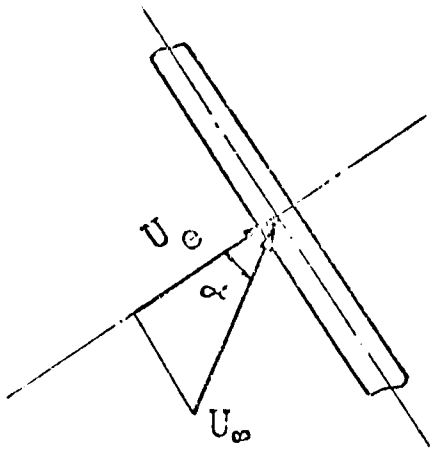

Fig.6.3.Effective cooling velocity in the cosine cooling law

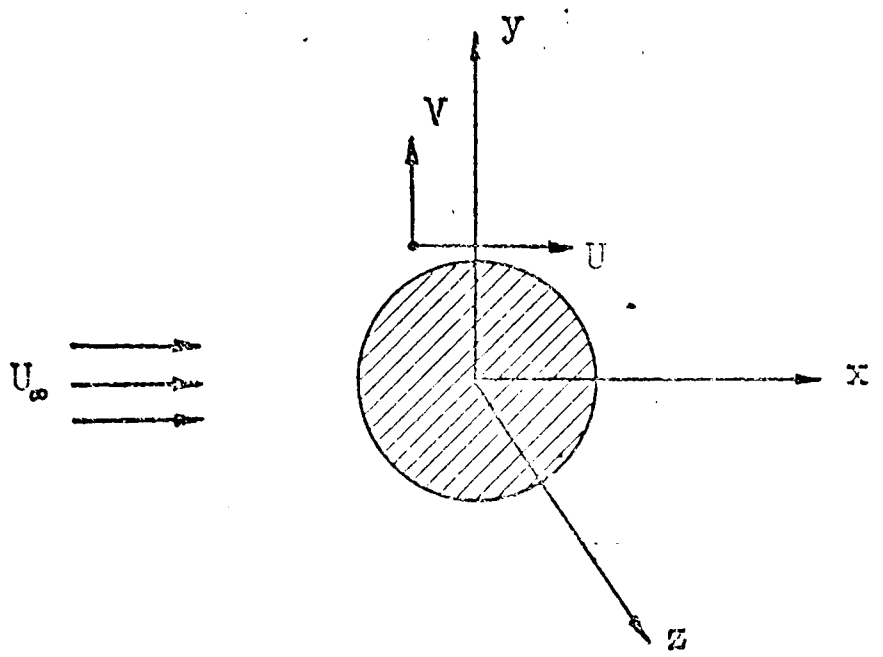

Fig.6.4a.Cross section of the hot-wire placed perpendicularly into the flow field

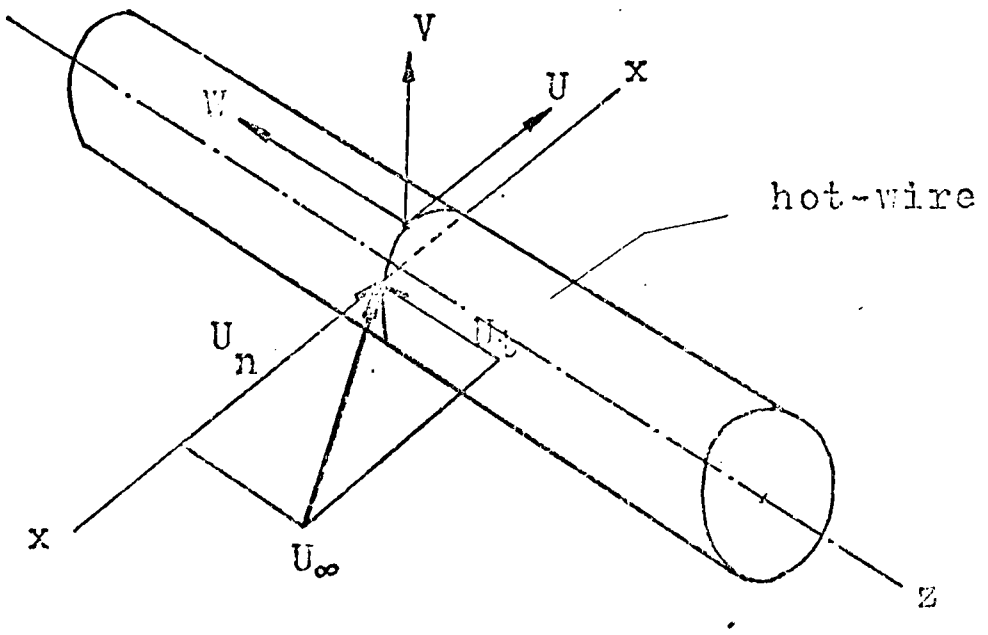

Fig.6.4b.The hot-wire placed obliquely into the flow field

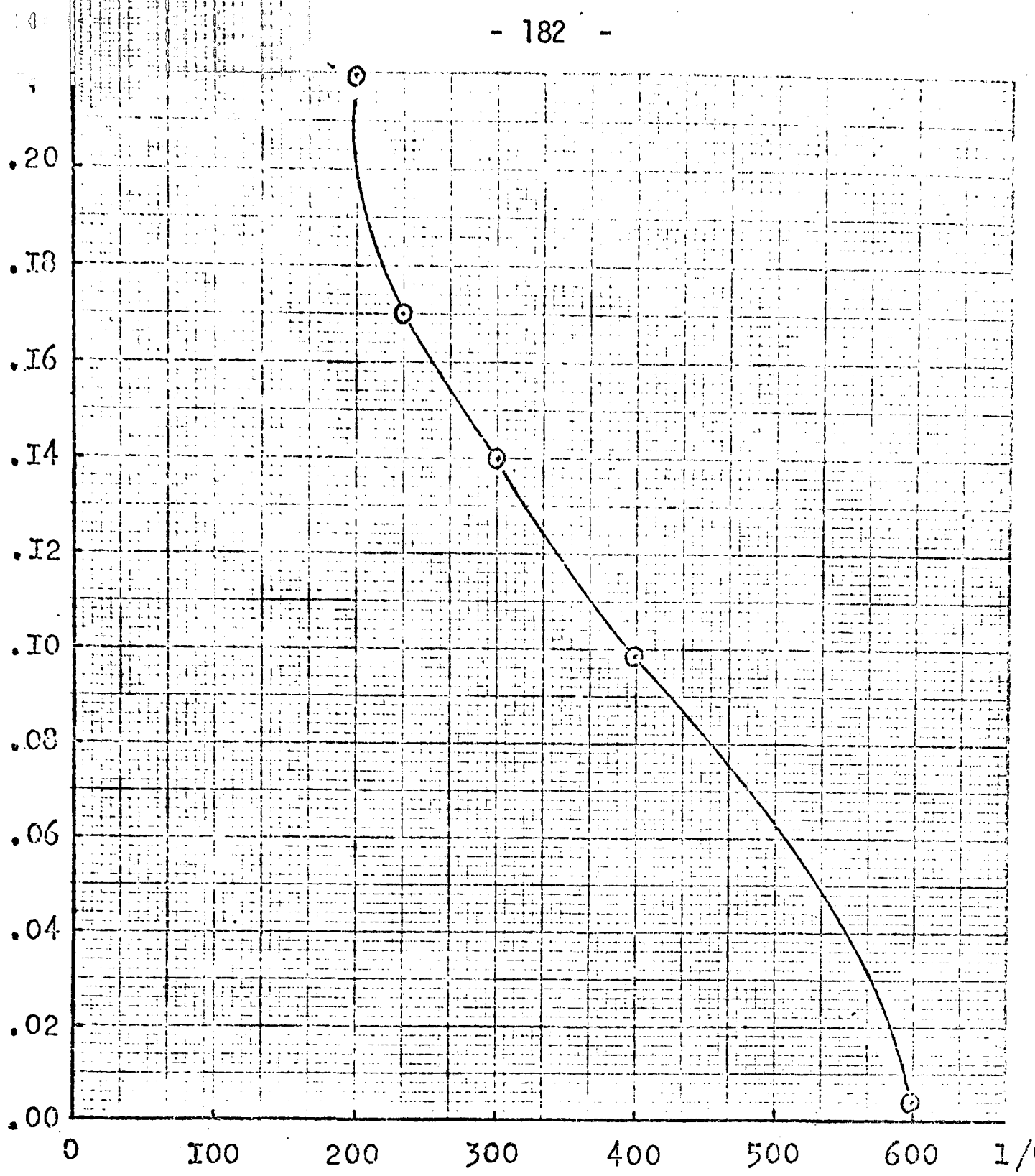

Fig.6.5.Variation of the yaw coefficient with the length-to-diameter ratio of the wire

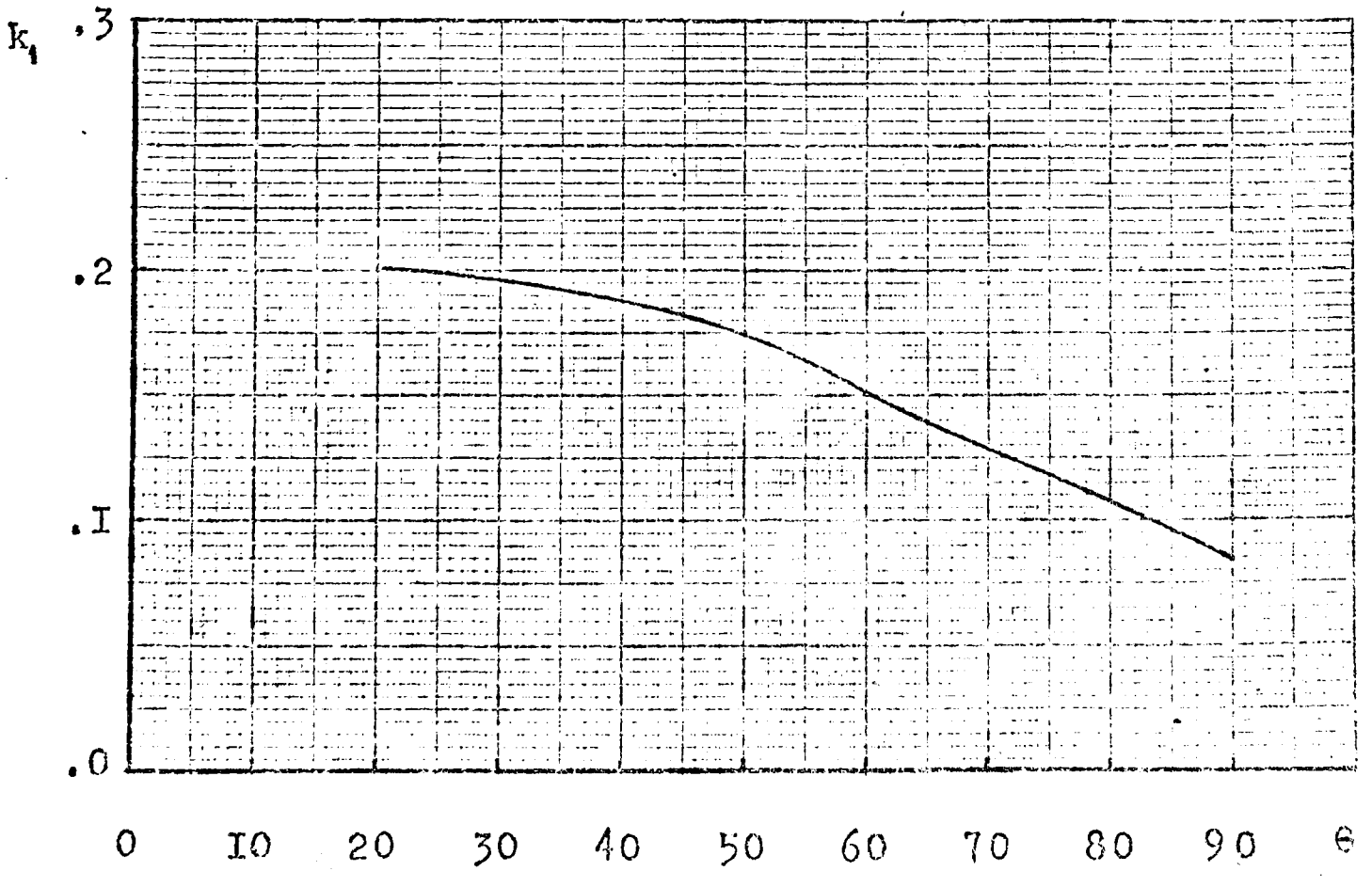

Fig.6.6.Variation of k_1 with yaw angle

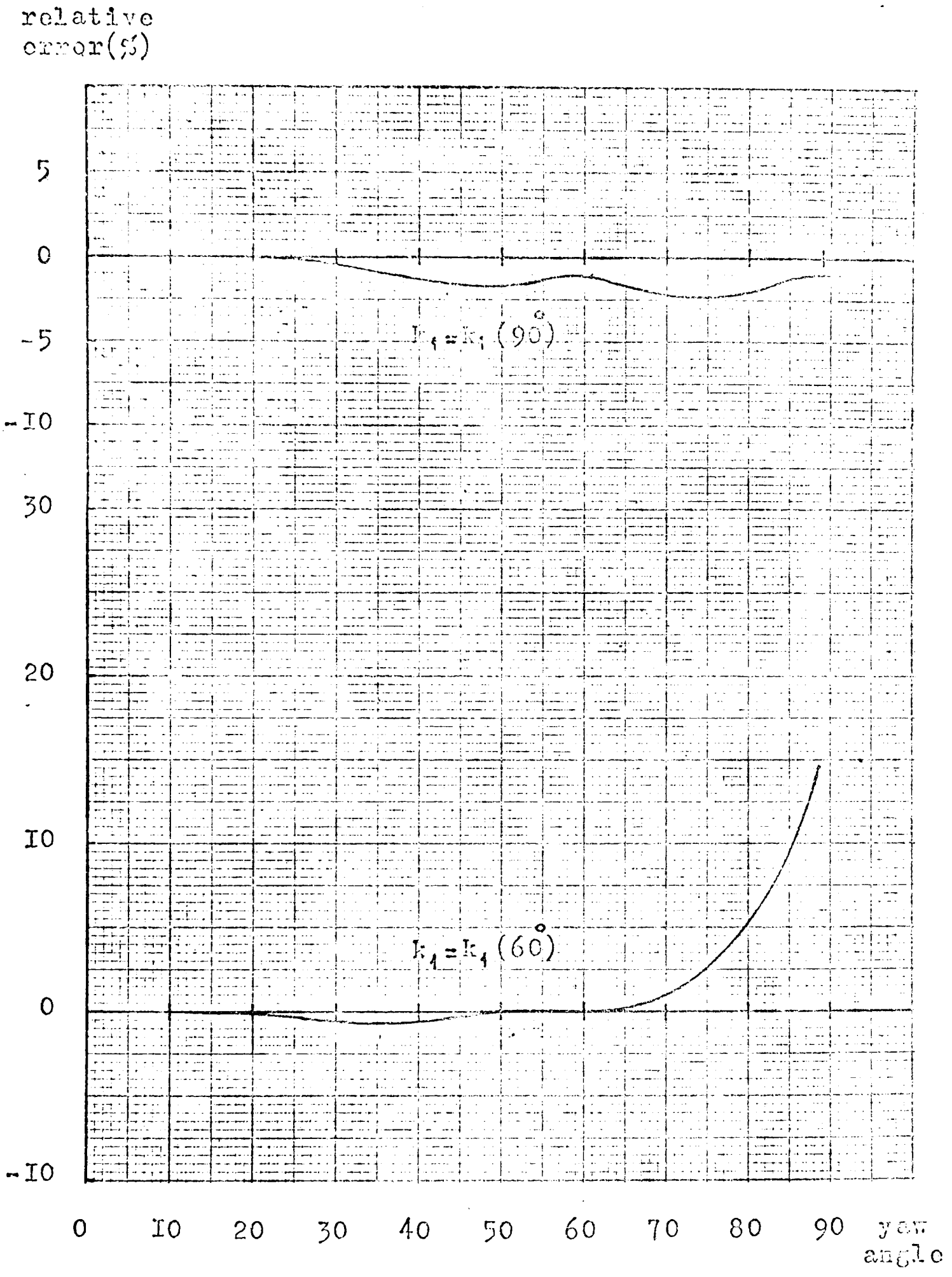

Fig.6.7 .Variation of the relative error in the calculation of velocity with yaw angle

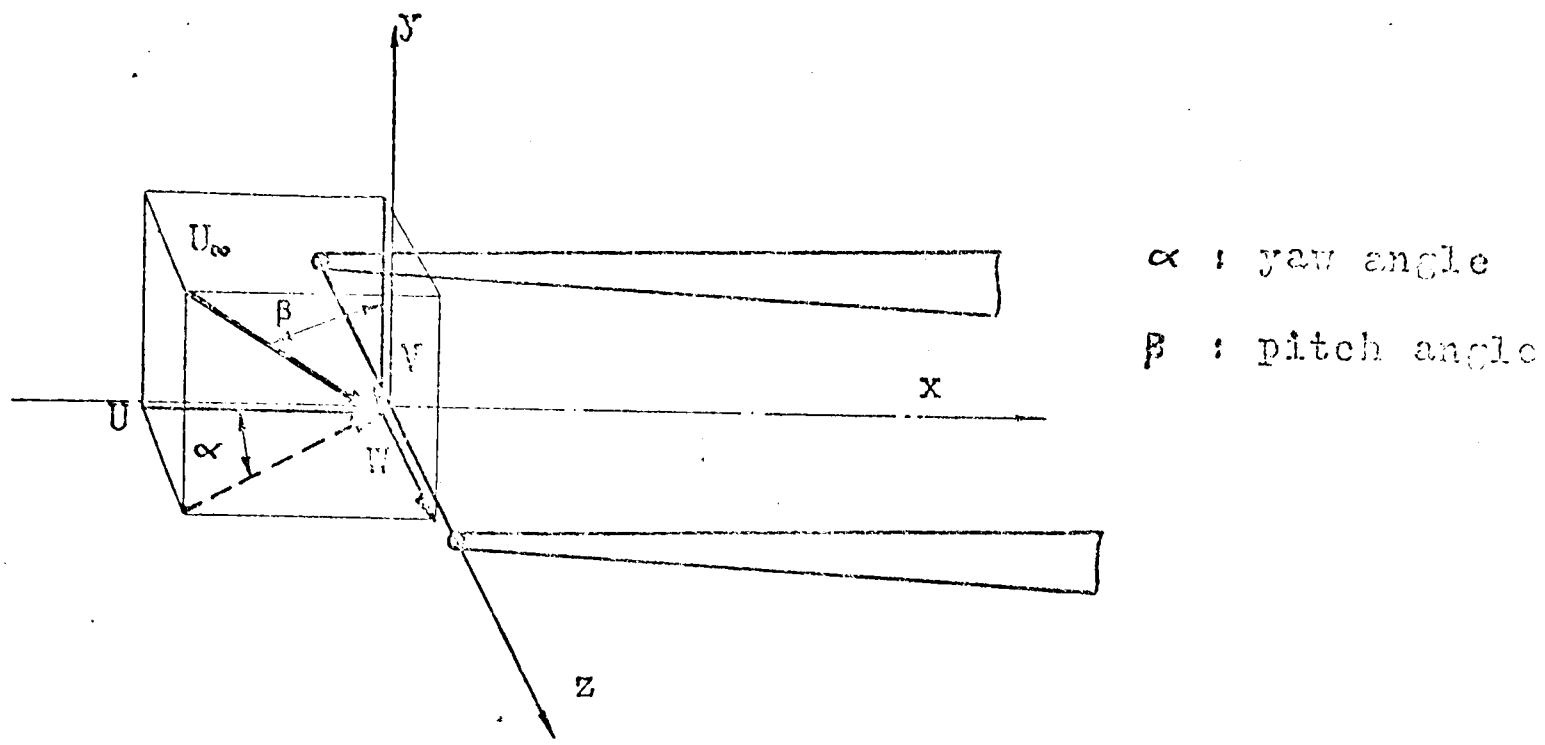

Fig.6.8.Overall directional characteristics of a hot-wire probe

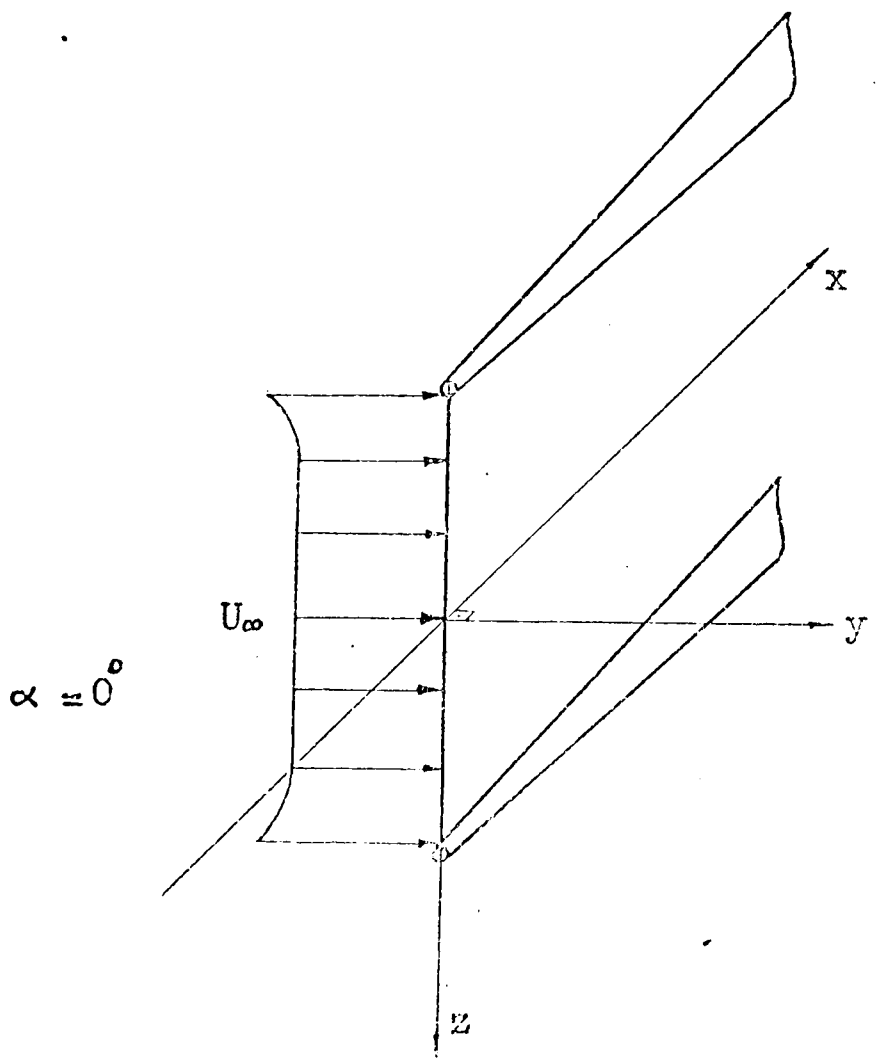

Fig.6.9.Increase in the velocity due to the thickness of the prong ends

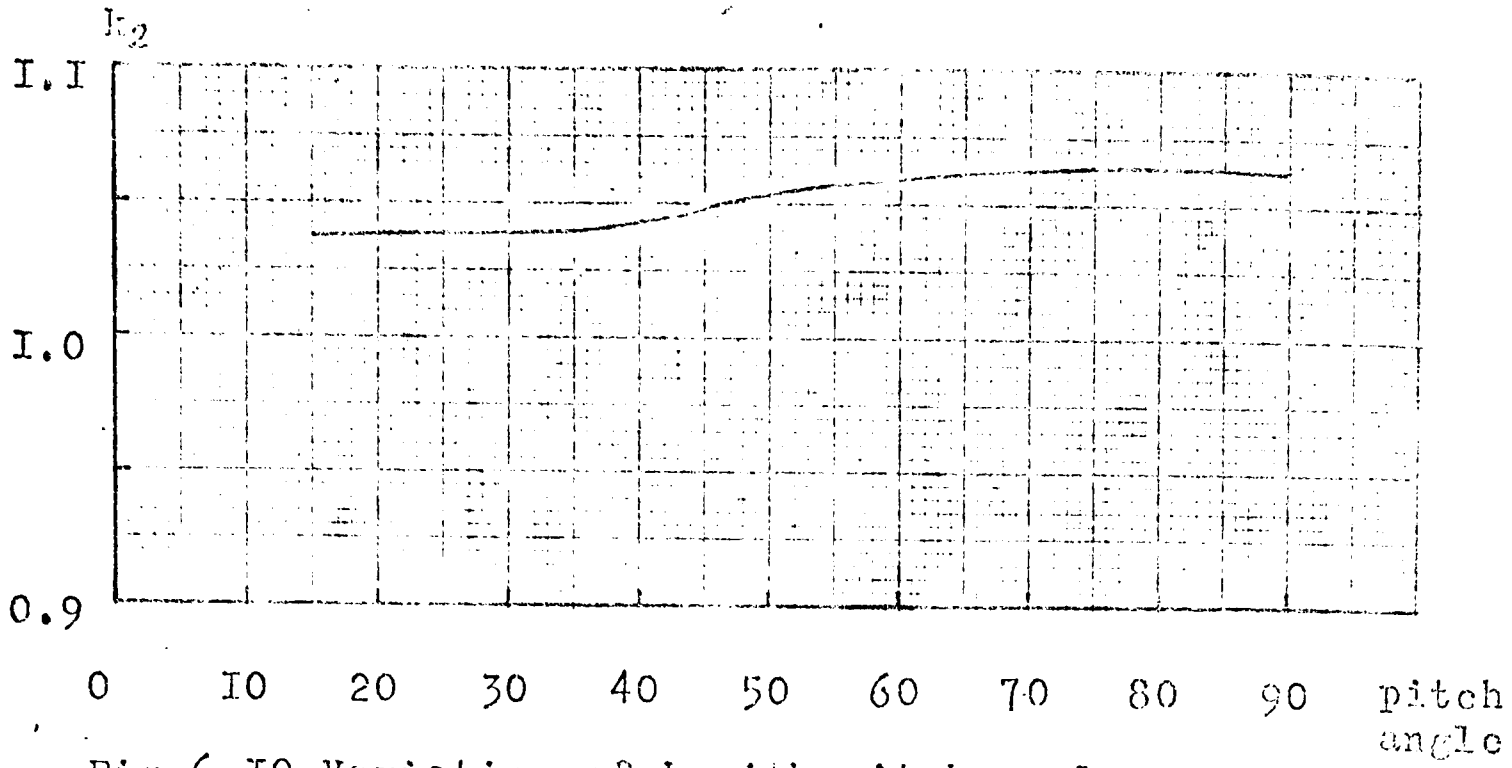

Fig.6.I0. Variation of k_2 with pitch angle

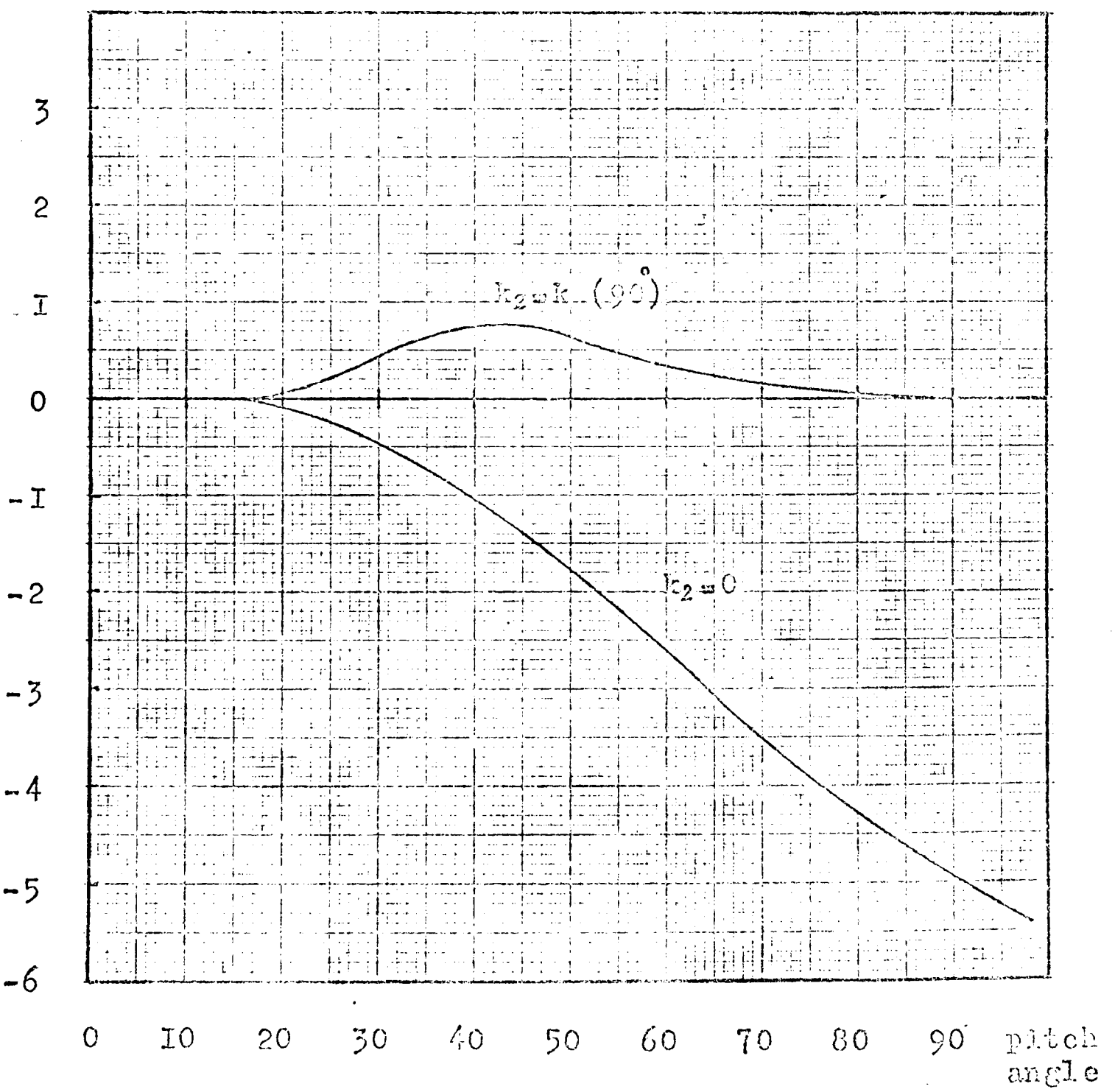

Fig.6.II. Variation of the relative error in the calculation of velocity with the pitch angle

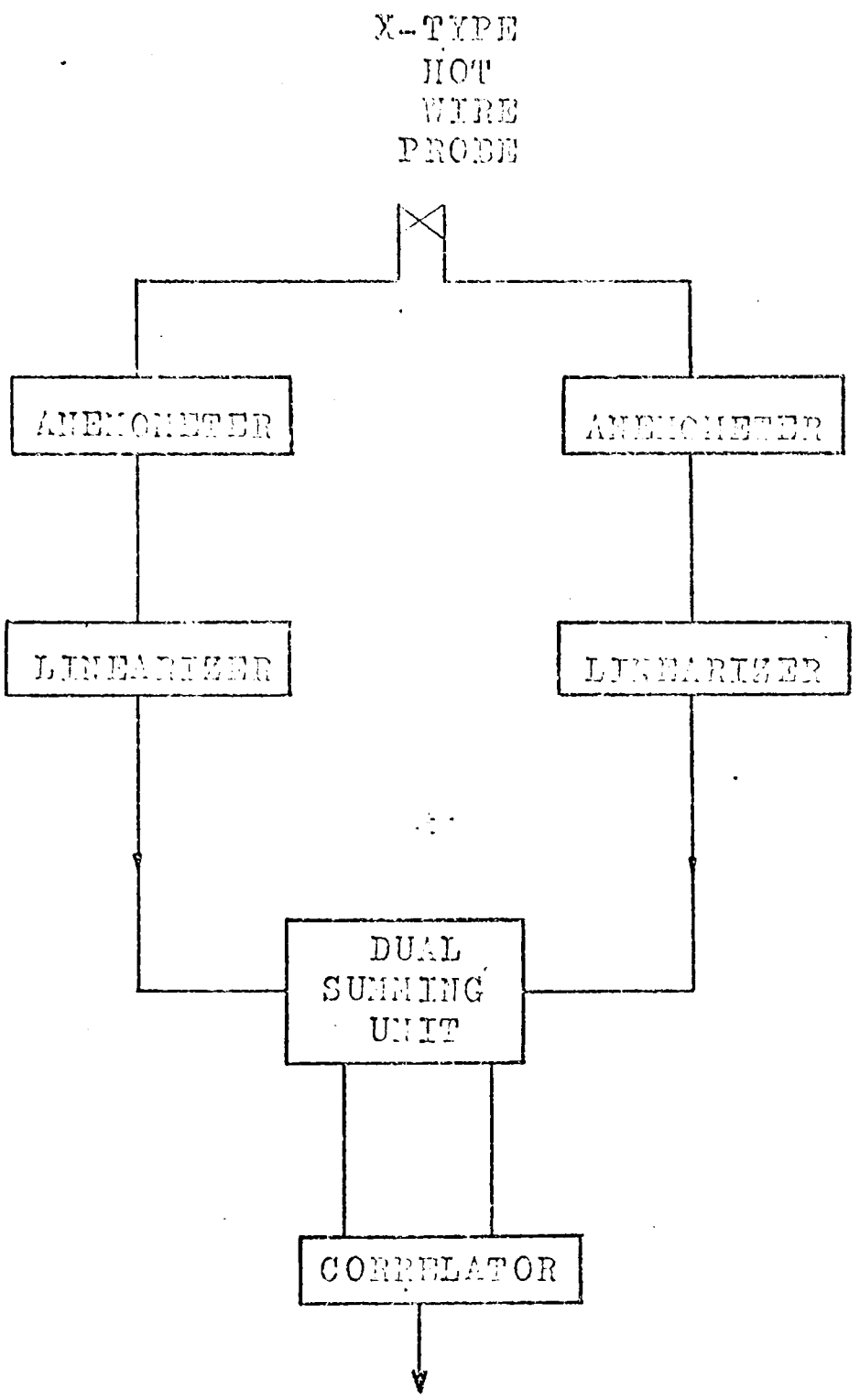

Fig.6.12.Measurement of Reynolds stresses using an X-type hot wire probe

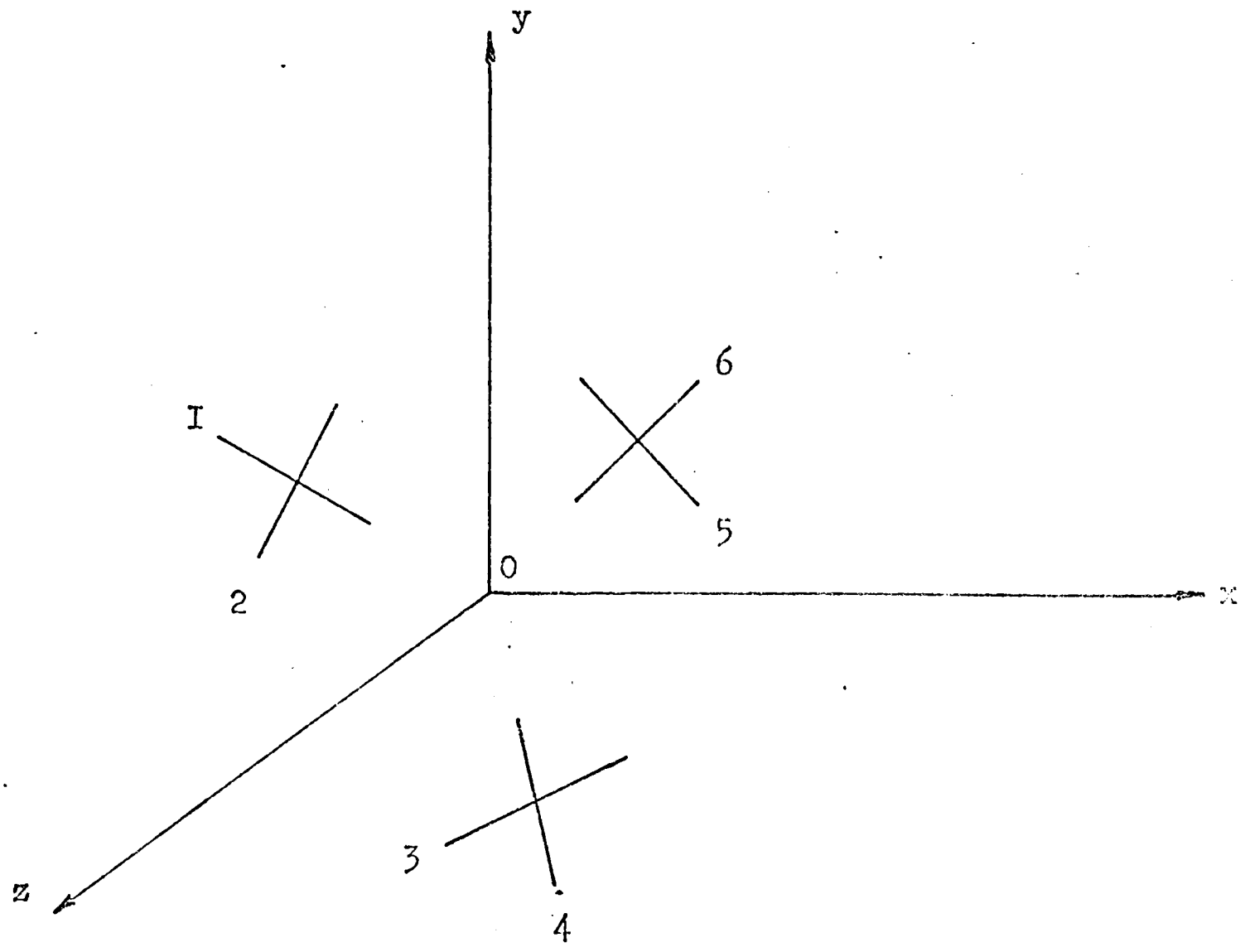

Fig.6.I3. Orientation of the hot-wires in six-orientation measurement technique

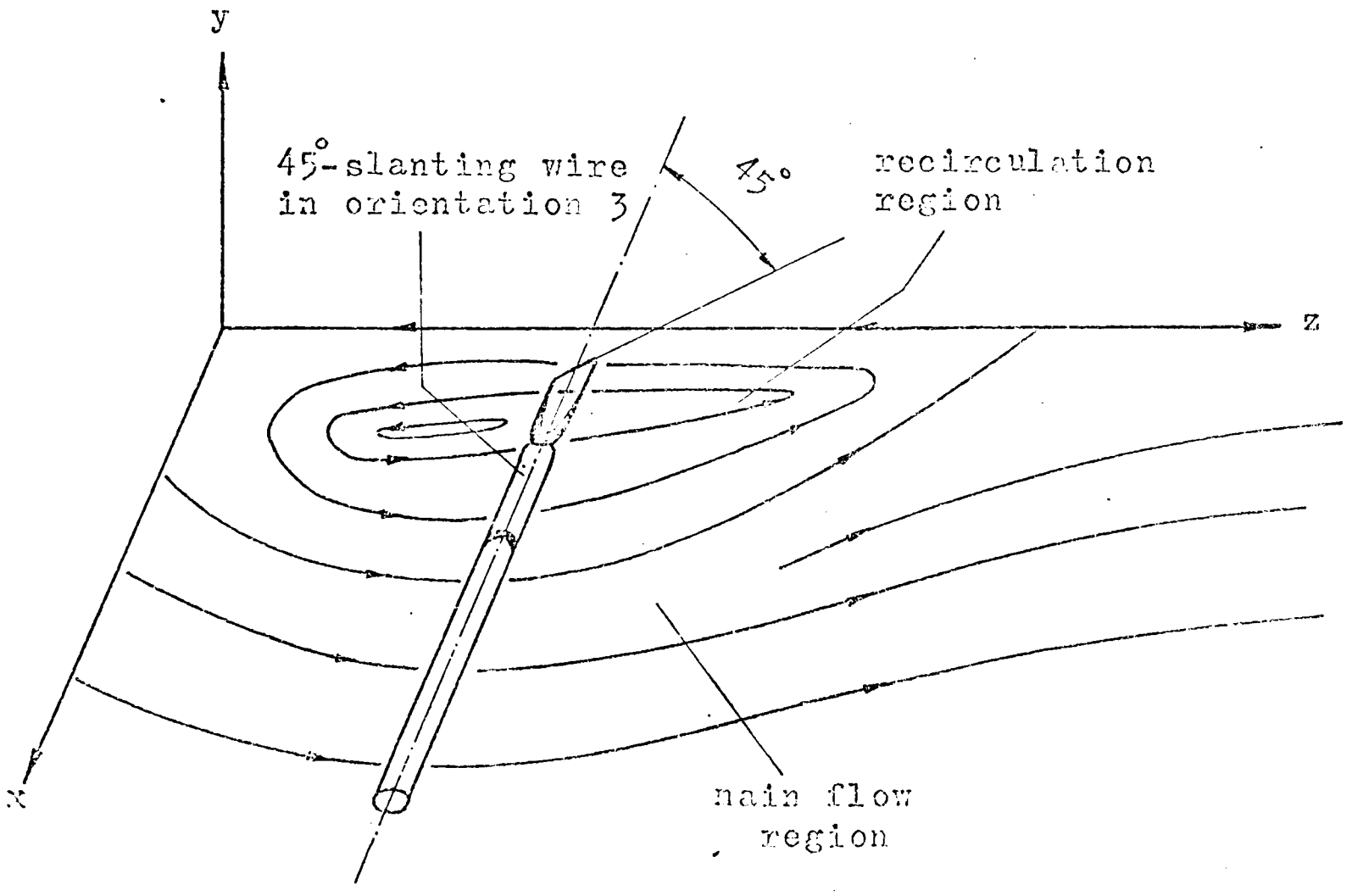

Fig.6.I4. Application of the six-orientation method to the recirculation region in a swirling flow field

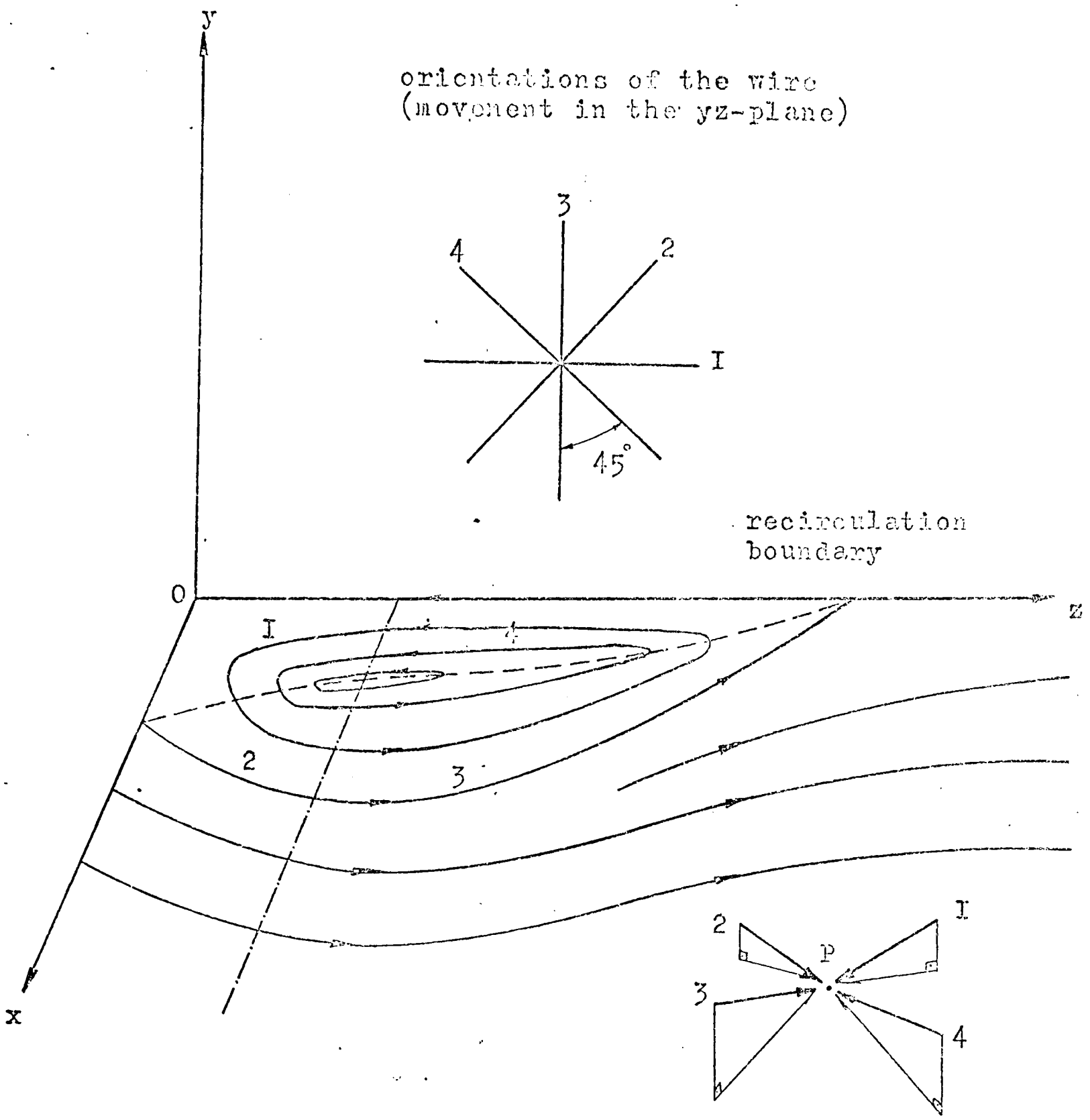

Fig.6.15.Application of the four-orintation technique to a swirling flow field with recirculation

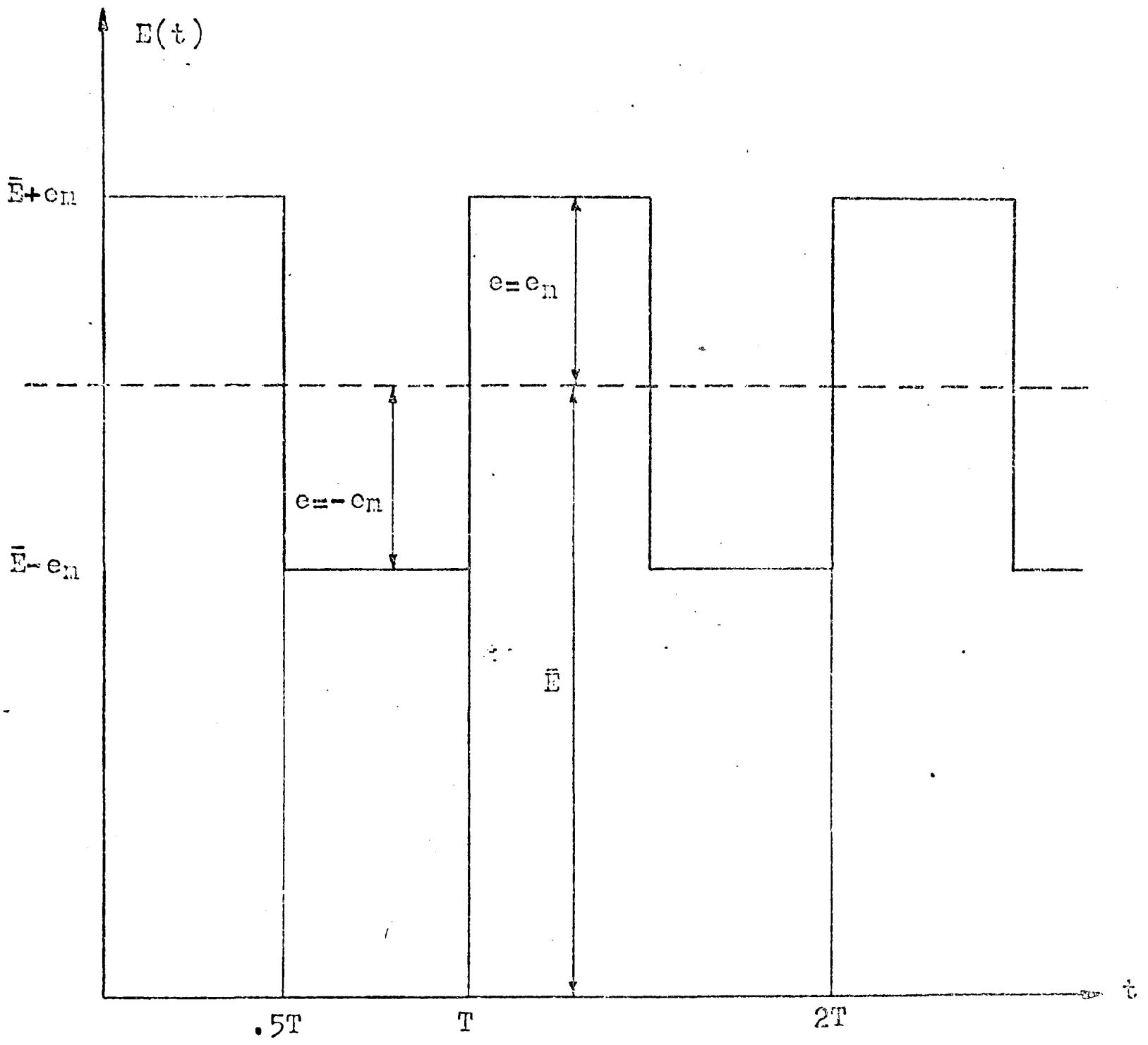

Fig.6.16.The square wave form assumed for instantaneous wire voltage

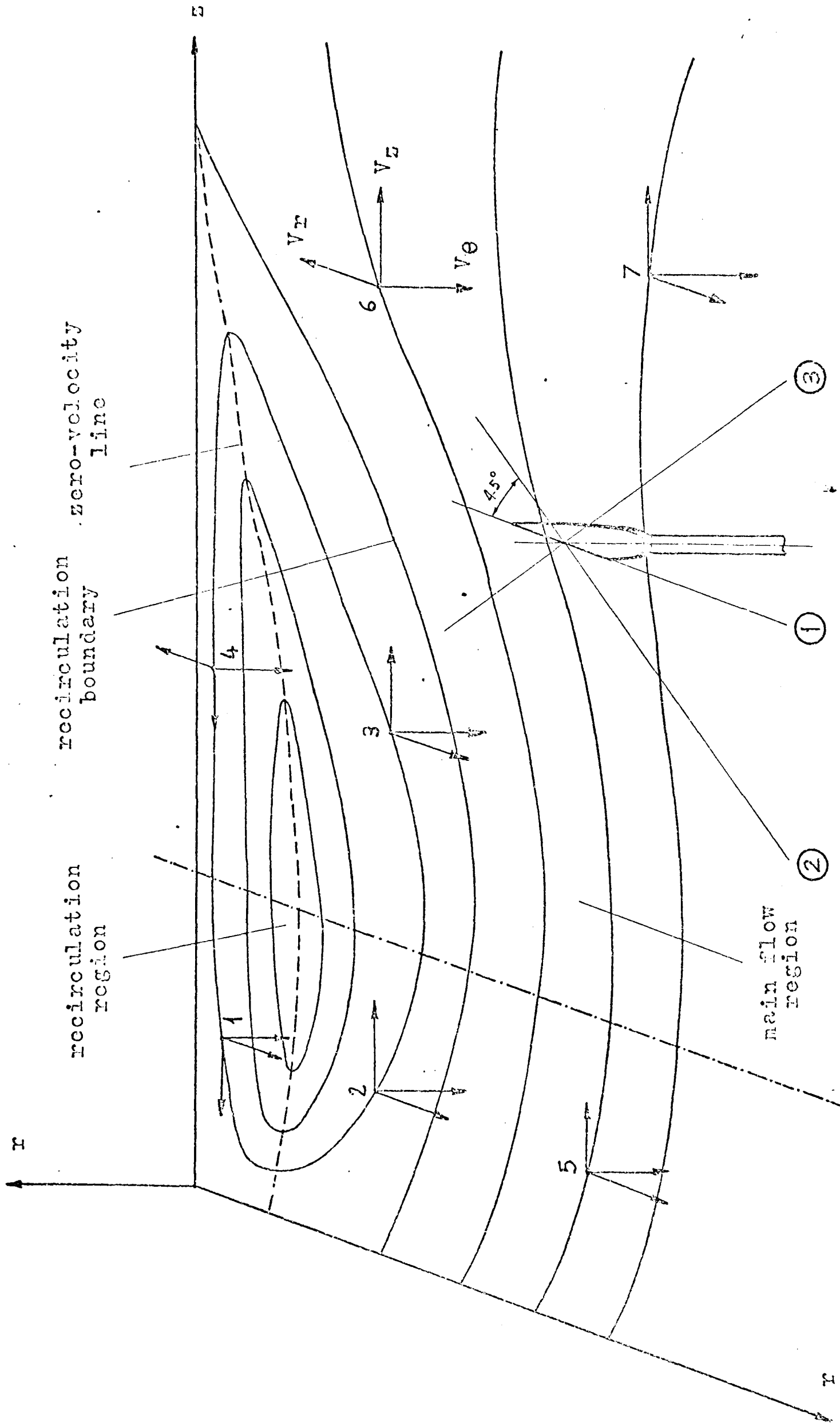

Fig.6.17. Orientation of the hot-wire probe in a recirculating flow field with recirculation zero-lines

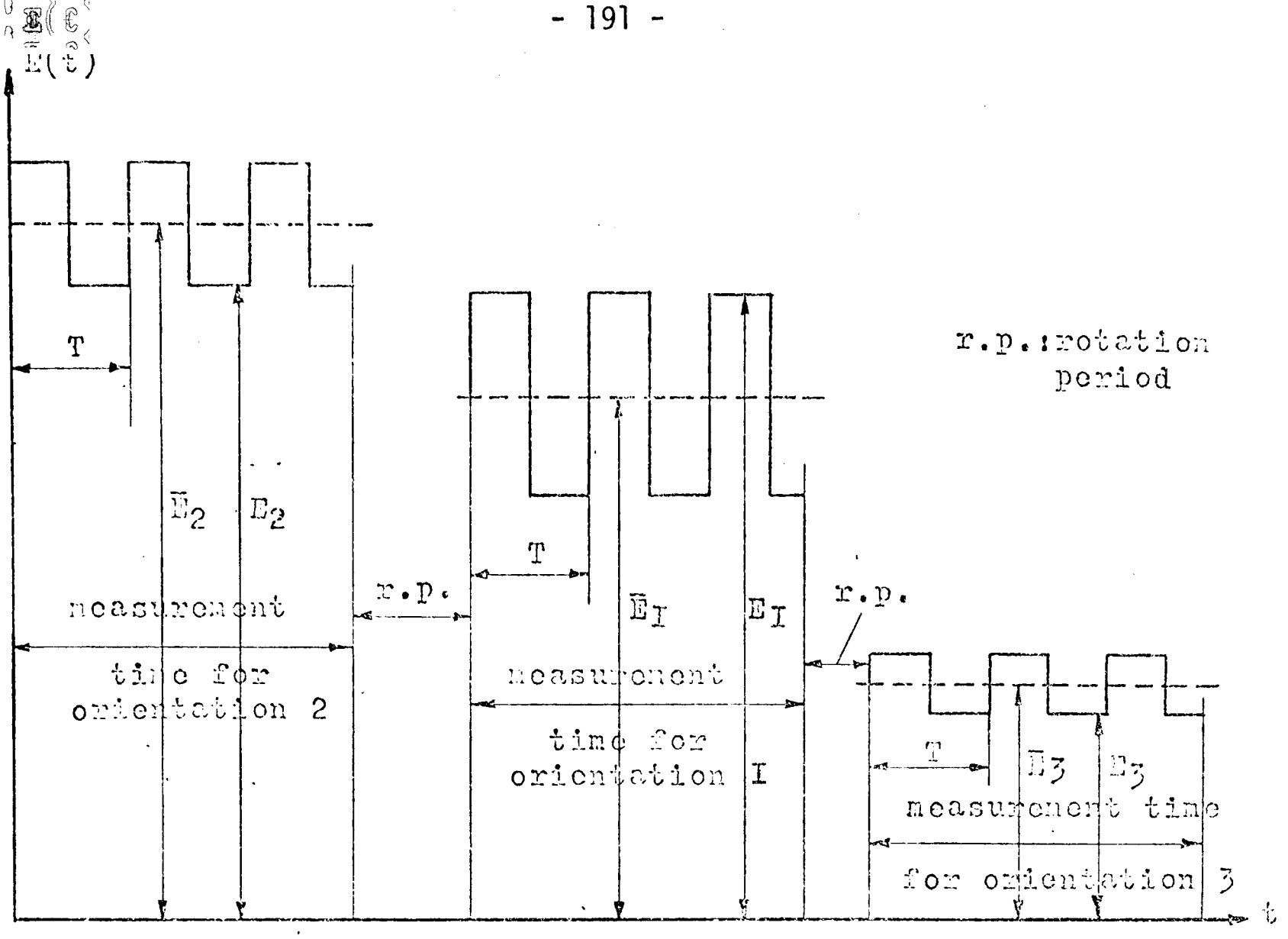

Fig.6.I8. Variation of instantaneous voltage for three orientations of a hot-wire probe placed in the recirculation region

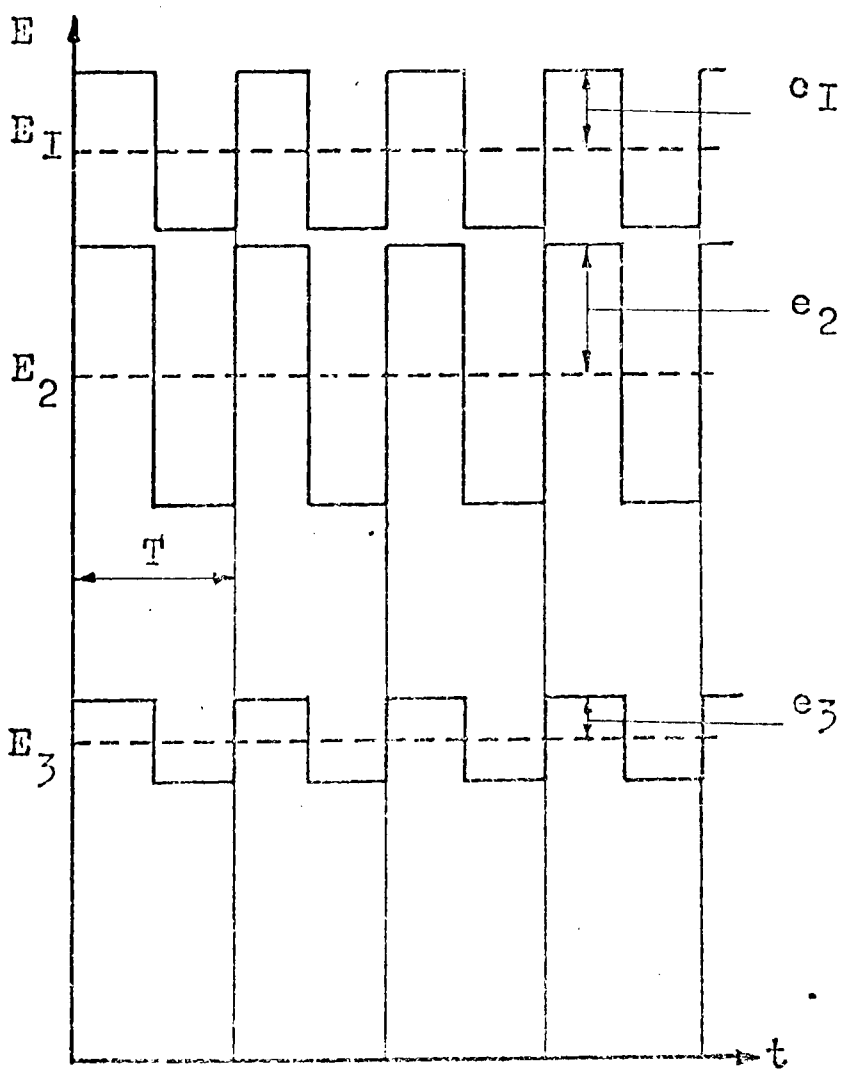

Fig.6.I9. The three voltages are assumed to occur simultaneously with the assumption of stationary turbulence

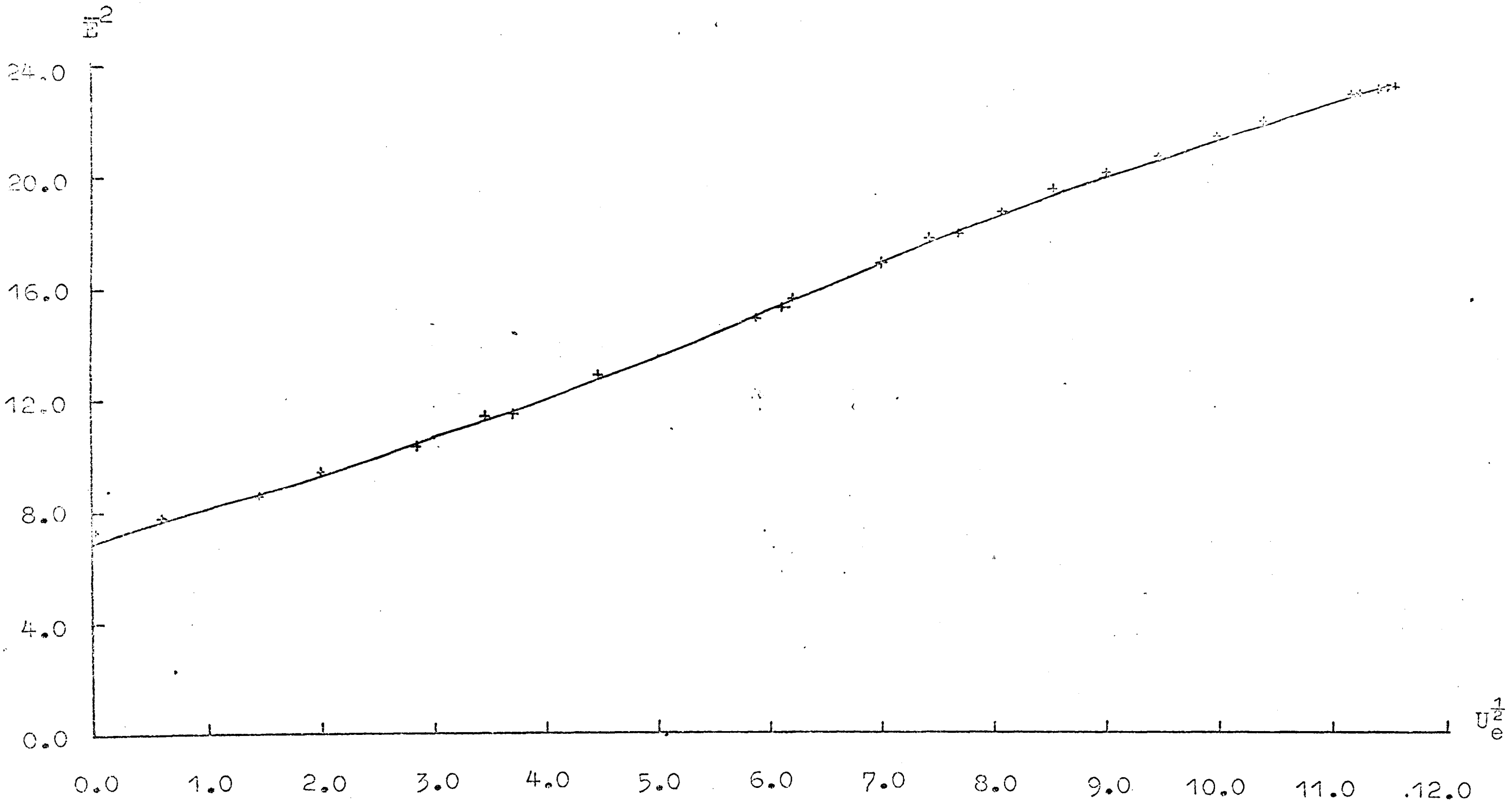

Fig.6.20. A typical calibration curve for the hot-wire probe

Fig.6.21.Variation of heat transfer from the wire with yaw and pitch angles

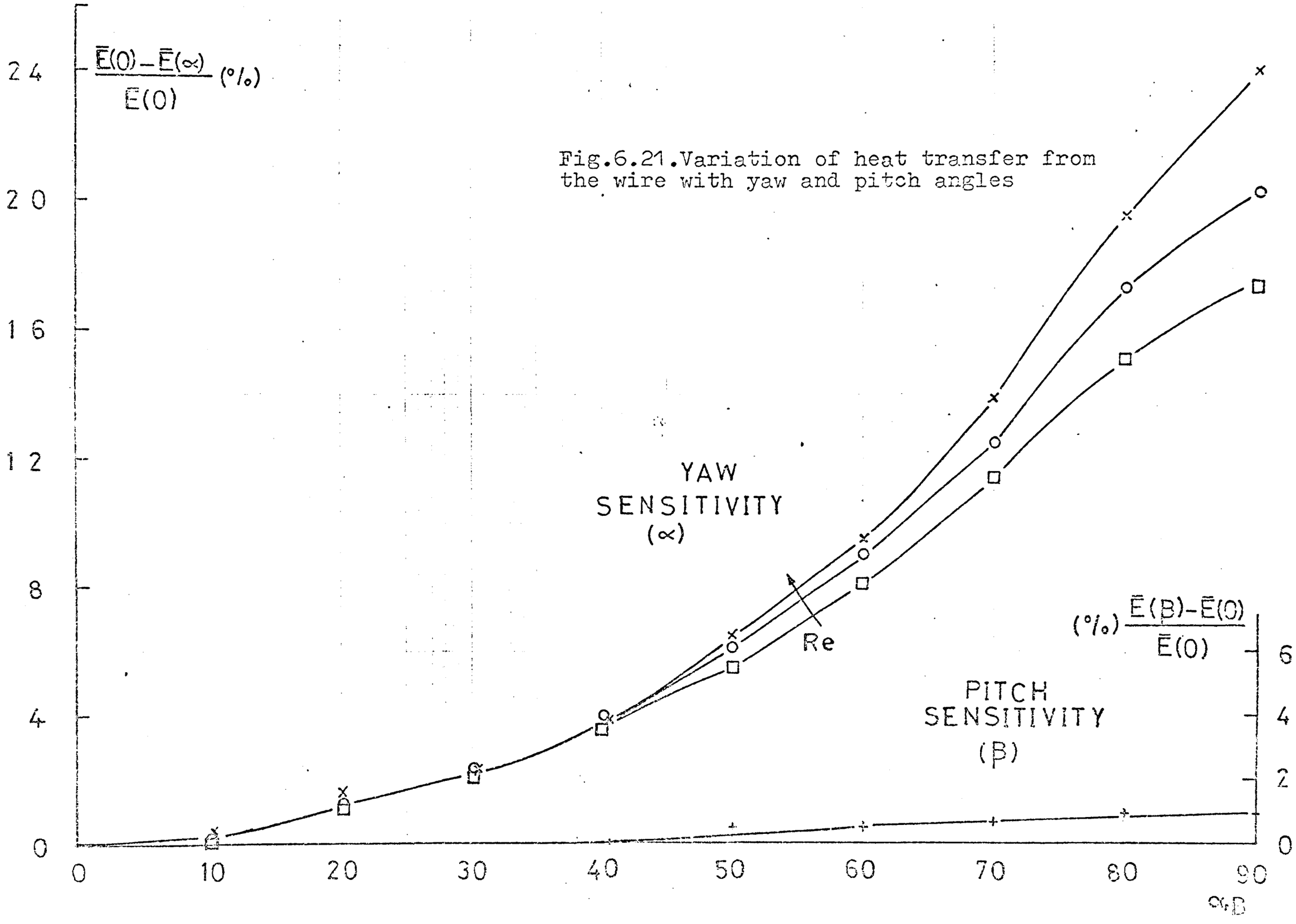

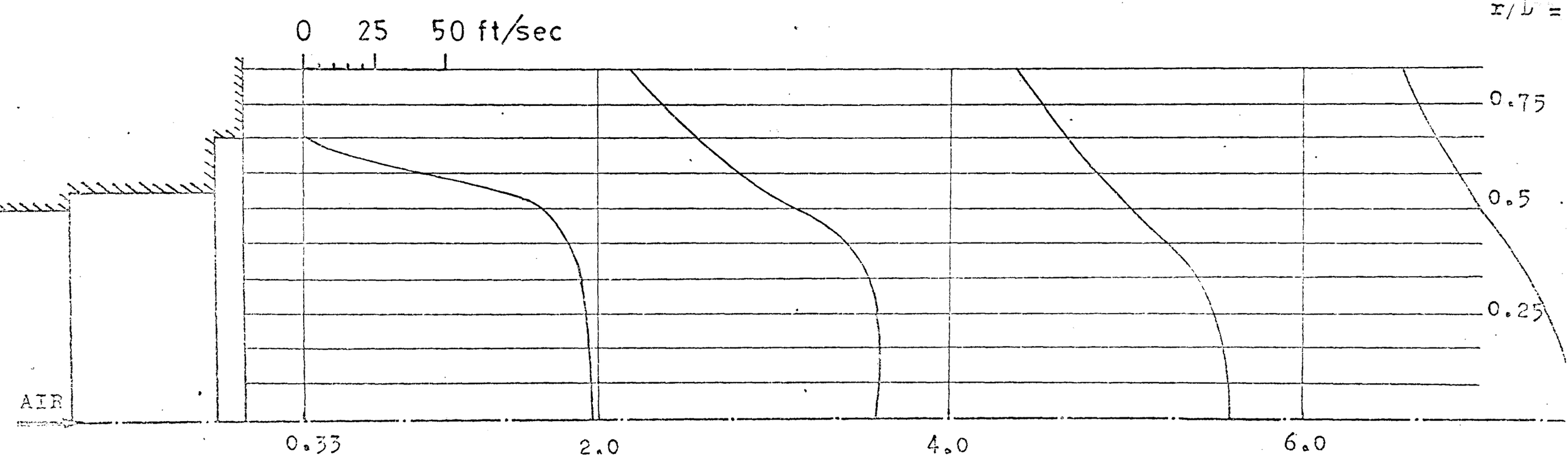

Fig.6.22.Distribution of axial velocity in a straight round jet

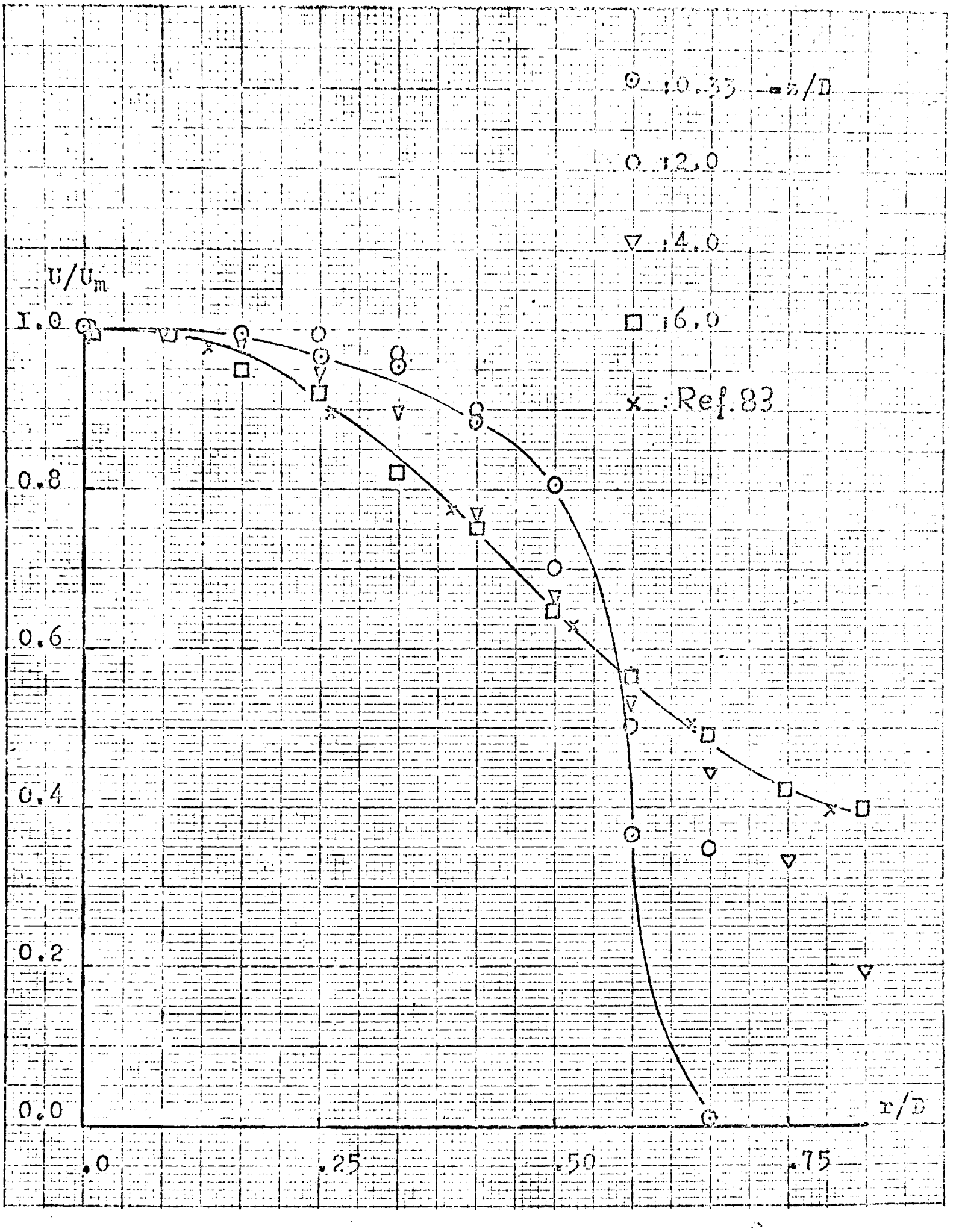

Fig.6.23.Radial distribution of normalized axial velocity

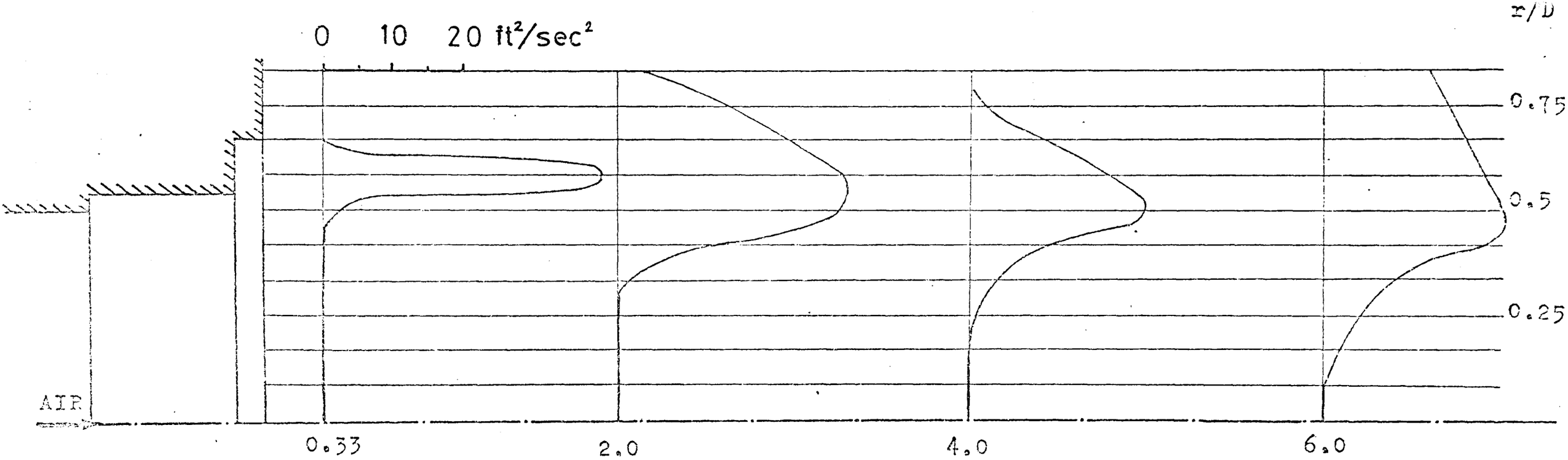

Fig.6.24.Distribution of the shear stress $\overline{uv}$ in a straight round jet

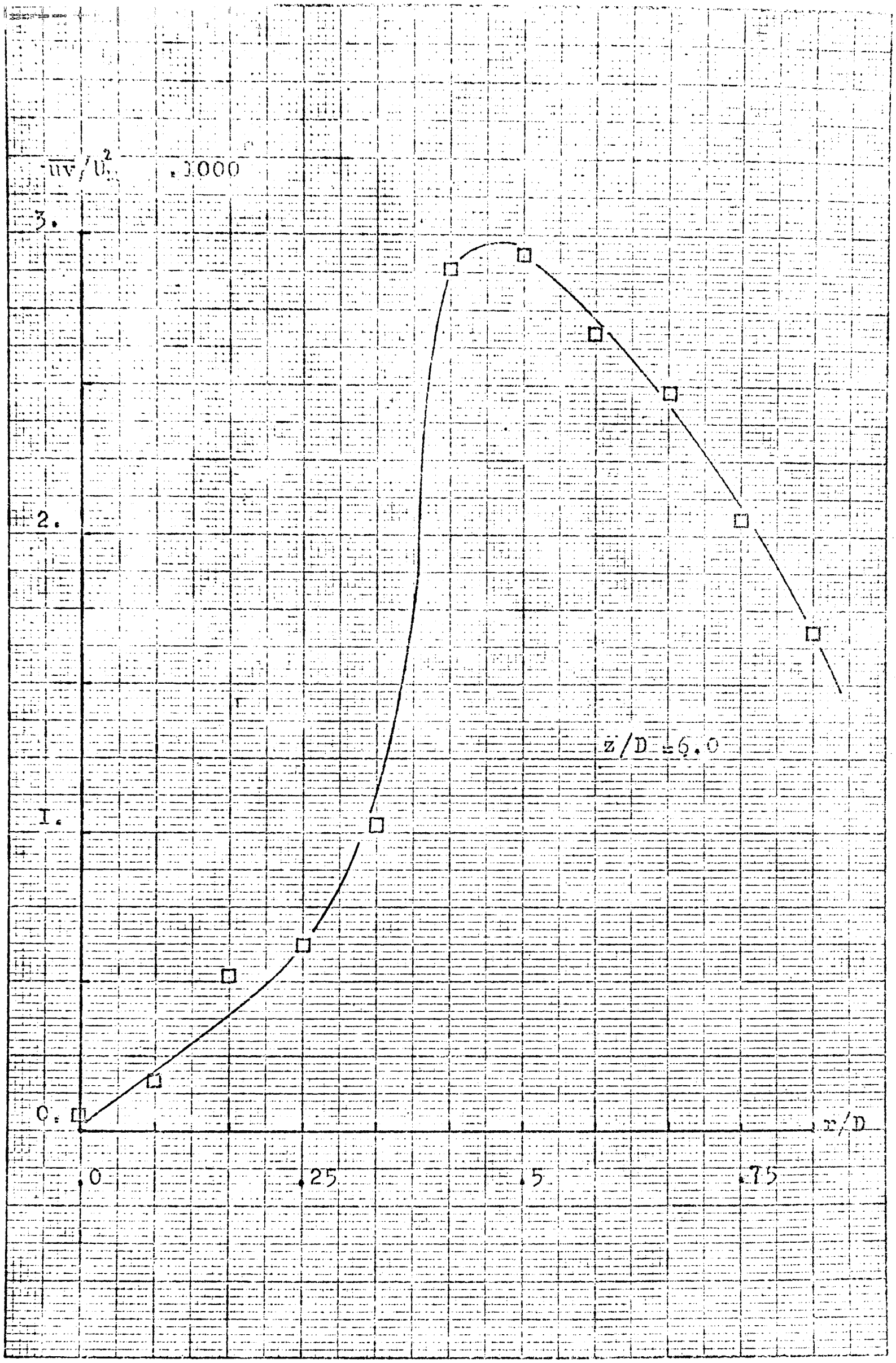

Fig.6.25.Radial distribution of the normalised shear stress

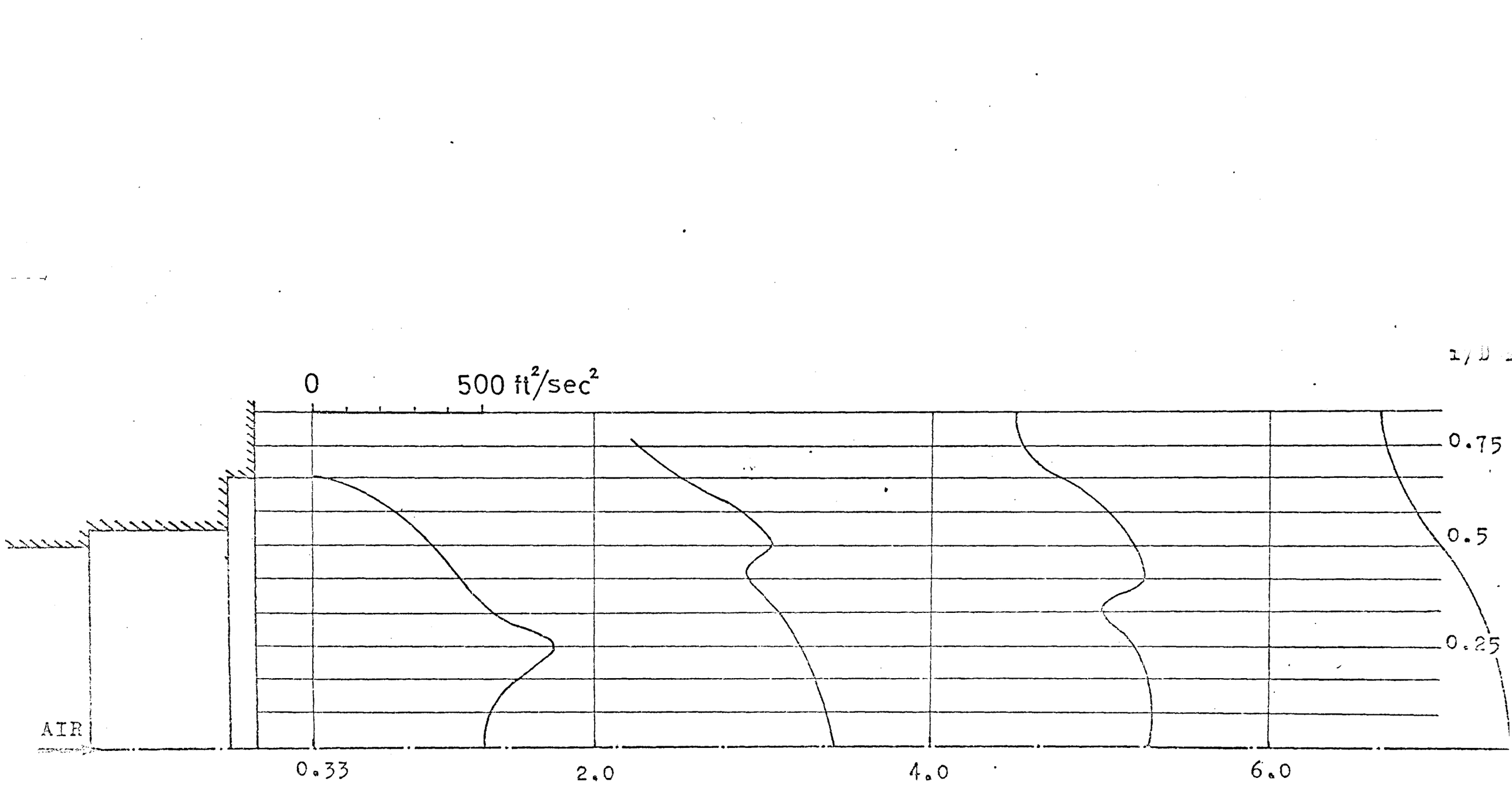

Fig.6.26.Distribution of the kinetic energy of turbulence in a straight round jet

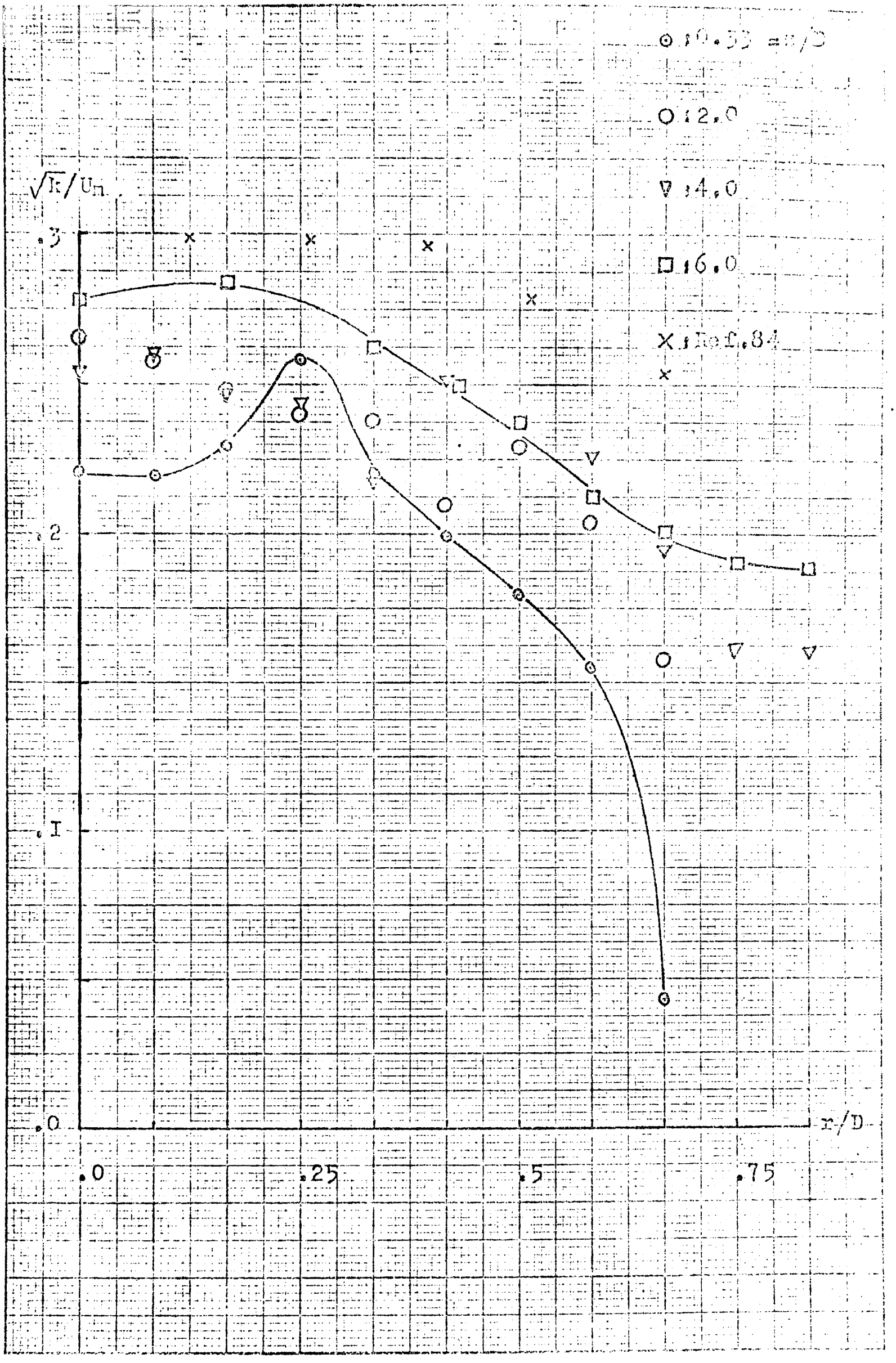

Fig.6.27. Radial distribution of the normalized turbulence kinetic energy

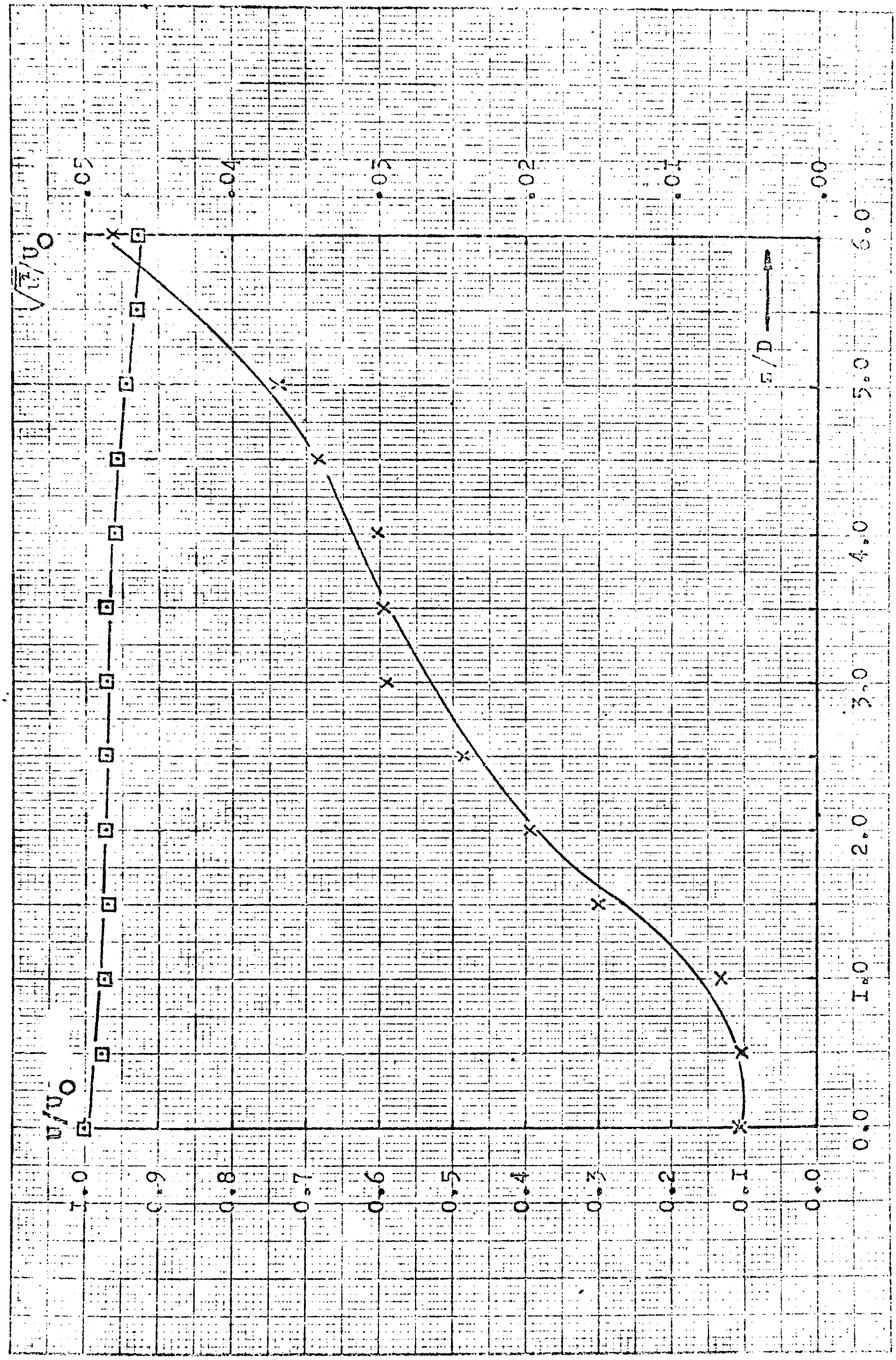

Fig.6.28.Distribution of the longitudinal turbulence intensity and normalized axial velocity on the axis of the straight jet

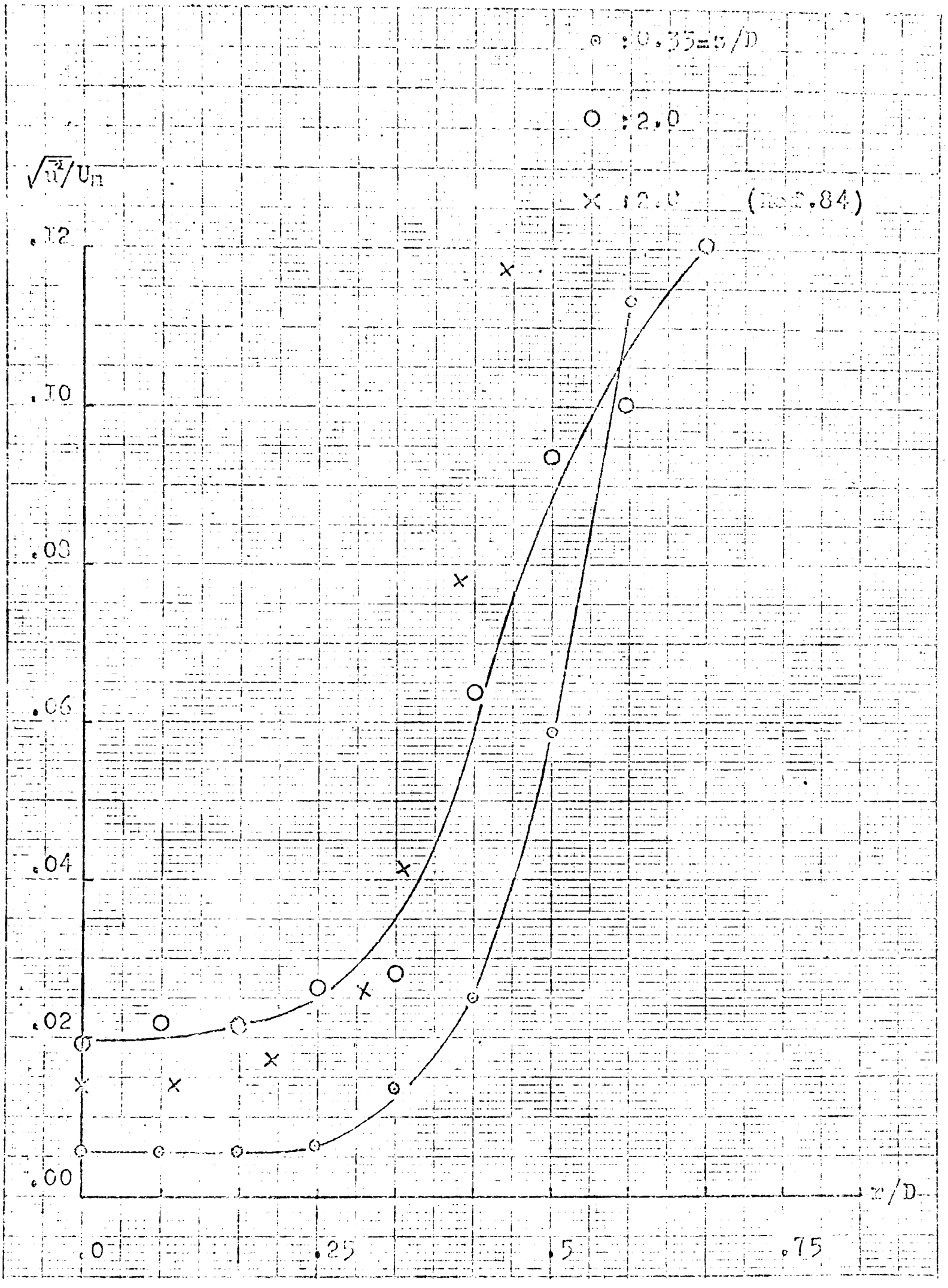

Fig.6.29. Profiles of the longitudanal turbulence intensity in the immediate downstream region of the nozzle

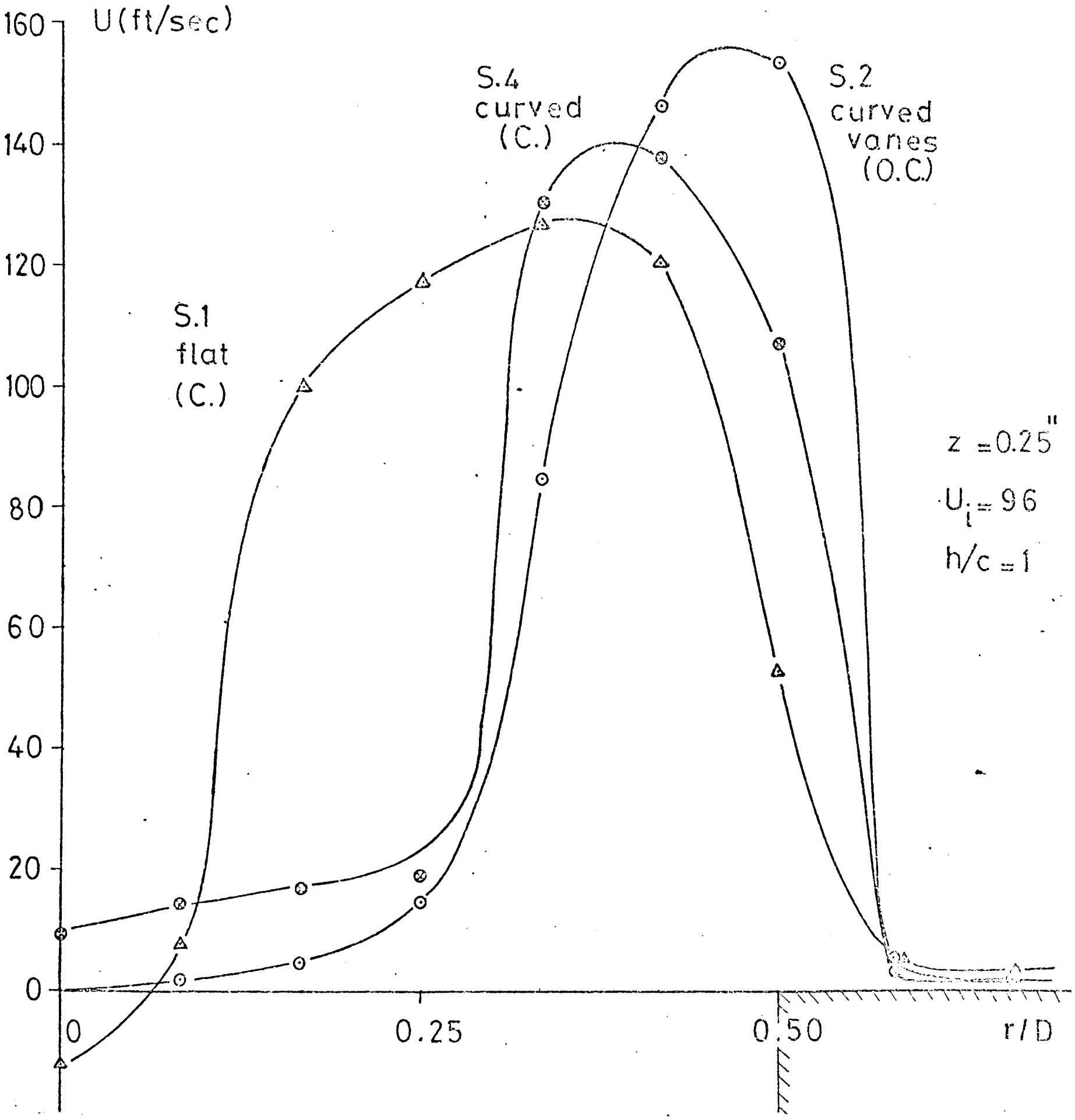

Fig.7.1.Typical profiles of the axial velocity component at the exit from the three types of swirler

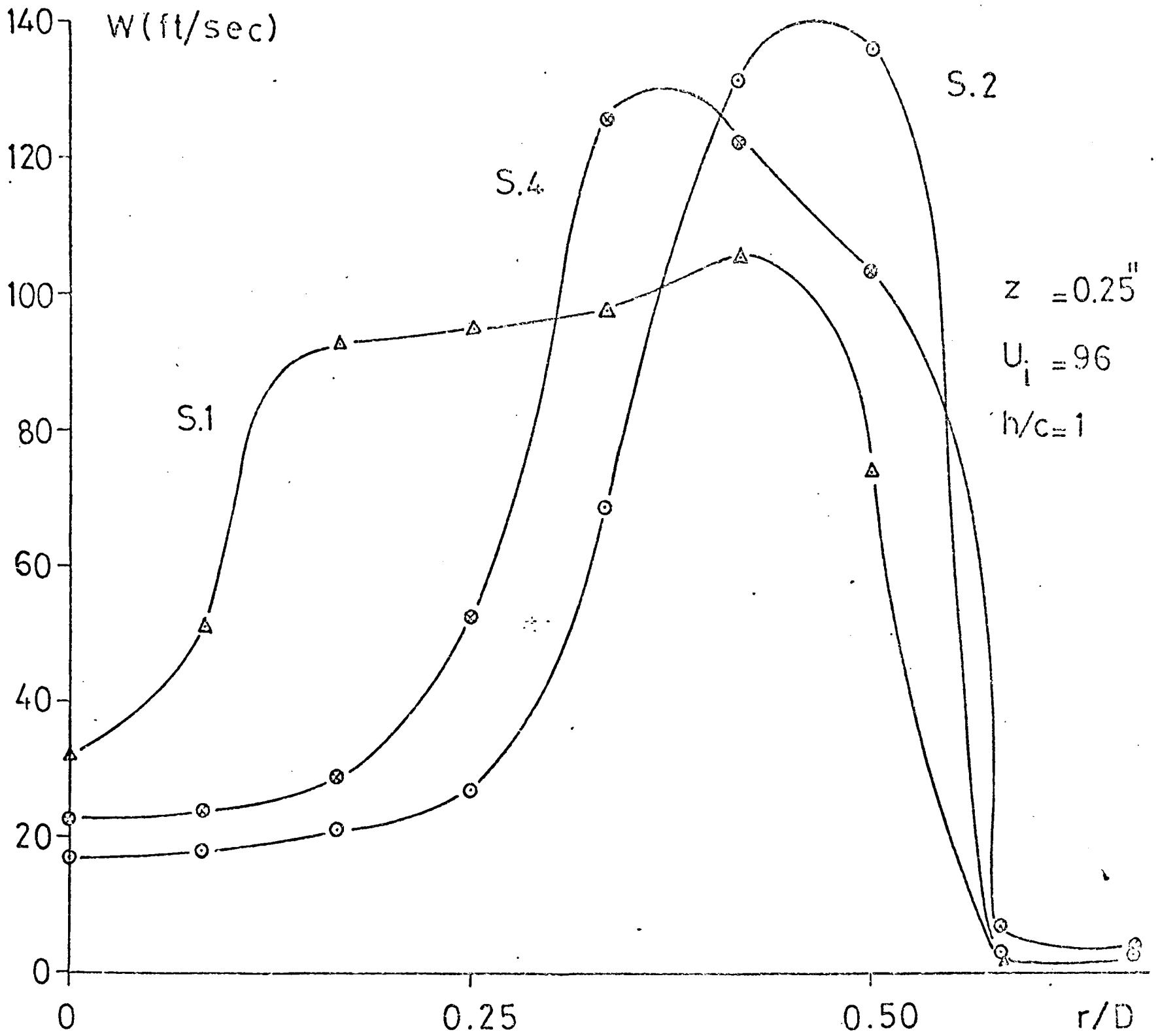

Fig.7.2.Radial distribution of the swirl velocity component at the exit of the three types of swirler

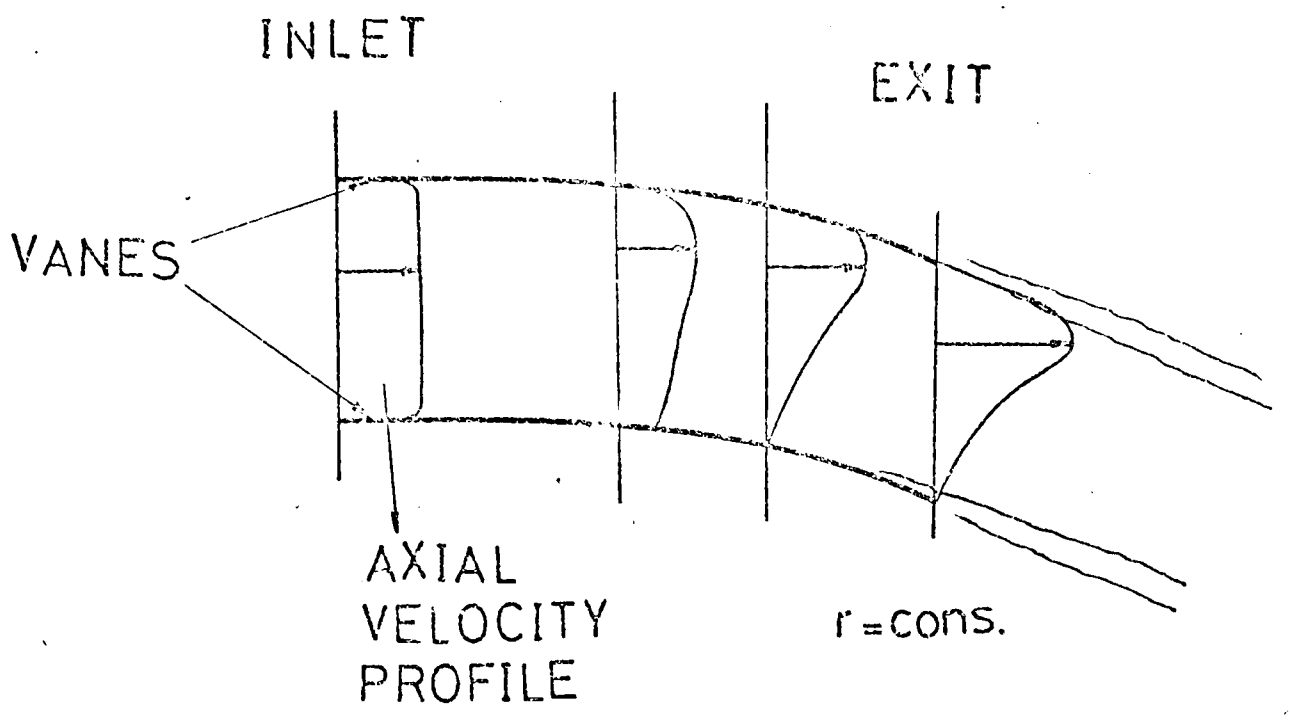

Fig.7.3a.Circumferential distribution of the axial velocity component in the swirler

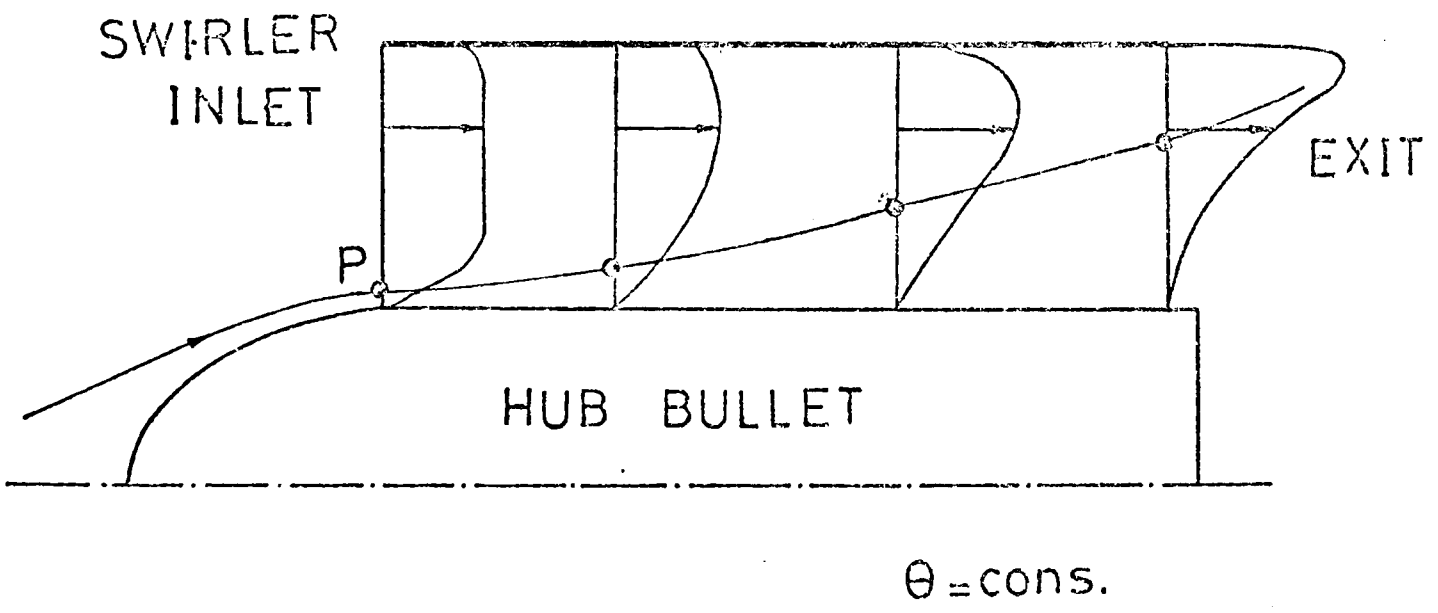

Fig.7.3b.Radial distribution of the axial velocity component in the swirler

Fig.7.4.Pressure drop for vane type swirlers

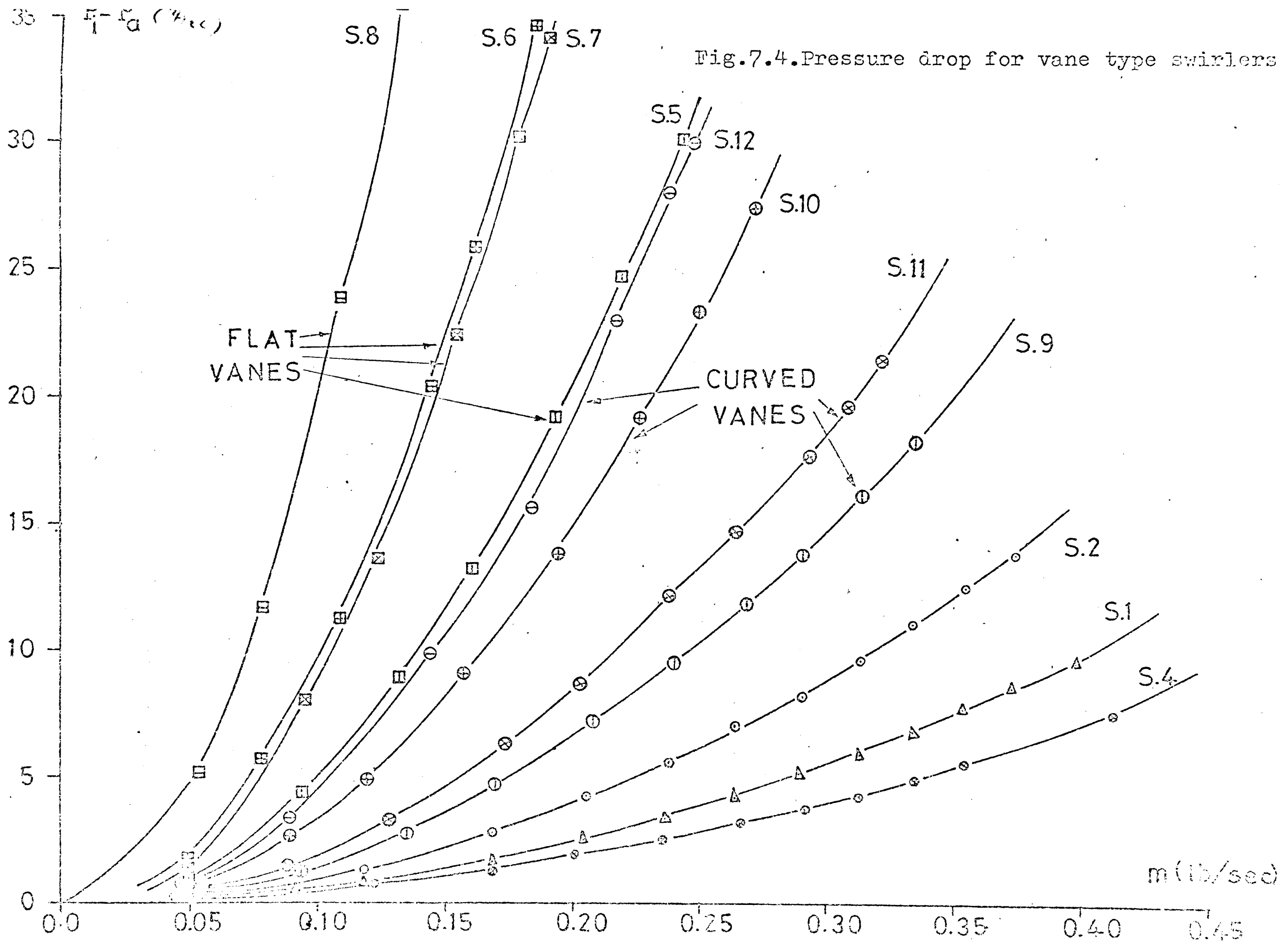

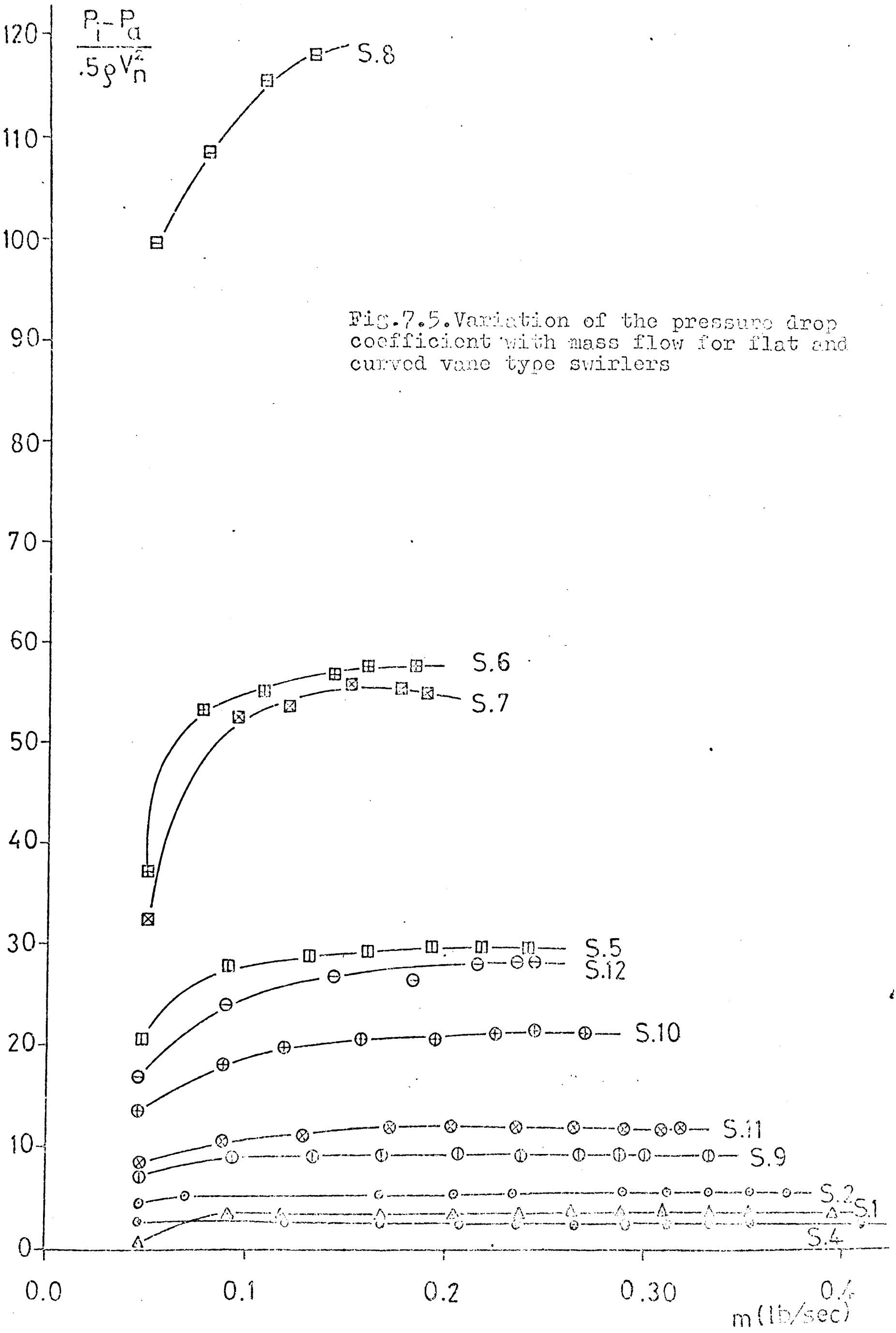

Fig.7.5. Variation of the pressure drop coefficient with mass flow for flat and curved vane type swirlers

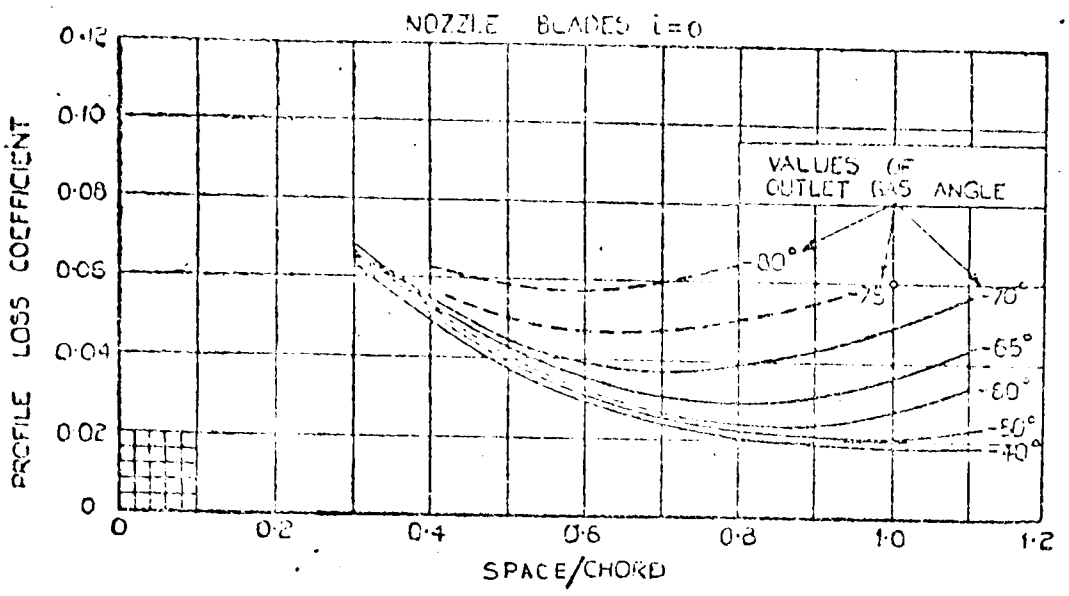

Fig.7.6a.Profile loss coefficient for conventional section blades at zero incidence (Re=2x10^5, M=.6 , thicknes/chord = 20%)

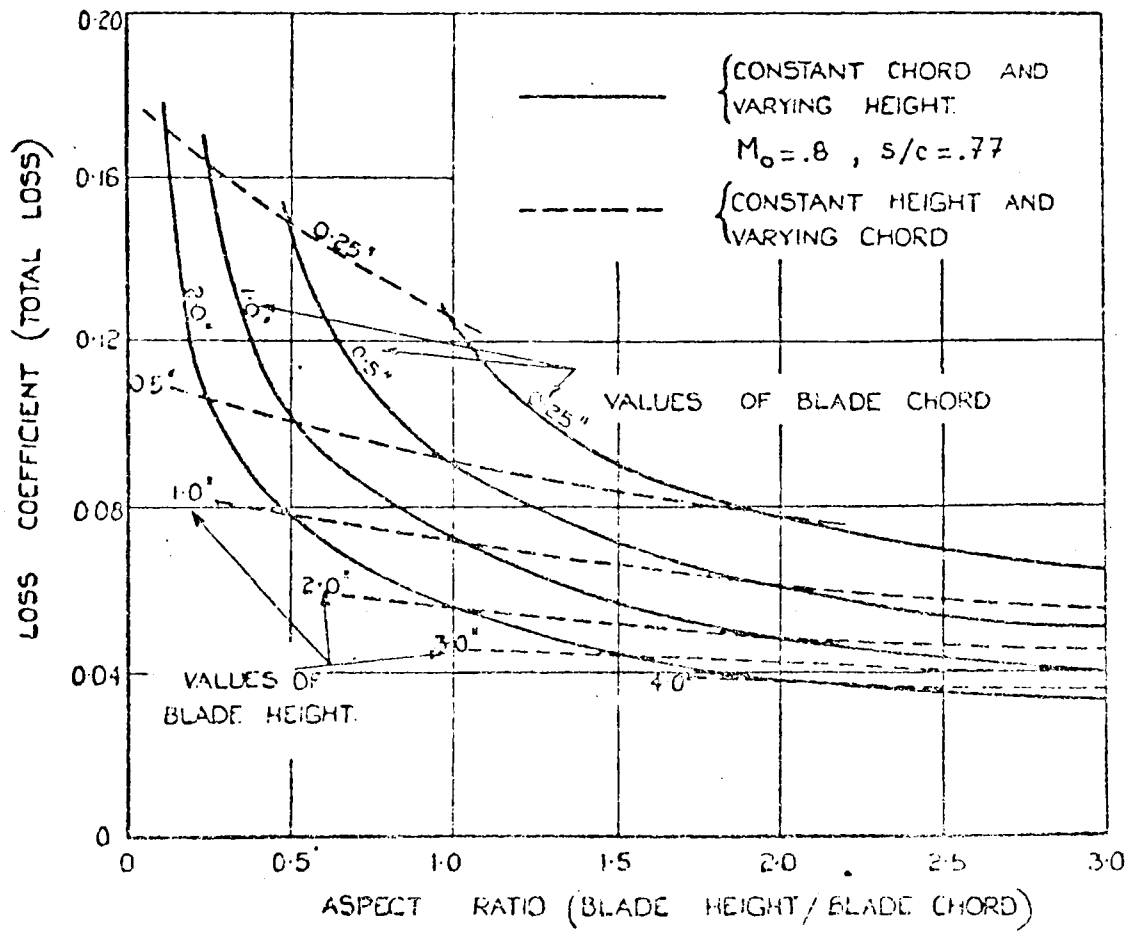

Fig.7.6b.Variation of loss coefficient with the aspect ratio

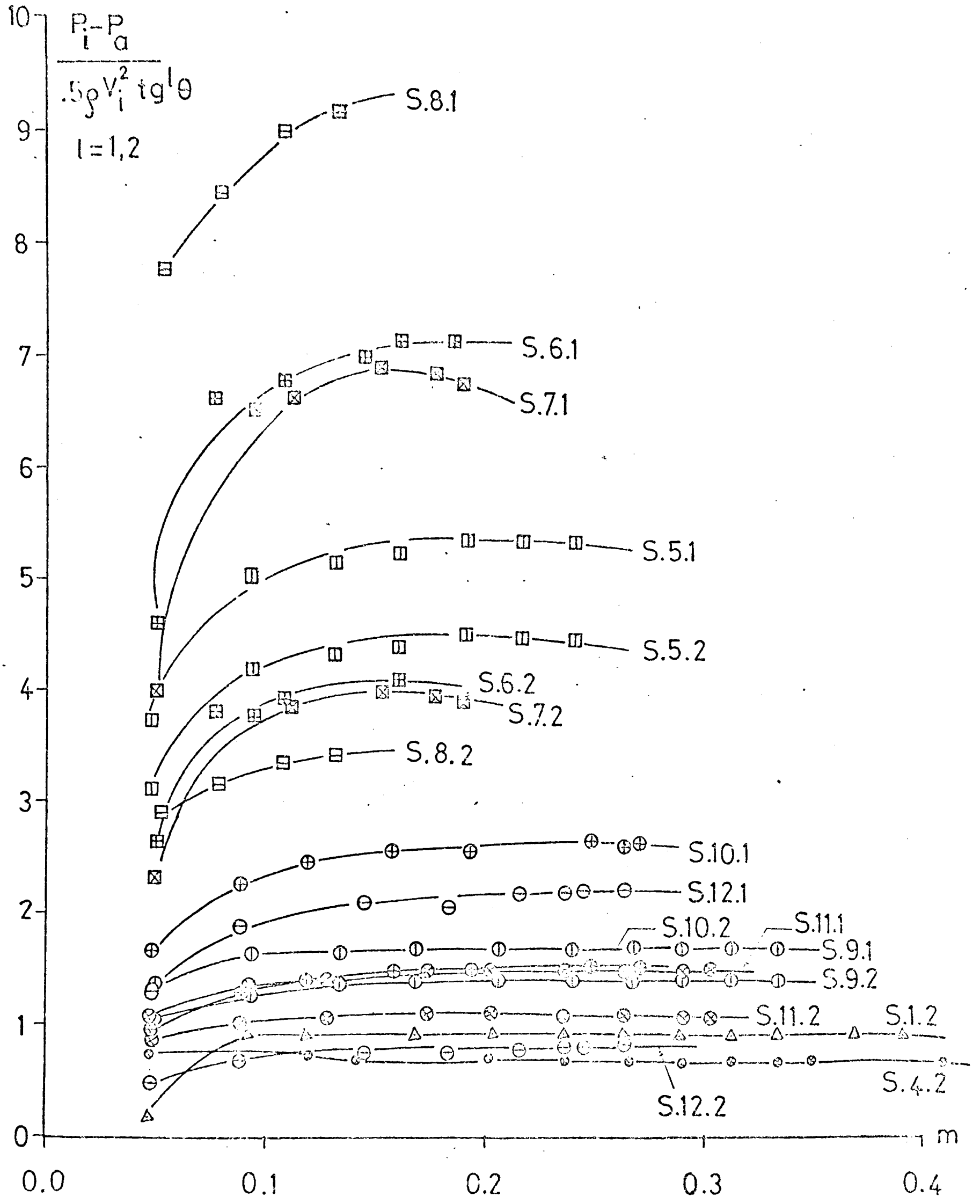

Fig.7.7.Normalized pressure drop coefficient for flat and curved vane type swirlers

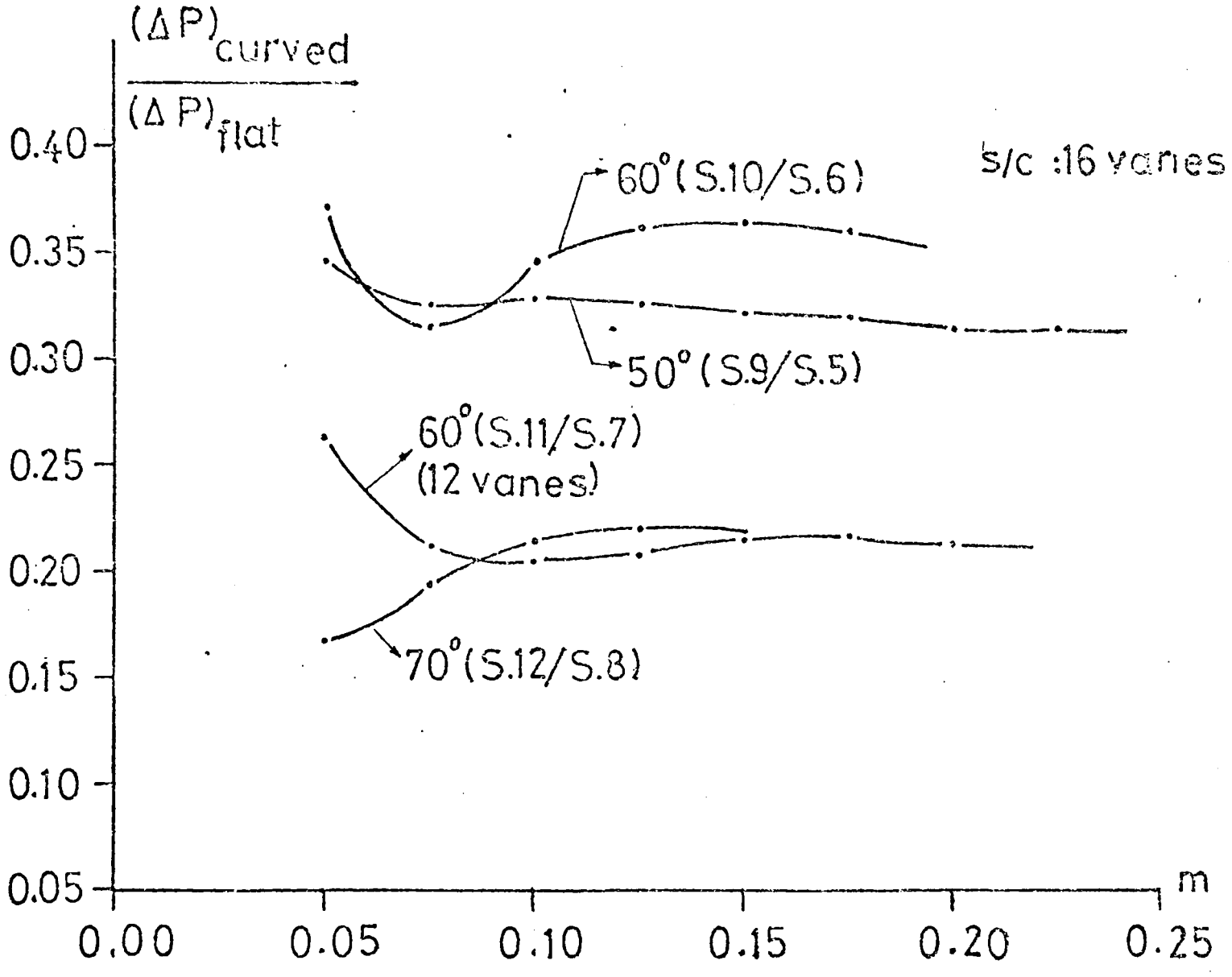

Fig.7.8.Comparison of the pressure drop coefficient for flat and curved vane type swirlers

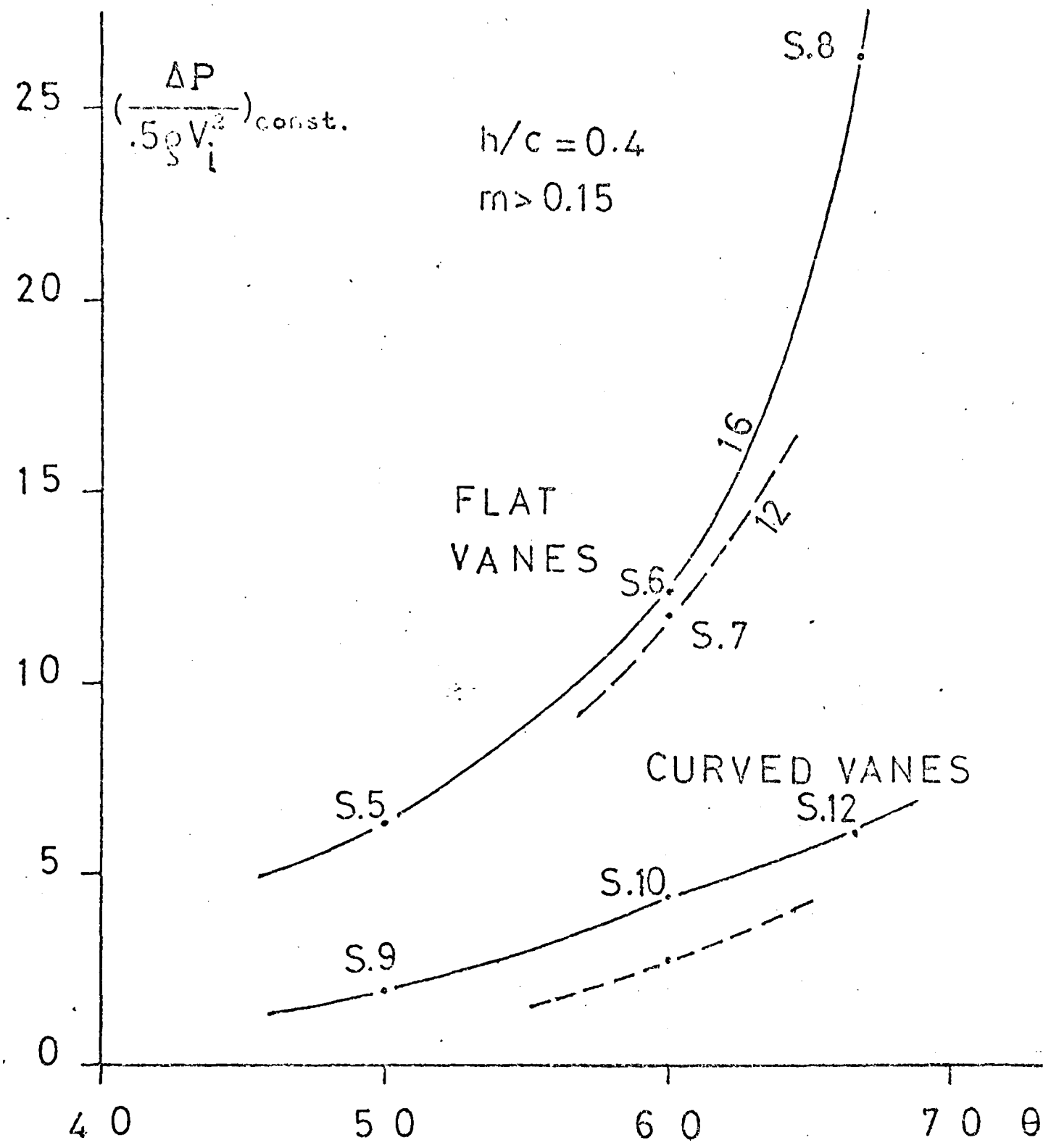

Fig.7.9. Variation of the pressure drop coefficient with vane angle for flat and curved vane type swirlers

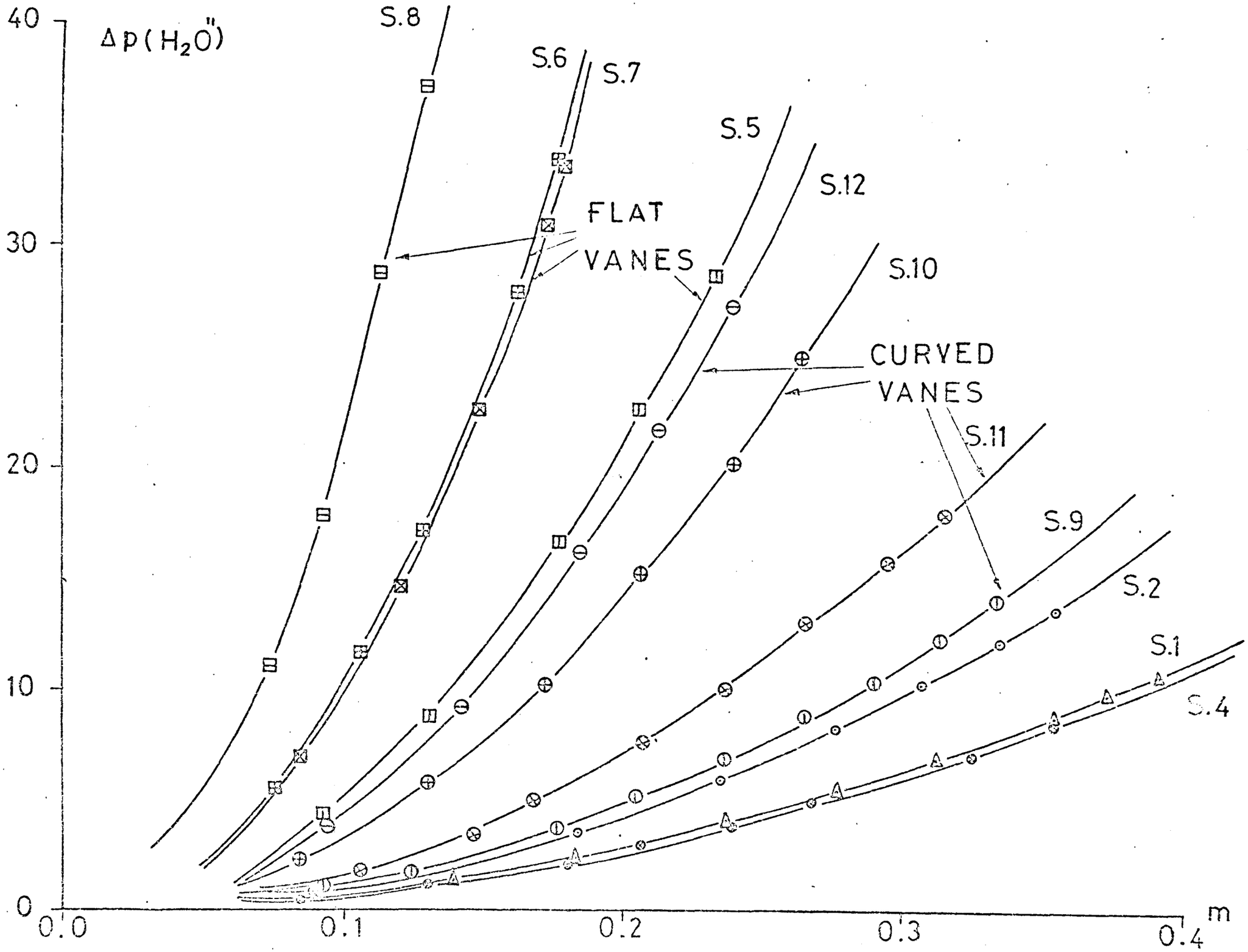

Fig.7.10.Variation of the static pressure drop with mass flow for the swirlers

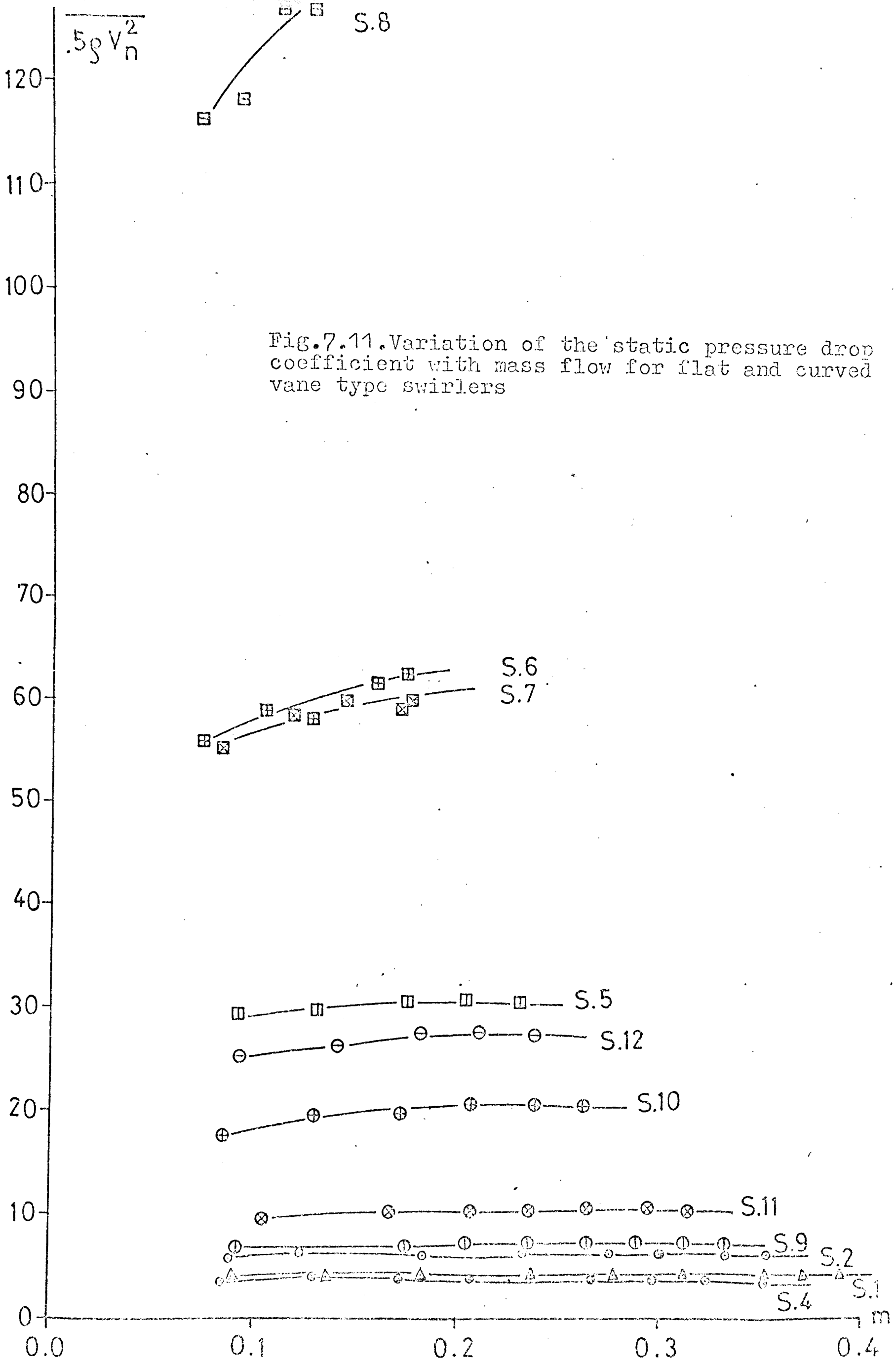

Fig.7.11.Variation of the static pressure drop coefficient with mass flow for flat and curved vane type swirlers

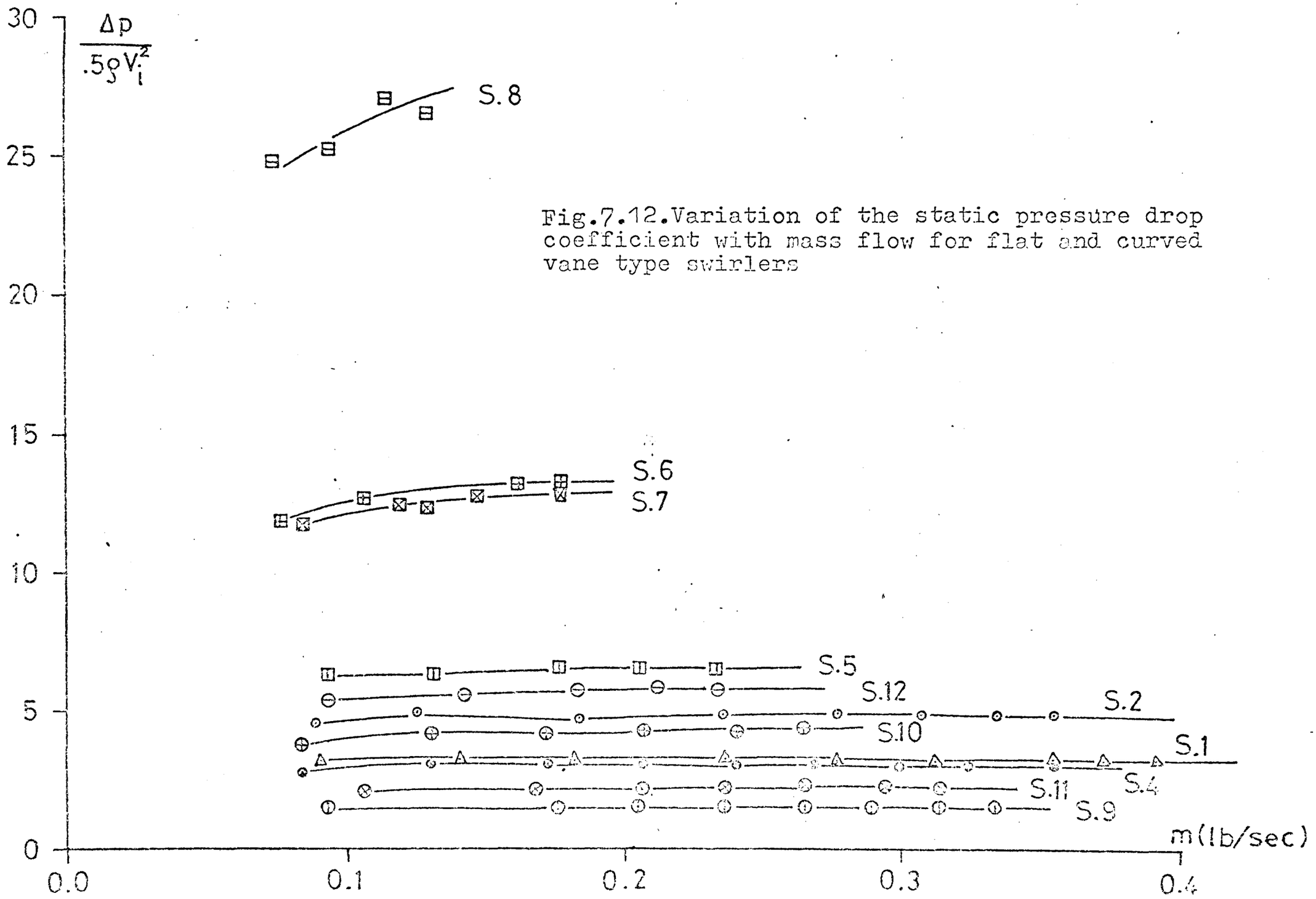

Fig.7.12.Variation of the static pressure drop coefficient with mass flow for flat and curved vane type swirlers

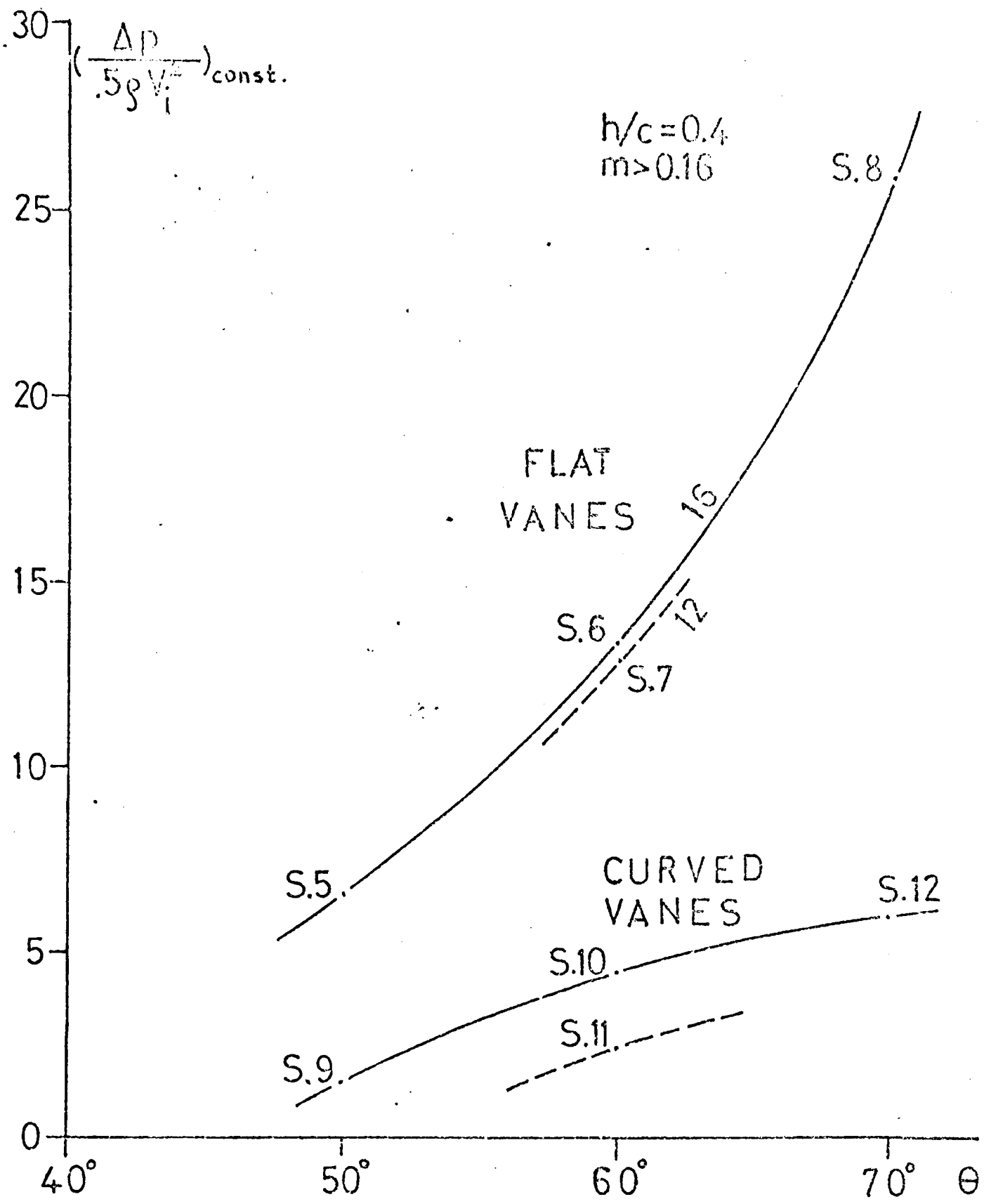

Fig.7.13.Variation of the static pressure drop coefficient with vane angle for flat and curved vane type swirlers

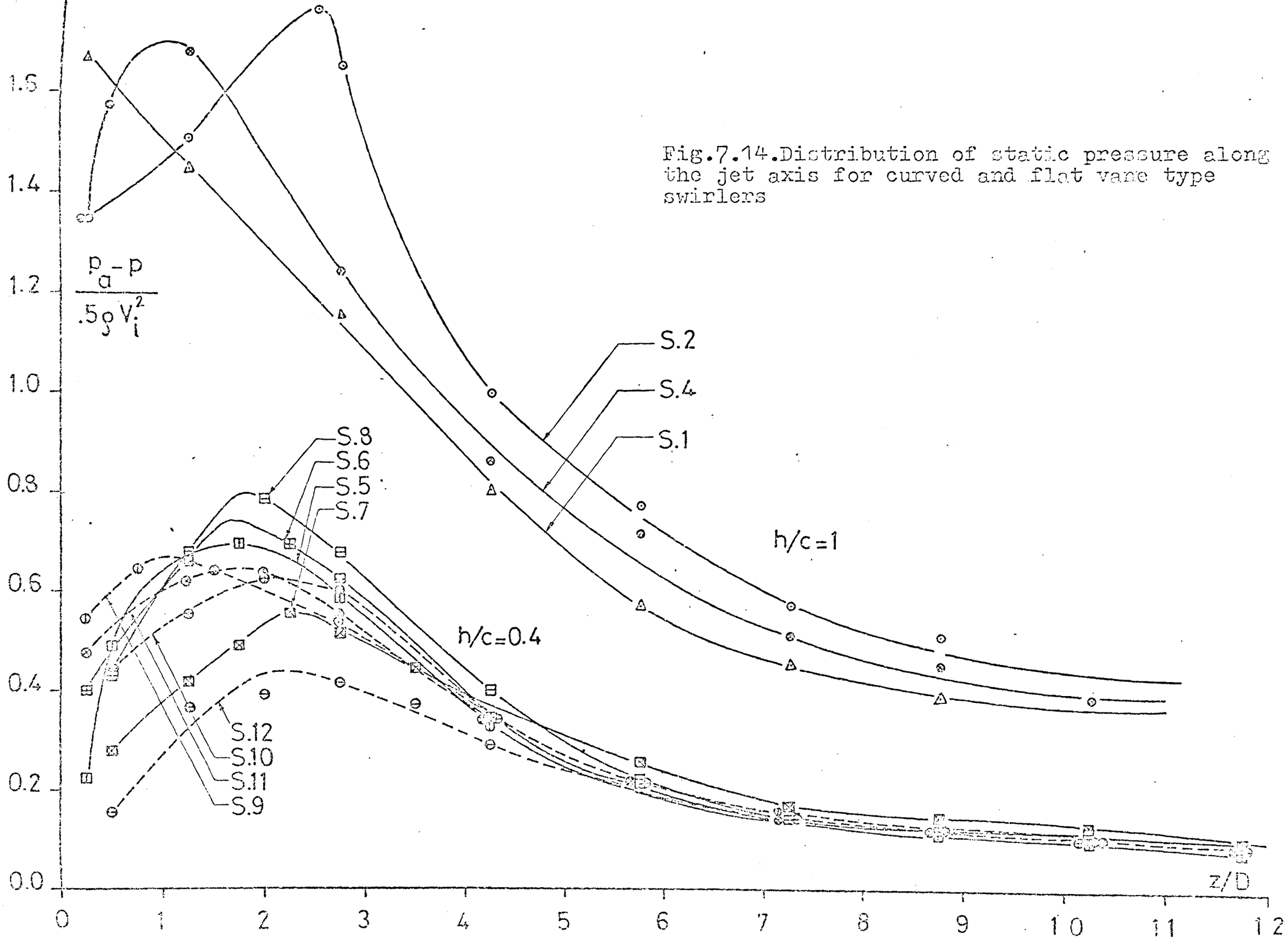

Fig.7.14.Distribution of static pressure along the jet axis for curved and flat vane type swirlers

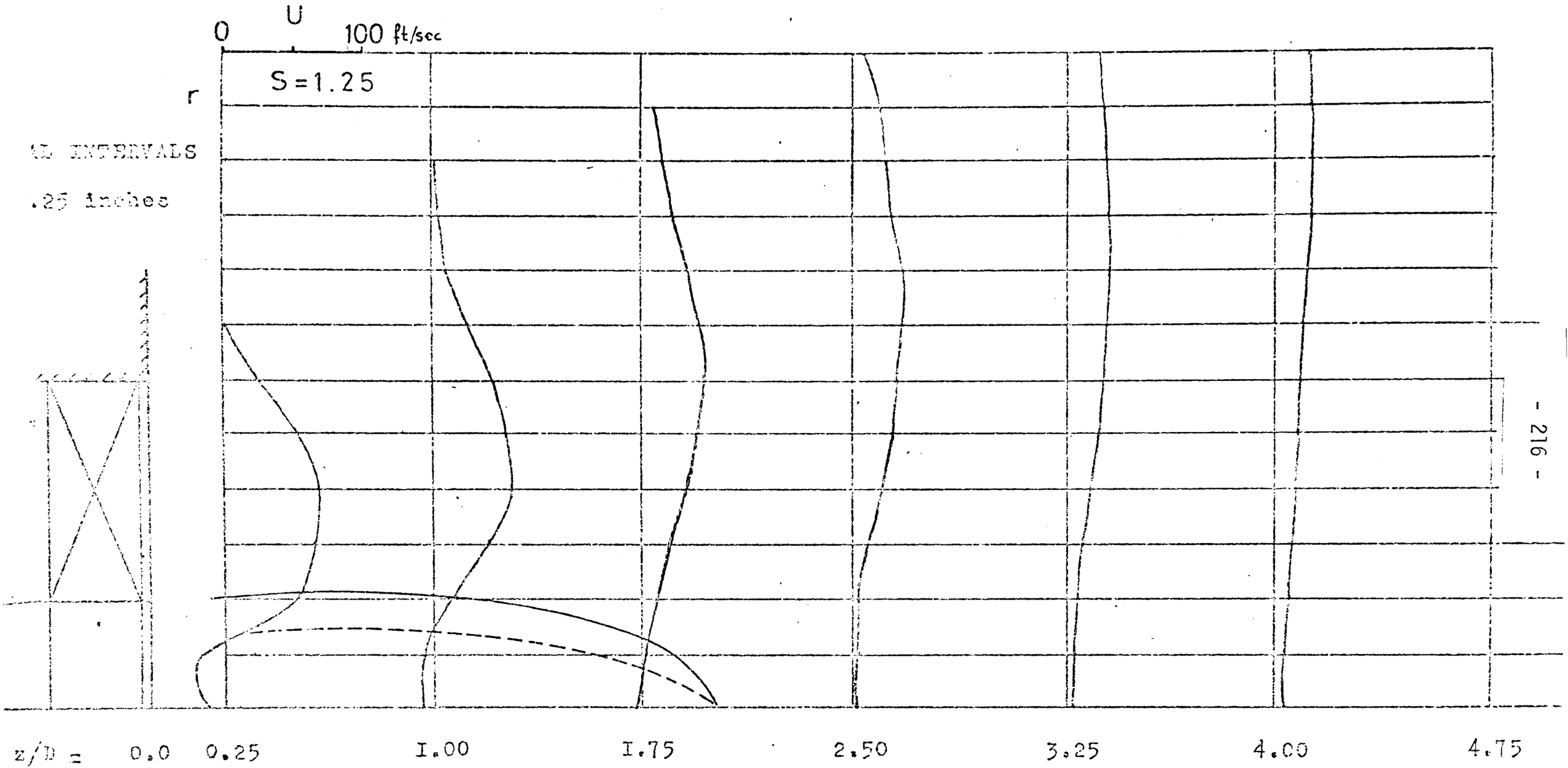

Fig.7.I5.Distribution of the axial velocity in the jet issuing from the swirler S.I

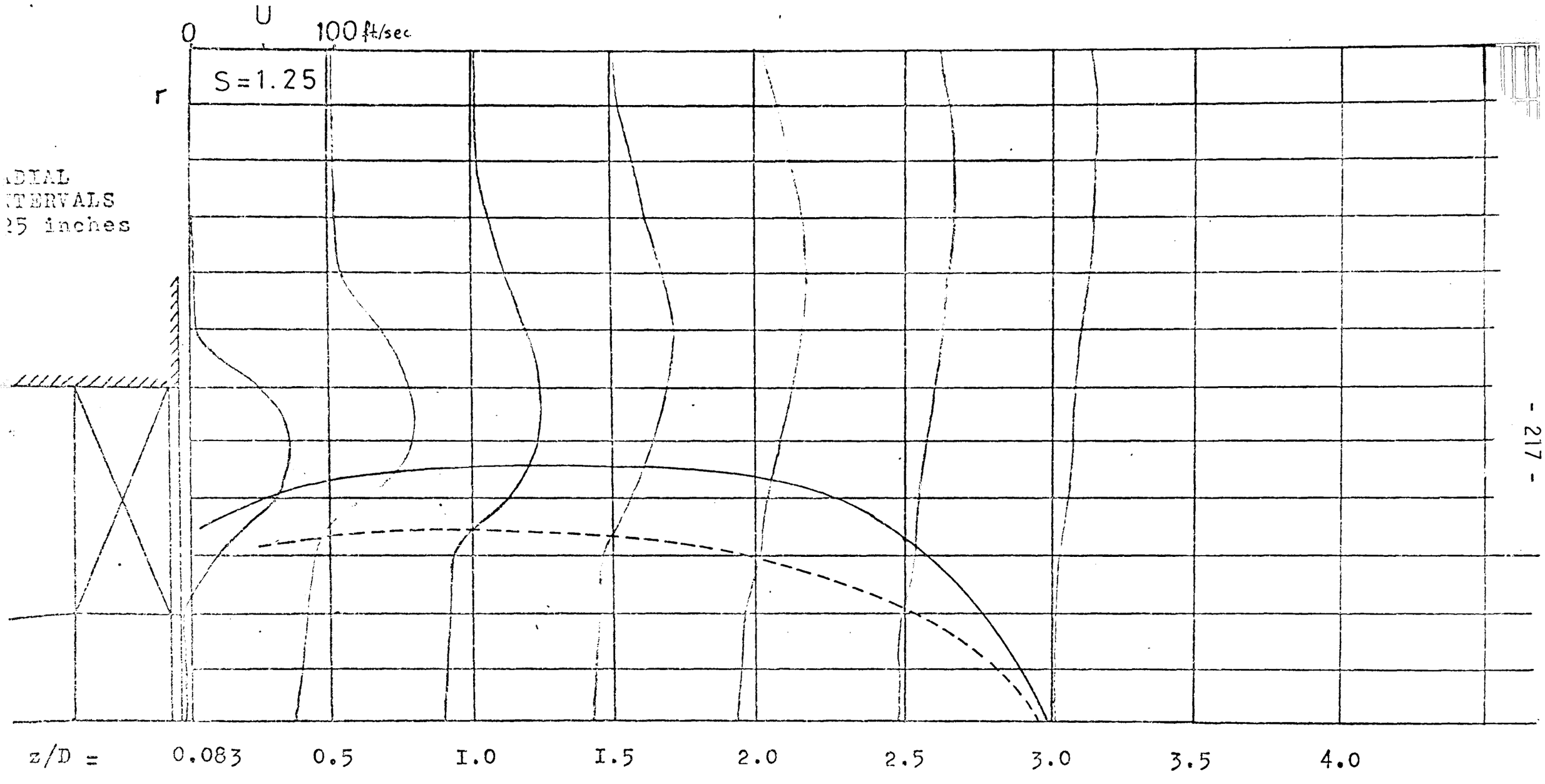

ADIAL
NTERVALS
25 inches

Fig.7.I6.Distribution of the axial velocity in the jet issuing from the swirler S.4

curves for AR=

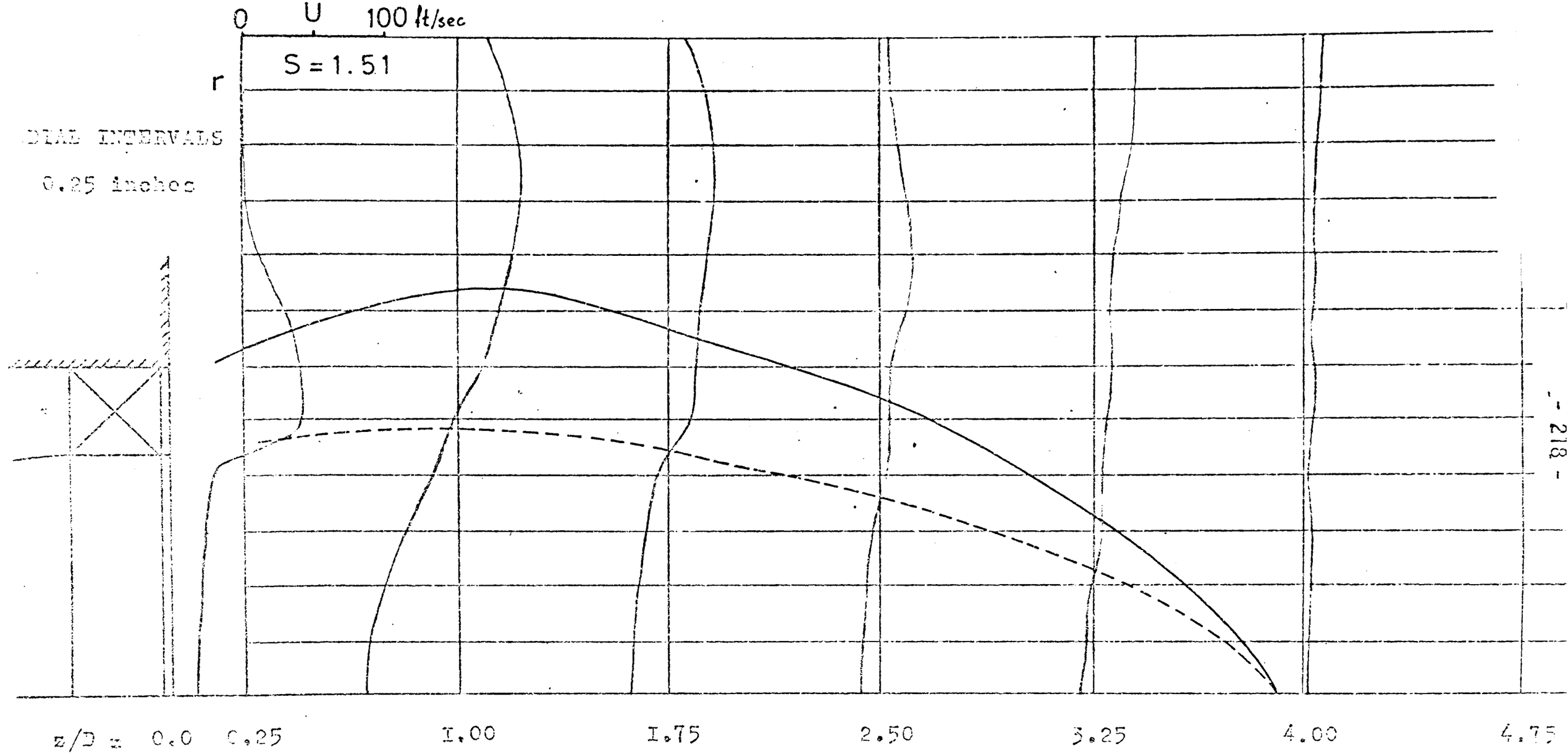

Fig.7.17.Distribution of the axial velocity in the jet issuing from the swirler S.6

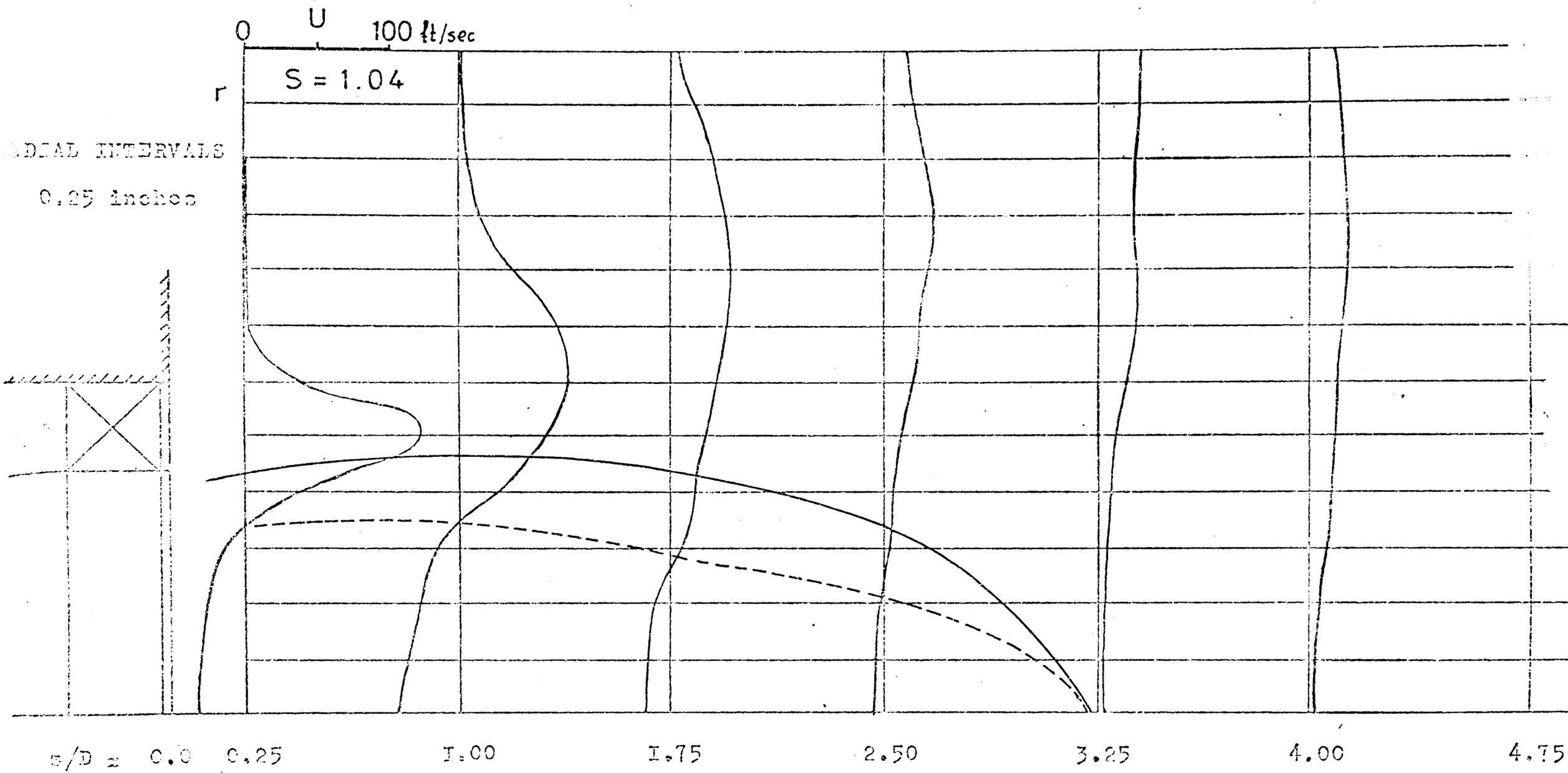

Fig.7.18.Distribution of the axial velocity in the jet issuing from the swirler S.9

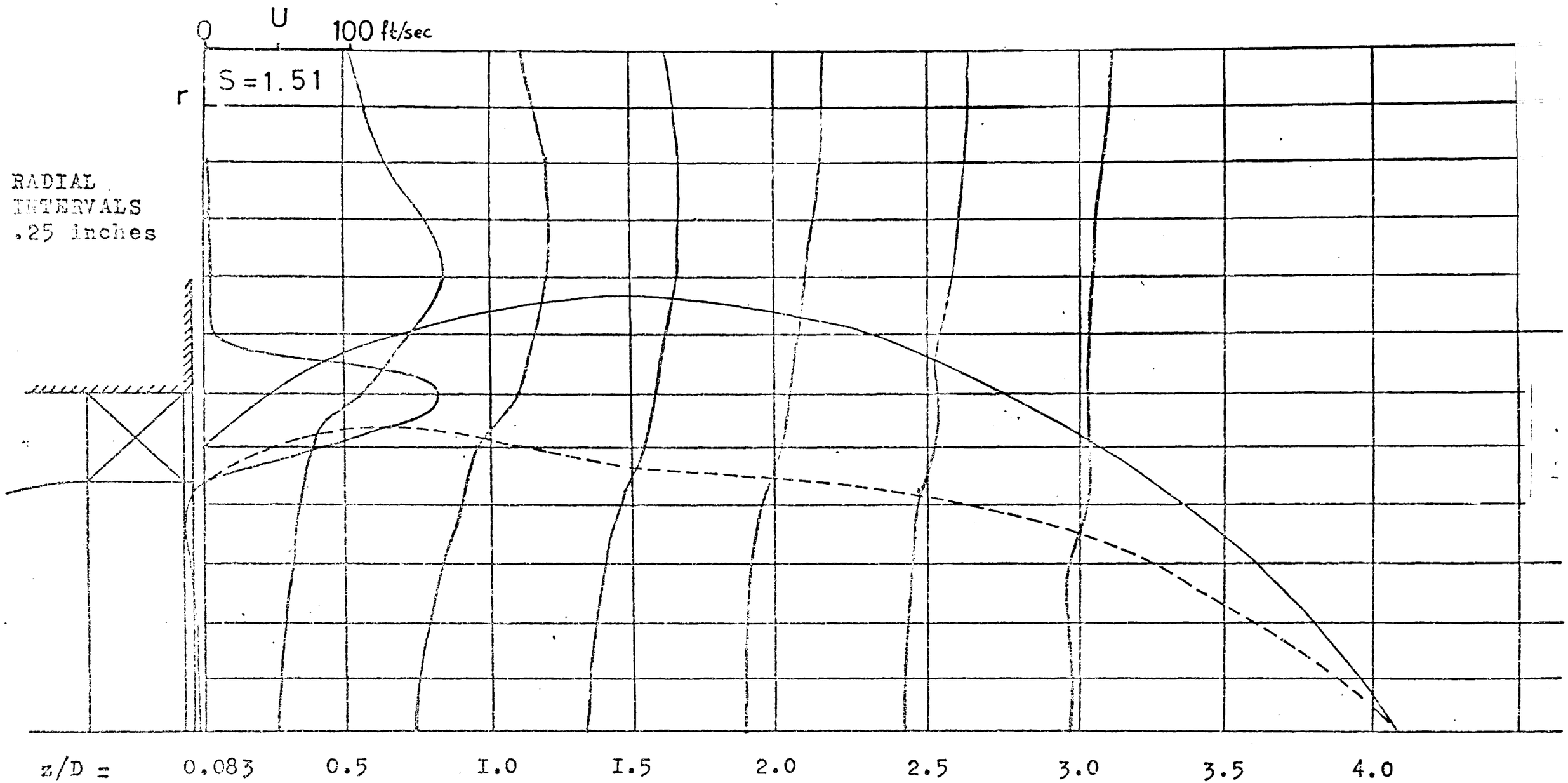

Fig.7.I9.Distribution of the axial velocity in the jet issuing from the swirler S.IO

60 0.4 16

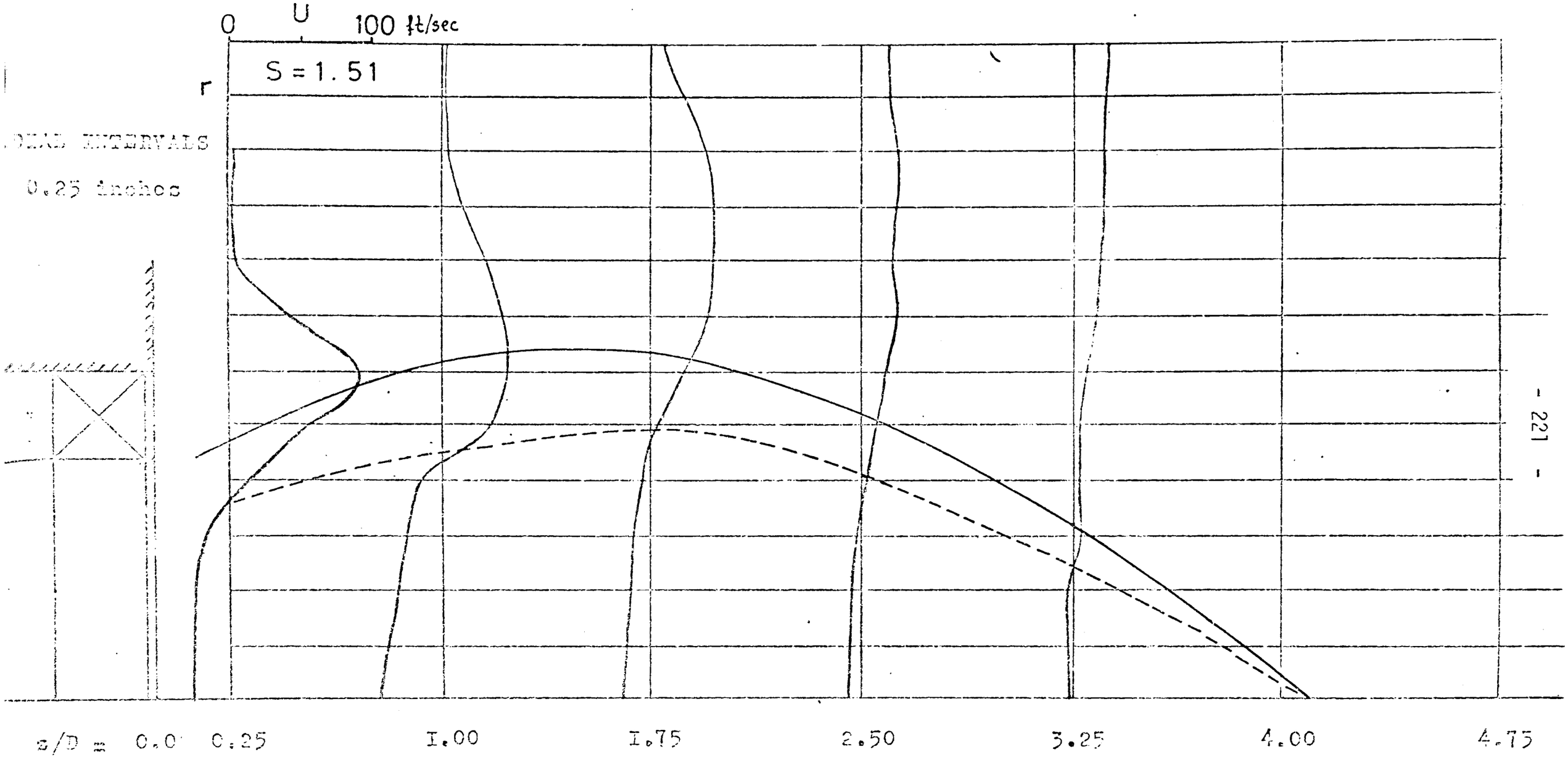

Fig.7.20.Distribution of the axial velocity in the jet issuing from the swirler S.II

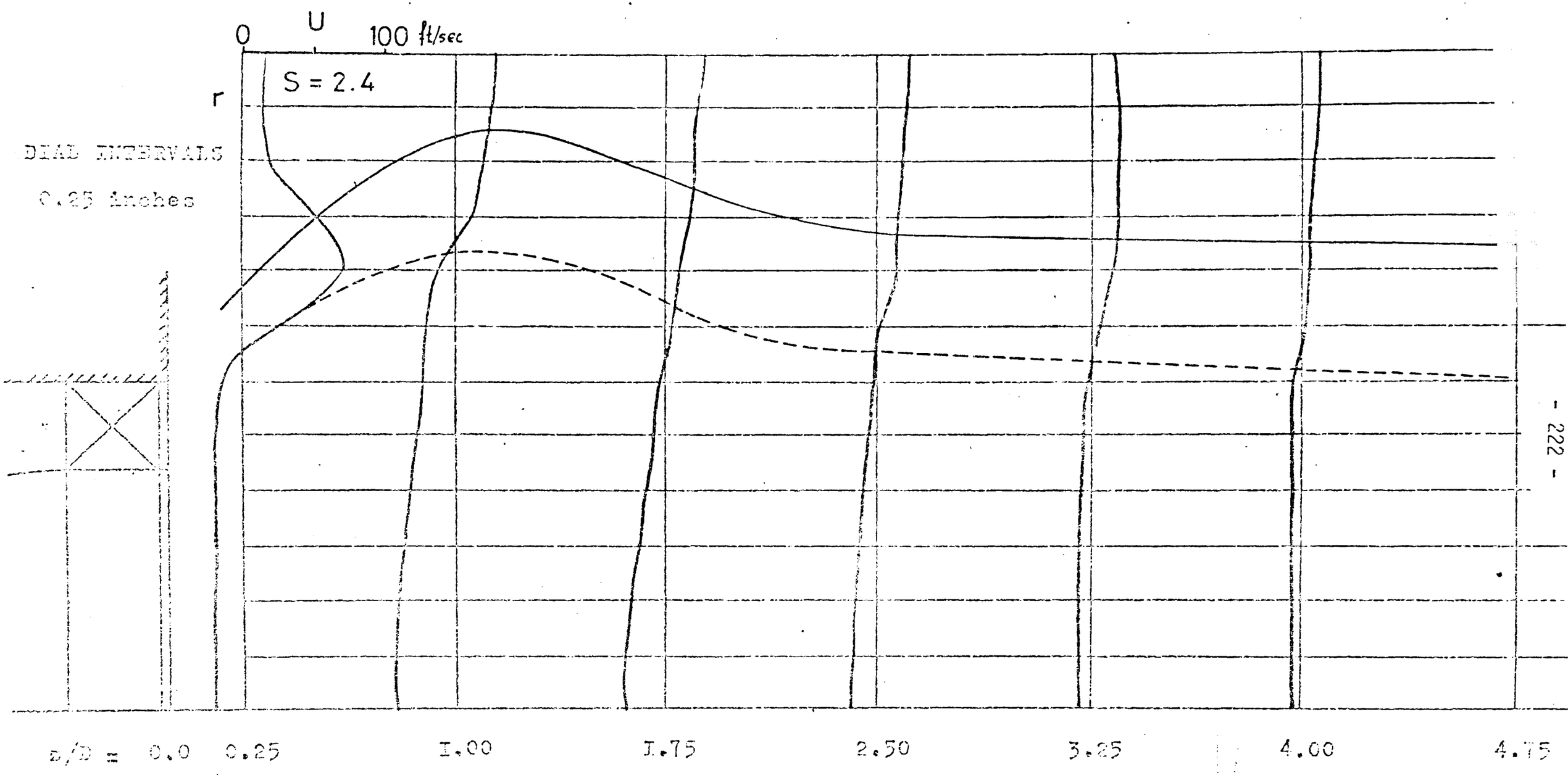

Fig.7.2I.Distribution of the axial velocity in the jet issuing from the swirler S.I2

16

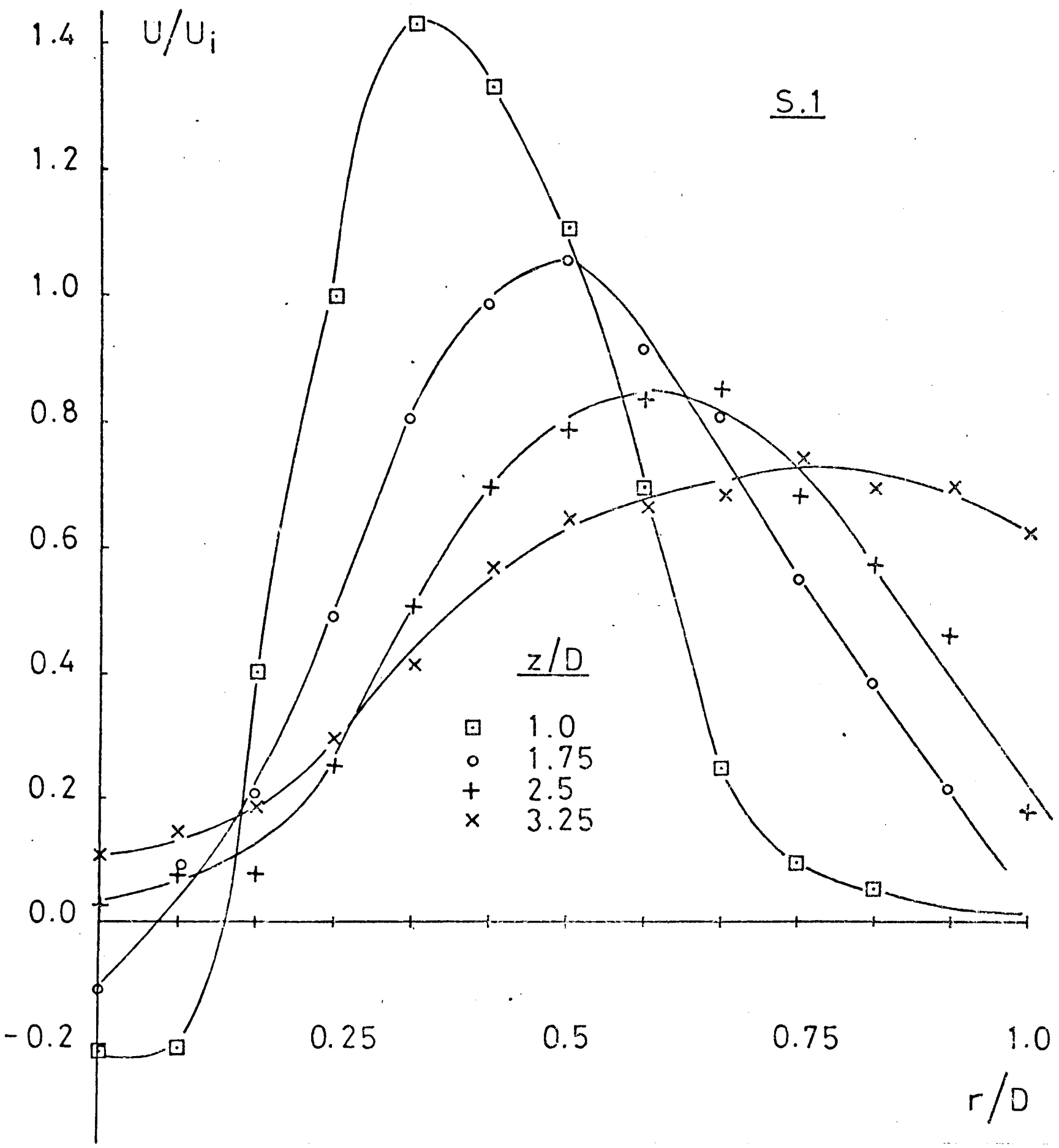

Fig.7.22.Variation of the profiles of the normalized axial velocity in the flow field of the swirler S.I

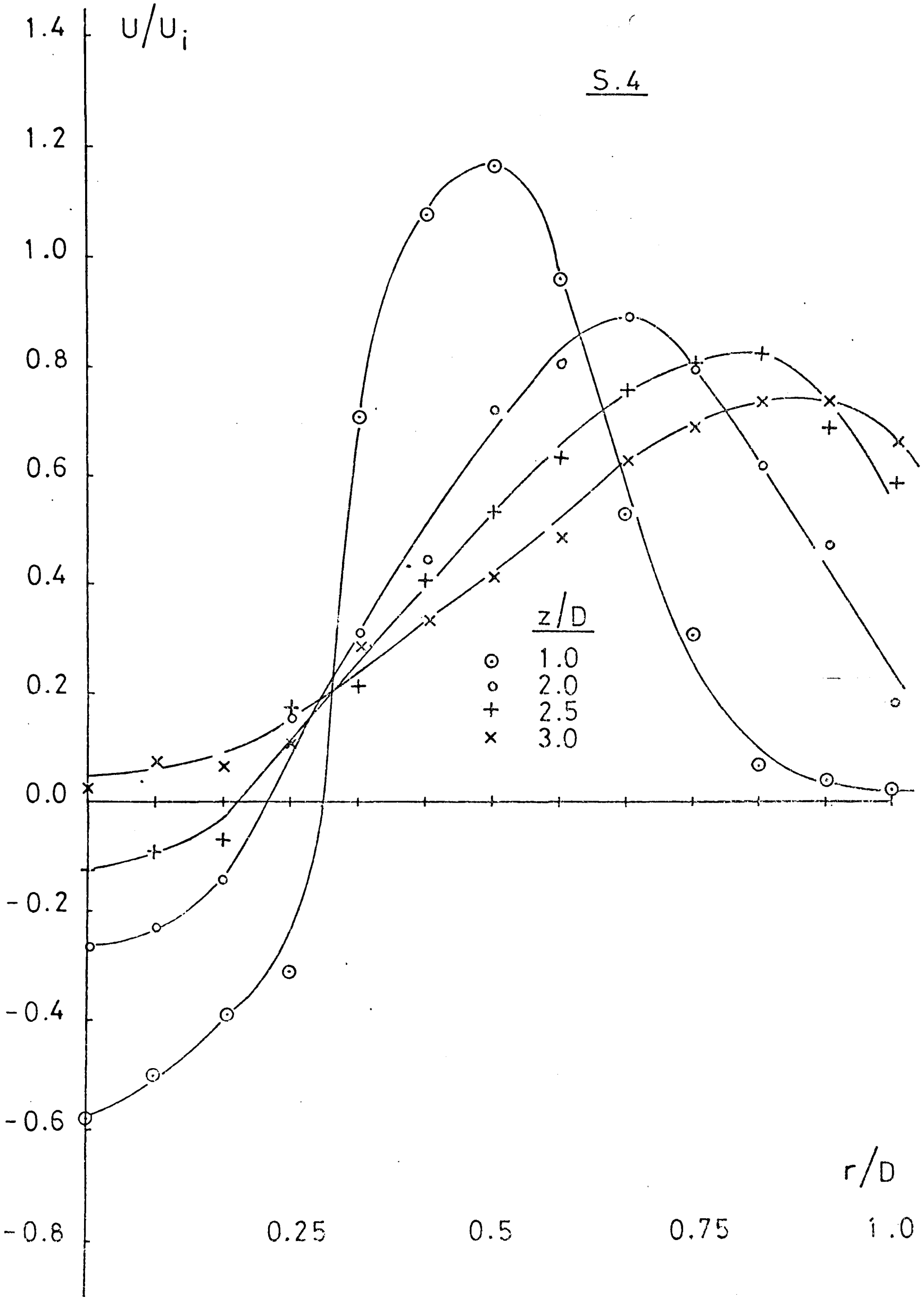

Fig.7.23.Variation of the profiles of the normalized axial velocity in the flow field of the swirler S.4

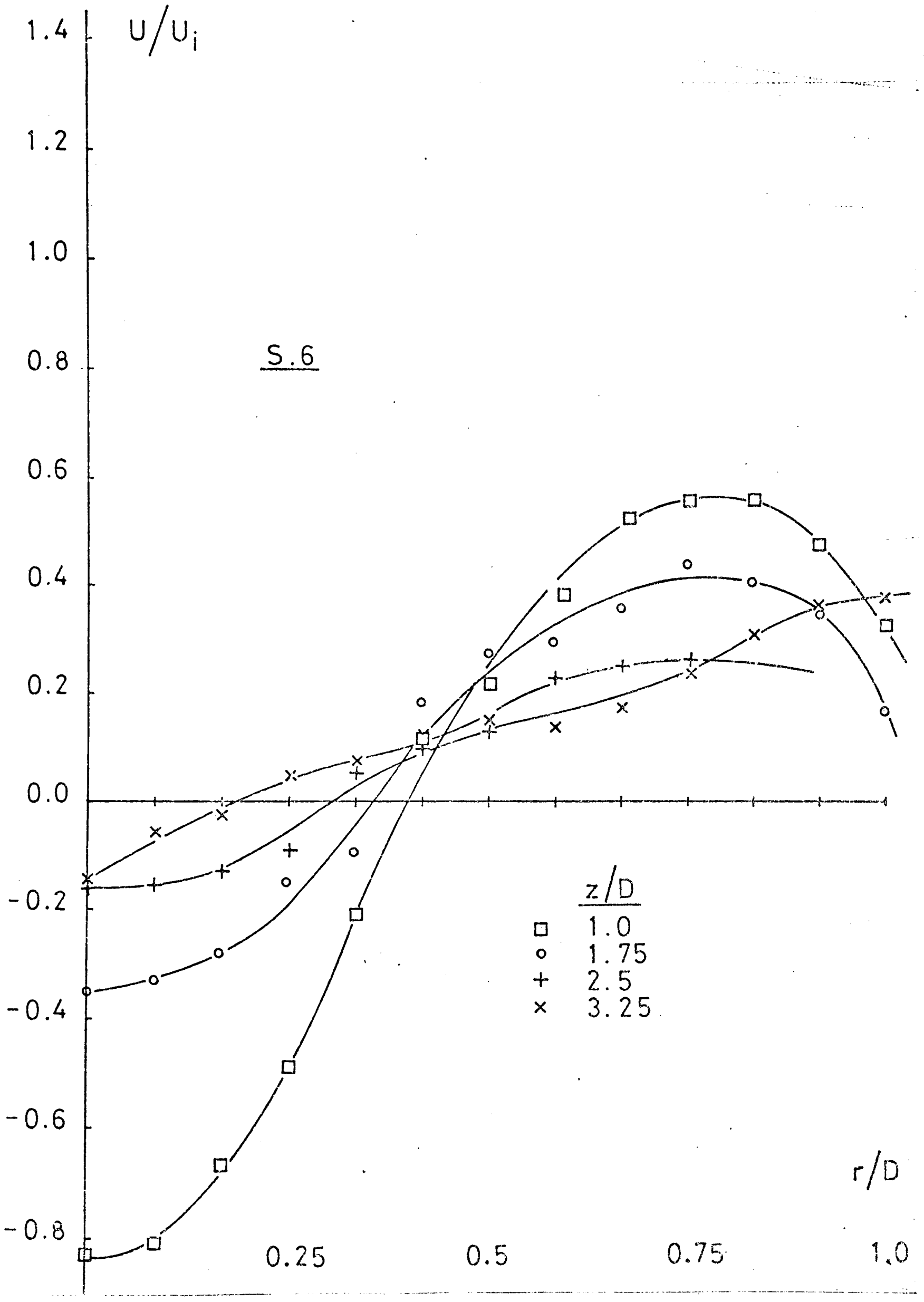

Fig.7.24.Variation of the profiles of the normalized axial velocity in the flow field of the swirler S.6

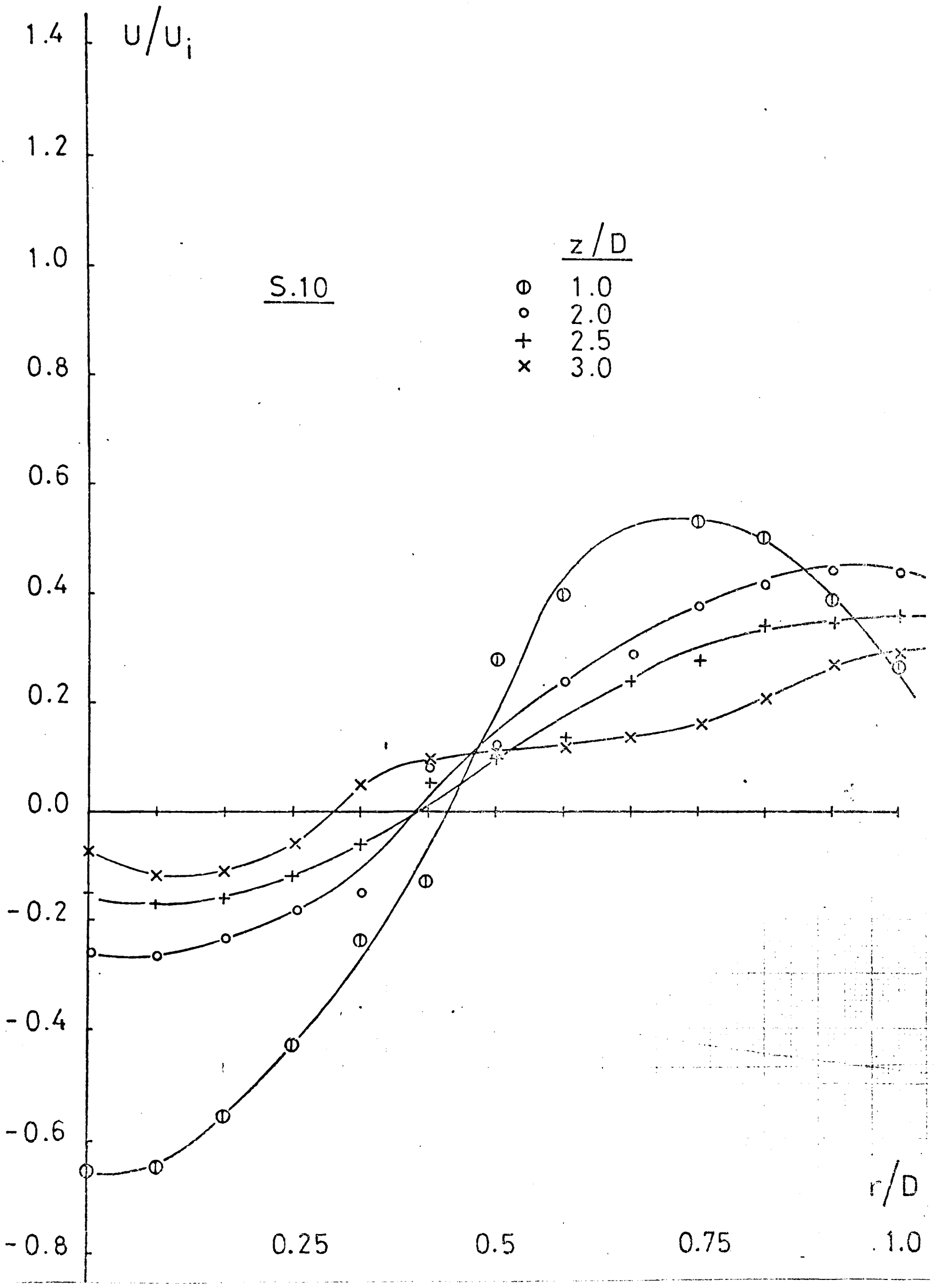

Fig.7.25.Variation of the profiles of the normalized axial velocity in the flow field of the swirler S.IO

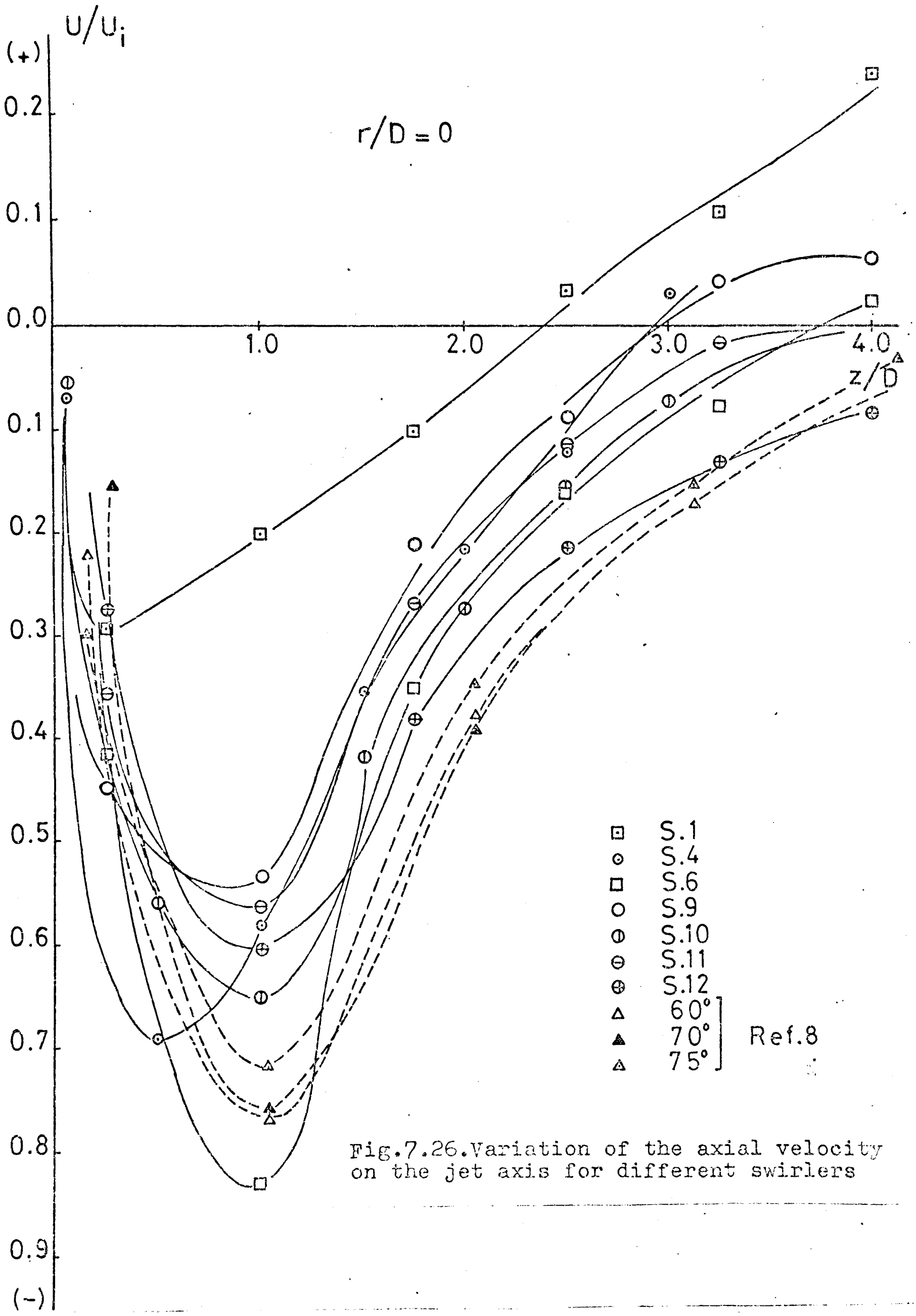

Fig.7.26.Variation of the axial velocity on the jet axis for different swirlers

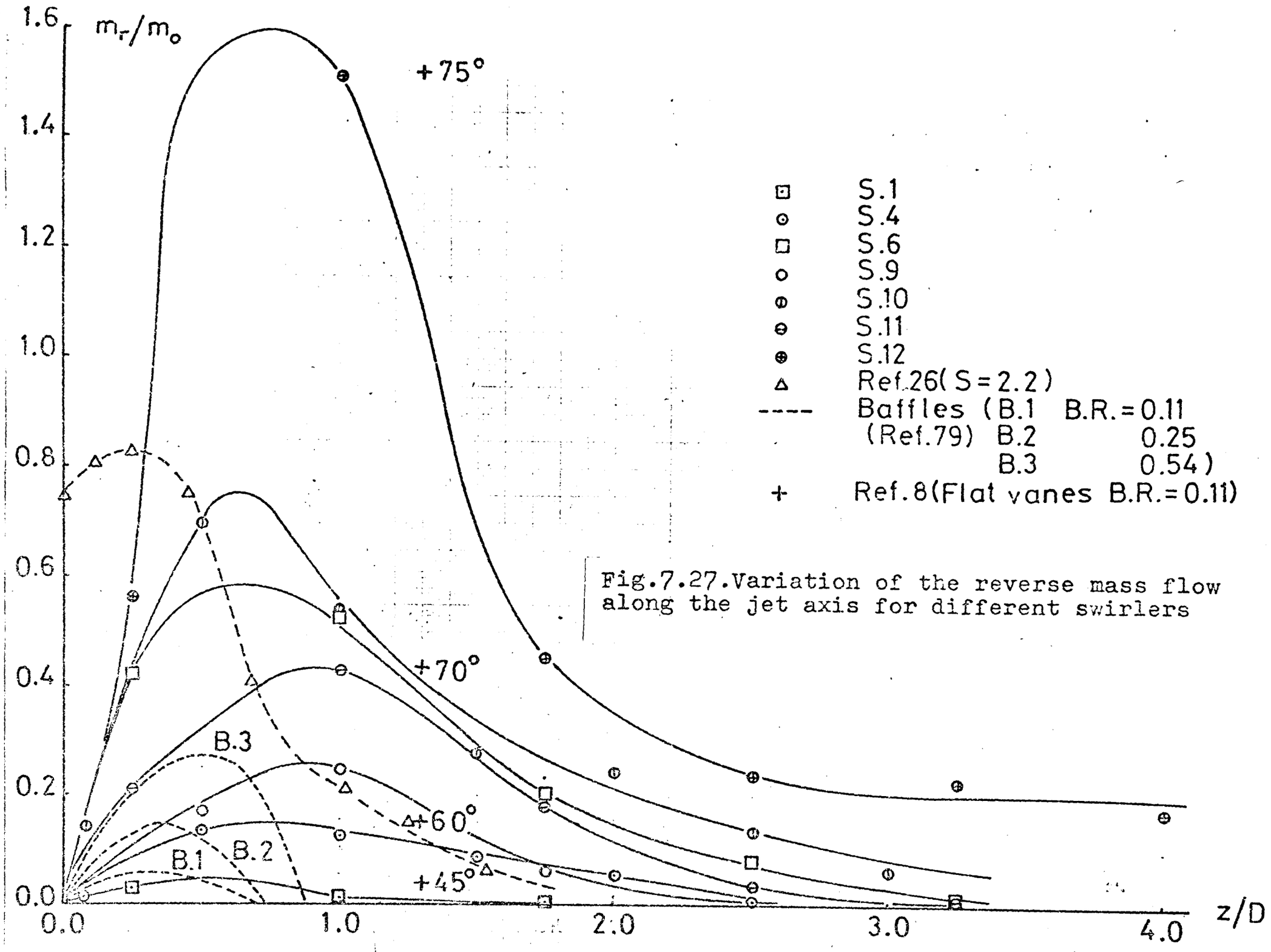

⊡ S.1
⊙ S.4
□ S.6
○ S.9
⊕ S.10
⊖ S.11
⊛ S.12
△ Ref.26(S = 2.2)
---- Baffles (B.1 B.R. = 0.11
(Ref.79) B.2 0.25
B.3 0.54)
\+ Ref.8(Flat vanes B.R. = 0.11)

Fig.7.27.Variation of the reverse mass flow along the jet axis for different swirlers

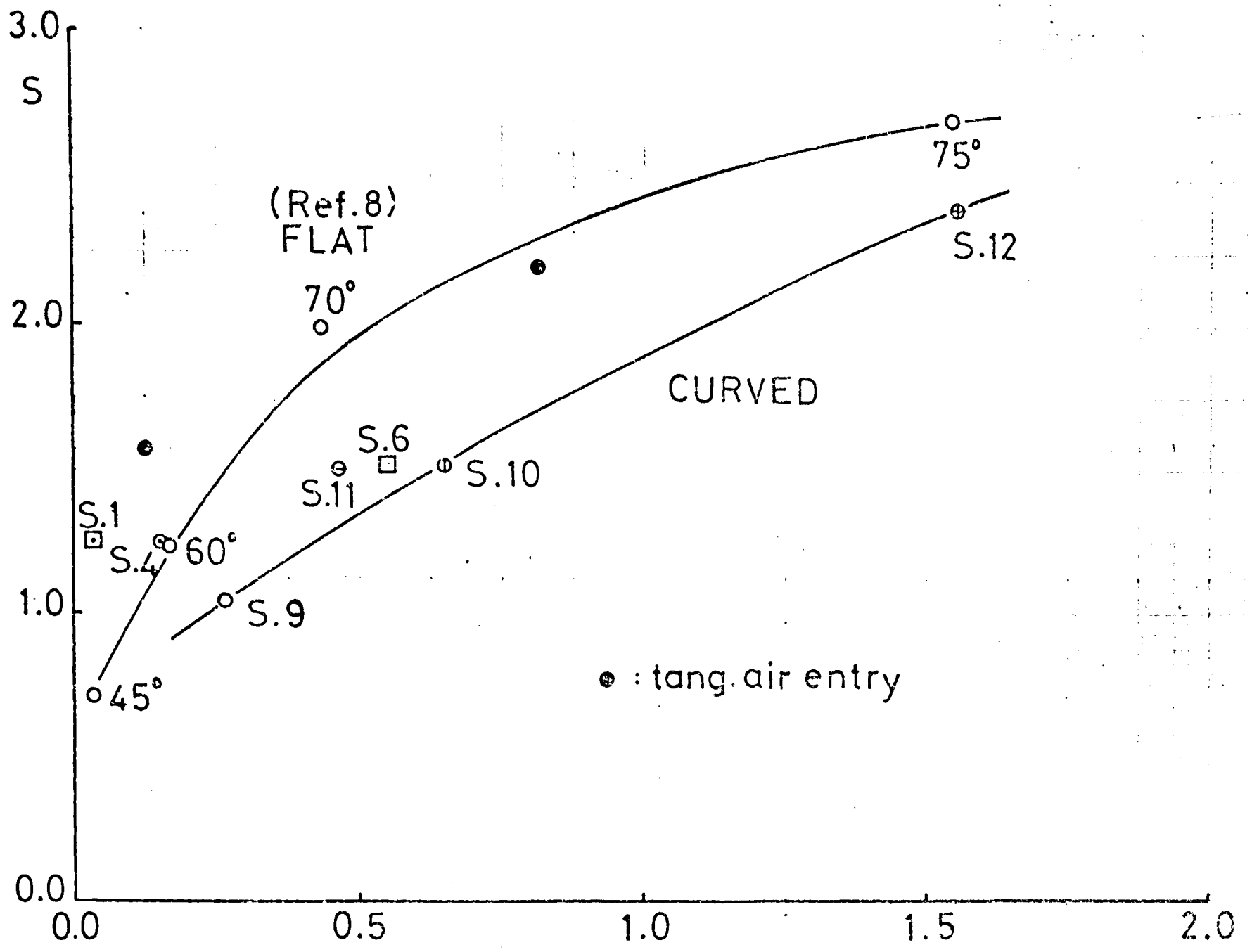

Fig.7.28.Variation of maximum reverse mass flow with swirl number

m_r/m_o

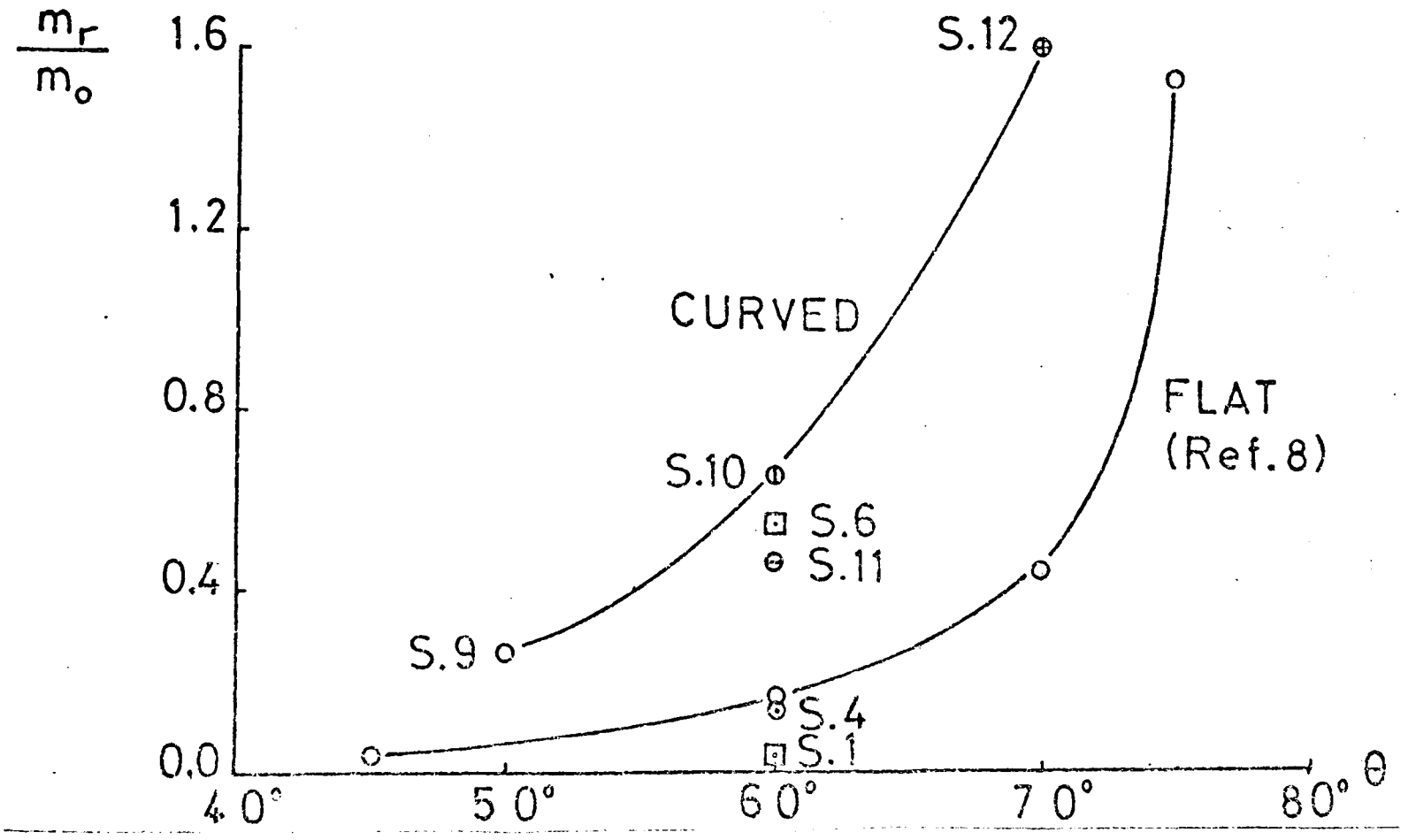

Fig.7.29.Variation of reverse mass flow with vane angle

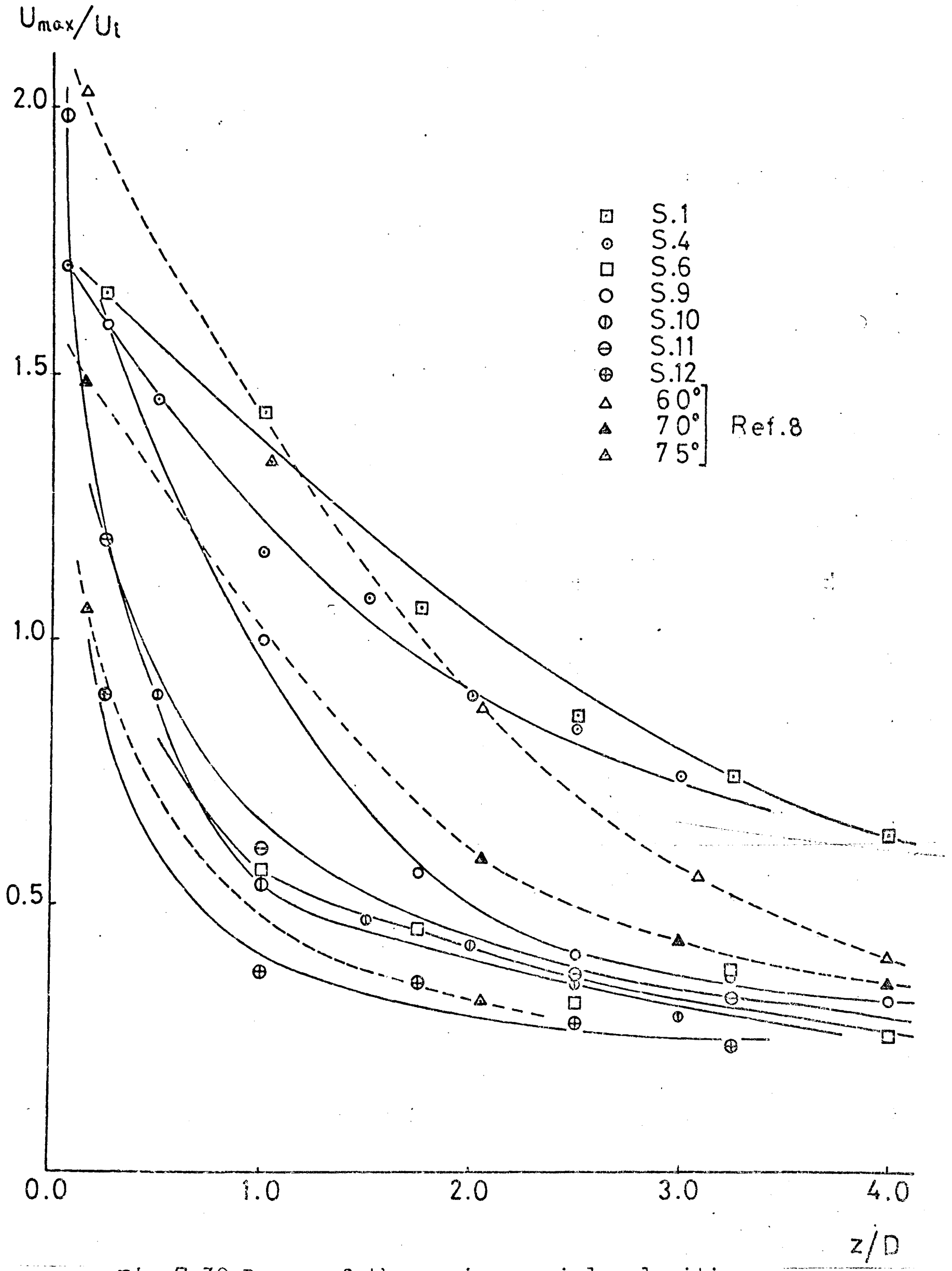

Fig.7.30.Decay of the maximum axial velocities along the jet axis for different swirlers

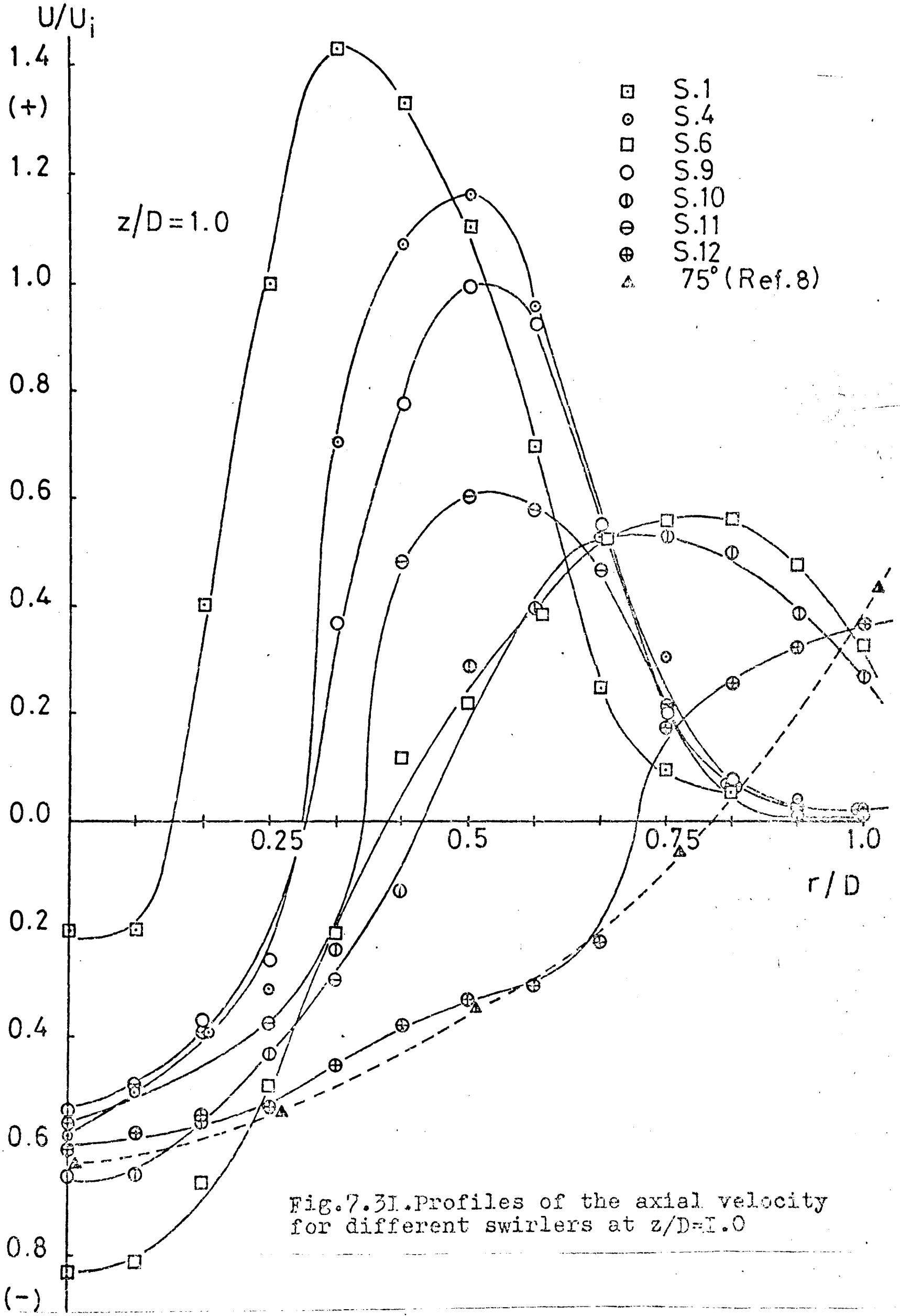

Fig.7.31.Profiles of the axial velocity for different swirlers at z/D=1.0

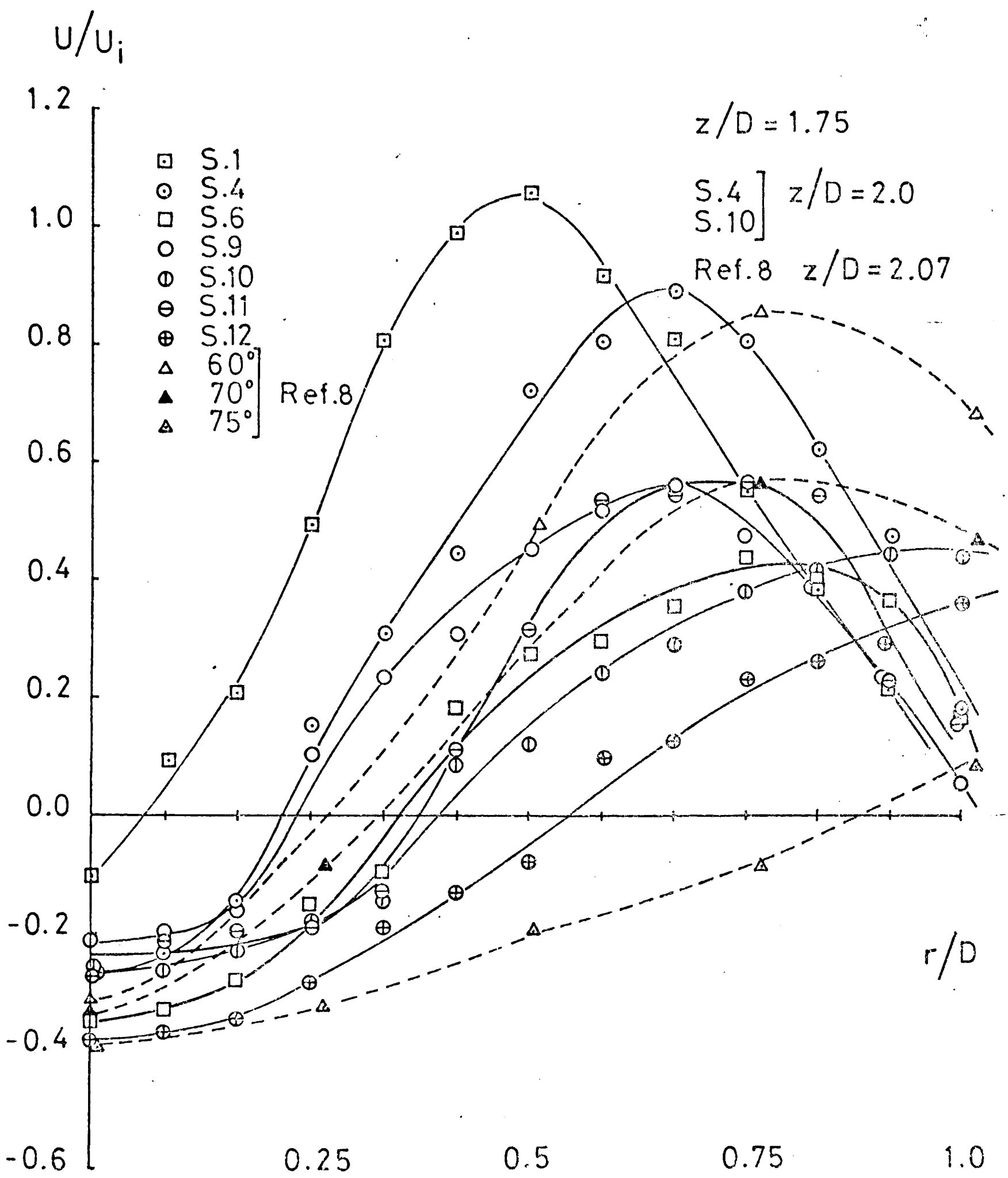

Fig.7.32.Profiles of the axial velocity for different swirlers at z/D=I.75

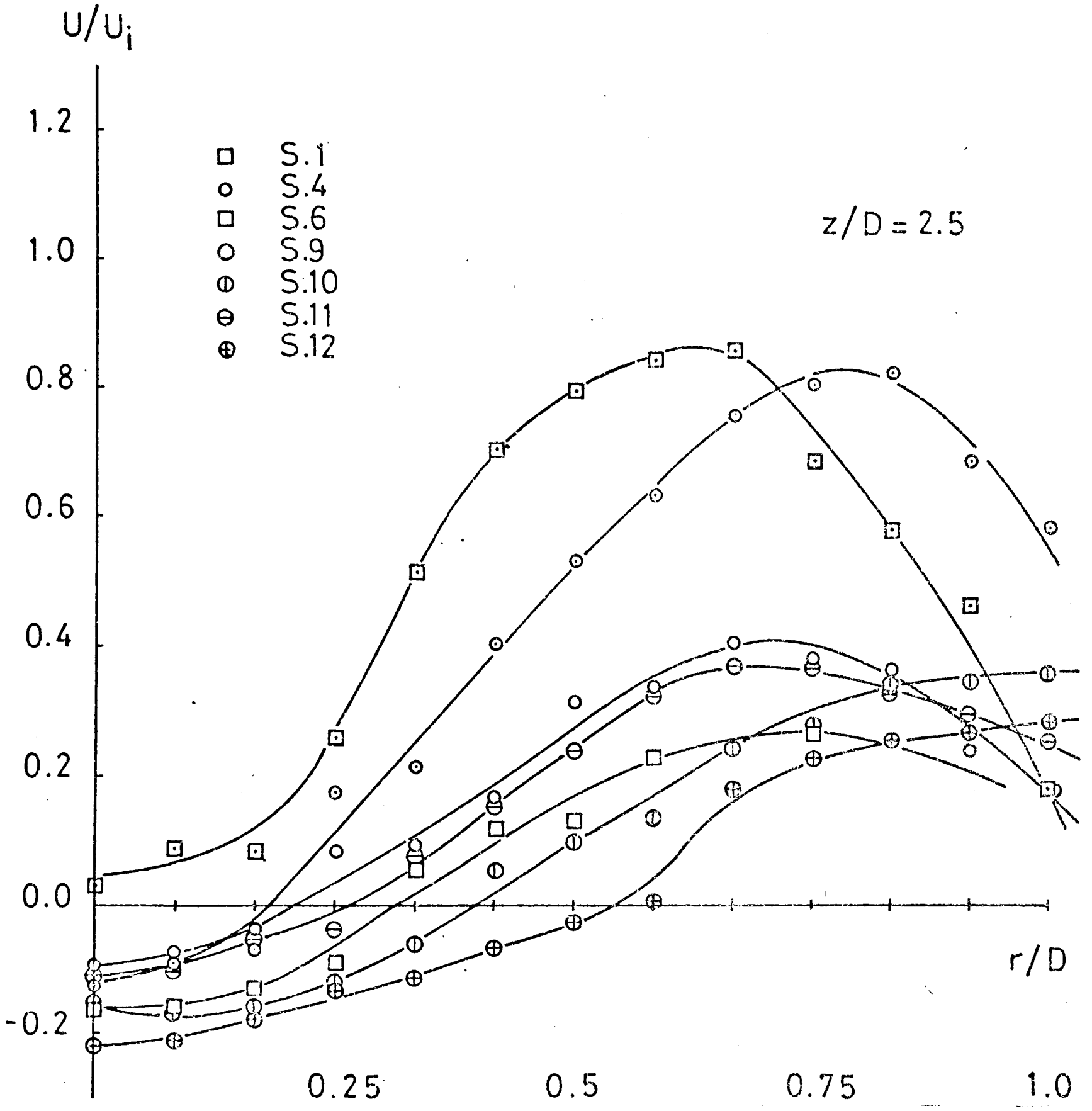

Fig.7.33.Profiles of the axial velocity for different swirlers at z/D=2.5

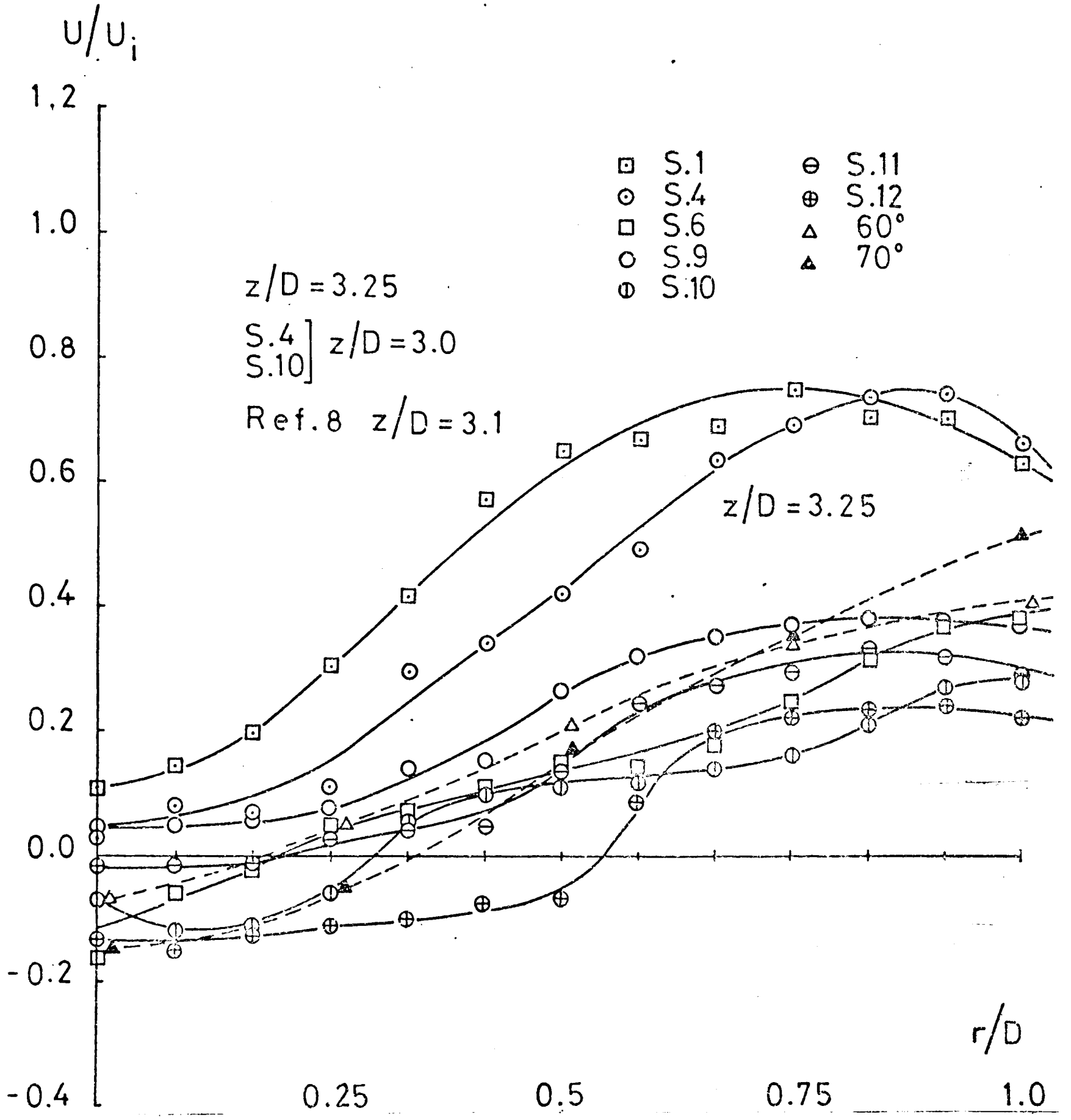

Fig.7.34.Profiles of the axial velocity for different swirlers at z/D=3.25

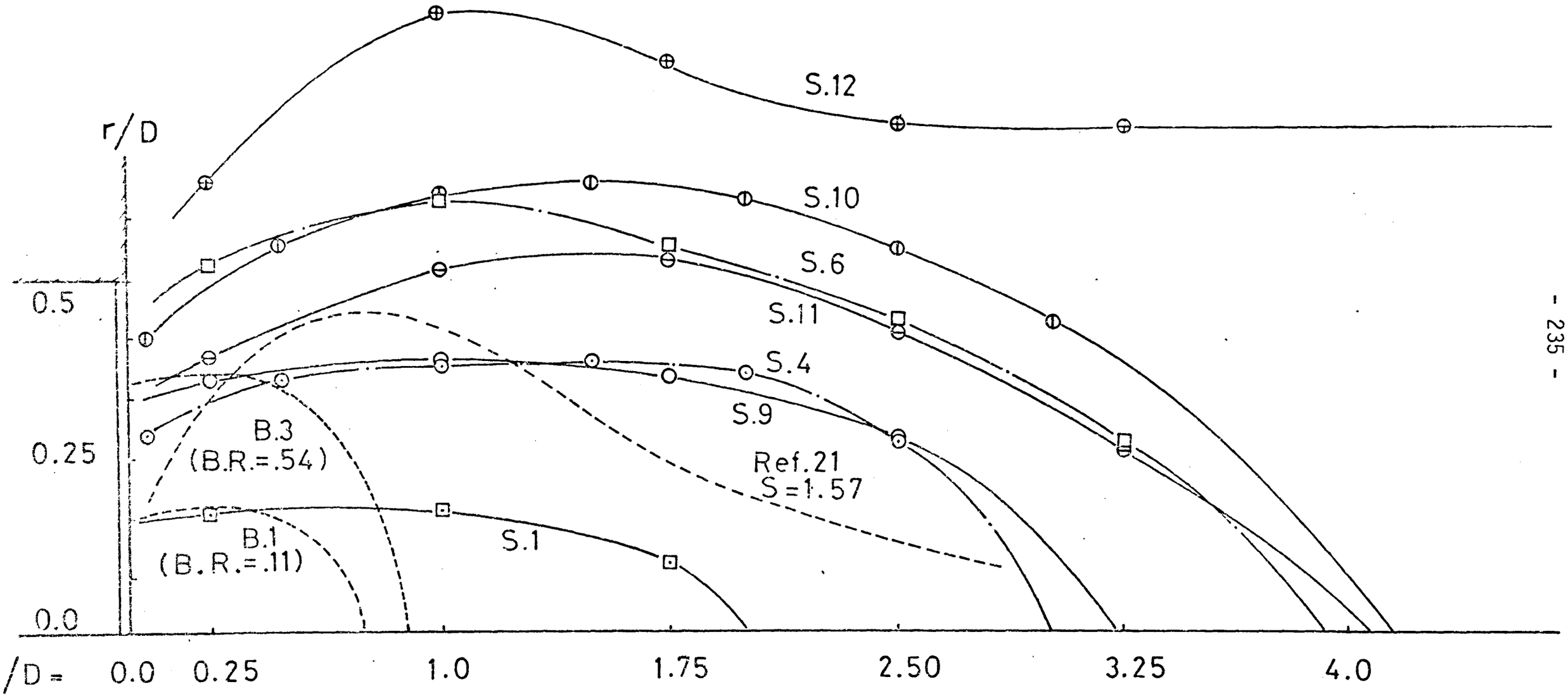

Fig.7.35.Comparison of the size of the recirculation regions for different swirlers

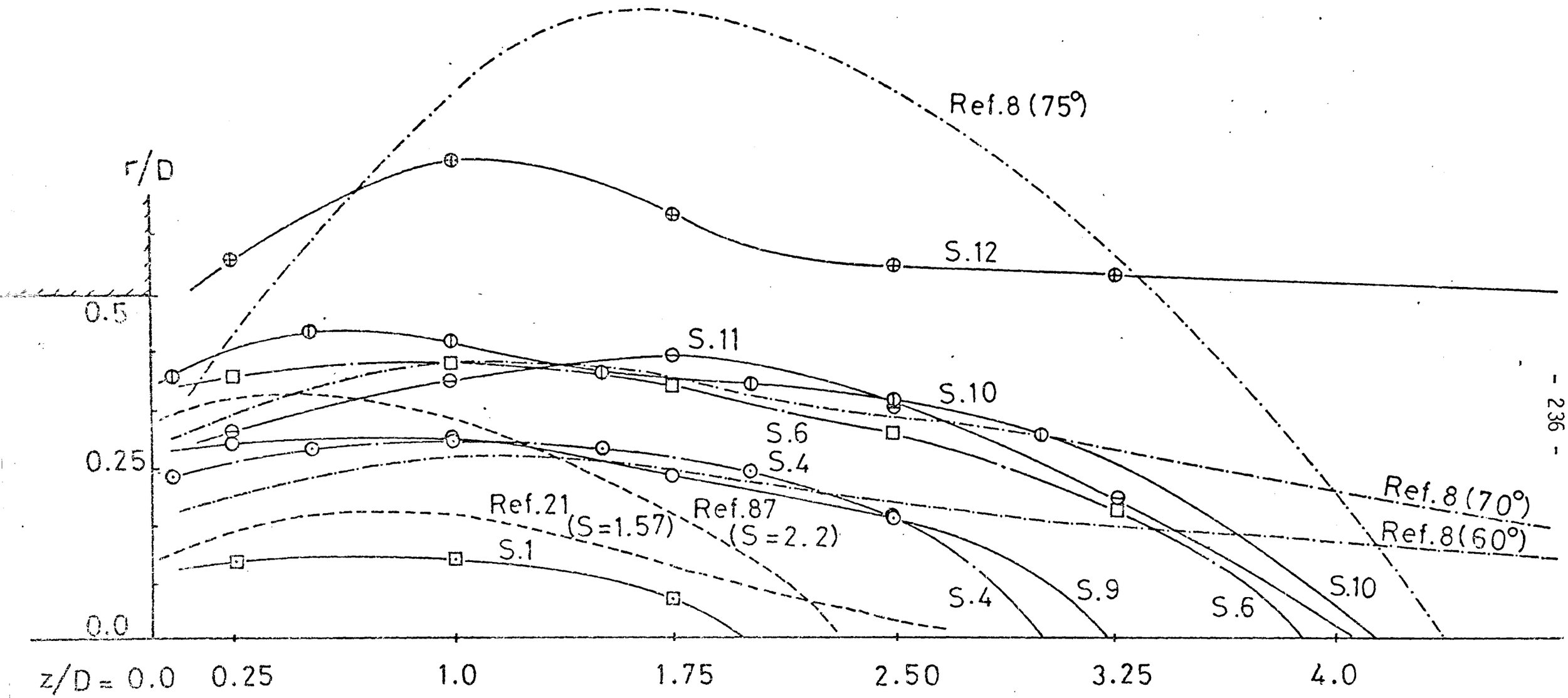

Fig.7.36.Comparison of the size of the reverse flow zones for different swirlers

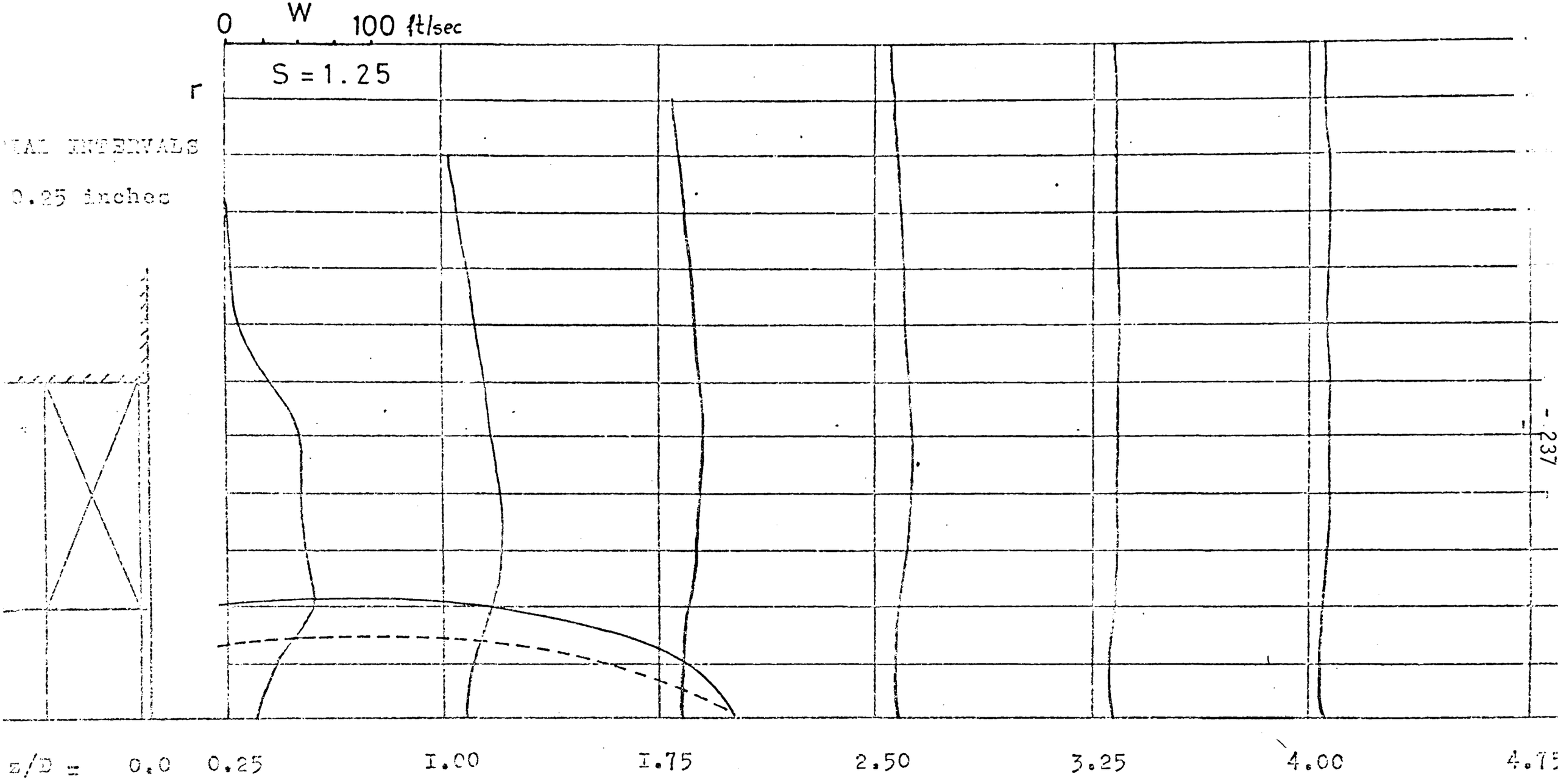

Fig.7.37.Distribution of the swirl velocity in the jet issuing from the swirler S.I

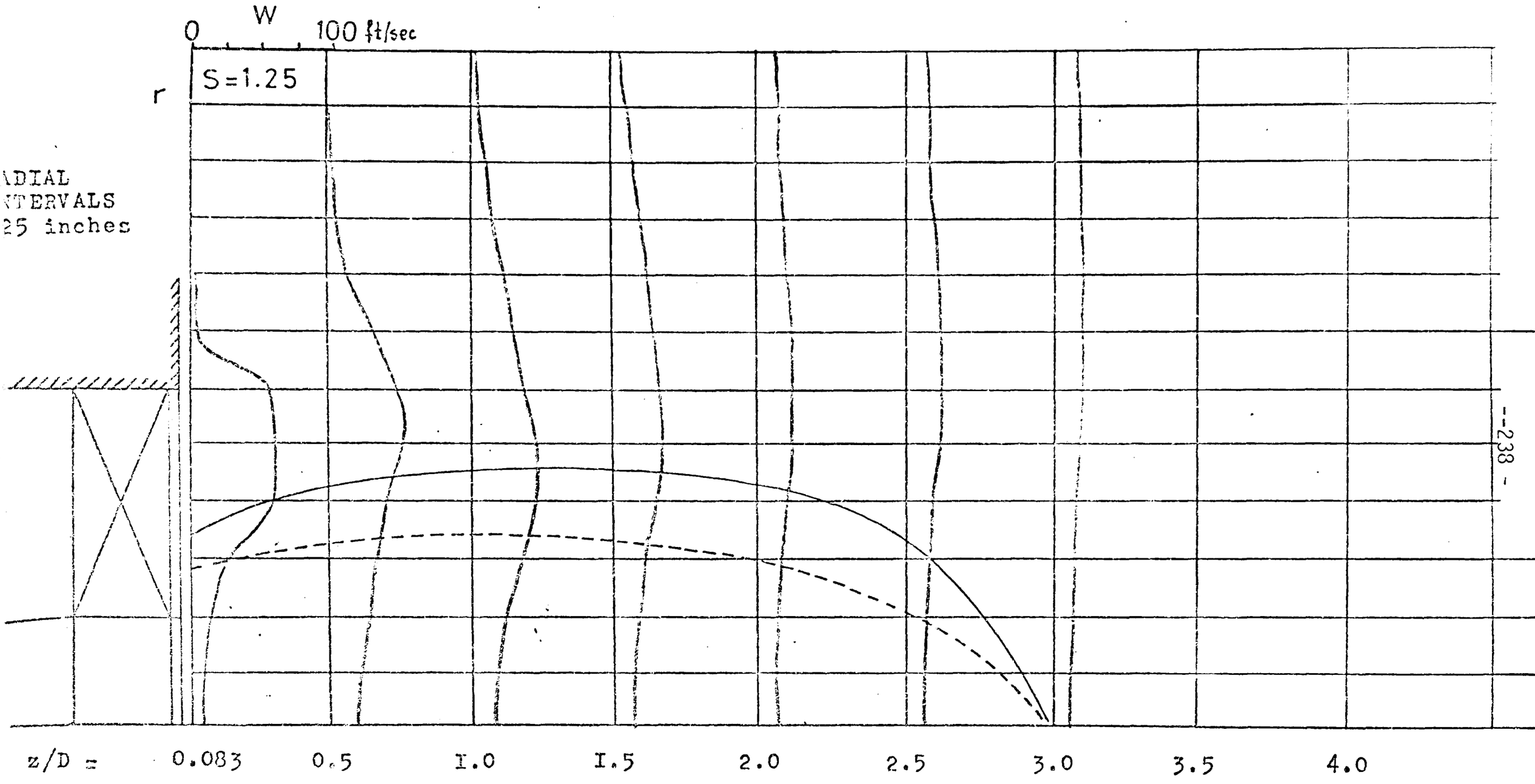

Fig.7.38.Distribution of the swirl velocity in the jet issuing from the swirler S.4

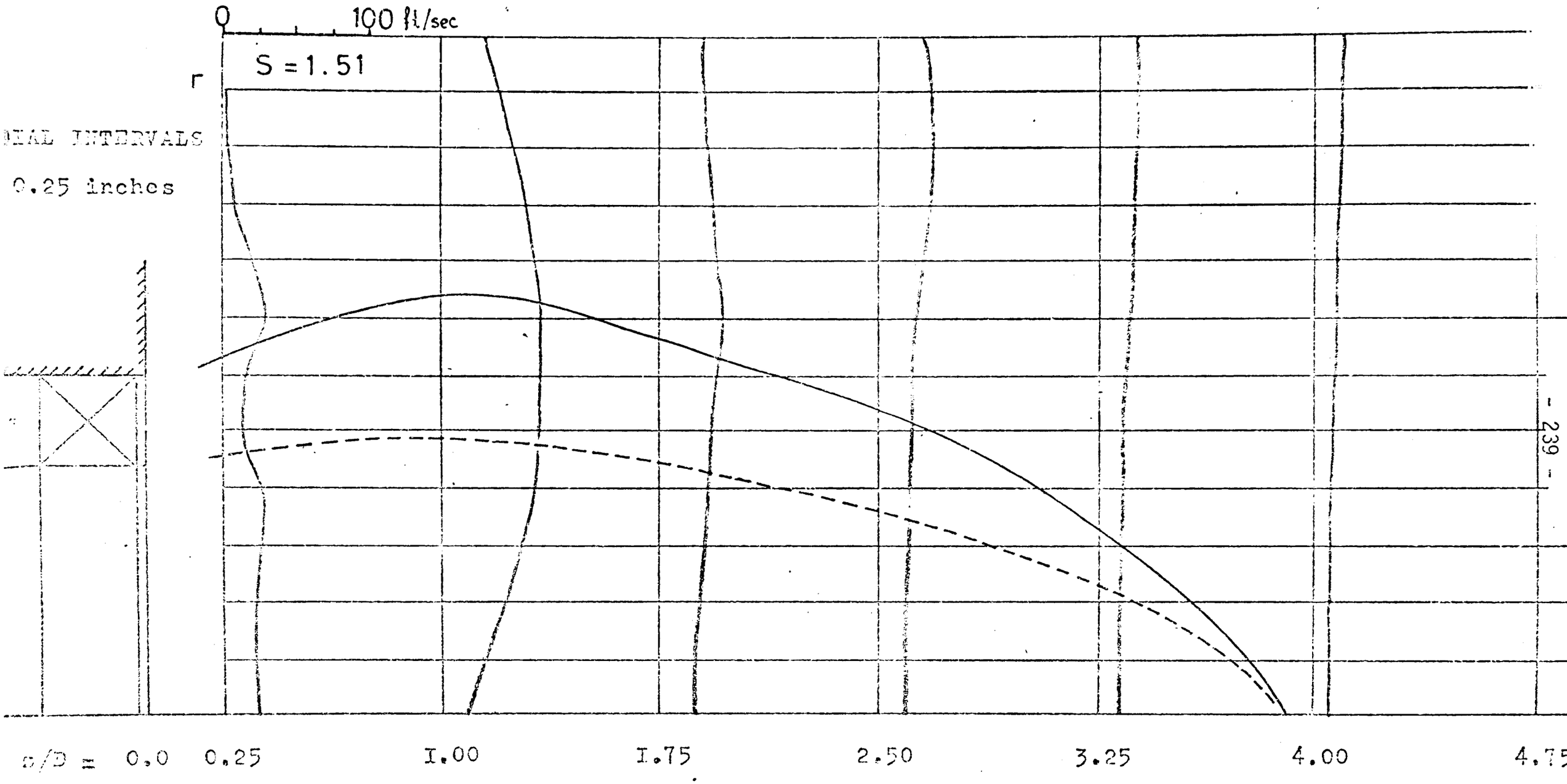

Fig.7.39.Distribution of the swirl velocity in the jet issuing from the swirler S.6

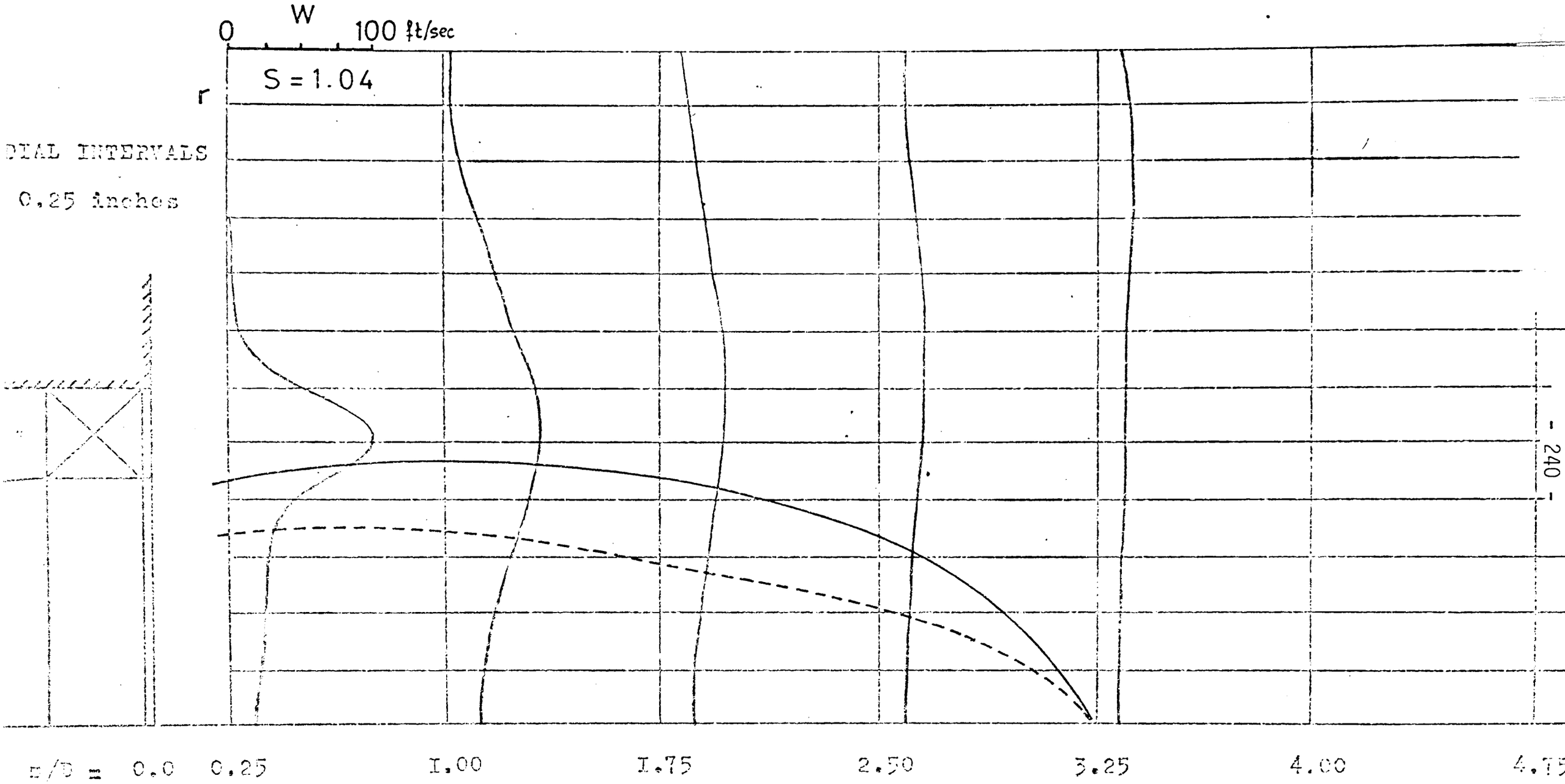

Fig.7.40.Distribution of the swirl velocity in the jet issuing from the swirler S.9

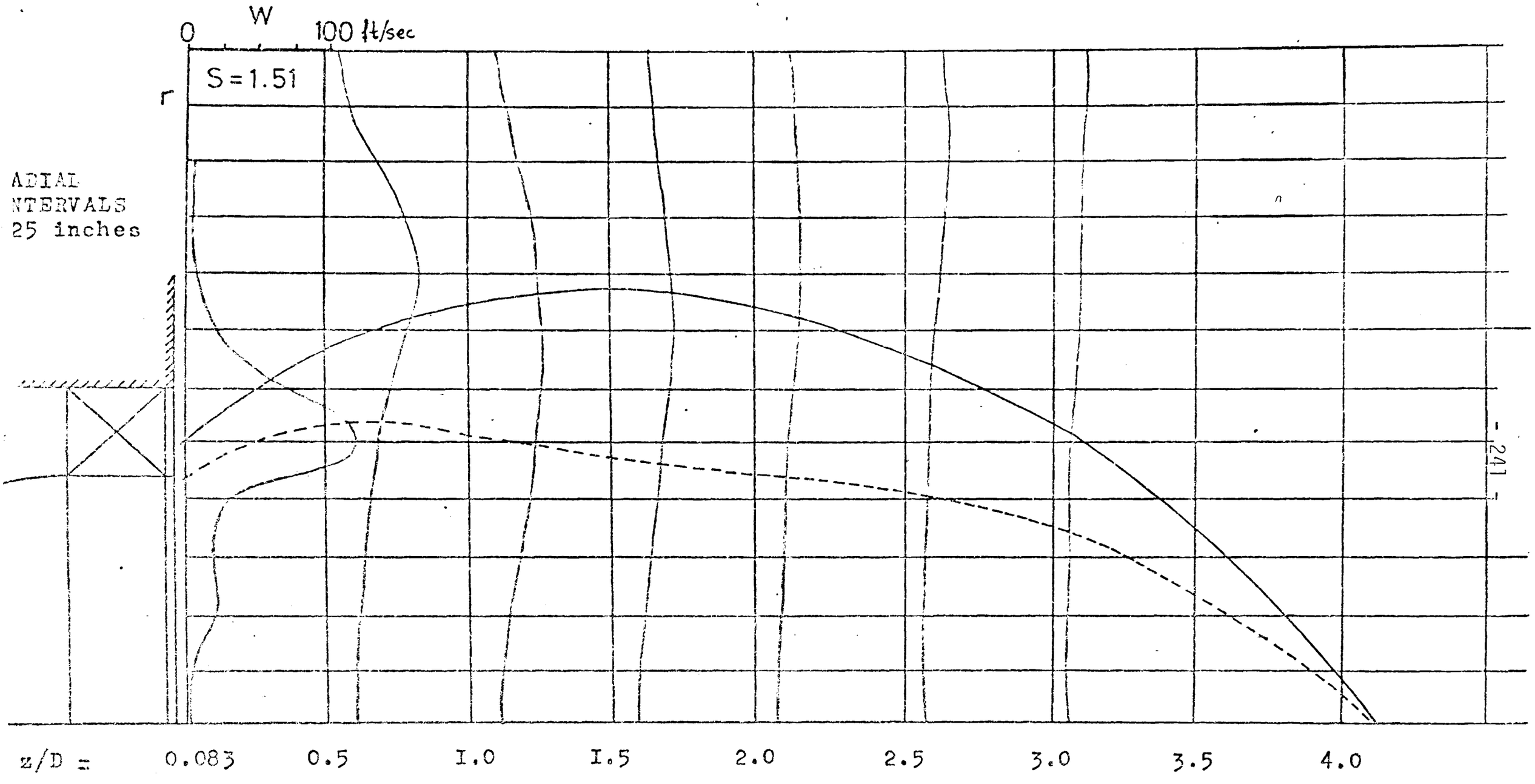

Fig.7.4I.Distribution of the swirl velocity in the jet issuing from the swirler S.IO

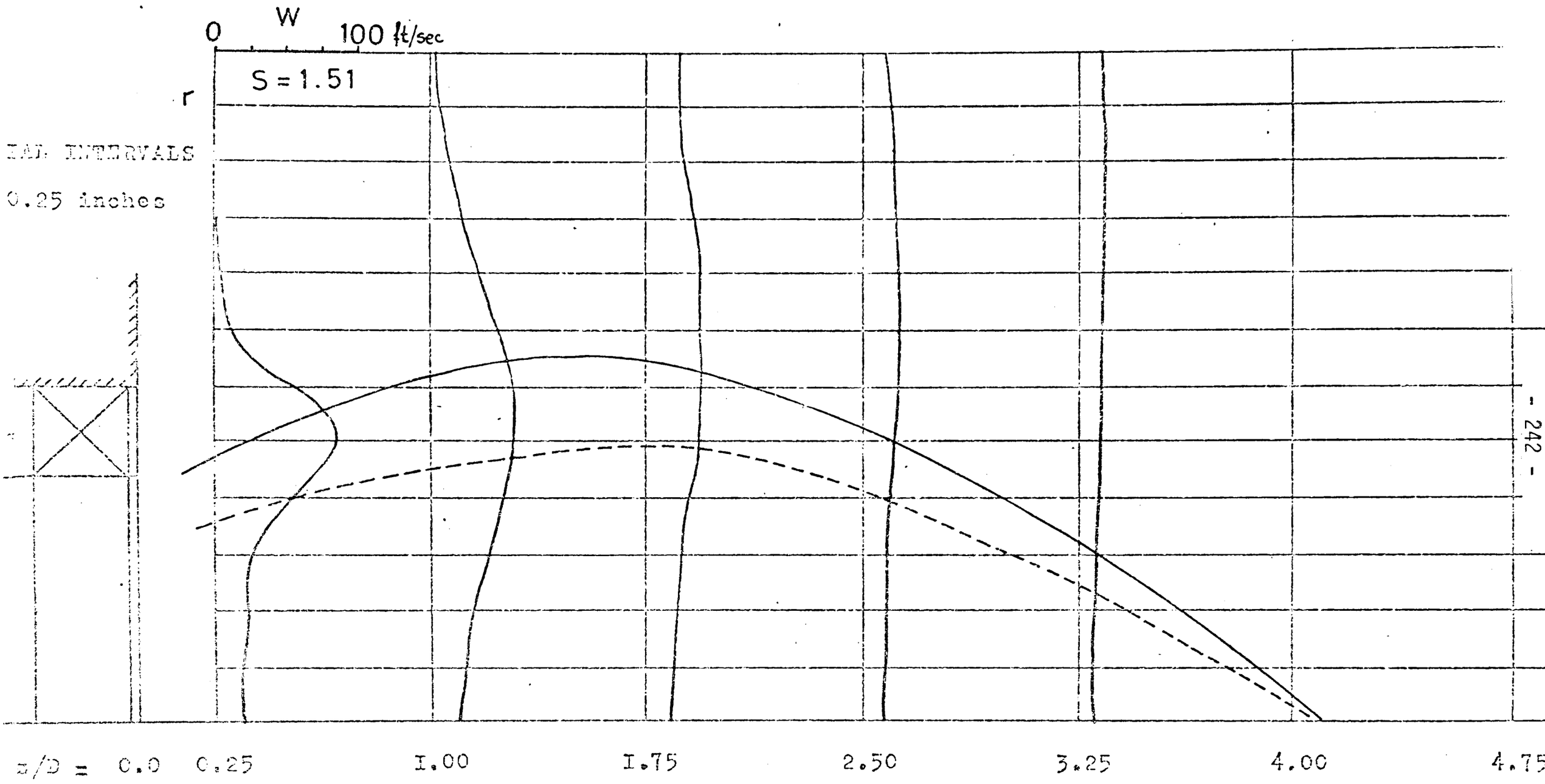

Fig.7.42.Distribution of the swirl velocity in the jet issuing from the swirler S.II

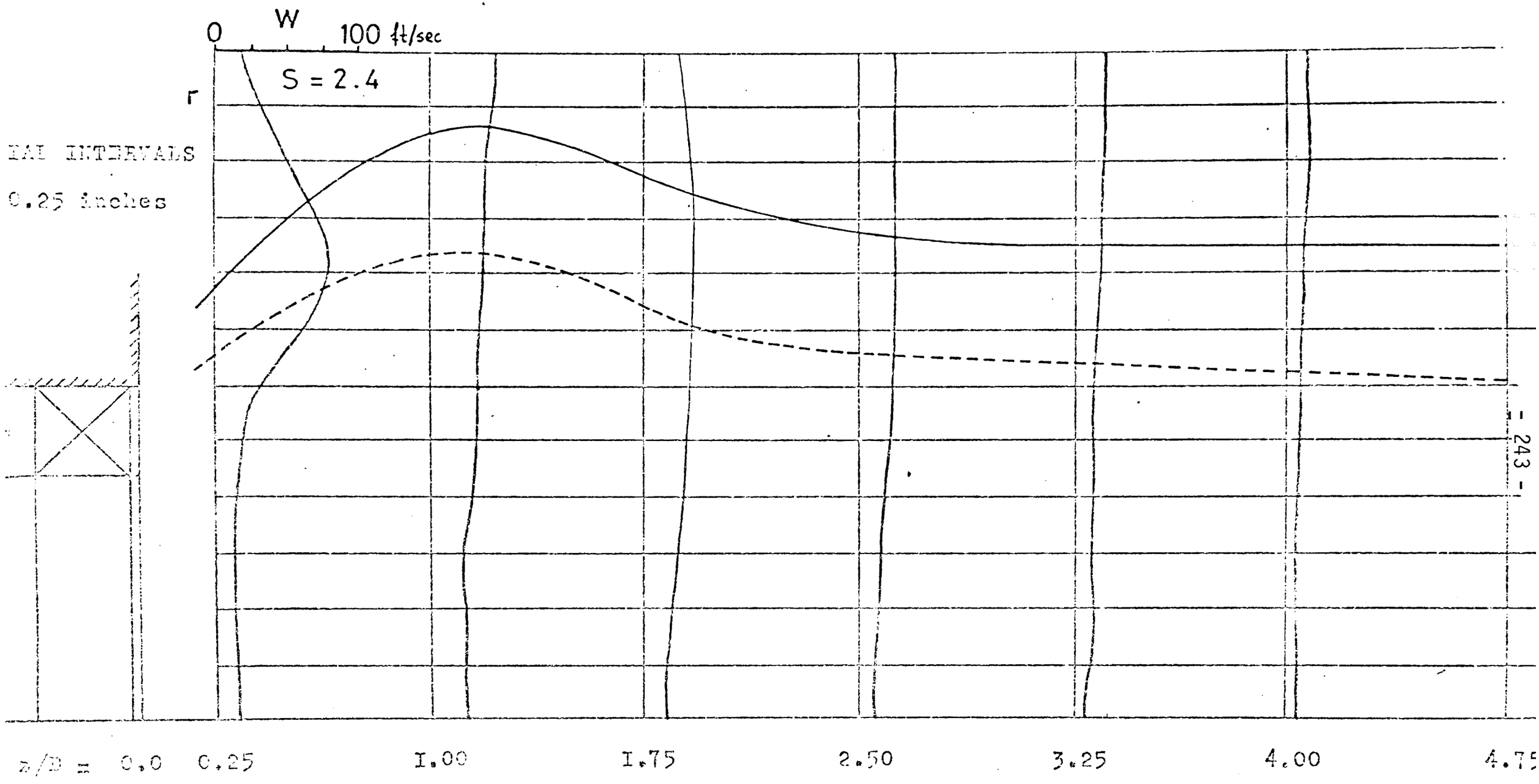

Fig.7.43.Distribution of the swirl velocity in the jet issuing from the swirler S.I2

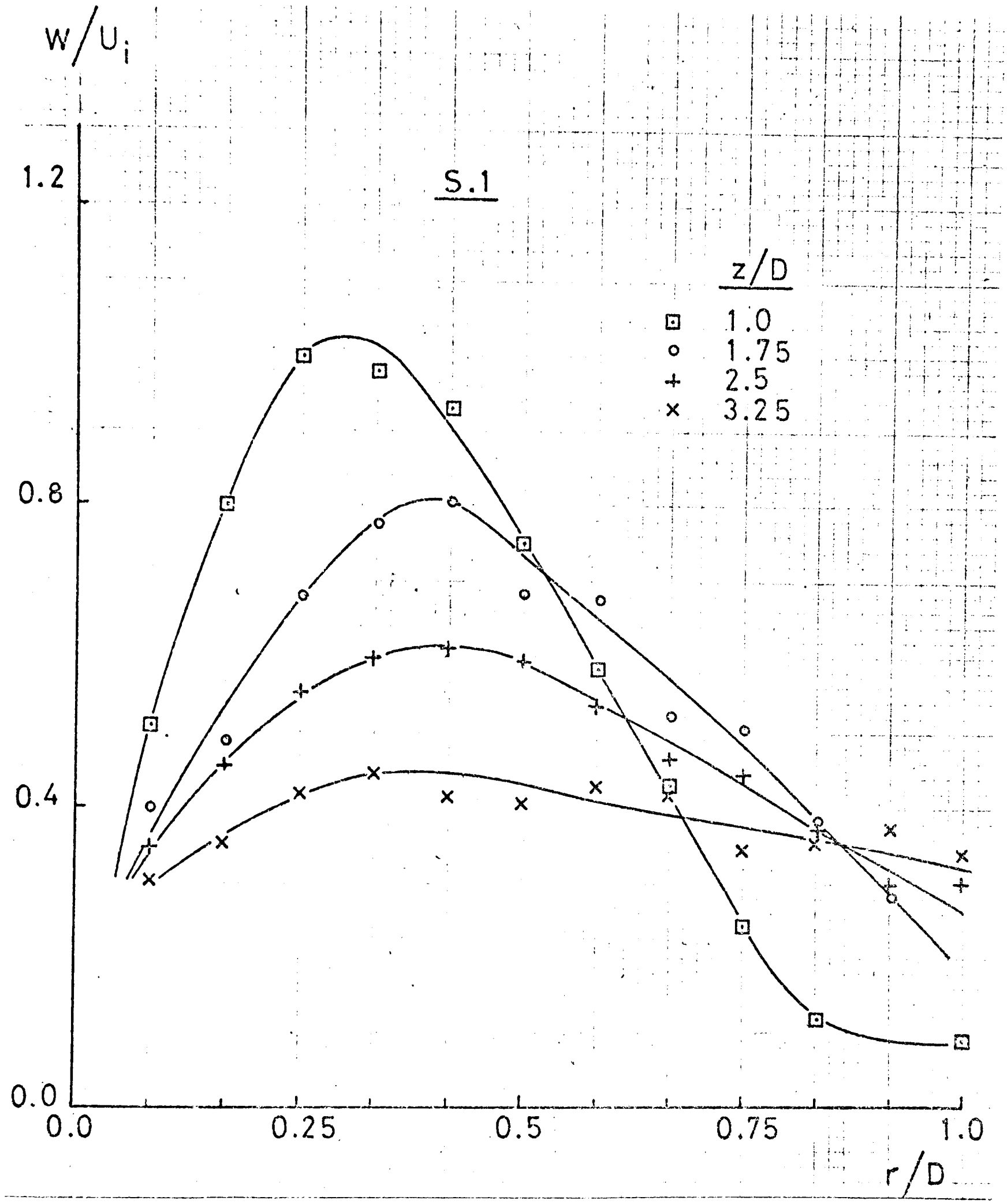

Fig.7.44.Variation of the profiles of the normalized swirl velocity in the flow field of the swirler S.I

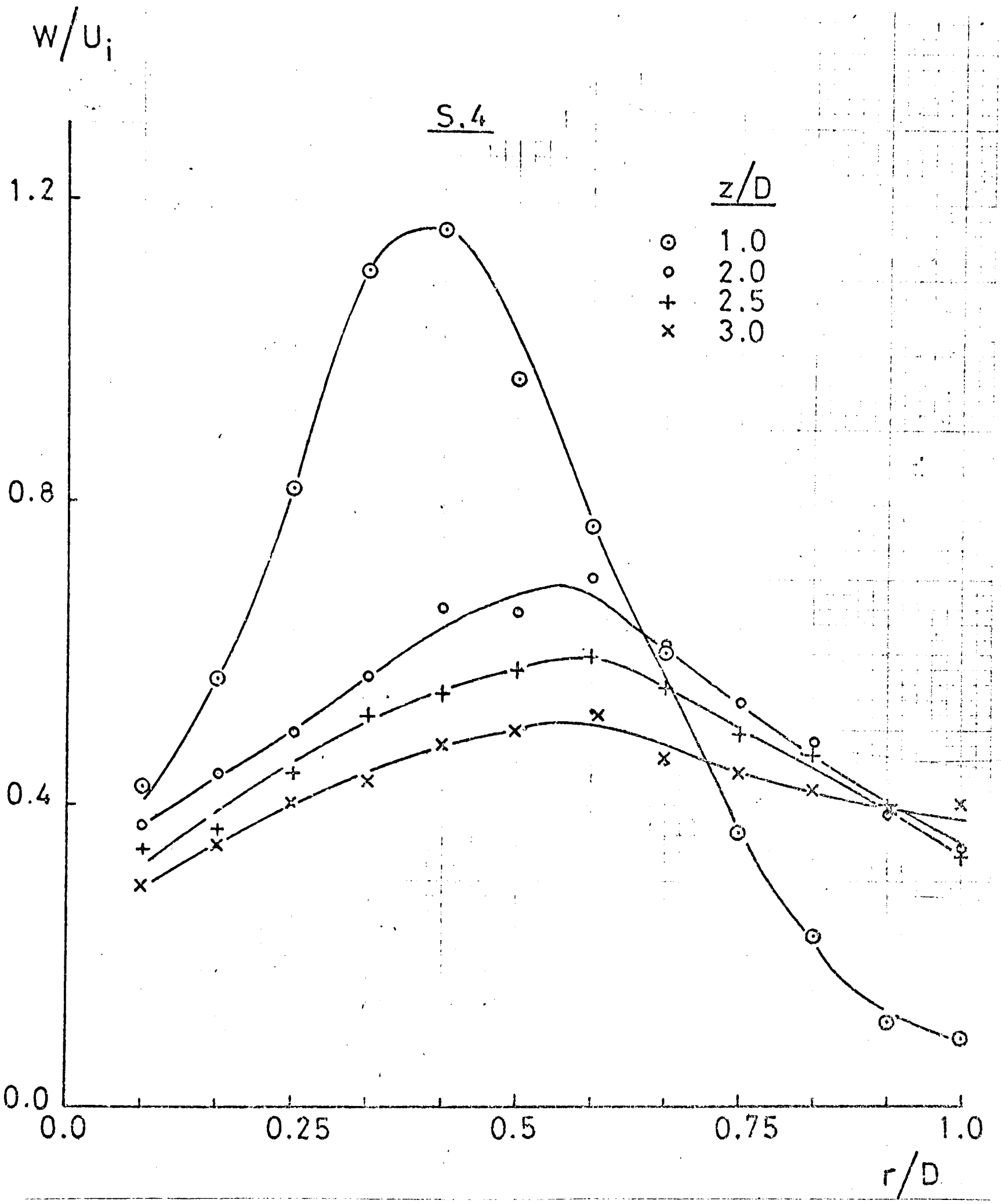

Fig.7.45.Variation of the profiles of the normalized swirl velocity in the flow field of the swirler S.4

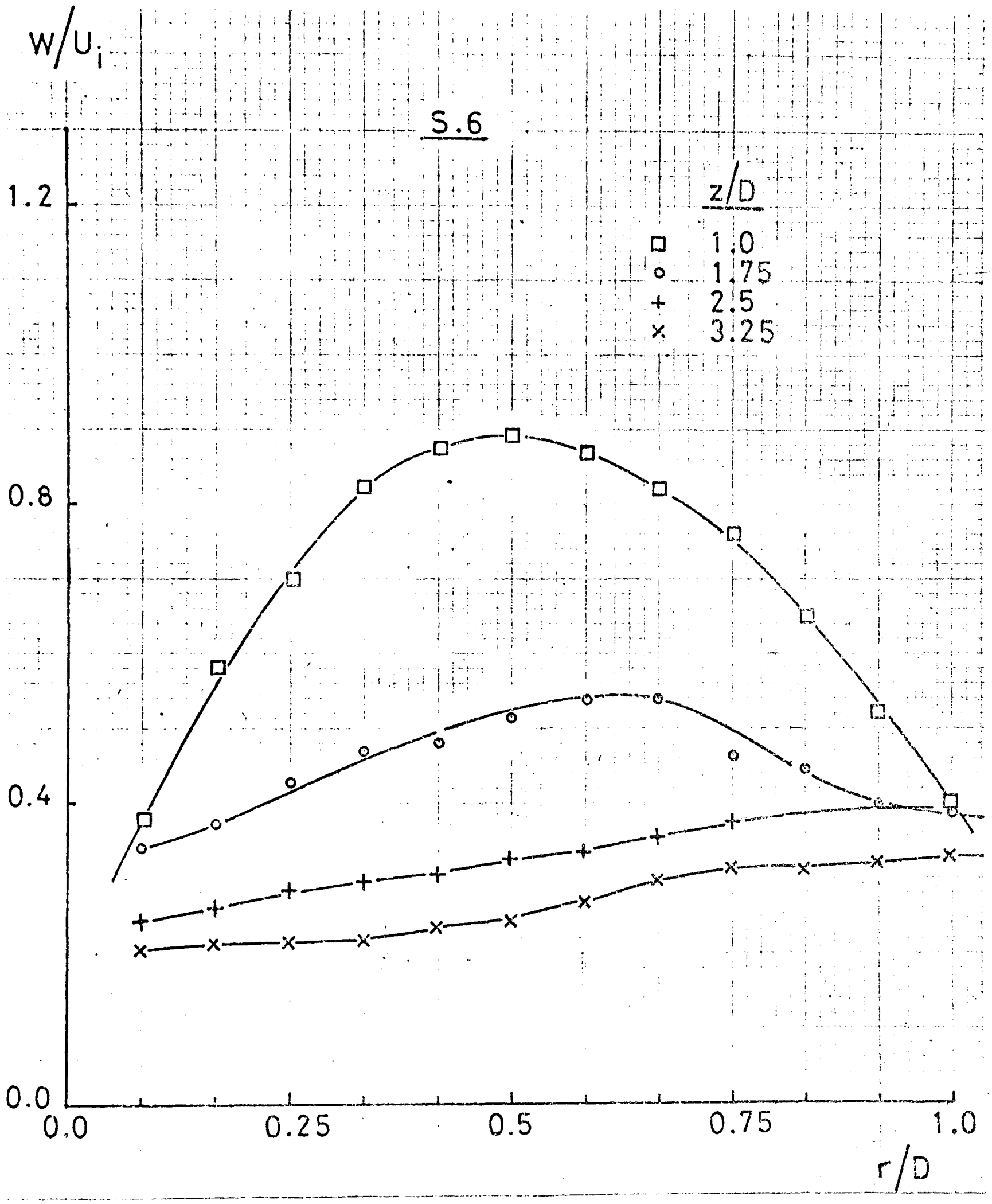

Fig.7.46. Variation of the profiles of the normalized swirl velocity in the flow field of the swirler S.6

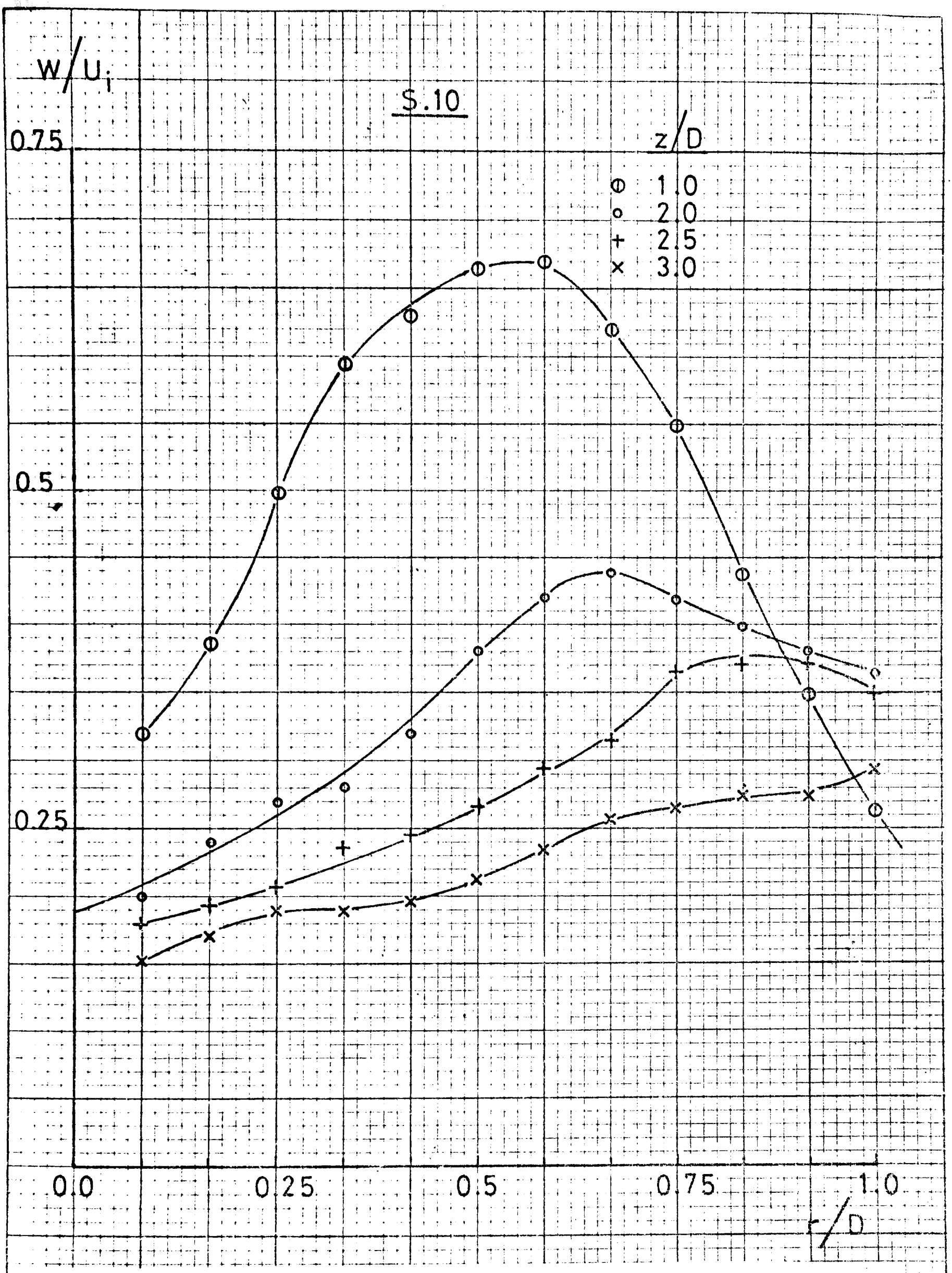

Fig.7.47.Variation of the profiles of the normalized swirl velocity in the flow field of the swirler S.IO

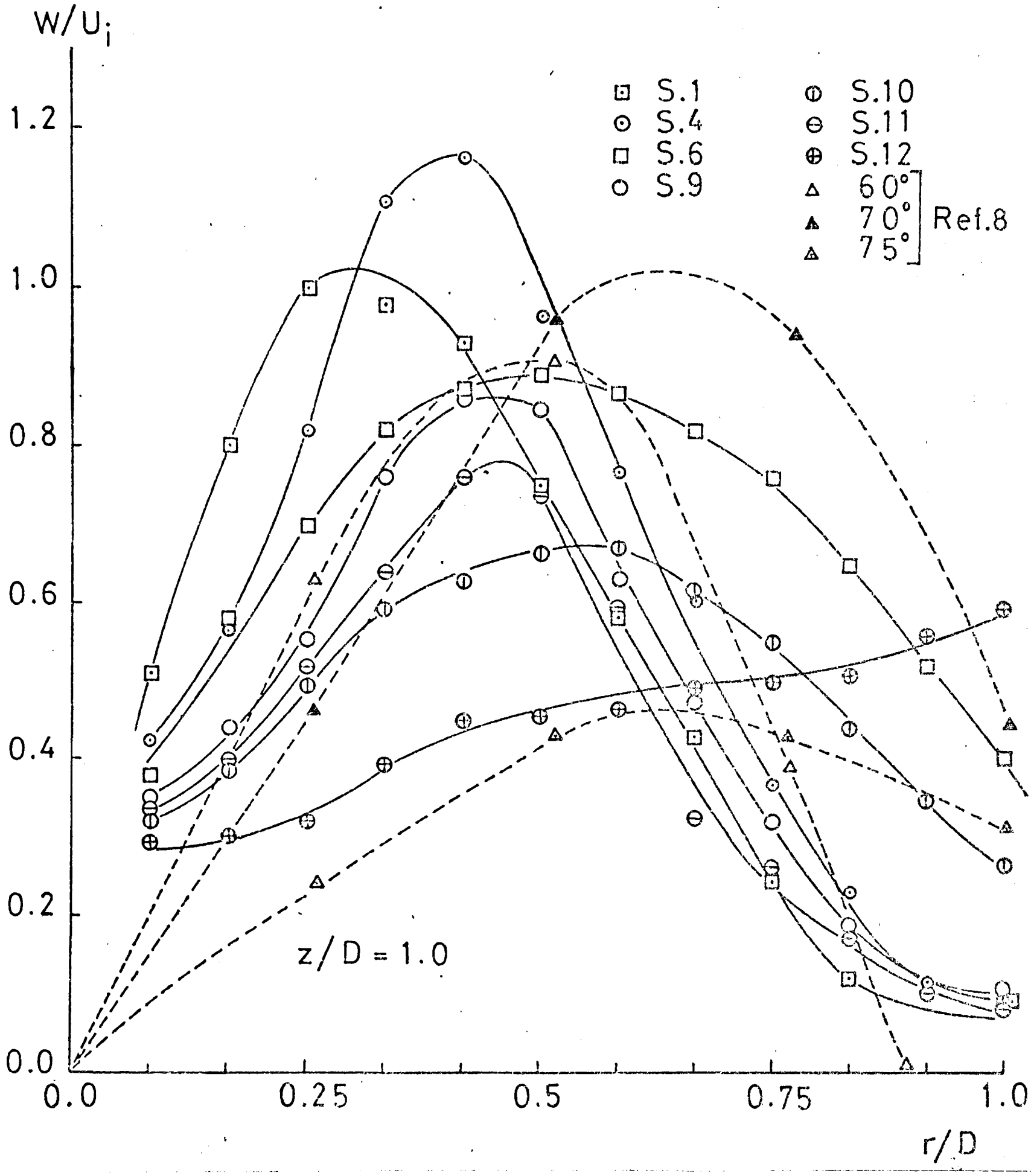

Fig.7.48.Profiles of the swirl velocity for different swirlers at z/D=I.0

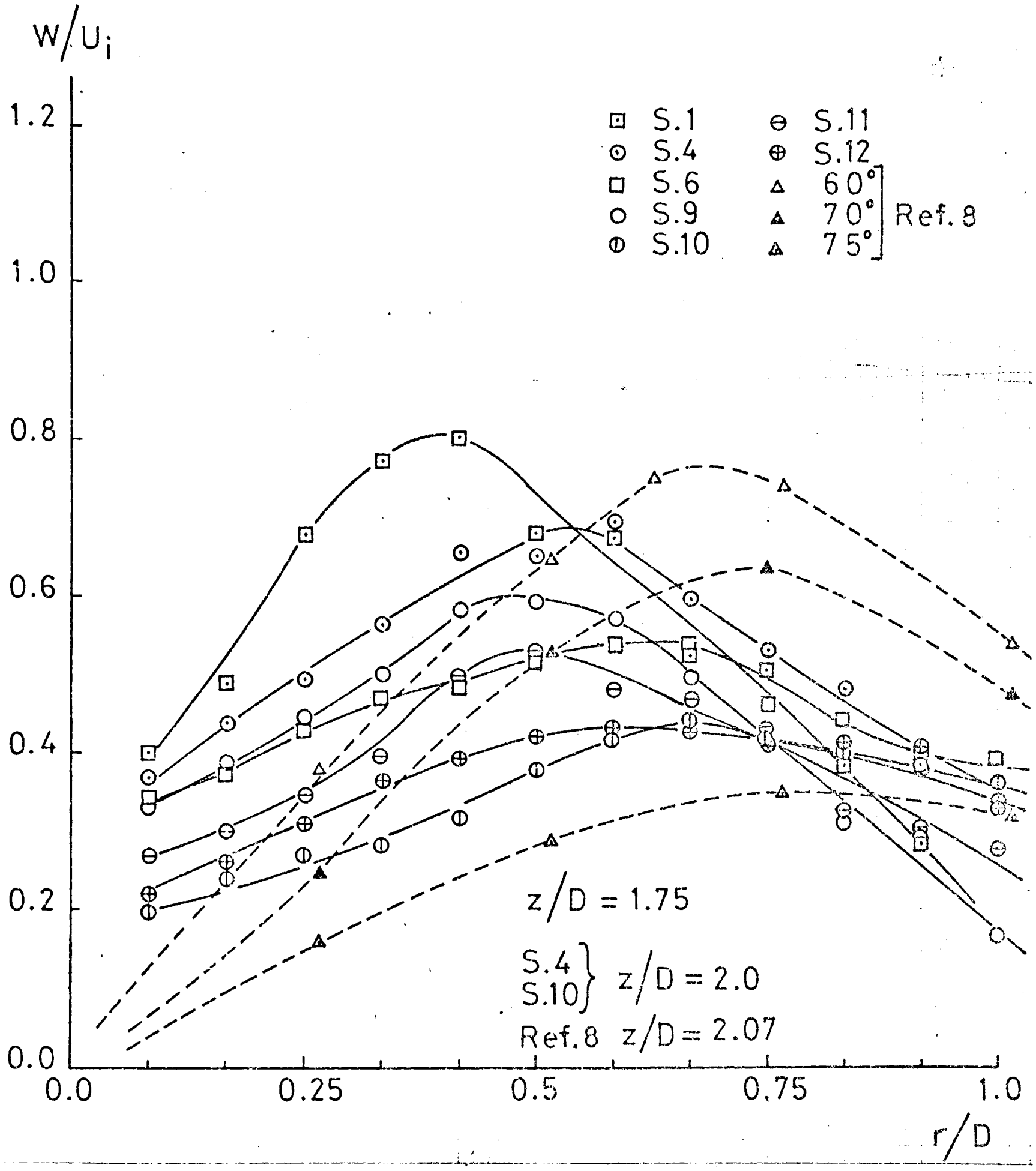

Fig.7.49.Profiles of the swirl velocity for different swirlers at z/D=I.75

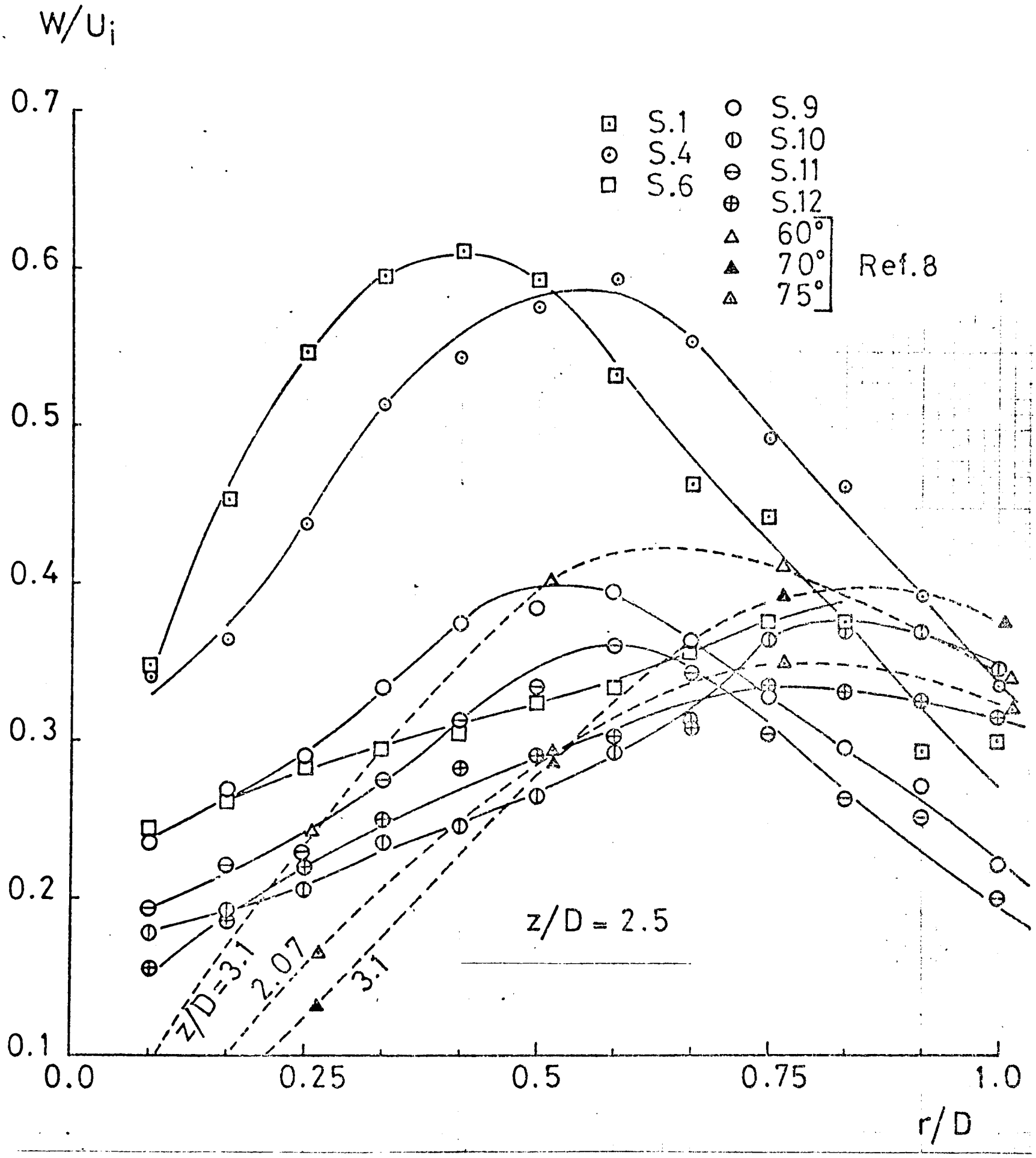

Fig.7.50.Profiles of the swirl velocity for different swirlers at z/D=2.5

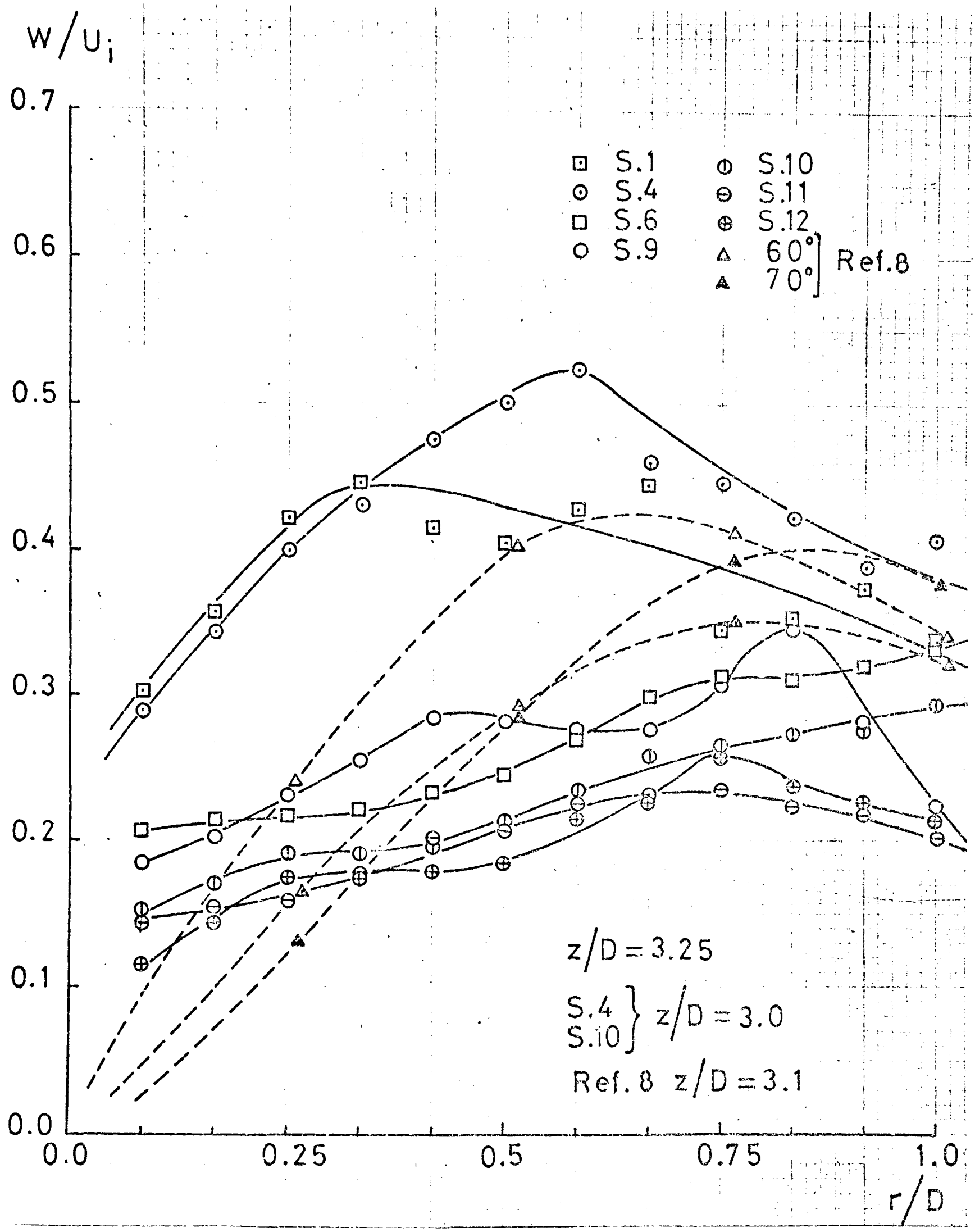

Fig.7.5I. Profiles of the swirl velocity for different swirlers at z/D=3.25

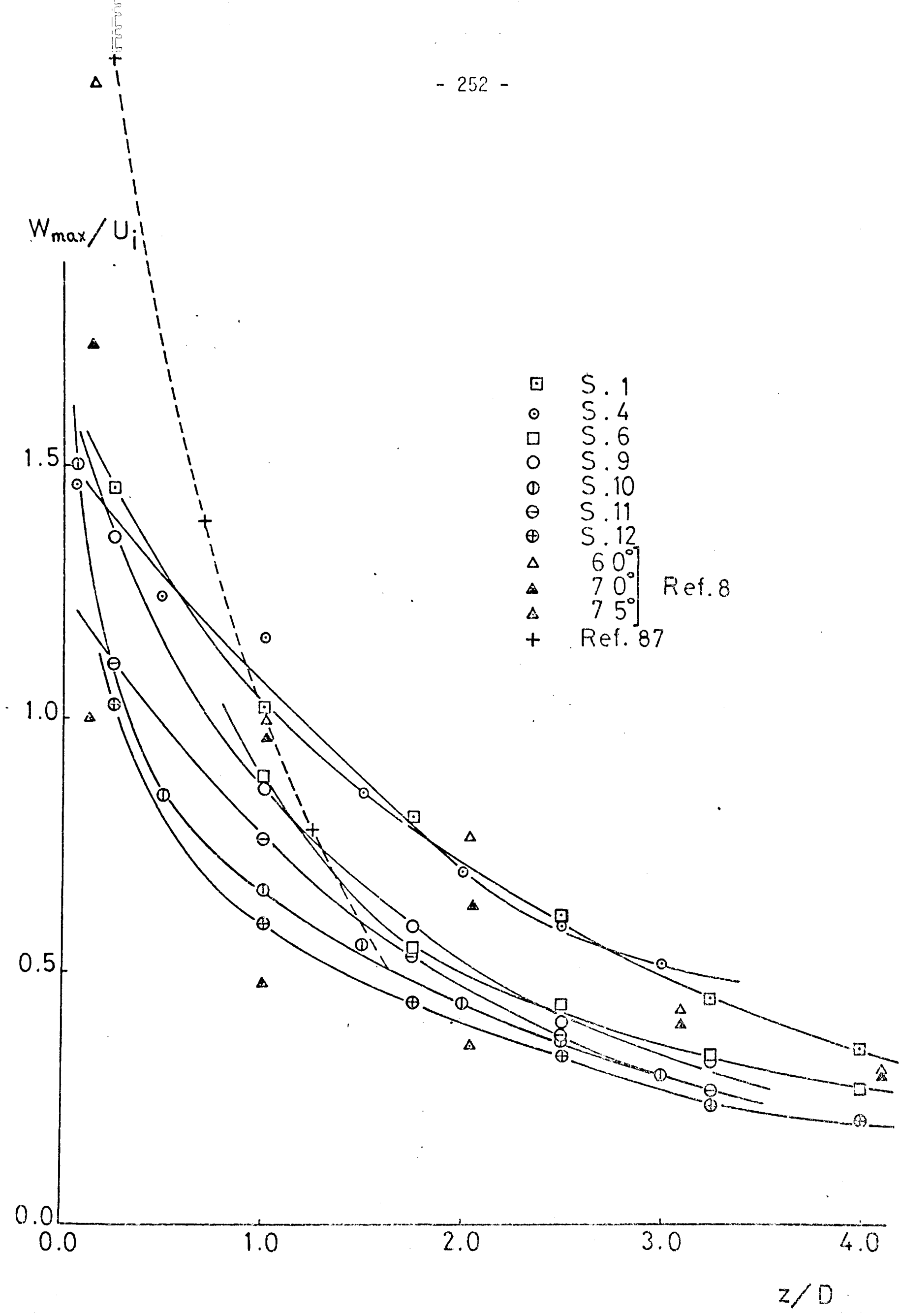

Fig.7.52. Decay of the maximum swirl velocities along the jet axis for different swirlers

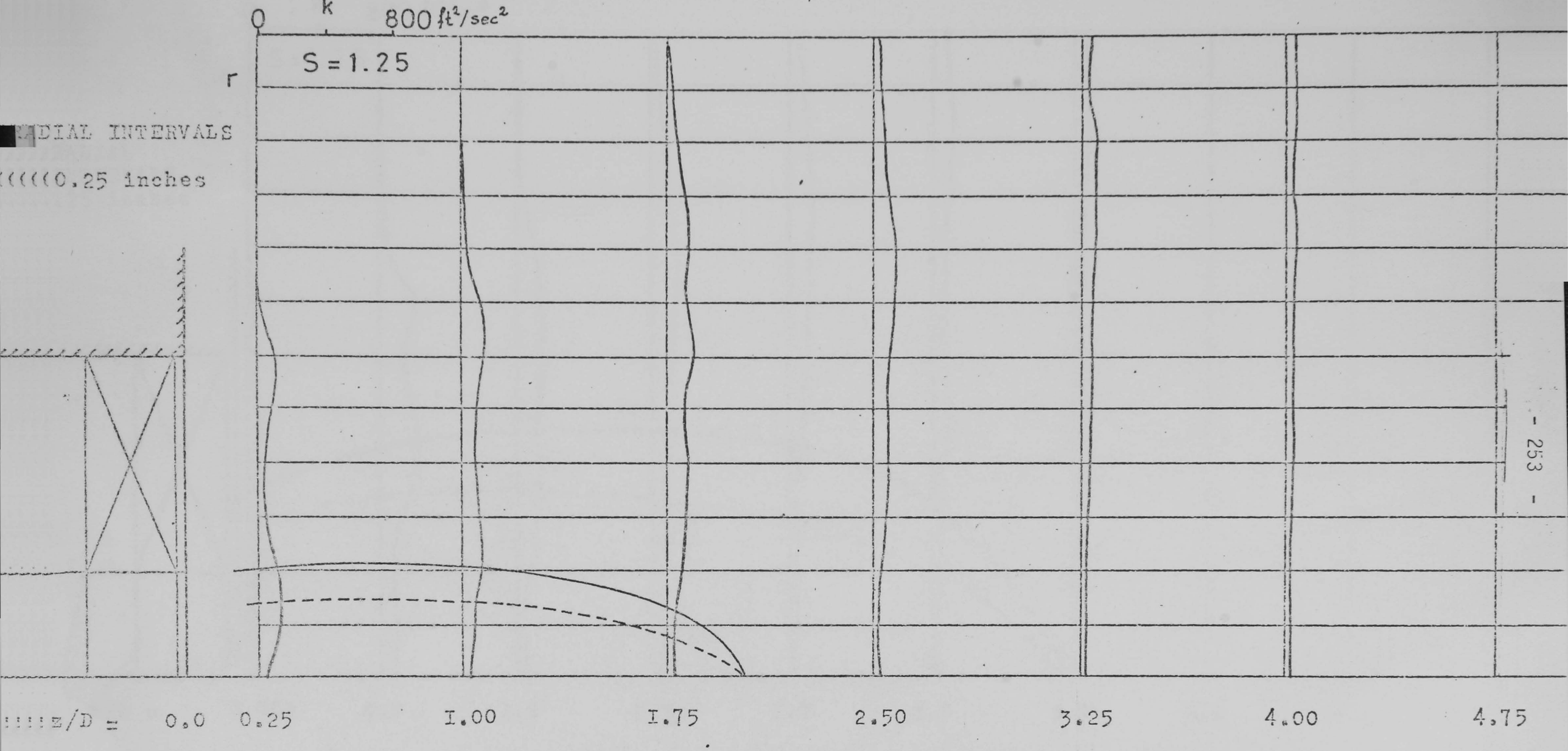

Fig.7.53.Distribution of the kinetic energy of turbulence in the jet issuing from the swirler S.I

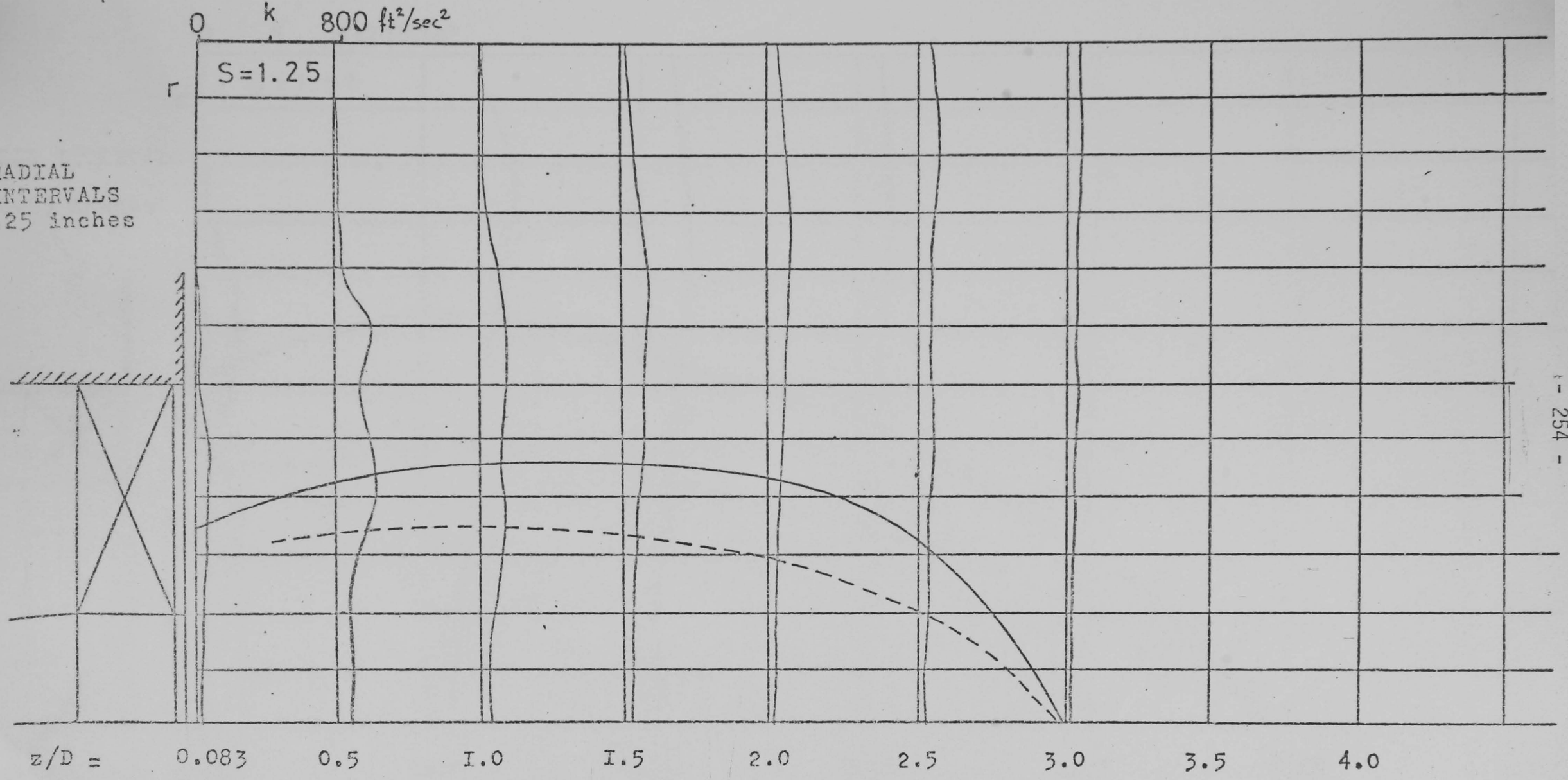

Fig.7.54.Distribution of the kinetic energy of turbulence in the jet issuing from the swirler S.4

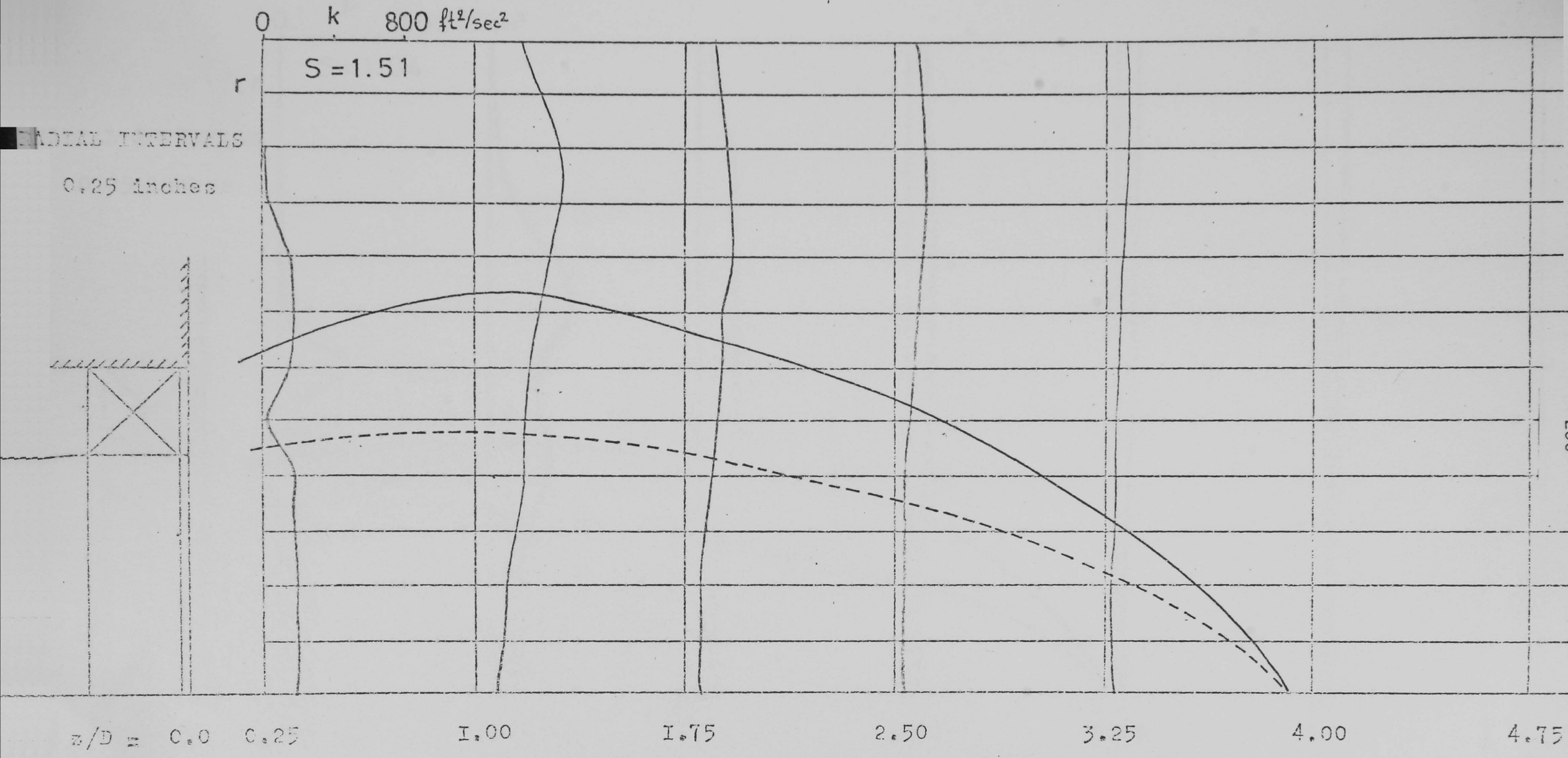

Fig.7.55.Distribution of the kinetic energy of turbulence in the jet issuing from the swirler S.6

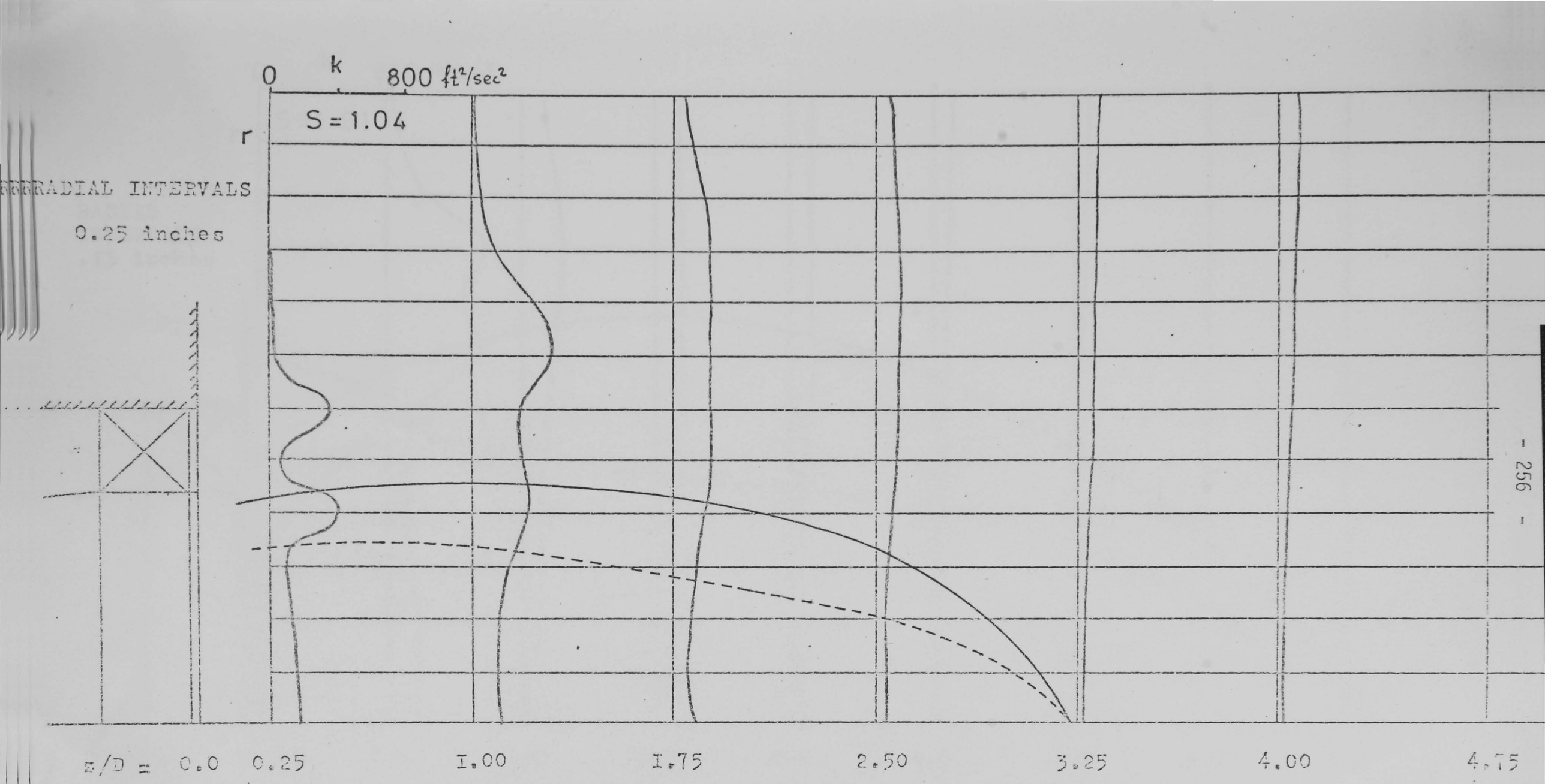

Fig.7.56.Distribution of the kinetic energy of turbulence in the jet issuing from the swirler S.9

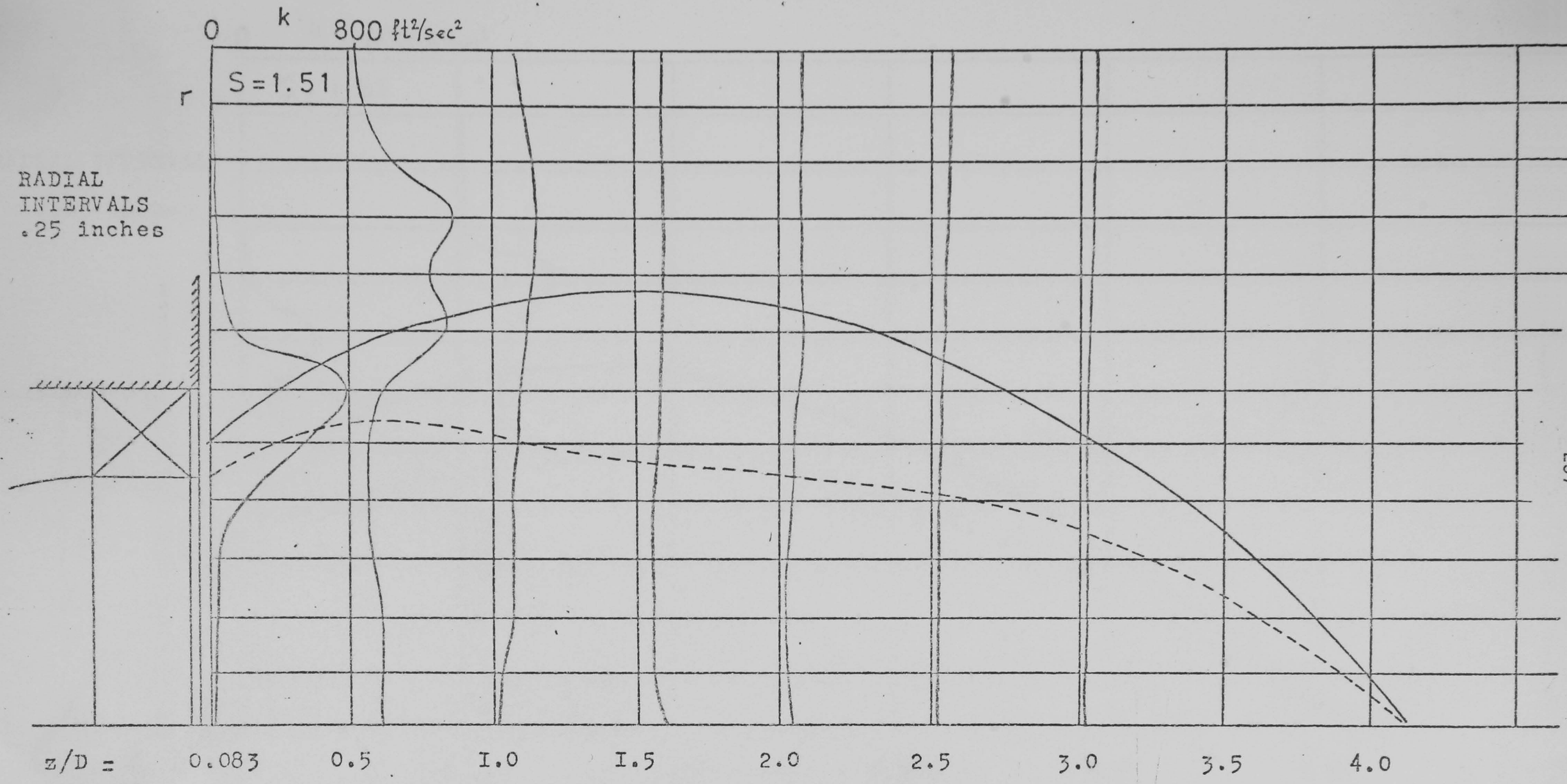

Fig.7.57.Distribution of the kinetic energy of turbulence in the jet issuing from the swirler S.IO

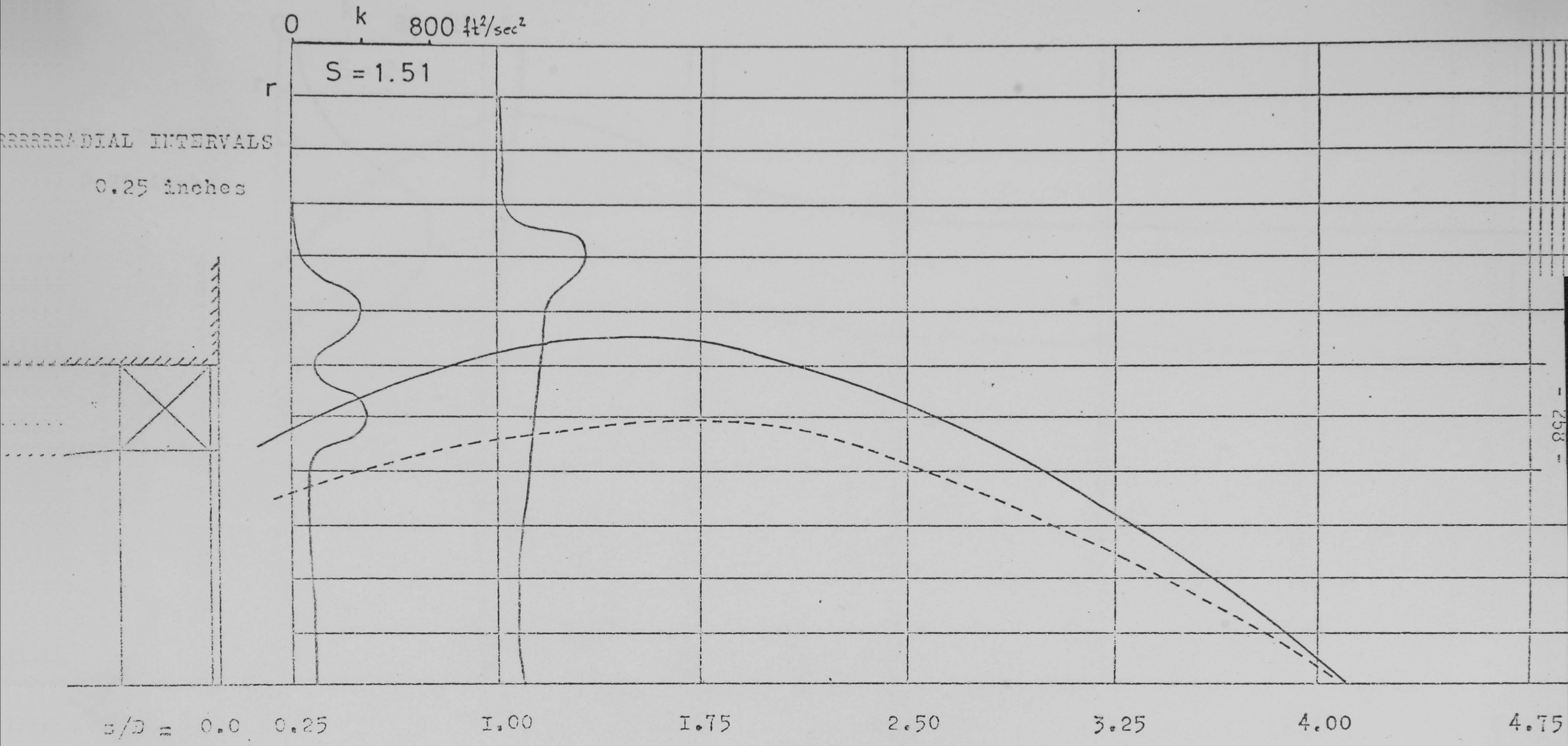

Fig.7.58.Distribution of the kinetic energy of turbulence in the jet issuing from the swirler S.II

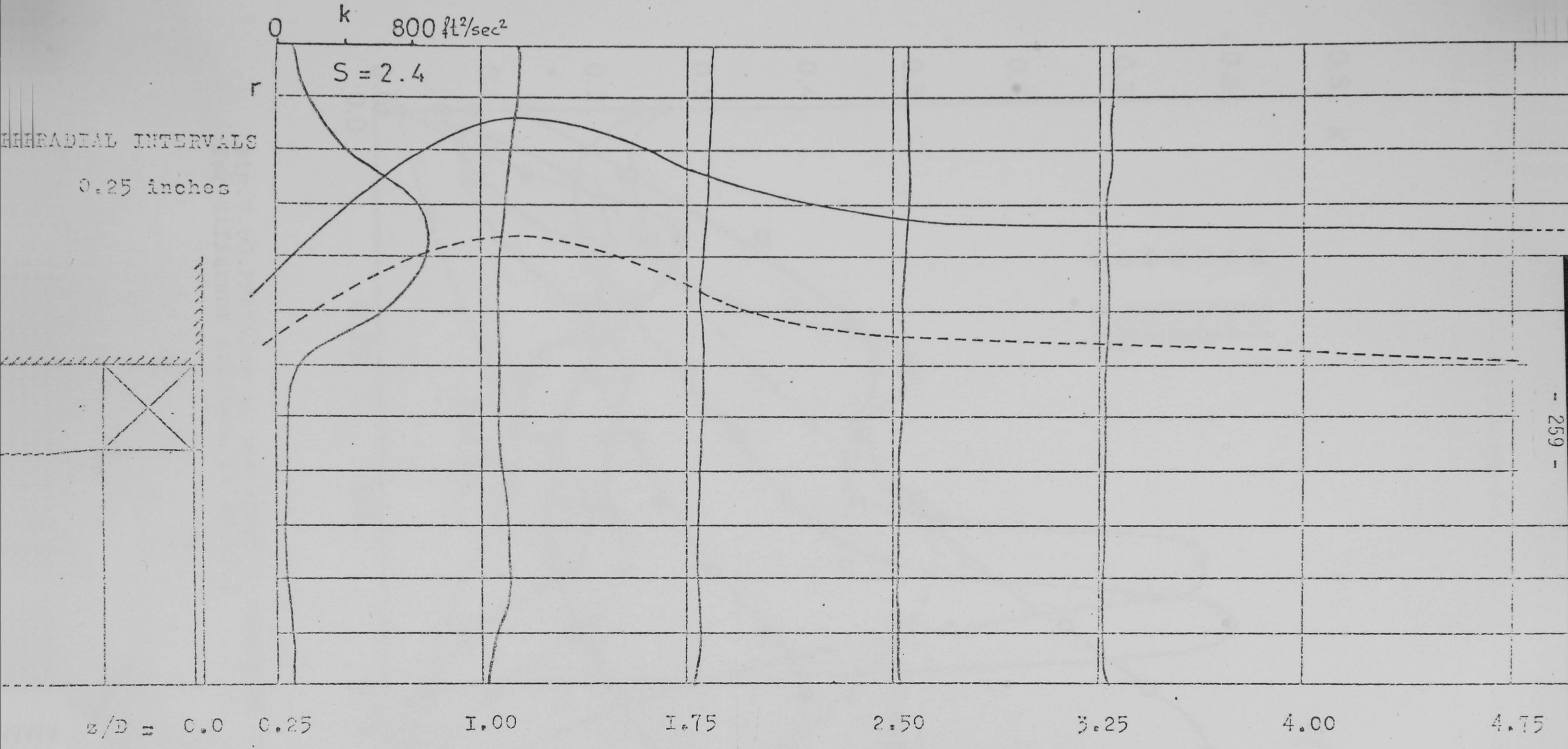

Fig.7.59.Distribution of the kinetic energy of turbulence in the jet issuing from the swirler S.I2

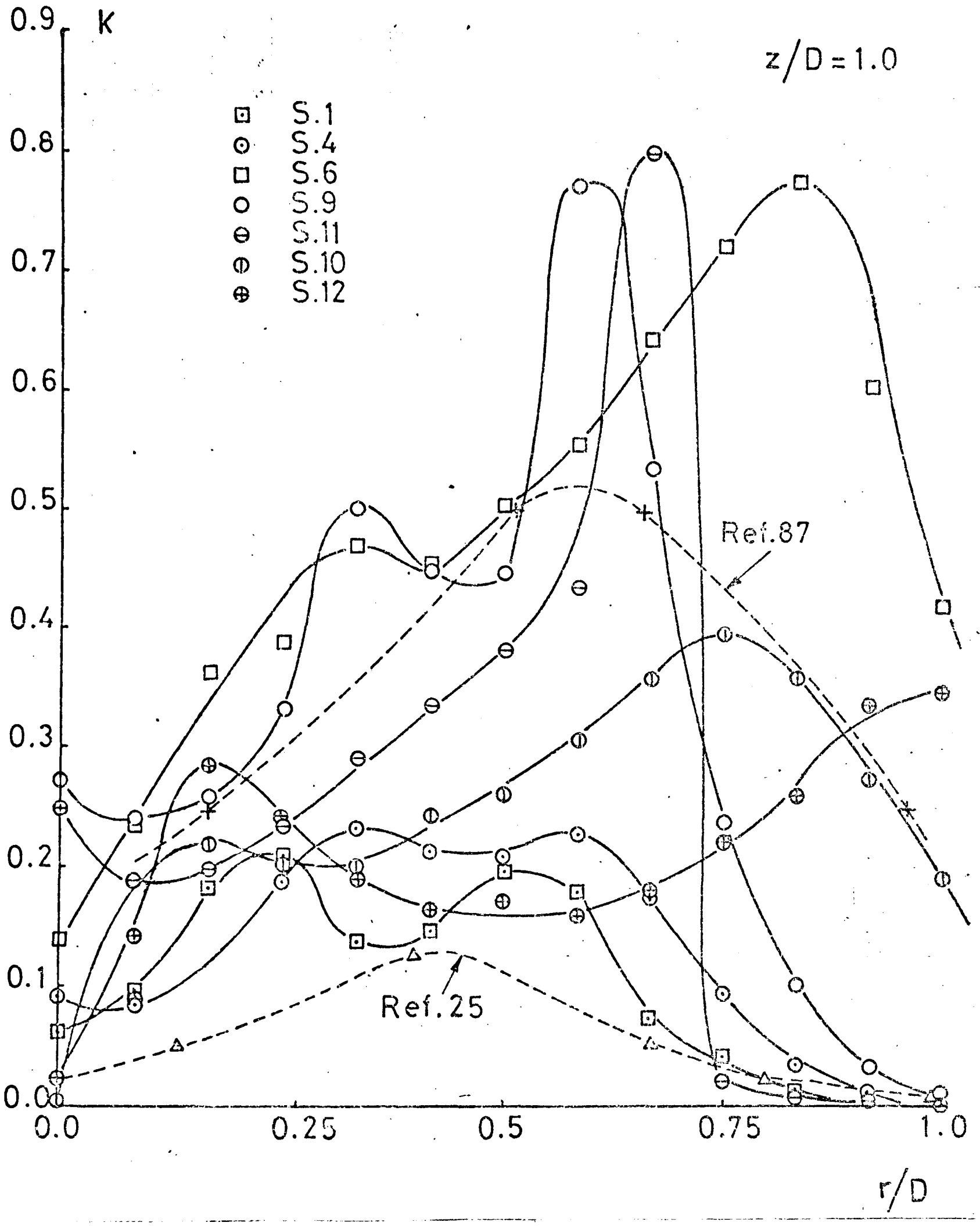

Fig.7.60.Profiles of the kinetic energy of turbulence for different swirlers at z/D=I.0

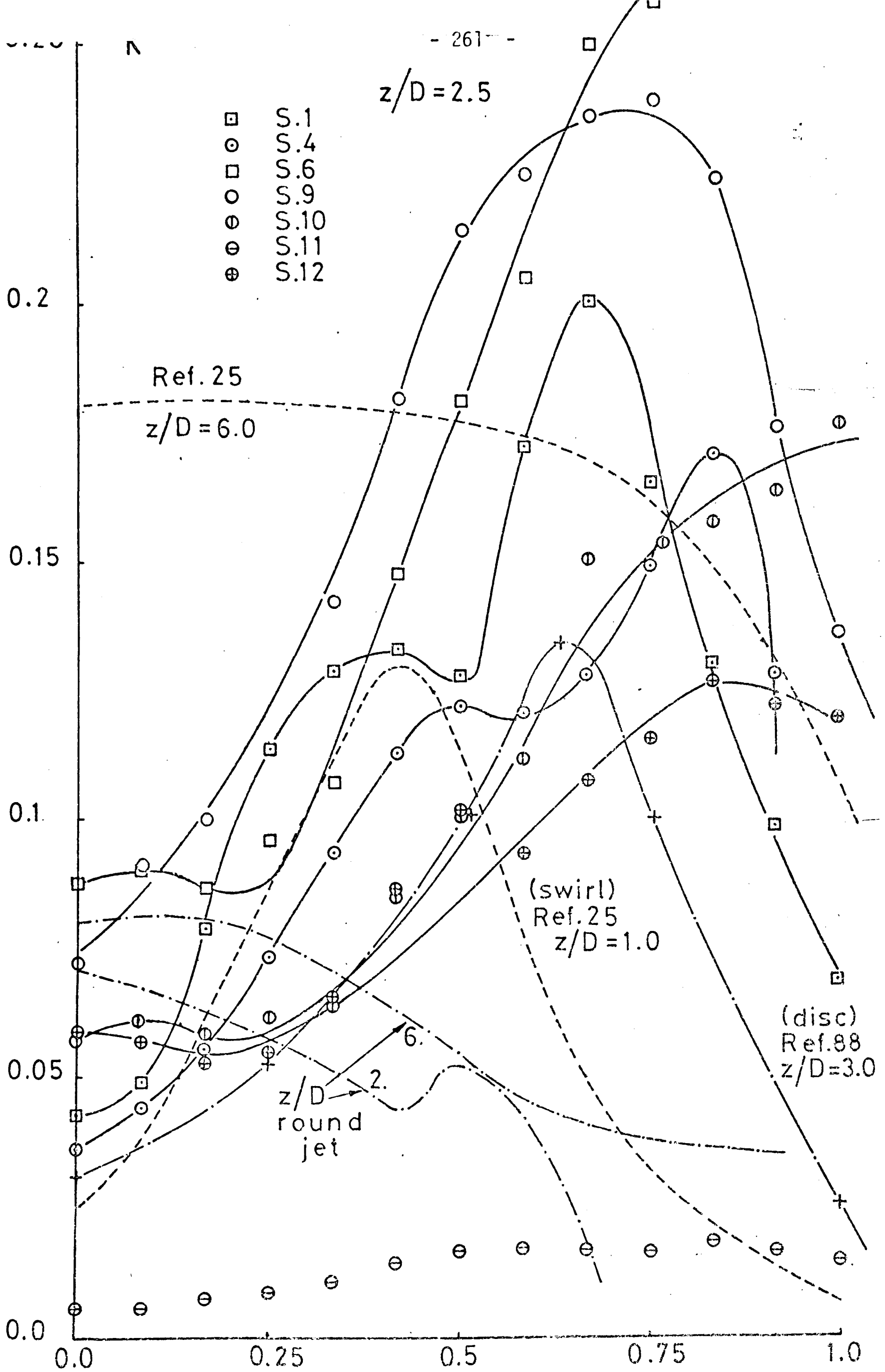

Fig.7.6I. Profiles of the kinetic energy of turbulence for different swirlers at z/D=2.5

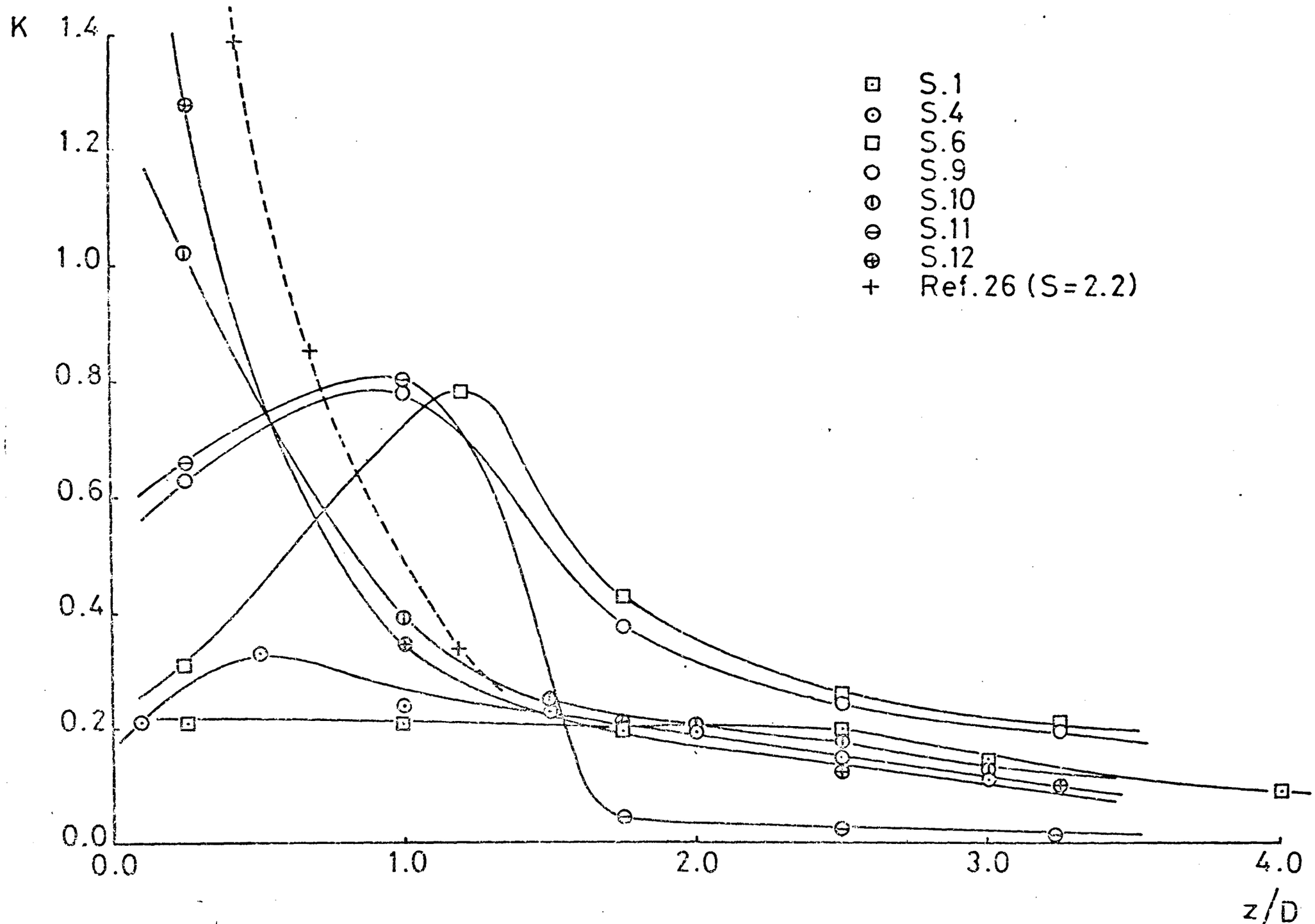

Fig.7.62.Decay of the maximum kinetic energy of turbulence along the jet axis for different swirlers

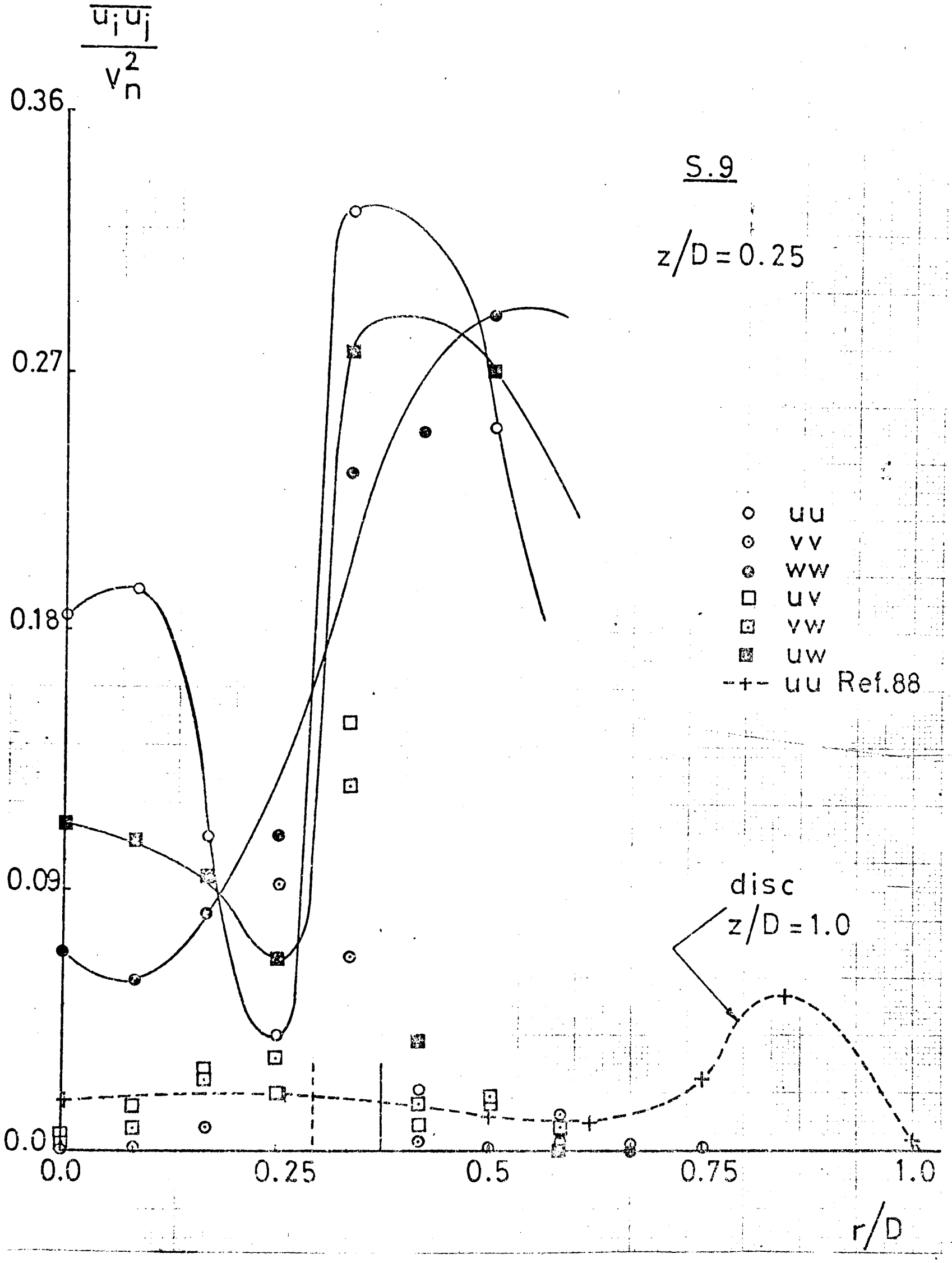

Fig.7.63.Profiles of the Reynolds stresses at z/D=0.25 in the flow field of the swirler S.9

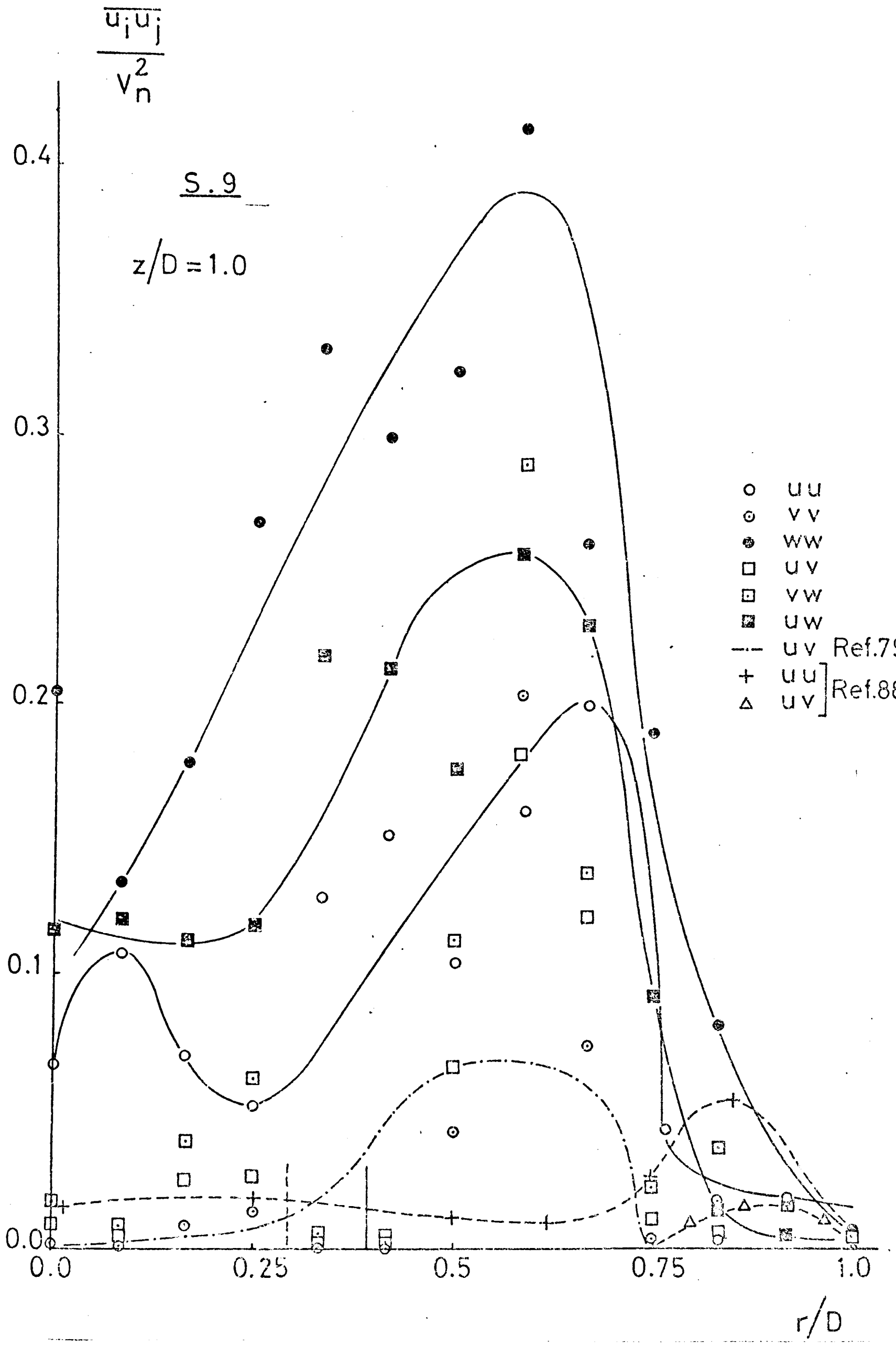

Fig.7.64.Profiles of the Reynolds stresses at z/D=I.0 in the flow field of the swirler S.9

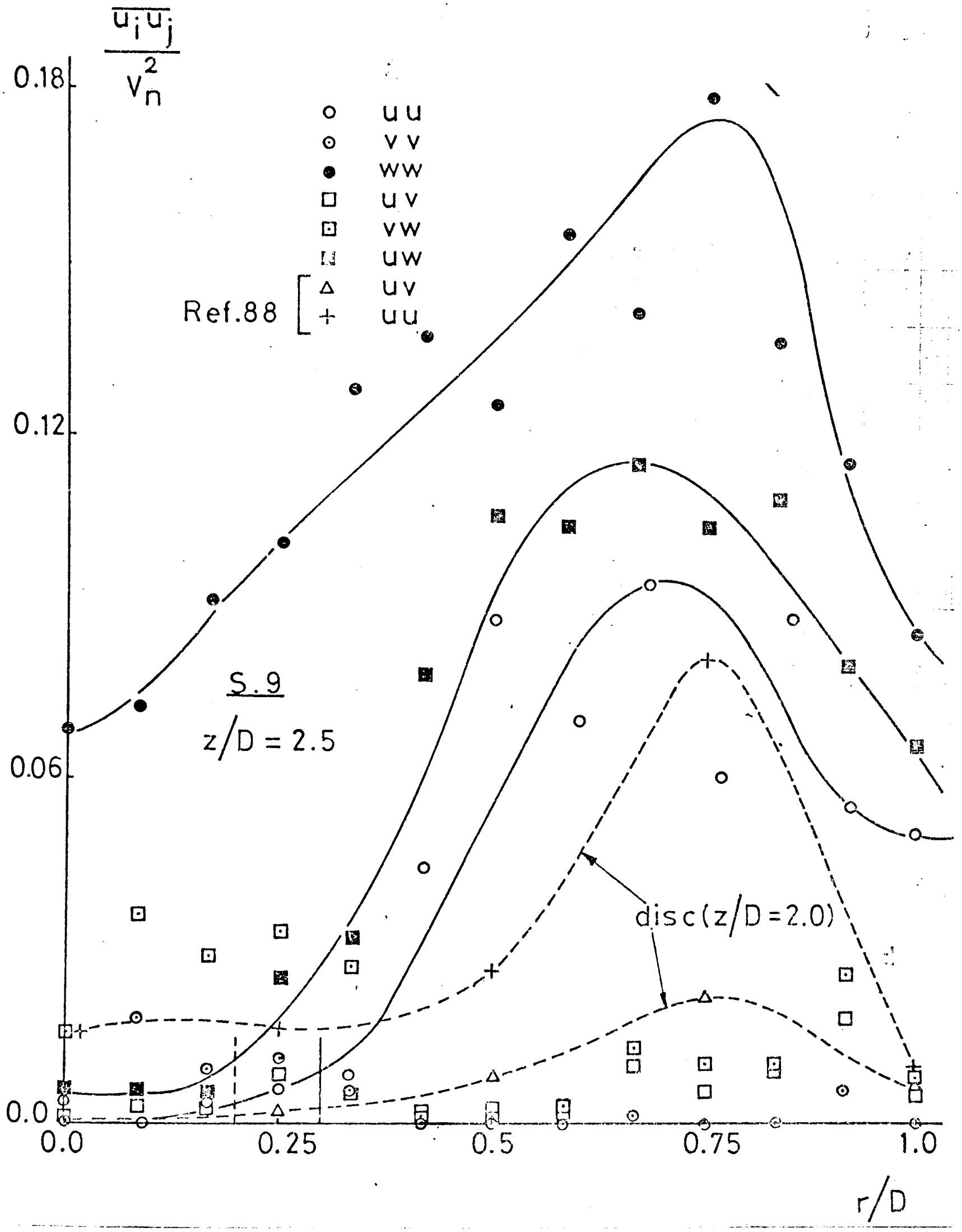

Fig.7.65.Profiles of the Reynolds stresses at z/D=2.5 in the flow field of the swirler S.9

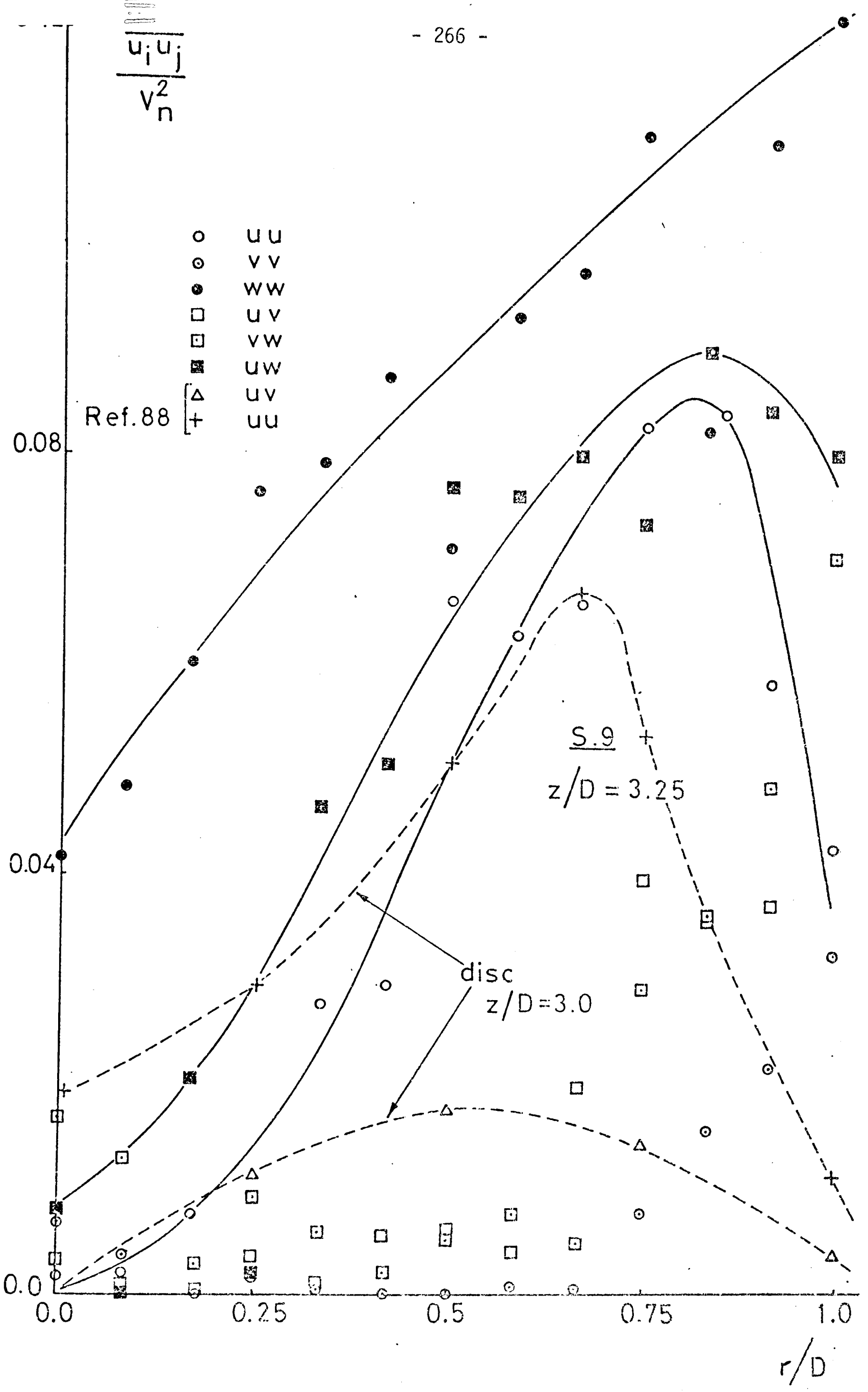

Fig.7.66.Profiles of the Reynolds stresses at z/D=3.25 in the flow field of the swirler S.9

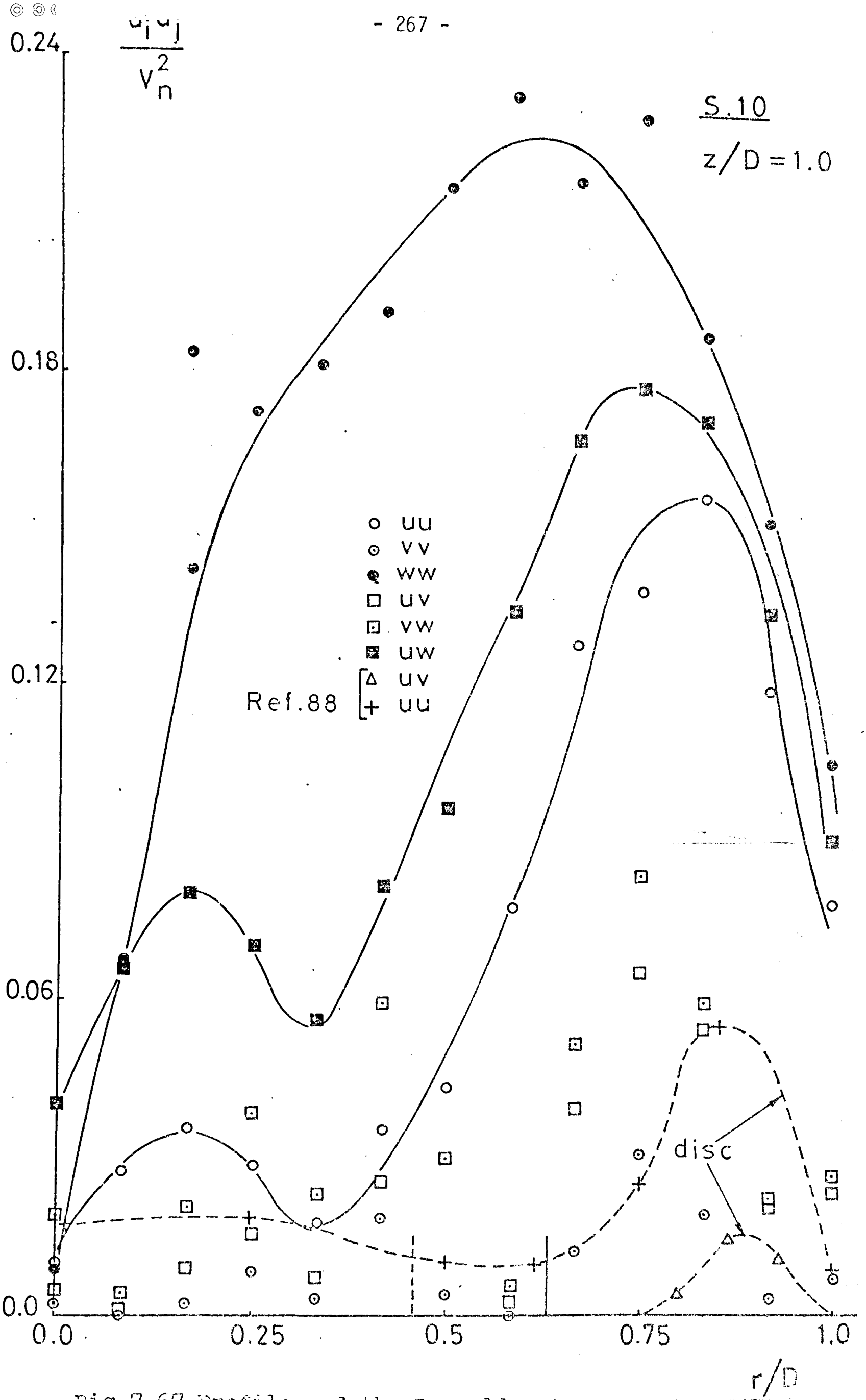

Fig.7.67.Profiles of the Reynolds stresses at z/D=1.0 in the flow field of the swirler S.IO

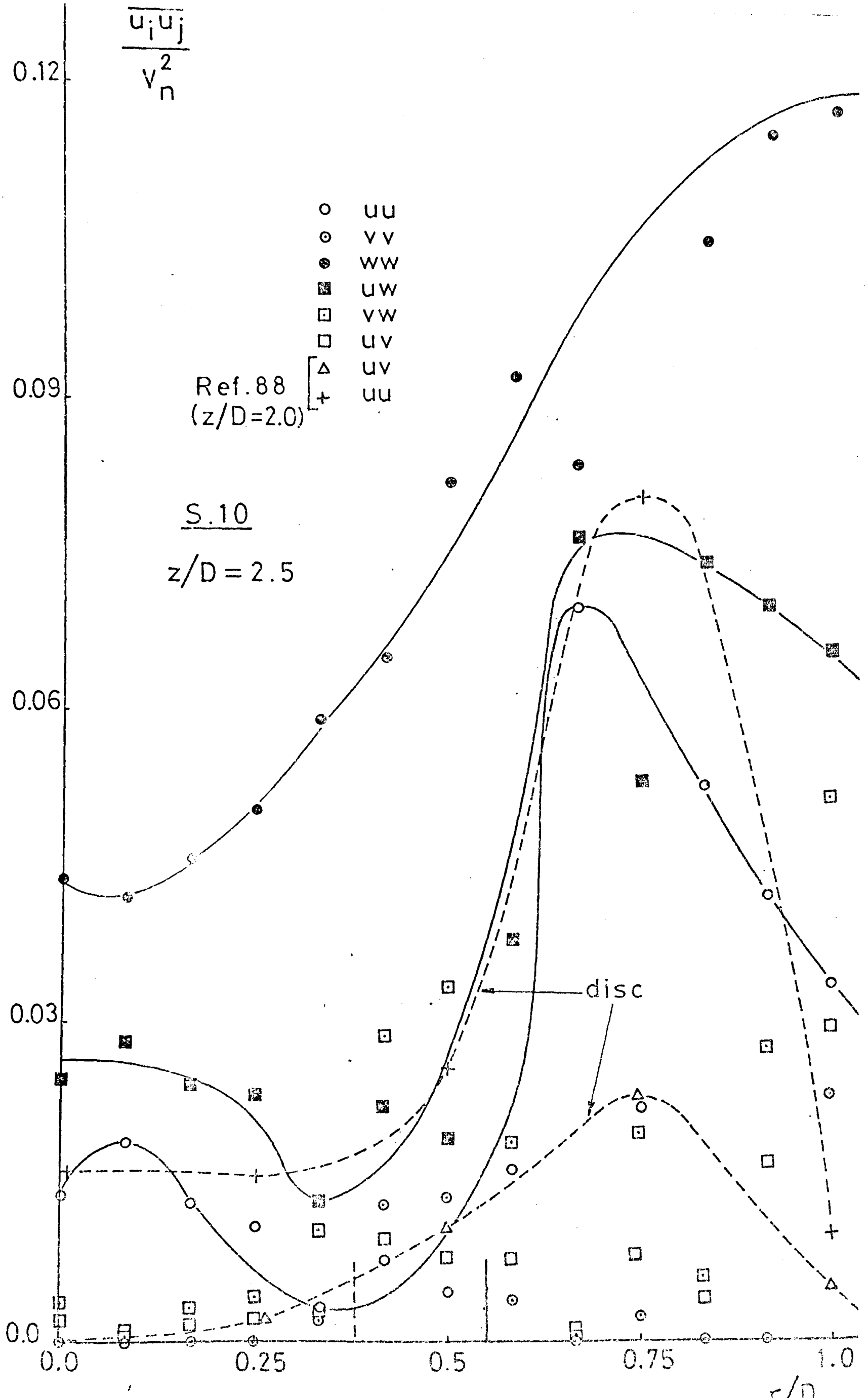

Fig. 7.63. Profiles of the Reynolds stresses at [illegible] field of the swirler S.IO

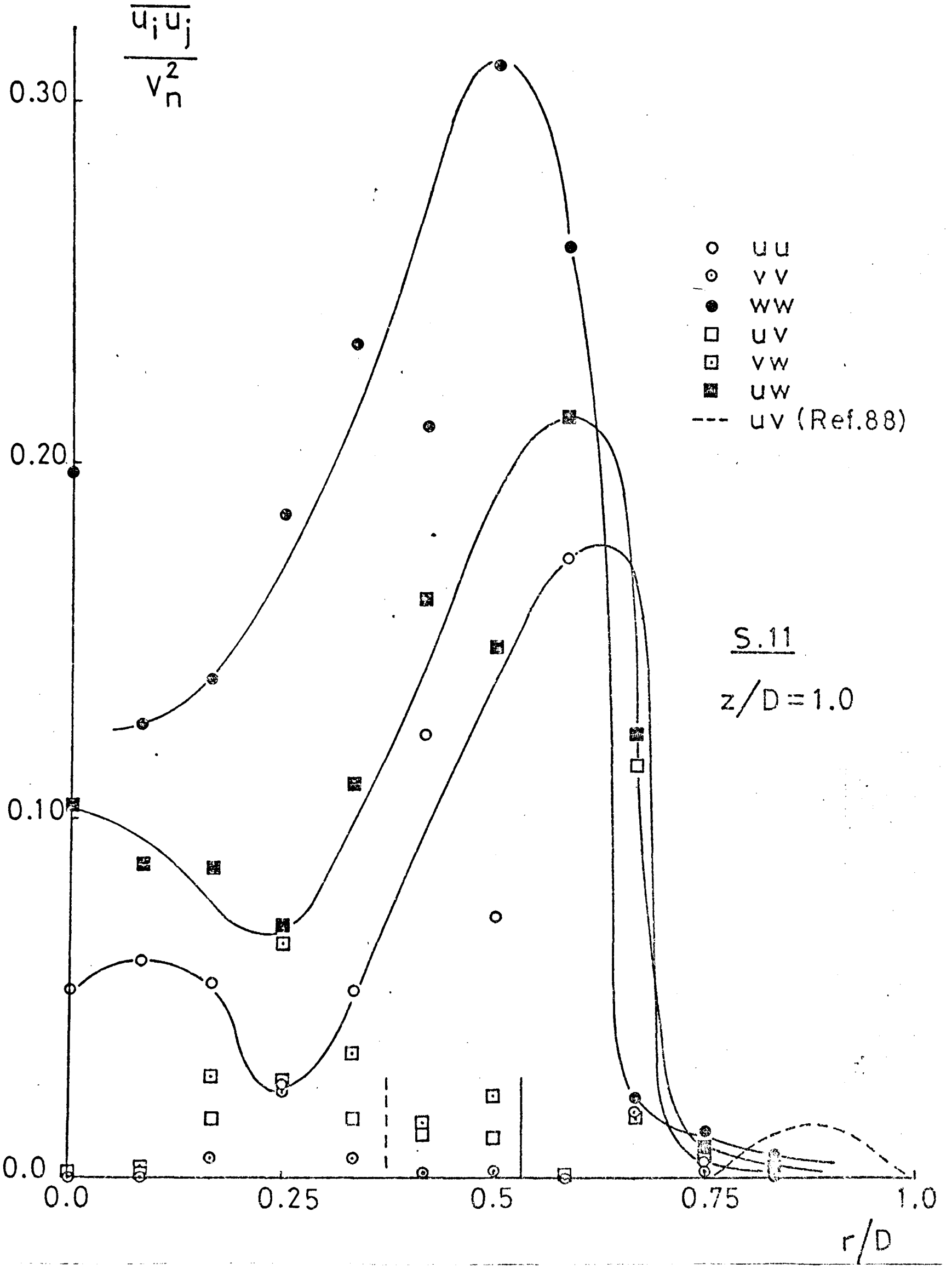

Fig.7.69.Profiles of the Reynolds stresses at z/D=1.0 in the flow field of the swirler S.II

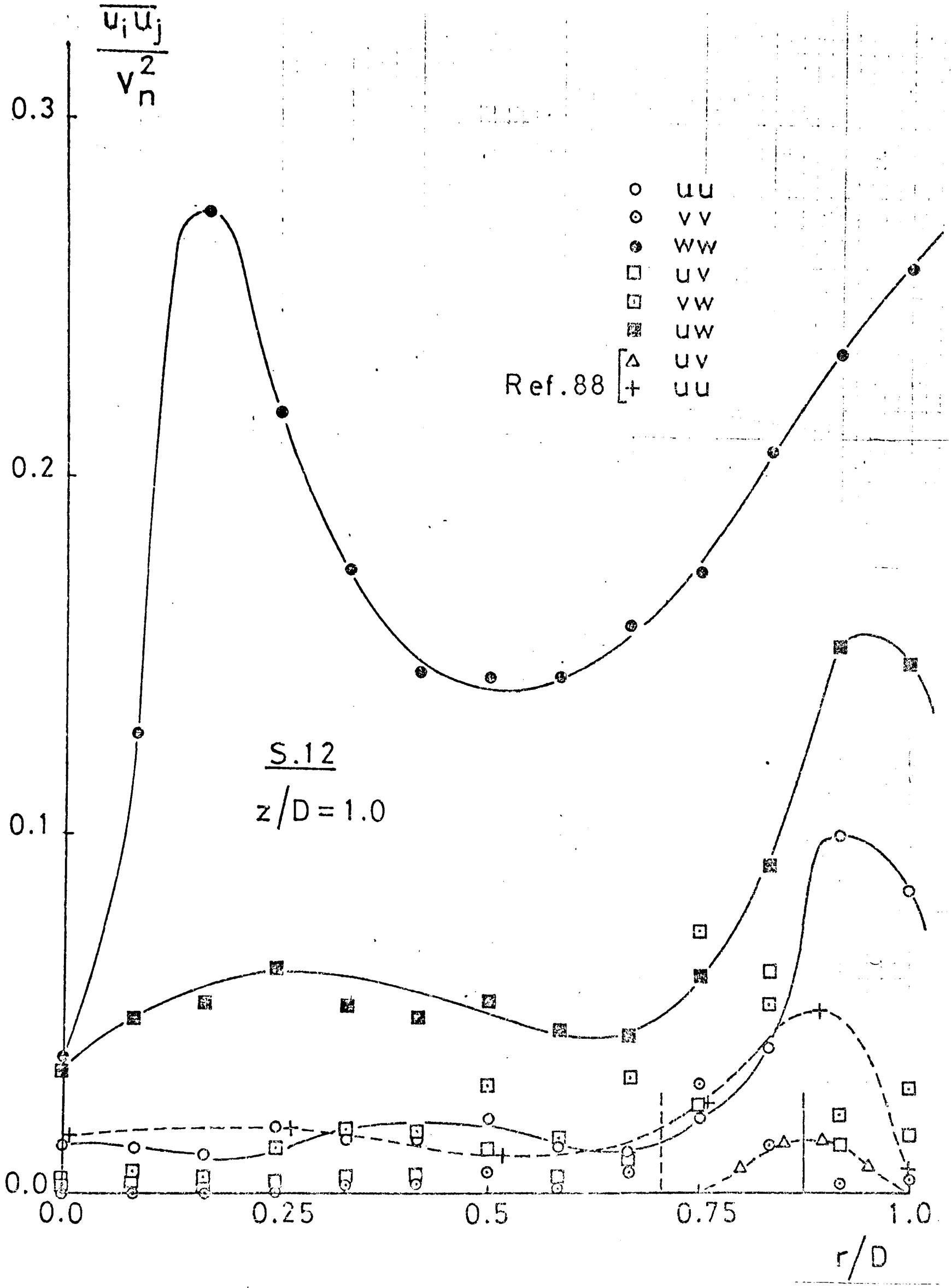

Fig.7.70.Profiles of the Reynolds stresses at z/D=I.0 in the flow field of the swirler S.12

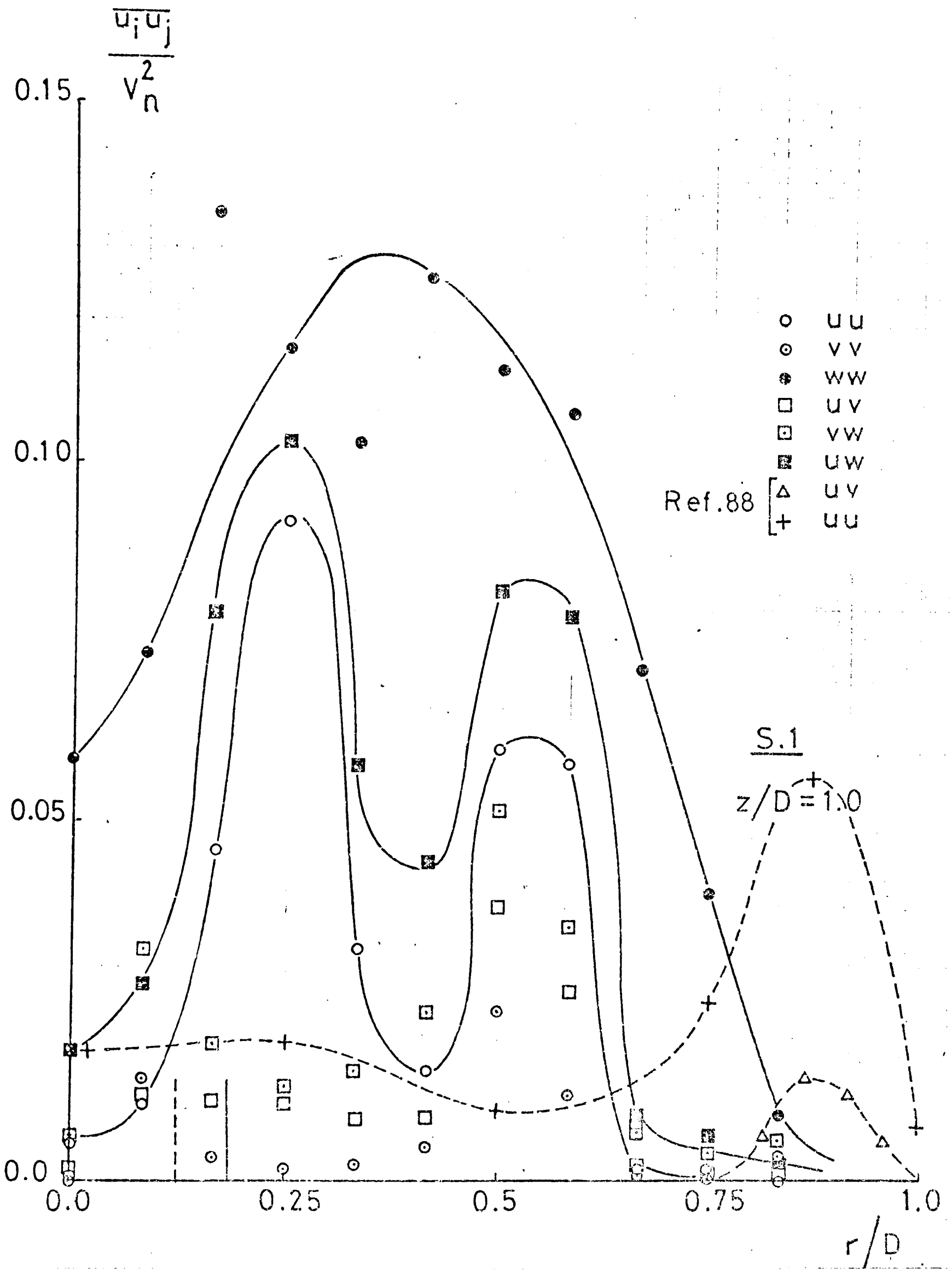

Fig.7.7I.Profiles of the Reynolds stresses at z/D=I.O in the flow field of the swirler S.I

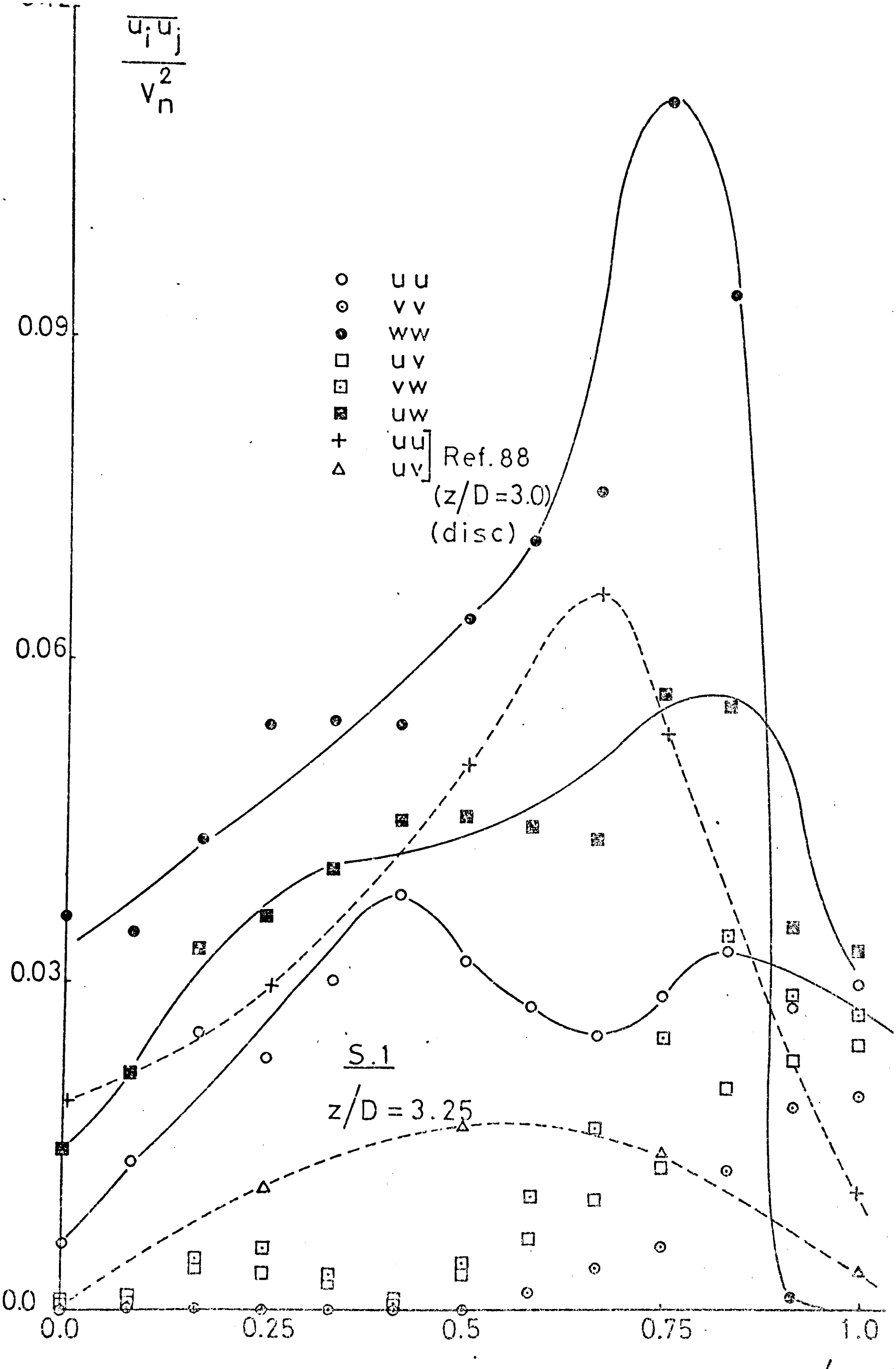

Fig.7.72.Profiles of the Reynolds stresses at z/D=3.25 in the flow field of the swirler S.I

$\frac{\overline{ww}}{V_n^2}$

Fig.7.73. Profiles of the dominant stress $\overline{ww}$ for different swirlers at z/D=I.0

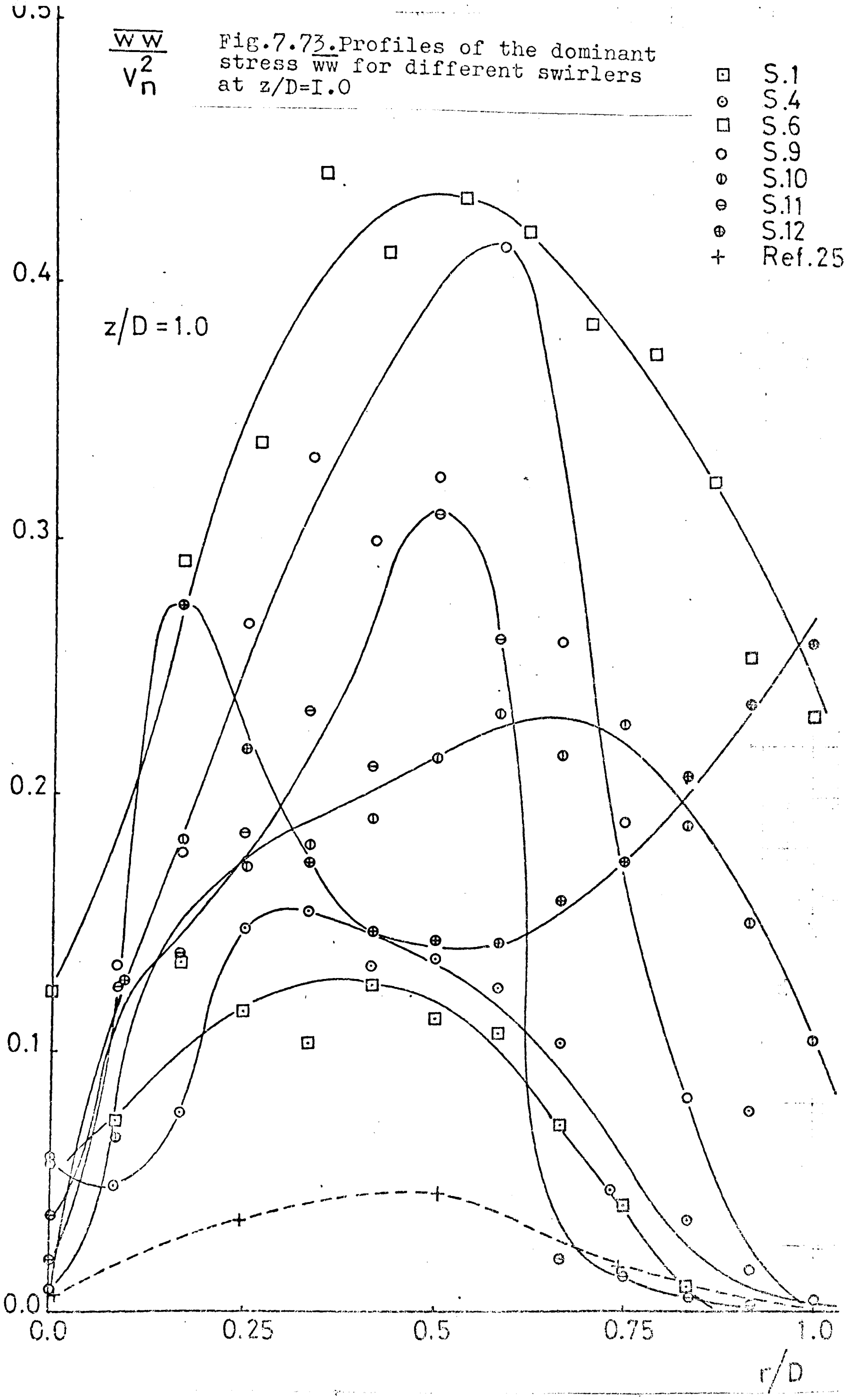

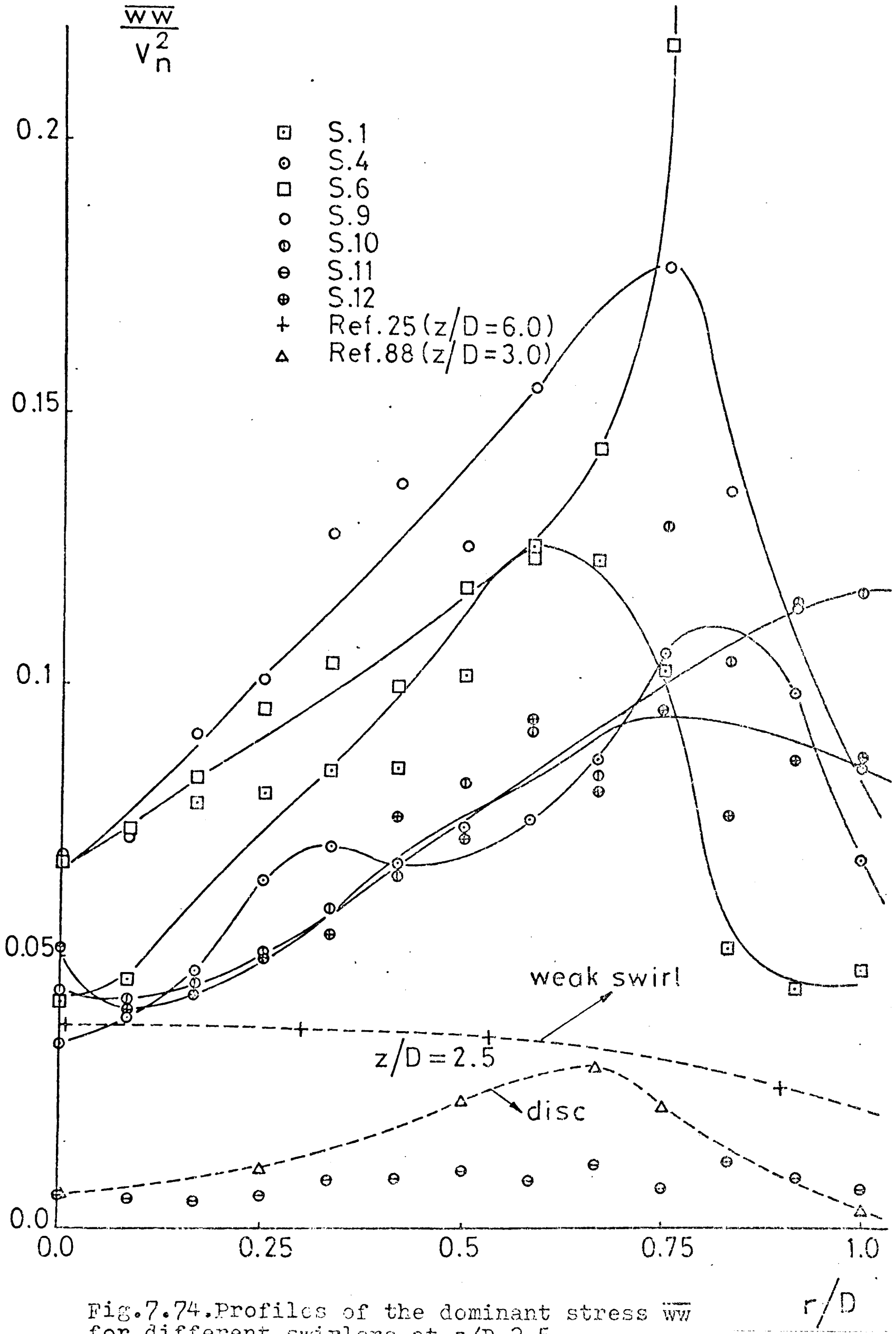

Fig.7.74.Profiles of the dominant stress $\overline{ww}$ for different swirlers at z/D=2.5

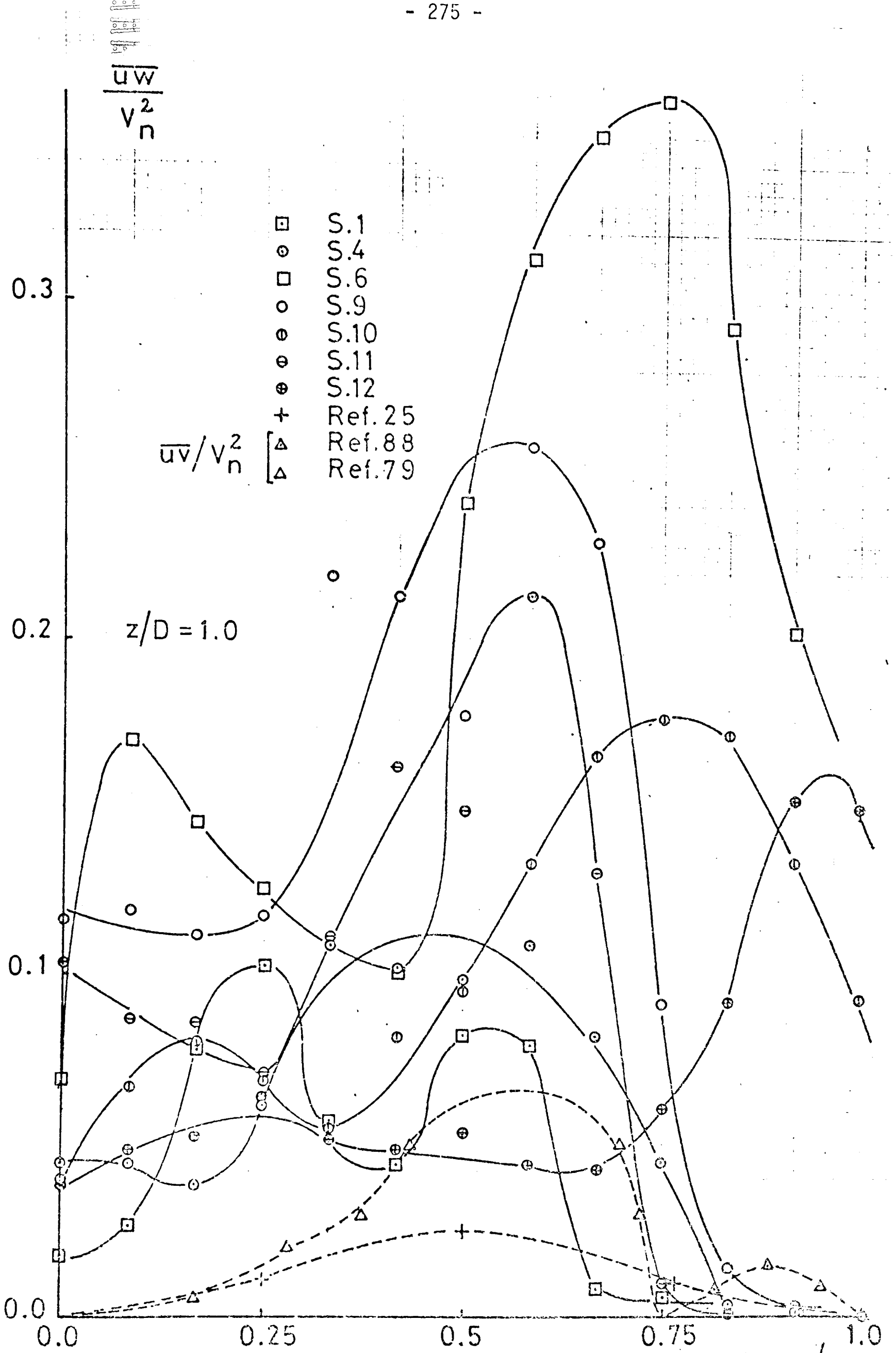

Fig.7.75.Profiles of the second dominant stress $\overline{uw}$ for different swirlers at z/D=I.O

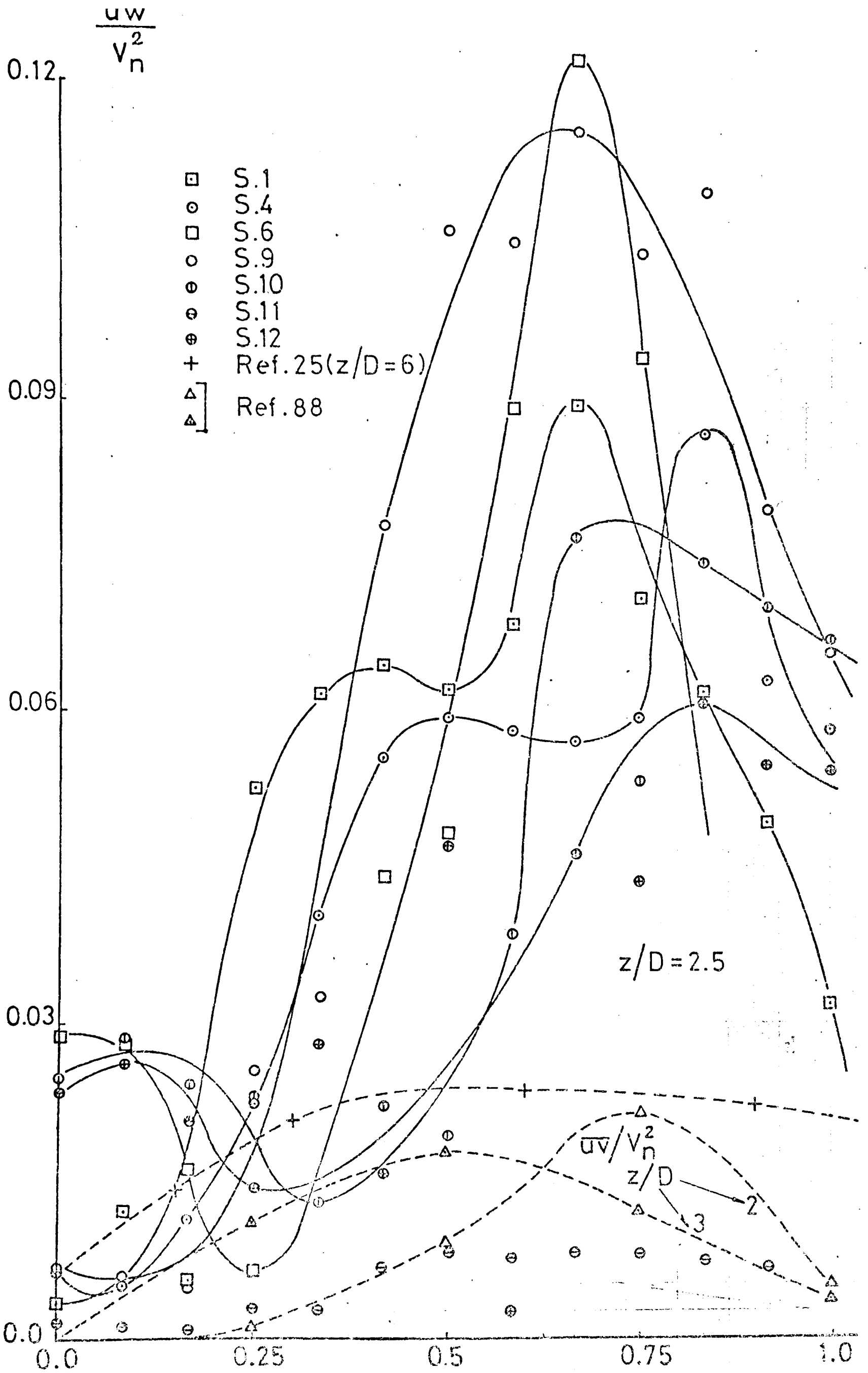

Fig.7.76.Profiles of the second dominant stress $\overline{uw}$ ers at z/D=2.5

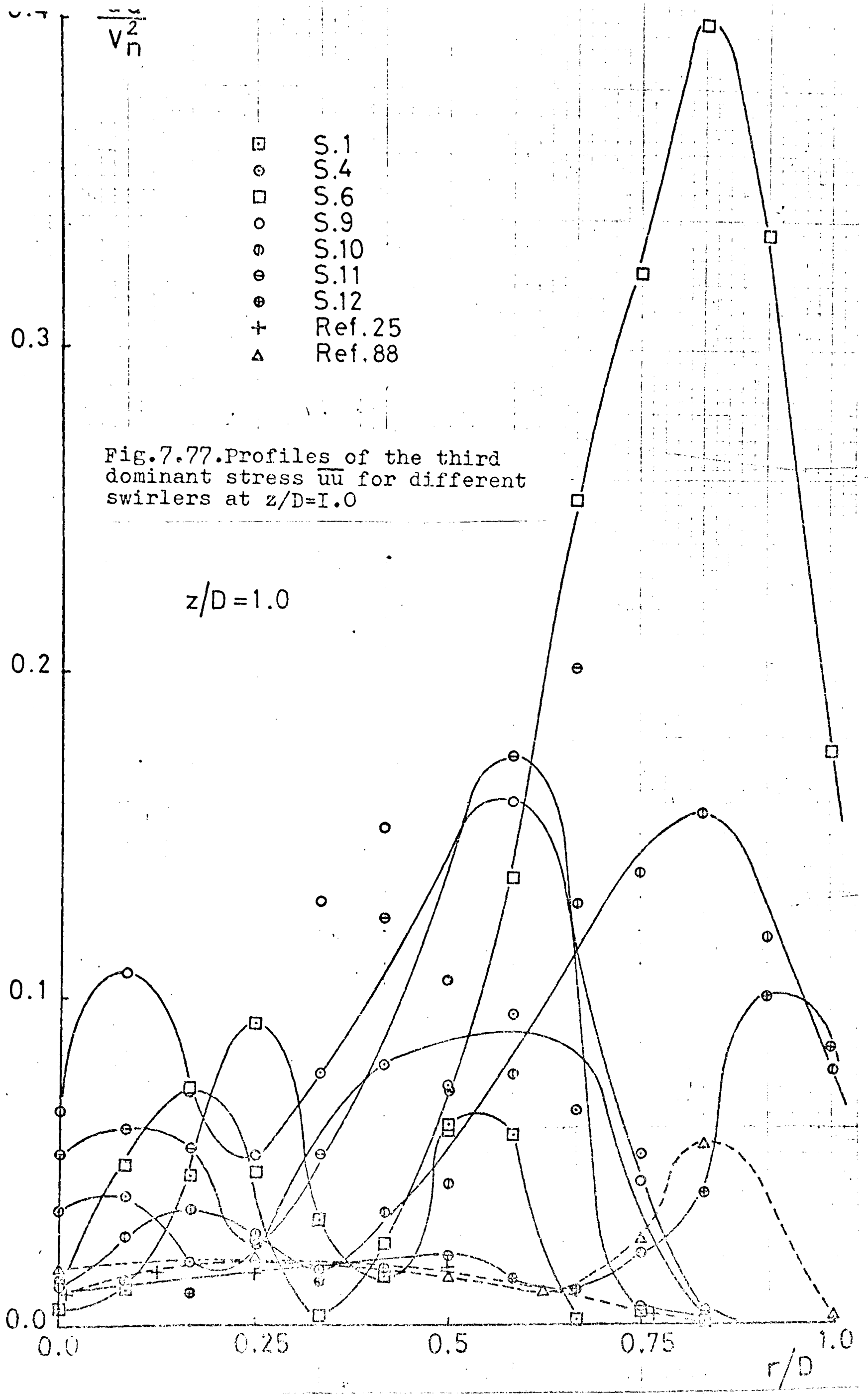

Fig.7.77.Profiles of the third dominant stress $\overline{uu}$ for different swirlers at z/D=I.O

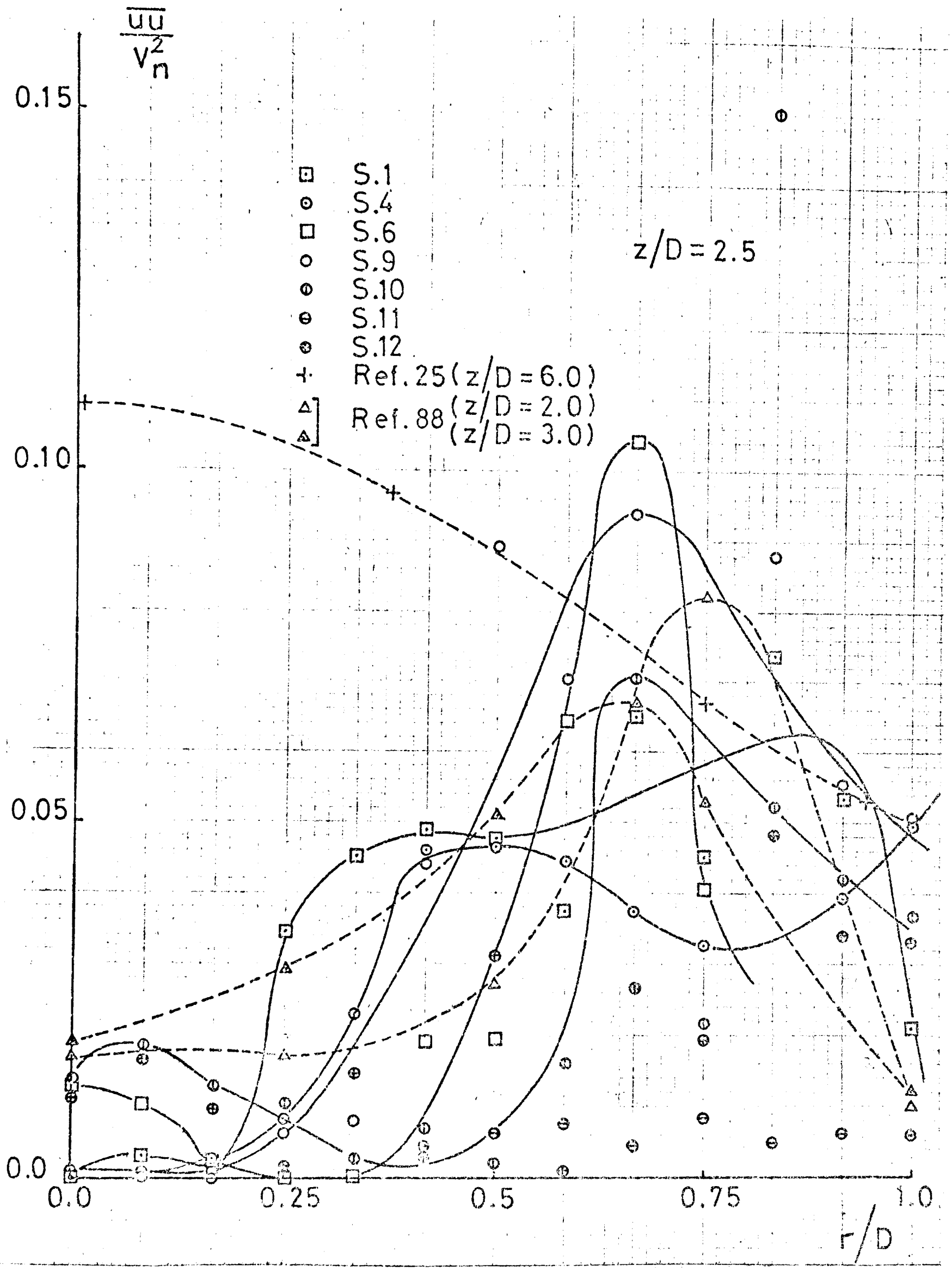

Fig.7.78.Profiles of the third dominant stress $\overline{uu}$ for different swirlers at z/D-2.5

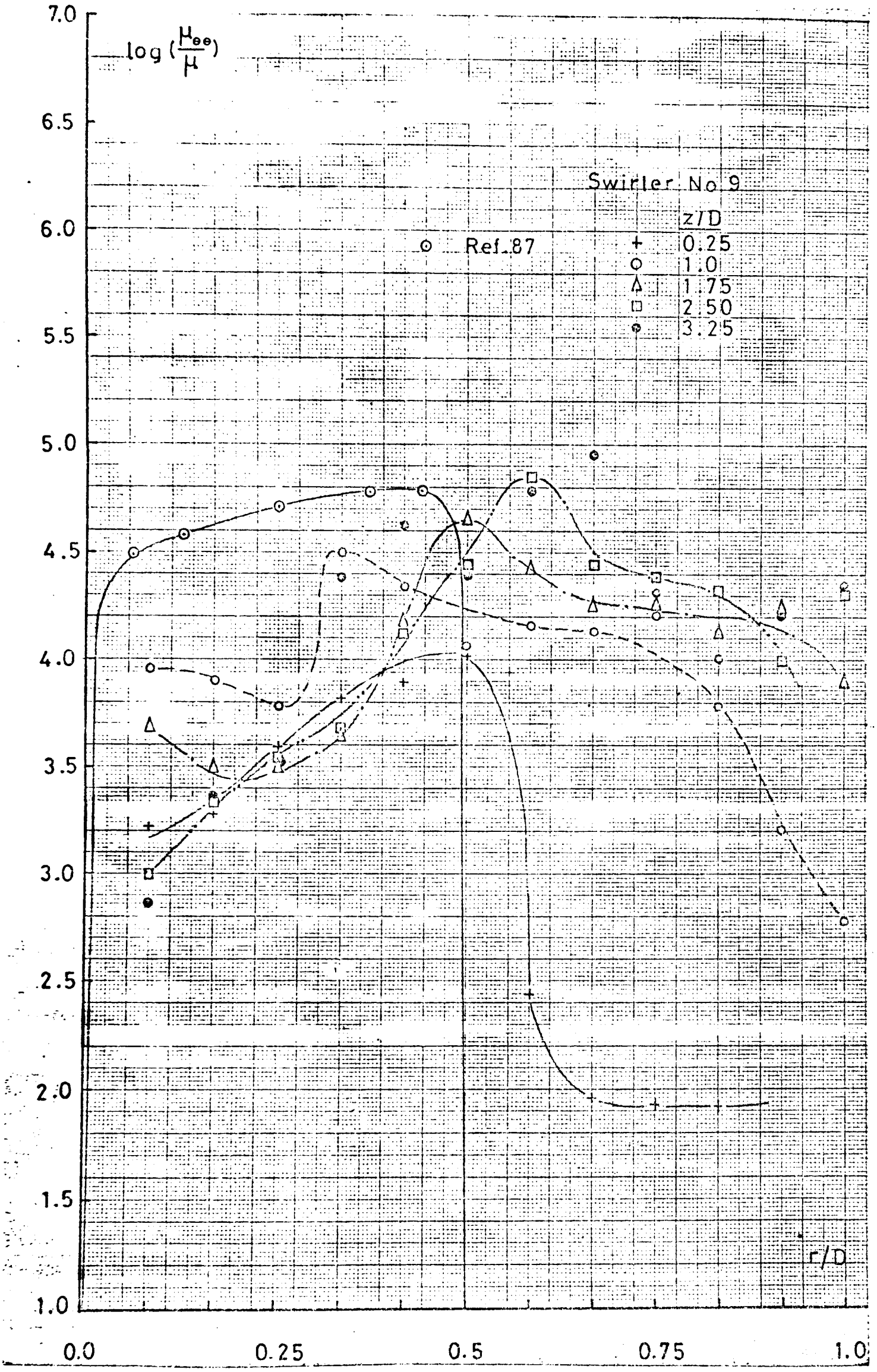

Fig.7.79.Profiles of the turbulent viscosity $\mu_{\theta\theta}$ in the flow field of the swirler S.9

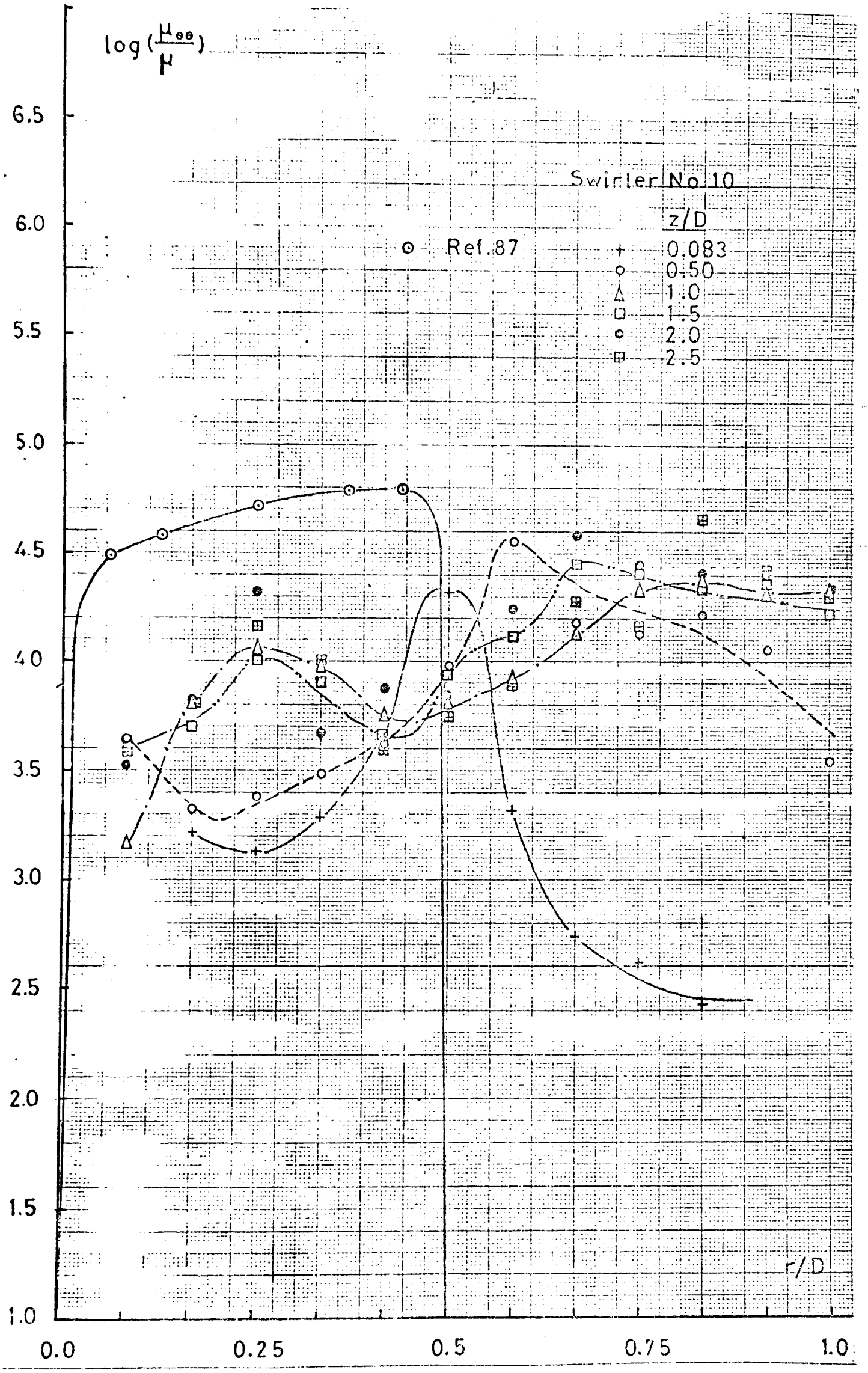

Fig.7.80.Profiles of the turbulent viscosity $\mu_{\theta\theta}$ in the flow field of the swirler S.IO

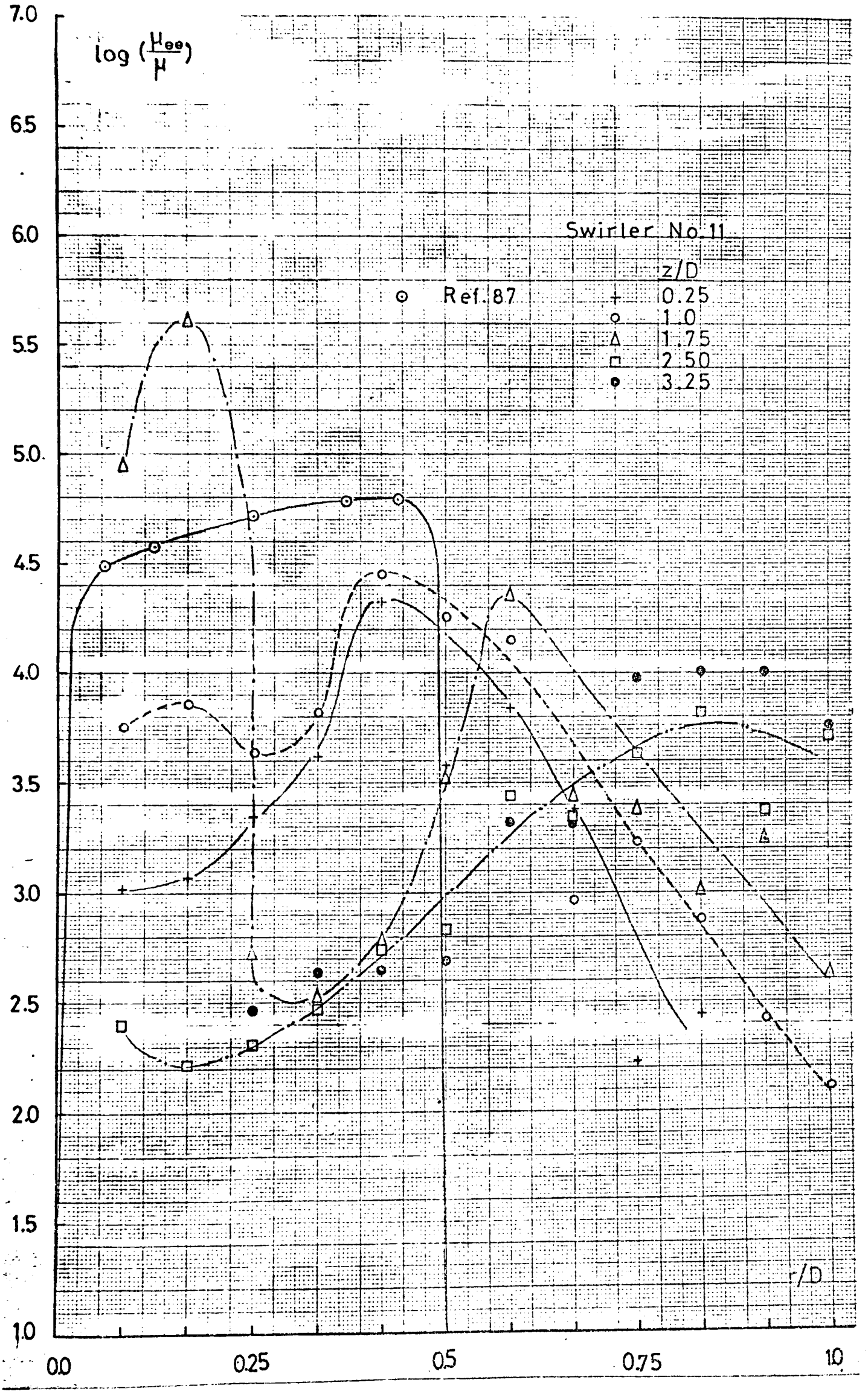

Fig.7.8I.Profiles of the turbulent viscosity $\mu_{\theta\theta}$ in the flow field of the swirler S.II

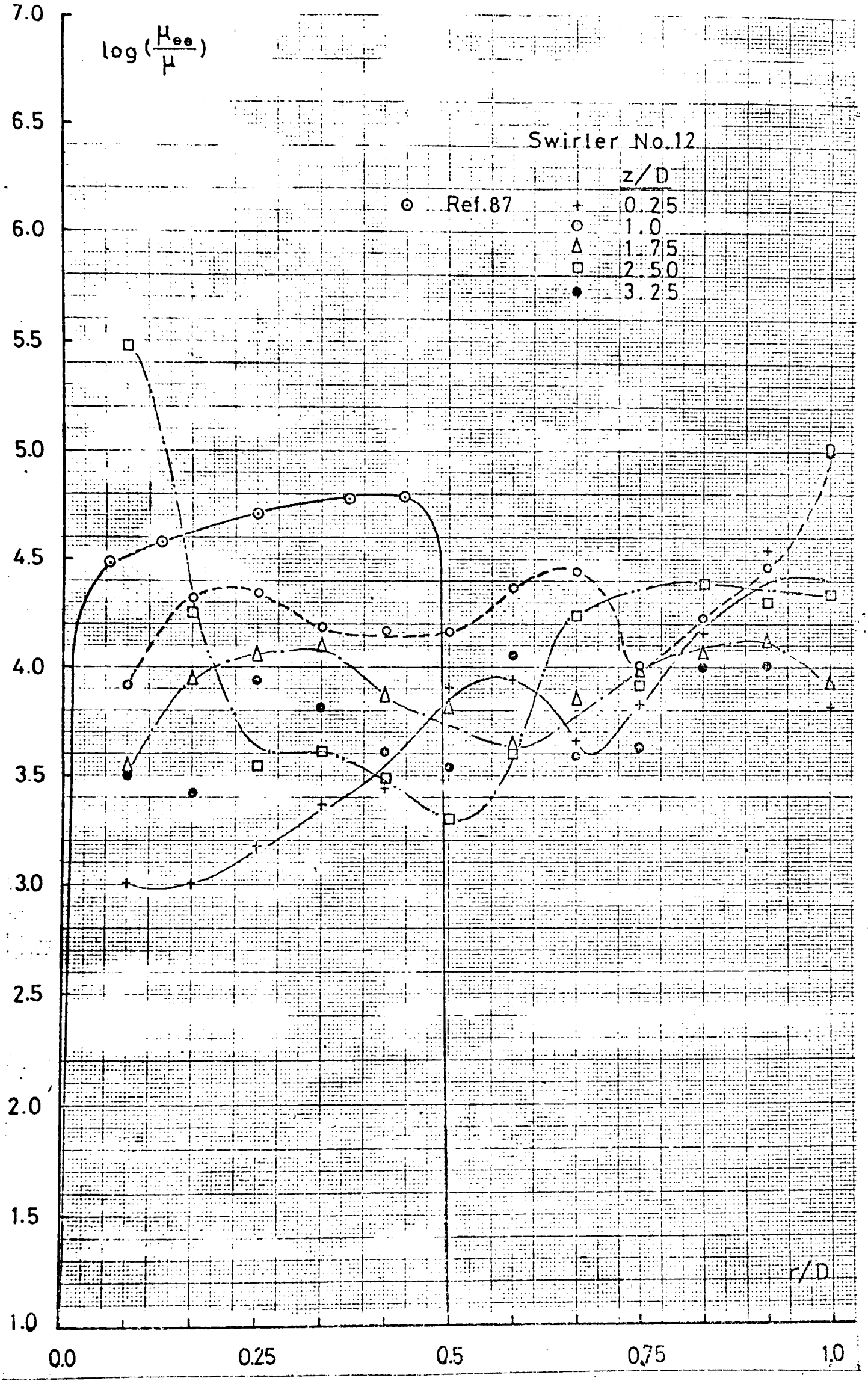

Fig.7.82.Profiles of the turbulent viscosity $\mu_{\theta\theta}$ in the flow field of the swirler S.I2

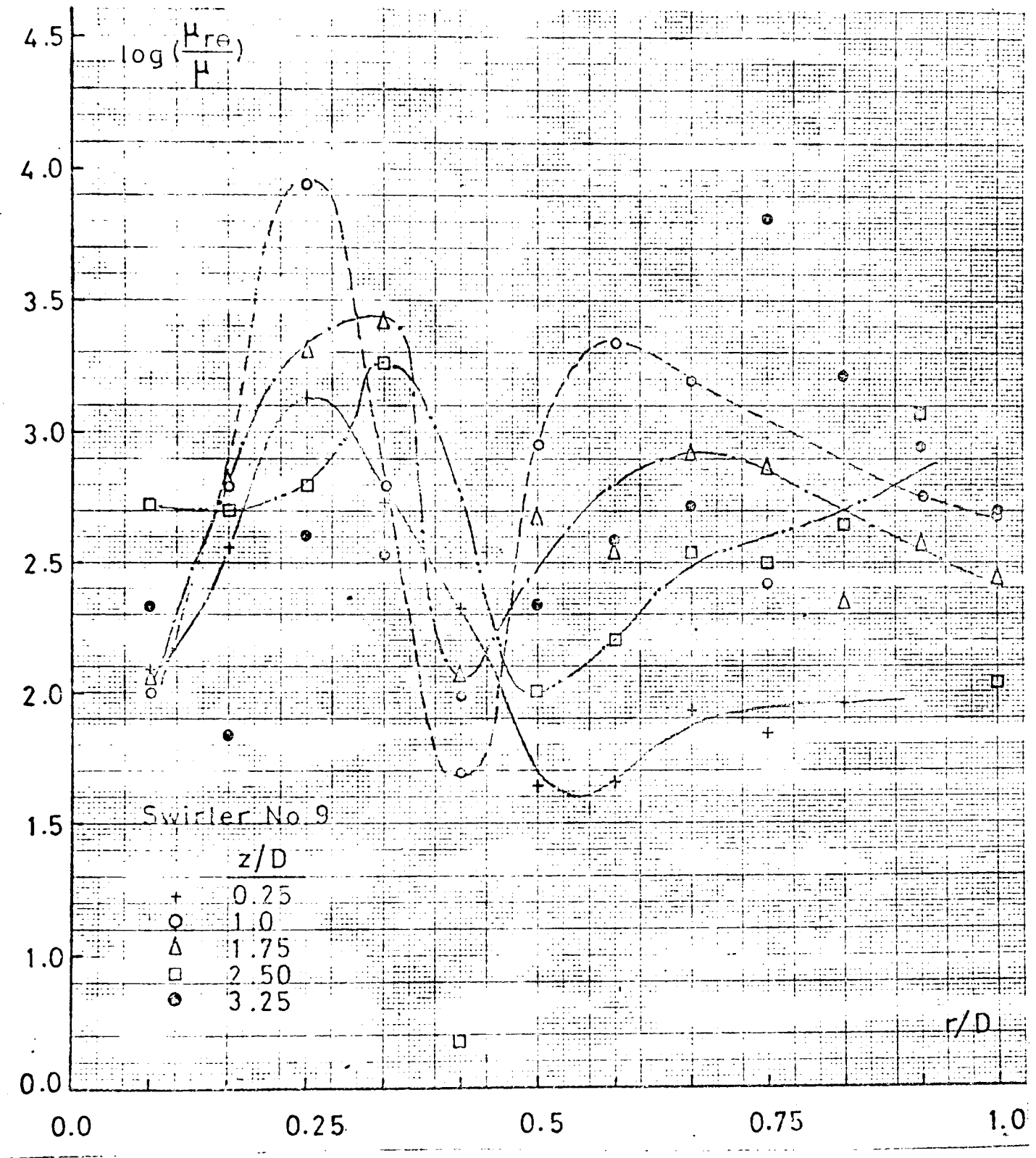

Fig.7.83. Profiles of the turbulent viscosity $\mu_{r\theta}$ in the flow field of the swirler S.9

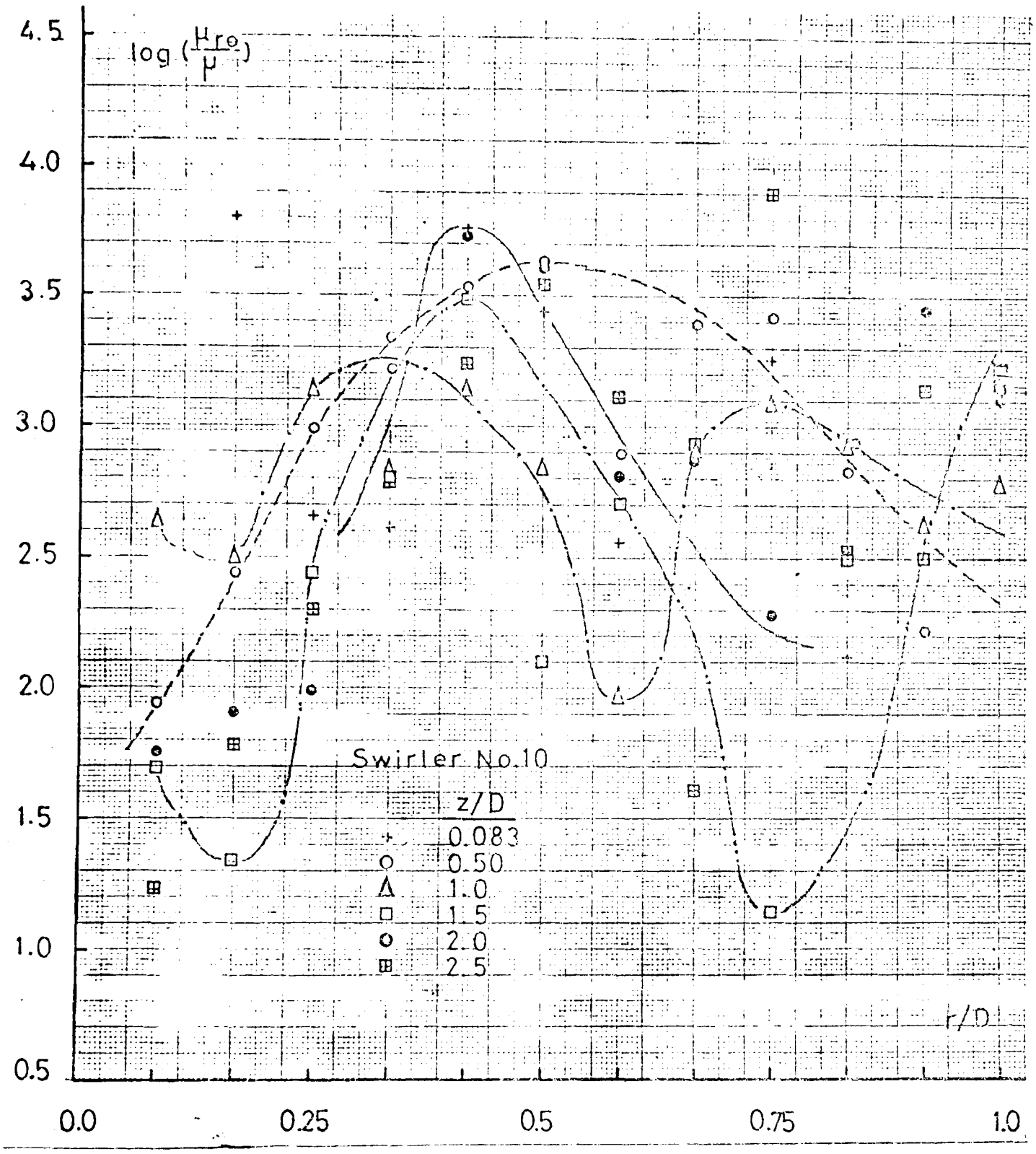

Fig.7.84.Profiles of the turbulent viscosity $\mu_{r\theta}$ in the flow field of the swirler S.IO

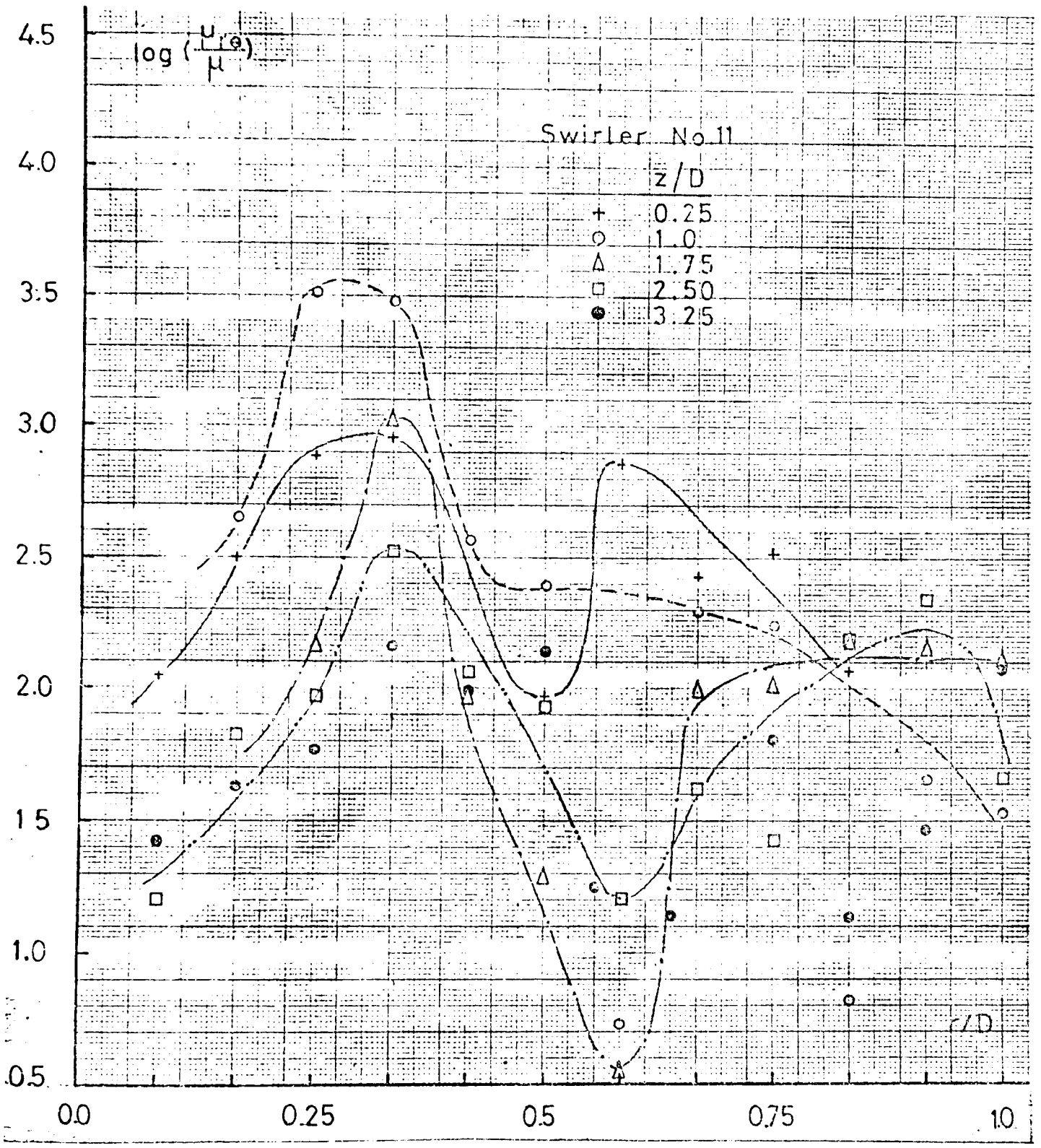

Fig.7.85.Profiles of the turbulent viscosity $\mu_{r\theta}$ in the flow field of the swirler S.II

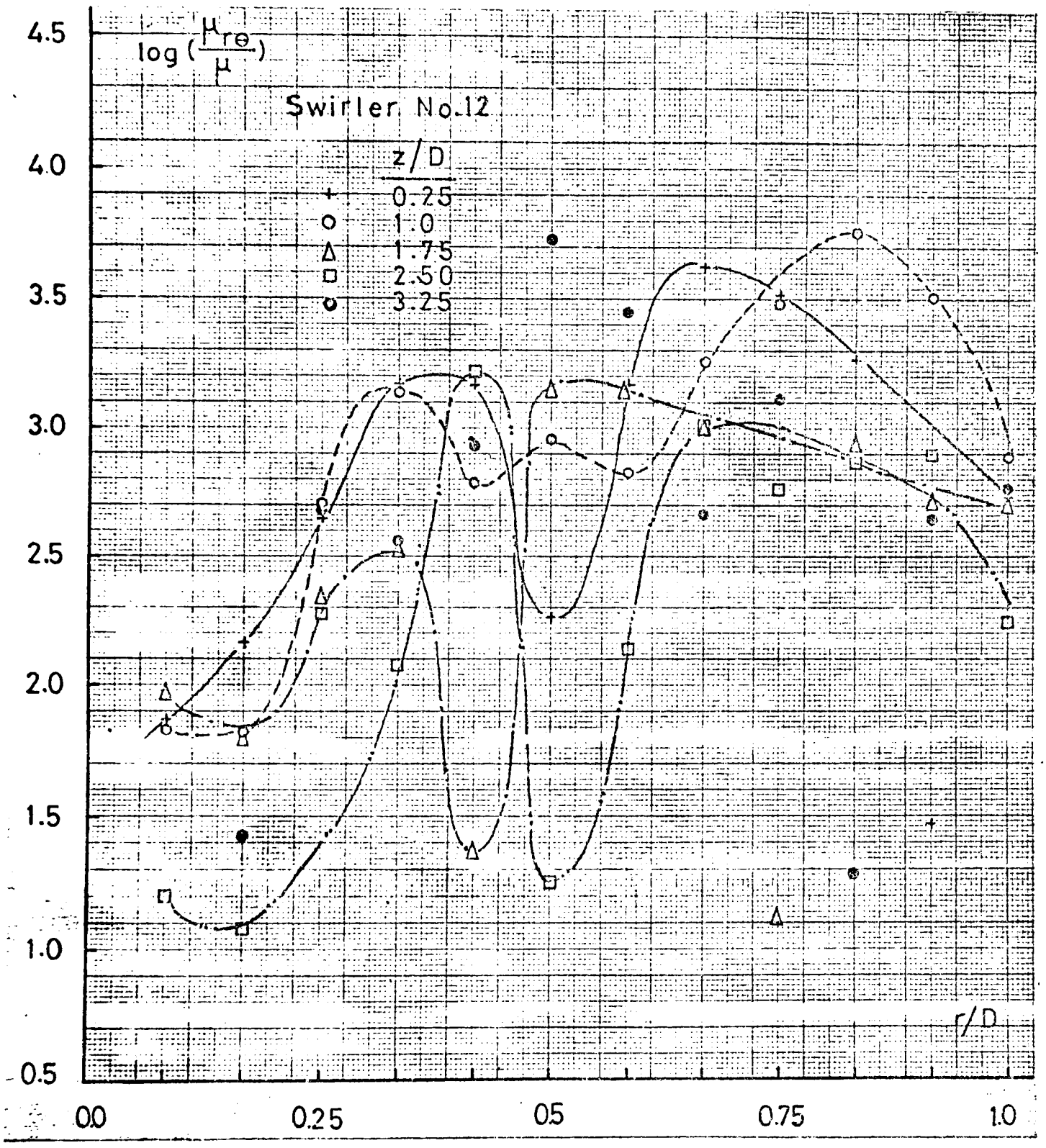

Fig.7.86.Profiles of the turbulent viscosity $\mu_{r\theta}$ in the flow field of the swirler S.I2

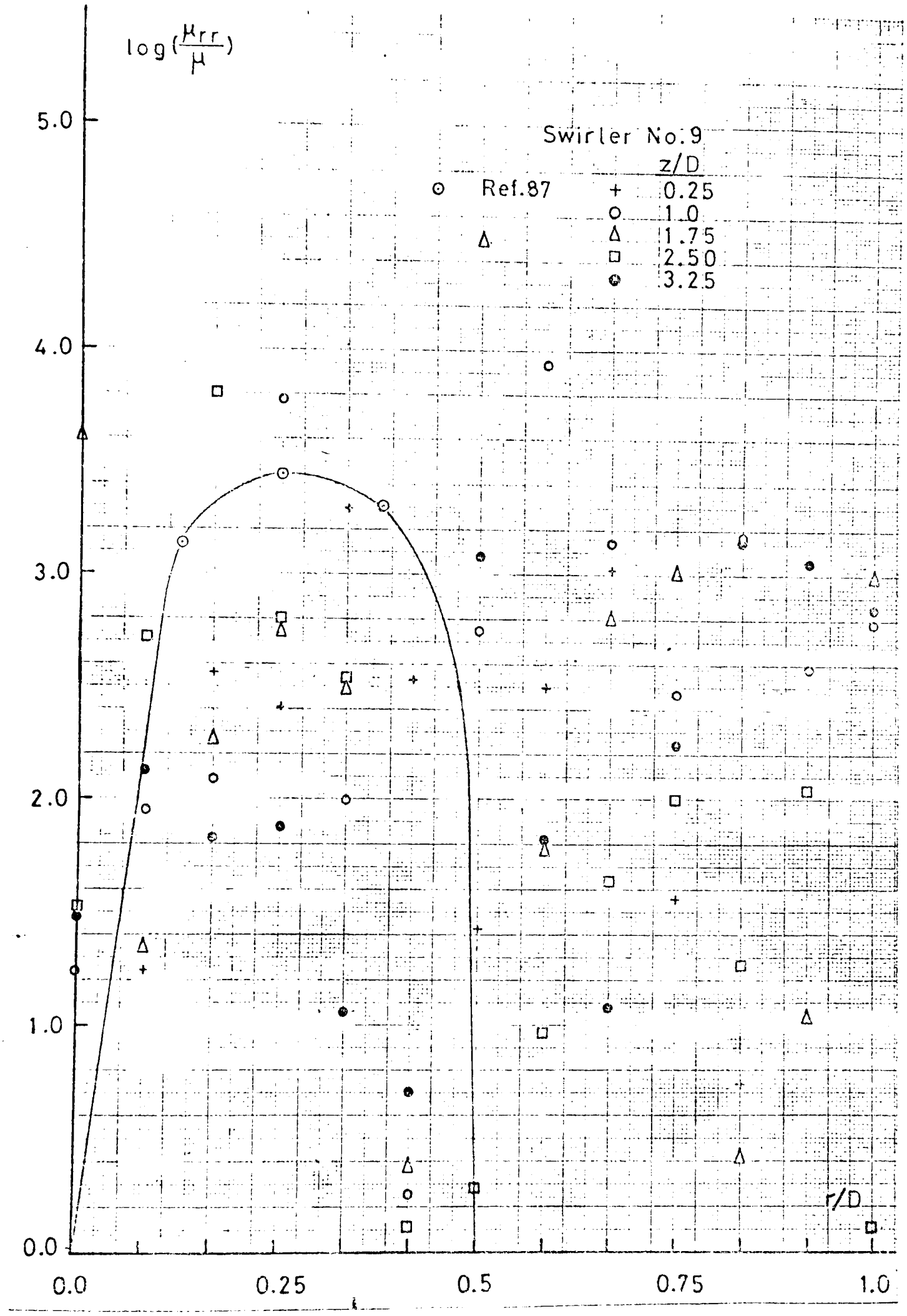

Fig.7.87.Profiles of the turbulent viscosity μ_{rr} in the flow field of the swirler S.9

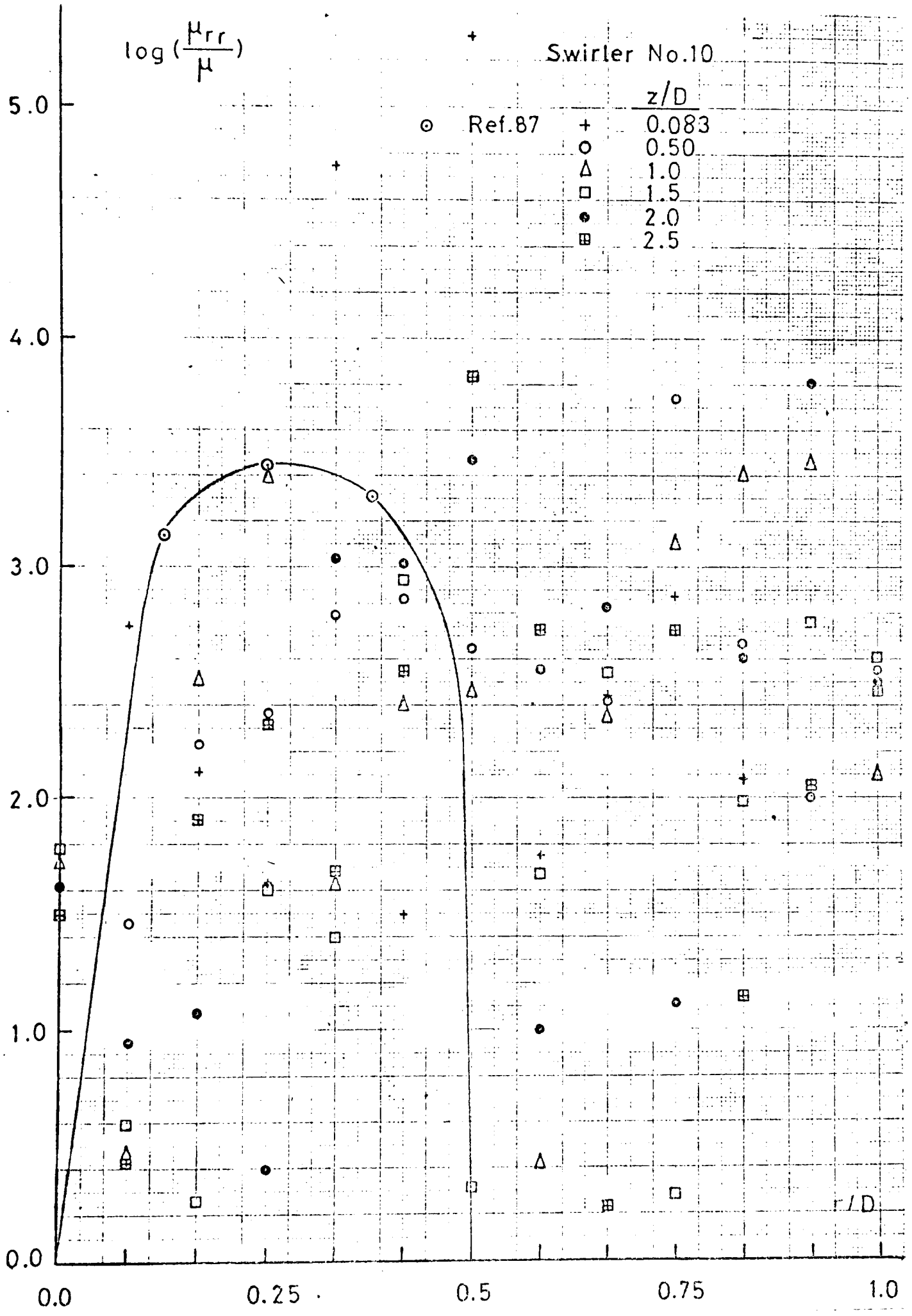

Fig.7.88.Profiles of the turbulent viscosity μ_{rr} in the flow field of the swirler S.IO

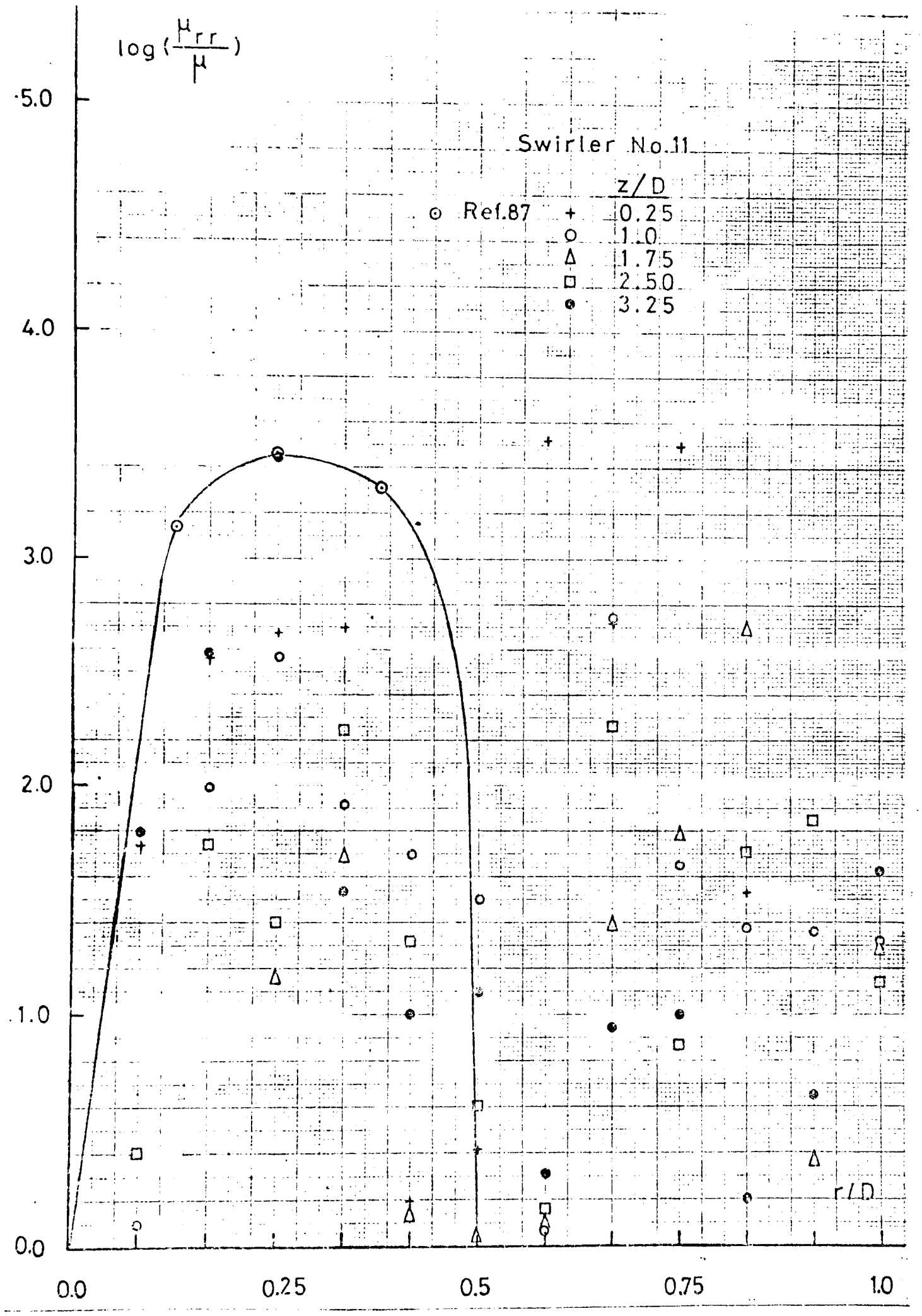

Fig.7.89.Profiles of the turbulent viscosity μ_{rr} in the flow field of the swirler S.II

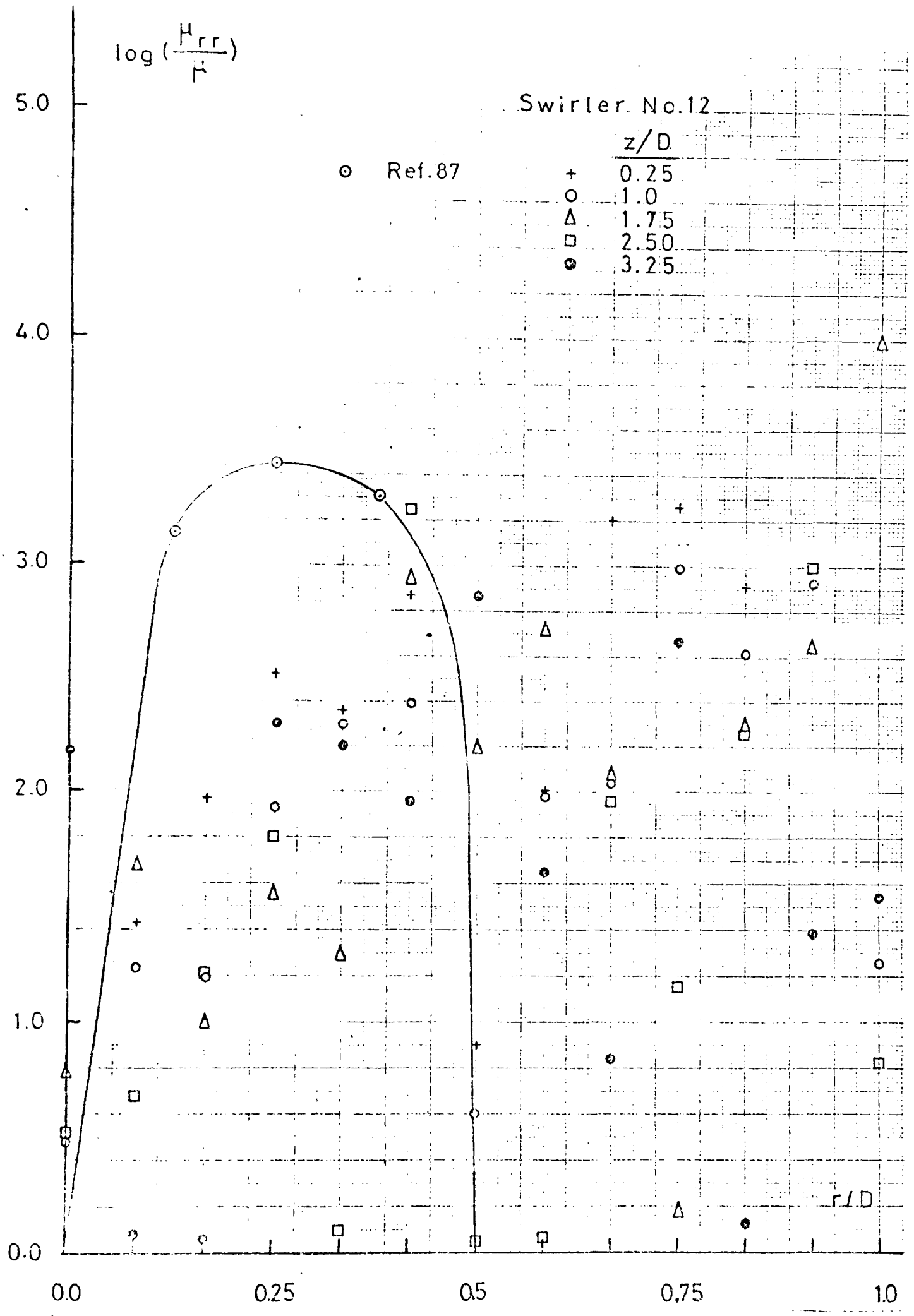

Fig.7.90.Profiles of the turbulent viscosity μ_{rr} in the flow field of the swirler S.I2

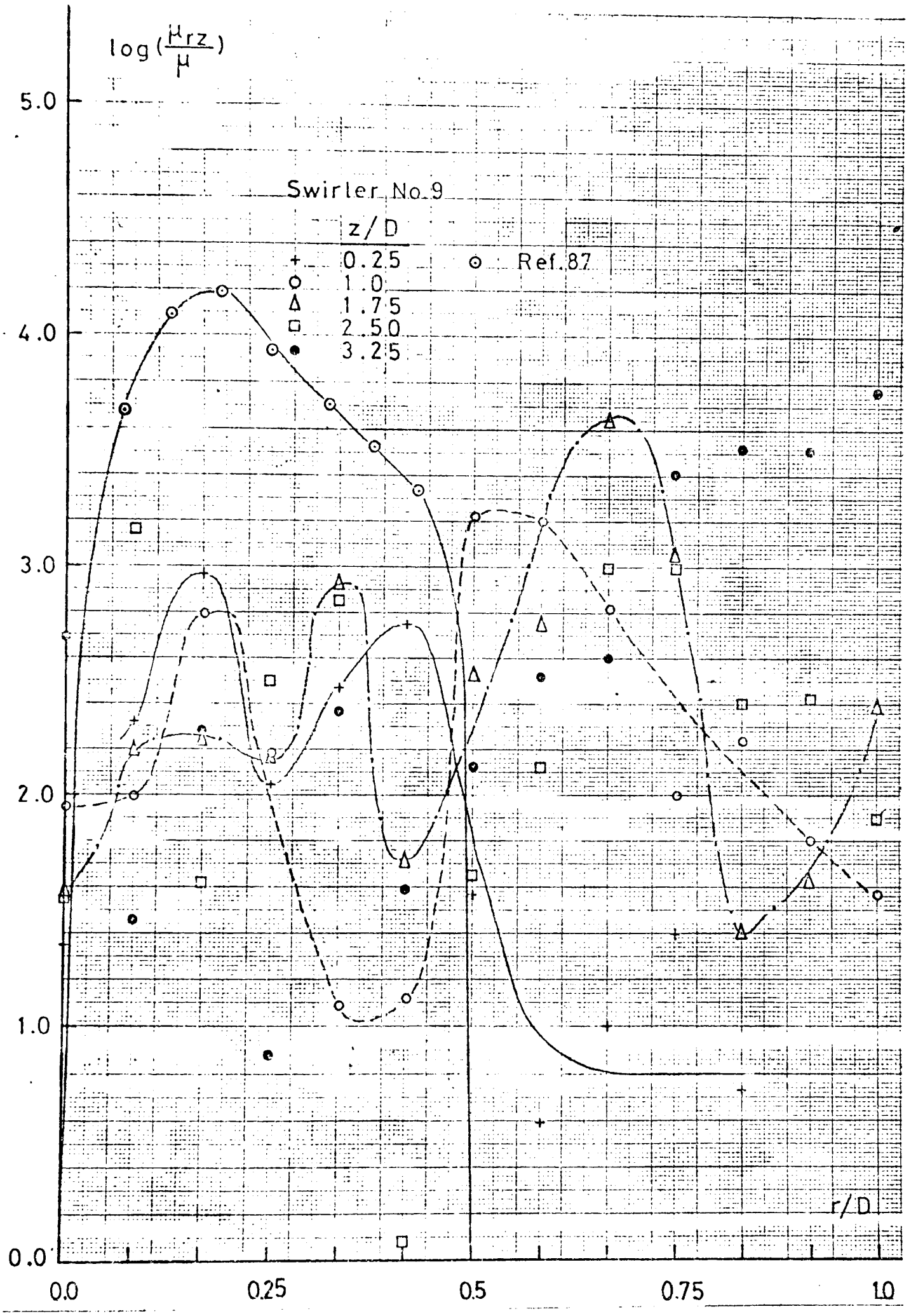

Fig.7.9I. Profiles of the turbulent viscosity μ_{rz} in the flow field of the swirler S.9

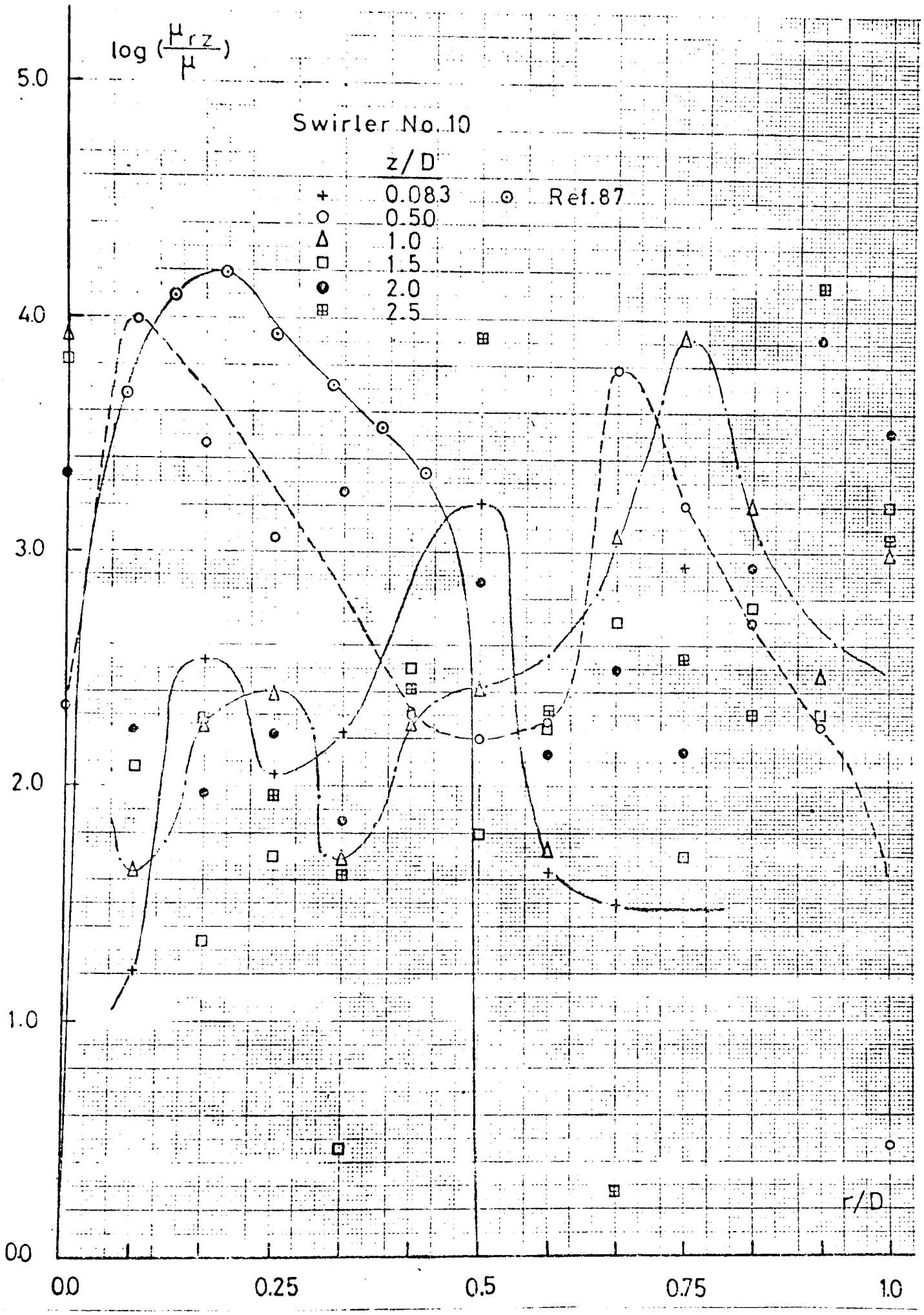

Fig.7.92.Profiles of the turbulent viscosity μ_{rz} in the flow field of the swirler S.IO

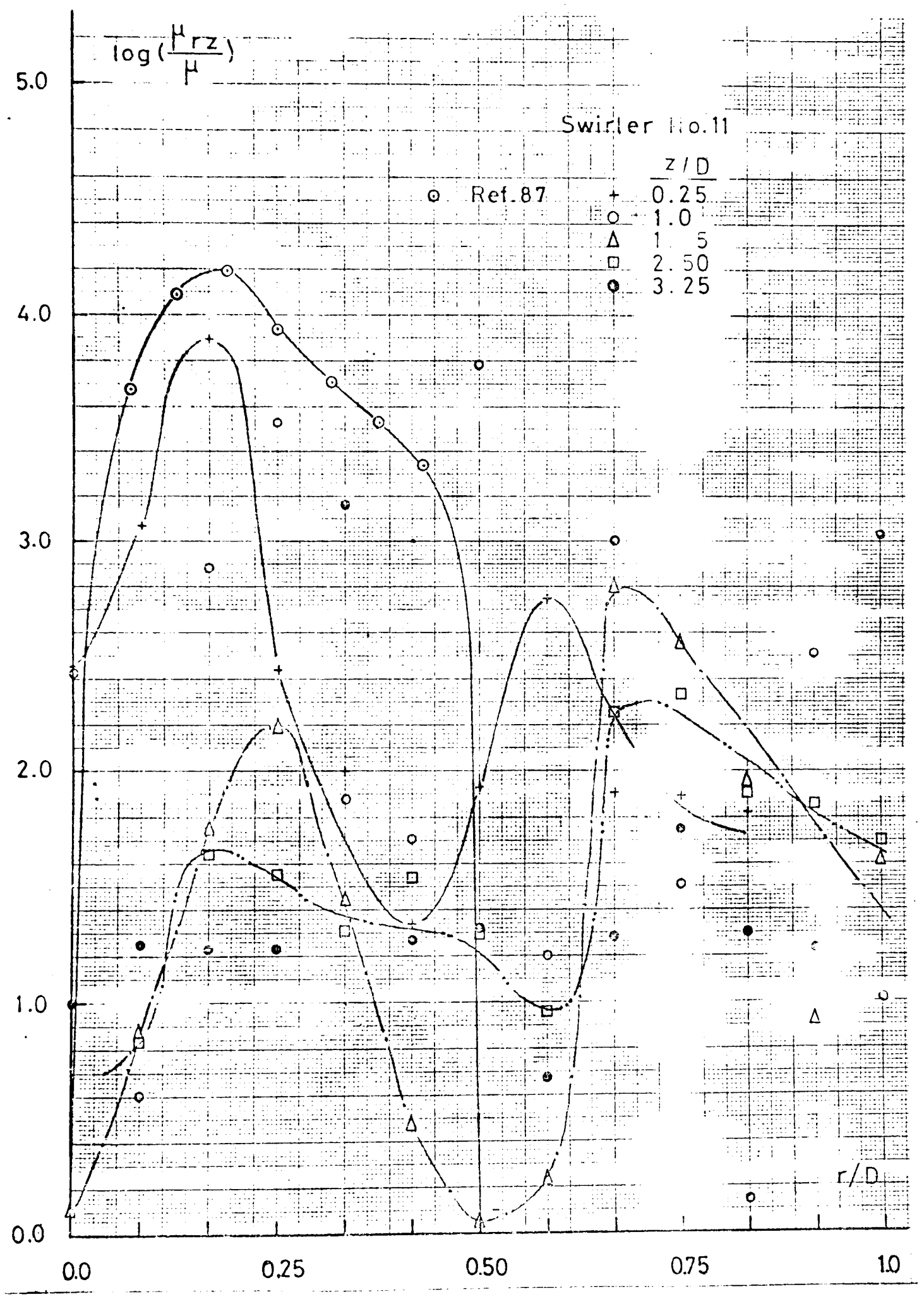

Fig.7.93.Profiles of the turbulent viscosity μ_{rz} in the flow field of the swirler S.II

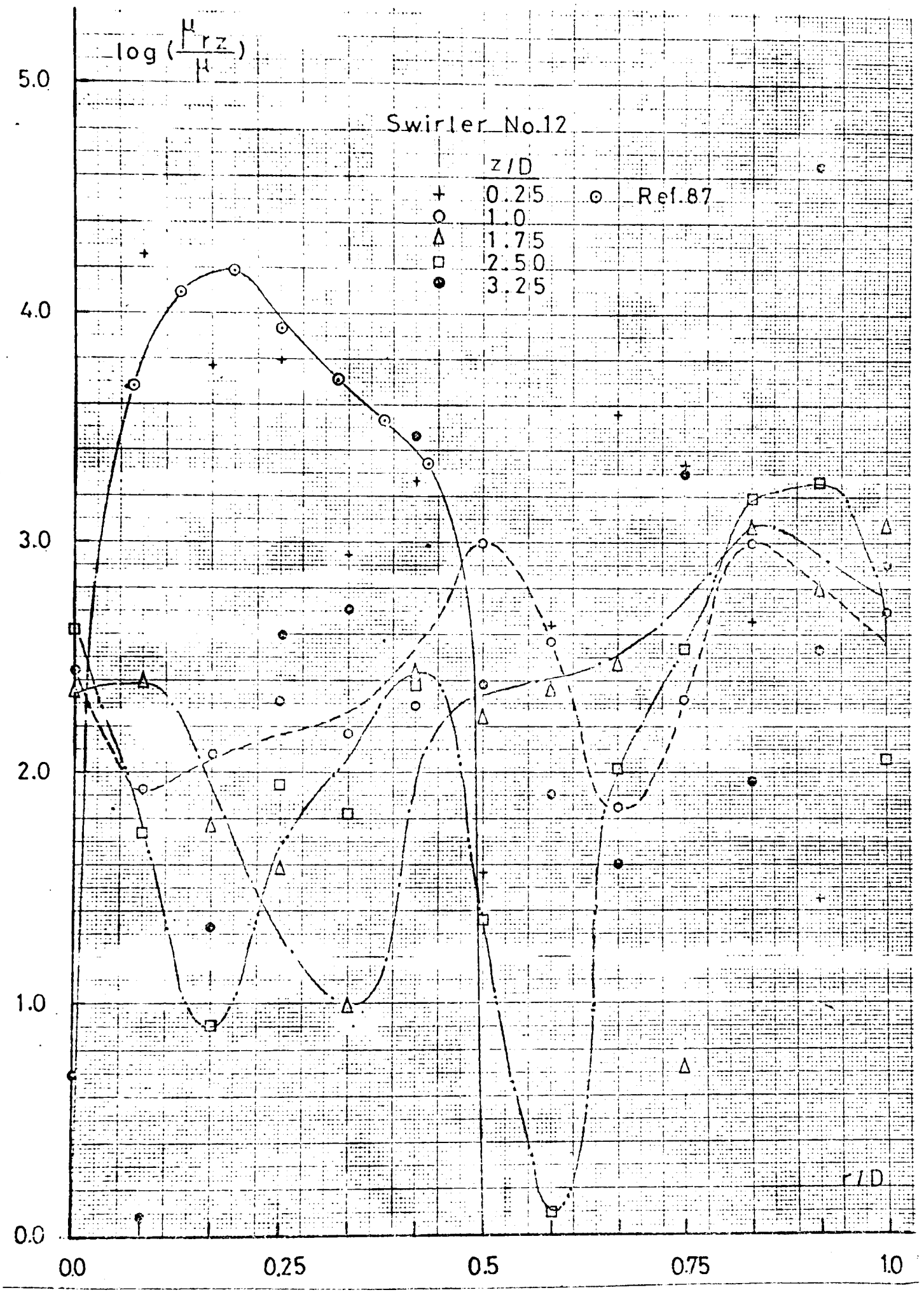

Fig.7.94.Profiles of the turbulent viscosity μ_{rz} in the flow field of the swirler S.I2

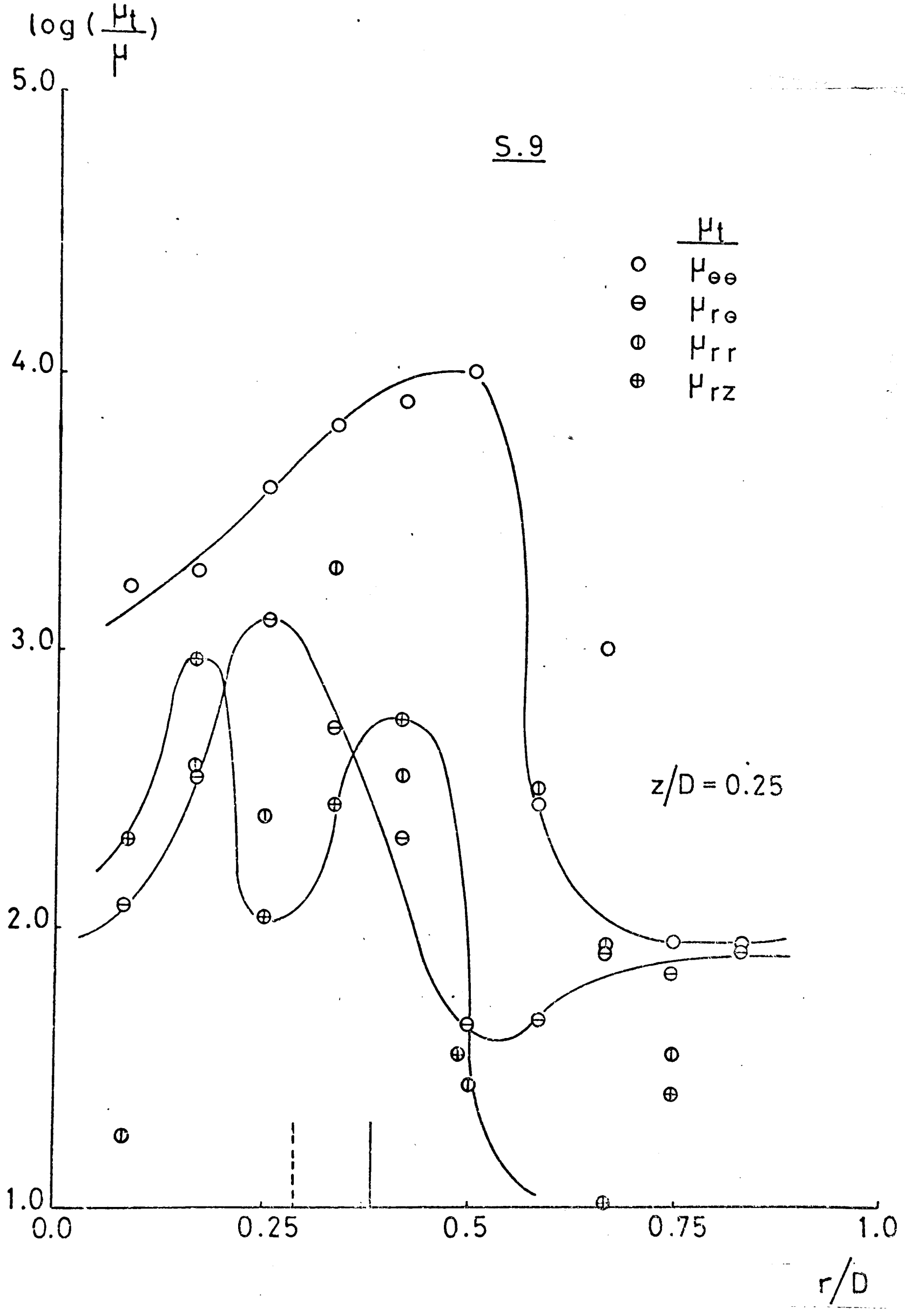

Fig.7.95.Comparison of the four turbulent viscosities at z/D=0.25 in the flow field of the swirler S.9

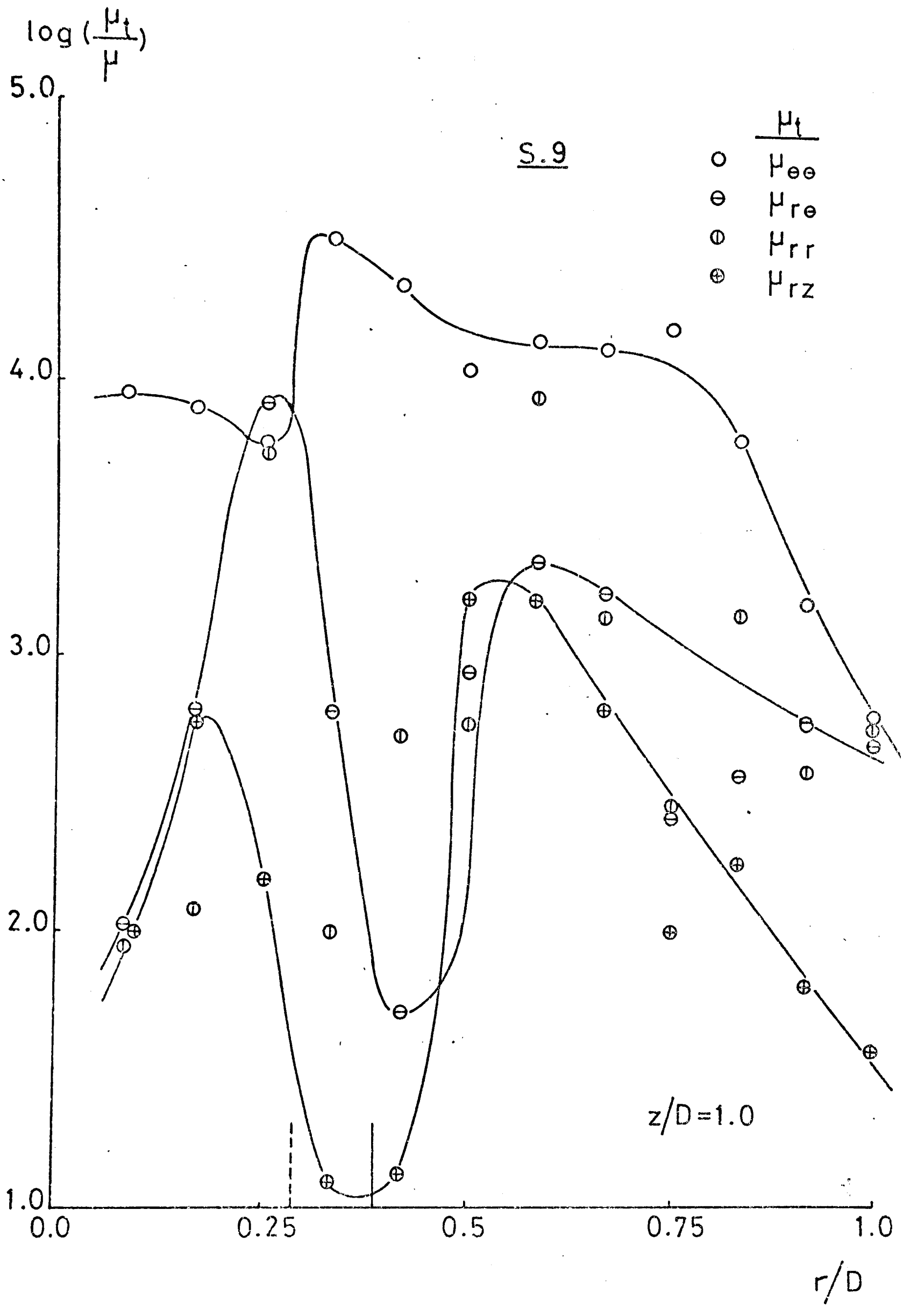

Fig.7.96.Comparison of the four turbulent viscosities at z/D=I.O in the flow field of the swirler S.9

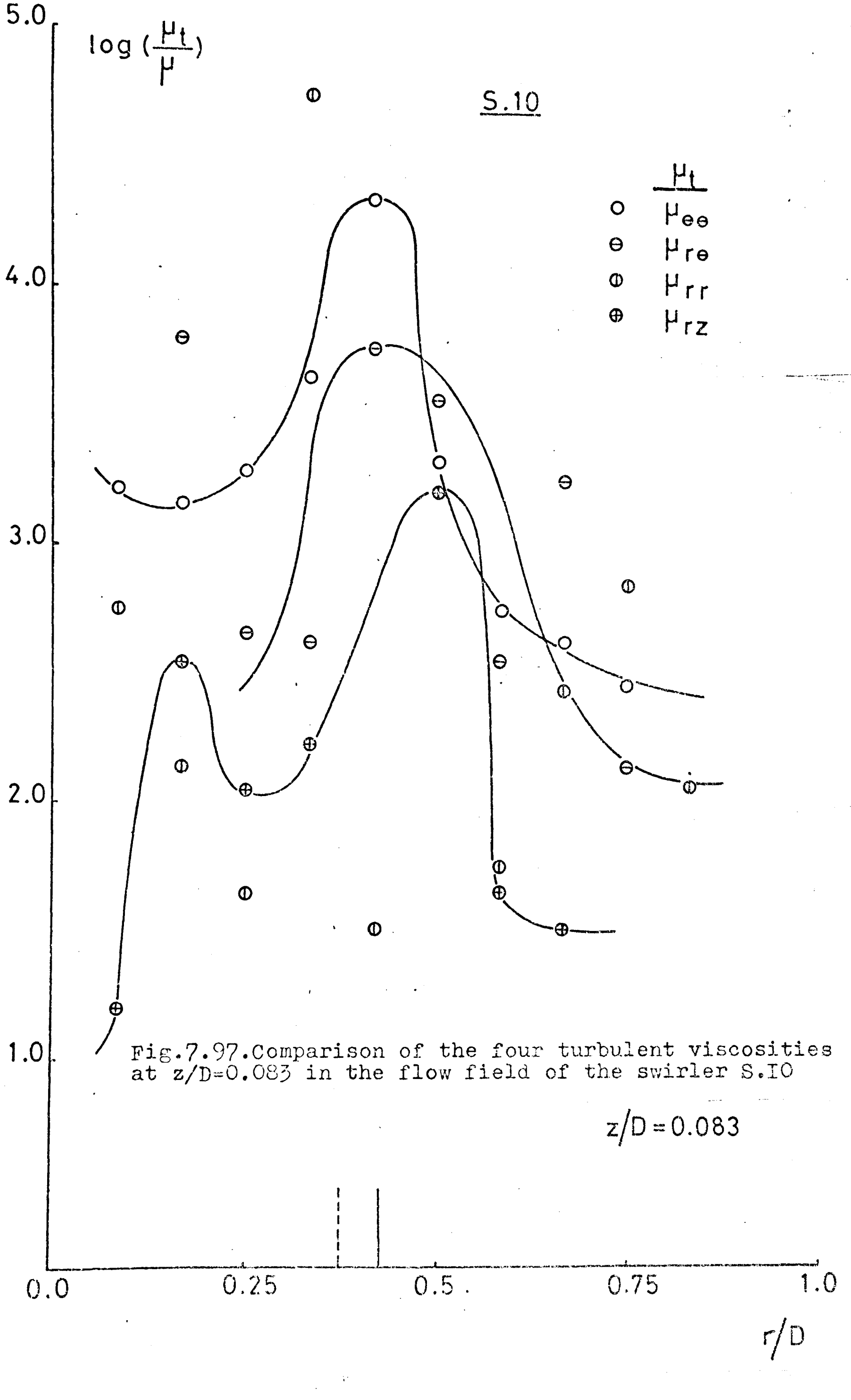

Fig.7.97.Comparison of the four turbulent viscosities at z/D=0.083 in the flow field of the swirler S.IO

S.10

Fig.7.98.Comparison of the four turbulent viscosities at z/D=I.5 in the flow field of the swirler S.IO

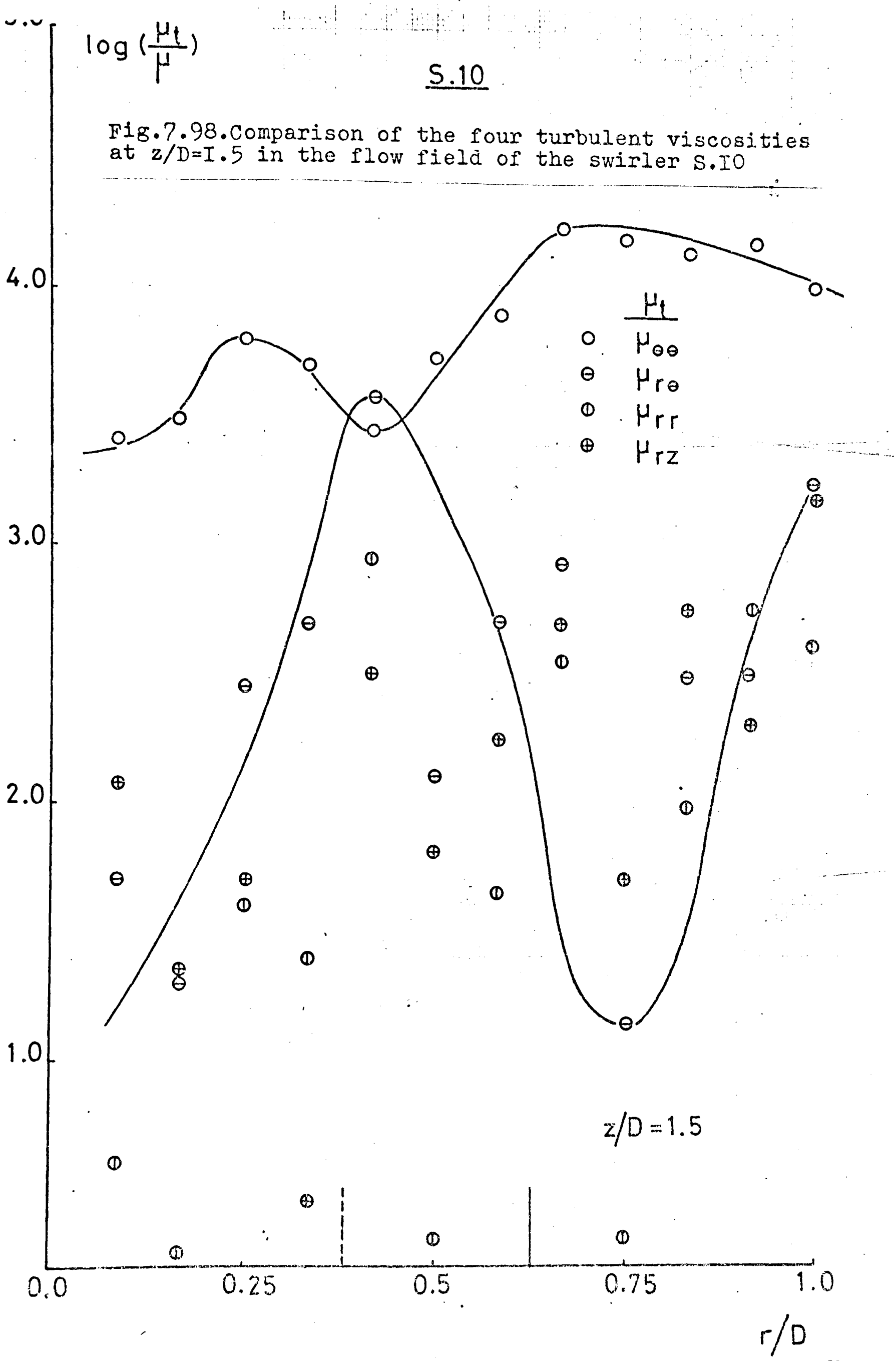

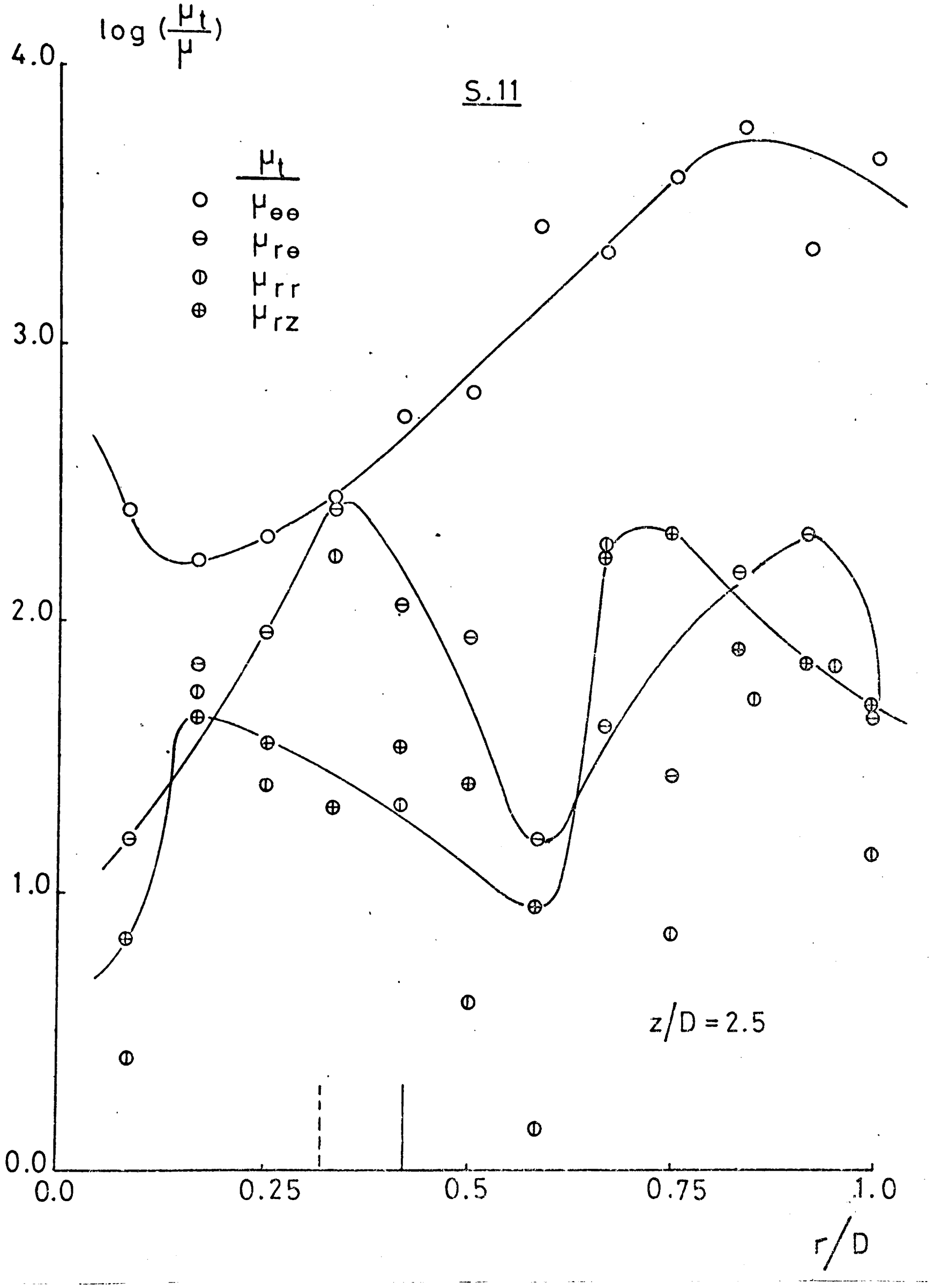

Fig.7.99.Comparison of the four turbulent viscosities at z/D=2.5 in the flow field of the swirler S.II

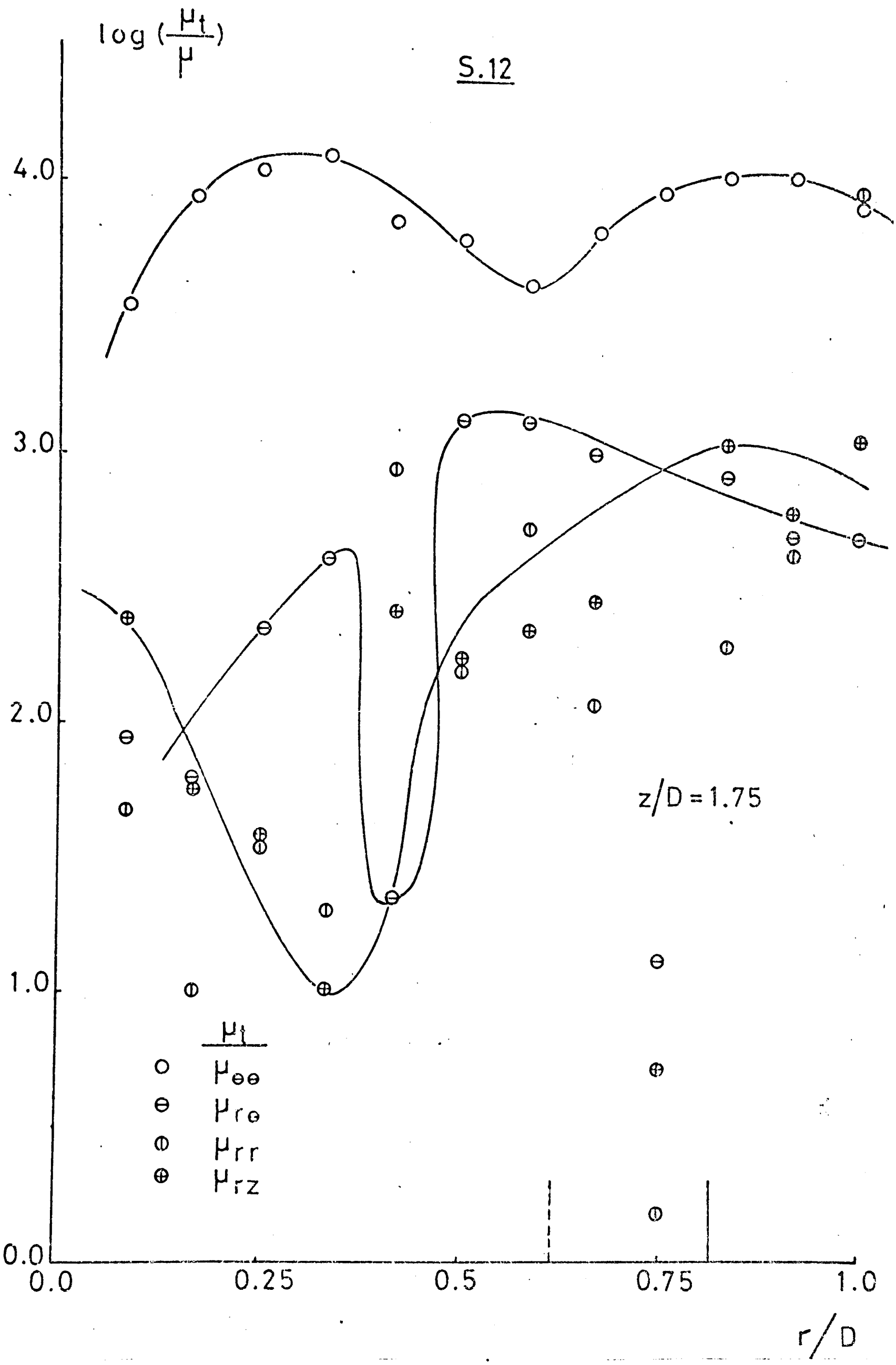

Fig.7.100.Comparison of the four turbulent viscosities at z/D=1.75 in the flow field of the swirler S.12

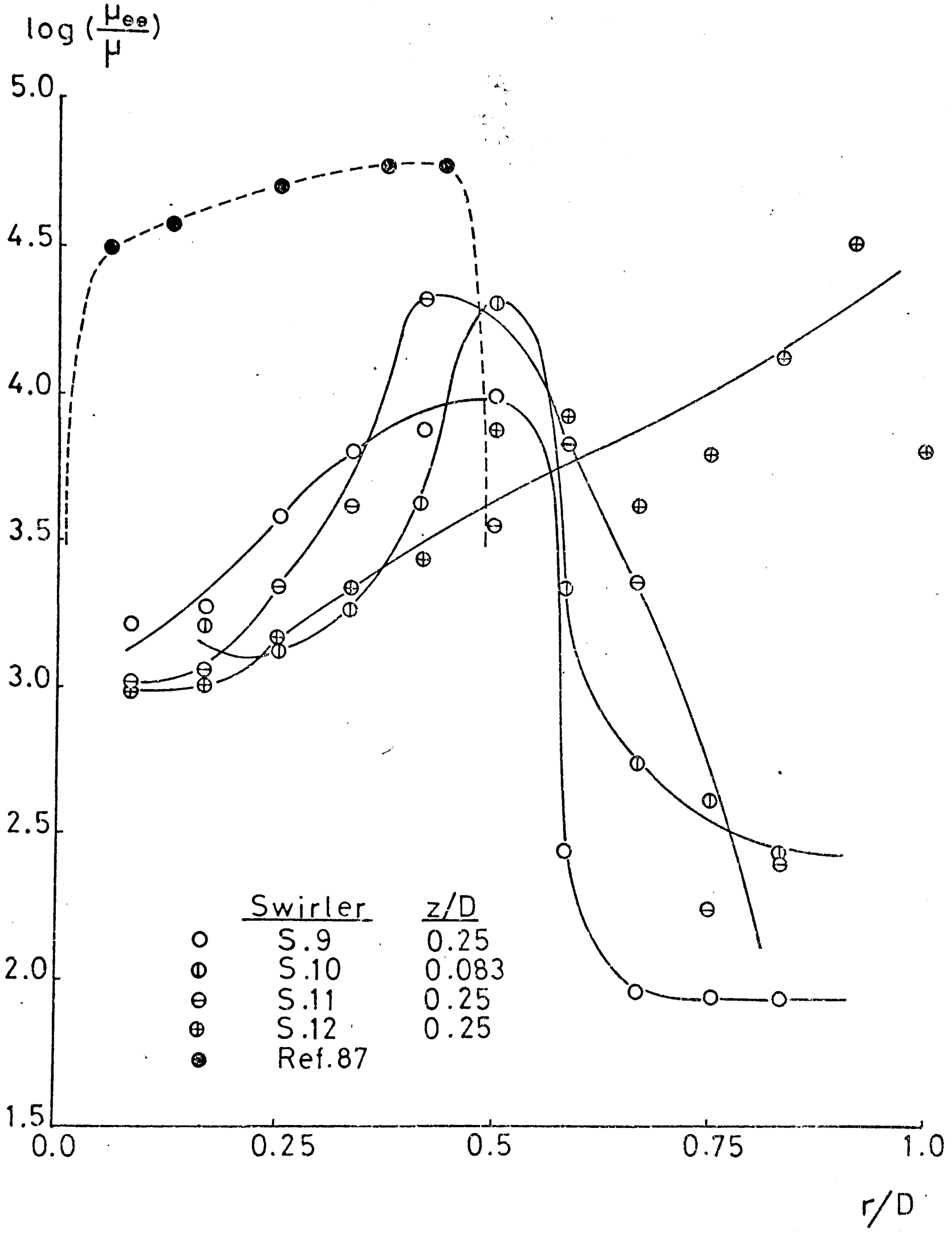

Fig.7.101.Comparison of the dominant viscosity $\mu_{\theta\theta}$ for different swirlers

Fig.7.102.Comparison of the dominant viscosity $\mu_{\theta\theta}$ for different swirlers

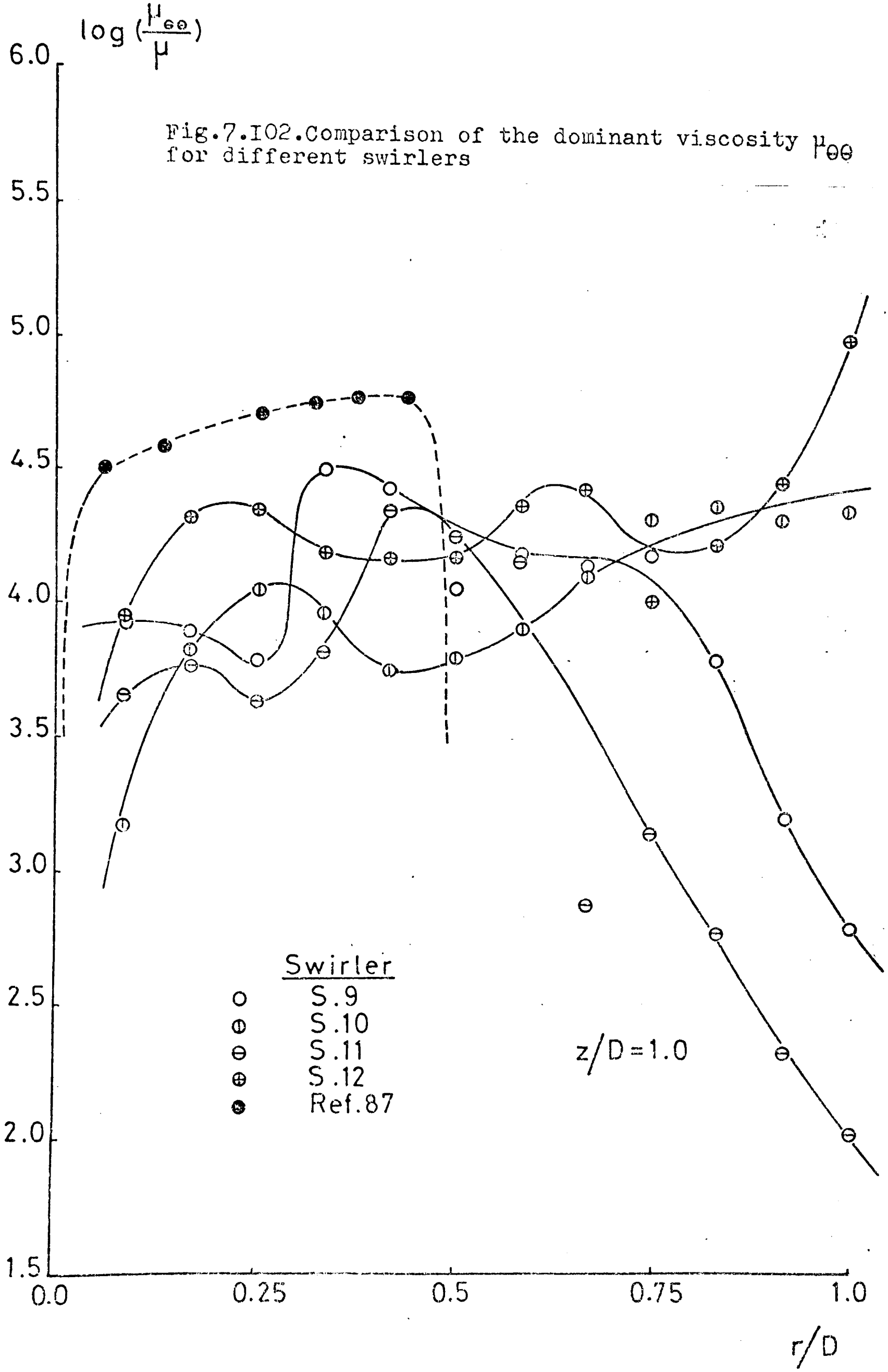

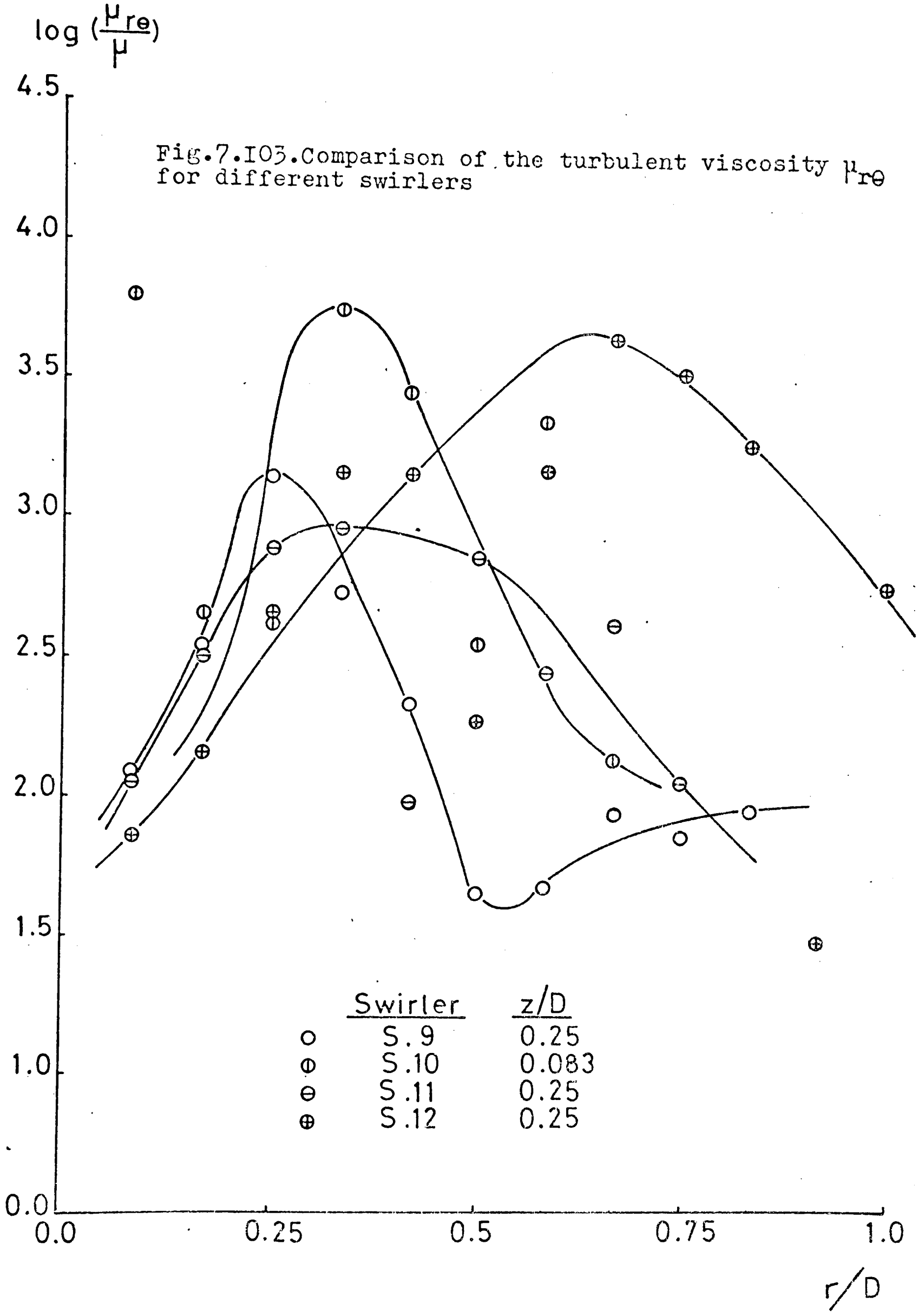

Fig.7.103.Comparison of the turbulent viscosity μ_{re} for different swirlers

Fig.7.I04.Comparison of the turbulent viscosity $\mu_{r\theta}$ for different swirlers

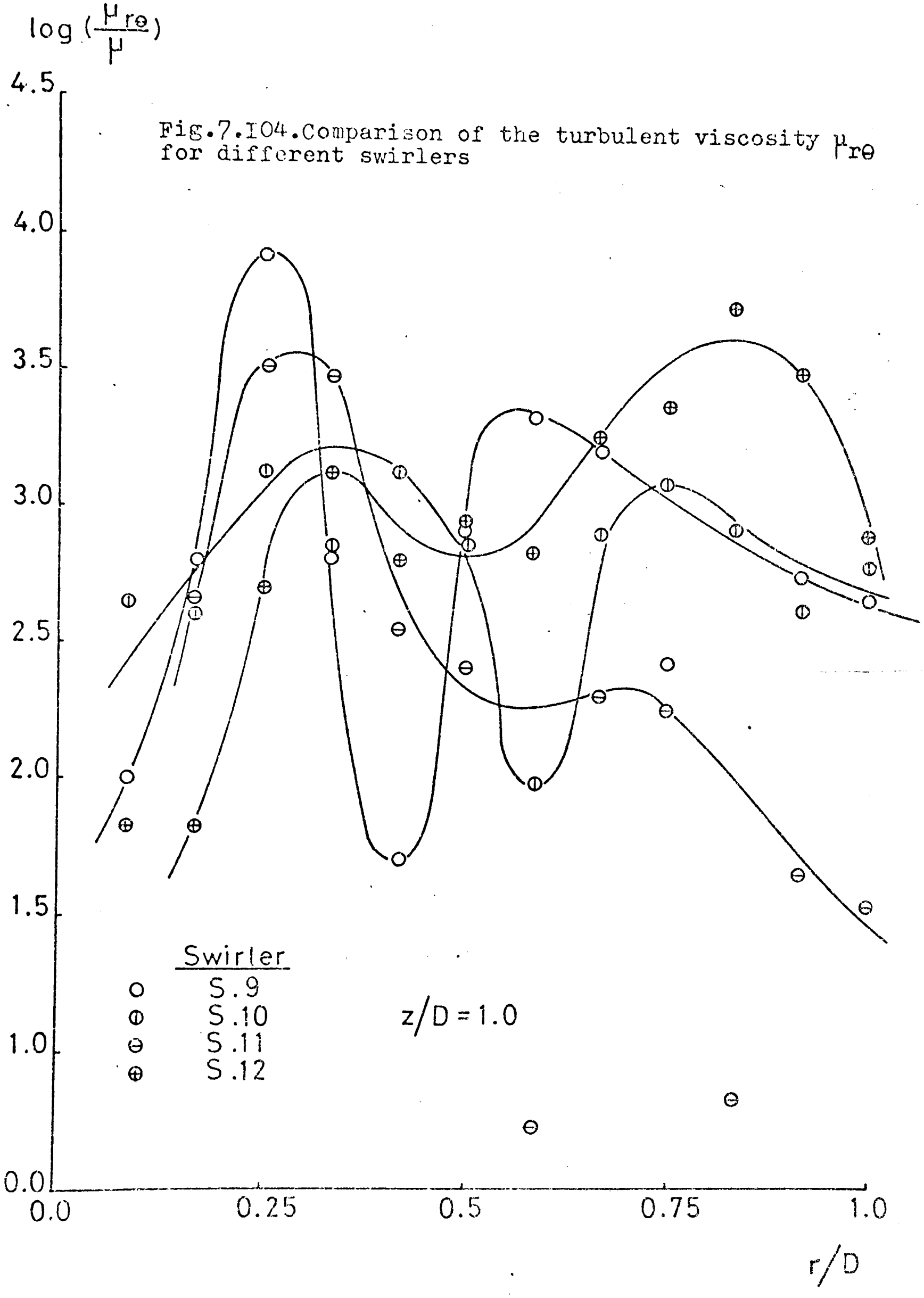

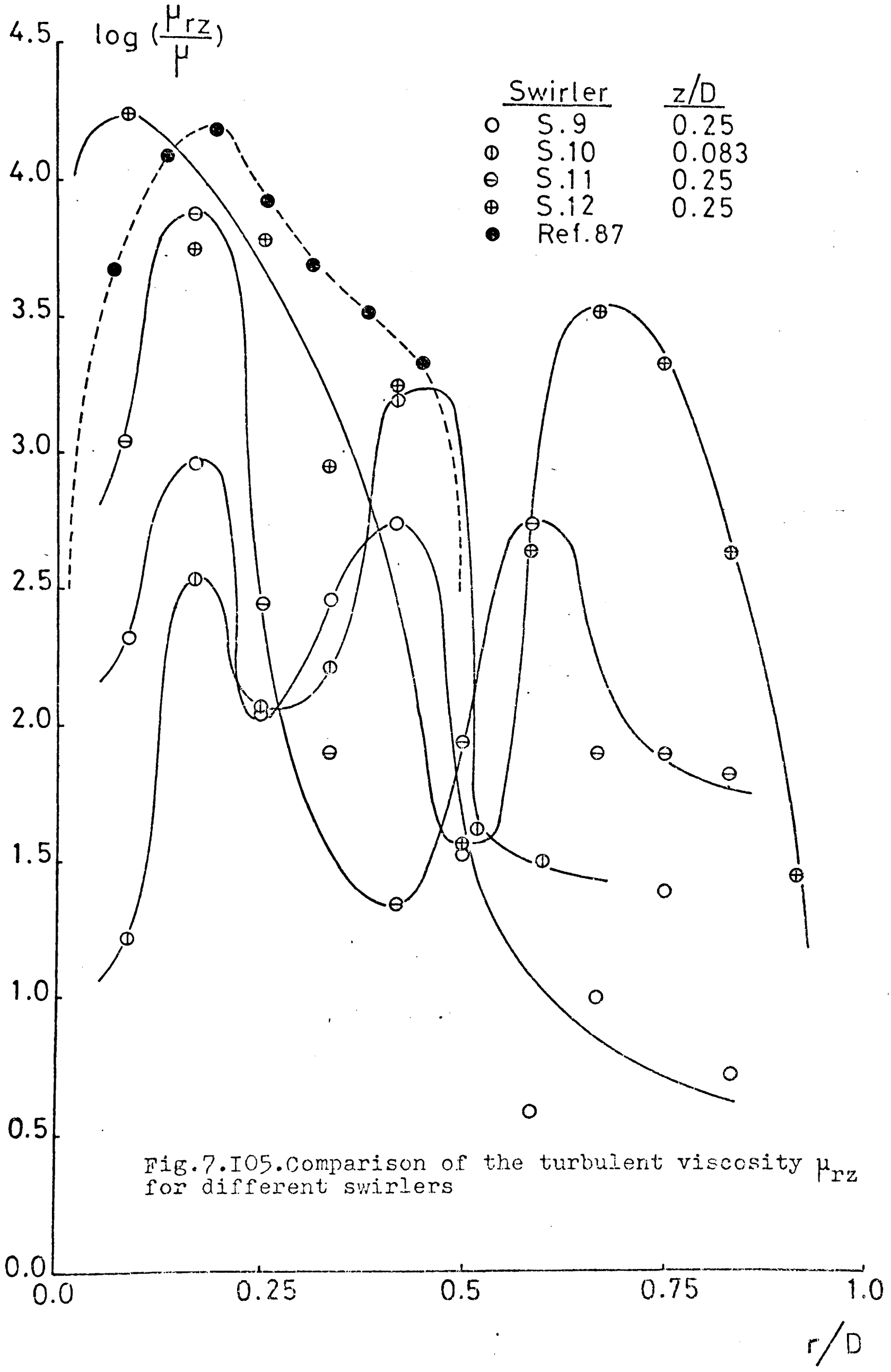

Fig.7.105.Comparison of the turbulent viscosity μ_{rz} for different swirlers

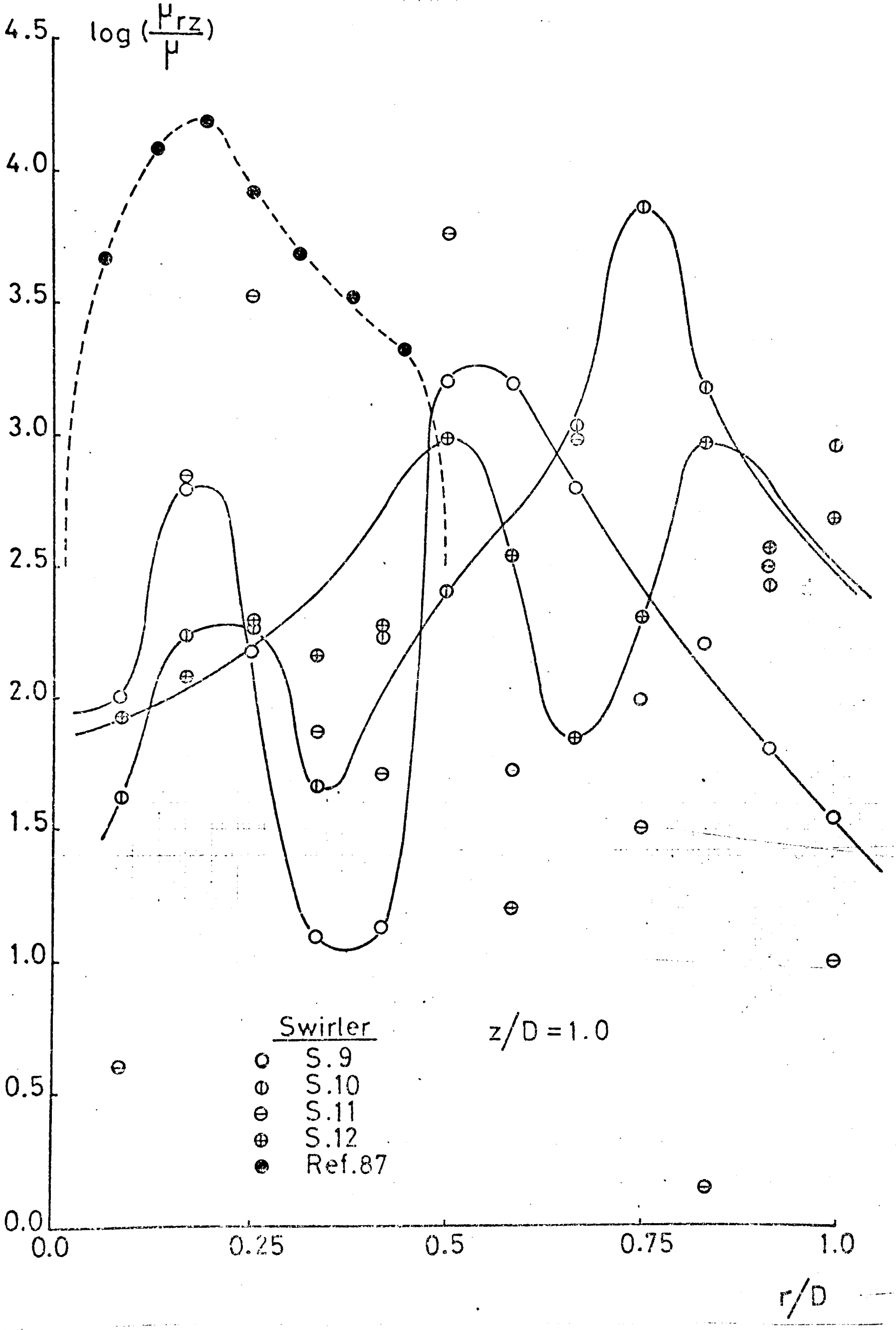

Fig.7.106.Comparison of the turbulent viscosity μ_{rz} for different swirlers